

Proceedings of the U.S. Nuclear Regulatory Commission

---

---

# Twelfth Water Reactor Safety Research Information Meeting

## Volume 2

- Pressurized Thermal Shock
- Code Assessment and Improvement
- 2D/3D Research Program
- Nuclear Plant Analyzer Program

Held at  
National Bureau of Standards  
Gaithersburg, Maryland  
October 22-26, 1984

---

---

**U.S. Nuclear Regulatory  
Commission**

Office of Nuclear Regulatory Research



## NOTICE

These proceedings have been authored by a contractor of the United States Government. Neither the United States Government nor any agency thereof, or any of their employees, makes any warranty, expressed or implied, or assumes any legal liability or responsibility for any third party's use, or the results of such use, of any information, apparatus, product or process disclosed in these proceedings, or represents that its use by such third party would not infringe privately owned rights. The views expressed in these proceedings are not necessarily those of the U.S. Nuclear Regulatory Commission.

Available from

GPO Sales Program  
Division of Technical Information and Document Control  
U.S. Nuclear Regulatory Commission  
Washington, D.C. 20555

Printed copy price: \$9.00

and

National Technical Information Service  
Springfield, VA 22161

Proceedings of the U.S. Nuclear Regulatory Commission

---

---

# Twelfth Water Reactor Safety Research Information Meeting

## Volume 2

- Pressurized Thermal Shock
- Code Assessment and Improvement
- 2D/3D Research Program
- Nuclear Plant Analyzer Program

Held at  
National Bureau of Standards  
Gaithersburg, Maryland  
October 22-26, 1984

---

---

Date Published: January 1985

Compiled by: Stanley A. Szawlewicz, Consultant

Office of Nuclear Regulatory Research  
U.S. Nuclear Regulatory Commission  
Washington, D.C. 20555



#### ABSTRACT

The papers published in this six volume report were presented at the Twelfth Water Reactor Safety Research Information Meeting held at the National Bureau of Standards, Gaithersburg, Maryland during the week of October 22-26, 1984. The papers describe progress and results of programs in nuclear safety research conducted in this country and abroad. Foreign participation in the meeting included twenty-six different papers presented by researchers from seven European countries, Japan, and Canada.

PROCEEDINGS OF THE  
TWELFTH WATER REACTOR SAFETY RESEARCH  
INFORMATION MEETING

October 22-26, 1984

Published in Six Volumes

GENERAL INDEX

VOLUME 1

- Plenary Session - I
- Integral System Tests
- Separate Effects
- International Programs in Thermal Hydraulics
- Calculation of Appendix K Conservatism

VOLUME 2

- Pressurized Thermal Shock
- Code Assessment and Improvement
- 2D/3D Research Program
- Nuclear Plant Analyzer Program

VOLUME 3

- Containment Systems Research
- Fuel Systems Research
- Accident Source Term Assessment
- Japanese Industry Safety Research

VOLUME 4

- Materials Engineering Research

VOLUME 5

- Mechanical Engineering
- Structural Engineering
- Seismic Research
- Process Control
- Instrumentation and Control Program
- Equipment Qualification and Nuclear Plant Aging

VOLUME 6

- Plenary Session - II
- Human Factors and Safeguards Research
- Health Effects and Radiation Protection
- Risk Analysis
- EPRI Safety Research

PROCEEDINGS OF THE  
TWELFTH WATER REACTOR SAFETY RESEARCH  
INFORMATION MEETING

held at the

NATIONAL BUREAU OF STANDARDS  
Gaithersburg, Maryland  
October 22-26, 1984

TABLE OF CONTENTS - VOLUME 2

PREFACE . . . . .	ix
PRESSURIZED THERMAL SHOCK	
Chairmen: C. E. Johnson, J. N. Reyes, NRC	
Integration of PTS Studies to Calculate Through-the-Wall Crack Probabilities	
D. L. Selby, ORNL . . . . .	1
TRAC-PF1 Analyses of Potential Pressurized-Thermal-Shock Transients at a Combustion Engineering PWR	
J. E. Koenig and R. C. Smith, LANL . . . . .	5
Analysis of H. B. Robinson Unit-2 Pressurized Thermal Shock Transients	
D. M. Ogden, C. D. Fletcher, C. B. Davis, INEL. . . . .	16
Review of Thermal-Hydraulic Calculations for Calvert Cliffs and H. B. Robinson PTS Study	
J. H. Jo, C. Yuelys-Miksis, U. S. Rohatgi, BNL . . . . .	42
Buoyancy Effects in Overcooling Transients	
T. G. Theofanous and K. Iyer, Purdue University . . . . .	55
IPTS Program Probabilistic Fracture-Mechanics Analysis and Results	
R. D. Cheverton and D. G. Ball, ORNL. . . . .	77
Results and Conclusions from the First Pressurized-Thermal-Shock Experiment	
R. H. Bryan, et al., ORNL . . . . .	89
Vessel Behavior Following a Through-Wall Crack	
F. A. Simonen, PNL . . . . .	115
Consequence Evaluation for Pressurized Thermal Shock	
R. J. Barrett and E. D. Throm, NRC . . . . .	136
CODE ASSESSMENT AND IMPROVEMENT	
Chairman: Fuat Odar, NRC	
The TRAC-PF1/MOD1 Computer Code	
D. R. Liles and J. H. Mahaffy, LANL . . . . .	148
Status of RELAP5/MOD2 Development and Assessment	
G. W. Johnsen, INEL . . . . .	153
The Status of the TRAC-BWR Program	
W. L. Weaver, III, and S. Z. Rouhani, INEL . . . . .	167

CODE ASSESSMENT AND IMPROVEMENT (Cont'd)

Independent Assessment of the TRAC-BD1/MOD1 Computer Code at the Idaho National Engineering Laboratory G. E. Wilson, et al., INEL . . . . .	176
RELAP5/MOD2 Assessment Calculation of Semiscale Test S-UT-8 D. M. Ogden and C. B. Davis, INEL . . . . .	189
TRAC-PF1/MOD1 Assessment at Los Alamos T. D. Knight, LANL . . . . .	211
TRAC-PF1/MOD1 Independent Assessment at Sandia National Laboratories L. D. Buxton, et al., SNL . . . . .	231
Assessment of TRAC-BD1 and RAMONA-3B Codes for BWR ATWS Application J. Neymotin, C. J. Hsu, P. Saha, BNL. . . . .	242
Investigation of Dispersed Flow Heat Transfer Phenomena and Assessment of TRAC-PF1/MOD1 Heat Transfer Correlations I. Vojtek, GRS, FRG . . . . .	266
2D/3D RESEARCH PROGRAM Chairman: G. Rhee, NRC	
Results of CCTF Upper Plenum Injection Tests Y. Murao, et al., JAERI . . . . .	306
Status of CCTF/SCTF Test Programs Y. Murao, et al., JAERI . . . . .	342
TRAC Analyses for CCTF and SCTF Tests and UPTF Design/Operation F. E. Motley, LANL . . . . .	373
NUCLEAR PLANT ANALYZER PROGRAM Chairman: C. Troutman, NRC	
Safety Analysis Code Input Automation Using the Nuclear Plant Data Bank H. Kopp, et al., Technology Development of California . . . . .	395
The Los Alamos Nuclear Plant Analyzer: An Interactive Power-Plant Simulation Program R. Steinke, et al., LANL . . . . .	409
Nuclear Plant Analyzer Development at the Idaho National Engineering Laboratory E. T. Laats, et al., INEL . . . . .	424
Development of BWR Plant Analyzer W. Wulff, et al., BNL. . . . .	431

## PREFACE

This report, published in six volumes, contains 176 papers out of the 205 that were presented at the Twelfth Water Reactor Safety Research Information Meeting. The papers are printed in the order of their presentation in each session. The titles of the papers and the names of the authors have been updated and may differ from those which appear in the final agenda for the meeting. The papers listed under the session on Human Factors and Safeguards Research did not appear in the agenda but were prepared for the panel discussions that made up that session.

## INTEGRATION OF PTS STUDIES TO CALCULATE THROUGH-THE-WALL CRACK PROBABILITIES

D. L. Selby  
Oak Ridge National Laboratory

This paper describes a NRC-sponsored research project formed to help confirm the technical basis for the proposed Pressurized Thermal Shock (PTS) rule, to aid in the development of guidance for licensee plant-specific PTS analyses, and to examine the effects of proposed corrective measures. The research project, still under way (10/84), consists of PTS pilot analyses for three PWRs: Oconee Unit 1, designed by Babcock and Wilcox; Calvert Cliffs Unit 1, designed by Combustion Engineering; and H. B. Robinson Unit 2, designed by Westinghouse. The study team consists of Oak Ridge National Laboratory (ORNL), Idaho National Engineering Laboratory (INEL), Los Alamos National Laboratory (LANL), Brookhaven National Laboratory (BNL), and Purdue University, with the results being integrated by Oak Ridge National Laboratory (ORNL).

The overall objectives of the PTS studies at ORNL are: (1) to provide for each of the three plants an estimate of the frequency of a PTS-induced through-the-wall crack (TWC); (2) to determine the dominant overcooling sequences, plant features, and operator and control actions, as well as the important uncertainties, in the PTS risk; and (3) to evaluate the effectiveness of potential corrective measures for reducing the TWC frequencies. ORNL is also to determine what parts of the studies might have generic applicability.

Thousands of hypothetical overcooling sequences were constructed for each plant analysis using computer-generated event trees based on quantified event initiating frequencies and branch probabilities. A screening frequency of  $1.0E-7$  per reactor year was used to screen out those sequences (scenarios) which had a very low probability of occurring. All remaining scenarios were considered explicitly, and those scenarios screened out were grouped into "residual" groups to ensure that their contributions to the TWC frequency were included in the study.

Full-scale thermal-hydraulics analyses were performed for a selected number of the scenarios. For Calvert Cliffs the analyses were performed by LANL using the TRAC computer code, and for H. B. Robinson they were performed by INEL using the RELAP5 code. For Oconee both LANL and INEL used their respective analysis tools to analyze selected Oconee transients. The remaining scenarios were analyzed with simpler models by Science Applications, Inc. (Oconee and Calvert Cliffs) and INEL (H. B. Robinson). In addition, mixing calculations were performed by Purdue University for some of the scenarios.

Probabilistic fracture-mechanics calculations were performed by ORNL for all the scenarios for which thermal-hydraulic analyses were performed. The results of these analyses, performed with the computer code OCA-P, were then integrated by ORNL to predict the TWC frequency for each plant. The best estimate values determined for each plant are as follows:

	TWC frequency at 32 EFPY*	TWC frequency at RTNDT+2σ = 270°F**
Oconee Unit 1	5E-6/yr	5E-6/yr
Calvert Cliffs Unit 1	1E-7/yr	2E-7/yr
H. B. Robinson Unit 2	<1E-11/yr	1E-8/yr

\*EFPY = effective full power years.

\*\*RTNDT = nil-ductility reference temperature.

It should be noted that the Oconee analysis was the first plant study performed, and the analysts felt that certain assumptions may have led to an overprediction of the actual PTS risk for this plant.

An uncertainty analysis performed for each plant indicated that a factor of about 100 is an appropriate 95% confidence interval, assuming a log-normal uncertainty distribution. The uncertainty in the flaw density in the pressure vessel was found to be the most important contributor to the overall uncertainty in the risk.

For Oconee the dominant risk sequences were basically secondary side initiating events. The vent valves tended to mitigate cooldowns dominated by high-pressure injection (HPI) flow under low loop-flow conditions. This virtually eliminated the importance of loss-of-coolant accidents (LOCAs) as PTS transients. The presence of an integrated control system tended to increase the probability of PTS-type events, and the full pressure head system provided a means by which repressurization could be performed rapidly relative to the other two plants. The most important operator action was determined to be the isolation of the steam generator during an excess steam flow event (either a steam-line pipe break or a steam-line valve failure). This action was especially important since Oconee does not have main steam isolation valves (MSIVs). Reduction of the vessel fluence appeared to be the most beneficial risk reduction action for this plant. Fluence rate reduction factors of 2, 4, and 8 reduced the estimated TWC frequencies by factors of approximately 5, 20, and 50, respectively, at 32 EFPY.

For the Calvert Cliffs plant, which does not have vent valves, the LOCA events were much more important than for the Oconee plant. In fact, the top three dominant risk sequences for Calvert Cliffs involved a small-break LOCA in which total loop flow stagnation was predicted. (It should be noted that each of these sequences occurred at low decay heat condition, and loop flow stagnation was not predicted for small-break LOCA events occurring at full power. In fact, none of the sequences occurring from full power were considered major contributors to the overall PTS risk.) The relative importance of each initiator class for Calvert Cliffs can be seen in Figure 1, in which the TWC frequency is plotted as a function of RTNDT, fluence, and EFPY for each initiator class as designated below:

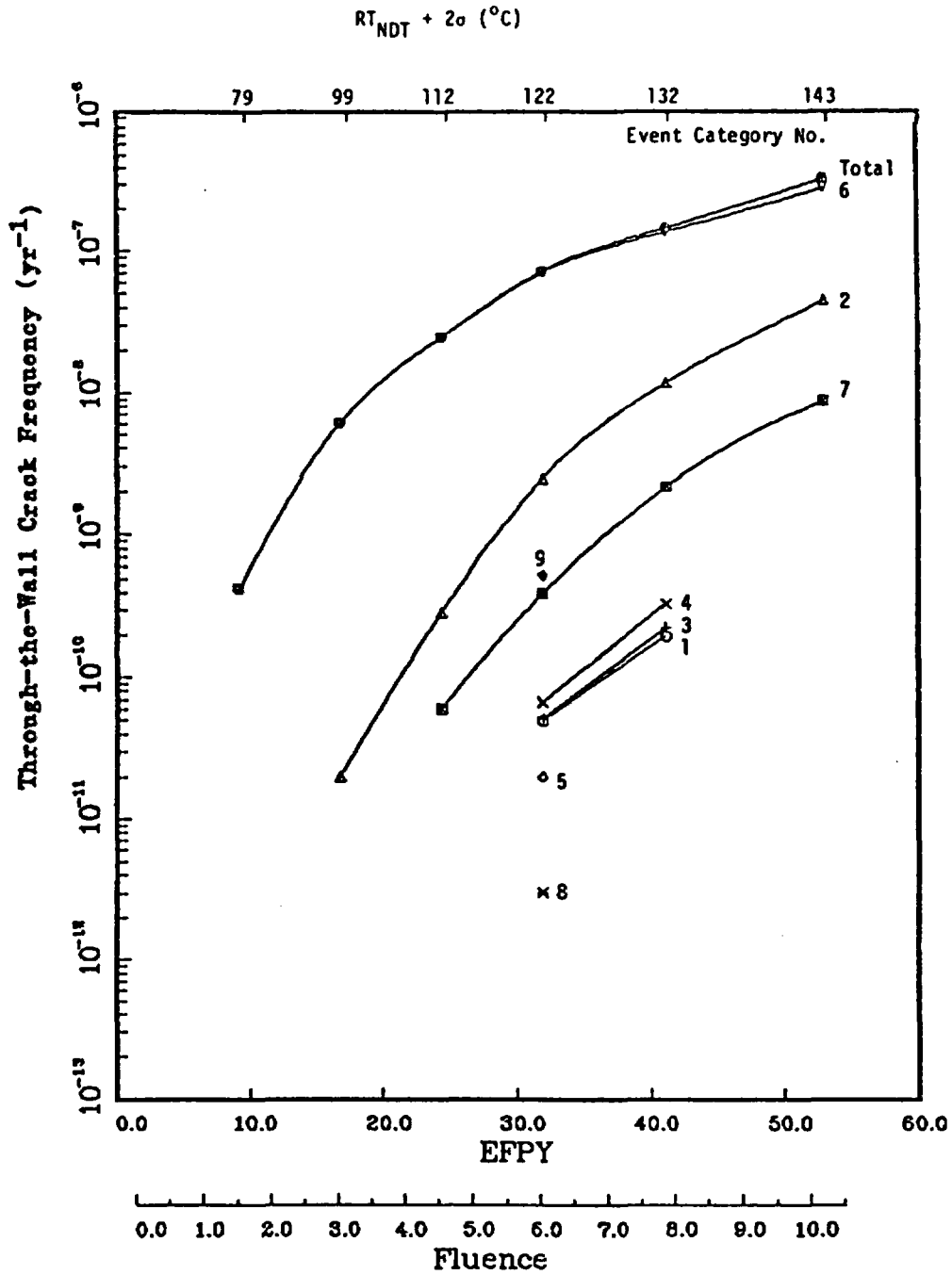


Figure 1. Risk associated with each category of events.

1. Large main steam-line break at low decay heat.
2. Small main steam-line break at low decay heat.
3. Large main steam-line break at full power.
4. Small main steam-line break at full power.
5. Small-break LOCA (<0.16 sq. ft.) at full power.
6. Small-break LOCA (<0.05 sq. ft.) at low decay heat.
7. Small-break LOCA (>0.016 and <0.05 sq. ft.) at full power.
8. Steam generator overfeed.

The HPI shutoff head design for Calvert Cliffs (1275 psi) had a major impact by slowing the repressurization process and thus reducing the PTS risk. Operator actions associated with the overcooling initiating events considered in this analysis appear to be less important with respect to PTS than in the analysis for the other two plants. This is due to the automatic function design of the MSIVs and auxiliary feed-water block valves. Heating of the HPI water was found to have a major impact on the risk values since the dominant risk sequences involved cooldowns associated with HPI water. Increasing the HPI water by about 30°F was found to decrease the TWC frequency by nearly a factor of 10. In addition, as in the Oconee analysis, fluence reductions were found to be a reasonable means for decreasing the potential for a through-the-wall crack.

Since the H. B. Robinson conclusions are still being developed, they are not presented in this paper. However, there are some general findings which can be addressed. First of all, the very low RTNDT value at 32 EFPY (<200°F) resulted in very low conditional failure probabilities, making the fracture mechanics calculations difficult. As a result, conservative extrapolations were used to bound the estimated TWC frequency at 32 EFPY, and most of the calculations were performed for a hypothetical H. B. Robinson plant which had a RTNDT value of 270°F. Secondary side initiating events were found to be the dominant sequences for this plant condition. The LOCA events did not result in stagnant flow for break sizes less than 2 in., and thus the cooldown was not severe. For LOCAs 2 in. in size or slightly larger, stagnation did occur very early and downcomer temperatures of approximately 100°F were obtained within 45 min. However, although many cracks were initiated, the pressure drop associated with the transient was rapid. Thus, there was no driving force on the crack and nearly all initiated cracks arrested.

The H. B. Robinson analysis will be completed and a separate report will be issued in the coming year for each plant studied. In addition, a comparison of the three studies will be made to provide a better understanding of the PTS issue.

TRAC-PF1 ANALYSES OF POTENTIAL PRESSURIZED-THERMAL-SHOCK  
TRANSIENTS AT A COMBUSTION-ENGINEERING PWR\*

Jan E. Koenig and Russell C. Smith

Energy Division  
Los Alamos National Laboratory  
Los Alamos, New Mexico USA 87544

ABSTRACT

Los Alamos National Laboratory participated in a program to assess the risk of a pressurized thermal shock (PTS) to the reactor vessel during a postulated overcooling transient in a pressurized water reactor (PWR). Using the Transient Reactor Analysis Code (TRAC), Los Alamos studied the thermal-hydraulic behavior of the three following accident categories: steamline breaks, runaway-feedwater transients, and small-break loss-of-coolant accidents. These accidents were simulated for a Combustion-Engineering (C-E) PWR, Calvert Cliffs, and included multiple operator and equipment failures. The results will be used by Oak Ridge National Laboratory (ORNL) to determine the vessel wall temperature and stresses corresponding to the bulk downcomer liquid temperature and pressure predicted by TRAC.

The study identified the importance of the initial plant conditions and loop flows to the PTS issue. If the plant was initially at hot-zero power (rather than full power), the same accident initiator could produce significantly lower downcomer temperatures because of the reduced decay heat and stored energy. Flow stagnation in all reactor coolant loops, which occurred in one transient, could lead to a vessel wall temperature that approached the relatively cold high-pressure-injection fluid temperature. However, routine operator actions would reduce the consequences of any of these simulated accidents if the pressure-temperature relationships prescribed in the operator guidelines are followed. ORNL will extend the results of the Los Alamos study by determining the probability of vessel failure and accident occurrence for an overall assessment of PTS risk.

---

\*Work supported by the US Nuclear Regulatory Commission.

## INTRODUCTION

Los Alamos National Laboratory participated in a program to assess the risk of a pressurized thermal shock (PTS) to a reactor vessel. Our role was to provide best-estimate thermal-hydraulic analyses of 13 postulated overcooling transients using TRAC-PF1.<sup>1</sup> These transients were all hypothetical and included multiple equipment and operator failures. Calvert Cliffs, a Combustion Engineering (C-E) plant, was the pressurized water reactor (PWR) modeled for this study. Calvert Cliffs/Unit 1, located on the Chesapeake Bay in Maryland, began operation in January 1975. Figure 1 shows the configuration of the primary side of the power plant. Unit 1 has a 2 x 4 loop arrangement: two hot legs and two steam generators (SGs) with four cold legs and four reactor coolant pumps (RCPs). The plant operates at 2700 MW<sub>th</sub>.

The reactor vessels of certain older plants containing copper impurities in the vessel welds risk cracking if subjected to a thermal shock concurrent with high system pressure (referred to as PTS). After years of irradiation, the vessel welds in these plants have become more brittle; and therefore, the temperature at which a crack may initiate or propagate increases. Overcooling transients can be postulated that may lead to a PTS. For this reason, in late 1981, the US Nuclear Regulatory Commission (NRC) identified PTS as an unresolved safety issue and developed a task action plan (TAP A-49) to resolve the issue.

An effort to assess the risk of PTS in representative plants of the three US PWR vendors was established. A Westinghouse plant (H. B. Robinson) and a Babcock & Wilcox plant (Oconee) were also studied as part of the program. For the C-E plant (Calvert Cliffs), several organizations participated: the plant owner, which is the Baltimore Gas and Electric Co. (BG&E); C-E; the NRC; Oak

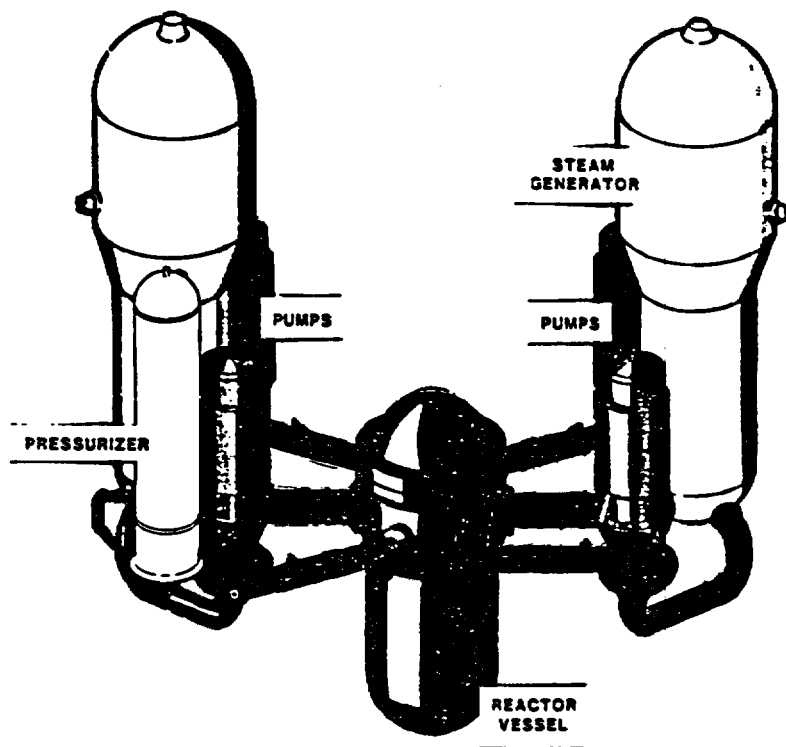


Fig. 1  
Primary side of Calvert Cliffs.

Ridge National Laboratory (ORNL); Brookhaven National Laboratory (BNL); and Los Alamos National Laboratory.

The NRC managed the multi-organizational project. BG&E and C-E supplied extensive information about the plant and its operation. Los Alamos used this information to prepare a comprehensive TRAC-PF1 model of Calvert Cliffs. ORNL identified 13 postulated overcooling transients that could lead to PTS, and Los Alamos simulated most of these transients for 7200 s (2 h) after their initiation. These transients were reviewed by BG&E, C-E, ORNL, and BNL. Our results were provided to ORNL, who plan to extend these results to other postulated PTS transients using a simplified mass-and-energy balance approach. For each of these postulated transients, ORNL plans to determine the stresses in the vessel wall and calculate the probability of vessel failure. ORNL then plans to publish a report<sup>2</sup> that incorporates the entire study and identifies the important event sequences, operator and control actions, and uncertainties.

The purpose of these calculations is to aid the NRC in confirming the screening criterion (the criterion to determine if a power plant is subject to a risk of PTS) in the proposed PTS rule (10 CFR 50.61). The current screening criterion of a power plant is a reference temperature for nil-ductility transition ( $RT_{NDT}$ ) of 405 K (270°F) at 40 effective full-power years. The NRC will also use these analyses to develop requirements for the licensees' plant-specific PTS safety-analysis reports and the acceptance criterion for proposed PTS preventive actions.

### TRAC-PF1 CALCULATIONS

TRAC-PF1 is a best-estimate finite-difference computer code capable of modeling thermal-hydraulic transients in both one and three dimensions. The code solves the field equations for mass, momentum and energy conservation of both vapor and liquid. The Calvert Cliffs model fully exercised the capabilities of TRAC-PF1.

We performed thermal-hydraulic analyses of three accident categories: runaway-feedwater transients, steamline breaks, and small-break loss-of-coolant accidents (SBLOCAs). These transients were initiated from either hot-zero power (HZP) or full power (FP). The RCPs were tripped 30 s after the safety-injection-actuation signal in all but one transient. Parameters that were significant in assessing the risk of PTS were the downcomer liquid temperature, the system pressure, and the occurrence of flow stagnation in the reactor coolant loops. This paper describes the factors that strongly affected these three parameters in the TRAC PF1 calculations. Table I lists a description of each of the 13 transients, the calculated minimum downcomer liquid temperature, and whether repressurization and/or loop flow stagnation were calculated by TRAC-PF1. This work is documented in detail in Ref. 3.

### FACTORS AFFECTING DOWNCOMER LIQUID TEMPERATURE

The initial conditions of the plant were important. When a transient was initiated from FP, the decay heat was high enough that a significant decrease in the downcomer bulk fluid temperature did not occur. Uncertainty in the amount of decay heat following FP shutdown exists because the decay heat is dependent on the operating history of the plant and thus, the system energy following FP shutdown can vary significantly. For the TRAC-PF1 calculations, it was assumed

TABLE I  
TRANSIENT RESULTS<sup>a</sup>

<u>Description<sup>b</sup></u>	<u>Minimum T</u>		<u>Repressuri-</u> <u>zation</u>	<u>Flow</u> <u>Stagnation</u>
	<u>K</u>	<u>°F</u>		
<b>Runaway-feedwater Cases:</b>				
1. Runaway MFW to two SGs from FP	480	404	yes	no
2. Runaway MFW to one SG from FP	490	422	yes	one loop
3. Runaway AFW to two SGs from FP	490	422	yes	no
<b>Steamline Breaks:</b>				
4. 0.1-m <sup>2</sup> MSLB				
a. From HZP	395	251	yes	one loop
b. From FP	468	383	yes	one loop
c. With two operating RCPs from HZP	446	343	yes	no
5. Double-ended MSLB				
a. With failure to isolate AFW to broken SG from HZP	377	219	yes	one loop
b. With two stuck-open MSIVs from HZP	376	217	yes	no
6. Small steamline break (stuck-open TBV)				
a. From FP	530	494	yes	no
b. With one stuck-open MSIV from FP	500	440	yes	no <sup>b</sup>
<b>SBLOCAs:</b>				
7. 0.002-m <sup>2</sup> hot-leg break from FP	440	332	(low flow)	one loop
8. One stuck-open pressurizer valve				
a. With one stuck-open atmospheric dump valve from FP	407	273	no	one loop
b. From HZP	350 <sup>b</sup>	171 <sup>b</sup>	no	both loops

<sup>a</sup>No operator intervention assumed except to trip the RCPs.

<sup>b</sup>Estimated.

TABLE I  
TRANSIENT RESULTS<sup>a</sup>

<u>Description<sup>b</sup></u>	<u>Minimum T</u>		<u>Repressuri-</u> <u>zation</u>	<u>Flow</u> <u>Stagnation</u>
	<u>K</u>	<u>°F</u>		
<b>Runaway-feedwater Cases:</b>				
1. Runaway MFW to two SGs from FP	480	404	yes	no
2. Runaway MFW to one SG from FP	490	422	yes	one loop
3. Runaway AFW to two SGs from FP	490	422	yes	no
<b>Steamline Breaks:</b>				
4. 0.1-m <sup>2</sup> MSLB				
a. From HZP	395	251	yes	one loop
b. From FP	468	383	yes	one loop
c. With two operating RCPs from HZP	446	343	yes	no
5. Double-ended MSLB				
a. With failure to isolate AFW to broken SG from HZP	377	219	yes	one loop
b. With two stuck-open MSIVs from HZP	376	217	yes	no
6. Small steamline break (stuck-open TBV)				
a. From FP	530	494	yes	no
b. With one stuck-open MSIV from FP	500	440	yes	no <sup>b</sup>
<b>SBLOCAs:</b>				
7. 0.002-m <sup>2</sup> hot-leg break from FP	440	332	(low flow)	one loop
8. One stuck-open pressurizer valve				
a. With one stuck-open atmospheric dump valve from FP	407	273	no	one loop
b. From FP	350 <sup>b</sup>	171 <sup>b</sup>	no	both loops

<sup>a</sup>No operator intervention assumed except to trip the RCPs.

<sup>b</sup>Estimated.

that the reactor had been in operation for an infinite length of time. An assessment of the effect of the uncertainty of the decay heat following FP shutdown is detailed in the full report (Ref. 3).

Plant features that significantly affected the rate and amount of primary cooldown were:

- (1) SG isolation capability - Valves on the main feedwater (MFW) lines and the steamlines terminate flows (except auxiliary feedwater) into both SGs if the secondary pressure is less than 4.6 MPa (668 psig) in either SG. This limits the cooling potential of a steamline break or stuck-open secondary valve. If the break was downstream of the main steam isolation valves (MSIVs), an overcooling transient was terminated upon receipt of the low-pressure signal (called the SG isolation signal or SGIS). If the break was upstream of the MSIVs, the primary overcooling was still limited to the energy-removal capability of one SG because the other SG was isolated after SGIS.
- (2) SG liquid inventory - The SGs at Calvert Cliffs have relatively large liquid inventories at steady state: ~102000 kg (225000 lb) at HZP and ~63000 kg (138600 lb) at FP. So, even with the capability to isolate one of the SGs, a steamline break would have severe overcooling potential.
- (3) Flow restrictors on the steamlines - Because of a flow restrictor located in each main steamline, the largest effective break size downstream of this restrictor (10 m (32.8 ft) from the SG exit) is 0.2 m<sup>2</sup> (2.0 ft<sup>2</sup>). Hence, the thermal-hydraulics of a 0.2-m<sup>2</sup> main steamline break (MSLB) and a double-ended MSLB (0.52 m<sup>2</sup> (5.6 ft<sup>2</sup>)) would be virtually the same because the effective break size would be the same.
- (4) Auxiliary feedwater (AFW) control logic - AFW is valved out to the SG at a lower pressure if a pressure differential greater than 0.8 MPa (115 psia) exists between the SGs. This limits the overcooling potential of a steamline break to the energy-removal capability of one SG because AFW will not be supplied to the "broken" SG.
- (5) Condenser/hotwell liquid inventory - This determined the overall cooling capability of the runaway-MFW transients.

#### FACTORS AFFECTING SYSTEM PRESSURE

The system pressure and rate of repressurization (if any) are important in assessing the risk of PTS. Because of an assumed operator failure to turn off the charging pumps, all secondary-side-initiated transients repressurized to the pressurizer power-operated relief valve (PORV) setpoint. Figure 2 shows a typical pressure history for a secondary-side transient (0.1-m<sup>2</sup> (1.0-ft<sup>2</sup>) MSLB from HZP). For a potential PTS problem to arise during an SBLOCA, the break size must be small enough for the system pressure to remain high but large enough for high-pressure-injection (HPI) flow to be necessary.

Plant features that strongly influenced the system pressure were:

- (1) Safety-injection and makeup/letdown (charging) flow - HPI flow is delivered by centrifugal pumps with a low shutoff head of 8.8 MPa (1285 psia) and charging flow is delivered by positive-displacement pumps. This means that while the primary can repressurize to the PORV setpoint, the repressurization rate would decrease drastically above 8.8 MPa. Also, the supply of cold water to the downcomer would be limited to charging flow when the system pressure is above the shutoff head of the HPI pumps. This feature was important for postulated secondary-side transients when the primary side repressurized.

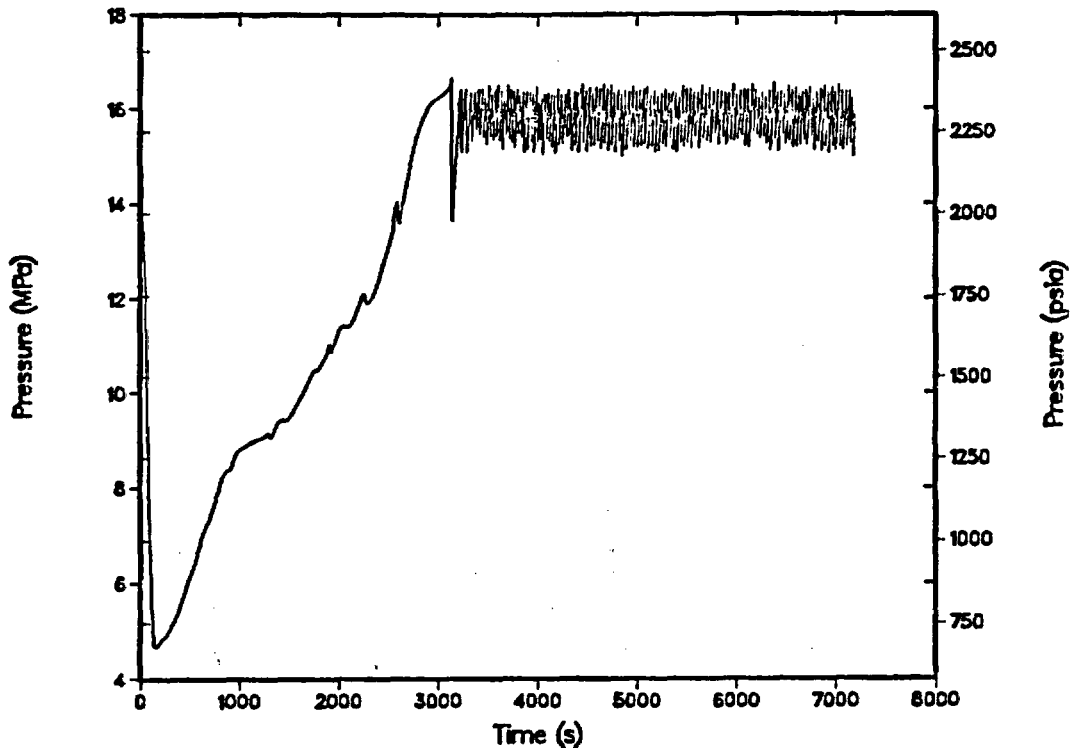


Fig. 2.  
Typical primary pressure history for a secondary-side transient.

- (2) Bypass flows into the upper head - Liquid enters the upper head via a controlled flow area through the control-element-assembly (CEA) shrouds and a small bypass leakage flow at the top of the downcomer. This flow was important for all transients when the upper head voided because it strongly affected the condensation rate and thus the depressurization and repressurization rate.

#### FACTORS AFFECTING LOOP FLOW STAGNATION

Flow stagnation is of particular importance to PTS because no mechanism is available to cause significant mixing of the cold-leg fluid with injected HPI fluid and consequently, the HPI fluid may concentrate along the vessel wall. TRAC-PF1 is not designed to predict flows of this nature and hence, calculations were performed at Purdue University<sup>4</sup> and at Los Alamos<sup>5</sup> (using SOLA-PTS code) to resolve the temperature and flow distributions during periods of flow stagnation during the transients.

Figure 3 illustrates the mechanism for producing loop flow stagnation. The SG must be in a reverse-heat-transfer mode for the loop flow to cease. When the driving head (density gradient) produced by heat input from the SG opposed the driving head produced by the heat input from the core, the net force to drive the flow was zero. The higher decay heat from FP transients produced a greater positive driving force for flow than the decay heat at HZP and flow stagnation was more likely in the HZP transients. Thus, the initial conditions also were an important factor in flow stagnation.

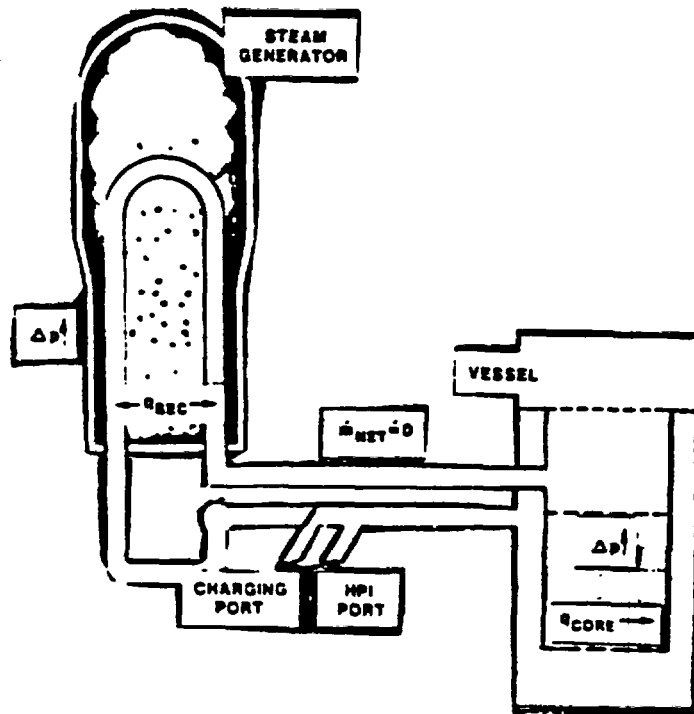


Fig. 3.  
Mechanism for producing loop flow stagnation.

Many transients produced loop flow stagnation in one loop because of asymmetric conditions on the secondary side (resulting from a steamline break or stuck-open valve); however, according to studies at Los Alamos,<sup>5</sup> if one loop is in natural circulation while the other loop is stagnant, the HPI fluid will still mix with the warmer fluid residing in the downcomer. Of the 12 transients initially specified by ORNL, flow stagnation in both loops did not occur. As our understanding of the significant phenomena improved, we were able to identify a transient that produced stagnation in both loops. This calculation is presented in the next section.

Plant features that were significant to flow stagnation were:

- (1) SG isolation capability - During a steamline break or runaway-feedwater transient, one SG may be isolated while the other is not. These asymmetric secondary conditions can lead to cooling of the primary fluid by one SG and heating by the other. The flow may stagnate in the loop where heat is being added by the SG. However, flow stagnation in one loop is currently judged not to be a PTS problem.
- (2) Number of reactor coolant loops - Thorough mixing in the downcomer might not occur if there are more than two loops. If stagnation were to occur in all but one loop of a three- or four-loop plant, it might be of PTS concern.

#### MOST SIGNIFICANT TRANSIENT

The most significant transient (from a thermal-hydraulic standpoint) was initiated by a stuck-open PORV while the plant was operating at HZP. This

transient produced stagnation in both loops leading to a low bulk downcomer temperature with a system pressure of  $\sim 7.2$  MPa (1058 psia).

The calculated downcomer liquid temperature, as shown in Fig. 4, may be divided into two phases. Phase 1 (0-260 s) was before the initiation of HPI flow. The system temperature remained constant at its initial value of 552 K (534°F). Because the primary and secondary sides were already in thermal equilibrium and the decay heat was low, only pressure changes, as shown in Fig. 5, occurred during this portion of the subcooled blowdown. When the pressure dropped below 8.8 MPa (1285 psia), HPI flow started and the primary cooldown began (Phase 2). The entire cooldown was due primarily to the replacement of the initial primary mass by the HPI and charging flow. After the top of the U-tubes in the SGs voided at  $\sim 600$  s, the loop flows ceased and subsequent heat addition from the SGs and pipe walls was small. The system began refilling when the HPI/charging flow exceeded the break flow. When the liquid on one side of the U-tubes spilled into the steam volume on the other side at 1800 s, a rapid condensation process began which caused a pressure drop of  $\sim 0.8$  MPa (117.5 psi). This initiated a small circulation of  $\sim 35$  kg/s (77 lb/s) in the loop without the break because a liquid flow path was re-established.

A minimum pressure of 6.0 MPa (882 psia) was reached before the upper head voided. The system pressure increased as the void in the upper head was compressed by the HPI/charging flow. After the steam in the upper head condensed, the pressure remained relatively constant (1200-2400 s) because of an approximate balance between the break flow and the HPI/charging flow. After 2400 s, significantly cooler liquid had reached the break, increasing the break mass flow and decreasing the system pressure. The pressure leveled off to less than the HPI head as the HPI flow increased and again balanced the break flow.

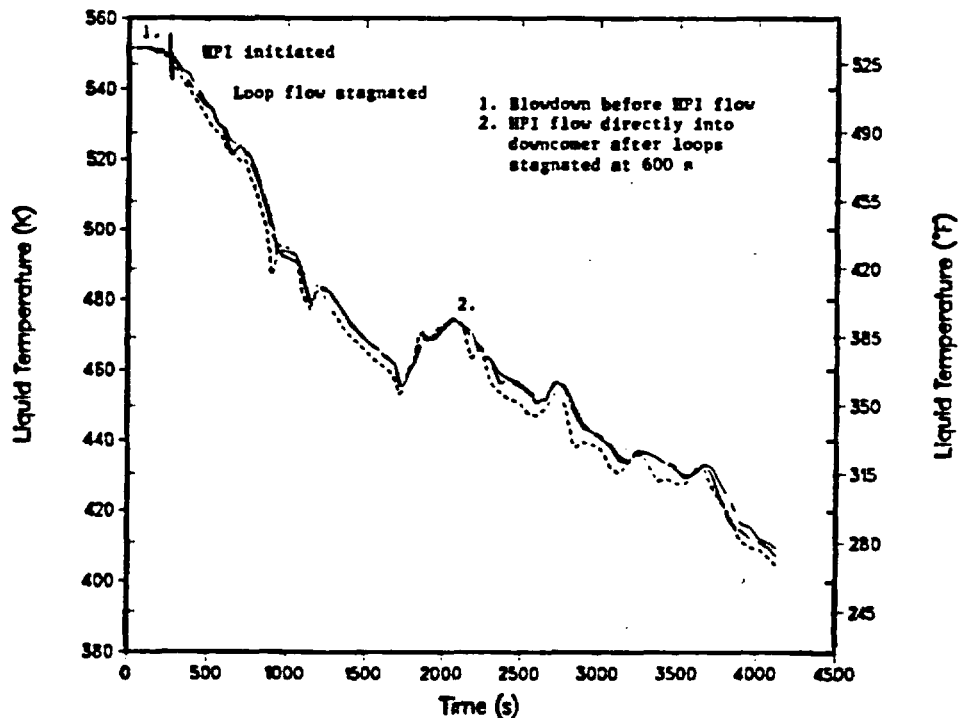


Fig. 4.  
Downcomer liquid temperature for stuck-open PORV from HZP.

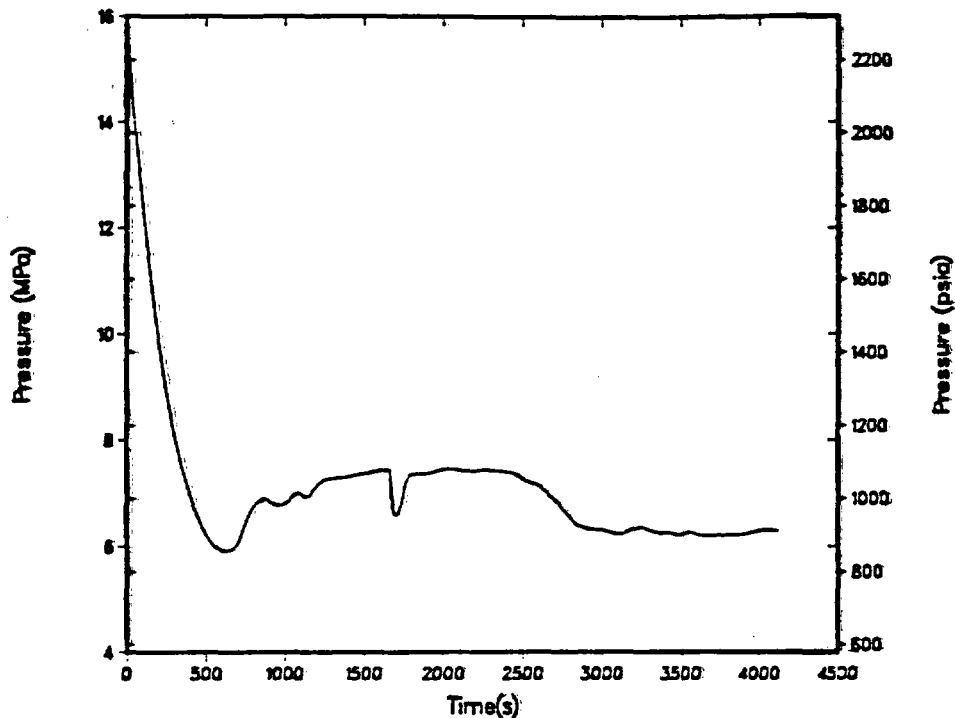


Fig. 5.

Primary pressure during a stuck-open PORV from HZP.

This transient demonstrated that flow stagnation in both loops was possible during an SBLOCA if the postulated transient is initiated from a low decay-heat level.

#### CONCLUSIONS

In general, those calculations initiated from FP conditions were thermal-hydraulically benign. If initiated from HZP, most of these transients could pose a PTS threat if there was no operator intervention. This is because of the increased likelihood of flow stagnation as well as the reduced heat content of the fluid and the system metal when the plant was at HZP.

Several plant features were identified as significant to the consequences of the postulated potential PTS transients:

1. SG isolation capability.
2. SG liquid inventory.
3. Flow restrictors in the steamlines.
4. AFW control logic.
5. Condenser/hotwell liquid inventory.
6. Safety-injection and makeup/letdown flow.
7. Bypass flows into the upper head.
8. Number of reactor coolant loops.

Steamline breaks possess the largest potential to produce rapid cooldown. If initiated when the SG water mass is large (as at HZP), the subsequent primary-side temperature reduction would be more than if the SG was at FP. SBLOCAs possess a larger potential for overall cooling of the primary system but the rate of cooldown will not be as large as the rate produced by steamline

breaks. Runaway-MFW transients can produce a rapid, but short-lived, cooldown of the primary system.

Simple routine operator actions would have reduced the consequences of any of these simulated accidents. The operator failure assumptions (particularly failure to throttle HPI and charging flow to control the system pressure-temperature relationship prescribed in the operator guidelines) were the single most important contributors to the generation of severe pressure-temperature conditions in all cases.

#### ACKNOWLEDGEMENT

The authors would like to acknowledge the many contributions of Gregory D. Spriggs, of Los Alamos, to this project.

#### REFERENCES

1. Safety Development Group, Energy Division, "TRAC-PF1: An Advanced Best-Estimate Computer Program for Pressurized Water Reactor Analysis," Los Alamos National Laboratory report LA-9944-MS, NUREG/CR-3567 (February 1984).
2. PTS Study Group of Oak Ridge National Laboratory, "Pressurized Thermal Shock Evaluation of the Calvert Cliffs-1 Nuclear Power Plant," Oak Ridge National Laboratory report to be published.
3. Gregory D. Spriggs, Jan E. Koenig, and Russell C. Smith, "TRAC-PF1 Analyses of Potential Pressurized-Thermal-Shock Transients in a Combustion-Engineering PWR," Los Alamos National Laboratory report LA-UR-84-2083 (August 1984).
4. T. G. Theofanus, H. P. Nourbakhsh, P. Gherson, K. Iyer, "Decay of Buoyancy Driven Stratified Layers With Applications to Pressurized Thermal Shock (PTS)," Purdue University report, NUREG/CR-3700 (May 1984).
5. Bart J. Daly, "Three-dimensional Calculations of Transient Fluid-Thermal Mixing in the Downcomer of the Calvert Cliffs-1 Plant Using SOLA-PTS," Los Alamos National Laboratory report LA-10039-MS, NUREG/CR-3704, (April 1984).

ANALYSIS OF H. B. ROBINSON UNIT-2  
PRESSURIZED THERMAL SHOCK TRANSIENTS

Donald M. Ogden  
C. Don Fletcher  
Cliff B. Davis

EG&G Idaho, Inc.

INTRODUCTION

The rapid cooldown of a pressurized water reactor (PWR) vessel during a transient or accident, accompanied by high coolant pressure is referred to as pressurized thermal shock (PTS). The United States Nuclear Regulatory Commission (USNRC) designated PTS unresolved safety issue (USI) A-49 and developed a task action plan (TAP A-49) to resolve the issue. The safety concern arises from the rapid cooling at the reactor vessel wall inner surface which produces thermal stresses within the wall. As long as the fracture toughness of the reactor vessel is high, overcooling will not cause vessel failure. However, USNRC staff analyses (SECY-85-465) showed certain older plants with copper and other impurities in vessel weldments may become sensitive to PTS as the nil-ductility transition temperature of the weld material gradually increases. In support of the USNRC PTS Integration Study for the resolution of USI A-49, the Idaho National Engineering Laboratory (INEL) has performed analyses of 180 overcooling sequences that were defined by the Oak Ridge National Laboratory (ORNL) for the H. B. Robinson Unit-2 (HBR-2) plant.

HBR-2 is a three loop Westinghouse PWR which is operated at Hartsville, South Carolina by Carolina Power and Light Company. It was one of three plants selected for evaluation by the PTS Integration Study which

was coordinated by ORNL. The analyses performed at the INEL produced vessel downcomer temperature, pressure and heat transfer coefficient histories (the primary parameters of interest for PTS) for the 180 overcooling sequences. The information was used by ORNL to perform fracture mechanics and multidimensional effects analyses to determine for each sequence the probability of vessel failure.

## MODELS AND METHODS

Analysis of the overcooling sequences for the HBR-2 plant was performed with the Reactor Excursion and Leak Analysis Package 5 (RELAP5) computer code. Detailed RELAP5/MOD1.6 and MOD2 models of the HBR-2 were developed. A nodal diagram for the detailed RELAP5 models is shown in Figure 1. The models simulated the reactor vessel, three steam generators, loop piping and pressurizer, steam lines from the generator to the turbine and feedwater system from the hotwell to the steam generator, primary coolant, feedwater, auxiliary feedwater and condensate pumps, the ECC systems including high pressure injection (HPI), low pressure injection (LPI), and accumulators; and power operated relief valves (PORVs), safety valves, steam dump valves, feedwater regulating valves, and main steam isolation valves (MSIVs). Included were the significant flow paths, volumes, heat transfer surface areas and metal masses. Control systems were modeled to simulate the steam dump control system with the load rejection, plant trip and steam pressure controllers; the steam generator level control system, pressurizer pressure control system; and the pressurizer level control system. The detailed models contained 224 volumes, 242 junctions, 218 heat structures and 300 control system components. In addition to the detailed models, several variations of simplified RELAP5 models were developed. These models combined volumes, metal masses, and heat transfer surface areas of the detailed RELAP5 models to produce very fast running models. The detailed models were benchmarked against plant startup data while the simplified models were benchmarked with results of the detailed model calculations.

## OVERVIEW OF ANALYSIS

The overcooling sequences defined by ORNL for analysis at the INEL can generally be grouped into five transient types: steamline break (SLB), loss-of-coolant accident (LOCA), combined LOCA and steamline break, steam generator tube rupture (SGTR) and steam generator overfill and overfeed. For each transient type, variations in break size, equipment failure and operator action or inaction were considered. Table 1 provides a general overview of the types of overcooling sequences considered for the HBR-2 plant.

The steamline break transients included double-ended guillotine and 1.0 ft<sup>2</sup> breaks upstream of the main steam isolation valves (MSIVs) but outside containment. Also included were failure open of one to five steam dump valves (SDVs) and one to three steamline power operated relief valves (PORVs). Both full power and hot standby initial power levels were included in the sequences. In addition to the steamline breaks or valve failures, some additional equipment failures or operator actions were investigated. These included both steam generator overfill and overfeed with auxiliary feedwater (AFW), failure of the operator to throttle charging flow and failure of the operator to isolate AFW to the affected steam generator.

Four breaks were analyzed for the LOCA transients, a 2.5 inch hot leg break, 2.0 inch hot leg break, 2.0 inch cold leg break and a failed open pressurizer PORV. The sequences included some transients for both full power and hot standby initial power levels. Second order effects analyzed included AFW overfill and overfeed and failure to throttle charging flow. Operator isolation of the 2.5 inch hot leg break and pressurizer PORV was also analyzed.

The combined LOCA and steamline break transients included combinations of primary and secondary system breaks. The primary coolant system breaks were either a failed open pressurizer PORV or a 2.5 inch hot leg break. The secondary system breaks involved either one to five failed open steam

dump valves, or one or two failed open steam line PORVS. Again both full power and hot standby initial power levels were included in the sequences. Effects of AFW overflow or overfeed and failure to throttle charging flow were also considered.

The ORNL sequences included steam generator tube rupture transients. A double-ended guillotine break of a single tube was assumed. The break was located at the tubesheet on the outlet side of the generator. Sequences were analyzed both for full power and hot standby initial conditions. The sequences included realistic operator actions based upon emergency operating procedures. Variations to the emergency operating procedures were analyzed which included no operator action.

The final class of sequences shown in Table 1 are steam generator overflow and overfeed with both AFW and MFW. These sequences were analyzed for full power conditions. Failure to throttle charging flow was considered as a secondary effect.

An overview of the results of the analyses of the overcooling transients for the HBR-2 plant is shown graphically in Figure 2. Plotted are the minimum downcomer temperature and the maximum subsequent downcomer pressure. The conditions for which PTS is a concern are low downcomer temperature and subsequent high pressure. This corresponds to the lower right corner of the plot. As shown in the figure, the steamline break sequences alone produced low temperatures with subsequent high pressures. The lowest temperature transients were initiated with large steamline breaks with failure to isolate AFW. The downcomer temperatures approached the affected steam generator secondary saturation temperature at atmospheric conditions. Natural circulation flow was maintained so that good mixing of the high pressure injection (HPI) flow occurred.

The LOCA sequences were generally less severe than the SLB sequences because the downcomer pressure remained much lower for those sequences with low temperatures. The medium break LOCA sequences resulted in downcomer temperatures approaching the HPI temperature ( $\sim 100^{\circ}\text{F}$ ). This was a result

TABLE 1. OVERVIEW OF TRANSIENTS ANALYZED

<u>Transient Type</u>	<u>Break Variations</u>	<u>Initial Power Level Variations</u>	<u>Variations of Additional Failures or Operator Actions</u>
Steamline break	Double-ended guillotine	Full power	AFW overfill/overfeed
	1.0 ft <sup>2</sup>	Hot standby	Failure to throttle charging
	Steam dump valves (SDVs)		AFW isolation failure
	Steamline PORVs		
LOCA	2.5 in. hot leg	Full power	AFW overfill/overfeed
	2.0 in. hot leg	Hot standby	Failure to throttle charging
	2.0 in. cold leg		Break isolation
	Pressurizer PORV		
LOCA/steamline break	Pressurizer PORV/SDVs	Full power	AFW overfill/overfeed
	Pressurizer PORV/steamline PORVs	Hot standby	Failure to throttle charging
	2.5 in. hot leg/SDVs		
	2.5 in. hot leg/steamline PORVs		
Steam generator tube rupture	Double-ended guillotine (one tube)	Hot standby	Various operator actions
		Full power	AFW overfill/overfeed

TABLE 1. (continued)

<u>Transient Type</u>	<u>Break Variations</u>	<u>Initial Power Level Variations</u>	<u>Variations of Additional Failures or Operator Actions</u>
Steam generator overfill/overfeed		Full power	MFW overfill Failure to throttle charging

of loop voiding and total stagnation of the loops. However, the pressures were also low because of the depressurization caused by the primary system break. The small break LOCA sequences generally resulted in higher pressures because of a slower depressurization due to the smaller break; however, the loops did not significantly void and loop stagnation did not occur. With natural circulation flow, there was good mixing in the downcomer and the temperature there remained relatively high. The isolatable LOCA sequences resulted in pressures higher than the small break LOCA sequences. The primary system refilled and subsequently repressurized but the downcomer temperatures remained relatively high because loop stagnation did not occur.

The combined LOCA/SLB sequences behaved similarly to the LOCA sequences in the primary pressure response but more like the SLB sequences in the downcomer temperature response. The increased cooling of the primary system due to the SLB produced the early depressurization seen in the SLB sequences, resulting in increased HPI flow which prevented significant loop voiding and stagnation. Thus, the natural circulation flow continued and the primary temperature was controlled by the affected steam generator pressure. Unlike the SLB sequences, however, the primary system break prevented primary system repressurization.

The results of the steam generator tube rupture (SGTR) sequences are shown near the middle of Figure 2. The primary system pressure generally was controlled near 1000 psia by the affected steam generator secondary. The minimum downcomer temperature occurred as a result of opening the steam dump valves (SDVs) and blowing down the unaffected steam generators. Because the SDV opening is an operator action, the minimum downcomer temperature was very dependent upon assumed operator action.

The least severe of all the sequences analyzed were the steam generator overfill or overfeed sequences. As seen in Figure 2, the primary temperatures remained near operating conditions. The AFW overfill sequences resulted in the lowest downcomer temperatures in this group but

these were relatively high at about 446°F. The primary system pressures were generally high but with little consequence because of the high downcomer temperatures.

The following sections provide a more detailed discussion of the five transient groups previously described. The general character of the transients, as well as the significant parametric effects are described. Most of the calculation results shown were those provided to ORNL for their fracture mechanics analysis. The downcomer and pressure histories were broken into a small number of representative segments and linearized within each segment. This was done for ease in transmitting results of calculations to ORNL and because the subsequent fracture mechanics analysis did not require the detail provided by the RELAP5 analysis. A small number of the figures contain curves generated directly from the RELAP5 analysis.

#### STEAMLINE BREAK ANALYSIS

Figures 3 through 5 show calculation results for a 1.0 ft<sup>2</sup> SLB transient at hot standby initial conditions. AFW isolation was assumed to occur at 10 minutes by operator action. The vessel downcomer pressure is overlaid with pressurizer level in Figure 3. The initiation of the secondary break causes an immediate safety injection actuation signal (SIAS) due to a high differential pressure between the affected steamline and steamline header. This causes main feedwater isolation and initiation of motor driven AFW. To simulate operator action, the reactor coolant pumps (RCPs) are tripped at 72 s on low primary system pressure. The initial period of depressurization is caused by the shrinking of the primary system fluid as it is cooled as indicated by the pressurizer level in Figure 3. Initially the RCPs are on or coasting down which provides good loop flow and couples the primary system very closely to the affected steam generator which is blowing down. When the loop flow degrades to natural circulation flow, primary to secondary heat transfer is reduced and the shrinking of the primary system fluid volume from the cooling is overcome by the volume addition from the high pressure injection (HPI) and charging flows. This terminates the depressurization and initiates a repressurization. This is

seen in an increasing pressurizer level and primary system pressure in Figure 3. The increasing pressure and pressurizer level results in termination of HPI and charging at approximately 1100 s, which is seen in Figure 3 as a slope change in the primary system pressure. After 1100 s the pressure increases because of the primary fluid expansion due to the core energy input.

The vessel downcomer temperature is overlaid with the affected steam generator secondary mass in Figure 4. The initial rapid decrease in temperature is a result of the blowdown of the affected steam generator. At 600 s the AFW is isolated and at approximately 1000 s the affected steam generator secondary is dry as seen in Figure 4. This eliminates the heat sink for the primary system resulting in a subsequent downcomer temperature increase.

Figure 5 shows the behavior of the primary loop flows for the three loops. After the period of flow coastdown, the loop with the affected steam generator establishes natural circulation flow which continues for the duration of the transient. The unaffected loops quickly stagnate as the primary temperature decreases below the unaffected steam generator secondary temperatures.

The effect of the steamline break size is illustrated in Figures 6 and 7, which show the downcomer pressure and temperature responses for a double ended guillotine steamline break compared with a failure open of a single steamline PORV (small steamline break). Both transients begin from hot standby conditions and assume operator isolation of AFW at 600 s. The initial depressurization is less rapid and smaller in magnitude for the small steamline break because the cooling is less severe, as seen in Figure 7. The first repressurization is terminated when recovery of level in the pressurizer terminates charging. The second repressurization is more rapid than for the large SLB. For the small SLB, the primary system pressure does not decrease enough to trip the RCPs. Thus, during the final repressurization, the RCPs are providing nearly the same energy as the core decay heat thereby contributing to the increased heatup and the repressurization rates.

The effect of initial power on the SLB transient is seen in Figures 8 and 9. Compared are two large SLB transients which begin from full power and hot standby conditions. Both transients assume isolation of the AFW at 600 s. The initial depressurization and cooldown are very similar. The full power SLB initially repressurizes slower. This is a result of turbine driven AFW initiation for the full power case which does not occur in the hot standby case. There is a major difference in the transients when the affected steam generators dry out. As seen in Figure 9, the full power transient primary system temperature increases more rapidly. This is due to the higher decay heat. Near 1000 s the heatup is significantly reduced. At this point heat transfer is established from the primary system to the unaffected steam generators. This mode of heat transfer does not occur for the hot standby case, primarily because of the slower heatup rate.

Figures 10 and 11 illustrate the effect of failure to throttle charging flow. Compared are large SLB transients beginning from hot standby conditions with isolation of AFW at 600 s. Charging is not throttled for one of the transients. The primary effect is in the pressure response. Upon dryout of the affected steam generator, the rapid repressurization continues for the transient with continued charging flow. The primary system heatup for this transient is slower because of the subcooling of the charging flow (Figure 11).

The effect of failing to isolate AFW to the affected steam generator is seen in Figures 12 and 13. Compared are two large SLB transients beginning from hot standby conditions. AFW is isolated at 600 s for one and not isolated in the other. The dominant effect is seen in the temperature response (Figure 13). When AFW is not isolated the primary system cooldown continues, with temperatures approaching the temperature of the affected steam generator secondary. The effect on the pressure response is a slower repressurization after charging is throttled.

## LOCA ANALYSIS

Figure 14 shows the downcomer temperature and pressure response for a 2.5 inch hot leg break beginning at full power conditions. Shortly after initiation of the break (16 s), the reactor scrams because of a reactor over-temperature  $\Delta T$  signal. At 27 s a safety injection actuation signal is generated because of low pressurizer pressure. Figure 15 shows that the break is removing more mass than the HPI and charging flows can provide. The effect is a continual depressurization and voiding of the primary system. At 400 s the hot legs of the unaffected loops are sufficiently voided to terminate natural circulation flow. At 1000 s voiding in the affected loop terminates natural circulation flow. With all loops stagnant, the downcomer temperature decreases steadily and approaches the HPI temperature ( $\sim 100^\circ\text{F}$ ) as seen in Figure 14.

Figure 16 shows the pressure and temperature responses for a small break LOCA transient (1 failed open pressurizer PORV) beginning at hot standby conditions. The early rapid depressurization is terminated by upper head flashing. Unlike the 2.5 inch break the voiding does not continue long, as the HPI flow soon exceeds the break flow (Figure 17), refilling the primary system. When subcooled break flow is established near 2000 s, the primary system begins a steady depressurization. During this period the downcomer temperature is decreasing as the break energy and subcooling of the HPI exceed the core decay heat. Natural circulation flow continues for the duration of the transient.

## COMBINED LOCA/STEAMLINE BREAK ANALYSIS

The combined primary LOCA and SLB transients behaved similarly to the SLB in the downcomer temperature response and similarly to the LOCA in the pressure response. Figure 18 compares the downcomer pressure histories for a LOCA transient (2.5 inch hot leg break) with a combined LOCA/SLB (2.5 inch hot leg break/1 failed open steamline PORV) transient. Both transients begin at full power. AFW is not isolated at 600 s but controlled to 40% steam generator level. Unlike the steamline break

transient there is not a repressurization for the combined LOCA/SLB transient. As seen in Figure 18 the pressure decreases even more rapidly than in the LOCA sequence because the primary system fluid is shrinking from the cooling of the SLB in addition to the loss of primary fluid at the break. Figure 19 compares the downcomer temperature response for the combined LOCA/SLB transient with a SLB transient (1 steamline PORV) at full power. The SLB transient is initiated with a reactor trip. The initial cooldown for the SLB transient, which is terminated just after 2000 s, is primarily due to the affected steam generator blowdown. When the AFW is throttled, the primary to secondary heat transfer is reduced which is seen as a slope change in Figure 19. The initial cooldown for the combined transient is also controlled primarily by the secondary blowdown. The cooldown rate is greater because of the increased HPI flow resulting from the lower primary system pressure. Near 1000 s the accumulators begin to inject which controls the cooldown until they empty near 1700 s. After the accumulators empty, the cooldown rate is very comparable to the SLB transient. AFW is throttled and the cooldown is being controlled by the primary to secondary heat transfer.

#### STEAM GENERATOR TUBE RUPTURE ANALYSIS

A double-ended guillotine break of a single tube was assumed for the steam generator tube rupture sequences. The break was modeled at the tubesheet on the outlet side of the steam generator. Initial plant conditions correspond to hot standby operation. A base case and four sensitivity calculations were performed. In the base case, the operator recognizes the transient as a tube rupture and (1) isolates the affected steam generator and (2) initiates a primary system cooldown by opening the steam dump valves and blowing down the unaffected steam generators. When a specified primary system subcooling is attained, the steam dump valves are closed and primary system pressure is controlled by periodic opening of the pressurizer PORV. Figure 20 shows the reactor vessel downcomer pressure and fluid temperature for the base case. The pressure and temperature responses are strong functions of the assumptions made for operator actions. Opening the steam dump valves causes rapid decreases in both

pressure and temperature. The effect of opening the pressurizer PORV is more pronounced on pressure than on temperature. The cooldown is terminated when HPI is secured by the operator. Figures 21 and 22 compare the pressure and temperature responses for the base case and one of the sensitivity calculations in which the steam dump valves remain open for an extra 10 minutes. The pressure responses are virtually identical except for a 600 s delay due to late steam dump valve closure. The temperature responses however, diverge due to the extra cooling in the sensitivity calculation and, as a result, the minimum temperature is 61 K (109°F) lower in the sensitivity calculation than in the base case.

### STEAM GENERATOR OVERFILL AND OVERFEED ANALYSIS

A series of calculations were performed to analyze the effects of auxiliary feedwater (AFW) overflow (completely filling the steam generators), AFW overfeed (at a high flow rate), main feedwater overflow, and failure to throttle charging flow following a reactor trip from full power operation. Results of these analyses indicate that such sequences are generally not severe for PTS because the period of primary system cooldown is short. Results typical for these sequences are shown in Figure 23 for an AFW overflow. The cooldown proceeded as the steam generators were filled with cold AFW. When the steam generators were full, and liquid began to spill into the steam lines, the AFW was terminated, and a primary system heatup started. As the primary system fluid heated, its expansion caused the pressure to increase to the opening setpoint pressure of the pressurizer PORV.

### CONCLUSIONS

The steamline break sequences produced downcomer temperatures approaching the affected steam generator secondary saturation temperature (212°F) and subsequent downcomer pressures as high as the primary system PORV setpoint (~2350 psia). The temperatures were a strong function of break size, initial operating power and operation of auxiliary feedwater. The highest downcomer pressures occurred for sequences where charging flow was not throttled.

The primary side LOCA sequences produced downcomer temperatures that approached the HPI temperatures of 100°F. These temperatures occurred for the medium break LOCAs where loop stagnation occurred. While the temperatures were low, the subsequent pressures were also low (144 psia). Pressures for the small break LOCAs were somewhat higher but the loop flows did not stagnate and thus the downcomer temperatures were much higher. The isolatable LOCAs (LOCAs in which the operator can terminate break flow) produced pressures equal to the safety relief valve setpoint (~2500 psia), however, loop stagnation did not occur and downcomer temperatures remained relatively high.

The combined steamline break/primary side LOCA sequences behaved similarly to the steamline breaks in their temperature response, but more nearly like the LOCAs in their pressure response. Thus, while downcomer temperatures were low, as with the steamline break events, the subsequent pressures were also low, as with the LOCA events.

A single tube double-ended break was assumed for the steam generator tube rupture (SGTR) sequences. A variety of assumed operator actions were analyzed. Generally, these scenarios produced downcomer pressures near that of the affected steam generator secondary (~1000 psia). The temperatures were moderately low (~400°F) and strongly dependent upon the assumed operation of the steam dump valves. The lowest temperatures occurred only during short periods when the steam dump valves were open.

The steam generator overfill/overfeed sequences were the most benign of all the sequences analyzed. The downcomer temperatures and pressures remained near operating conditions. Neither the rate of feed or the degree of overfeed contributed significantly to reducing the downcomer temperature.

Results of the analyses performed at the INEL represent a major part of the information required by ORNL for the assessment of PTS in the HBR-2 plant. ORNL will integrate these results with those of fracture mechanics and multidimensional effects studies and publish a final report.

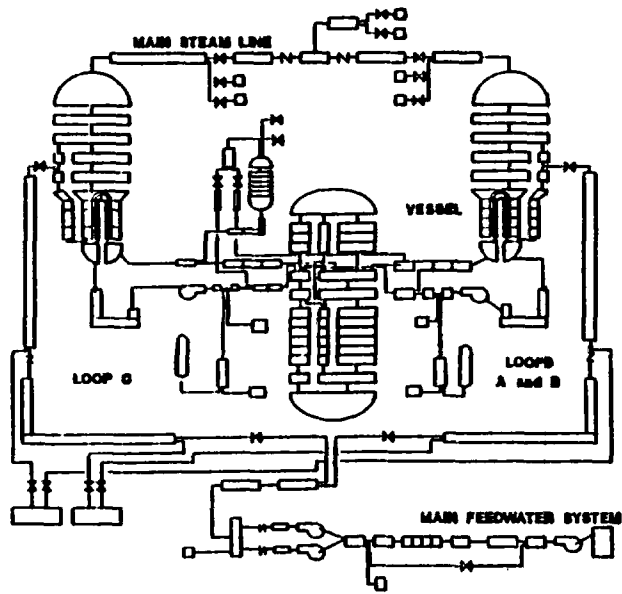


Figure 1. RELAP5 nodalization diagram of H.B. Robinson plant

EE00011

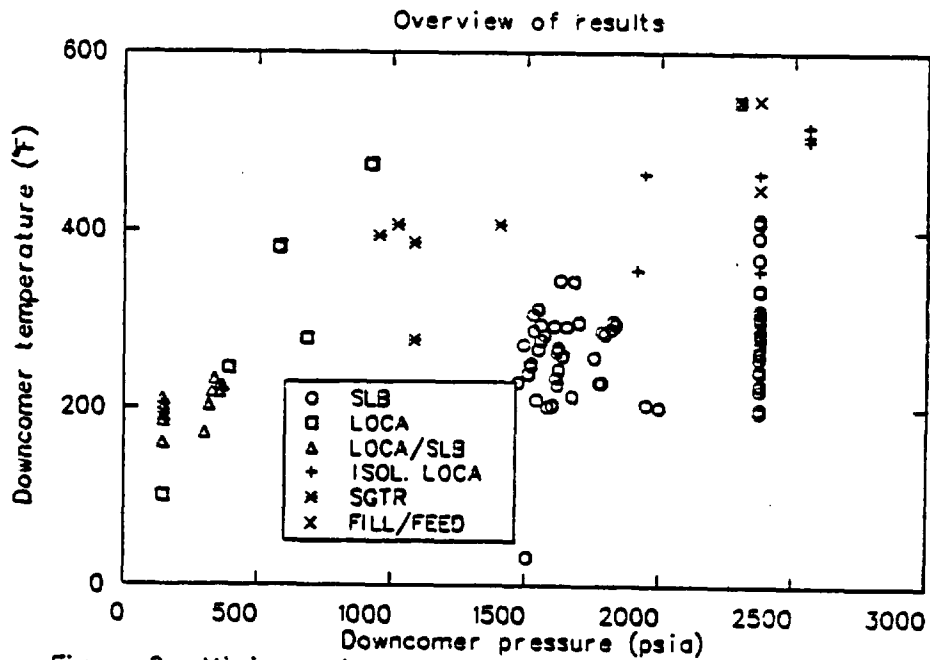


Figure 2. Minimum downcomer temperature and maximum subsequent downcomer pressure.

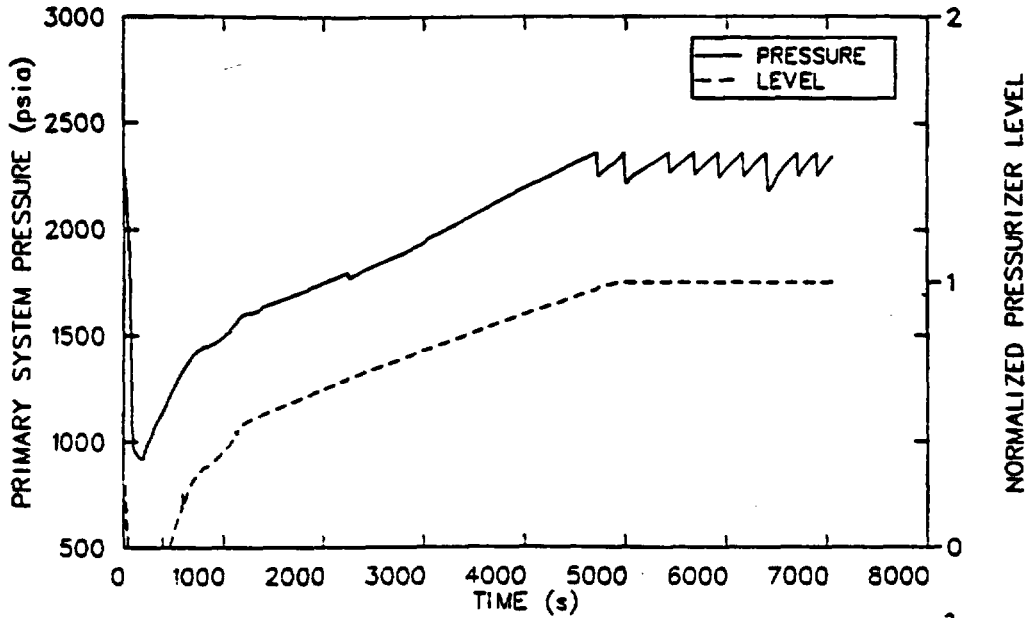


Figure 3. Primary system pressure and pressurizer level, 1.0 ft<sup>2</sup> main steam line break from hot standby conditions.

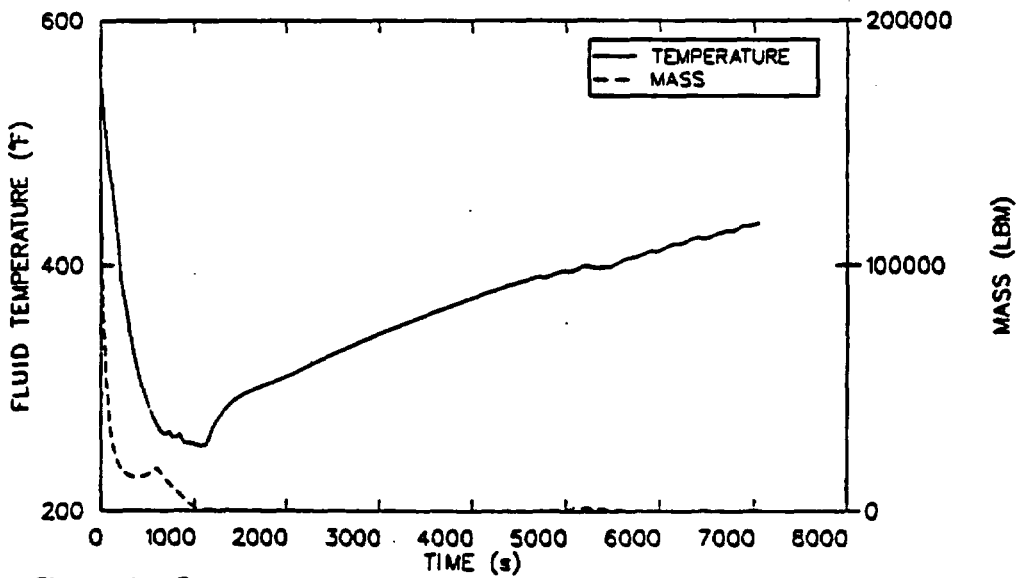


Figure 4. Reactor vessel downcomer fluid temperature and affected steam generator mass, 1.0 ft<sup>2</sup> main steam line break from hot standby conditions.

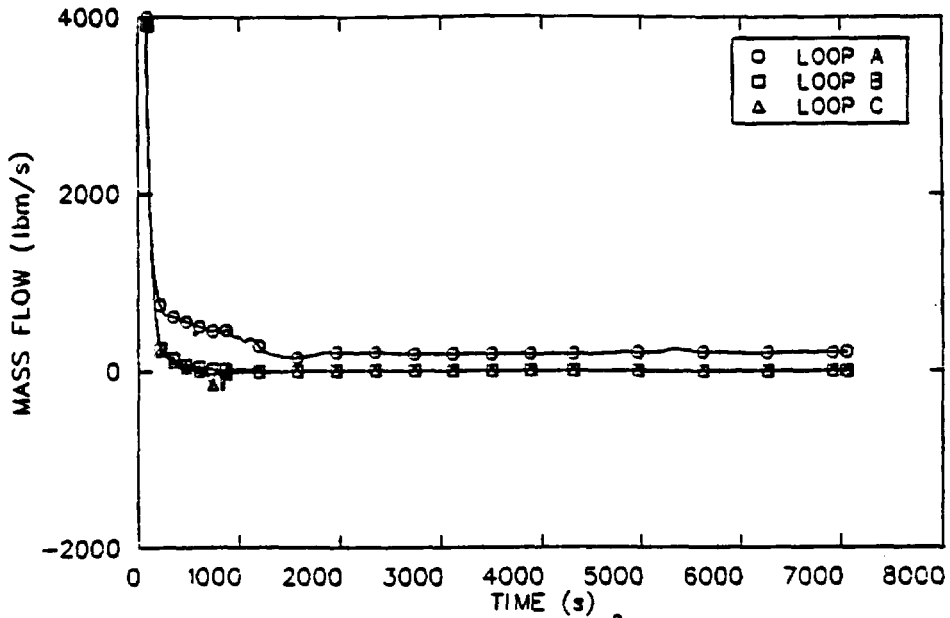


Figure 5. Loop mass flow rates, 1.0 ft<sup>2</sup> main steam line break from hot standby conditions.

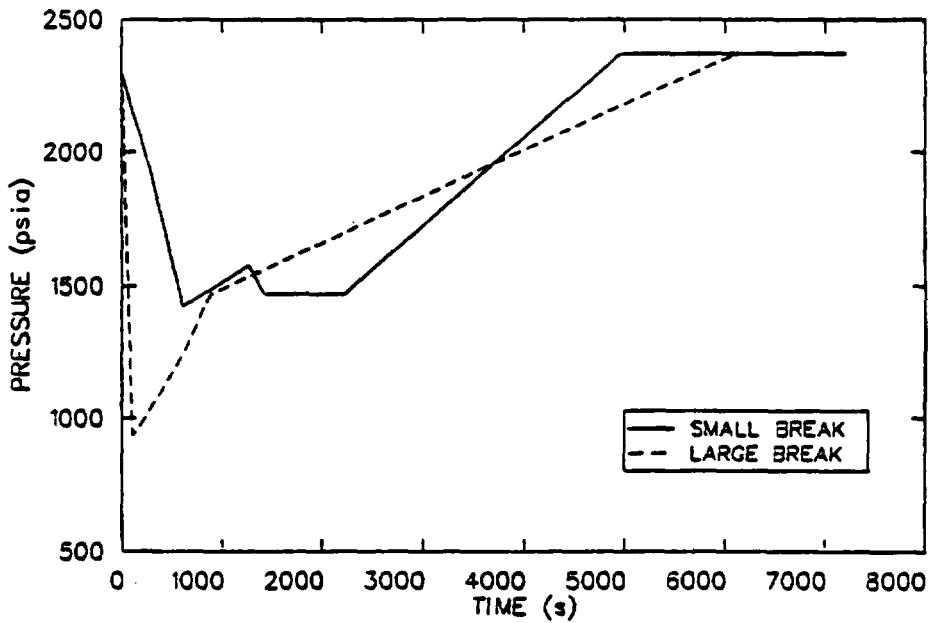


Figure 6. Primary system pressures, large and small steam line break from hot standby conditions.

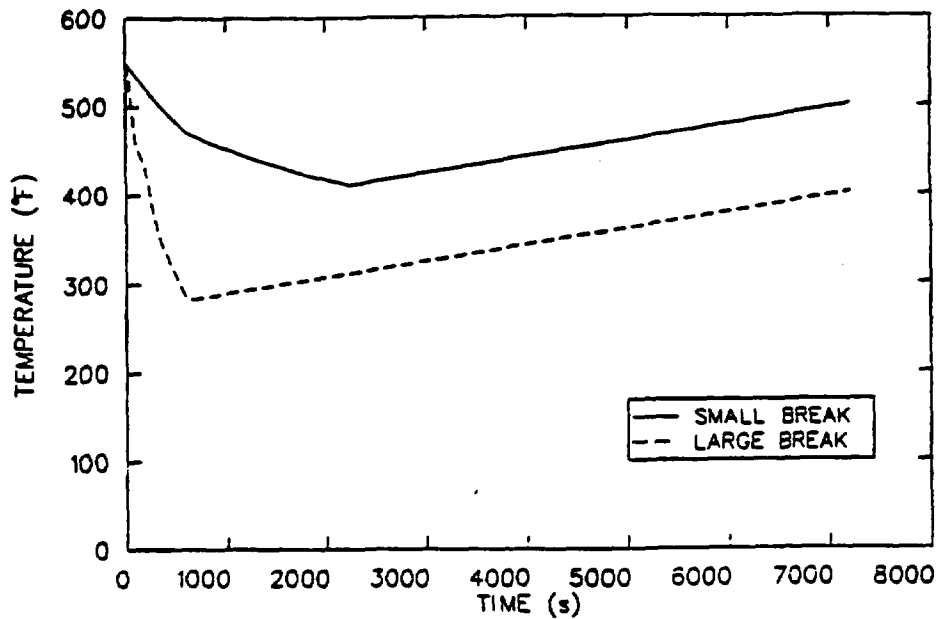


Figure 7. Reactor vessel downcomer fluid temperatures, large and small steam line breaks from hot standby conditions.

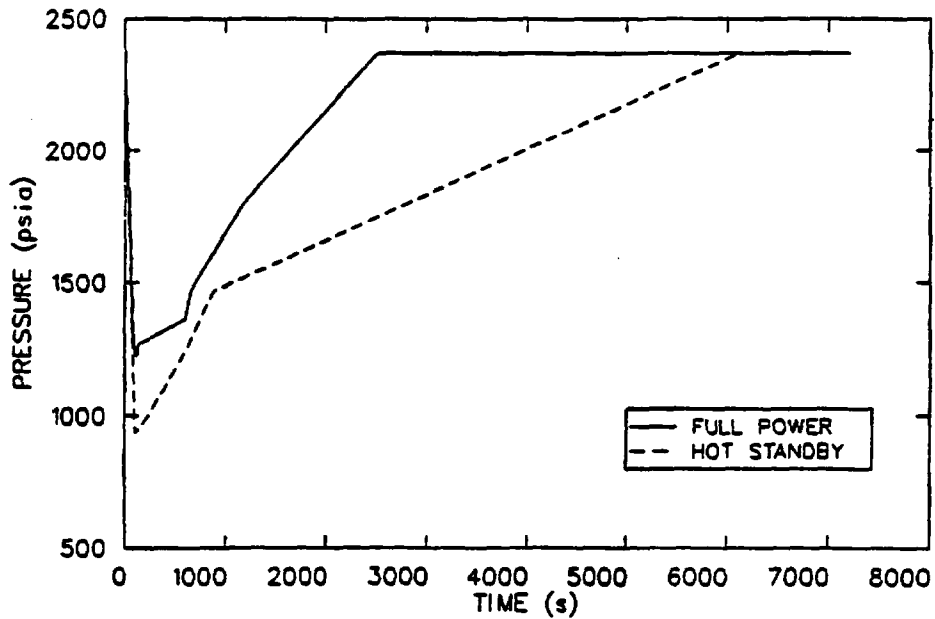


Figure 8. Primary system pressures, large steam line breaks from full power and hot standby conditions.

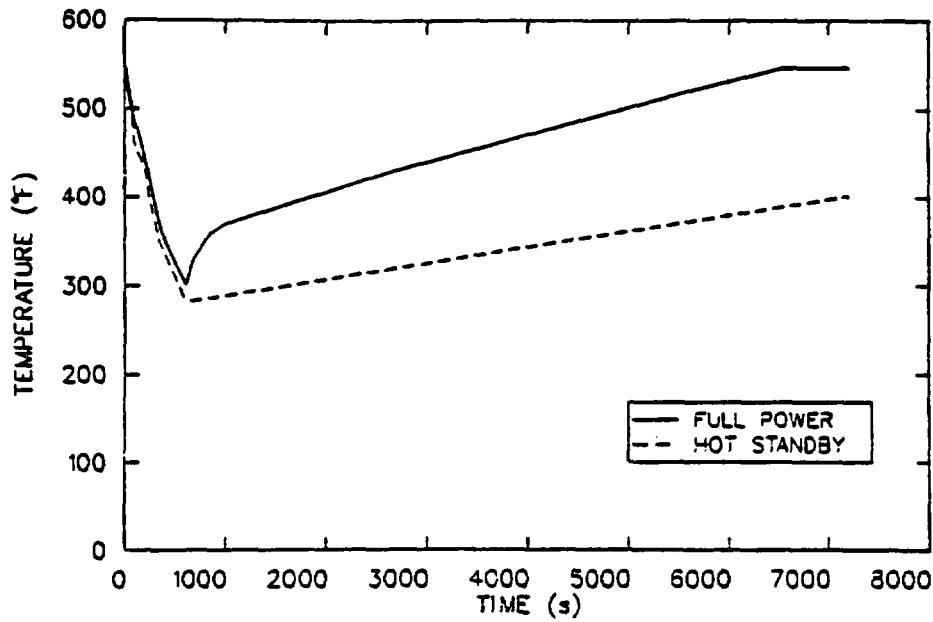


Figure 9. Reactor vessel downcomer fluid temperatures, large steam line breaks from full power and hot standby conditions.

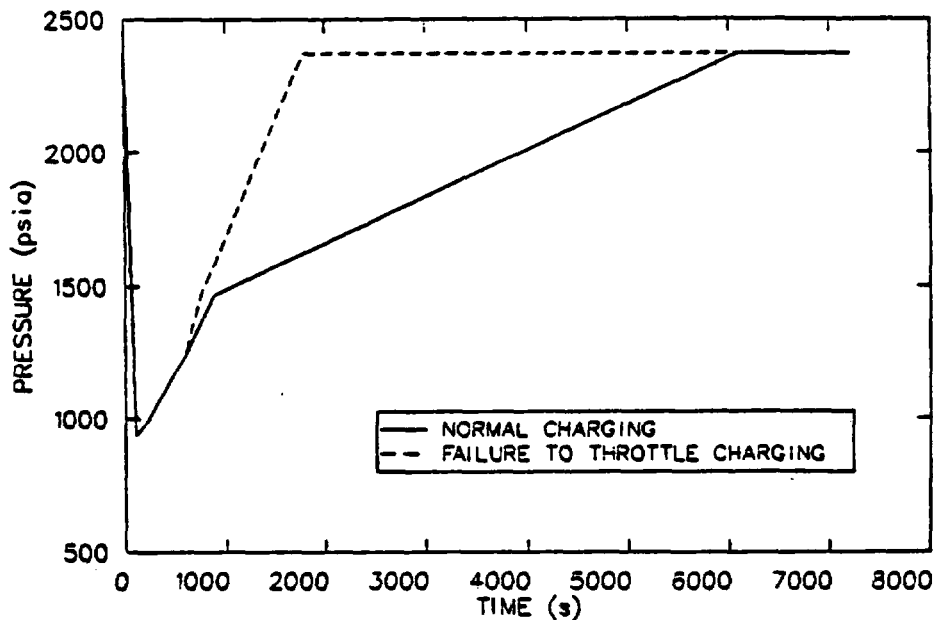


Figure 10. Primary system pressures, large steam line breaks from hot standby conditions, effect of failure to throttle charging.

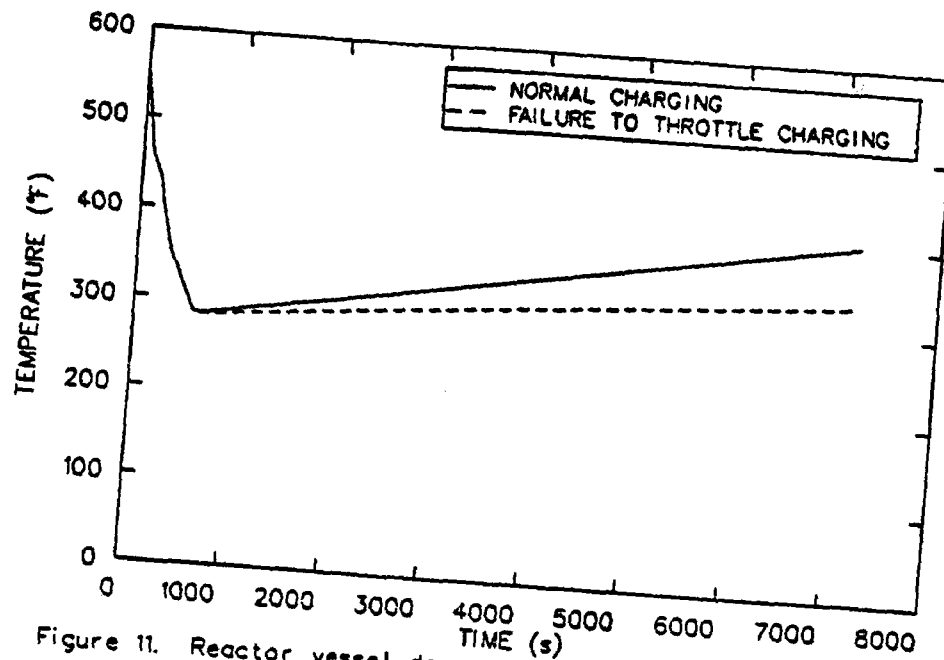


Figure 11. Reactor vessel downcomer fluid temperatures, large steam line breaks from hot standby conditions, effect of failure to throttle charging.

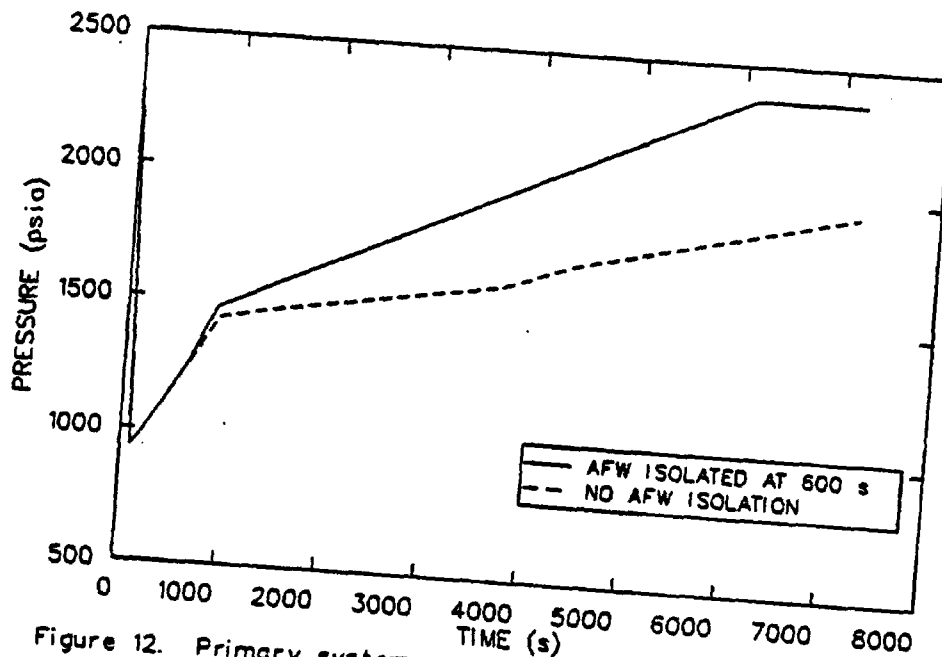


Figure 12. Primary system pressures, large steam line breaks from hot standby conditions, effect of AFW isolation.

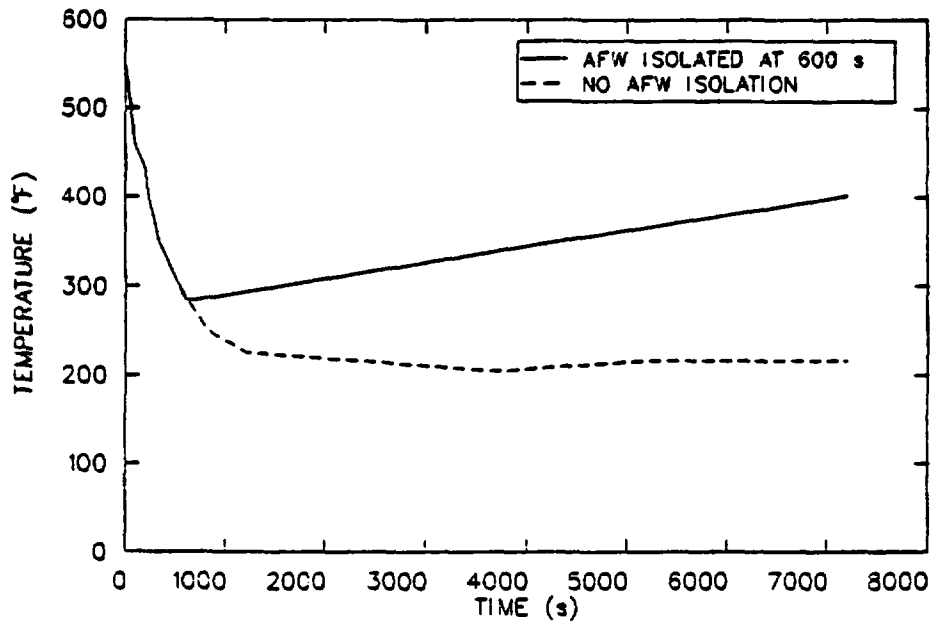


Figure 13. Reactor vessel downcomer fluid temperatures, large steam line break from hot standby conditions, effect of AFW isolation.

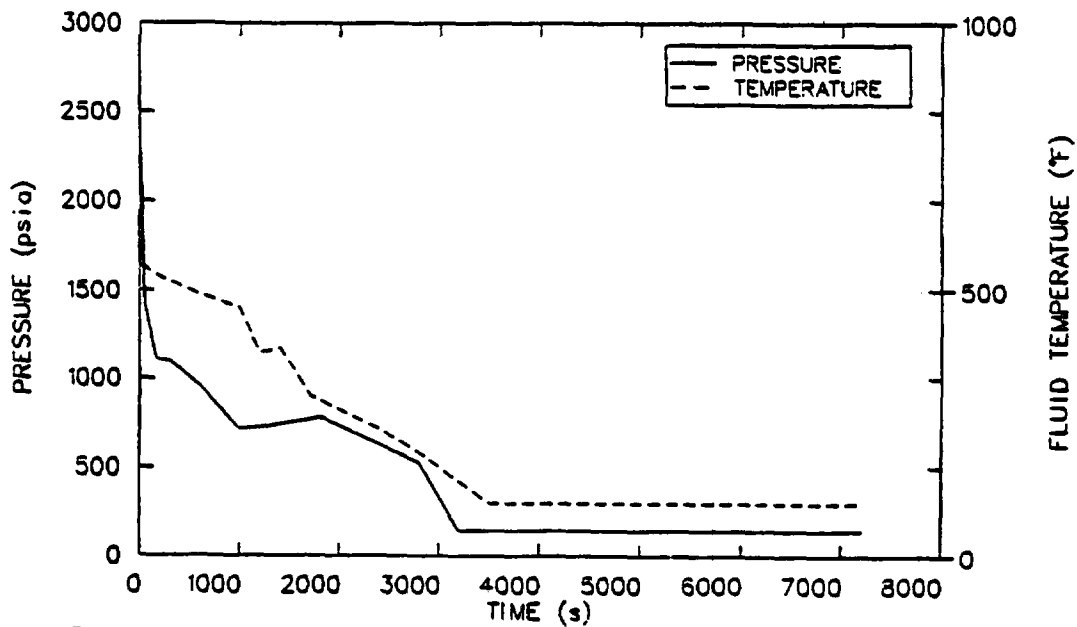


Figure 14. Reactor vessel downcomer pressure and temperatures, 2.5 in. hot leg break from full power.

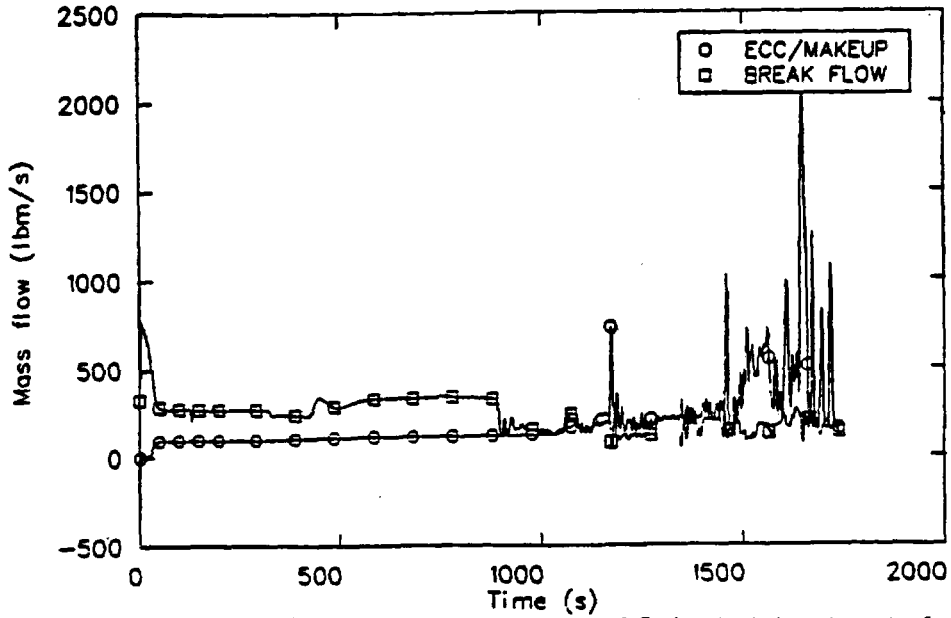


Figure 15. ECC/Makeup and break flow 2.5 in. hot leg break from full power.

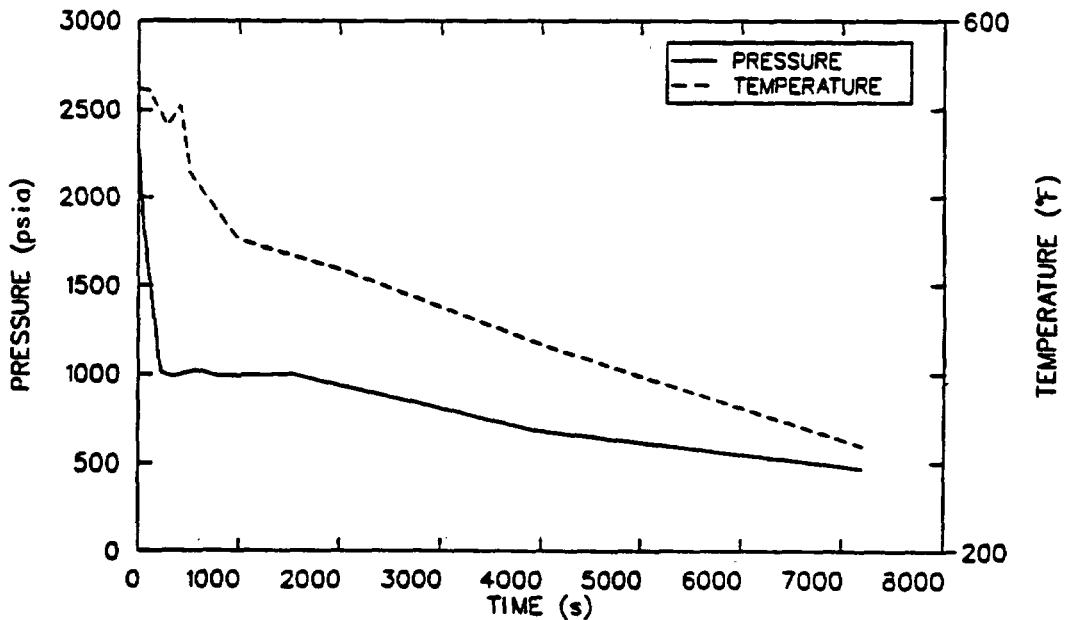


Figure 16. Reactor vessel downcomer pressure and fluid temperature, stuck-open PORV from hot standby conditions.

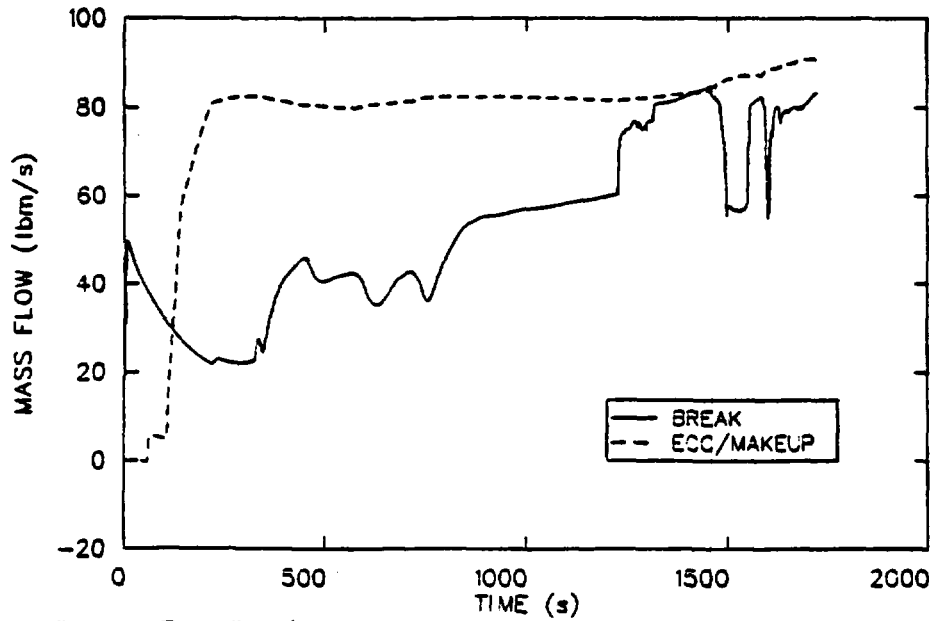


Figure 17. ECC/Makeup and break mass flow rates, stuck-open PORV from hot standby conditions.

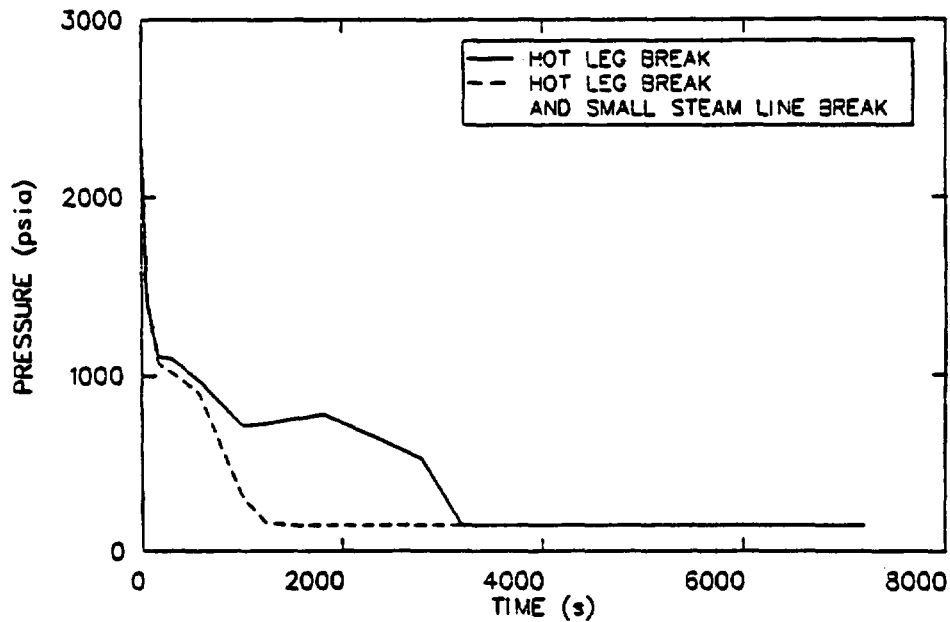


Figure 18. Primary system pressures, 2.5 in. hot leg break from full power conditions, effect of combining with small steam line break.

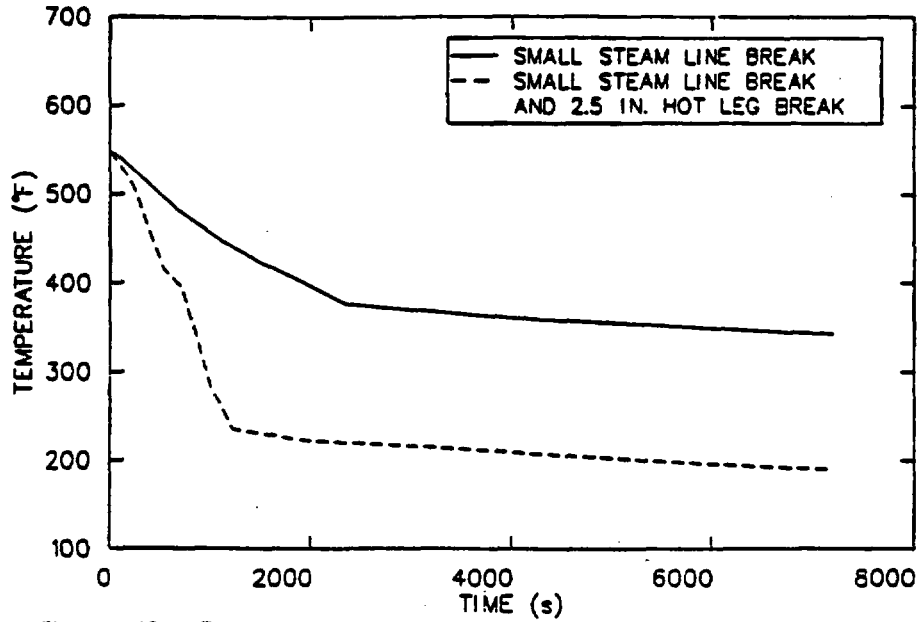


Figure 19. Reactor vessel downcomer fluid temperatures, small steam line break with and without 2.5 in. hot leg break.

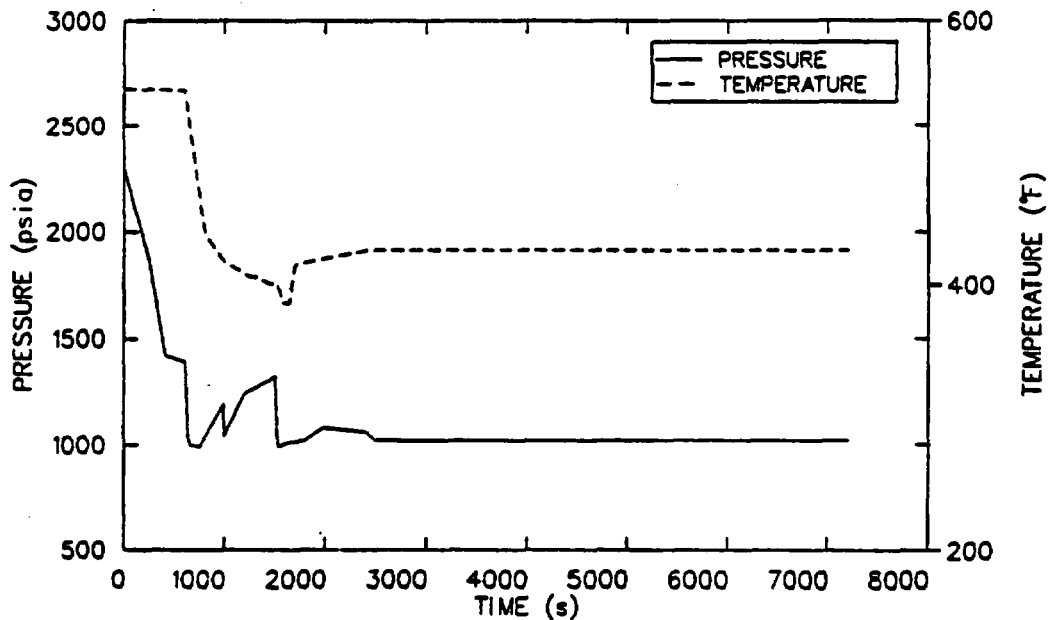


Figure 20. Reactor vessel downcomer pressure and fluid temperature, steam generator tube rupture.

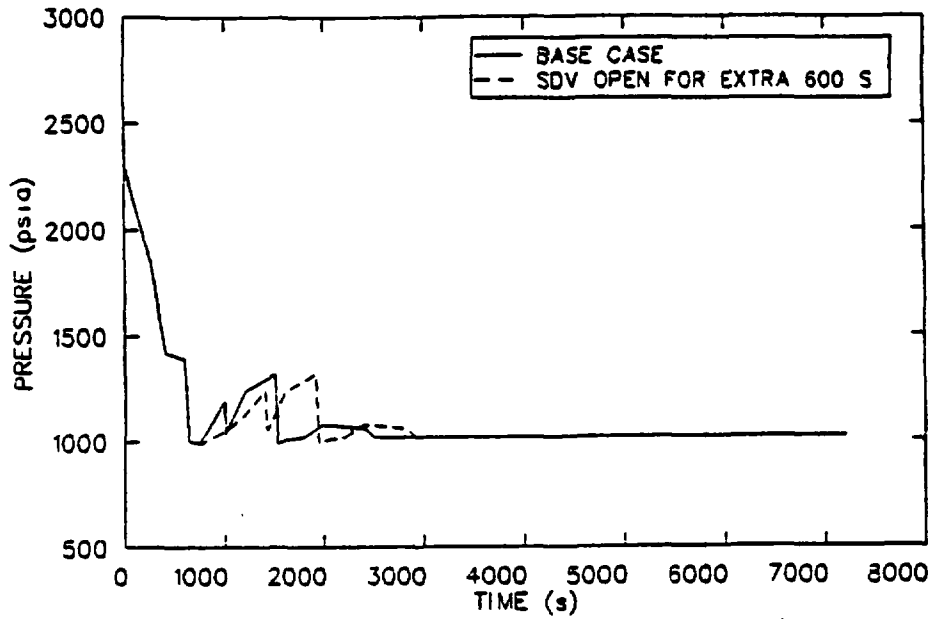


Figure 21. Primary system pressures, steam generator tube rupture, effect of delaying steam dump valve closure.

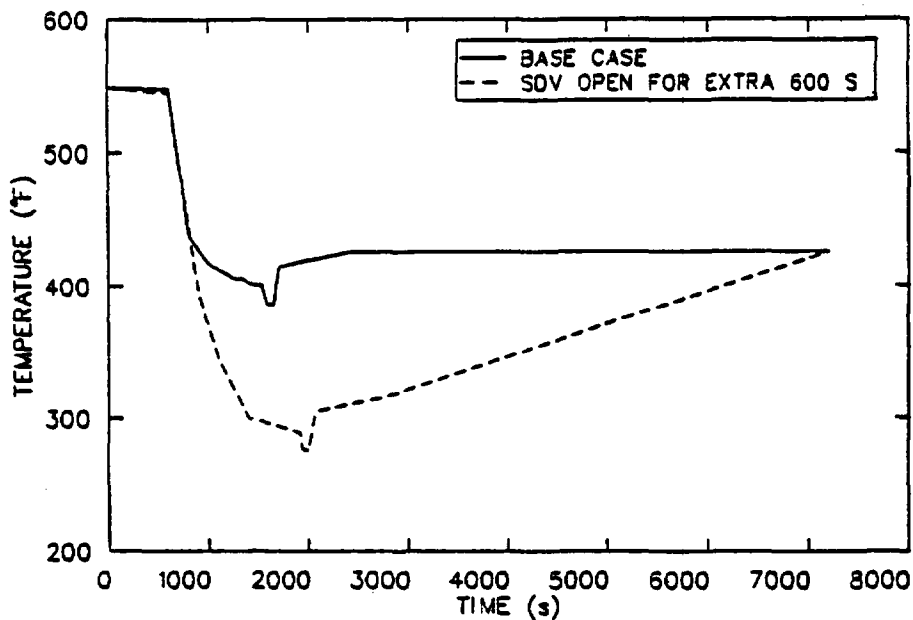


Figure 22. Reactor vessel downcomer fluid temperatures, steam generator tube rupture, effect of delaying steam dump valve closure.

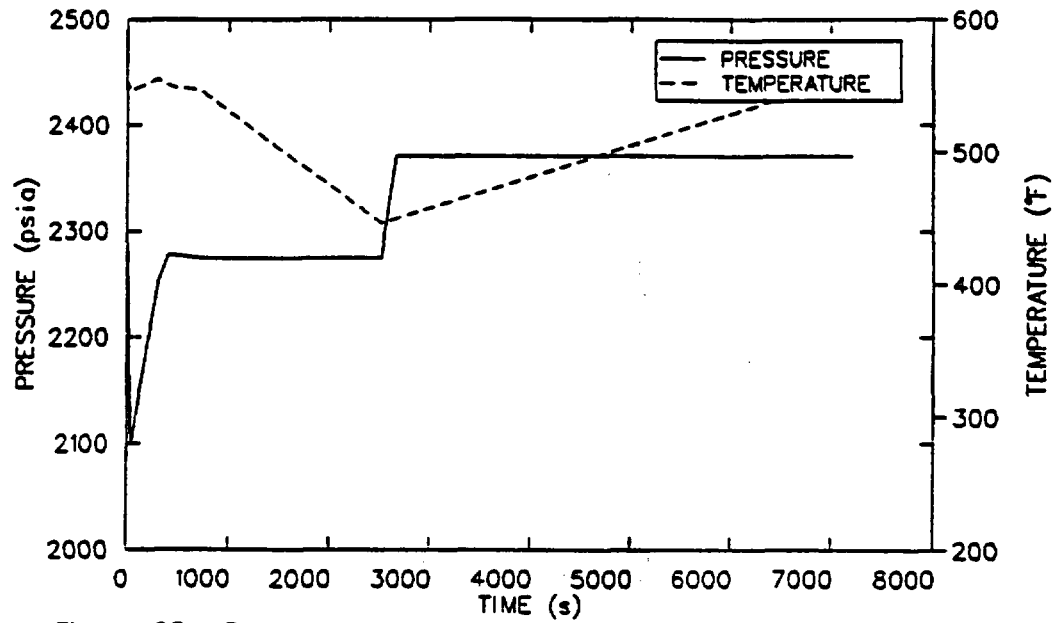


Figure 23. Reactor vessel downcomer pressure and fluid temperature, auxiliary feedwater overfill following reactor trip from full power.

REVIEW OF THERMAL-HYDRAULIC CALCULATIONS FOR CALVERT CLIFFS  
AND H. B. ROBINSON PTS STUDY\*

J. H. Jo, C. Yuelys-Miksis and U. S. Rohatgi

Department of Nuclear Energy  
Brookhaven National Laboratory  
Upton, New York 11973

1. INTRODUCTION

Rapid cooling of the reactor pressure vessel during a transient or accident accompanied by high coolant pressure is referred to as pressurized thermal shock (PTS).

Rapid cooling at the reactor vessel wall inner surface produces thermal stresses within the wall. As long as the fracture toughness of the reactor vessel is high, overcooling transients will not cause vessel failure. However, study<sup>1</sup> showed certain older plants with copper impurities in vessel weldments may become sensitive to PTS in a few years as the nil-ductility transition temperature of the weld material gradually increases. The purpose of the thermal-hydraulic analyses is to better understand the behavior of a plant during various kinds of postulated severe overcooling transients with multiple failures of equipment and without operator corrective action. For each of these postulated transients, the reactor vessel temperature distribution and stresses during the transient and the conditional probability of vessel failure was calculated if the transient should occur, to estimate the likelihood of PTS driving a crack through the reactor vessel wall and to identify important event sequences, operator and control actions, and uncertainties.

The Nuclear Regulatory Commission (NRC) has selected three plants representing PWRs supplied by three vendors in the United States for detailed PTS study. These are: Oconee-1 (Babcock and Wilcox), Calvert Cliffs-1 (Combustion Engineering), and H. B. Robinson-2 (Westinghouse Electric). Oak Ridge National Laboratory (ORNL) has identified several groups of transients with multiple equipment failure and with no corrective operator action which could lead to severe overcooling in these plants. It should be noted that these transient scenarios were purely hypothetical and not necessarily probable. The transients were chosen to give as much insight as possible in a minimum set of calculations to the effect of certain operator and equipment failures, even when the probability of the combination of these failures was extremely low. The thermal-hydraulic calculations for these transients were calculated at the Los Alamos National Laboratory (LANL) and the Idaho National Engineering Laboratory (INEL) using the latest versions of the TRAC-PWR and RELAP5 codes, respectively. The Oconee-1 transients were divided between LANL and INEL, with some transients common to both. The Calvert Cliffs and Robinson transient calculations were performed by LANL and INEL, respectively.

\* This work was performed under the auspices of the U. S. Nuclear Regulatory Commission.

Brookhaven National Laboratory (BNL) reviewed and compared the plant input decks developed at LANL and INEL, and reviewed the calculation results. This paper presents the results of the BNL review of the selected Calvert Cliffs and H. B. Robinson calculations performed at LANL and INEL.

LANL performed TRAC calculations of thirteen transients and INEL performed RELAP5 calculations of eleven transients. Input decks and steady-state results for these calculations were reviewed and a quick preliminary review of all calculations was also performed at BNL. BNL also selected six transients for each plant and performed detailed in-depth review of the calculations of these transients.

In order to provide a quantitative review of these calculations, a simple method has been developed to predict the primary system temperature based on the mass and energy balances. In this approach, the whole reactor system, including the secondary sides of the steam generators (SG) and the metal structures, is lumped into a single volume and the energy balance is applied to that volume. However, separate mass balance equations are used for the primary system and the secondary side of each SG. This approach assumes that the temperature differences between the cold and hot legs of the primary loops and between the primary and secondary sides of SGs are relatively small. It was shown that the primary temperatures calculated by both codes were indeed in close agreement with those obtained by simple hand calculations for most transients.

These balance equations are:

$$\frac{d}{dt} (M_p) = W_{HPI} + W_c - W_{BR}$$

$$\frac{d}{dt} (M_{si}) = W_{fwi} - W_{sti}$$

$$\begin{aligned} \frac{d}{dt} (M_p + M_m + \sum M_{si})h &= Q_d + Q_{pm} + Q_{mis} + W_{HPI} h_{HPI} \\ &+ W_c h_c - W_{BR} h_{BR} + \sum W_{fwi} h_{fwi} \\ &- \sum W_{sti} h_{sti} \end{aligned}$$

where M, W, Q, h are total mass, mass flow rate, heat (or power) and enthalpy, respectively and the subscripts p, s, m, HPI, c, BR, fw, st, d, pm, mis denote primary, secondary, metal structure, HPI, charging, break, feedwater, steamline, decay, pump and miscellaneous, respectively.

The primary and secondary pressures have been more difficult to analyze with this simple approach, especially when the cold water is entering into the pressurizer or the secondary sides of the SGs. Due to the significant non-equilibrium effect, the pressure prediction depends largely on the condensation or evaporation rate, which is difficult to estimate by simple analysis. Many factors affect the condensation and evaporation rates, such as temperature of the liquid and vapor, mass flow rate, mixing of the incoming water with the bulk water, and the mode of heat transfer between the liquid, vapor and wall. Therefore, in some transient calculations, attempts have been made to compare the pressurizer water levels obtained by the codes and BNL simple calculations instead of the pressures. It has been observed that the trend of the pressurizer pressure calculated by the codes is very closely approximated by the trend of the water level in the pressurizer in many transients. Whenever possible and applicable, calculation for the pressurizer pressure has been made based on the adiabatic and/or equilibrium assumptions. The adiabatic approach assumes no mass and energy transfer between the liquid and vapor phases (no condensation or evaporation). The pressure thus calculated is expected to be the lower bound of the actual pressure when the pressurizer is being emptied and the upper bound when the pressurizer is being filled. On the other hand, the equilibrium approach assumes that the phases are in complete equilibrium, and it is expected to provide the upper bound pressure when emptying and the lower bound when filling. The actual pressure is expected to be somewhere in between these two extreme pressures.

A similar nonequilibrium effect has also been observed in the secondary side pressure of SG, especially when the SG is being filled with the cold auxiliary feedwater (AFW). In several transients, the secondary pressure remains high while the temperature declines. This indicates high non-equilibrium effect. It appears that further code assessment work is needed to verify the code calculation of the U-tube steam generator pressure when the cold auxiliary feedwater is introduced into it. However, it is not expected that this uncertainty would affect the transient calculations significantly.

A similar approach was used for the extrapolation of the calculations and predicting the ultimate state of the system beyond the calculated time. Review of only one typical transient calculation for each plant will be discussed in this paper as illustration. Review of the remaining transients can be found in References 2 and 3.

## 2. REVIEW OF TRAC CALCULATION OF 1-FT<sup>2</sup> STEAM LINE BREAK IN HZP CONDITION FOR CALVERT CLIFFS

This transient was initiated by a 1-ft<sup>2</sup> break at the main steam line during the hot zero power (HZP) operation. No other equipment failure or operator action was assumed.

Figure 1 shows the downcomer liquid temperature calculated by TRAC with the system average temperature obtained by BNL hand calculation. Two BNL-calculated temperatures are shown in the figure. One is calculated with the assumption that heat transfer between the wall of the reactor (and other structures) and liquid is instantaneous and, thus, the metal temperature changes with the liquid temperature. The other calculation assumes that the heat

transfer is so slow that the metal temperature does not change. The real temperature should be between these two extreme temperatures. The TRAC downcomer temperature initially agrees well with the temperature calculated without the metal mass accounted for, and then it eventually approaches that calculated with the metal mass accounted for, as expected. This indicates that the metal takes a considerably longer time to cool and plays an important role in determining the minimum downcomer liquid temperature. The liquid temperatures calculated by TRAC at the various locations are shown in Figure 2, along with the BNL system average temperatures, with and without the metal heat transfer during the initial 1500 seconds. The figure shows that the downcomer temperature may be representative of the system average temperature and, again, both TRAC and BNL calculations agree very well.

Figure 3 shows the system pressures as calculated by TRAC and BNL. The BNL pressure is calculated based on the assumption of adiabatic compression during the filling stage, which yields the highest rate of pressure increase during compression. The actual pressure is expected to be lower than this, as is the case in this calculation. Figure 4 compares the water level in the pressurizer as calculated by TRAC, BNL and RETRAN. As expected, the pressure and the water level behave similarly.

Figure 5 shows the TRAC pressure of the secondary sides of both steam generators. The saturation pressures corresponding to the BNL average temperature and the TRAC intact steam generator temperature are also shown in the figure. These would be the expected pressures of the steam generators if the equilibrium condition prevails. The broken steam generator pressure stays at the atmospheric pressure as it becomes empty, as expected. However, the intact steam generator pressure remains much higher than the saturation pressure and also shows several sharp turns. A similar steam generator pressure response is observed in several other transients when the steam generator is being filled with cold AFW. This is apparently related to the severe non-equilibrium effect caused by the TRAC condensation model. It appears that the TRAC condensation model underpredicts the condensation rate and, thus, over-estimates the non-equilibrium effect. However, this uncertainty is not expected to alter the course of the rest of the transient significantly, since the SG pressure is not involved in the control of the system after the initial 100 seconds into this transient.

The TRAC calculation was terminated at 7200 seconds. After 7200 seconds, the system temperature is expected to continue to decrease until it eventually reaches 357°K where the decay heat balances with the cooling by the charging and the AFW.

There is a corresponding RETRAN calculation performed by ENSA for BG&E, the owner of the Calvert Cliffs plant, available for this transient for the initial 1000 seconds. Figure 6 shows good agreement between the downcomer temperature calculated by RETRAN and those obtained by TRAC and BNL calculations. Figure 7 shows that the RETRAN pressure is virtually identical to the TRAC pressure, while the BNL pressure based on the adiabatic assumption is higher than these, as expected. Figure 8 shows the pressure in the steam generators from both RETRAN and TRAC calculations. The saturation pressure corresponding to the system average temperature calculated by BNL is also shown in the figure. The BNL saturation pressure matches the broken SG pressures for both

TRAC and RETRAN calculations very closely. However, the intact SG pressure for TRAC increases while the RETRAN pressure continues to decrease. As discussed earlier, further work is needed to clarify this uncertainty.

In summary, both TRAC and RETRAN codes present reasonable results except for the TRAC intact SG pressure, which may have an insignificant effect on the final results.

### 3. REVIEW OF RELAP5 CALCULATION OF STEAM LINE BREAK AT HZP CONDITION FOR H. B. ROBINSON

This transient, as the one discussed in the previous section, was initiated by a 1 ft<sup>2</sup> break in a main steam line at hot standby operation. The break is upstream of the main steam isolation valve and there is no failure of any automatic equipment. The operator is assumed to trip the reactor coolant pumps when the safety injection actuation signal is generated and the primary system pressure falls to 1300 psig and to stop the auxiliary feedwater flow 600 seconds after the initiation of the transient.

The RELAP5 code was used to calculate the transient to 1800 seconds and the key parameters were extrapolated to 7200 seconds. Figure 9 shows the downcomer temperatures calculated by RELAP5 with the system average temperature obtained by the BNL hand calculation. In addition, the figure shows the INEL extrapolation of the downcomer temperature. The BNL temperature shown is that calculated without accounting for the heat stored in the metal structure. This assumes that the heat transfer between the liquid and the reactor and component metal structures is relatively slow to affect the temperature of the metal at the early stage of the transient. Calculations were also performed with the assumption that the wall heat transfer is instantaneous, so that the metal and the liquid temperatures change simultaneously. The actual temperature would be close to that calculated without the metal structure initially and eventually approach that calculated with the metal latent heat accounted for since the metal cooling is considerably slower than that for the liquid.

In the code calculations, there was stagnation in Loops B and C which prevented the injected cooling water from circulating, hence, keeping the cold leg temperatures very low. This lack of natural circulation forced the Loop B and C hot leg temperatures to remain very high. In the affected Loop A there is greater natural circulation and therefore its hot leg temperature is lower than the other loops and its cold leg temperature is closer to the downcomer temperature.

Figure 10 to 12 show the hot and cold leg temperatures of each loop with the BNL calculated temperatures with and without the metal latent heat. Due to stagnation in the loops, there are large temperature spreads between the hot and cold legs in Loops B and C and the BNL calculated temperatures fall between the two extremes. In Loop A the BNL system average without the metal heat accounted for is very close to the hot leg temperature. Since the BNL values are system average temperatures, these results are to be expected. Figure 10 also compares the temperature spread between the hot leg and the cold leg as calculated by RELAP5 and BNL. This spread is based on the flow rates calculated by RELAP5. As can be seen, the INEL calculated temperature spread is realistic and to be expected.

Figure 13 shows the cold leg temperatures as extrapolated by INEL and the BNL temperatures with and without the heat stored in the metal structures. The INEL extrapolations approach the system average temperature with the metal, as would be expected, in Loops B and C, but not in Loop A. These extrapolations assume a constant rate of temperature increase or decrease based upon the temperatures calculated at 1800 seconds. However, these calculations appear to have been prematurely terminated since the key parameters still have not stabilized and there is insufficient information to accurately extrapolate the results. As found in the previous section the effect of the metal latent heat is significant up to 4000 seconds after which the heat transfer rate may decrease.

Figure 14 shows the system pressures as calculated by RELAP5 and BNL. The BNL pressures are calculated with the assumption of adiabatic compression during the filling stage which is expected to provide the upper bound of the actual pressure. Also shown is the saturation pressure corresponding to the BNL calculated system average temperature. As expected, the RELAP5 pressure remained below the BNL pressure. Similar results were observed in the Calvert Cliff case discussed previously, as can be seen in Figure 3. However, RELAP5 exhibited less non-equilibrium effect than did TRAC. The secondary pressure of the broken loop corresponds very closely with the equilibrium pressure, as expected. The pressure in the intact steam generators remains high, indicating that these loops are completely stagnated.

#### 4. SUMMARY AND CONCLUSIONS

Thermal-hydraulic transient calculations performed by LANL using the TRAC-PP1 code and by INEL using the RELAP5 code for the USNRC PTS study of the Calvert Cliffs and H. B. Robinson Nuclear Power Plants have been reviewed at BNL including the input decks and steady state calculations. Furthermore, six transients for each plant have been selected for the in-depth review. Simple hand calculations based on the mass and energy balances of the entire reactor system, have been performed to predict the temperature and pressure of the reactor system, and the results have been compared with those obtained by the code calculation.

In general, the temperatures and pressures of the primary system calculated by the codes have been very reasonable. The secondary pressures calculated by TRAC appear to indicate that the codes have some difficulty with the condensation model and further work is needed to assess the code calculation of the U-tube steam generator pressure when the cold auxiliary feedwater is introduced to the steam generator. However, it is not expected that this uncertainty would affect the transient calculations significantly.

#### REFERENCES

1. U. S. Nuclear Regulatory Commission Paper, "Pressurized Thermal Shock," SECY-82-465, November 23, 1982.
2. Jo, J. H., "Review of TRAC Calculations for Calvert Cliffs PTS Study," Brookhaven National Laboratory report to be published.
3. Yuelys-Miksis, C., "Review of RELAP5 Calculations for H. B. Robinson PTS Study," Brookhaven National Laboratory report to be published.

CAUTION: The scenario simulated contains significant conservatisms in operator actions and equipment failures.

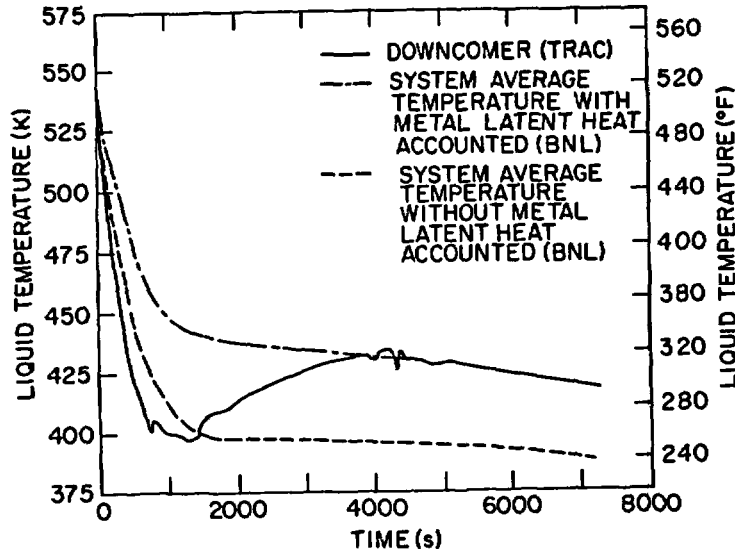


Figure 1 Liquid Temperature  
1-ft<sup>2</sup> Steamline Break in HZP Condition for Calvert Cliffs

CAUTION: The scenario simulated contains significant conservatisms in operator actions and equipment failures.

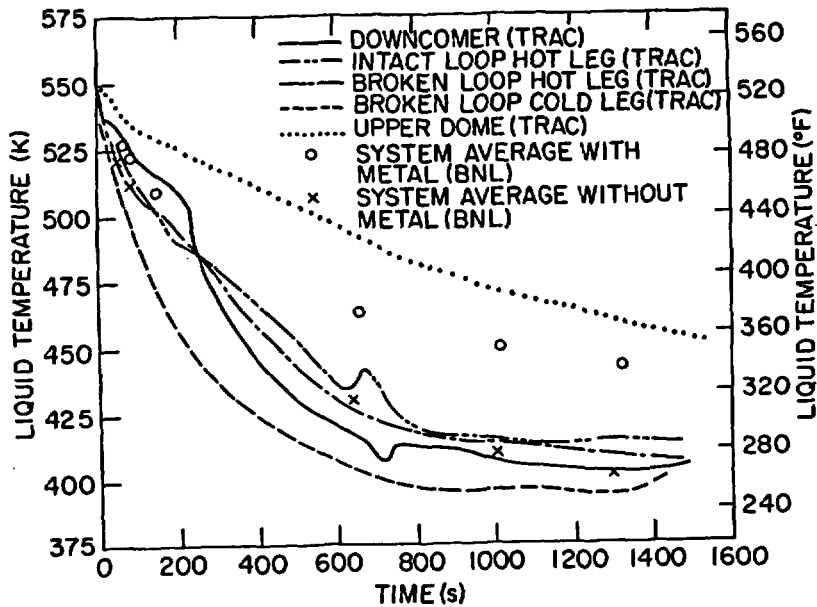


Figure 2 Liquid Temperature  
1-ft<sup>2</sup> Steamline Break in HZP Condition for Calvert Cliffs

CAUTION: The scenario simulated contains significant conservatisms in operator actions and equipment failures.

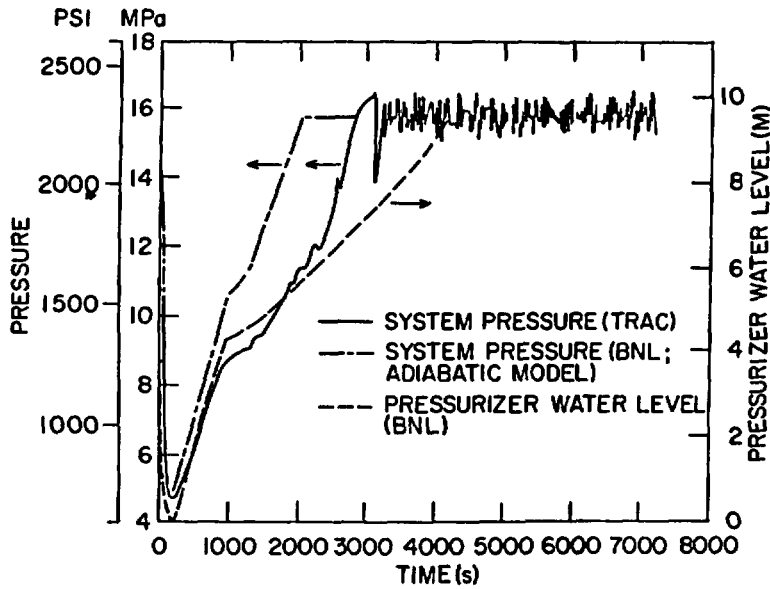


Figure 3 System Pressure  
1-ft<sup>2</sup> Steamline Break in HZP Condition for Calvert Cliffs

CAUTION: The scenario simulated contains significant conservatisms in operator action and equipment failures.

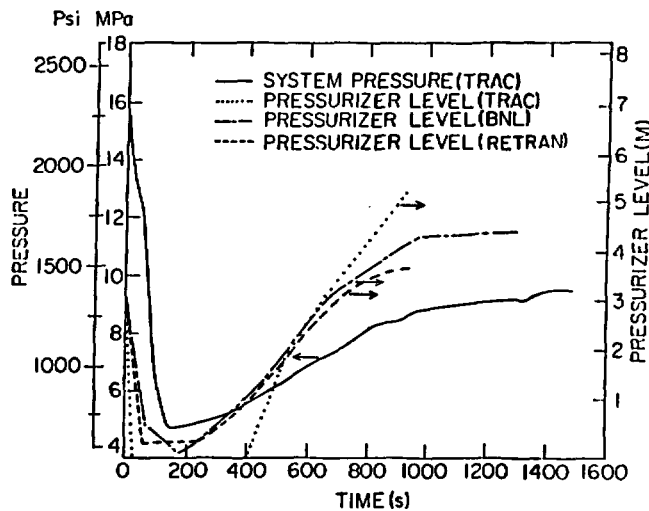


Figure 4 System Pressure and Pressurizer Level  
1-ft<sup>2</sup> Steamline Break in HZP Condition for Calvert Cliffs

CAUTION: The scenario simulated contains significant conservatisms in operator actions and equipment failures.

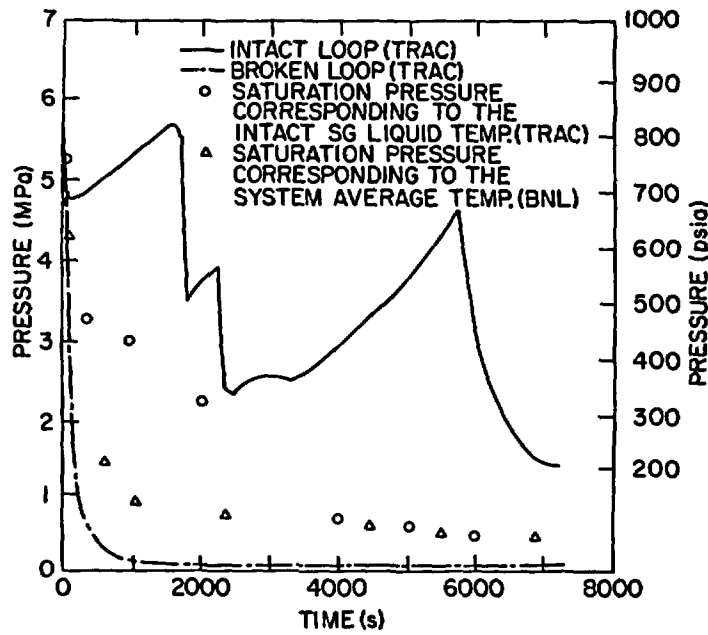


Figure 5 Steam Generator Pressure  
1-ft<sup>2</sup> Steamline Break in HZP Condition for Calvert Cliffs

CAUTION: The scenario simulated contains significant conservatisms in operator action and equipment failures.

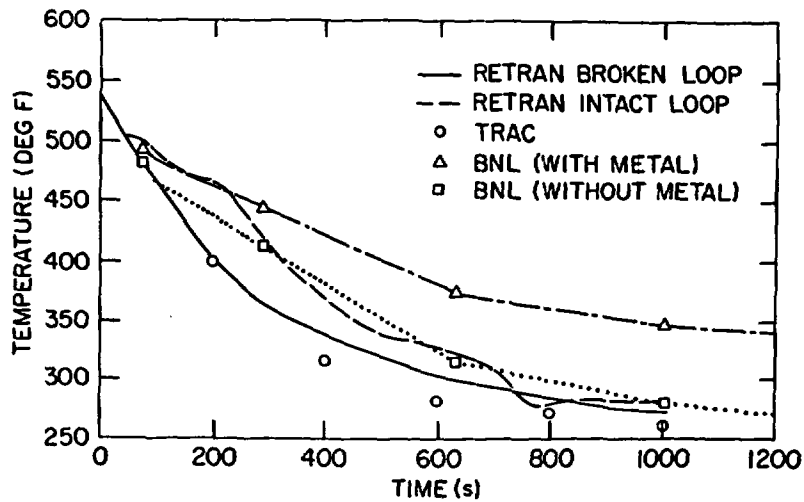


Figure 6 Liquid Temperature in the Downcomer  
1-ft<sup>2</sup> Steamline Break in HZP Condition for Calvert Cliffs

CAUTION: The scenario simulated contains significant conservatisms in operator actions and equipment failures.

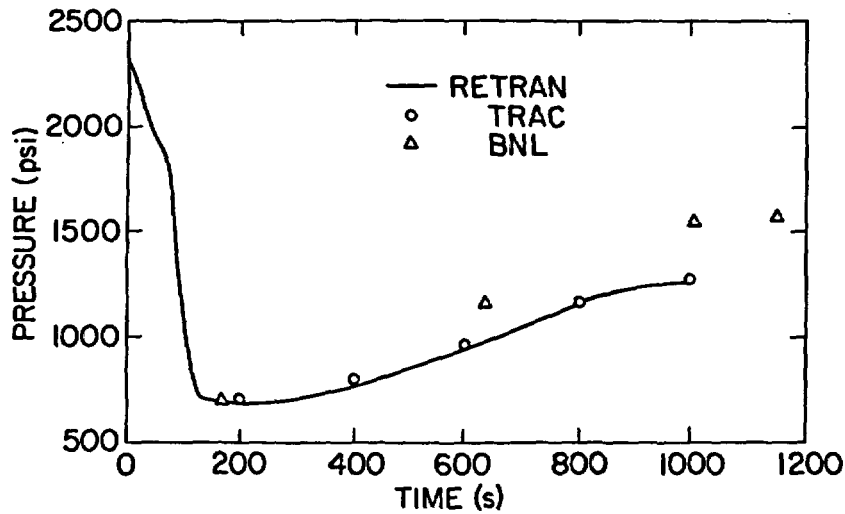


Figure 7 System Pressure  
1-ft<sup>2</sup> steamline Break in HZP Condition for Calvert Cliffs

CAUTION: The scenario simulated contains significant conservatisms in operator action and equipment failures.

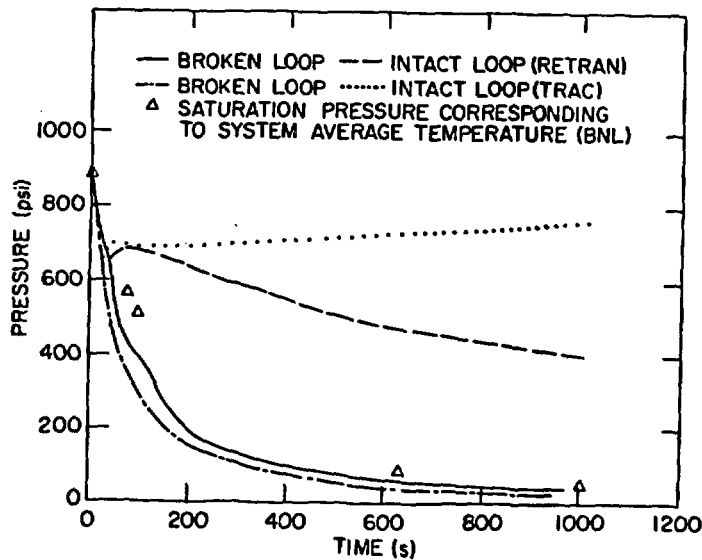


Figure 8 Steam Generator Pressure  
1-ft<sup>2</sup> steamline Break in HZP Condition for Calvert Cliffs

CAUTION: The scenario simulated contains significant conservatisms in operator actions and equipment failures.

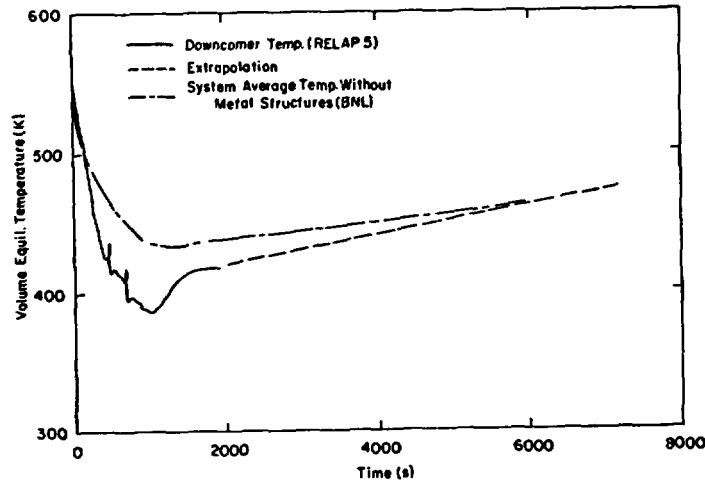


Figure 9 Liquid Temperature in the Downcomer 1-ft<sup>2</sup> Steamline Break in HZP Condition for H. B. Robinson

CAUTION: The scenario simulated contains significant conservatisms in operator actions and equipment failures.

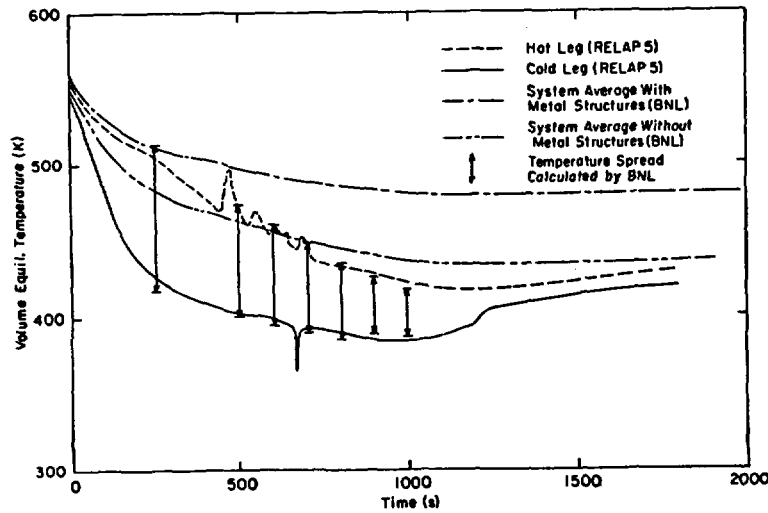


Figure 10 Liquid Temperature 1-ft<sup>2</sup> Steamline Break in HZP Condition for H. B. Robinson

CAUTION: The scenario simulated contains significant conservatisms in operator actions and equipment failures.

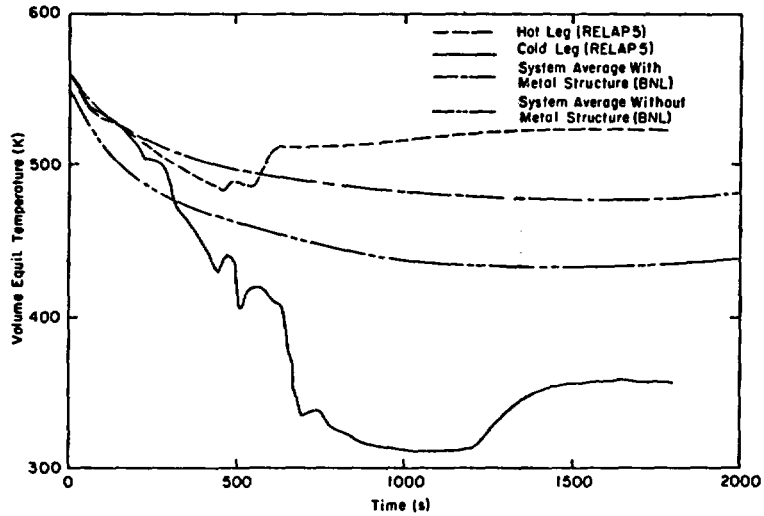


Figure 11 Liquid Temperature  
1-ft<sup>2</sup> Steamline Break in HZP Condition for H. B. Robinson

CAUTION: The scenario simulated contains significant conservatisms in operator action and equipment failures.

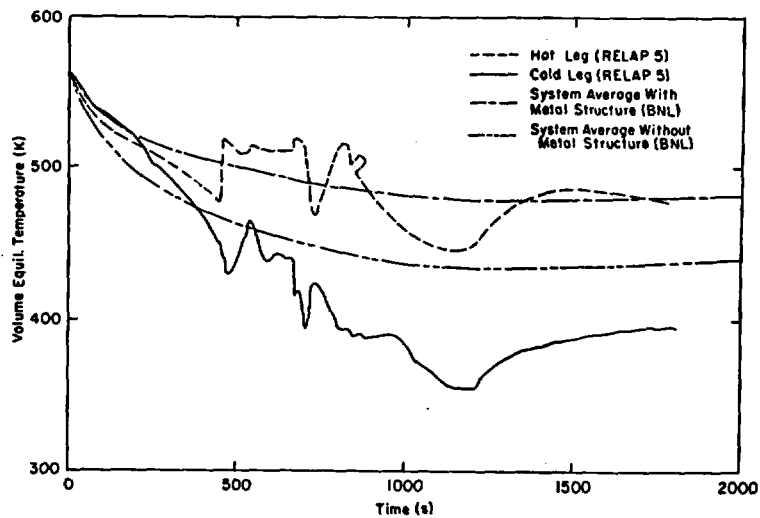


Figure 12 Liquid Temperature  
1-ft<sup>2</sup> Steamline Break in HZP Condition for H. B. Robinson

CAUTION: The scenario simulated contains significant conservatisms in operator action and equipment failures.

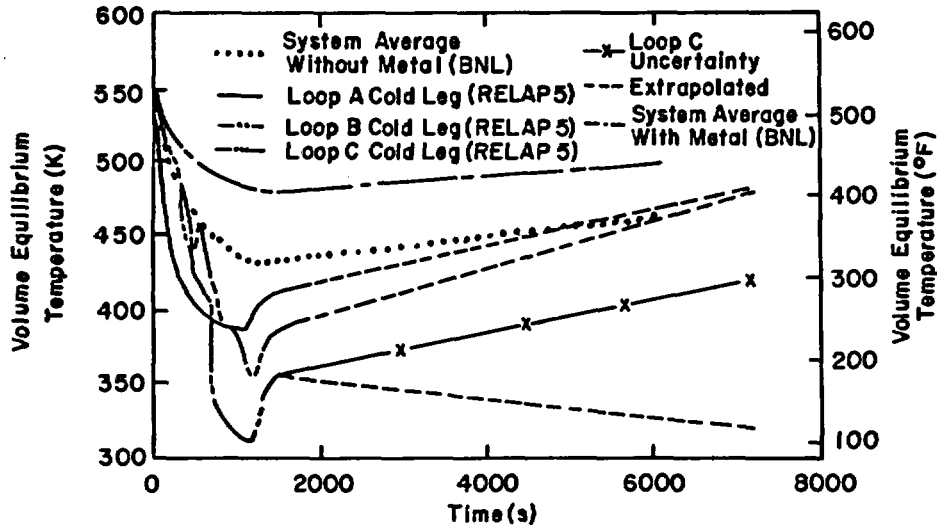


Figure 13 Liquid Temperature  
1-ft<sup>2</sup> Steamline Break in HZP Condition for H. B. Robinson

CAUTION: The scenario simulated contains significant conservatisms in operator actions and equipment failures.

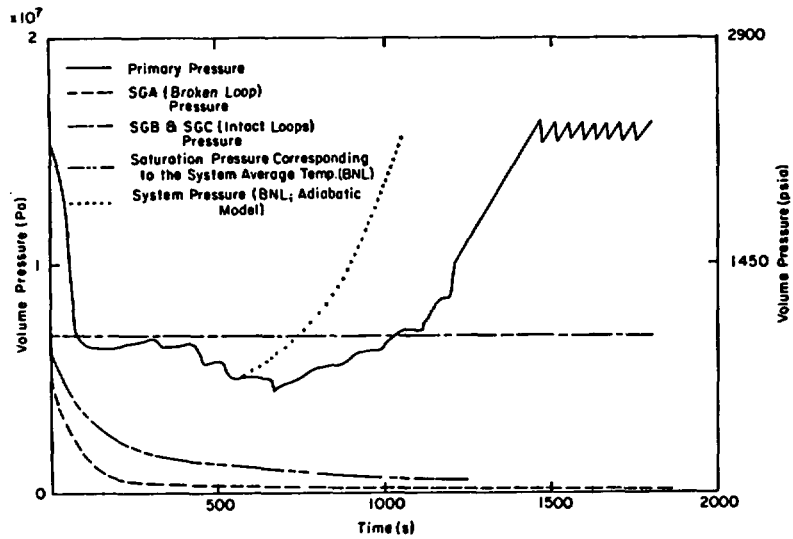


Figure 14 Primary and Secondary Pressure  
1-ft<sup>2</sup> Steamline Break in HZP Condition for Calvert Cliffs

## Buoyancy Effects in Overcooling Transients

By

T. G. Theofanous and K. Iyer

School of Nuclear Engineering  
Purdue University

This presentation is a short report on Purdue's contribution to the NRC PTS study. Our task was to include stratification/thermal-mixing effects in the thermal-hydraulic scenarios developed by TRAC and RELAP5 calculations. The results from our study provided the input to the fracture mechanics calculations carried out at ORNL.

Last year, in the 11th Water Reactor Safety Information Meeting, we presented a method for predicting the onset of stratification in the cold leg, due to HPI. Use of these criteria with the thermal-hydraulic behavior predicted by TRAC and RELAP5 leads to the conclusion that the only practically significant situation where stratification need to be considered is that involving loop flow stagnation. Of principal interest are, therefore, transients leading to complete flow stagnation. Our analyses, and this presentation was, therefore, principally oriented to this condition. The Calvert Cliffs analyses by TRAC have also shown that an asymmetric downcomer condition, obtained by flow stagnation in only one or two of the loops, is also possible. We have demonstrated that the basic analyses tools developed for the fully stagnated case can be fruitfully employed to address the asymmetric situations also.

Our analysis was based on the Regional Mixing Model (RMM) and the associated computer code REMIX. These analytical tools were supported by reactor-specific simulations in Purdue's 1/2 scale PTS facility. Details of these analytical and experimental tools, as well as of all reactor-specific calculations may be found in a set of three NUREG/CR reports: NUREG/CR-3700, -3701, -3702.

Figure 1. This figure illustrates the basic structure of our Regional Mixing Model. The key aspect of this model is its unique closure scheme, whereby the height of the cold stream  $h_c$  and the entrainment in Mixing Region 1 (MR1) are made consistent with a counter-current flow condition at the exit of the cold leg (i.e. the sum of the squares of the Froude numbers of the two streams is equal to unity). After the stratification in the cold leg has been predicted, the downcomer plume characteristics may be found by an entrainment process in MR3 (which was determined experimentally at 1/2 scale to be about 1-to-1) and a subsequent plume decay.

Figure 2. For injection Froude numbers of less than 0.6, we expect backflow of hot stream water into the injection line. The approximate extent of this backflow region was found visually from experiments. Although the behavior is unsteady, we postulate that the plume length available for entrainment in MR1 should be increased by an effective length,  $L_{eff}$ , taken to be equal to one-half the backflow penetration. This approximate, empirical trend, for  $Fr < 0.6$ , as shown in Figure 2, was incorporated in REMIX.

Figure 3. This figure shows schematically the generic configuration of Purdue's 1/2-scale thermal-mixing facility. Reactor-specific configurations can be assembled by using approximate attachments to the cold leg of the configuration-0. The test section is transparent (acrylic) and the density effect is simulated by using brine injection into fresh water. The scale was chosen such that with full density difference, and a Froude number similarity the Reynolds numbers similarity is off by less than one order of magnitude, and certainly well within the turbulent regime. Mixing was determined by the use of concentration probes with a frequency response of  $\sim 1,000$  Hz. Thus not only means but also concentration fluctuations could be obtained. Velocities were measured with hot film probes. All probes were put on traversing devices such that measurements could be recorded

continuously as the probe traversed the domain of interest. Thus an essentially complete resolution of the steep gradients between the hot and the cold streams, in the cold leg, could be secured. At position TRI the traverse is along a vertical diameter in the cold leg. At position TR2 the traverse is along the downcomer gap and just beneath the cold leg centerline. A stationary concentration probe measures continuously the exiting stream concentration. We label this as "ambient" or "mixed mean" concentration.

Figure 4. This figure illustrates the pump and loop seal attachment to configuration-0 in order to create the Westinghouse(w) or Combustion Engineering(CE) configuration. For the B&W configuration an upward sloping cold leg attachment with a horizontally oriented injection line was utilized.

Figures 5-8. These figures provide a sample of the kinds of agreement obtained between the REMIX and the experimental data. Run-CE was obtained with injection Froude number of 0.22 and Run-W with 0.4.

Figures 9-10. From the temporal variations of concentrations at each location, synchronous spatial concentration distributions could be obtained. Such plots clearly show the stratification in the cold leg. The counter current flow behavior, and the good agreement with REMIX predictions are also evident.

Figures 11-12. Here predictions are given for the temperature transients in Calvert Cliffs (CE) and H.B. Robinson(W) assuming complete stagnation in loop flow at time zero. We note that the maximum stratification (i.e. difference between the temperature of cold stream in the cold leg and that of the "ambient" or "well Mixed") is  $\sim 30^{\circ}\text{K}$ . On the other hand in the downcomer and outside a narrow strip, just beneath the cold leg, about one cold leg diameter wide and about 1-2 diameters long, the fluid

temperature follows the ambient within  $\approx 15-20^\circ\text{C}$ . These calculations took into account heat released from the vessel wall as the primary fluid cooled down. As it turns out, the large effective volume for mixing, including the lower plenum and pump and loop seal, slows down sufficiently the cooldown to allow the wall heat to come into play. That is a synergistic effect with beneficial results in moderating the cooldown rate is observed.

Figure 13. Here we show a typical result for a transient in Calvert Cliffs with asymmetric loop behavior. Loop B1 stagnates while loop A1 continues, in natural circulation. We apply REMIX in B1 and a mixing volume made up only by cold leg, pump, and loop seal. The reason for excluding the downcomer and lower plenum is that since the flow in loop A1 cools quite fast and is colder than the cold stream in the stagnated loop, the downcomer environment present a stable condition for any flow exiting B1. Thus, in this case, the downcomer response is clearly controlled by the flow and temperature in loop A1 rather than that of the stagnated loop. Therefore, TRAC results are directly applicable to fracture mechanics calculations.

Figures 14-17. Here the procedure for estimating downcomer heat transfer coefficients is illustrated. Mixed convection, of course, is a complicated, scarcely investigated topic at this time. Fortunately, conduction limitations in the wall limit the extent of importance of this mechanism such that predictions can be made with confidence. We use the Fewster-Jackson correlation with an imposed downcomer velocity transient (given by the system codes, or predicted for the plume region from REMIX) together with a conduction calculation in the vessel wall. For example, figure 14 shows the upper, lower, and average flow velocity in the downcomer as deduced from TRAC calculations. As we can see in figure 15 only for the lower bound of velocity the Nusselt number (Nu) is strongly affected by free convection (NU0 is the Nusselt number in the presence of only forced convection). The predicted heat transfer coefficient histories for the three velocity transients are shown in figure 16. Although the range in these values is not small, the effect on vessel wall surface temperature is

exceedingly small as shown in figure 17. In fact these trends were generalized by estimating the response to a good number of exponential decays in temperature combined with a wide range of imposed downcomer velocities. These results indicate that the Fewster-Jackson correlation is adequate, and that within the initial portion of the plume region forced convection dominates heat transfer.

### CONCLUSIONS

The REMIX code and a simple convection/conduction coupling model were used to predict stratification and vessel wall temperatures under complete loop flow stagnation conditions in postulated reactor PTS scenarios. Insights gained by these first applications and comparisons to experimental data indicate that such predictions can be made with high degree of confidence.

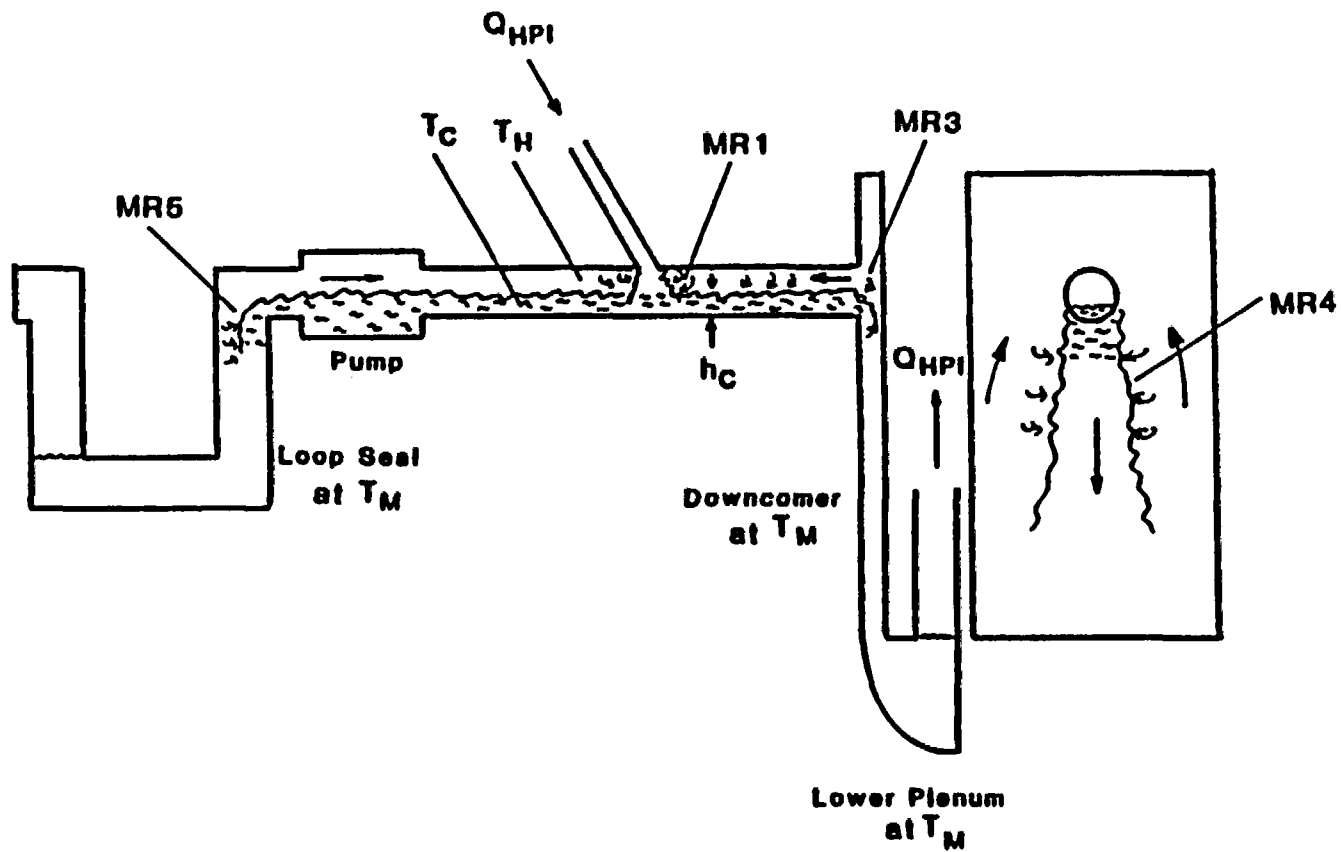


Fig. 1

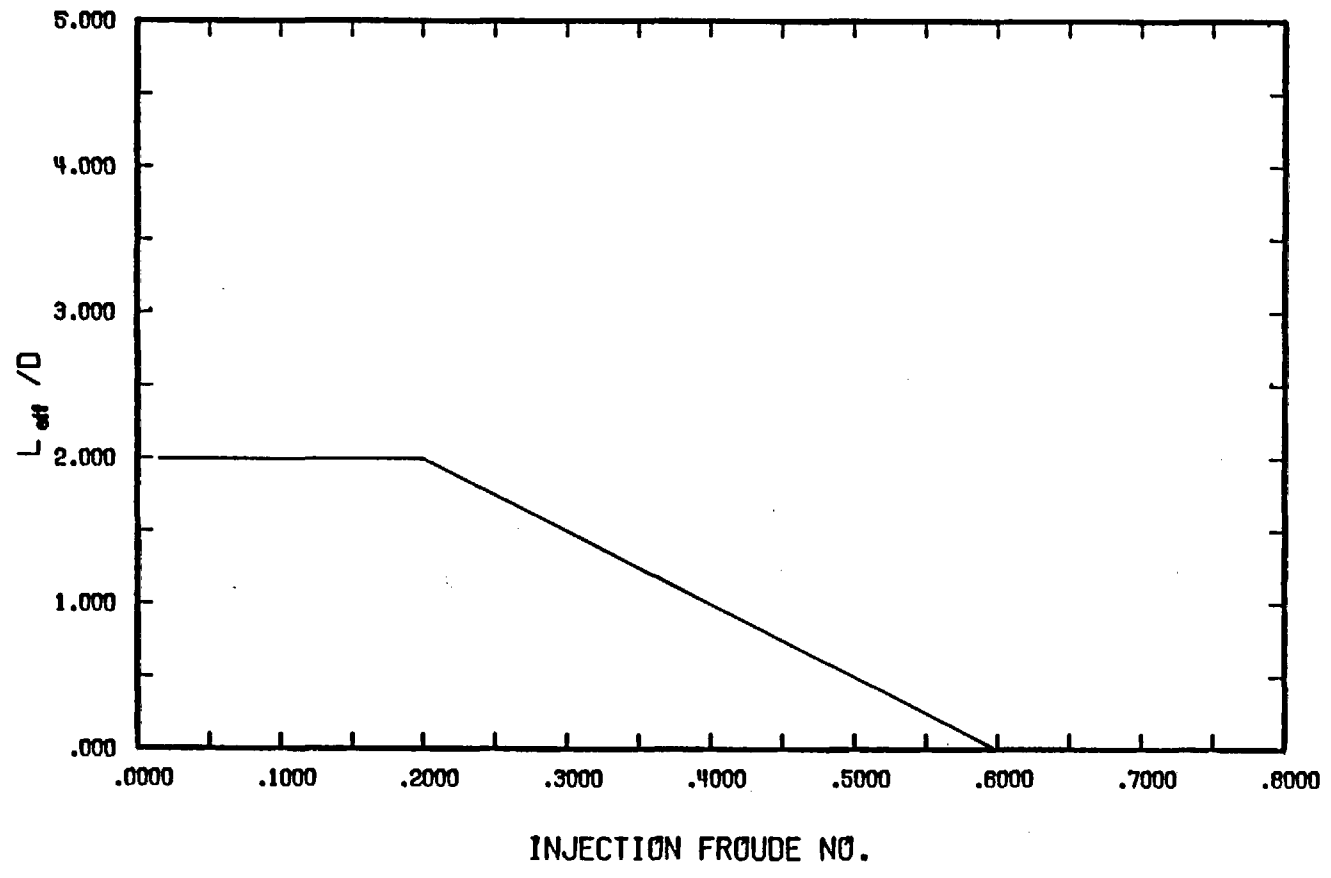


Fig. 2

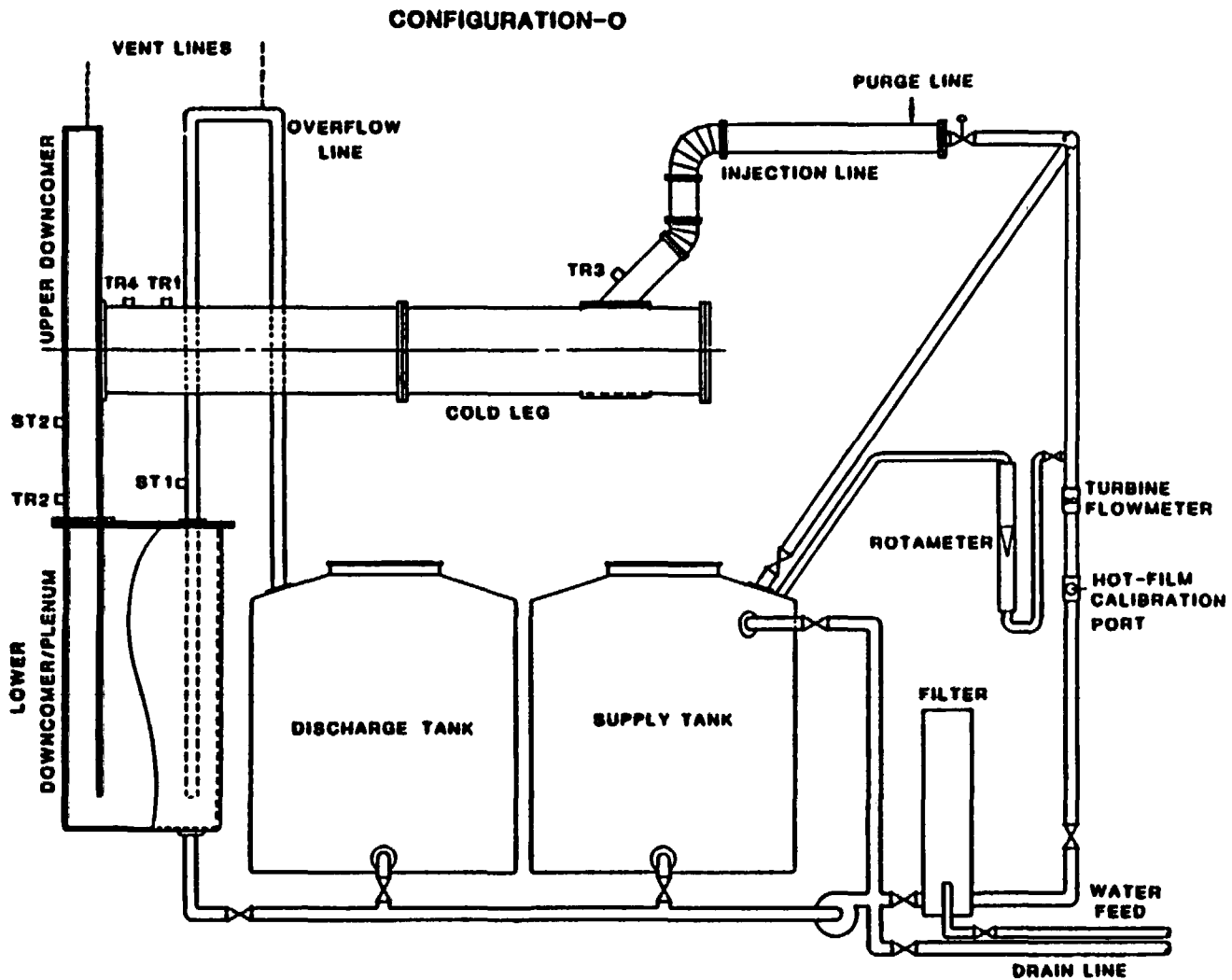


Fig. 3

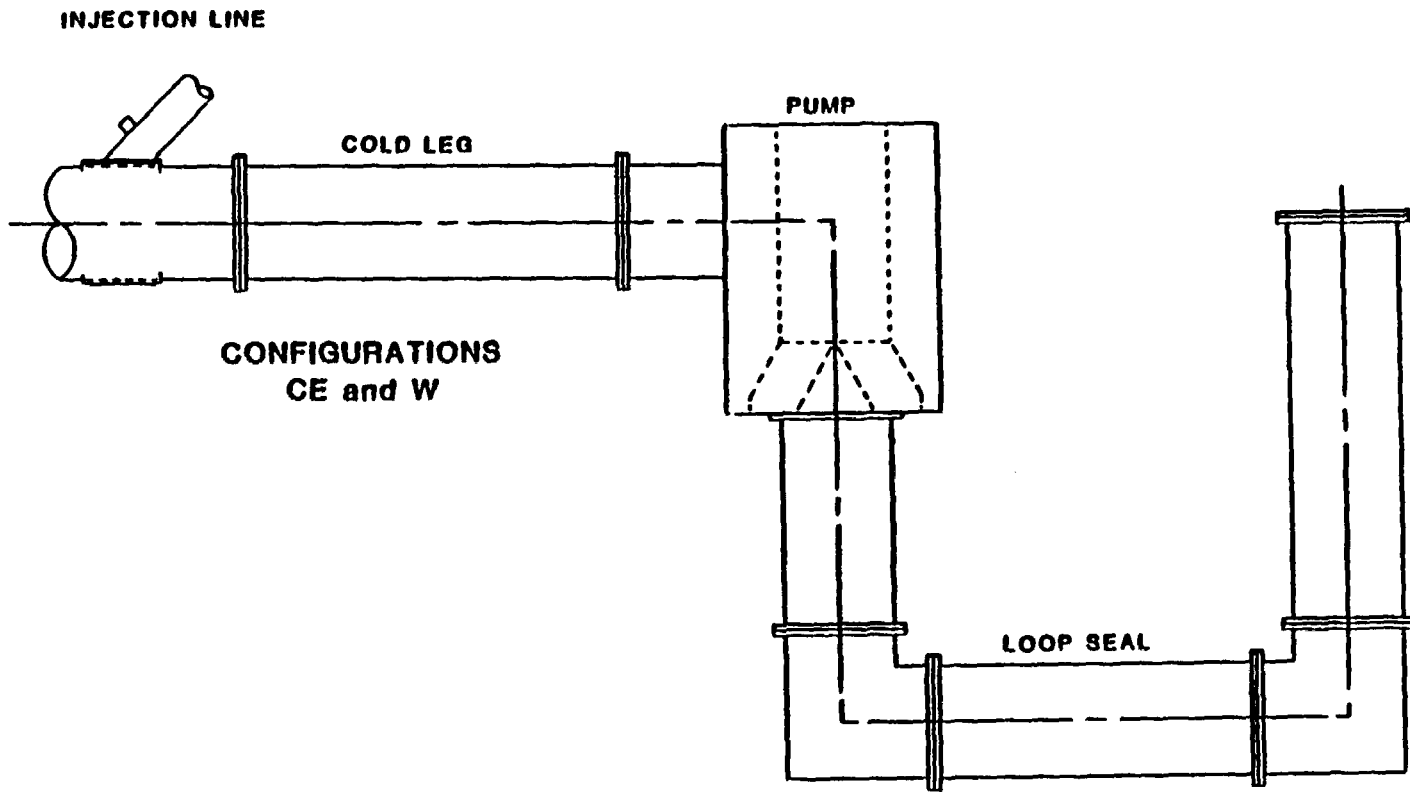


Fig. 4

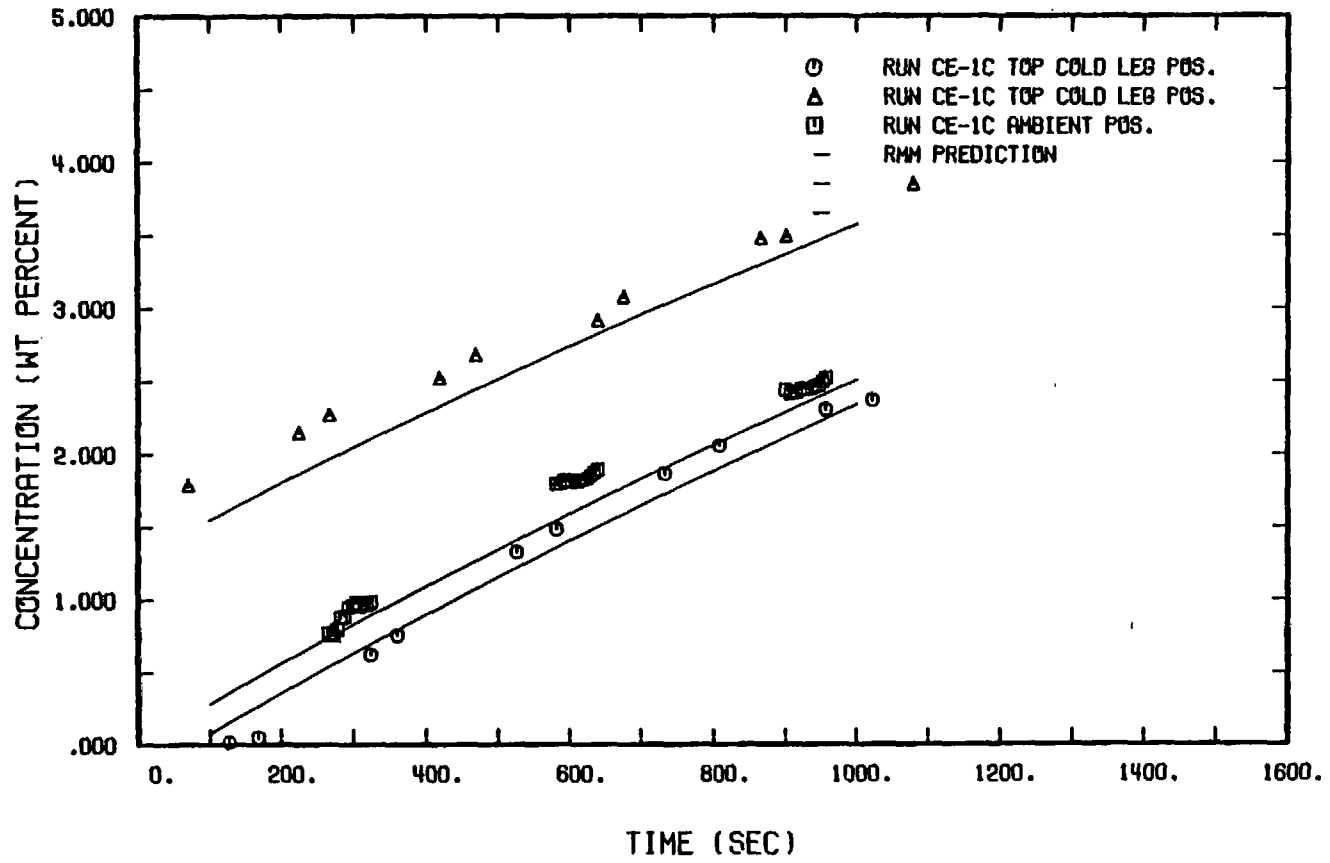


Fig. 5

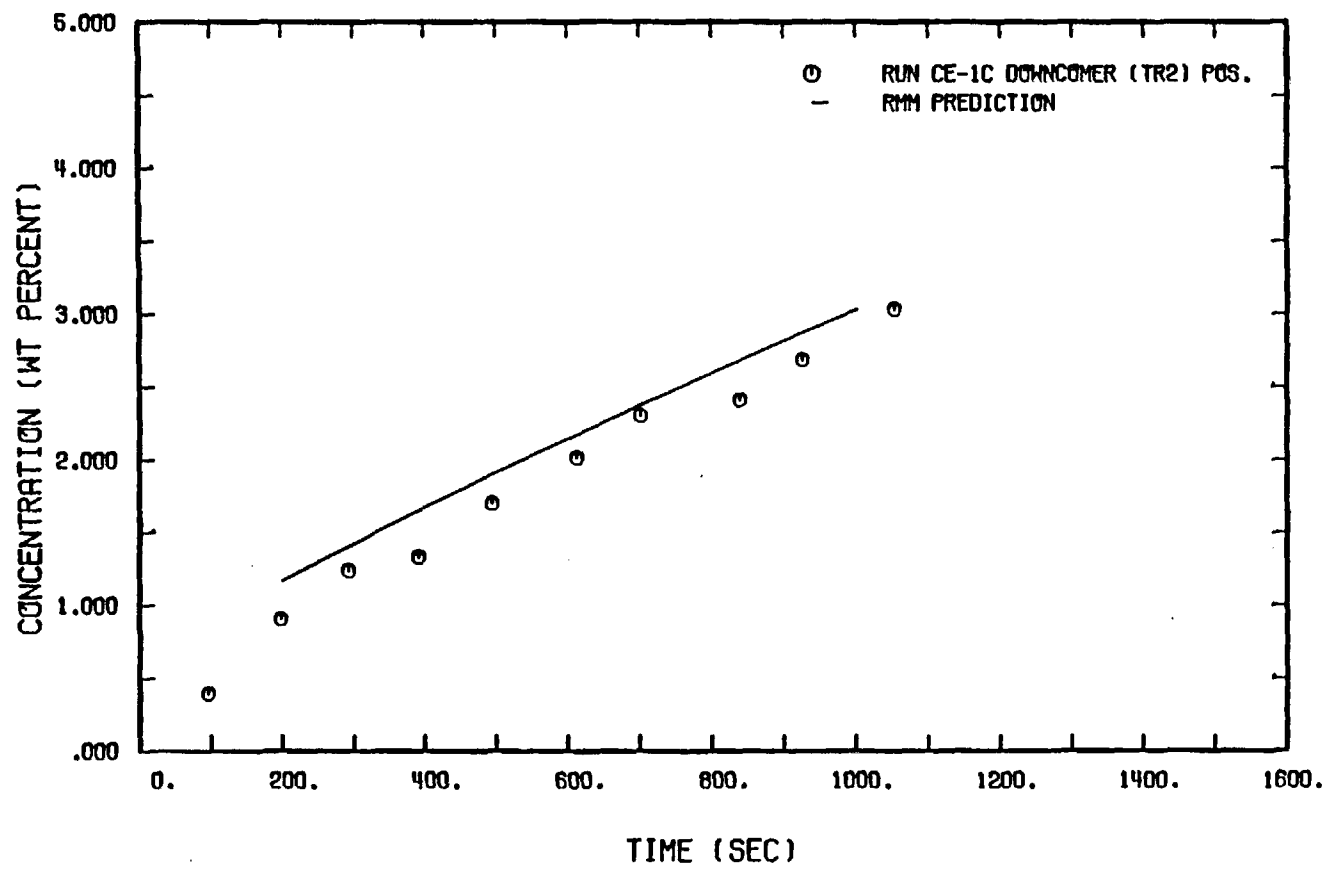


Fig. 6

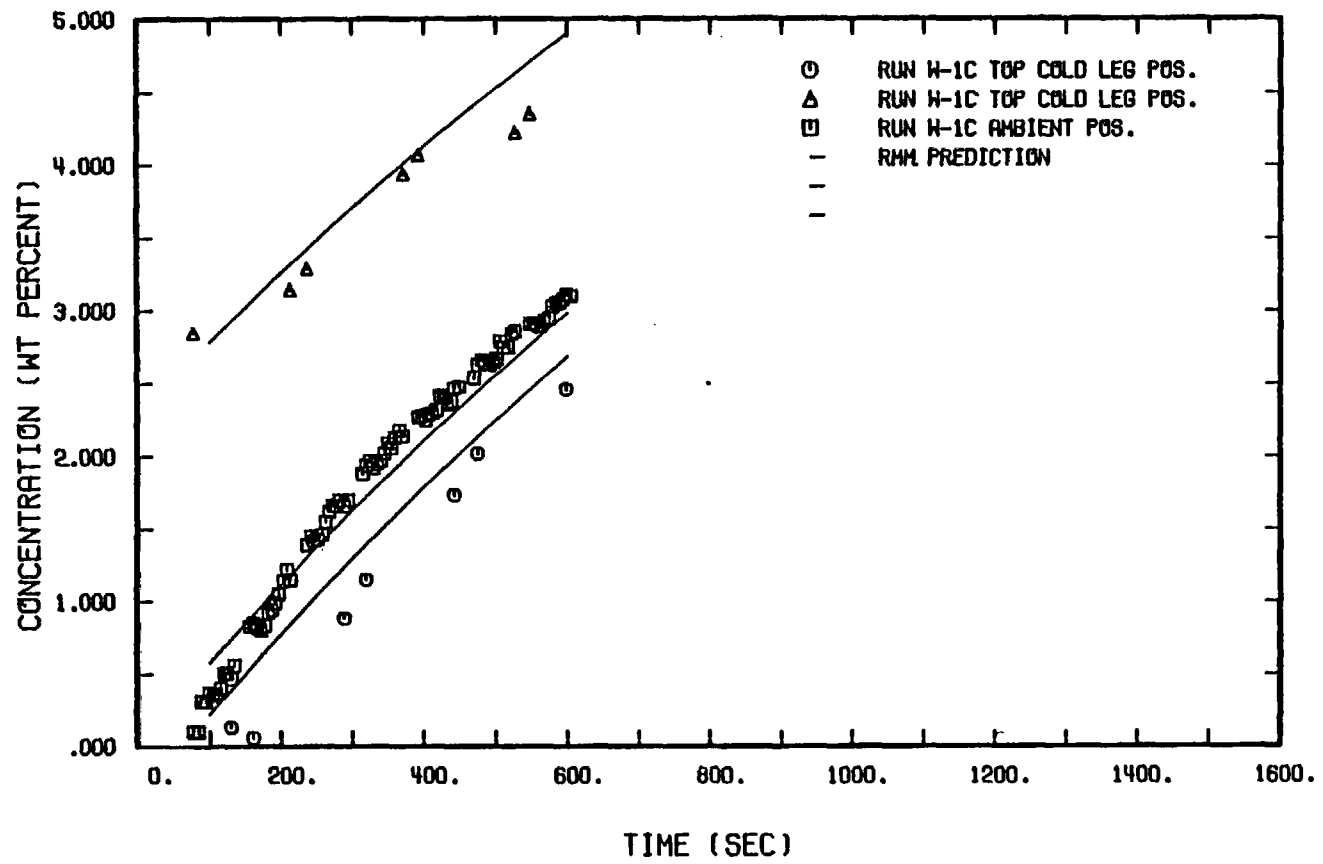


Fig. 7

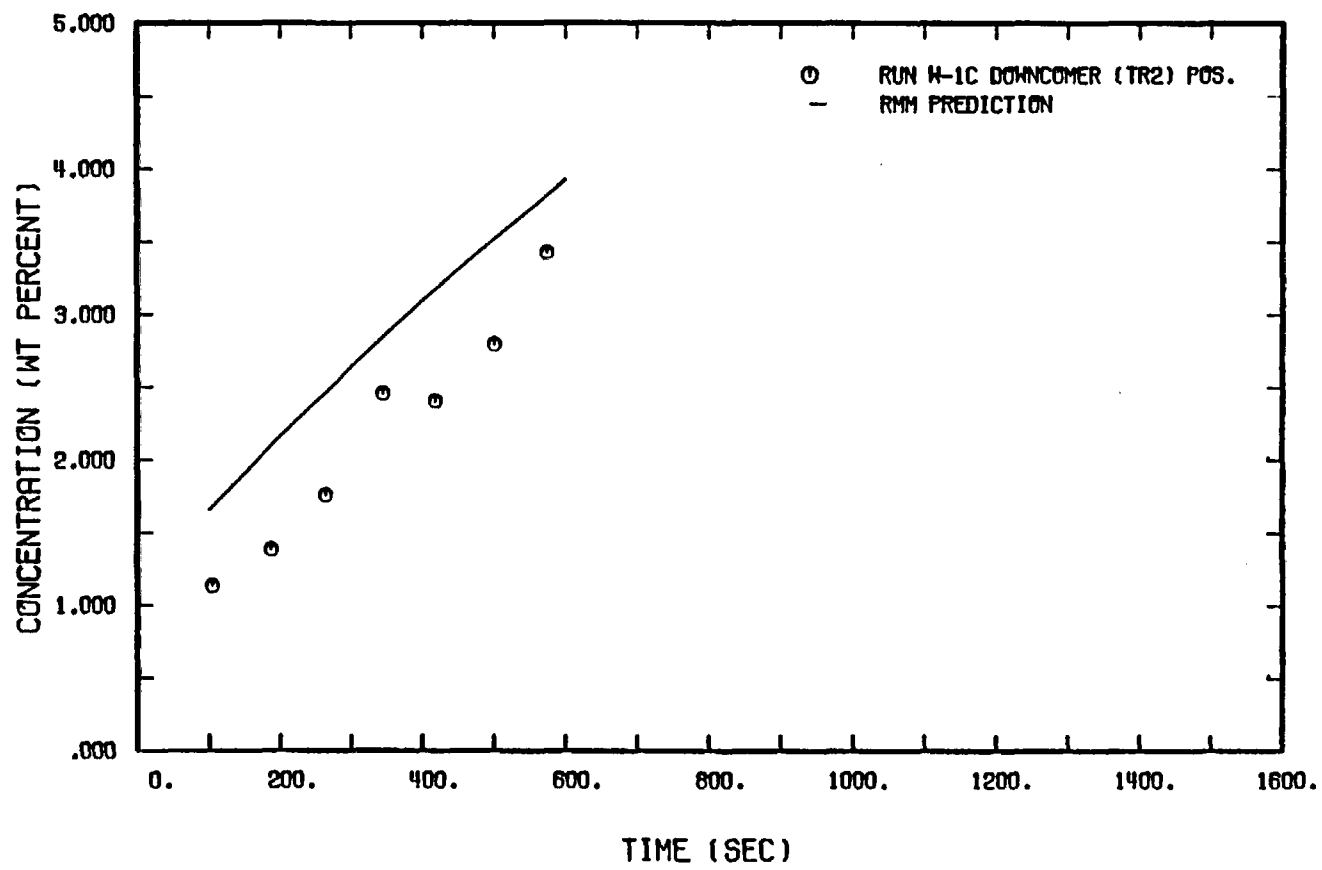


Fig. 8

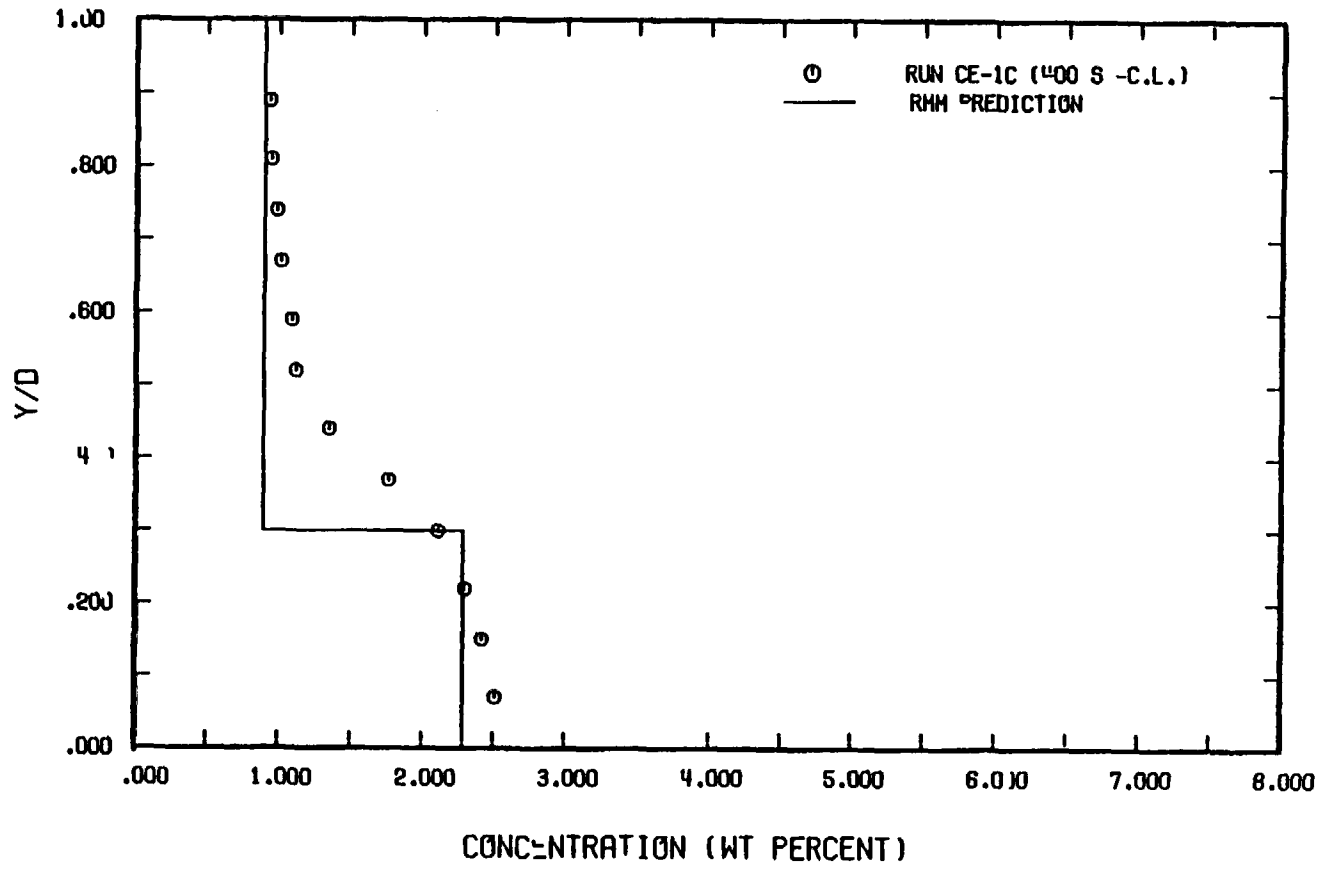


Fig. 9

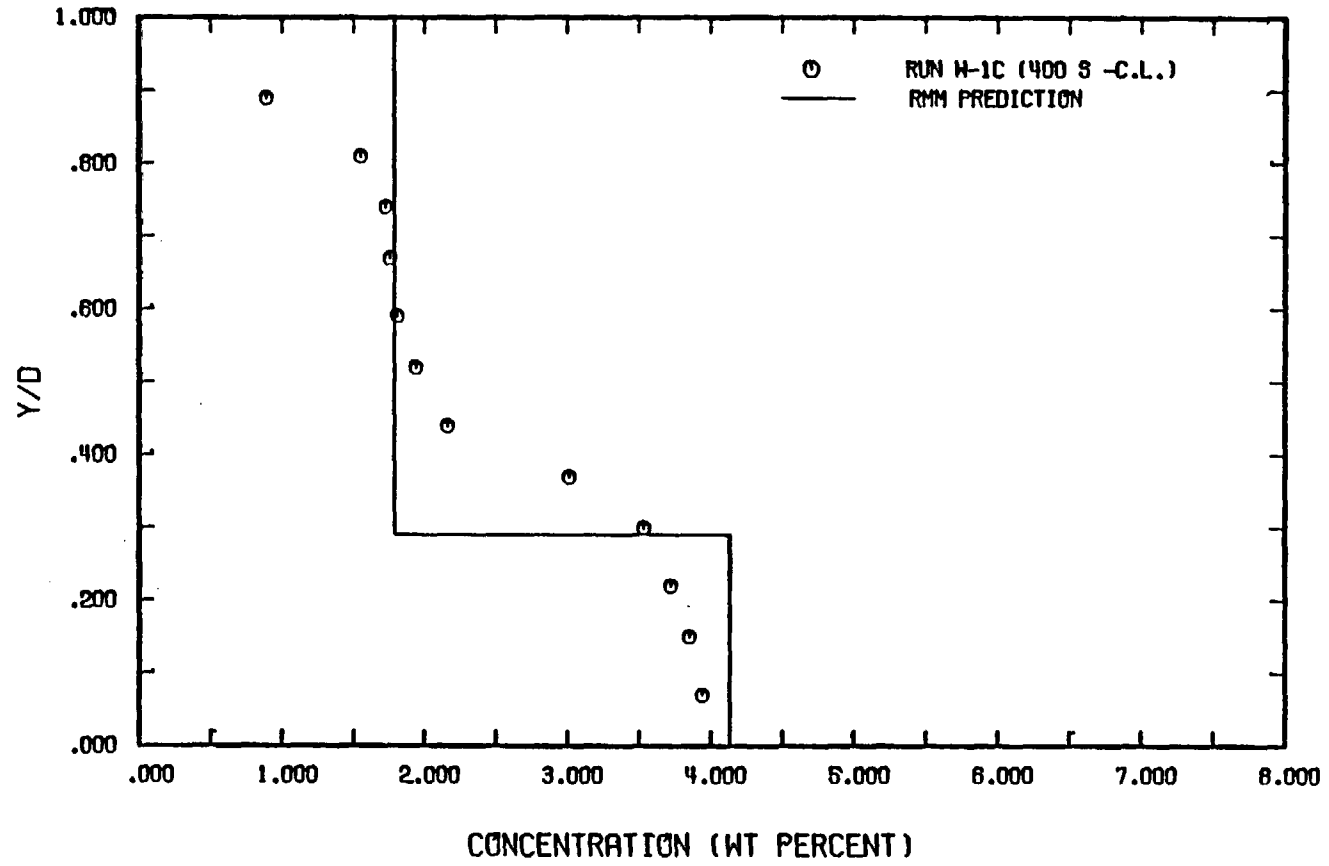


Fig. 10

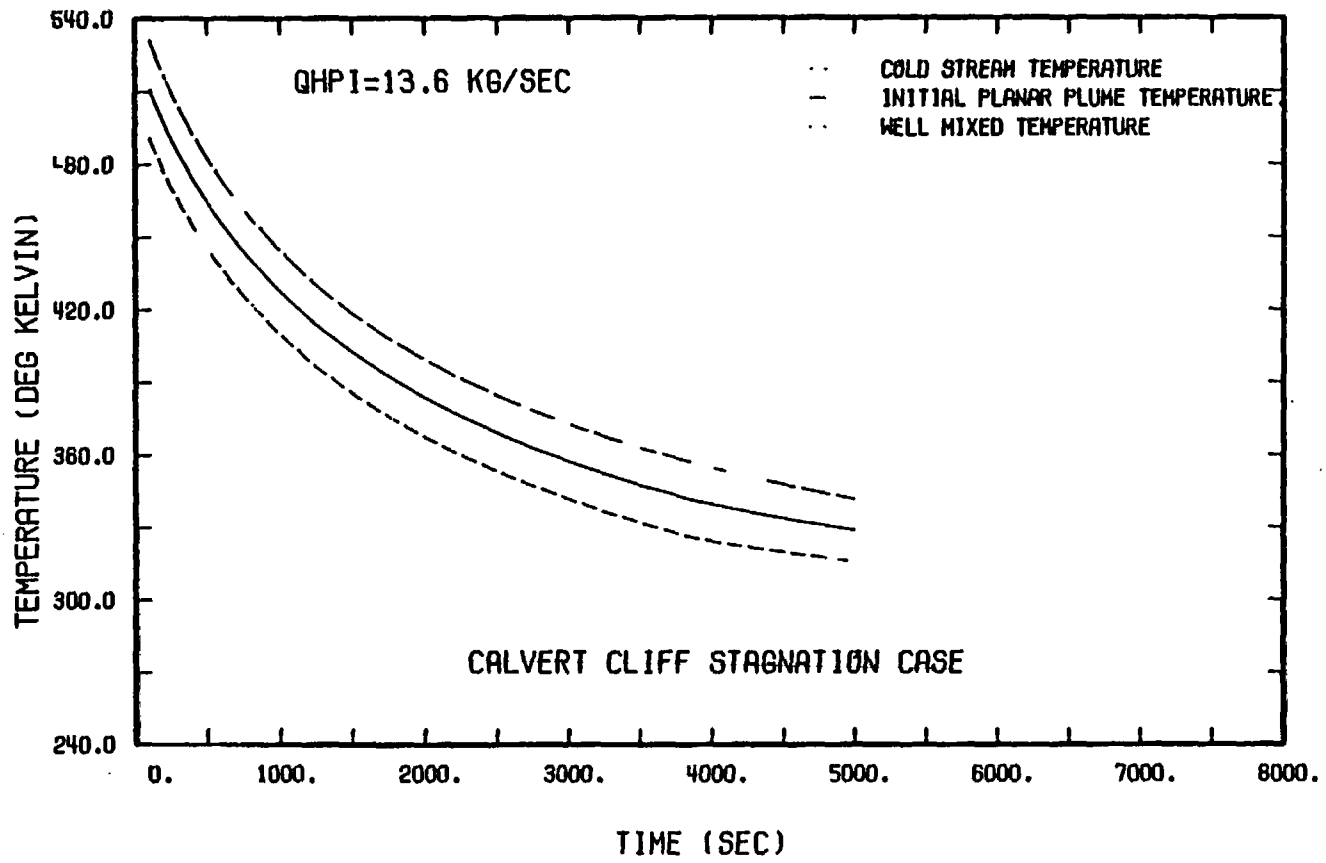


Fig. 11

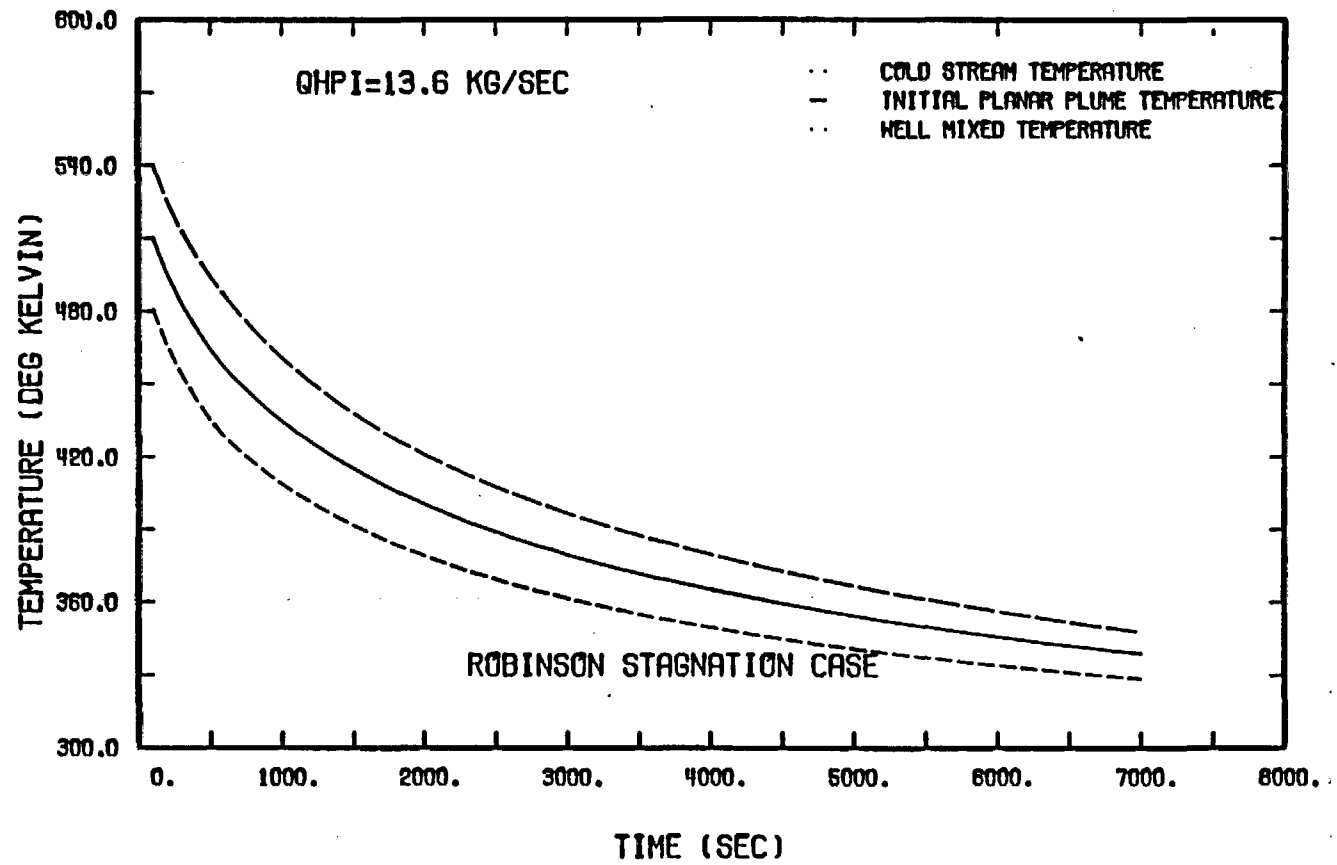


Fig. 12

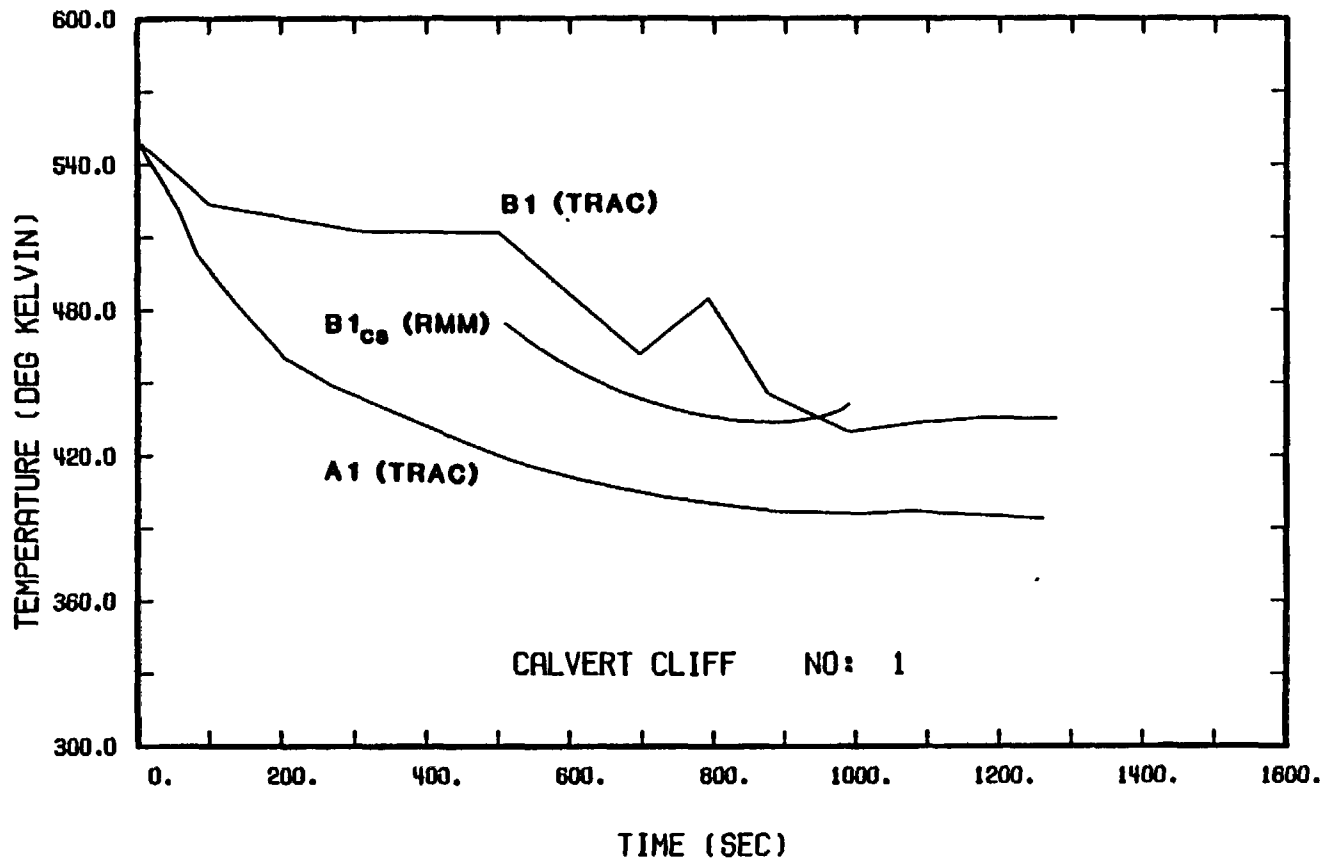


Fig. 13

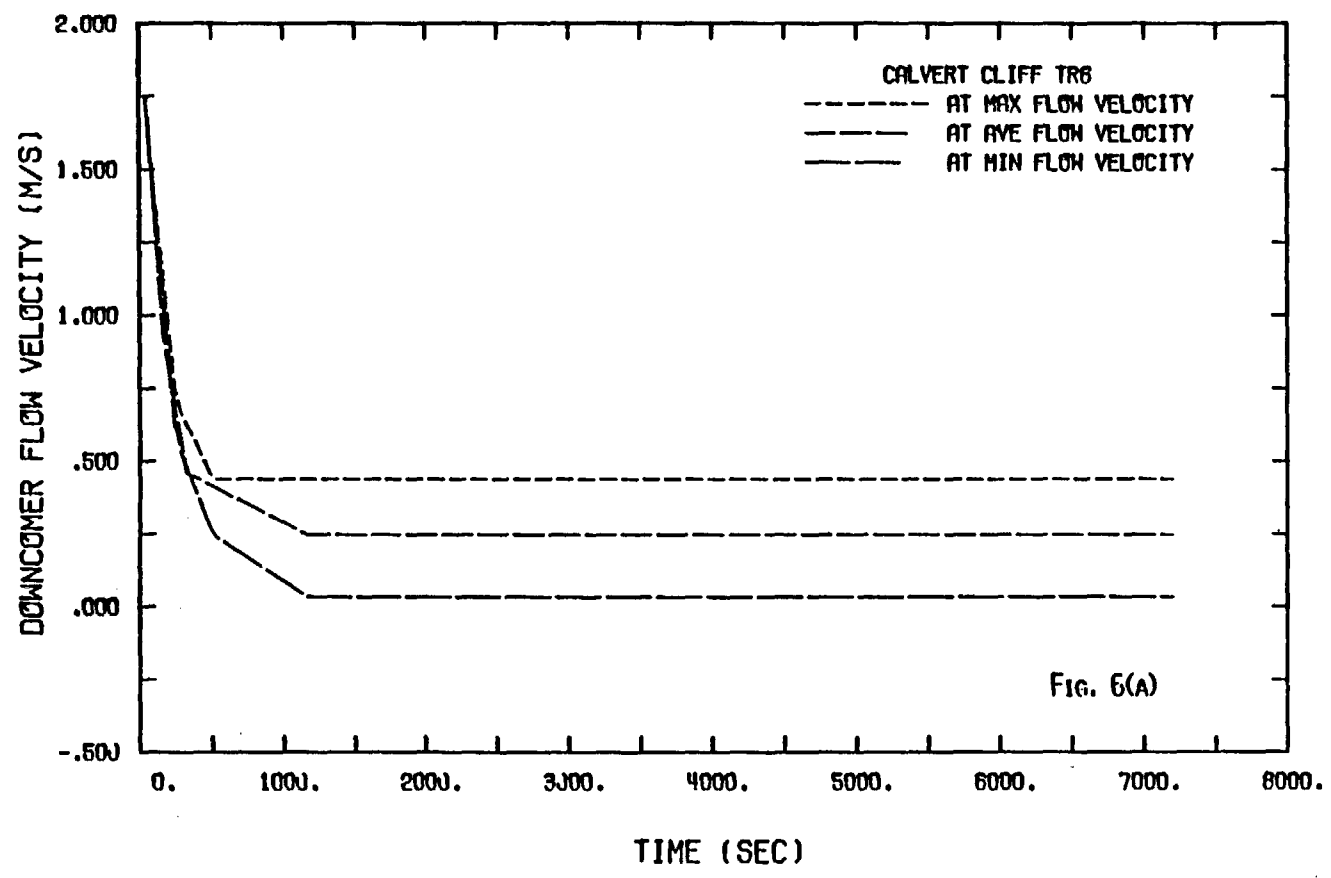


Fig. 14

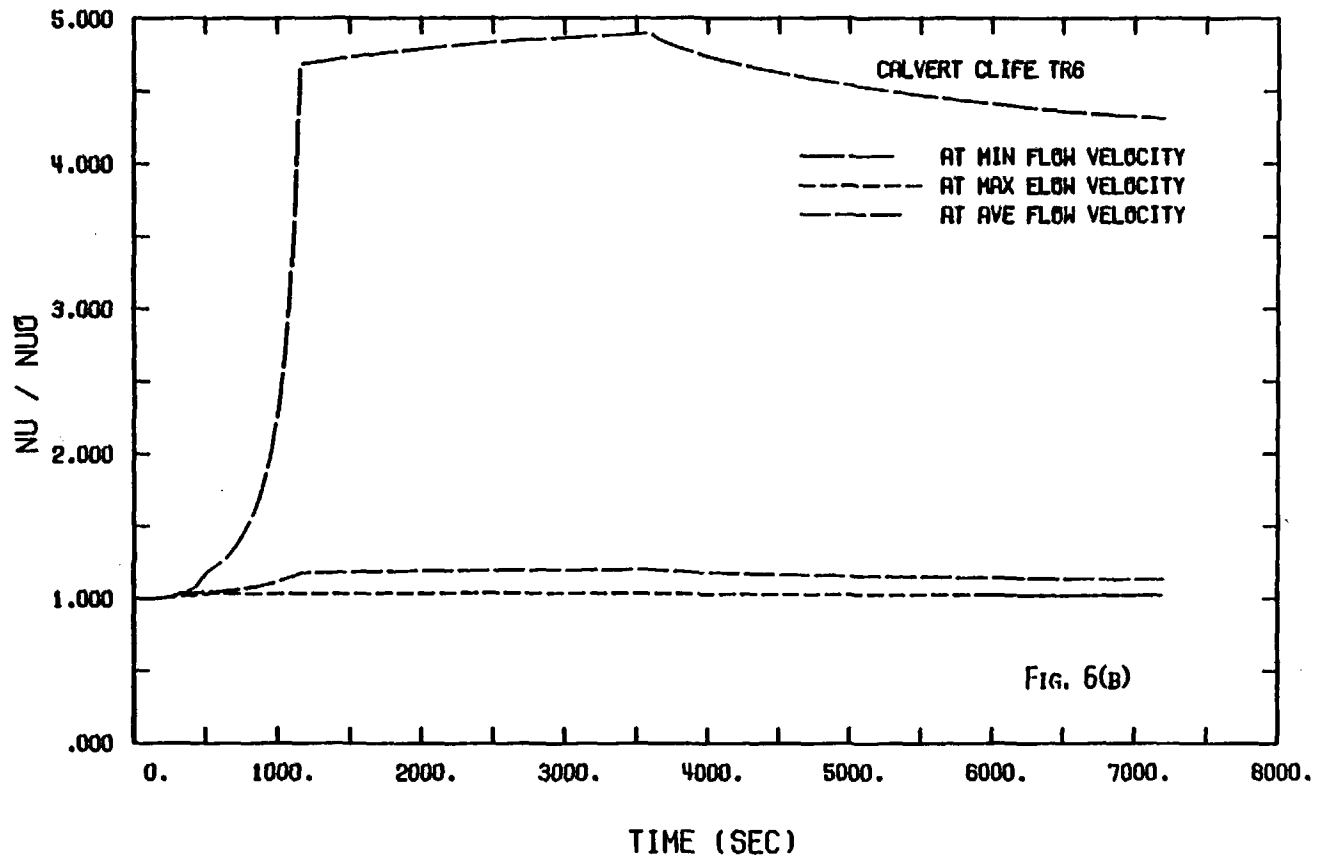


Fig. 15

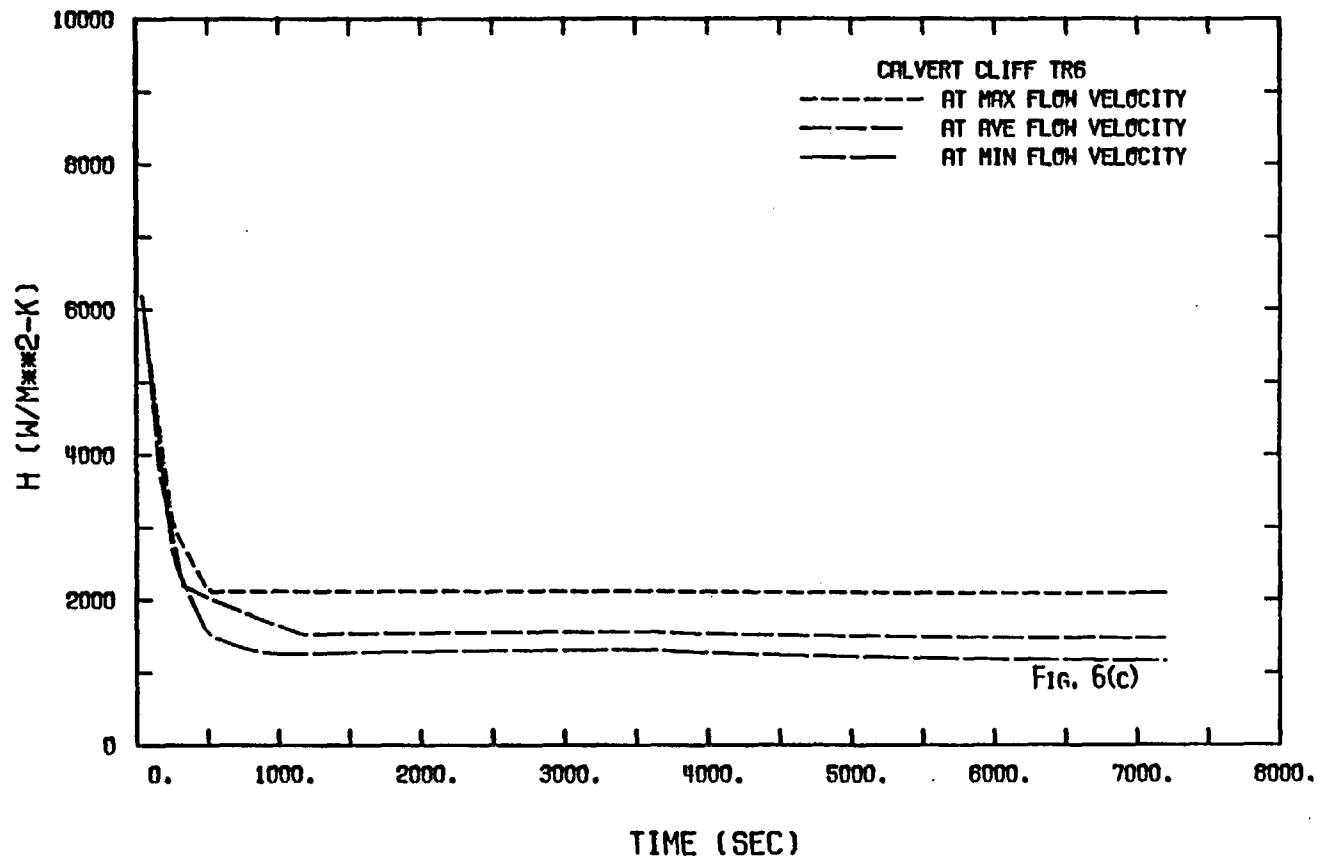


Fig. 16

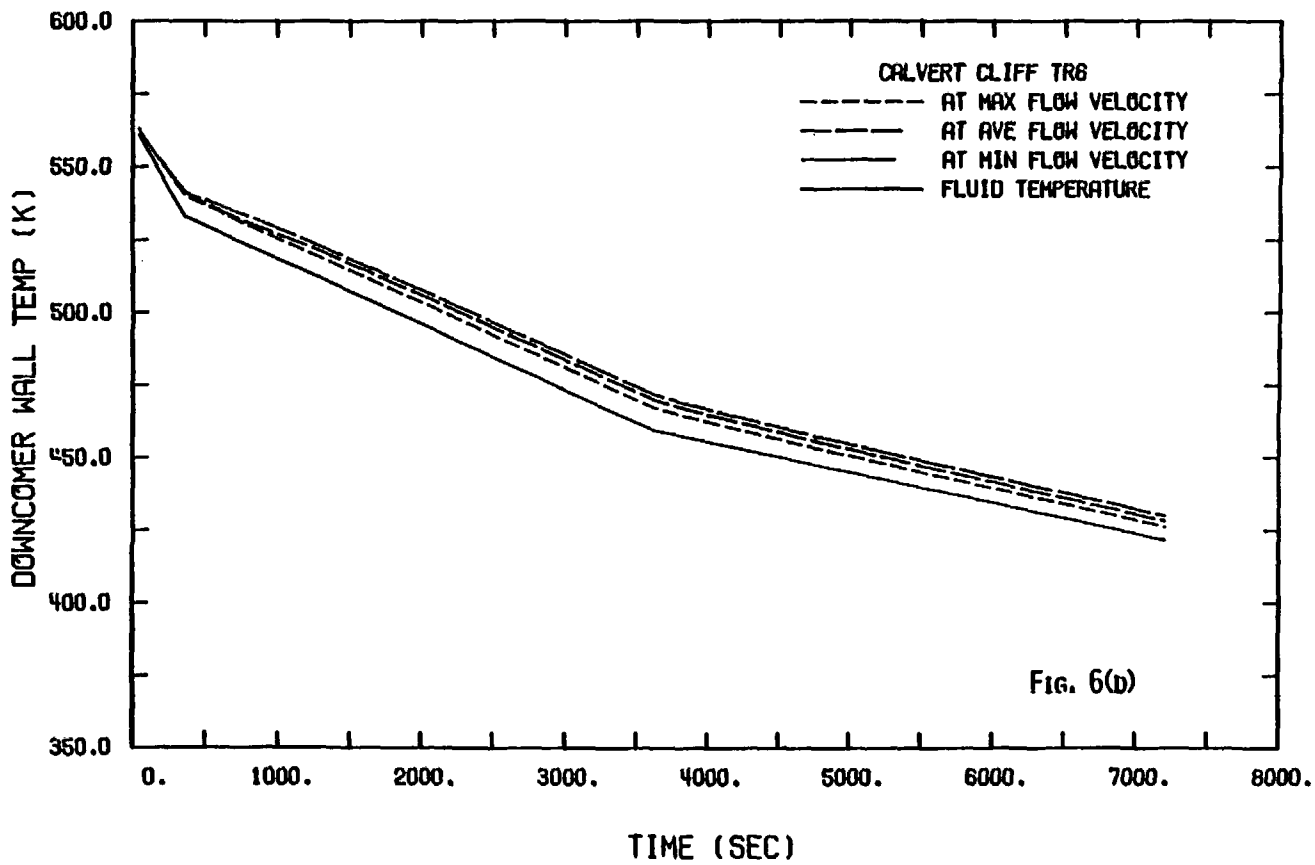


Fig. 17

IPTS PROGRAM PROBABILISTIC FRACTURE-MECHANICS  
ANALYSIS AND RESULTS\*

R. D. Cheverton and D. G. Ball<sup>†</sup>

Oak Ridge National Laboratory  
Oak Ridge, Tennessee 37831

SUMMARY

The pressurized-thermal-shock (PTS) issue is concerned with the possibility of failure of a PWR pressure vessel during a transient that subjects the vessel to severe thermal shock. The ingredients necessary for failure to occur are (1) the occurrence of the transient, (2) the presence of a sharp, crack-like defect (flaw) on the inner surface, (3) exposure of the vessel wall to "high" fast-neutron fluxes, and (4) "high" concentrations of copper and nickel. The transient provides both thermal and pressure loadings that may cause the initially shallow flaw to propagate through the vessel wall, provided that the radiation-induced reduction in fracture toughness, which is enhanced by the presence of copper and nickel, is sufficient. The need for high-neutron fluxes limits the area of the vessel of concern to the beltline region, and the accumulative nature of radiation damage introduces a time dependence: the longer the vessel is in service, the greater the probability of failure.

The overall estimated frequency of vessel failure is determined by postulating appropriate transients, estimating their frequency of occurrence, and calculating the probability,  $P(F|E)$ , of vessel failure for each of these transients. The probabilistic fracture-mechanics (PFM) model used for estimating  $P(F|E)$  and the scope and results of the fracture-mechanics studies for the Integrated Pressurized Thermal-Shock (IPTS) Program are the subject of this paper.

The scope of the PFM studies includes estimates of (1)  $P(F|E)$  for reactor pressure vessels similar to those at Oconee-I, Calvert Cliffs-1, and H. B. Robinson-2, using PTS transients postulated for these plants; (2) the effect of including warm prestressing (WPS) in the calculation of  $P(F|E)$ ; (3) the sensitivity of  $P(F|E)$  to fracture toughness, radiation damage, and the primary-system temperature and pressure transients; and (4) the benefit of specific suggested remedial measures (reduction in fluence rate, application of in-service inspection, limit on repressurization, and annealing).

---

\*Research sponsored by the Office of Nuclear Regulatory Research, U.S. Nuclear Regulatory Commission under Interagency Agreements 40-551-75 and 40-552-75 with the U.S. Department of Energy under Contract DE-AC05-84OR21400 with Martin Marietta Energy Systems, Inc.

By acceptance of this article, the publisher or recipient acknowledges the U.S. Government's right to retain a nonexclusive, royalty-free license in and to any copyright covering the article.

<sup>†</sup>Computer Services Division, Martin Marietta Energy Systems, Inc.

The conditional probability of vessel failure is calculated using the OCA-P code,<sup>1</sup> which is based on linear-elastic fracture mechanics, uses a specified maximum value of the crack-arrest toughness to account for upper-shelf behavior, and employs Monte Carlo techniques to facilitate the probabilistic aspect. Parameters simulated in the Monte Carlo analysis are the crack initiation and arrest fracture-toughness values ( $K_{Ic}$ ,  $K_{Ia}$ ), the nil-ductility reference temperature (RTNDT), fast-neutron fluence, copper concentration, and flaw depth. Warm prestressing was not included, except to the extent of investigating its effect for a few specific transients. The radiation-damage trend curve,  $\Delta RTNDT = f(Cu, Ni, F_0)$ , and the standard deviations for all simulated parameters were the same as those used in the NRC studies that lead to the NRC PTS screening criteria.<sup>2</sup>

Results of the analysis for Oconee-1 indicated that, at 32 EFPY,  $P(F|E) = 2 \times 10^{-3}$  and  $6 \times 10^{-4}$  for the two most dominant types of transients (those that contribute the most to the overall frequency of failure). For these exact transients, the inclusion of WPS in the analysis reduced  $P(F|E)$  by factors of  $\sim 10^{-3}$  and  $\sim 3 \times 10^{-1}$ , respectively.

Values of  $P(F|E)$  at 32 EFPY for the Calvert Cliffs-1 two most dominant transients were  $2 \times 10^{-4}$  and  $4 \times 10^{-3}$ . Consideration of WPS for these exact transients reduced  $P(F|E)$  by factors of  $10^{-3}$  and unity, respectively. Warm prestressing had no significant effect for the latter transient because of very late repressurization.

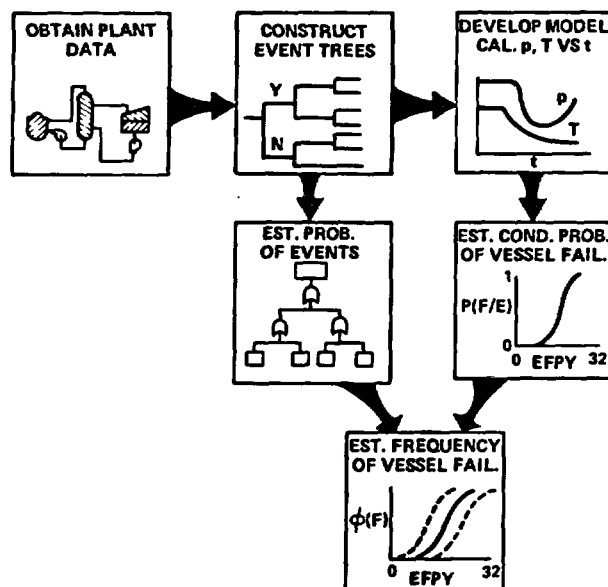
Recently reported revised values for copper and nickel concentrations and  $RTNDT_0$  for the H. B. Robinson-2 vessel are so low that, at 32 EFPY,  $P(F|E) < 10^{-7}$  for all postulated high-frequency transients. In order to better illustrate the methods of analysis, a hypothetical vessel, similar to the H. B. Robinson-2 vessel, but with higher copper and nickel concentrations and higher  $RTNDT_0$ , is being analyzed.

There are rather large uncertainties in the calculated values of  $P(F|E)$  because of uncertainties in the flaw density, the effect of cladding on the surface extension of flaws, and the role of WPS, among other things. Cladding and WPS effects that were not considered will tend to decrease  $P(F|E)$ , perhaps by several orders of magnitude.

#### References

1. R. D. Cheverton and D. G. Ball, *OCA-P, A Deterministic and Probabilistic Fracture-Mechanics Code for Application to Pressure Vessels*, NUREG/CR-3618 (ORNL-5991), Union Carbide Corp., Nuclear Div., Oak Ridge Natl. Lab. (May 1984).
2. U.S. Nuclear Regulatory Commission Paper, Pressurized Thermal Shock (PTS), SECY-82-465, November 23, 1982.

**IPTS PROGRAM CONSISTS OF FIVE MAJOR EFFORTS, INVOLVES  
THREE NATIONAL LABS (ORNL, LANL, INEL)**



MARTIN MARIETTA

**SCOPE OF PROBABILISTIC FRACTURE—  
MECHANICS ANALYSIS**

- P(F|E)
- SENSITIVITY OF P(F|E) TO SIMULATED PARAMETERS
- EFFECT OF WARM PRESTRESSING (WPS)
- EFFECT OF REMEDIAL MEASURES
  - REDUCTION IN FLUENCE RATE
  - IN-SERVICE INSPECTION
  - LIMIT ON REPRESSURIZATION
  - ANNEALING

MARTIN MARIETTA

## PROBABILISTIC FRACTURE-MECHANICS ANALYSIS PERFORMED WITH OCA-P

- BASED ON MONTE CARLO METHODS
  - MANY VESSELS SIMULATED
  - DETERMINISTIC FM ANALYSIS FOR EACH
  - $P(F|E) = \frac{\text{NUMBER OF FAILURES}}{\text{NUMBER OF VESSELS}}$
- BASIC INPUT FROM SYSTEMS ANALYSIS:  
 $T_c, p, h = f(t)$
- PERFORMS THERMAL, STRESS, AND FM ANALYSIS

MARTIN MARIETTA

---

## SEVEN FM PARAMETERS SIMULATED IN IPTS STUDIES

- FLUENCE AT INNER SURFACE
- COPPER CONCENTRATION
- RTNDT<sub>0</sub>
- ΔRTNDT
- K<sub>Ic</sub>, K<sub>Ia</sub>
- FLAW DEPTH

MARTIN MARIETTA

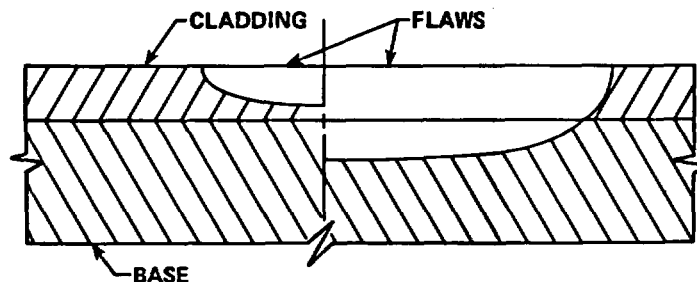
## OCA-P FM MODEL INCLUDES SOME SIMPLIFYING ASSUMPTIONS FOR EXPEDIENCY

- LEFM
- 1-D THERMAL AND STRESS ANALYSIS
- CLADDING A DISCRETE REGION
- $(K_{Ic}, K_{Ia})$  SAME FOR CLAD AND BASE MATERIALS
  - SURFACE EXTENSION OF FLAW POSSIBLE
  - VERY SHALLOW FLAWS PROPAGATE
- $(K_{Ia})_{max} = 200 \text{ ksi}\sqrt{\text{in.}}$
- WPS NOT INCLUDED

MARTIN MARIETTA

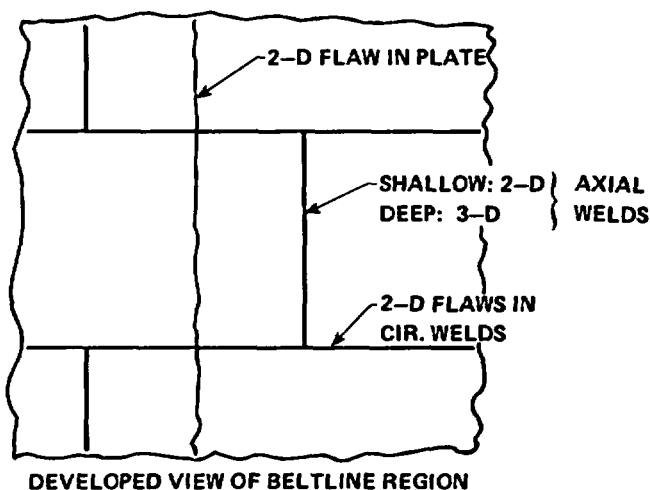
## FLAWS CONSIDERED EXTEND FROM INNER SURFACE INTO OR THROUGH CLADDING

- RESULT OF CLADDING PROCESS, STRESS-CORROSION CRACKING, etc.
- VERY LITTLE NDE DATA
- LARGE UNCERTAINTY IN FLAW DENSITY



MARTIN MARIETTA

## TWO FLAW GEOMETRIES (2-D, 3-D) AND THREE FLAW REGIONS (PLATE, AXIAL AND CIRCUMFERENTIAL WELDS) CONSIDERED



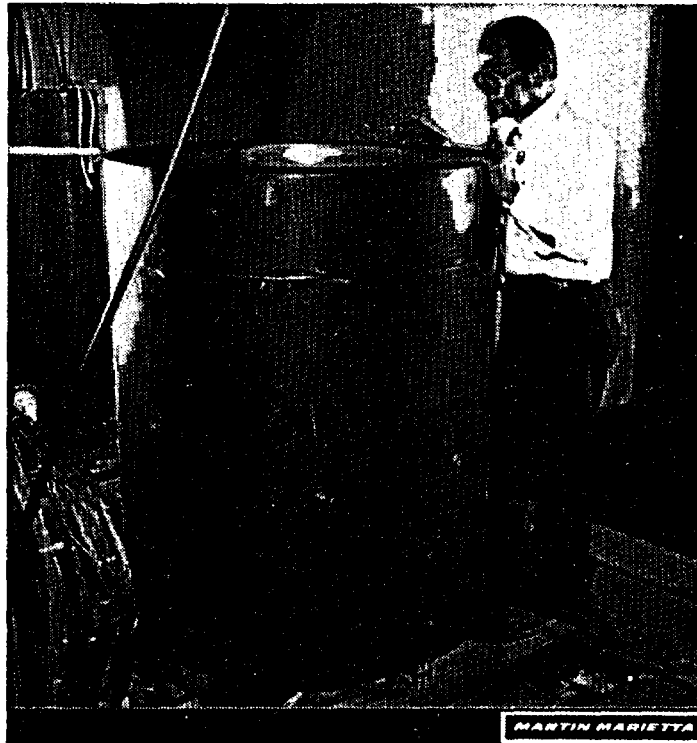
MARTIN MARIETTA

## LARGE-SCALE THERMAL-SHOCK AND PRESSURIZED-THERMAL-SHOCK EXPERIMENTS CONDUCTED TO VERIFY FM METHODS OF ANALYSIS

- LEFM VALID
  - CRACK-ARREST CONCEPT VALID
  - WARM PRESTRESSING DEMONSTRATED
  - CLADDING RESTRAINT
  - ARREST ON UPPER SHELF
- UNDER INVESTIGATION

MARTIN MARIETTA

**TSEs AND PTSEs CONDUCTED WITH LARGE STEEL CYLINDERS  
(1-m OD X 152-mm WALL X 1.2-m LENGTH)**



---

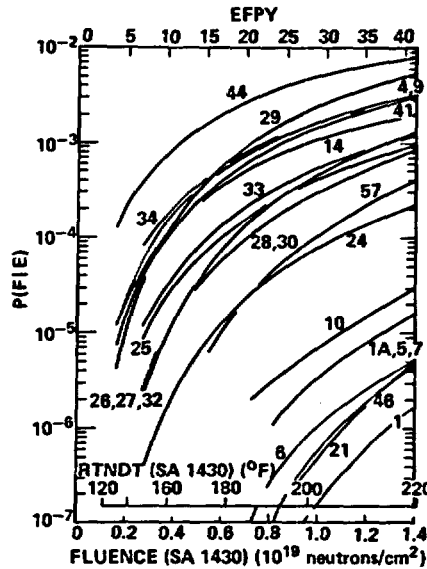
ORNL WS-35624 ETD

**AXIAL WELDS ARE DOMINANT CONTRIBUTOR TO P(F|E)  
FOR OCONEE-1, CC-1, HBR-HYPO**

- Cu IN WELDS RELATIVELY HIGH
- $K_I$  (AXIAL) >  $K_I$  (CIRCUMFERENTIAL)
- FLAW SURFACE DENSITY ASSUMED EQUAL FOR ALL REGIONS

**MARTIN MARIETTA**

**P(F|E) INCREASES WITH EFPY AND COVERS WIDE RANGE OF VALUES FOR TRANSIENTS ANALYZED (TYPIFIED BY OCONEE-1 RESULTS)**



MARTIN MARIETTA

**RTNDT FOR EACH PLANT AND  $\Phi(F)$  FOR CC-1 AND HBR-2 APPEAR TO SATISFY NRC SCREENING CRITERIA AT 32 EFPY**

PLANT	RTNDT ( $2\sigma$ ) AT 32 EFPY ( $^{\circ}F$ )	$\Phi(F)$ AT 32 EFPY (F/Ry)
OCONEE-1	265	$5 \times 10^{-6}$
CALVERT CLIFFS-1	252	$1 \times 10^{-7}$
H. B. ROBINSON-2	135	$<10^{-11}$
HBR-HYPO	270	$1 \times 10^{-8}$

MARTIN MARIETTA

**P(F|E) AT 32 EPFY FOR DOMINANT TRANSIENTS:  
<math>10^{-10}</math> TO**

TRANSIENT	P(F E) AT 32 EPFY			
	PLANT			
	OCONEE-1	CC-1	HBR-2	HBR-HYPO
MOST SEVERE	$5 \times 10^{-3}$	$4 \times 10^{-3}$	$<10^{-10}$	$7 \times 10^{-4}$
1st DOMINANT	$2 \times 10^{-3}$	$3 \times 10^{-4}$	$<10^{-10}$	$3 \times 10^{-7}$
2nd DOMINANT	$6 \times 10^{-4}$	$1 \times 10^{-5}$	$<10^{-10}$	$9 \times 10^{-7}$

**MARTIN MARIETTA**

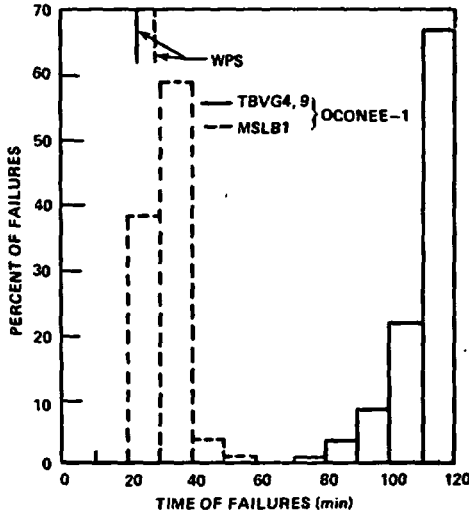
**P(F|E) EXPECTED TO BE PARTICULARLY SENSITIVE  
TO ASSUMPTIONS REGARDING**

- DURATION OF TRANSIENT
  - TWO-HOUR DURATION SPECIFIED
  - DECREASING TIME DECREASES P(F|E)
- WARM PRESTRESSING
  - NOT INCLUDED
  - INCLUSION DECREASES P(F|E)
- FLAW SURFACE DENSITY
  - $P(F|E) \propto$  FLAW DENSITY
  - 1 FLAW/5 m<sup>2</sup> SPECIFIED
  - LARGE UNCERTAINTY

**MARTIN MARIETTA**

RESULTS INDICATE BENEFIT OF SHORTER DURATION,  
INCLUSION OF WPS

• BENEFIT TRANSIENT DEPENDENT



MARTIN MARIETTA

WPS ( $\dot{K}_I = 0$ ) APPLIED TO DOMINANT TRANSIENTS MAY REDUCE  
 $P(F|E)$  AND  $\Phi(F)$  SIGNIFICANTLY

TRANSIENT (IN ORDER OF DOMINANCE)	PLANT		
	OCONEE-1	CC-1	HBR-HYPO
	$P(F E)_{WPS}/P(F E)$		
1	$<10^{-3}$	$<2 \times 10^{-3}$	$9 \times 10^{-3}$
2	$3 \times 10^{-1}$	1	$<2 \times 10^{-3}$
3	$<10^{-3}$	$<1 \times 10^{-2}$	$<2 \times 10^{-3}$
4	$<10^{-3}$	$1 \times 10^{-1}$	$<2 \times 10^{-3}$
5	$3 \times 10^{-1}$	$<5 \times 10^{-1}$	$5 \times 10^{-2}$
	$\Phi(F)_{WPS}/\Phi(F)$		
	$1 \times 10^{-1}$	$2 \times 10^{-1}$	$7 \times 10^{-3}$

MARTIN MARIETTA

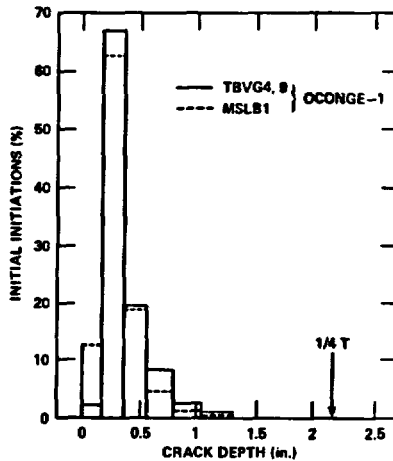
# BENEFIT OF WPS ( $K_I \leq 0$ ) IS PLANT DEPENDENT

PLANT	$\Phi(F)_{WPS}/\Phi(F)$
OCONEE-1	$1 \times 10^{-1}$
CC-1	$2 \times 10^{-1}$
HBR-HYPO	$7 \times 10^{-3}$

MARTIN MARIETTA

## MOST INITIAL INITIATIONS WITH VERY SHALLOW FLAWS

- SHALLOW FLAWS MORE LIKELY
- THERMAL STRESS AND RADIATION DAMAGE
- SHALLOW FLAWS DIFFICULT TO DETECT



MARTIN MARIETTA

## SUMMARY

- AXIAL WELDS ARE DOMINANT CONTRIBUTOR TO P(F|E)
- SHALLOW FLAWS RESPONSIBLE FOR FAILURES
- P(F|E) PARTICULARLY SENSITIVE TO
  - DURATION OF TRANSIENT
  - WPS ( $R_1 \leq 0$ )
  - FLAW SURFACE DENSITY
- P(F|E) INSENSITIVE TO  $(K_{Ia})_{max}$ 
  - 200-300 ksi  $\sqrt{\text{in.}}$
- NRC SCREENING CRITERIA SATISFIED AT 32 EFPY
  - RTNDT ( $2\sigma$ )  $< 270^\circ\text{F}$
  - $\Phi(F) \leq 10^{-6}$

MARTIN MARIETTA

## RESULTS AND CONCLUSIONS FROM THE FIRST PRESSURIZED-THERMAL-SHOCK EXPERIMENT\*

R. H. Bryan            B. R. Bass  
S. E. Bolt            J. W. Bryson  
J. G. Merkle        G. C. Robinson  
                         G. D. Whitman

Oak Ridge National Laboratory  
Oak Ridge, Tennessee 37831

### Introduction

The first pressurized-thermal-shock experiment (PTSE-1) in the Heavy-Section Steel Technology (HSST) Program is the most recent of a long succession of fracture-mechanics experiments that are on a scale that allows important aspects of fracture behavior of reactor pressure vessels to be simulated. Such experiments are the means by which theoretical models of fracture behavior can be evaluated for possible application to fracture analysis of vessels in nuclear plants. The principal issues of concern in the pressurized-thermal-shock experiments are: (1) warm prestressing phenomena, (2) crack propagation from brittle to ductile regions, (3) transient crack stabilization in ductile regions, and (4) crack shape changes in bimetallic zones of clad vessels.

The facility and plan for performing pressurized-thermal-shock experiments were developed to conform to the following criteria.

1. The tests shall be designed to challenge the predictions of analytical methods that are applicable to full-scale reactor pressure vessels (RPV) under combined loading.
2. The scale of the tests shall be large enough to attain effectively full-scale restraint of the flawed region.
3. Material in the flawed region shall be characterized by specimen tests prior to each vessel test.
4. Test conditions and materials shall be selected to produce:
  - (a) realistic RPV stress fields and gradients around the flaw and
  - (b) realistic fracture-toughness conditions in the zone of action.

---

\*Research sponsored by the Office of Nuclear Regulatory Research, U.S. Nuclear Regulatory Commission under Interagency Agreements 40-551-75 and 40-552-75 with the U.S. Department of Energy under Contract DE-AC05-84OR21400 with Martin Marietta Energy Systems, Inc.

By acceptance of this article, the publisher or recipient acknowledges the U.S. Government's right to retain a nonexclusive, royalty-free license in and to any copyright covering the article.

5. Loading conditions and controls shall be used to prevent bursting the vessel (except when desired) to minimize damage to the test facility.
6. The test facility shall be capable of producing (with realistic stresses) a variety of fracture possibilities:
  - (a) cleavage initiation of small flaws,
  - (b) cleavage initiation and arrest below the upper shelf,
  - (c) cleavage initiation with arrest on the upper shelf,
  - (d) arrest in a high  $K_I$  gradient,
  - (e) warm and anti-warm prestressing states in succession, and
  - (f) progressive (upper-shelf) tearing, tearing instability, and re-stabilization.

Three experiments have been planned to help resolve the four principal issues. The emphasis of each experiment is:

PTSE-1 — to demonstrate effectiveness of warm prestressing and to investigate rapid crack propagation into the ductile upper shelf and subsequent tearing stability;

PTSE-2 — to study additional aspects of warm prestressing and to investigate the transition from cleavage fracture to unstable ductile tearing;

PTSE-3 — to investigate the influence of stainless steel cladding in restricting the growth of short flaws.

PTSE-1 was designed to investigate the first three issues under conditions relevant to a flawed reactor vessel during an overcooling accident. The crack was long, sharp, and shallow, as is assumed in regulatory evaluations. The material properties were typical of pressure vessel steel after moderate neutron embrittlement, the  $RT_{NDT}$  being 91°C. Temperatures in the vessel during the test were in the range from ~15°C to 290°C. The stress levels and gradients around the outside surface flaw in the test vessel were approximately those that would occur in a PWR vessel with a flaw on the inside surface during a severe pressurized-thermal-shock transient.

The flawed vessel was enclosed in a shroud as shown in Fig. 1. The shroud was electrically heated to bring the vessel to the desired initial temperature. A thermal transient was initiated by suddenly injecting chilled water or a methanol-water mixture into the outer vessel. The annulus between the cylindrical surfaces of the two vessels was designed to permit coolant velocities that would produce the appropriate convective heat transfer from the test vessel for a period of about 10 minutes. Pressurization of the test vessel was controlled independently by a system capable of increasing pressures to about 100 MPa.

The plan for PTSE-1 was to initiate and arrest a fast-running crack, make the arrested crack supercritical ( $K_I > K_{IC}$ ) while in a warm prestressed state, and subsequently reinitiate the crack so as to drive it as near to completely ductile material as practical. The necessity to preserve evidence of crack geometry precluded the deliberate bursting of the test vessel.

Extensive materials property tests and fracture analyses preceded the transient test of the PTSE-1 vessel. The initial 1-m-long by 12-mm-deep flaw was axially oriented on the outside (cooled) surface of the 148-mm-thick vessel. The transient test was performed in three phases; in each phase the vessel was initially in an isothermal state ( $\sim 290^\circ\text{C}$ ). Each phase consisted of a pressure transient and a thermal transient, which were coordinated to produce an evolution of stress and toughness states that would fulfill the objectives of the plan. Fracture analyses performed to define the transients were based on fracture-toughness data from tests of small specimens. Much of the expected action in the experiment would take place in a temperature range above that for which there were prior data; consequently, transients were selected so as to attain the desired objectives in the presence of uncertainty.

### Description of Experiment

Crack behavior in an experiment depends on characteristics of both the test facility and the vessel itself. The interdependence of these factors is illustrated in Fig. 2. Methods of fracture analysis used in designing the experiment took account of all of these factors. The ORMGEN/ADINA/ORVIRT system<sup>1-3</sup> of finite element computer programs was used in conjunction with the OCA/USA program<sup>4</sup> to define fracture properties and transients that would meet PTSE-1 objectives.

The test vessel and flaw geometry are described in Fig. 3 and Table 1. Vessel V-8 of the HSST intermediate test vessel series was repaired with a plug of especially tempered steel of SA508, class 2 composition welded into the region to be flawed. The 1-m-long sharp flaw was implanted in the plug of special material by cracking a shallow electron beam weld under the influence of hydrogen charging. The vessel was extensively instrumented to give direct measurements of crack-mouth opening displacement, temperature profiles through the vessel wall, and internal pressure during the transient (see Fig. 4). Pretest fracture analyses were based on computed temperature profiles and hypothetical pressure transients, while posttest analyses employed measured temperatures and pressures. Material properties of the vessel are given in Table 2 and Figs. 5 and 6.

Fracture initiation and arrest toughnesses were determined, respectively, by 25-mm and 37-mm compact specimen tests. Figures 5 and 6 show the raw  $K_C$  and  $K_a$  data together with adjusted data and a set of curves used in OCA/USA fracture analyses. The A curve of Fig. 5 was used in analyses made prior to execution of the first transient PTSE-1A; curve B was used subsequently.

A tentative transient was defined for the first experiment: to (1) initiate and arrest a cleavage fracture, (2) experience warm prestressing that is eventually relieved by increasing pressure, and (3) reinitiate a cleavage

fracture that is arrested on the ductile upper shelf. The course of the experiment is illustrated in Fig. 7, which shows the evolution of crack-tip conditions.  $K_I$ ,  $K_{IC}$ , and  $K_{Ia}$  vs time curves are shown for three crack depths:  $a_0$ , the initial crack depth;  $a_1$ , an intermediate depth; and  $a_2$ , the final depth. In the phase  $t < t_1$ , the initial crack is subcritical and should not propagate. At  $t = t_1$ ,  $K_I$  is first equal to  $K_{IC}$ , (point A) and the crack should propagate. If it does not propagate at  $t_1$ , it may still propagate at some time prior to  $t_2$ , at which time the initial crack would become simply warm prestressed ( $K_I < 0$ ). In the interval  $t_1 < t < t_2$ ,  $K_I/K_{IC}$  for the initial crack may become much greater than unity, but the loading rate  $\dot{K}_I$  diminishes. A crack propagating at  $t = t_1$  would arrest at a depth  $a_1$ , for which  $K_I = K_{Ia}$  (point B).  $K_I$  for the intermediate crack would continue to rise until  $t = t_3$ , at which time the intermediate crack would be warm prestressed (point C). The crack would again become critical at  $t = t_4$  (point D), but it would not propagate immediately because of its warm prestressed state. When  $t_5 < t < t_7$  (after point E) the nominal warm prestressing condition ( $\dot{K}_I \leq 0$ ) no longer obtains; and, since  $K_I > K_{IC}$ , the crack should again propagate, for example at point F, unless it is inhibited by a complex type of warm prestressing. This running crack should again arrest at a depth  $a_2$  for which  $K_I = K_{Ia}$  (point G).

In any persistent transient there is generally a time  $t_I$  beyond which an arrested crack in the upper-shelf regime would not be stable, either because of a tearing instability or a net ligament tensile instability. Since it is essential to the interpretation of the experiment to preserve evidence of the arrested crack geometry, it is necessary that  $t_I$  be predictable and that the transient be terminated at some time  $t_7 < t_I$  (point H).

An OCA/USA analysis of the first transient (PTSE-1A) projected the crack trajectory shown in Fig. 8. Prior to initial warm prestressing (at  $\sim 120$  s) the crack would propagate by one or more jumps to a depth with an  $a/w$  between 0.18 and 0.22, where  $a$  is the crack depth and  $w$  is the thickness of the vessel wall. The deeper crack would be inhibited by simple warm prestressing ( $\dot{K}_I < 0$ ) until  $t \approx 230$  s, after which it would be capable of propagating again to a depth with a final  $a/w$  between 0.42 and 0.48. The planned pressure transient is curve A of Fig 9 and other actual test conditions are given in Table 3.

The actual pressure transient in the A test varied slightly from the plan, the crack was slightly deeper than had been estimated, and the actual toughness was higher than had been estimated; consequently the crack did not propagate during the transient. The  $K_I$  trajectory reconstructed from experimental data is shown in Fig. 10. Since temperature (on the abscissa) decreases monotonically with time one can discern from this plot two episodes of simple warm prestressing ( $\dot{K}_I < 0$ ) each followed by simple anti-warm prestressing ( $\dot{K}_I > 0$ ) while  $K_I$  is greater than  $K_{IC}$ .

Plans for the B and C transients were based upon the evidence from PTSE-1A that the vessel was tougher than estimated and that, to overcome warm prestressing, a higher  $K_I$  value would have to be attained. Accordingly, the B curve of Fig. 5 was adopted for further analysis, lower coolant temperatures were specified for the thermal transient (Table 3), and a transient to higher pressure was selected (curve B, Fig. 9). A two-step pressure transient

was not performed during the B test because a second pressure increase of a useful magnitude was not within the capabilities of the pressurization system. The B transient resulted in a crack jump to a depth of 24.4 mm. The conditions of initiation and arrest are shown in Fig. 11.

The final transient, PTSE-1C, was performed under the conditions given in Table 3 and with the planned pressure transient described by curve C of Fig. 9. The crack jumped to a depth of 41 mm under conditions presented in Fig. 12.

The vessel was examined visually and ultrasonically after the final test. At the outside surface the crack extended axially about 110 mm at the upper end of the vessel and about 120 mm at the lower end (Fig. 13). The crack branched at the lower end, as shown in the photograph, Fig. 14. Test instrumentation indicated that all of the axial extensions occurred at the time of the first crack jump, that is, in transient PTSE-1B.

The flawed region was cut from the vessel, chilled in liquid nitrogen, and broken apart so as to reveal the fracture surfaces, shown in Fig. 15. Details of a segment of one surface are shown in Fig. 16. Fractographic examination of the surfaces and measurement of the flaw geometry indicated that the initial flaw tore slightly prior to the initial cleavage fracture. The initial crack extension was essentially a pure cleavage fracture throughout the first half of the extension and predominantly cleavage (~90%) with finely dispersed ductile tearing in the remaining extension. The crack extension in the second crack jump was mixed mode throughout with ~85% cleavage. At the termini of the two crack extensions there were no coherent regions of ductile tearing, contrary to predictions based on the measured tearing resistance,  $J_R$ , of the material.

### Conclusions and Recommendations

The first experiment is a basis for quantitative conclusions on initiation and arrest toughnesses, which are summarized in Table 4. The values of  $K_{IC}$  and  $K_{Ia}$  inferred from test data are shown in Fig. 17 in comparison with the pretest estimates and with the  $K_{IC}$  and  $K_{Ia}$  relationships suggested in Sect. XI of the ASME *Boiler and Pressure Vessel Code*. Pretest estimates of fracture toughness are reasonably close to the PTSE-1 values. Furthermore, the Sect. XI toughness relationships are conservative relative to actual material characteristics. The experiment demonstrated that arrest toughness substantially above the 220 MPa·√m cutoff of Sect. XI could be realized. The arrest values in PTSE-1 also are consistent with arrest measurements made in wide-plate tests and reported by the Japan Welding Council,<sup>5</sup> as illustrated in Fig. 18. The highest PTSE-1 value of arrest occurred at a temperature ~30 K above the onset of the Charpy upper shelf. This is believed to be very close to the threshold temperature above which cleavage fracture cannot persist. This result also suggests that the methods of linear elastic fracture mechanics have an important role in fracture evaluation at high (upper-shelf) temperatures.

The PTSE-1A and -1B transients were a demonstration that simple warm prestressing ( $K_I < 0$ ) strongly inhibits crack initiation. With allowance for uncertainty in the true  $K_{IC}$  values it is evident that  $K_I$  exceeds  $K_{IC}$  during warm prestressing

by 50% to 90%. Thus, the effectiveness of simple warm prestressing has now been demonstrated in two experiments with thick cylinders, thermal shock experiment TSE-5A and PTSE-1. In the A transient, simple anti-warm prestressing ( $K_I > 0$ ) prevailed during two periods of 40-s and 60-s duration without crack initiation, although  $K_I$  exceeded  $K_{IC}$  by 30% to 50%. Clearly simple anti-warm prestressing is not a sufficient condition to alleviate the effects of warm prestressing.

A narrow band of ductile tearing formed ahead of the initial cleavage fracture. This was not unexpected, since analysis as well as prior intermediate vessel tests<sup>6-8</sup> indicated the potential for stable tearing prior to cleavage. The complete absence of ductile tearing after crack arrest is not consistent with tearing analysis based on pretest data on tearing resistance. This result suggests that the data or the method of analysis or both are very conservative.

The conclusions drawn from PTSE-1 suggest that procedures used for evaluating overcooling accidents in pressurized-water reactors should take into consideration realistically the fracture mechanisms that have been clearly demonstrated but not yet generally accepted. Account should be taken for the inhibiting effect of simple warm prestressing. Furthermore, it is not premature to allow consideration of crack-arrest toughness values above the ceiling suggested in Sect. XI of the ASME Code. These two measures would make evaluations less conservative without being unrealistic. In a change toward conservatism, the phenomenon of ductile tearing below upper-shelf temperatures should be explicitly considered in vessel evaluations to ensure that the procedure is never unconservative.

#### Acknowledgments

The authors gratefully acknowledge the essential contributions of H. A. Domian et al of the Babcock & Wilcox Alliance Research Center; A. R. Rosenfield et al of the Battelle Columbus Laboratories; T. M. Cate, D. P. Edmonds, F. R. Gibson, R. W. McCulloch and K. R. Thoms of the Oak Ridge National Laboratory; and D. A. Steinert of the Computing and Telecommunications Division.

## REFERENCES

1. B. R. Bass and J. W. Bryson, *Applications of Energy Release Rate Techniques to Part-Through Cracks in Plates and Cylinders, Volume 1. ORMGEN-3D: A Finite Element Mesh Generator for 3-Dimensional Crack Geometries*, NUREG/CR-2997, Vol. 1 (ORNL/TM-8527/V1), Oak Ridge National Laboratory, Oak Ridge, Tenn., December 1982.
2. K. J. Bathe, *ADINA - A Finite Element Program for Automatic Dynamic Incremental Nonlinear Analysis*, Report 82448-1, Massachusetts Institute of Technology, Cambridge, Mass., September 1975 (revised December 1978).
3. B. R. Bass and J. W. Bryson, *Applications of Energy Release Rate Techniques to Part-Through Cracks in Plates and Cylinders, Volume 2. ORVIRT: A Finite Element Program for Energy Release Rate Calculations for 2-D and 3-D Crack Models*, NUREG/CR-2997, Vol. 2 (ORNL/TM-8527/V2), Oak Ridge National Laboratory, Oak Ridge, Tenn., February 1983.
4. R. H. Bryan and J. G. Merkle, "Upper-Shelf Arrest Analysis Based on J<sub>R</sub>-Controlled Tearing," *Heavy-Section Steel Technology Program Quart. Prog. Rep. January-March 1983*, NUREG/CR-3334, Vol. 1 (ORNL/TM-8787/V1), Oak Ridge National Laboratory, Oak Ridge, Tenn., September 1983, pp. 111-124.
5. Japan Welding Council, *Structural Integrity of Very Thick Steel Plate for Nuclear Reactor Pressure Vessels*, JWES-AE-7806, 1977 (in Japanese).
6. R. W. Derby et al., *Test of 6-in.-thick Pressure Vessels. Series 1: Intermediate Test Vessels V-1 and V-2*, ORNL-4895, Oak Ridge National Laboratory, Oak Ridge, Tenn., February 1974.
7. R. H. Bryan et al., *Test of 6-in.-thick Pressure Vessels, Series 2: Intermediate Test Vessels V-3, V-4, and V-6*, ORNL-5059, Oak Ridge National Laboratory, Oak Ridge, Tenn., November 1975.
8. J. G. Merkle et al., *Test of 6-in.-thick Pressure Vessels. Series 4: Intermediate Test Vessels V-5 and V-9*, ORNL/NUREG-7, Oak Ridge National Laboratory, Oak Ridge, Tenn., August 1977.

Table 1. Geometric parameters of PTSE-1 Vessel.

Parameter	Value
Inside radius, mm	343
Wall thickness (w), mm	147.6
Flaw length, mm	1000
Flaw depth (a), mm	12.2
a/w	0.083

Table 2. Properties of PTSE-1 vessel material (A508, class 2 steel with special tempering treatment).

Property	Value
$K_{Ic}$	Fig. 5
$K_{Ia}$	Fig. 6
$J_R$ Parameters <sup>a</sup>	
c	2.60
n	0.359
Onset of Charpy upper shelf, °C	150
Ductile threshold temperature, °C	175
RTNDT, °C	91
Yield stress, MPa	600
Stress-strain	Curve from data <sup>b</sup>
Young's Modulus, GPa	200 and 209.6 pretest 202.3 posttest <sup>c</sup>
Coefficient of thermal expansion, $K^{-1}$	$1.3 \times 10^{-5}$ & $1.445 \times 10^{-5}$ pretest $1.441 \times 10^{-5}$ posttest <sup>c</sup>
Poisson's Ratio	0.3
Thermal conductivity, $W \cdot m^{-1} \cdot K^{-1}$	41.54
Heat capacity, $J \cdot kg^{-1} \cdot K^{-1}$	502.4
Density, $kg/m^3$	7833

<sup>a</sup> $J_R = c (\Delta a)^n$ ;  $J_R$  in MJ/m<sup>2</sup>,  $\Delta a$  in m

<sup>b</sup>Piecewise linear fit.

<sup>c</sup>These average values are based on experimental measurements of  $E(T)$  and  $\alpha(T)$  for the vessel material, and they give values of  $K_I$  within 1% of the values based upon the temperature-dependent properties.

Table 3. Conditions for PTSE-1A, -1B, and -1C transients

	Test		
	PTSE-1A	PTSE-1B	PTSE-1C
Thermal transient parameters			
Initial vessel temperature, °C	277.6	290.7	287.4
Coolant temperature T(t), °C	15 to 34 <sup>a</sup>	-22 to 0 <sup>a</sup>	-29 to 14 <sup>a</sup>
h(t), W·m <sup>-2</sup> ·K <sup>-1</sup>	8000 to 6000 <sup>a</sup>	5500 to 6500 <sup>a</sup>	4000 to 5500 <sup>a</sup>
Pressure transient (planned)	Curve A, Fig. 9	Curve B, Fig. 9	Curve C, Fig. 9
Initial flaw depth			
a, mm	12.2	12.2	24.4
a/w	0.083	0.083	0.165

<sup>a</sup>Initial and final (t ≈ 300 s) values.

Table 4. Summary of fracture conditions in PTSE-1.

Experiment	Event	Crack Depth (mm)	Crack Tip Temperature (°C)	$K_I$ (MPa $\cdot\sqrt{m}$ )
PTSE-1A	1st max $K_I$ (AT $K_I \approx K_{Ic}$ )	12.2	105	152
	2nd max $K_I$	12.2	78	154
	3rd max $K_I$	12.2	57	139
PTSE-1B	Initiation	12.2	104	177
	Arrest	24.4	163	201
	Subsequent max $K_I$	24.4	118	247
PTSE-1C	Initiation	24.4	125	254
	Arrest	41	179	299
	Subsequent max $K_I$	41	156	340

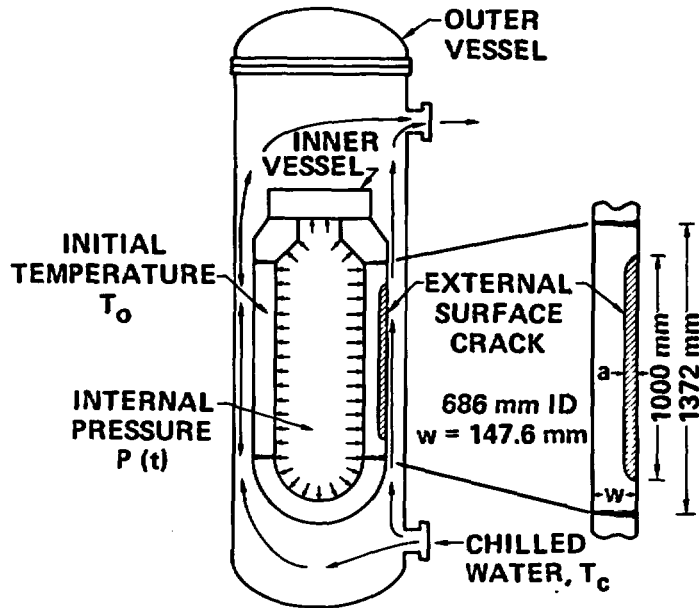


Fig. 1. Schematic drawing of flawed test vessel inside shroud.

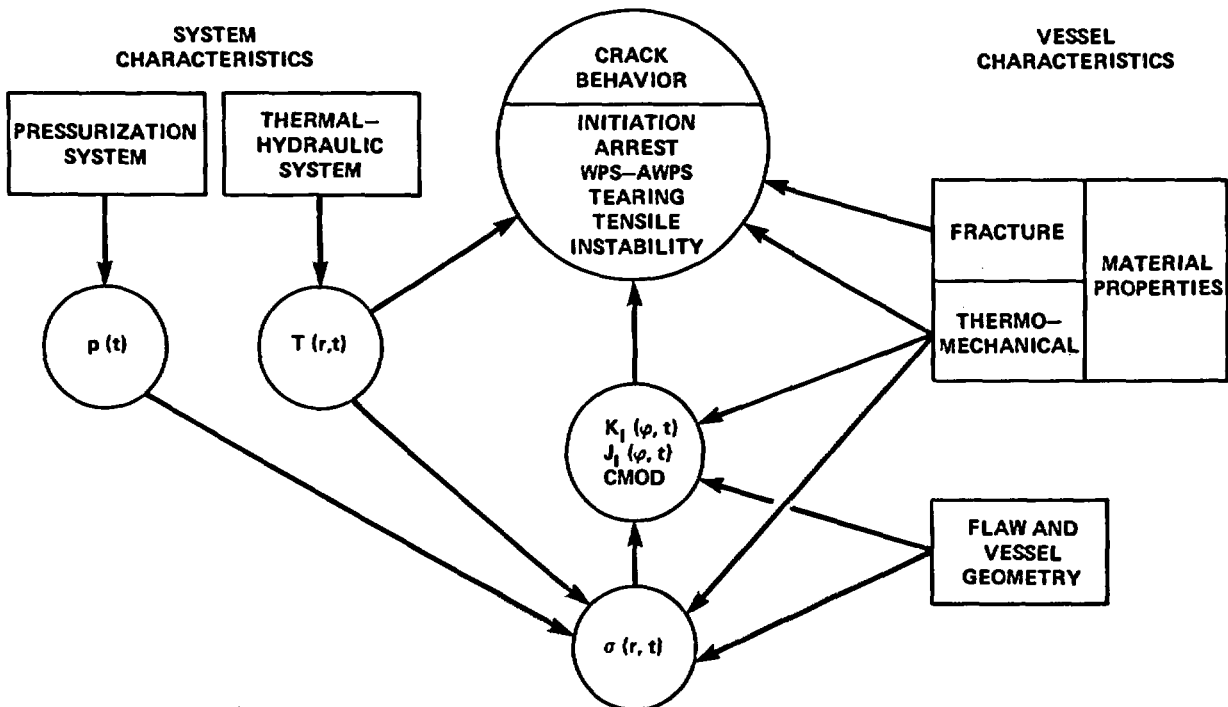


Fig. 2. Interdependence of crack behavior, system characteristics, and vessel characteristics.

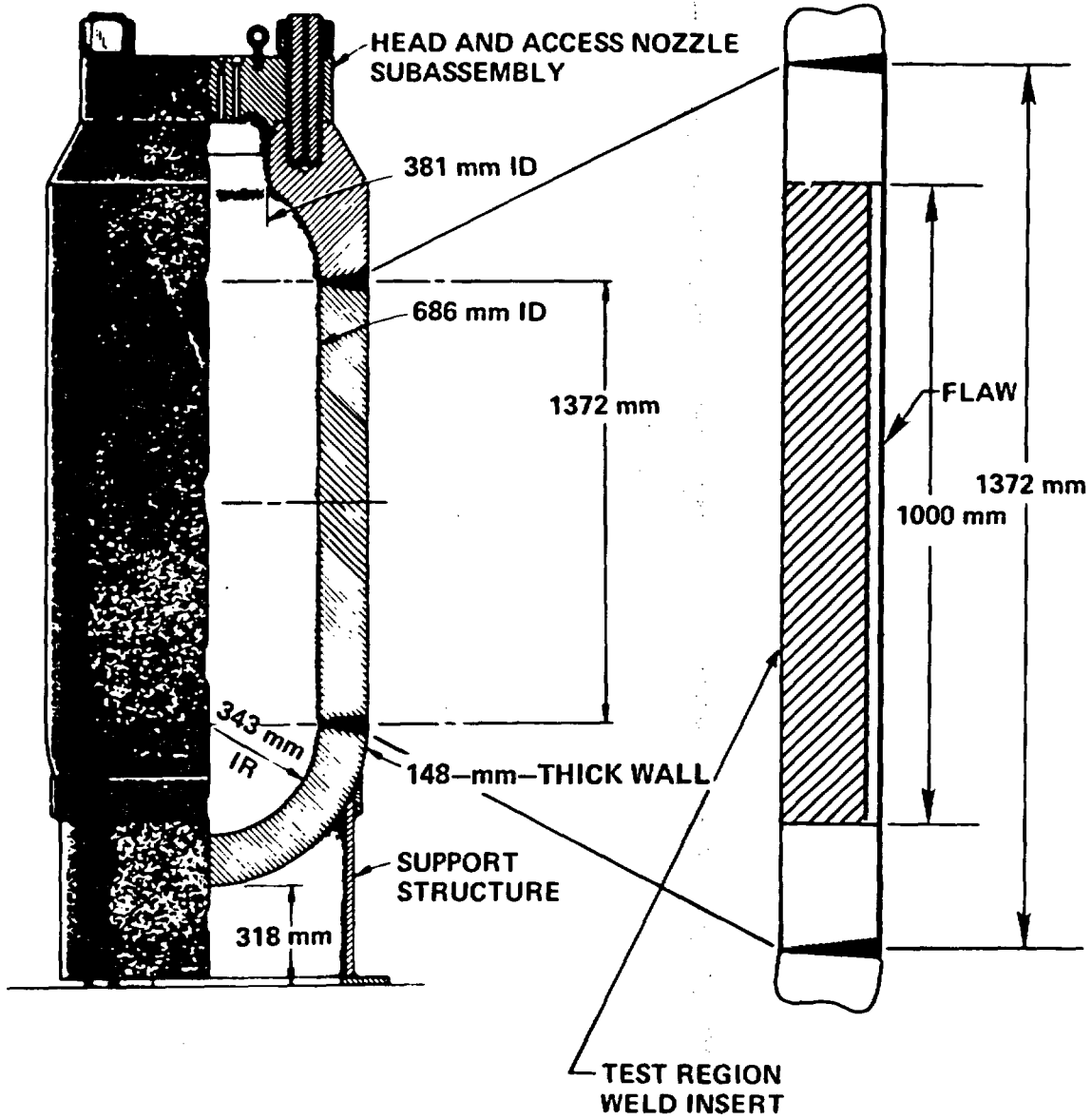


Fig. 3. Geometry of PTSE-1 test vessel.

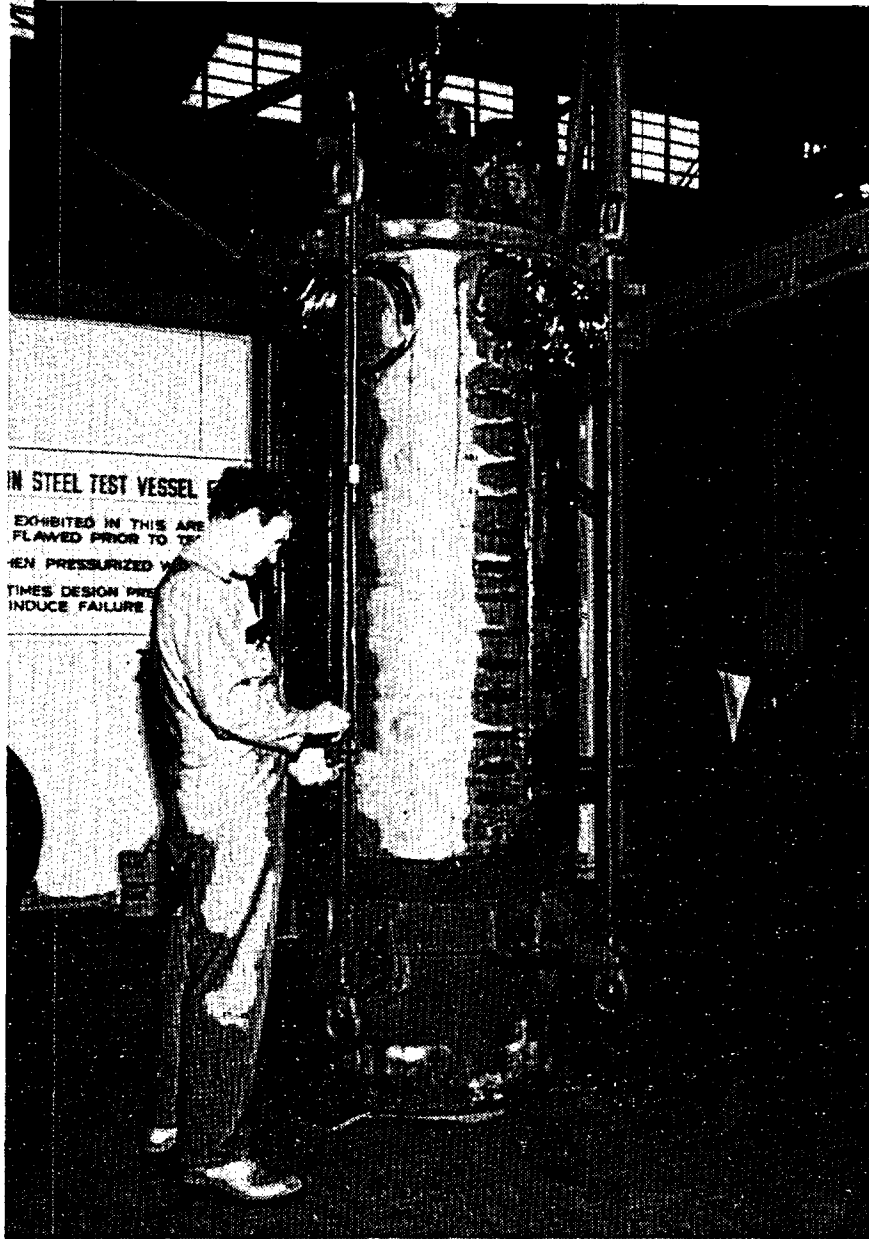


Fig. 4. Instrumented PTSE-1 test vessel. Ten crack-mouth-opening displacement gages are visible along the flaw.

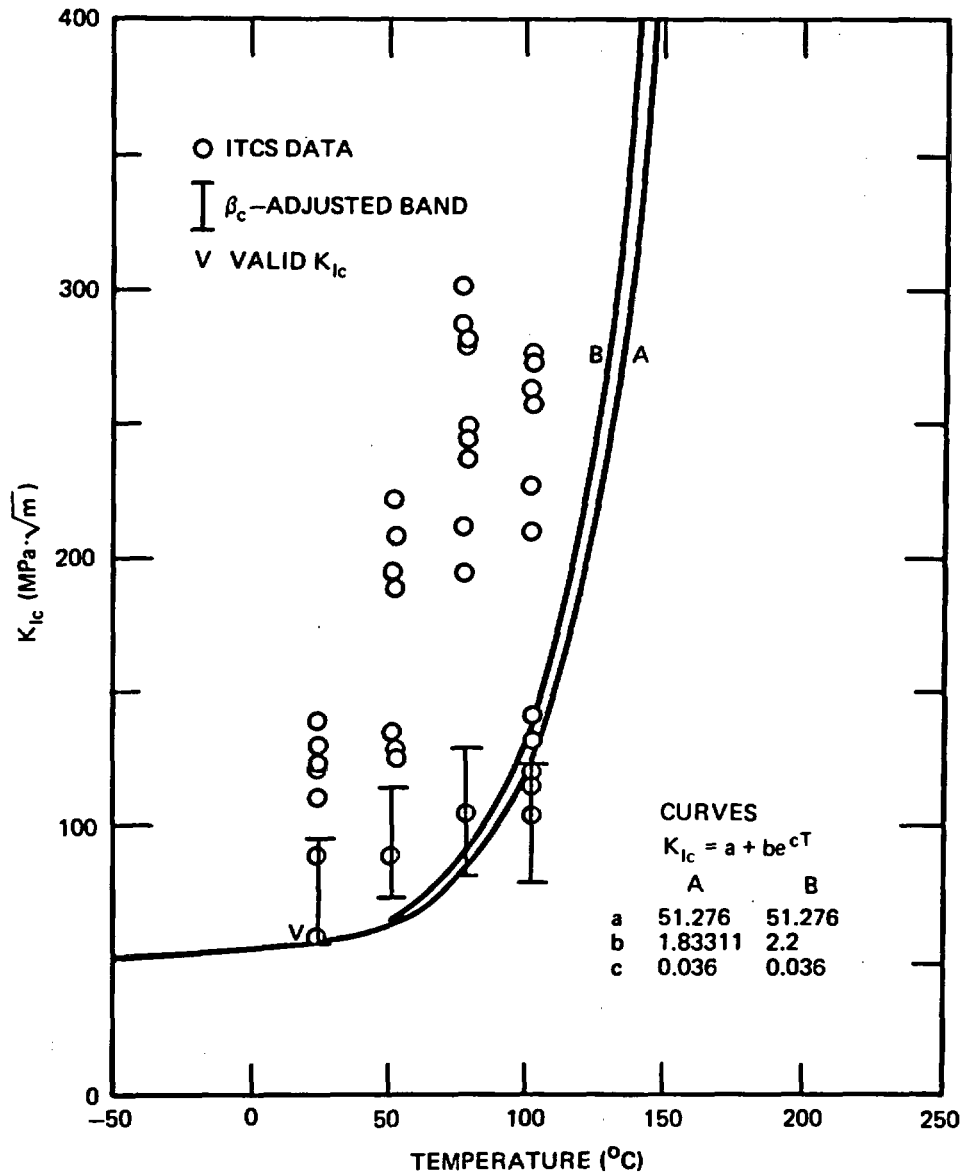


Fig. 5. Pretest  $K_{Ic}$  information. Compact specimen (CS) data are from 25-mm-thick specimens. Curve A is the exponential expression of Section XI of the ASME *Boiler and Pressure Vessel Code* translated to be a lower bound to the adjusted data at and below 77.2°C.

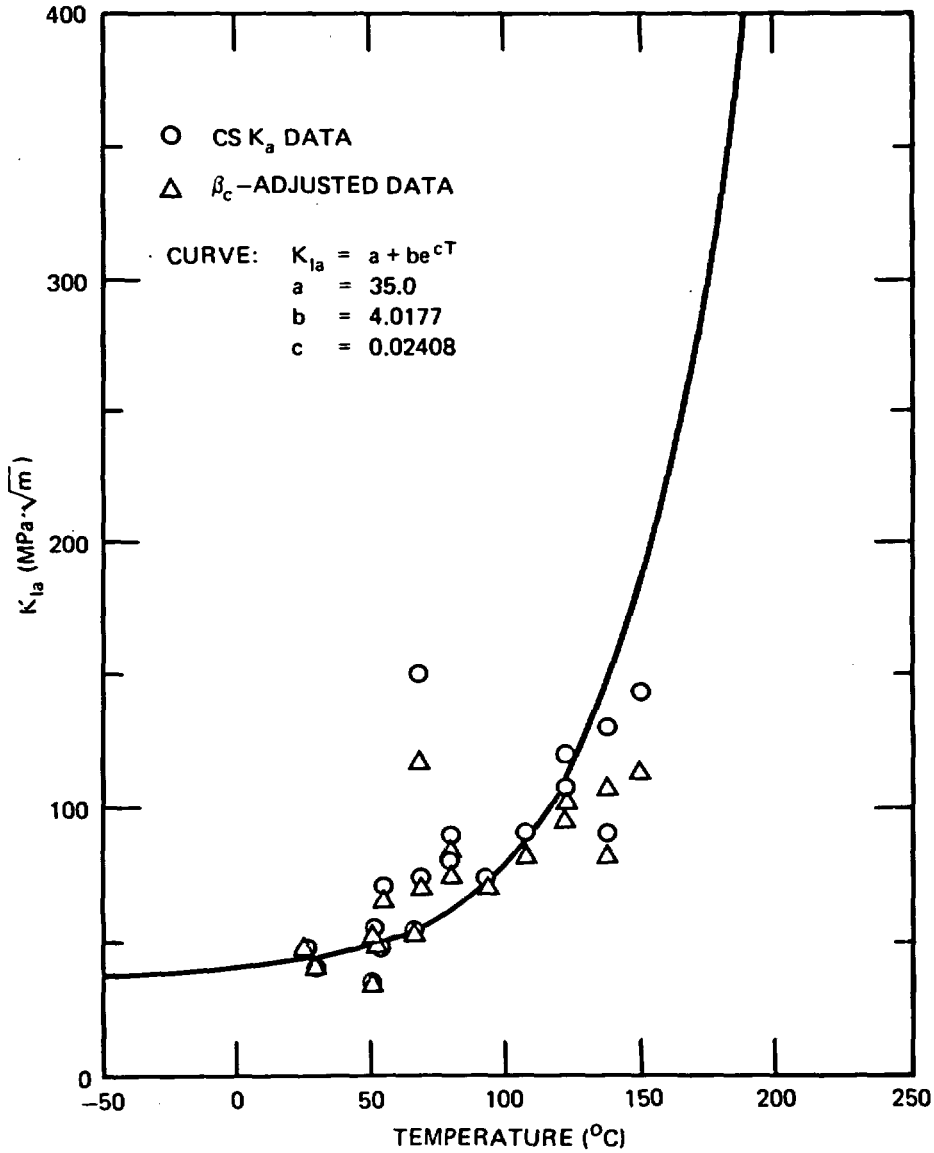


Fig. 6. Pretest  $K_{Ia}$  information. Compact specimen (CS) data are from 37-mm-thick specimens. The curve is a least-squares fit to the adjusted data with the highest point (at 67°C) excluded.

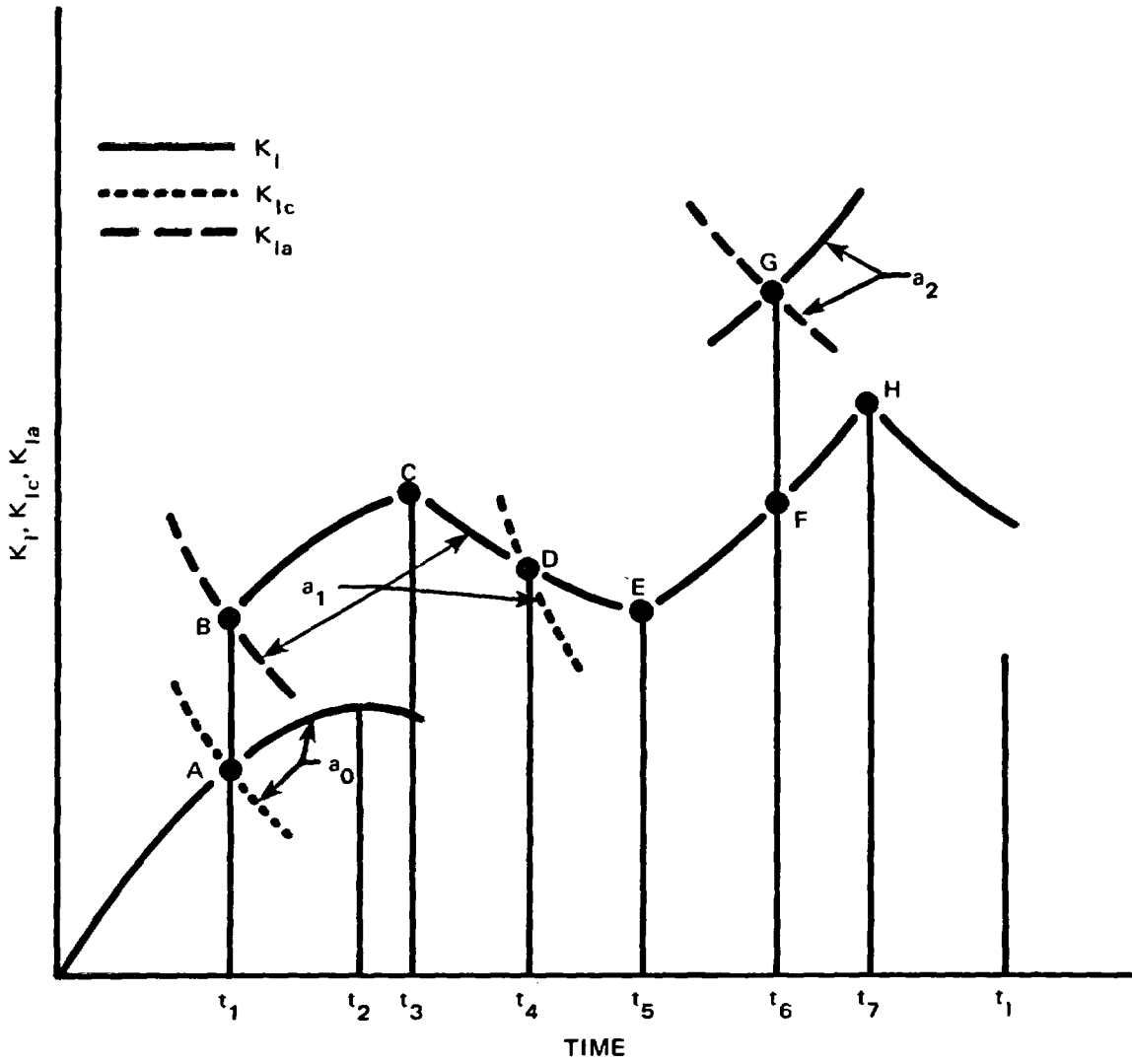


Fig. 7. Idealized PTSE-1 transient.

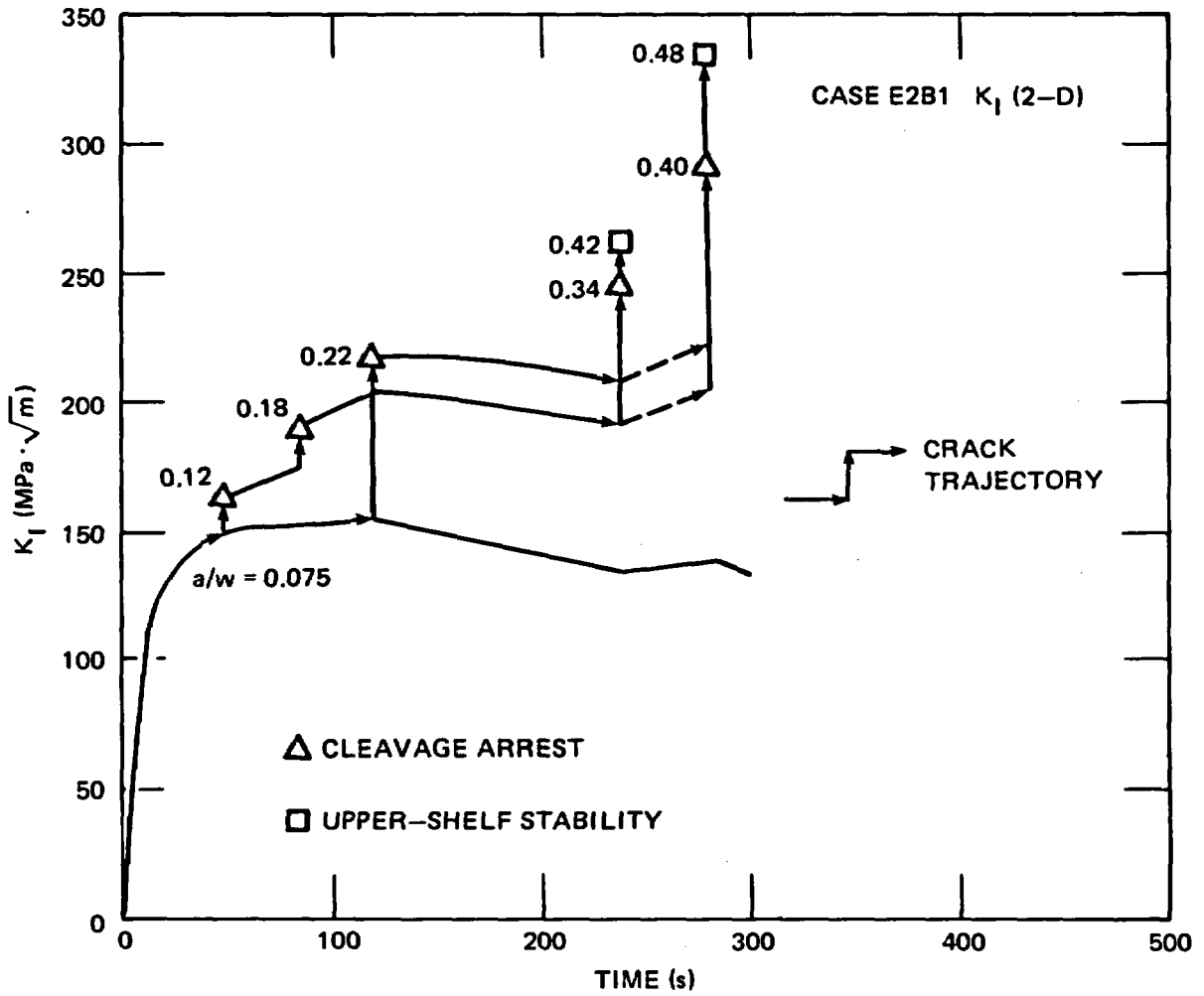


Fig. 8. Results of pretest analysis of the planned PTSE-1A transient.

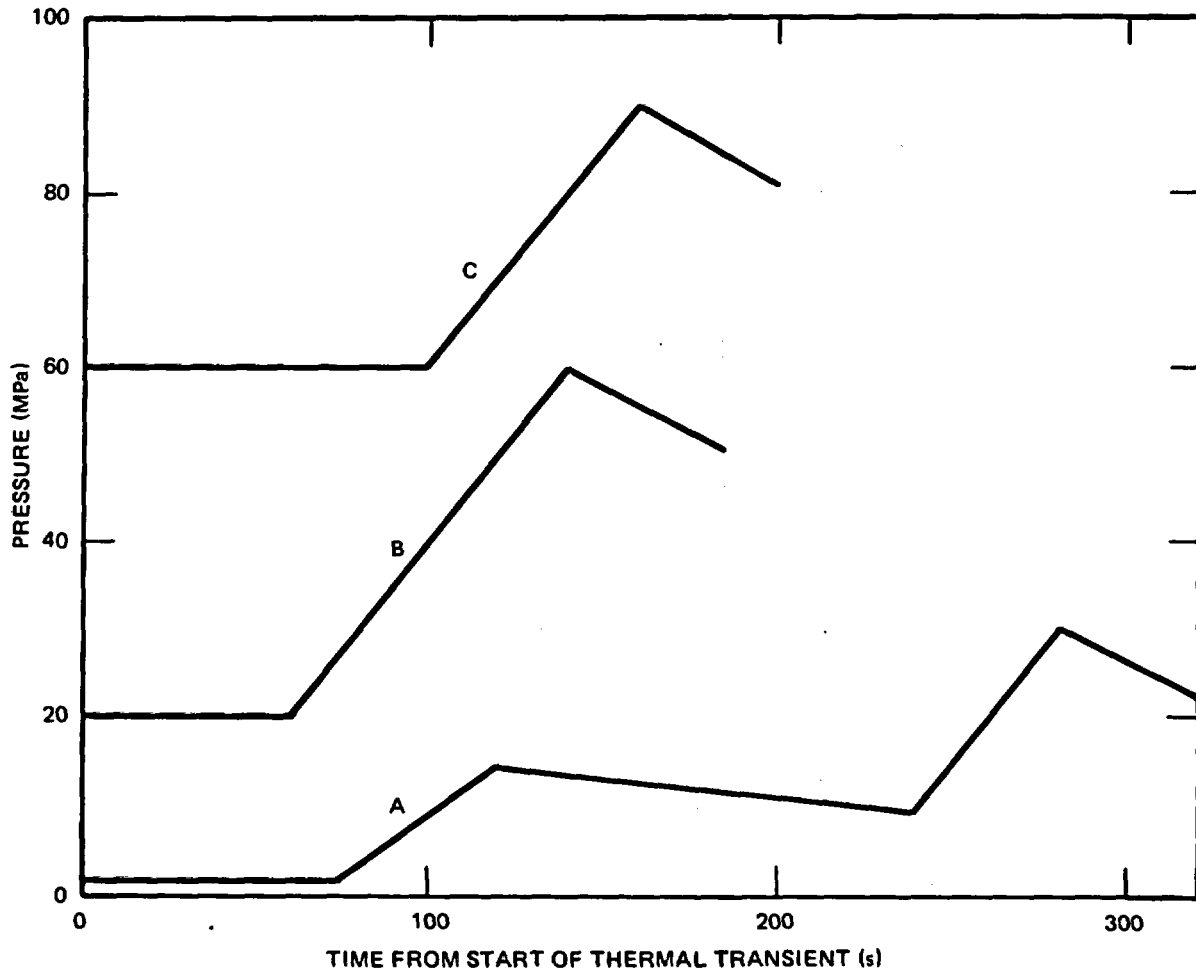


Fig. 9. Planned pressure transients for PTSE-1A, -1B, and -1C.

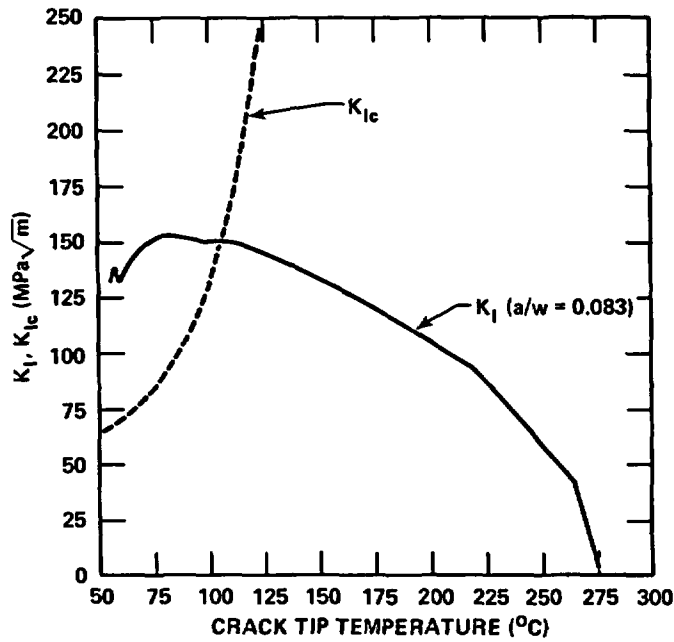


Fig. 10. Results of OCA/USA analysis of PTSE-1A based on measured temperature, pressure, and flaw depth. The  $K_{IC}$  expression is curve B of Fig. 5.

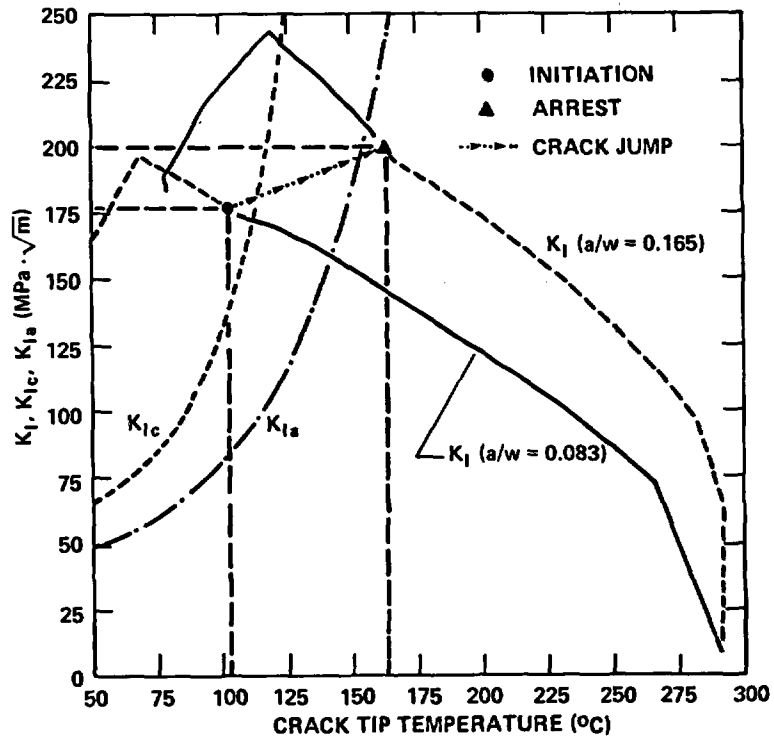


Fig. 11. Results of OCA/USA analysis of PTSE-1B based on measured temperature, pressure, flaw depth, and time of the crack jump.

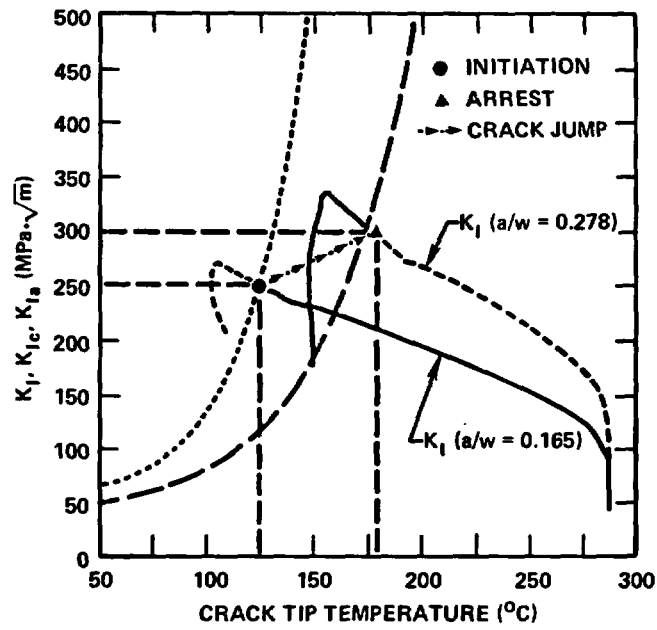


Fig. 12. Results of OCA/USA analysis of PTSE-1C based on measured temperature, pressure, flaw depth, and time of the crack jump.

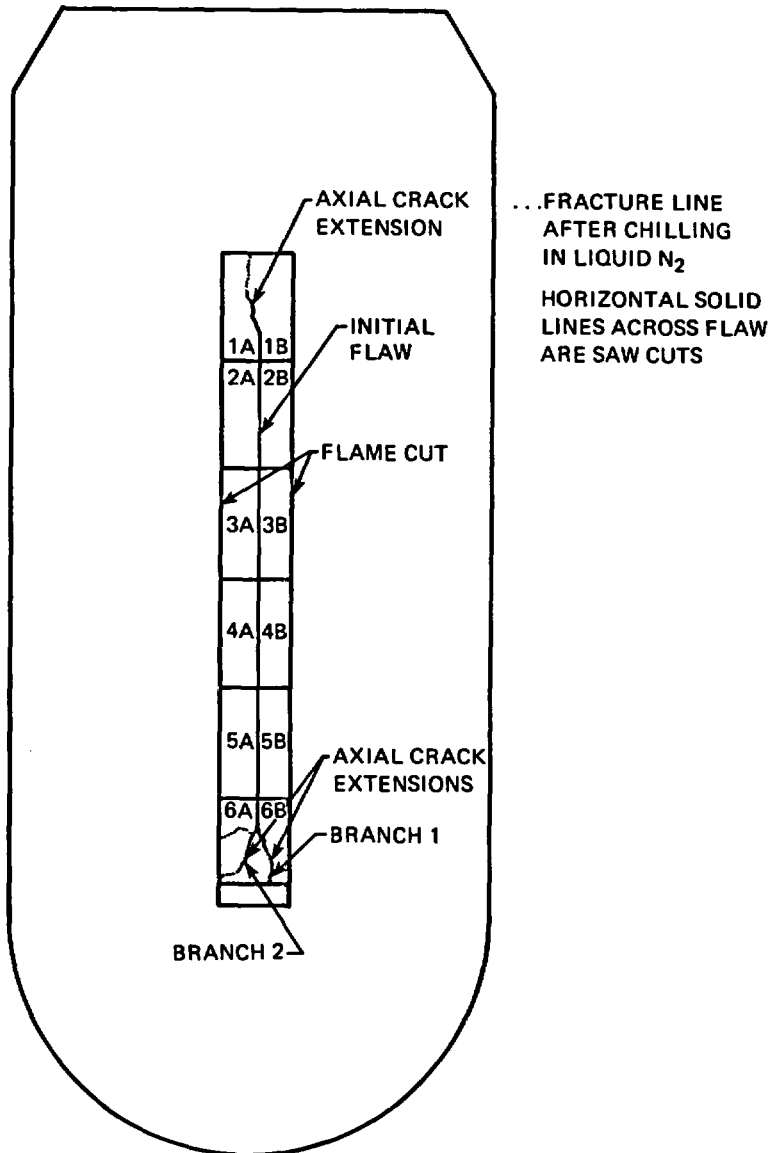


Fig. 13. Diagram of the intersection of the flaw with the outside surface of the test vessel. Locations of segments of the flaw and axial extensions of the flaw are shown.

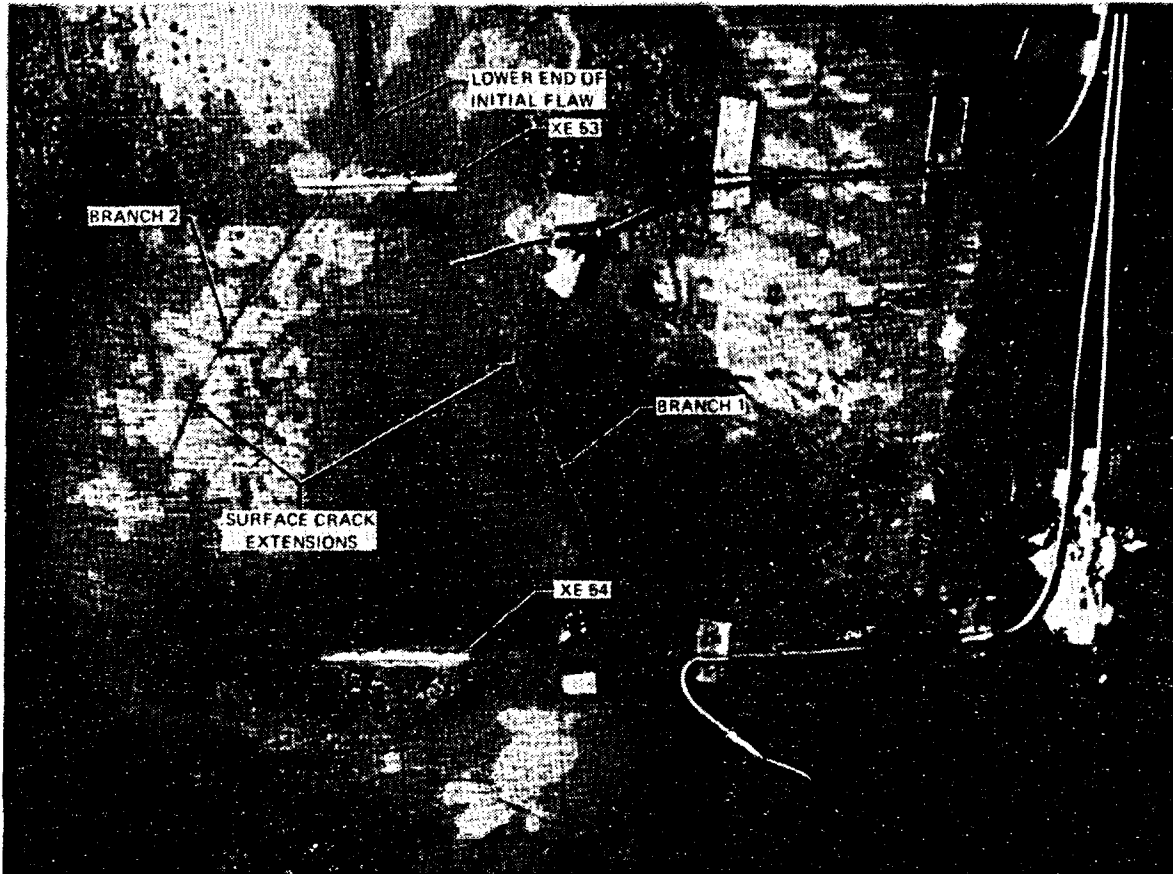


Fig. 14. Photograph showing the branching of the PTSE-1 flaw at the lower end. Strain gages XE53 and XE54 were located 10 mm and 100 mm, respectively, from the end of the initial flaw.

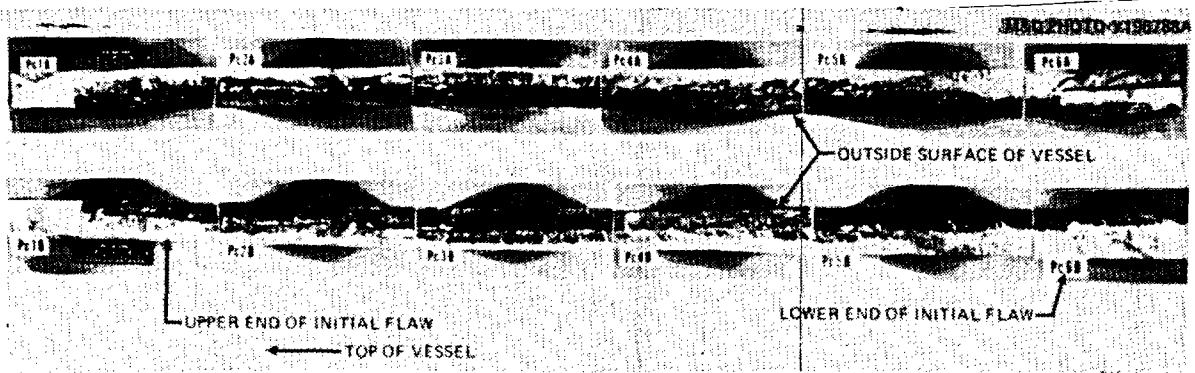


Fig. 15. Montage of fracture surfaces from PTSE-1. Only branch 1 surfaces are shown in pieces 6A and 6B. See Fig. 13 for key to location.

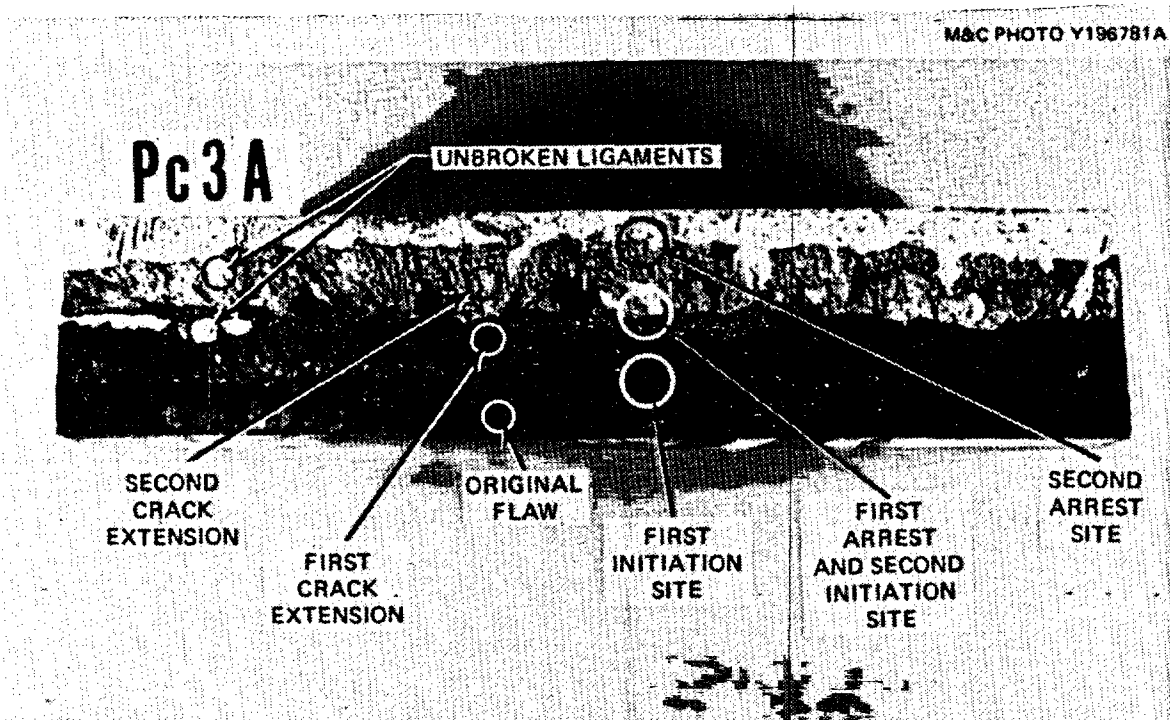


Fig. 16. Typical portion of fracture surface from PTSE-1 (surface A in segment 3).

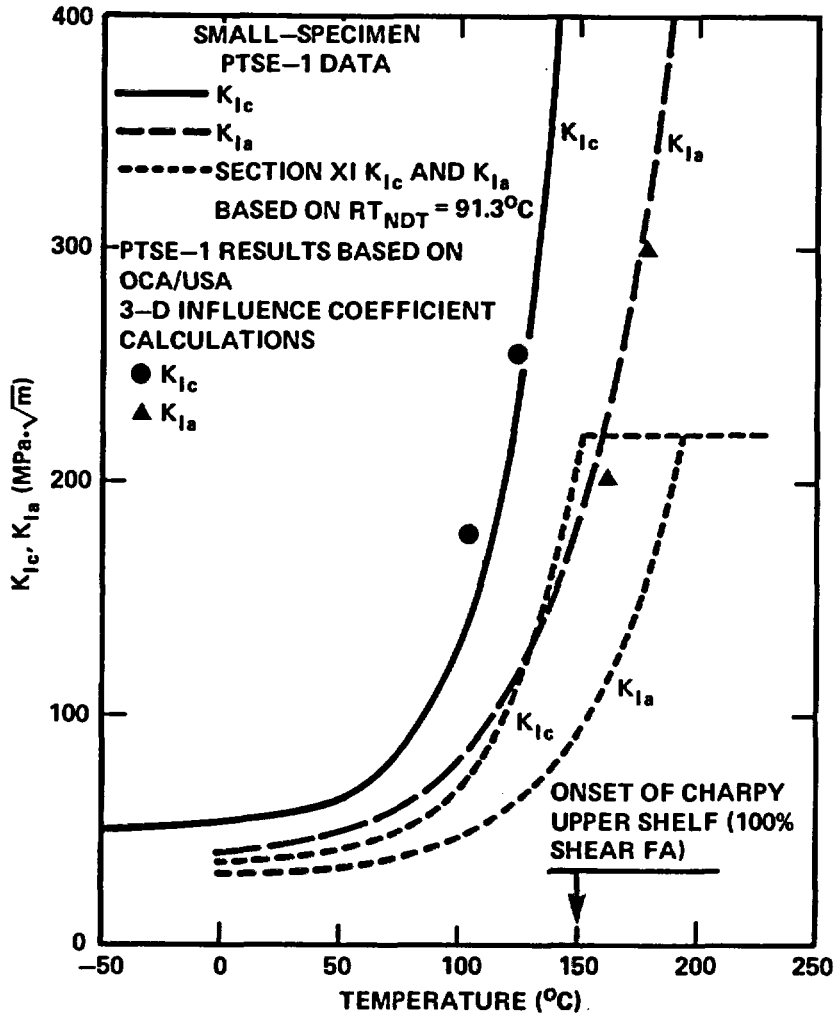


Fig. 17. Comparison of curves representing small-specimen  $K_{Ic}$  and  $K_{Ia}$  data with Section XI curves and results of PTSE-1 experiment.

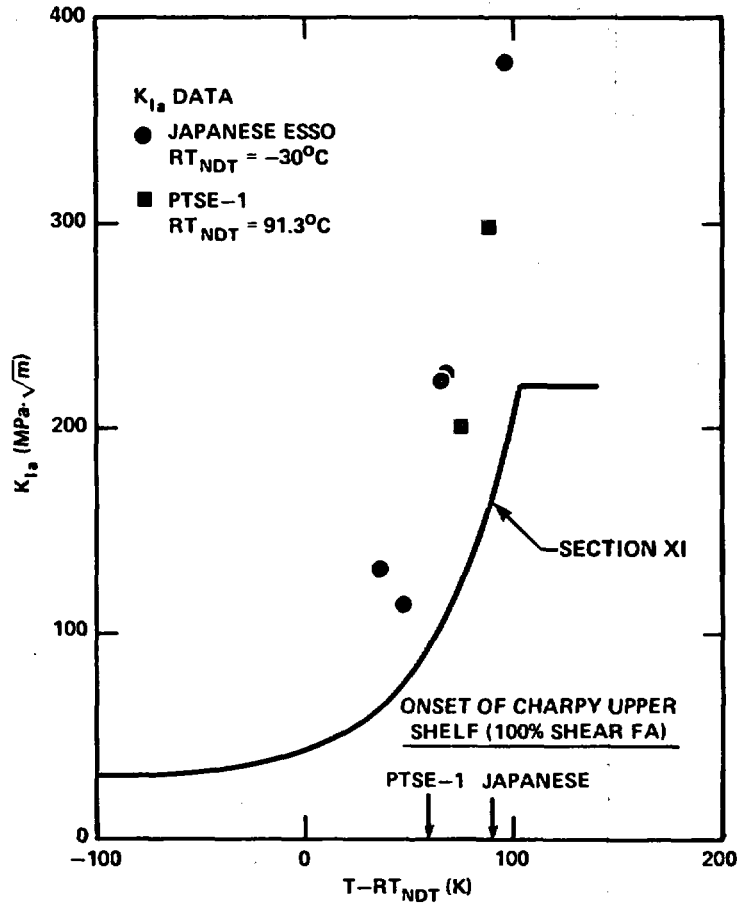


Fig. 18. Comparison of PTSE-1 arrest toughness results with Japanese wide-plate test results and Section XI curve.

## VESSEL BEHAVIOR FOLLOWING A THROUGH-WALL CRACK<sup>(a)</sup>

F. A. Simonen  
Pacific Northwest Laboratory<sup>(b)</sup>  
Richland, Washington 99352

### ABSTRACT

A fracture mechanics model has been developed to predict the behavior of a reactor pressure vessel following the occurrence of a through-wall crack during a pressurized thermal shock event. This study has been coordinated with the Integrated Pressurized Thermal Shock (IPTS) Program at Oak Ridge National Laboratory. The fracture mechanics model uses as inputs the critical transients and probabilities of through-wall cracks from the IPTS Program. The model has been applied to predict the modes of failure for plant specific vessel characteristics. A Monte Carlo type of computer code has been written to predict the probabilities of alternate failure modes. This code treats the fracture mechanics properties of the various welds and plates of a vessel as random variables. The computer code also calculates the crack driving force as a function of the crack length and the internal pressure for critical times during the transient. The fracture mechanics model has been applied in calculations that simulate the Oconee-1 reactor pressure vessel. The model predicted that about 50% of the through-wall axial cracks will turn and follow a circumferential weld giving a potential for missiles. Missile arrest calculations predict that vertical as well as all potential horizontal missiles will be arrested and will be confined to the vessel enclosure cavity. In future work, plant specific analyses will be continued with calculations that simulate Calvert Cliff 1 and H.B. Robinson 2 reactor vessels.

### INTRODUCTION

In recent years the issue of Pressurized Thermal Shock (PTS) has been investigated in great detail by the U.S. Nuclear Regulatory Commission (NRC), the utility industry, and nuclear steam supply system contractors. The concern in PTS has been with brittle fracture of welds in reactor pressure vessels under conditions of both rapid cooling and high system pressures.

This paper describes a contribution by the Pacific Northwest Laboratory (PNL) to NRC's effort to resolve the PTS safety issue (A-49). The PNL study is being closely coordinated with NRC's Integrated Pressurized Thermal Shock (IPTS) Program (Ref. 1) at Oak Ridge National Laboratory (ORNL). In the IPTS

- (a) A report on work performed for Division of Safety Technology, Office of Nuclear Regulatory Regulation, U.S. Nuclear Regulatory Commission (NRC FIN: B2510).
- (b) Operated for the U.S. Department of Energy by Battelle Memorial Institute.

Program the probabilities of PTS-type thermal transients are being estimated. Detailed thermal hydraulic calculations are being performed for three operating reactors. The final step in ORNL's calculations is to predict probabilities that these cooling transients will result in a through-wall crack in the reactor pressure vessel.

An important step in the overall PTS risk assessment by NRC staff involves a probabilistic evaluation of whether a through-wall crack in a vessel will result in core melt. The present study at PNL makes predictions of the failure modes of a vessel, given that a crack has penetrated through a weld. The failure modes of interest range from "catastrophic" vessel rupture to a crack in a single axial weld that gives only a small opening in the vessel wall.

In the failure mode evaluations, PNL was requested by NRC to address the following types of questions:

- Will a crack in an axial weld extend into the plate material of the next shell course?
- Will this axial crack turn and follow the circumferential weld joining adjacent shell courses?
- Does a through-wall crack in a circumferential weld necessarily lead to a complete circumferential fracture of the vessel?
- Given a complete circumferential fracture, what is the effect of the fluid thrust forces and attached piping on the motion of the vessel fragments?
- What are the sizes, velocities, and hazards of other potential fragments of the vessel?

This paper describes a fracture mechanics model and results of an application of this model to the Oconee-1 reactor vessel. The calculations address the potential for missile generation during fracture of the Oconee vessel and evaluates the consequences of such missiles. In future work the fracture mechanics model will be applied in calculations for the Calvert Cliffs 1 and H.B. Robinson 2 reactor vessels. In all these plant-specific calculations, data from the IPTS Program (Refs. 2, 3) are being supplied by ORNL as major inputs to the vessel failure mode calculations.

#### FRACTURE OF CIRCUMFERENTIAL WELDS

The growth of a part-through crack in a circumferential weld was treated early in the present study. The potential to arrest the lengthwise growth of circumferential cracks was considered. Circumferential temperature and fluence gradients were the potential factors to cause such arrest. However,

the analyses indicated that the magnitudes of these gradients for PTS scenarios were insufficient, and that all through-wall circumferential cracks would extend 360 degrees around the vessel.

Further analyses considered the fracture of a vessel due to the turning of a crack in an axial weld to follow a circumferential weld in the vessel. Figure 1 shows the results of numerical evaluations of the crack tip stress intensity factors for such turning behavior. The calculated crack driving force for circumferential growth is about one-half that for further growth in the axial direction. This factor of one-half for the vessel is consistent with published solutions for flat plates (Ref. 4).

The failure mode analysis assumes that micro-structural features can and will cause axial cracks to turn and follow circumferential welds. However, it is required that the applied value of stress intensity factor as calculated by the above procedure exceed the fracture toughness of the material of the circumferential weld. Detailed analyses of the continued circumferential growth of this crack was not possible. Hence, it was conservatively assumed that the turning of an axial crack will always result in a complete circumferential fracture of the vessel.

#### THROUGH-WALL THERMAL GRADIENT

Detailed calculations of stress intensity factors were performed for axial cracks subjected to PTS-type thermal stresses. The results indicated that such thermal stresses can be neglected for through-wall cracks. Their contribution was small relative to the contribution of pressure stresses. Such stresses also tend to offset the contribution of the bulging effects induced by pressure loading.

The variation in fracture toughness through the wall of the vessel was treated by calculating a root mean square average of the toughness distribution through the wall of the vessel. In this case the thermal gradient effect was included with the toughness variation due to the variations in the neutron fluence, which decreases from the vessel inside surface towards the outside surface.

#### ELASTIC-PLASTIC SOLUTIONS

The failure mode analyses involved predictions of stress intensity factors and crack opening areas for axial cracks. For elastic behavior, published fracture mechanics solutions were available for the vessel dimensions and crack lengths of concern to PTS. However, it was necessary to correct these solutions for plastic deformation. Figure 2 shows the "ad-hoc" plasticity correction factor developed as part of this study.

Finite element analysis for vessel parameters showed that the Battelle-Columbus Laboratory (BCL) strip yield model (Ref. 5) was inadequate. It was found that a modification of the BCL-type of analysis gave significantly

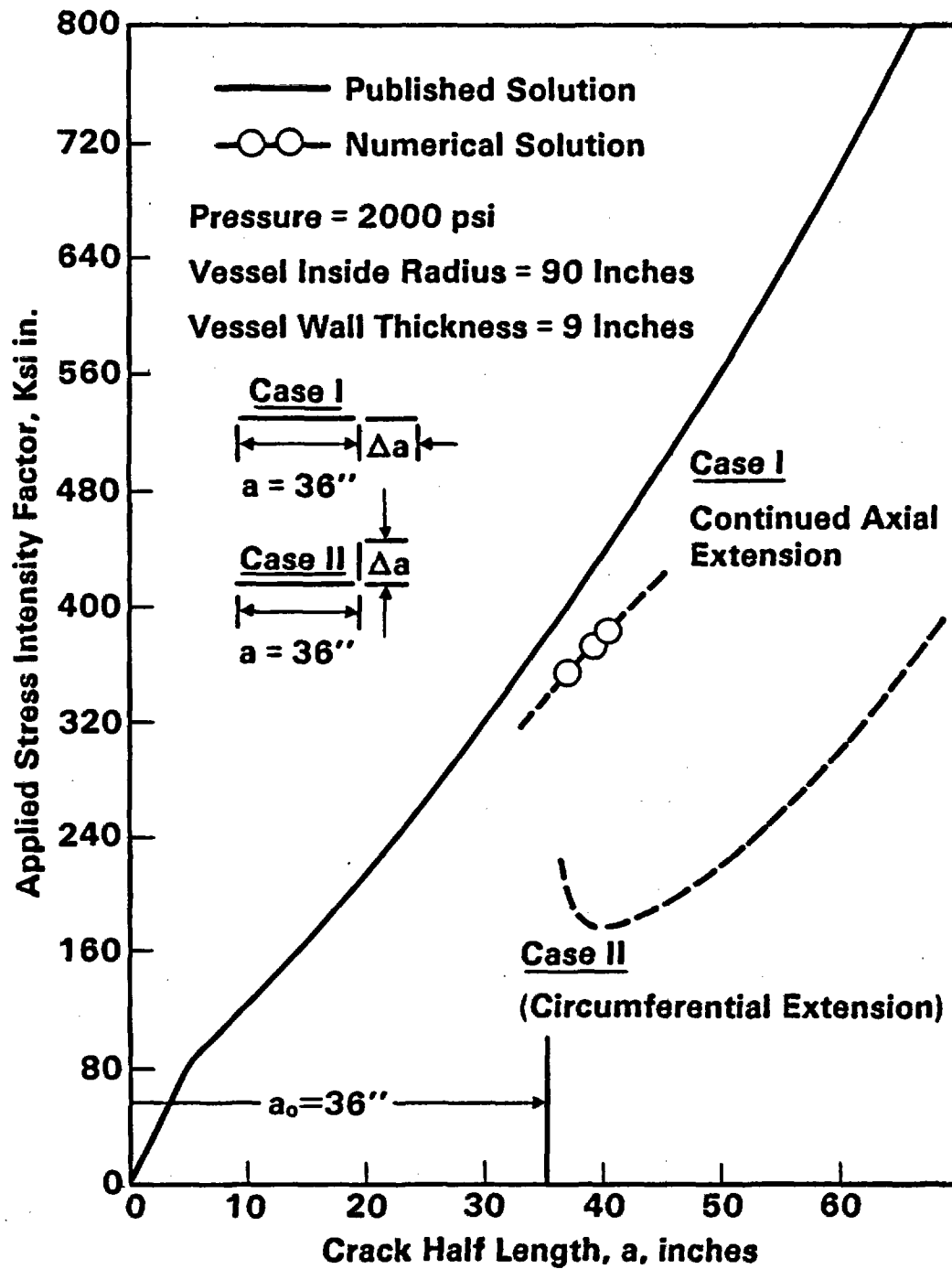


**FIGURE 1.** Comparison of Stress Intensities for Axial and Circumferential Crack Extensions

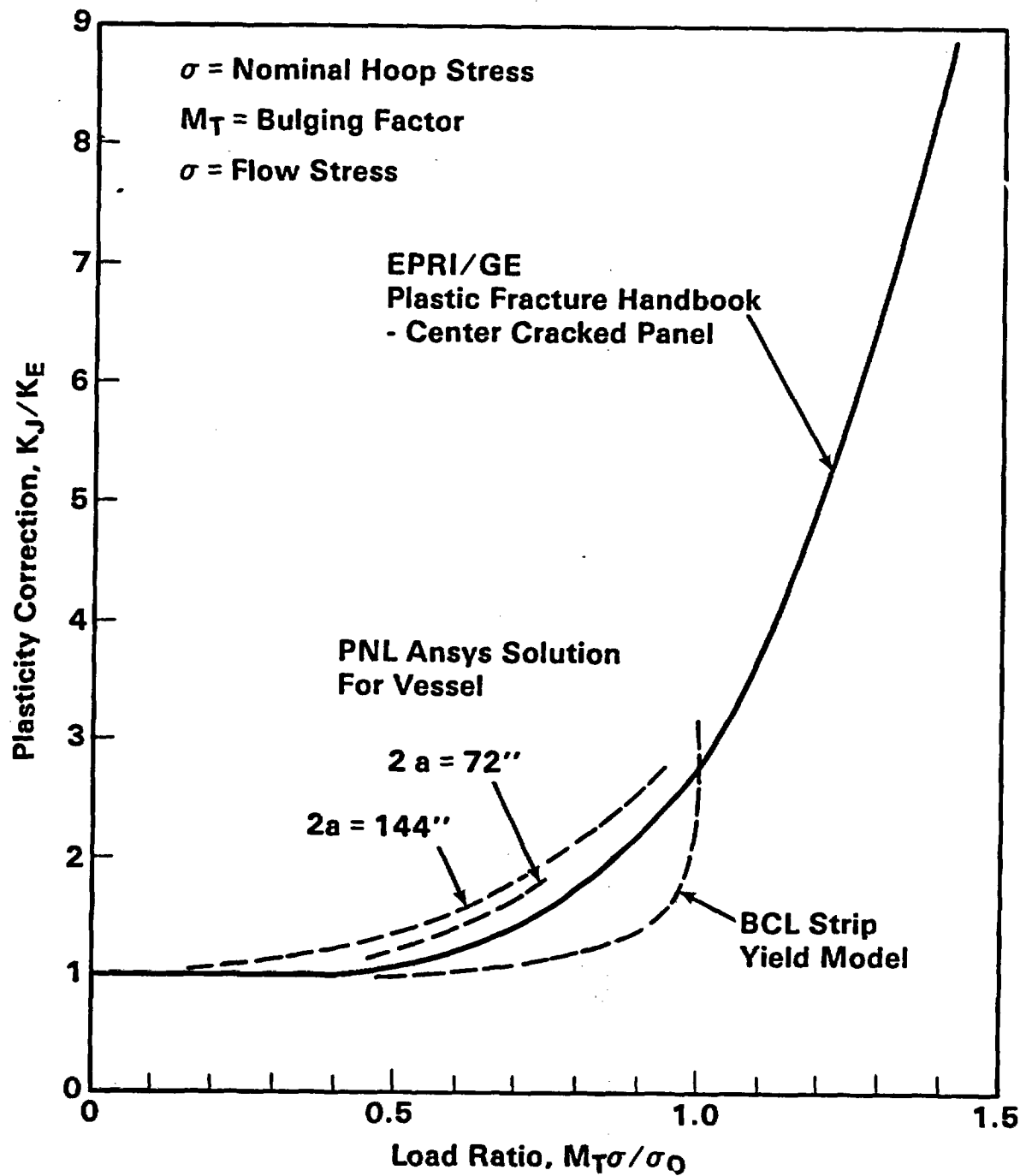


**FIGURE 2.** Plasticity Correction Factor for Pressure Vessel with Axial Crack improved predictions. The strip yield aspect of the model (based on flat plate solutions) was replaced as indicated in Figure 2 by results of more recent elastic plastic solutions from Reference 6.

## IRRADIATION DAMAGE

The present model uses the same equations for the shift in  $RT_{NDT}$  (reference temperature for nil ductility transition) as in the ORNL/IPTS evaluations (Ref. 3). However, it was also necessary to estimate the impact of irradiation on the upper shelf properties of Charpy Energy (CVN) and material flow stress.

Predictive equations for  $\Delta USE$  (change in upper shelf energy) and increase in flow stress were reviewed. For  $\Delta USE$ , equations from Reference 7 were selected:

$$\begin{aligned}\Delta USE (\%) &= (24.97 + 79.65 \text{ Cu} - 43.29 \text{ Si}) f^{0.15}, \text{ for welds} \\ &= (-1.19 + 102.49 \text{ Cu}) f^{0.27}, \text{ for plates}\end{aligned}$$

where: Cu = weight % copper  
Si = weight % silicon  
f = fluence,  $10^{19}$  n/cm<sup>2</sup>.

The increase in flow stress ( $\Delta\sigma_0$ , MPa) was taken to be the same as the increase in yield strength as predicted by Odette and Lombrozo (Ref. 8):

$$\begin{aligned}\Delta\sigma_0 &= 1.5 \Delta RT_{NDT} \\ \Delta RT_{NDT} &= \text{Shift in } RT_{NDT}, \text{ }^\circ\text{C}.\end{aligned}$$

## UPPER SHELF ANALYSIS

The use of elastic-plastic fracture mechanics has been accepted by NRC (Ref. 9) in the resolution of the A-11 issue and has been applied to predict fracture behavior of reactor vessels. Elastic-plastic methods were required in the present study to predict the continued growth and arrest of through-wall cracks into plates and welds of upper shelf materials. However, it was necessary to modify the methods of Reference (9).

The correlation of the J-resistance curve to the CVN energy was that given in Reference (9). This correlation predicted allowable values of  $K_J = \sqrt{EJ}$  which were about 200 ksi  $\sqrt{\text{in.}}$  for irradiated welds (CVN = 50 ft-lb). This is essentially the value used by ORNL for upper shelf toughness in linear elastic fracture mechanics evaluations. In contrast, the corresponding allowable  $K_J$  was about 700 ksi  $\sqrt{\text{in.}}$  for an unirradiated plate material with perhaps better than average toughness properties (CVN = 140 ft-lb).

The  $J_{50}$  approach for crack stability predictions was judged to be too conservative for the present probabilistic evaluations of through wall (as opposed to part-through flaws). Consequently the allowable value of applied J was that corresponding to  $\Delta a = 2.0$  inch of crack growth. There is some

limited data from large specimens (10) to support the CVN correlation of (9) to  $\Delta a = 2.0$  inch. Axial cracks were assumed to be stable for  $J$ -applied less than this allowable value of  $J$  unstable for greater values of  $J$ -applied. The arrest values of allowable  $J$ -applied were conservatively assumed to be the same as the initiation values.

### DYNAMIC EFFECTS

The sudden opening of an axial crack in a pressurized reactor vessel is a dynamic event. There will be dynamic interactions between the vessel and the pressurized water. A major effort was made to model these interactions, and typical results are summarized in Figure 3.

The detailed finite analyses supported the approximation that one can neglect dynamic effects. This trend is consistent with results for cracks in reactor piping (Ref. 11). Eventually the structural dynamic effects associated with the sudden opening of the crack is offset by the local depressurization of the fluid. In the simplified fracture mechanics model only static solutions are used, but for the full pressure that exists prior to any opening of the crack.

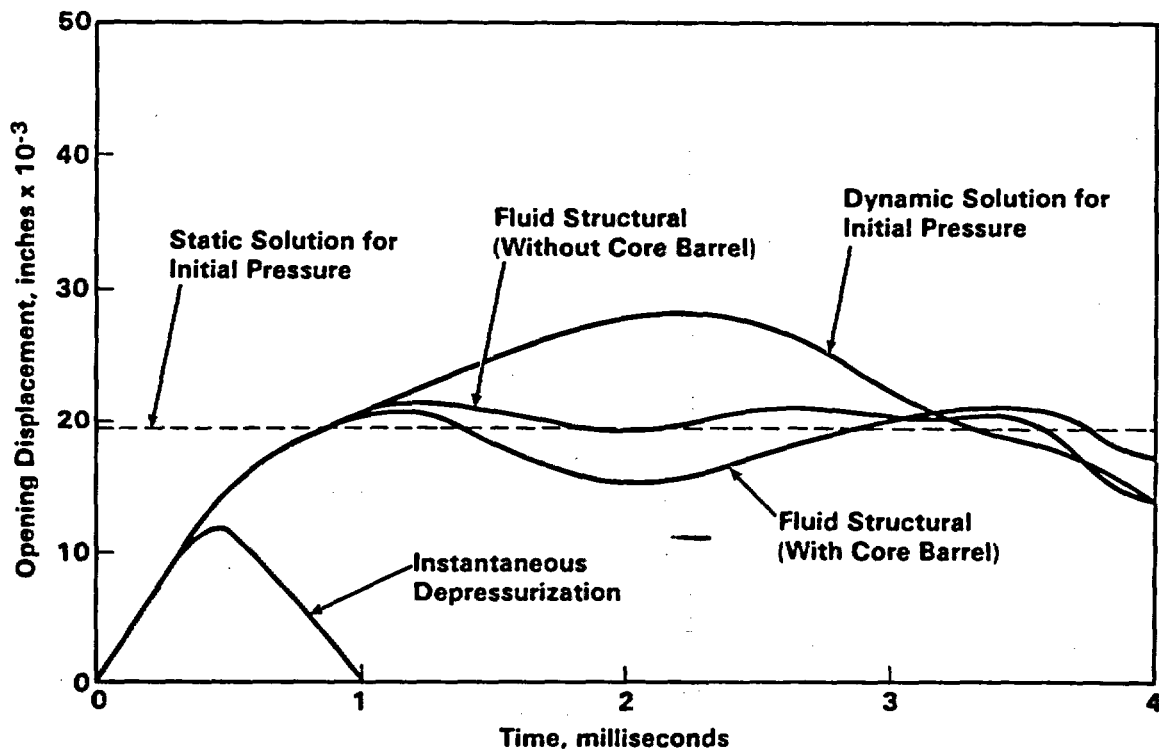


**FIGURE 3.** Fluid Structural Interaction for Opening of 72 Inch Long Crack

## LEAK RATE/DEPRESSURIZATION EFFECTS

The present evaluations of vessel failure modes treat the sustained leakage through an open axial crack that may occur once crack growth arrests. This leakage is balanced against the make-up of water from injection pumps. An equilibrium pressure is calculated and used to determine if an arrested crack may reinitiate later in a PTS transient.

A leak rate model was developed based on the flow of subcooled water through the crack. Existing equations for saturated flow through stress corrosion cracks (Ref. 12) were considered as an alternative but found to be inappropriate.

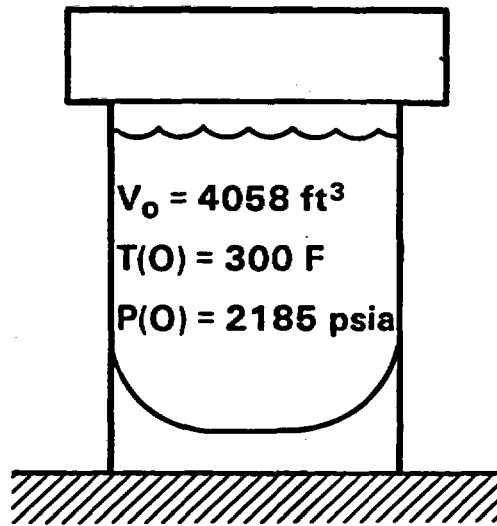
The depressurization model has been applied in evaluations of the Oconee-1 vessel. It appears that the leakage through an axial crack will result in a bleed-down in pressure to 200 psi within about 5 minutes. It is unlikely that the growth of arrested cracks will reinitiate for such a low level of pressure.

## MISSILE CONSIDERATIONS

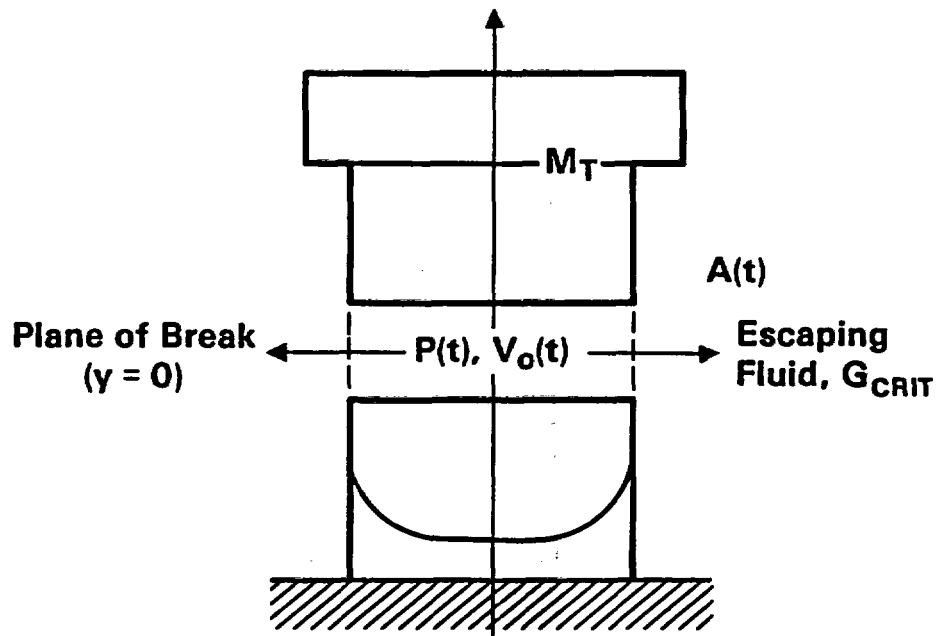
Two classes of missiles have been considered: i) a vertical missile resulting from the fracture of a circumferential weld, and ii) horizontal missiles resulting from the fragmentation of a vessel. It should be recognized that detailed analysis of fragmentation phenomenon are beyond the "state-of-the-art" in fracture mechanics modeling. Therefore, a range of missiles has been postulated which are consistent with empirical data. Calculations were then performed to determine if such missiles could penetrate and escape from the vessel cavity.

A complete fracture of a circumferential weld would result in a large fragment. Figure 4 shows how this missile was modeled for the bottom supported Oconee reactor vessel. Figure 5 shows results that predict the vertical acceleration and subsequent arrest of this upper head missile. In this worst case condition of maximum fluid thrust, a volume of steam is postulated within the upper portion of the vessel. Nevertheless, the restraint forces from the attached primary coolant loop piping is capable of arresting this worst case missile after less than a foot of vertical motion.

To define the sizes of horizontal missile fragments, a set of documents were collected to obtain data about both service failures and burst tests of vessels. In general, fragmentation occurs when the vessel is "brittle" and the pressurizing medium is "energetic" rather than hydraulic in nature. The results of our evaluation indicated that the vessels and fluid conditions of interest to the PTS issue fall somewhat short of observed fragmentation conditions. Nevertheless, a conservative evaluation was performed by assuming a spectrum of possible missiles.



(a) Initial Conditions ( $t = 0$ )



(b) After Rupture

**FIGURE 4.** Model of Ruptured Vessel

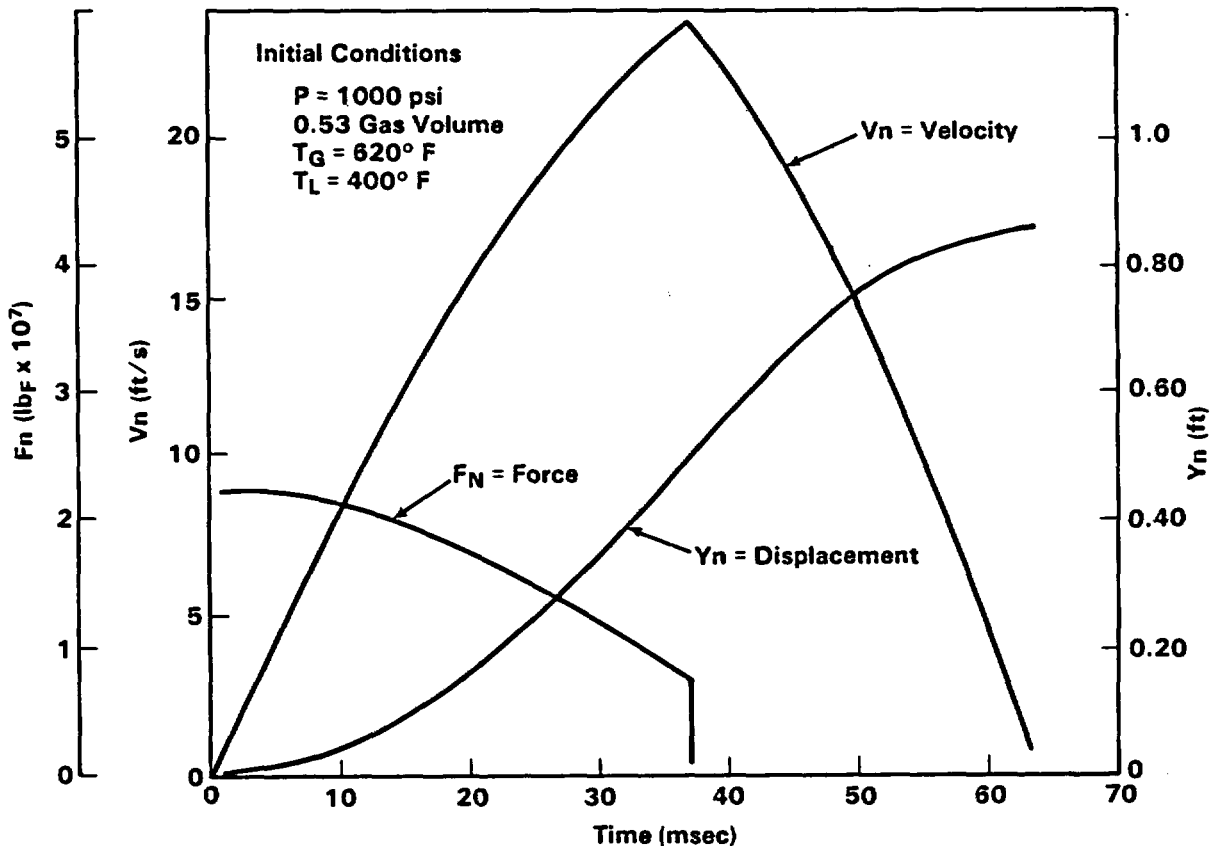


**FIGURE 5.** Force, Velocity, and Displacement Characteristics

Figure 6 shows a mass-velocity relationship, which was derived from an energy balance argument. The entire stored energy of compression of the 2000 psi subcooled fluid within the vessel was assumed to be transferred as kinetic energy to the missile. However, for small missiles (less than about 200 lb), the velocity is bounded by the free jet velocity of water through an opening in the vessel. It can also be noted in Figure 6 that this analysis predicts velocities for large missiles that are consistent with the more detailed upper head missile study.

Figure 7 shows calculated concrete penetration depths for a 1380 lb horizontal missile as a function of impact velocity. Other calculations predict that this penetration depth is relatively insensitive to missile weight. In effect, the greater mass of the larger missiles is offset by associated lower velocities. The 24x24 inch fragment of vessel wall was selected as perhaps a worst case. It is about as large a fragment that could rotate to an "edge-on" impact orientation within the confined space between the vessel and the surrounding concrete shield. The best estimate of the actual impact velocity (from Figure 6) is about 200 ft/sec. At this velocity, the 1380 lb fragment penetrates less than a foot of concrete, whereas the actual concrete thickness is on the order of 4 feet.

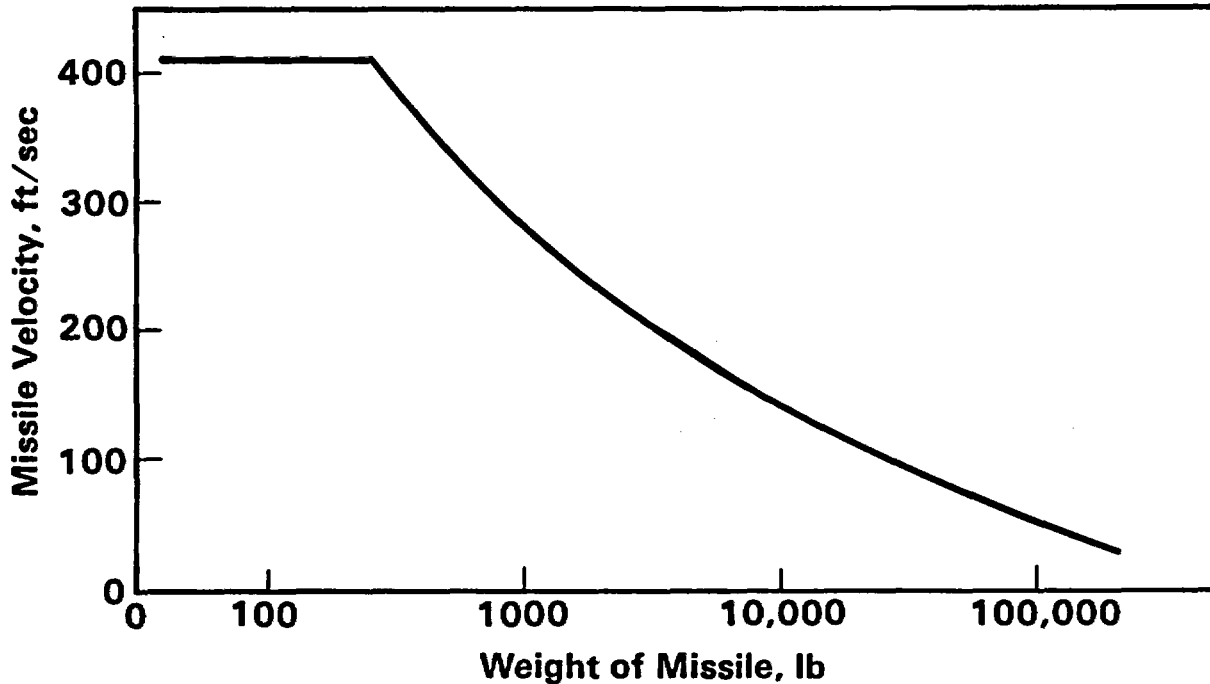


**FIGURE 6.** Velocity of Horizontal Fragments When Accelerated by 2000 psi Subcooled Water

#### PROBABILISTIC MODEL

The probabilistic model performs a Monte Carlo simulation of the growth of a through-wall crack in a reactor pressure vessel. In this model, the parameters that govern the fracture toughness of each weld and plate in the vessel are simulated as random variations. These simulations of toughness are performed in much the same manner as in ORNL's calculations for the IPTS Project (Ref. 3).

The essential assumption in the present probabilistic model is that there is no correlation between the random variations in properties of the various welds and plates of a given vessel. Such an assumption is believed to be reasonable since the different classes of materials of a given vessel (e.g. plates, axial welds and circumferential welds) are fabricated at different facilities and by different processes. The shift in  $RT_{NDT}$  is simulated by sampling from prescribed distributions of copper, fluence and initial  $RT_{NDT}$ . In a similar manner, upper shelf toughness is simulated through copper and fluence uncertainties. The simulation procedure was designed to be consistent with that used by ORNL to calculate probabilities of through-wall cracks (Ref. 3).

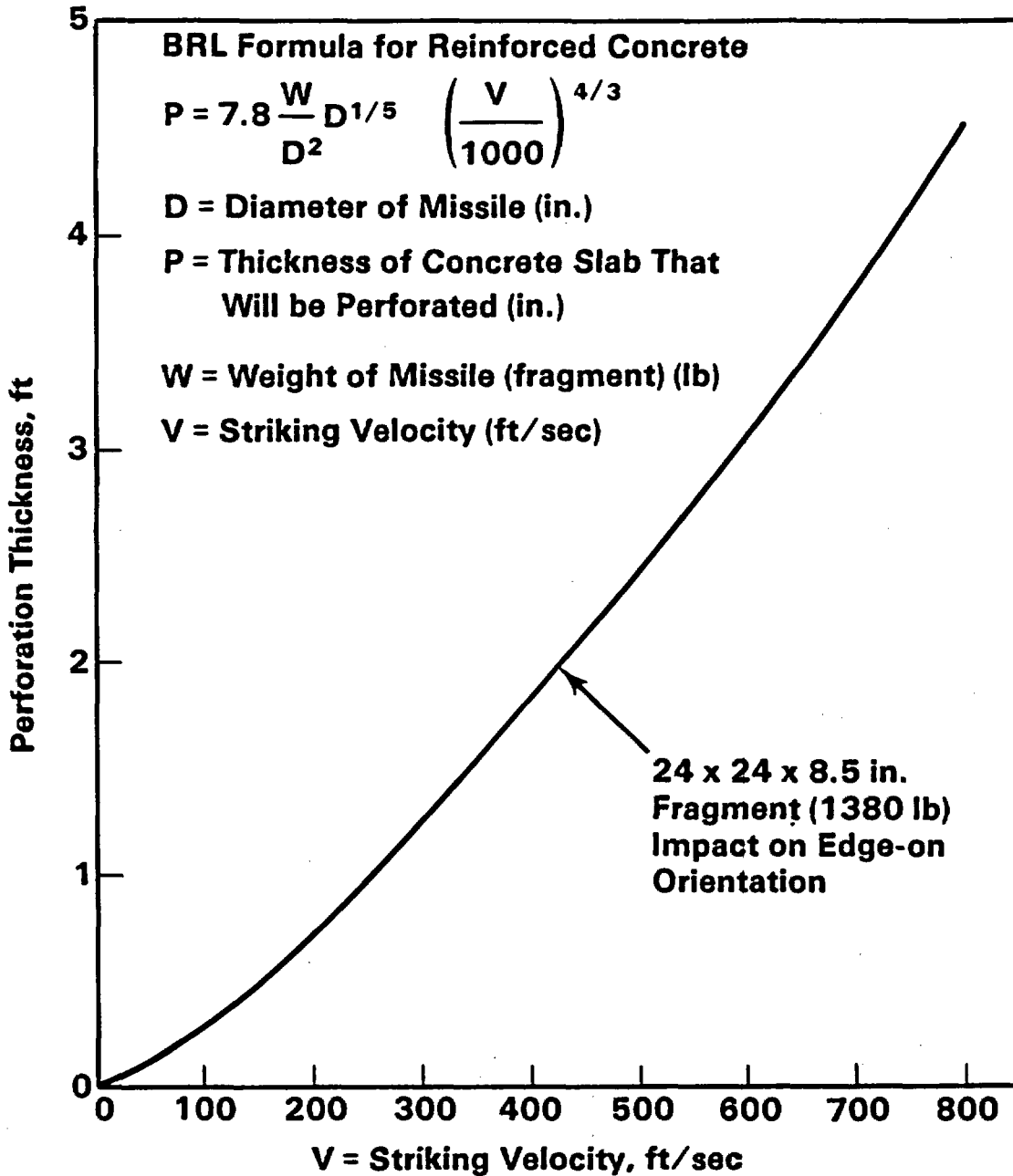


**FIGURE 7.** Penetration Potential of Representative Vessel Fragment in Horizontal Direction

Figure 8 is a flow chart of the probabilistic code. The inputs to this code are: 1) vessel dimensions, 2) elastic and thermal properties, 3) pressures and temperatures for the transient, 4) truncation values for  $K_{Ic}$  and  $K_{Ia}$ , 5) maximum  $\Delta a$  for the J-resistance curve 6) copper content, 7) nickel content, 8) flow stress, 9) initial  $RT_{NDT}$ , 10) fluence variation, 11)  $K_{Ic}$  variation, and 12)  $K_{Ia}$  variation.

The through wall axial crack is allowed to grow in the axial direction from node to node in analytical the model. Each node has its own material identification and fluence level. As such, there can be dramatic increases (and decreases) in material toughness from one node to the next node.

The final probabilistic inputs are the length of the axial crack and the time during the transient at which the crack attains a through-wall status. The primary outputs of the probabilistic code are as follows: 1) final crack opening areas, 2) final position of the ends of the axial crack, 3) locations of cracked circumferential welds, and 4) the time in the transient that the through-wall crack attain its final size. Each computer run treats 1) one fluence level, 2) one axial weld, and 3) one pressure-temperature transient. The relative contribution of each of these three items to the occurrence of through-wall cracking was obtained from the ORNL/IPTS calculations. The probabilities for each failure mode is obtained by combining the various conditional probabilities.

#### OCONEE-1 CALCULATIONS

The above fracture mechanics model was applied to the Ocone-1 vessel using the critical transients and through-wall crack probabilities from the ORNL/IPTS study (Refs. 2, 3). The material and property definitions for the Ocone vessel are given in Table 1. Figure 9 shows the arrangement of plates and welds for the vessel.

The outputs of the Ocone calculations were 1) probability of large axial or circumferential break, 2) probability of other less severe failure modes, and 3) missile characteristics and missile arrest.

Table 2 lists the critical transients from the ORNL study of the Ocone vessel (Ref. 2) and their fractional contributions to the probability of through-wall crack. Note that the numbers for each column of Table 2 sum to a total of 1.00. Transient 26 differs significantly from the other two transients. For transient 26, the through-wall cracks tend to occur at relatively low pressures. Consequently, transient 26 may be typical of a transient for which through-wall axial cracks do not extend beyond the length of a single axial weld.

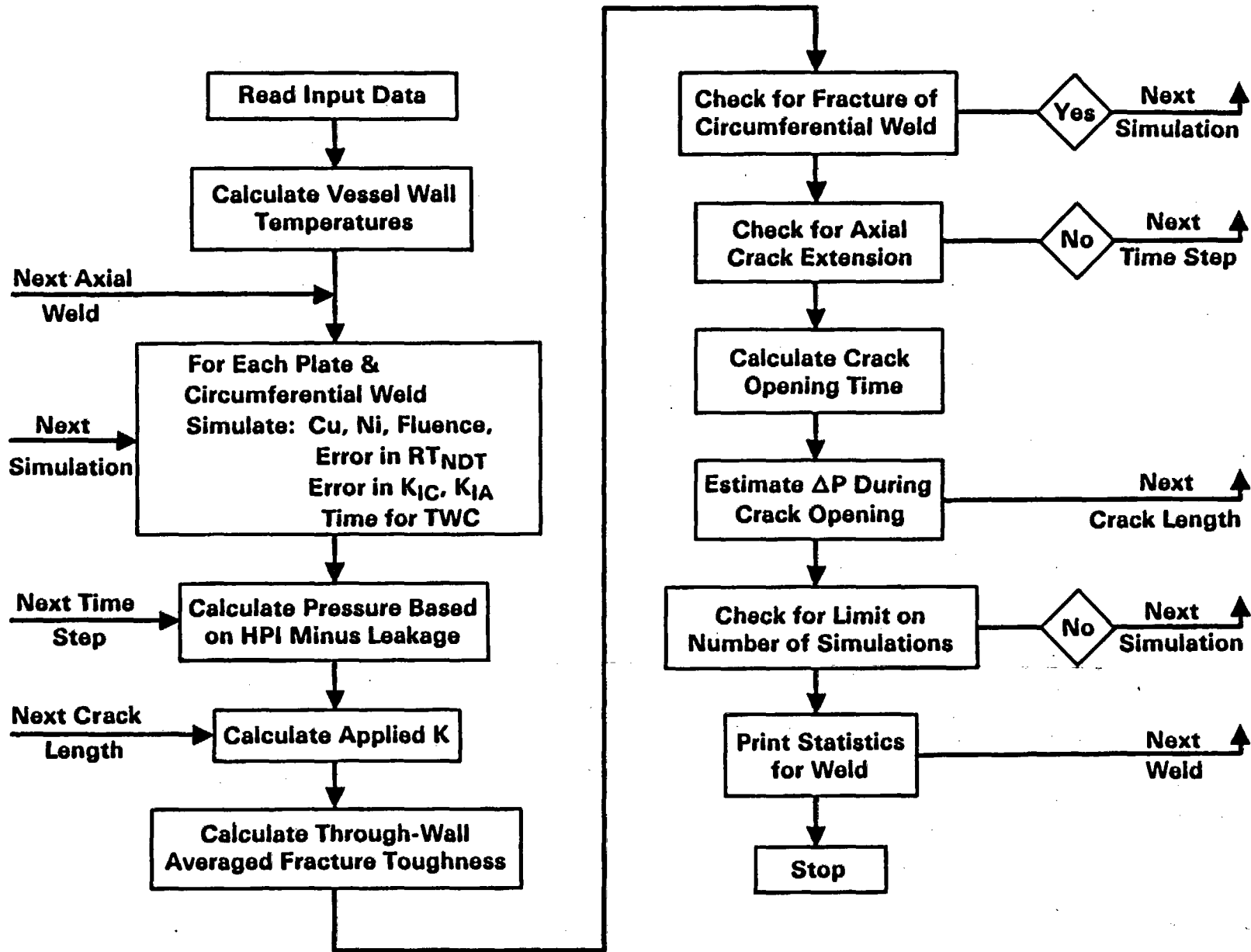
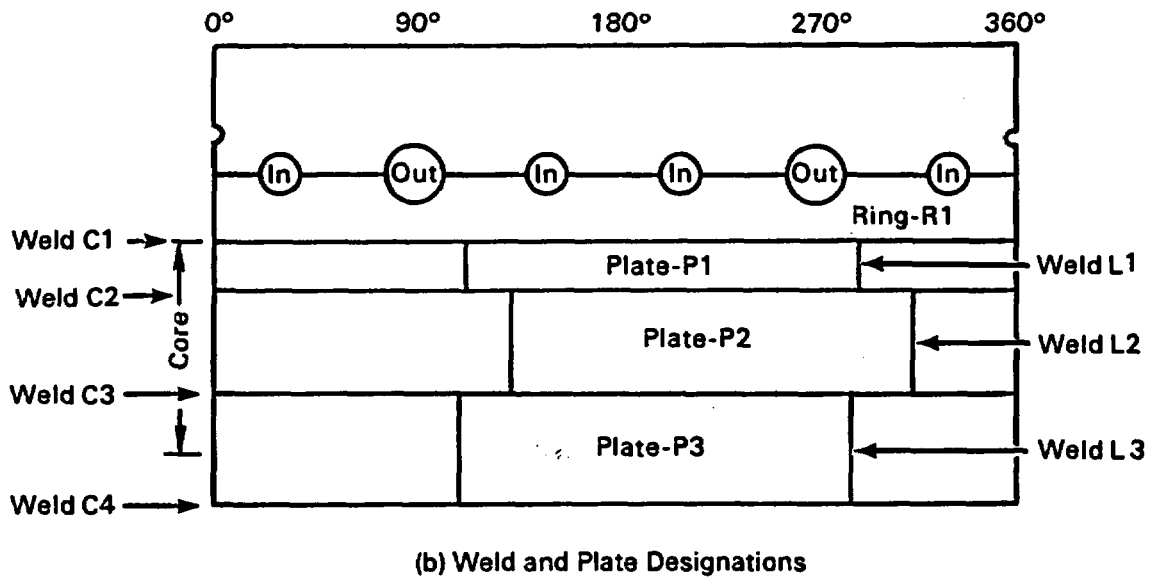
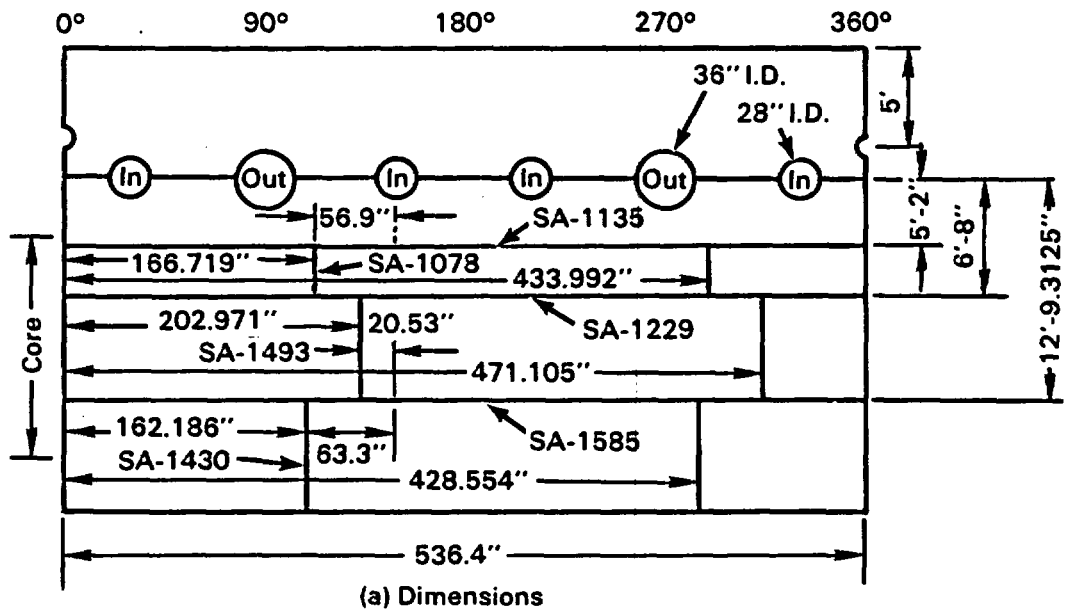


FIGURE 8. Flow Chart for Probabilistic Analysis of Vessel Failure Modes

**TABLE 1. Material Properties Used by PNL in Failure Mode Analysis of the Oconee-1 Vessel**

Material Number	Designation	Copper (wt%)		Nickel (wt%)		Initial RT <sub>NDT</sub> (°F)		σ of K <sub>IC</sub>	Silicon (wt%)	σ of K <sub>IC</sub>	σ of	Unirradiated Flow Stress (ksi)	Unirradiated Charpy Energy (ft-lb)	σ of Fluence,
		Mean	σ	Mean	σ	Mean	σ	(Fraction of Mean)		(Fraction of Mean)	ΔRT <sub>NDT</sub> (°F)			(Fraction of Mean)
1	L1	0.31	0.03	0.64	0.00	20.0	16.0	0.15	0.600	0.15	24.0	76.0	70.0	0.30
2	L2	0.29	0.03	0.55	0.00	20.0	16.0	0.15	0.600	0.15	24.0	76.0	70.0	0.30
3	L3	0.29	0.03	0.55	0.00	20.0	16.0	0.15	0.600	0.15	24.0	76.0	70.0	0.30
4	C1	0.25	0.03	0.54	0.00	20.0	16.0	0.15	0.600	0.15	24.0	76.0	70.0	0.30
5	C2	0.26	0.03	0.61	0.00	20.0	16.0	0.15	0.600	0.15	24.0	76.0	70.0	0.30
6	C3	0.21	0.03	0.59	0.00	20.0	16.0	0.15	0.600	0.15	24.0	76.0	70.0	0.30
7	C4	0.31	0.03	0.59	0.00	20.0	16.0	0.15	0.600	0.15	24.0	76.0	70.0	0.30
8	R1	0.16	0.03	0.60	0.00	60.0	10.0	0.15	0.600	0.15	12.0	76.0	120.0	0.30
9	P1	0.15	0.03	0.60	0.00	40.0	10.0	0.15	0.600	0.15	12.0	76.0	120.0	0.30
10	P2	0.12	0.03	0.60	0.00	40.0	10.0	0.15	0.600	0.15	12.0	76.0	120.0	0.30
11	P3	0.11	0.03	0.60	0.00	40.0	10.0	0.15	0.600	0.15	12.0	76.0	120.0	0.30



**FIGURE 9.** Developed View of Inner Surface of Ocone-1 Reactor Vessel Showing Weld Locations

**TABLE 2. Critical Transients Used in Failure Mode Analysis of the Oconee-1 Vessel**

<u>Transient</u>		<u>Fractional Contribution to Probability of Through-Wall Crack</u>	
<u>Number</u>	<u>Designation</u>	<u><math>f = 0.545 \times 10^{19}</math></u>	<u><math>f = 1.417 \times 10^{19}</math></u>
44	TBV(6A) or LANL10	0.77	0.53
26	MSLB1	0.14	0.29
4	TBVG4	0.09	0.18

Table 3 and Figure 10 summarize the results of the failure mode calculations for the Oconee vessel. These results show the following trends.

1. About 50% of the through-wall axial cracks extend and follow a circumferential weld.
2. For most other cases, the axial cracks arrest at the length of the axial weld and do not extend either into the adjacent plate material nor does the crack follow the adjacent circumferential weld.
3. Cracks tend to arrest for short axial welds (weld L1) and low pressure transients (transient 26).
4. Missiles that may result from fracture of the Oconee-1 vessel will be confined to the vessel cavity.

#### ACKNOWLEDGEMENTS

The author gratefully acknowledges the contributions of other PNL staff members. Foremost among these other PNL staff are L. T. Pedersen (Project Manager), Mark Garnich (finite element calculations), S. H. Bian and K. Nomura (fluid mechanics), E. P. Simonen (material properties), and W. E. Anderson (fracture mechanics).

NRC staff providing encouragement and support include R. Woods (Task Action Manager for Issue A-49), M. Vagins, J. Strosnider, C. E. Johnson, and R. E. Johnson. From Oak Ridge National Laboratory, J. G. Merkle, R. D. Cheverton and D. G. Ball provided valuable input and advice. Finally, it was a privilege to discuss many of the difficult fracture mechanics issues with Dr. G. R. Irwin at the University of Maryland.

**TABLE 3. Results of Failure Mode Analyses for Individual Welds and Transients (for Fluence of  $1.417 \times 10^{19}$  at Weld SA1430)**

**(a) Transient #44/TBV(6A)/LANL10**

Axial Weld	Contribution of weld to $\phi$ (TWC), fraction of total	Vessel Failure Mode - (Fraction of Total)					
		Circumferential Failures (Weld Location)			Axial Failures Opening Area, in <sup>2</sup>		
		C1 @ 64"	C2 @ 46"	C3 @ 26"	0 to 10	10 to 100	100 to 1000
L1	0.13	0.050	0.080	0.055	0.815	0.0	0.0
L2	0.38	0.0	0.625	0.375	0.0	0.0	0.0
L3	0.49	0.0	0.130	0.355	0.175	0.0	0.340

**(b) Transient #26/MSLB1**

Axial Weld	Contribution of weld to $\phi$ (TWC), fraction of total	Vessel Failure Mode - (Fraction of Total)					
		Circumferential Failures (Weld Location)			Axial Failures Opening Area, in <sup>2</sup>		
		C1 @ 64"	C2 @ 46"	C3 @ 26"	0 to 10	10 to 100	100 to 1000
L1	0.15	0.0	0.0	0.0	1.000	0.0	0.0
L2	0.31	0.055	0.170	0.120	0.645	0.0	0.10
L3	0.54	0.0	0.0	0.005	0.995	0.0	0.0

**(c) Transient #4/TBVG4**

Axial Weld	Contribution of weld to $\phi$ (TWC), fraction of total	Vessel Failure Mode - (Fraction of Total)					
		Circumferential Failures (Weld Location)			Axial Failures Opening Area, in <sup>2</sup>		
		C1 @ 64"	C2 @ 46"	C3 @ 26"	0 to 10	10 to 100	100 to 1000
L1	0.13	0.010	0.020	0.025	0.945	0.0	0.0
L2	0.35	0.005	0.625	0.370	0.0	0.0	0.0
L3	0.52	0.0	0.120	0.205	0.270	0.0	0.405

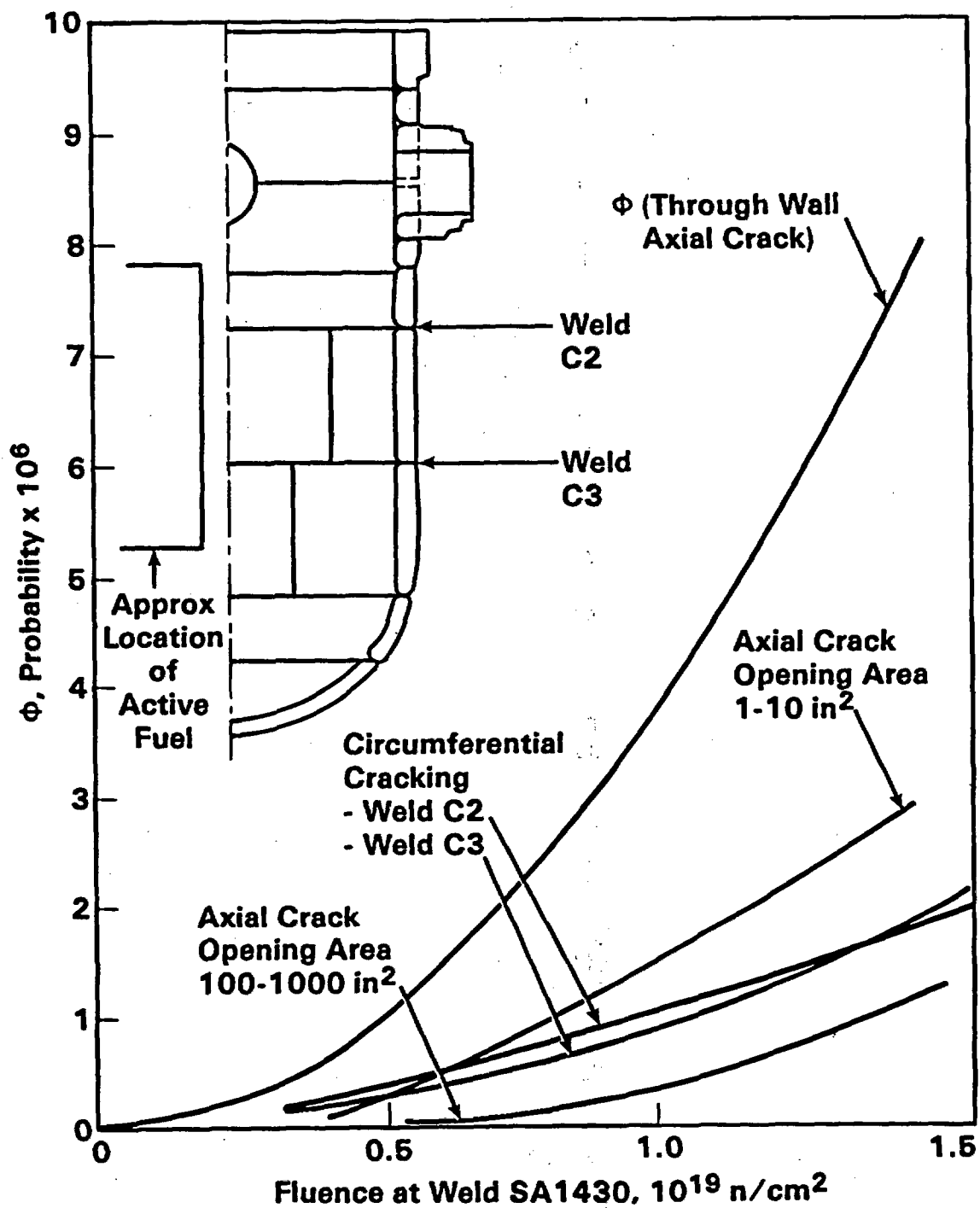


FIGURE 10. Oconee-1 Failure Mode Prediction

## REFERENCES

1. White, J. D. 1983. "Integration of PTS Studies to Calculate Through-Wall Crack Probabilities", NUREG/CP-0047, Trans. of the Eleventh Water Reactor Safety Research Information Meeting, Gaithersburg, Maryland, October 24-28, 1983.
2. White, J. D. 1984. "Results of PTS Probabilistic Analysis Based on Oconee, Calvert Cliffs and H. B. Robinson", Proceedings of the Twelfth Water Reactor Safety Research Information Meeting, Gaithersburg, Maryland, October 22-26, 1984.
3. Cheverton, R. D. 1984. "PTS Fracture Mechanics Methodology and Conclusions", Proceedings of the Twelfth Water Reactor Safety Research Information Meeting, Gaithersburg, Maryland, October 22-26, 1984.
4. Hassan, M. A., S. L. Pu, and J. Underwood. 1974. "Strain Energy Release Rate for a Crack Under Combined Mode I and Mode II", Fracture Analysis ASTM STP 560, American Society for Testing and Materials, pp. 2-28.
5. Maxey, W. A., J. F. Kiefner, R. J. Eiber, and A. R. Duffy. 1971. "Ductile Fracture Initiation, Propagation, and Arrest in Cylindrical Vessels", Fracture Toughness, Proceedings of the 1971 National Symposium on Fracture Mechanics, Part II, ASTM STP-415, American Society for Testing and Materials.
6. Kumar, J., M. D. German and C. F. Shih. 1981. "An Engineering Approach for Elastic-Plastic Analysis", EPRI NP-1931, Electric Power Research Institute, Palo Alto, California.
7. "Evaluation of Irradiation Response of Reactor Pressure Vessel Materials", EPRI NP-2720, submitted by Combustion Engineering, Inc., to Electric Power Research Institute, November 1982.
8. Odette, G. R. and P. Lombrozo. 1983. "A Physically Statistically Based Correlation for Transition Temperature Shifts in Pressure Vessel Surveillance Welds," Transactions of the American Nuclear Society, pp. 224-225, June 1983.
9. Johnson, R. 1982. "Resolution of the Task A-11 Reactor Materials Toughness Safety Issue," NUREG-0744, October 1982.
10. Shih, C. F. and W. R. Andrews. 1981. "Methodology for Plastic Fracture", EPRI NP-1735, Electric Power Research Institute, Palo Alto, California, March 1981.

11. Ayres, D. J. 1975. "Elastic-Plastic Dynamic Analysis of Opening Area of an Axial Crack in a Pipe Under Pressure", Paper L-716, 3rd International Conference on Structural Mechanics in Reactor Technology, London, U.K., September 1975.
12. Mayfield, M. E., et al. 1980. "Cold Leg Integrity Evaluation", NUREG/CR-1319, February 1980.

## "Consequence Evaluation for Pressurized Thermal Shock"

Richard J. Barrett  
Edward D. Throm  
Reactor Systems Branch  
Division of Systems Integration  
Office of Nuclear Reactor Regulation  
U.S. Nuclear Regulatory Commission

The purpose of this paper is to illustrate the logic and methods required to estimate the societal consequences of a large break LOCA resulting from pressurized thermal shock (PTS). The analysis includes an assessment of containment response, radionuclide behavior and offsite consequences. Our intent is to demonstrate the type of analysis that might be performed for a plant that is approaching the PTS screening criterion. Much of the data and many of the assumptions used in our analysis are based on experience with previous risk studies. Hence, the results are approximate. A licensee performing a PTS risk study would be expected to use more accurate data and plant specific calculations as the basis for a consequence analysis.

The containment and site characteristics are intended to model Oconee Unit 1, a plant for which the frequency and phenomenology of PTS events have been studied in some detail (references 1 and 2). Much of the data we use is taken from two probabilistic assessments for Oconee Unit 3 (references 3 and 4). Although there are differences between the plants, we have assumed that the Unit 3 data are applicable to unit 1.

The ORNL estimates of through wall crack frequency as a function of time are shown in figure 1. The values range from the current value of  $5 \times 10^{-7}$  per reactor year (at 10 effective full power years) to an end of life value of  $5 \times 10^{-6}$  (32 EFPY). The end of life  $RT_{NDT}$  approaches the 210°F mean surface screening criterion. An approximate average value of  $3 \times 10^{-6}$  is used in this paper. The PNL report (reference 2) estimates about a 50% chance that the event will lead to failure of a circumferential weld, and a 50% chance that the crack will arrest at the end of axial weld, of which 20% may result in large break area. For the purpose of this paper, we assume that all these events lead to core melt.

Given a core melt, the estimation of risk involves several major steps. First we must define the plant damage state, which describes the status of the primary system and major safety systems. Based on the plant damage states one can deduce the containment response and the magnitude of the radiological releases. Finally, using the calculated releases, we estimate the offsite consequences.

### Plant Damage States

For the purpose of calculating containment response to a core melt accident, the accident sequences are generally grouped into categories called plant damage states. The categories are defined according to those parameters which

affect containment response. Among the important parameters are, the mode of reactor coolant system (RCS) depressurization (blowdown or boildown), the RCS pressure at the time of vessel failure, the amount of water in the reactor cavity at the time of failure, and the status of operation of containment heat removal. There are also special Plant Damage States for sequences in which containment is bypassed.

Because the core melt results from a large break LOCA, the RCS would depressurize primarily due to blowdown and the RCS pressure would be low at the time when the molten core melts through the bottom of the reactor vessel. Because core injection and containment sprays would be operable in almost all cases, the cavity is assumed to be always full of water. Consequently, the most important distinction to make in the plant damage states is whether or not containment heat removal operates following core melt. Plant damage state AC is defined as a LBLOCA with containment heat removal, and plant damage state A is LBLOCA without heat removal.

Two special plant damage states involving containment bypass are also included. Plant damage states V and V<sub>2</sub> designate bypass of containment by way of interfacing systems LOCA and steam generator tube ruptures, respectively. The tube rupture can either be an initiating event or a consequence of the PTS event. The plant damage states are summarized in Table 1.

Table 1  
Plant Damage States

- A - LBLOCA with no containment heat removal.
- AC - LBLOCA with successful containment heat removal.
- V - Containment bypass due to interfacing systems LOCA as a result of the PTS event.
- V<sub>2</sub> - Containment bypass due to steam generator tube rupture, either as the event initiator or as a consequence of the PTS event.

#### Plant Damage State Frequencies

The Oconee 3 plant, like most other PWR plants with large dry containments, has two diverse means of containment heat removal: fan coolers and sprays. The Oconee 3 RSSMAP study (reference 3), funded by NRC, evaluated the failure modes and probabilities for failure of the sprays during the injection and recirculation phases, and for failure of the fan coolers. Using the assumption that these system failure rates are independent of the initiating event and that there is not a station blackout, the spray failure probability was estimated at  $3.3 \times 10^{-3}$  during the injection phase, with an additional probability of  $6.9 \times 10^{-3}$  of failure during recirculation. The failure probability of the fan cooler system was estimated at  $1.6 \times 10^{-3}$ . If we were to assume complete independence of these two failure probabilities, the likelihood of both systems failing would be less than  $10^{-4}$ . For the purpose of this study, however, we assume a probability of  $10^{-3}$  for loss of containment heat removal. This approach was taken in order to account for unidentified common modes of failure, perhaps related to the PTS event phenomenology. Moreover, it will be shown

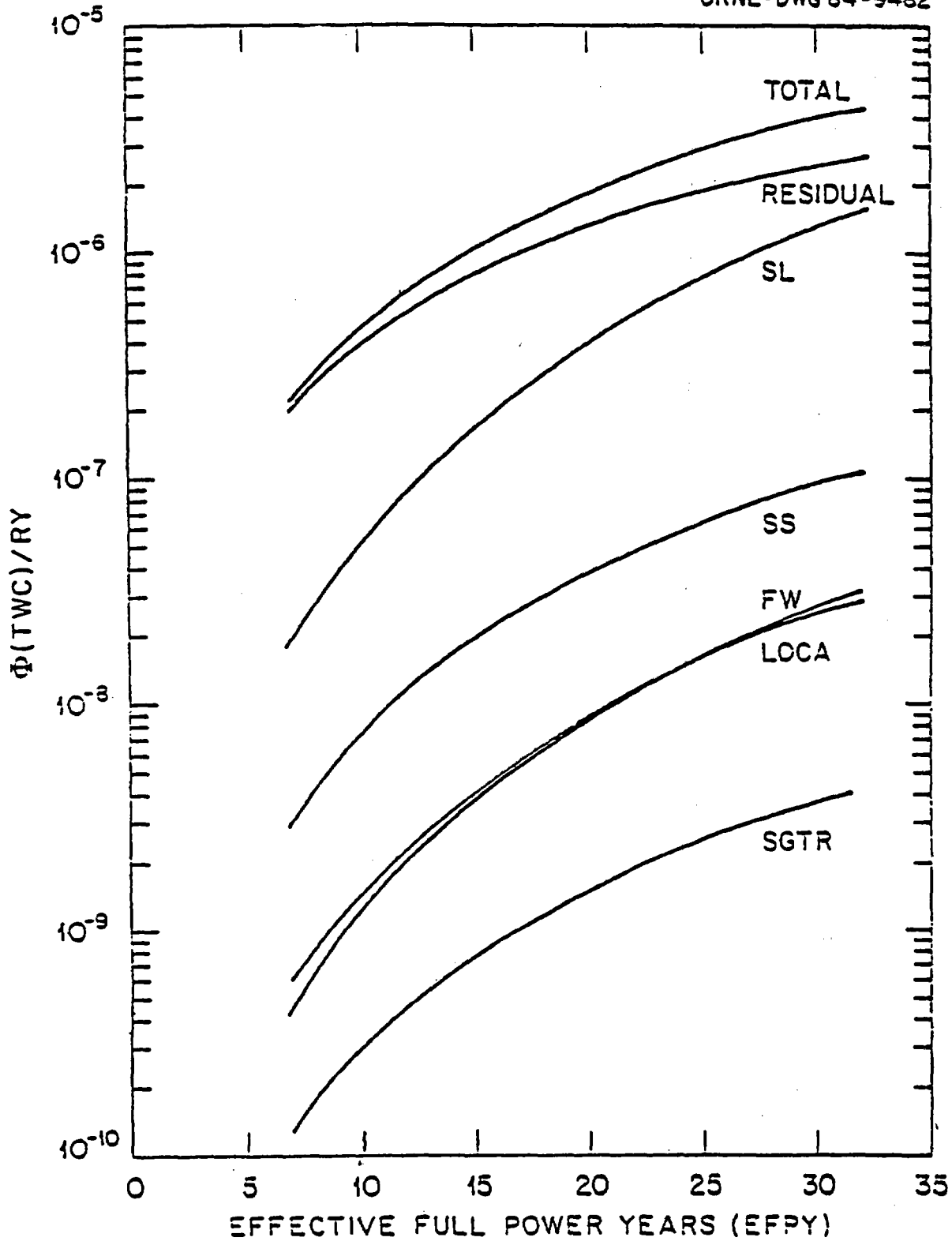


Figure 1 . Total and component frequencies of vessel through wall crack as a function of effective full power years.

that the results are insensitive to the choice of a lower failure probability. For the purpose of a plant specific analysis, the licensee should examine failure modes for heat removal, such as clogging of the filters in the fan coolers or missile damage.

The probability of a PTS event leading to a LOCA outside of containment (V sequence) is judged to be very low. Structural mechanics analyses conducted by PNL concluded that there would be minimal motion of the reactor vessel due to the loads caused by failure of the circumferential welds. The probability that this motion would lead to a break in the small piping of the reactor coolant system is low, and, if one were to occur, the most likely location would be inside containment. We have assigned a conditional probability of  $10^{-3}$  to the V plant damage state. This probability should be evaluated for each plant.

For similar reasons, we assign a  $10^{-3}$  likelihood that the PTS event will result in a steam generator tube rupture. Moreover approximately one in a thousand PTS core melt events is presumed to be initiated by a steam generator tube rupture (reference 1). Therefore, we assign a conditional probability of  $2 \times 10^{-3}$  for the V<sub>2</sub> plant damage state.

The remainder of PTS core melt accidents are assumed to result in the AC plant damage state. The conditional plant damage state frequencies are given in Table 2.

Table 2  
Conditional Probabilities of Plant Damage States  
for PTS Core Melt Accidents

<u>PDS</u>	<u>Conditional Probabilities</u>
A	.001
AC	.996
V	.001
V <sub>2</sub>	.002

Containment Response

The Oconee containment is a large dry design constructed of reinforced concrete with a ½" steel liner. The free volume is 2.05 million cubic feet. The design pressure is 74 psia, and the median failure pressure has been estimated to be in excess of 165 psia (reference 4).

There are numerous postulated failure mechanisms for containment. We will discuss each failure mode and assign a conditional probability of each plant damage state resulting in that failure. Together, these conditional probabilities comprise the C-matrix shown in table 3.

Table 3

## Containment Failure Matrix (C-matrix)

Plant Damage State/Mode	Failure				V	V <sub>2</sub>	no failure
	$\alpha$	$\delta$	$\gamma$	$\beta$			
A	10 <sup>-4</sup>	1.0		10 <sup>-2</sup>			
AC	10 <sup>-4</sup>			10 <sup>-2</sup>			1.0
V					1.0		
V <sub>2</sub>						1.0	

The interfacing systems LOCA and the steam generator tube rupture events result in bypass of the containment. Each of these events is carried as a unique containment failure mode (V and V<sub>2</sub>), and assigned a conditional probability of one.

For the A and AC plant damage states the picture is much more complicated. Several modes of containment failure are possible.

The  $\alpha$  failure mode refers to direct containment failure by missile penetration. Missiles could be generated in a PTS event, but reference 2 concludes that they would all remain within the reactor cavity. A second mechanism for generating missiles would be steam explosions in the reactor vessel after core melt. The NRC staff recognizes that steam explosions are likely to occur, but we place a very low likelihood on the  $\alpha$  failure mode. In several recent risk studies (for Zion, Indian Point and Millstone 3) we have assumed a conditional probability of 10<sup>-4</sup>. We also assume that value here. The probability of missiles which penetrate containment should be examined on a plant specific basis.

Steam production from reaction of molten fuel with water in the reactor cavity can fail the containment by overpressurization ( $\delta$  failure). This would occur only when containment cooling is lost, and would require at least 8 hours to reach the failure pressure. With containment cooling, the pressure in containment is likely to remain below 25 psia. If there is no source of water for steam production, the containment can be overpressurized by noncondensable gas production due to reaction of the fuel with the concrete in the reactor cavity. The rate of pressurization by noncondensibles is much slower, leading to failure after a day or longer. We assigned  $\delta$  conditional failure probabilities of zero for plant damage state AC and one for plant damage state A.

Hydrogen is produced on a continuous basis throughout the course of a severe accident. Hydrogen burns can produce large pressure spikes. If containment heat removal is in operation, there will be hydrogen burns, but their magnitude will fall short of the energy required to take the containment pressure from 25 psia to the failure pressure of 165 psia (the magnitude is limited by the mass of oxygen in containment). If containment heat removal fails, the steam in containment will suppress hydrogen burn propagation. We assign zero conditional probability of hydrogen burn failure ( $\gamma$  failure).

Failure of the operators to isolate the large leak paths from containment can lead to an early release of radionuclides from containment with no warning time for evacuation ( $\beta$  failure). In several recent PRA's for large dry containments, the conditional probability of this release has been estimated at  $10^{-2}$ . Basemat meltthrough ( $\epsilon$  failure) is a relatively benign failure mode. If sprays are available, we assume basemat melt-through is precluded. For the A sequence, we have already assumed the more serious  $\delta$  failure mode will occur.

The containment failure matrix is summarized in Table 3.

Given the containment failure matrix in Table 3 and the plant damage state frequencies in Table 2, one can relate core melt frequency to containment failure modes. In Table 4, we show the frequencies of containment failure modes with two assumptions for core melt frequency; the average core melt frequency for Oconee 1 operation ( $3 \times 10^{-6}$  per reactor years) and the estimated core melt frequency for the hypothetical situation in which Oconee 1 has exceeded the screening criterion ( $6 \times 10^{-6}$  per reactor year).

### Radiological Source Terms

The radiological release fractions for various containment failure modes have been calculated as part of the NSAC/Duke Power PRA for Oconee 3 (reference 4). The calculations were performed with the CORRAL code, and the calculated release fractions are comparable to those used in the Reactor Safety Study (reference 5). Table 5 lists the important source term information for each failure mode; namely, the release fractions for each class of radionuclides, the warning time and the energy of the release. The NSAC study did not specify a source term for the  $\alpha$  failure mode, because of the low probability of such an event. We will discuss the  $\alpha$  failure mode in the section on sensitivity analysis.

The overpressure source term in Table 5 is defined conservatively insofar as it refers to early overpressure failure, whereas we would expect late overpressure failure for a PTS event in Oconee.

The NSAC/Duke Power analyses of containment response, radiological releases and offsite consequences have not been reviewed by the NRC staff. They are quoted here because the study used standard methods and because the results appear reasonable and are comparable to results from previously reviewed risk studies.

Table 4

Estimated Frequencies of Containment Failure Modes (per reactor year)

	<u>Estimated Oconee Operating Lifetime Average</u>	<u>Oconee Operation Beyond the Screening Criterion</u>
$\alpha$	$3 \times 10^{-10}$	$6 \times 10^{-10}$
$\delta$	$3 \times 10^{-9}$	$6 \times 10^{-9}$
$\beta$ (with sprays)	$3 \times 10^{-8}$	$6 \times 10^{-8}$
V	$3 \times 10^{-9}$	$6 \times 10^{-9}$
V <sub>2</sub>	$6 \times 10^{-9}$	$1 \times 10^{-8}$
No Failure	$3 \times 10^{-6}$	$6 \times 10^{-6}$

Table 5

Radiological Release Characteristics For Various Containment Failure Modes

Release Category	Containment Failure Modes	Warning Time (hr)	Release Energy (10 <sup>6</sup> Btu/hr)	Release Fractions						
				Xe-Kr	I	Cs	Te	Ba	Ru	La
1A	δ	1.5**	289(77)†	1.0	0.61	0.66	0.7	0.072	0.13	8.8(-3)*
2	β (no sprays) V V <sub>2</sub>	0.5	33	1.0	0.31	0.32	0.3	0.036	0.027	4.1(-3)
3	β (with sprays)	0.5	33	1.0	0.041	0.011	0.01	1.4(-3)	8.4(-4)	1.4(-4)

\*8.8(-3) = 8.8 x 10<sup>-3</sup> = 0.0088

†The 1A release consists of an early puff followed by a more gradual low energy release.

\*\*Release categories were extracted from the NSAC sponsored PRA. More definitive PTS work would model late containment failure and hence extended warning time.

## Consequence Analysis

Given a set of radiological release fractions, determination of the offsite consequences requires a set of calculations with a consequence analysis code such as CRAC. Such an analysis requires detailed demographic and meteorological data for the plant site, as well as a model for the emergency response to a severe accident. For the purpose of this paper, we have used the conditional consequences calculated in reference 4. The mean values of conditional consequences listed in Table 6 are approximate values based on examination of complementary cumulative distribution functions in reference 4. They are comparable in magnitude to consequences calculated for other plants which have been reviewed by the NRC staff.

The values for early fatalities are representative of scenarios in which the emergency response plan is put into operation. If evacuation is impaired, as may be the case for seismically initiated events, the conditional values of early fatalities can be much greater.

For a plant specific analysis, it is very important to accurately estimate the evacuation response, as this is an important factor in determining early fatalities.

Table 6

Conditional Mean Values of Offsite Consequences for Various Containment Failure Modes

Release Category	Failure Mode	Early Fatalities (per event)	Latent Cancer Fatalities (per event)	Public Exposure (Person-Rem per event)
1A	$\delta$	50	$10^4$	$6 \times 10^7$
2	$\beta$ (no sprays) V V <sub>2</sub>	10	$5 \times 10^3$	$2 \times 10^7$
3	$\beta$ (with sprays)	—	$5 \times 10^2$	$2 \times 10^6$

### Risk Estimates

The failure frequencies of Table 4 were weighted with the estimated consequences in Table 6 to calculate the risk of early and latent fatalities and public radiation exposure (Table 7). These risks are minimal by almost any standard. For instance, the NSAC/Duke Power report estimates the background rate of accidental fatalities within ten miles of the plant to be about 30 per year. The estimated prompt fatality rate in Table 7 is less than one millionth of that figure. In a similar fashion, the estimated latent cancer fatalities in Table 7 can be compared to the total annual cancer fatality rate within 50 miles of the plant (1,700 per year). The annual rate from PTS related core melts ( $2 \times 10^{-4}$  per reactor year) is about seven orders of magnitude less.

It should be noted that the comparison of early fatalities with background fatalities should be done for the populace within 1 mile of the plant where the early fatality risk is greatest. For Oconee, the comparison was done for 10 miles, because there are no people within 1 mile of the site boundary.

Table 7

Estimated Risk for Oconee Operation Beyond the Screening Criterion

<u>Failure Mode</u>	<u>Early Fatalities</u> (per reactor year)	<u>Latent Fatalities</u> (per reactor year)	<u>Public Exposure</u> (Person-rem per reactor year)
δ	3(-7)	6(-5)	.4
β	-	3(-5)	.1
V	6(-8)	3(-5)	.1
V <sub>2</sub>	<u>1(-7)</u>	<u>6(-5)</u>	<u>.2</u>
Total	<u>5(-7)</u>	<u>2(-4)</u>	<u>.7</u>

Finally, from the viewpoint of evaluating the cost effectiveness of design changes to prevent or mitigate PTS events, the NRC procedure is to monetize the public exposure at a rate of \$1 thousand per person-rem. The 0.7 person rem per reactor year would be equivalent to \$700 per year, or a present value of about \$7 thousand over the life of the plant.

Uncertainties and Sensitivities

The uncertainties in this type of risk analysis are known to be large but not well quantified. For the purpose of examining sensitivity of the results to variations in the controlling parameters, we have performed a calculation based on reasonable upper bound values of the containment failure modes and offsite consequences.

First, although the PNL analysis (reference 2) showed that no missiles will penetrate the reactor cavity, there is always some small probability of an occurrence. We postulated an upper bound probability of 0.1 that a missile will breach containment. Presumably, this probability could be greater for some plants. We assigned the event to the α failure mode. By the same logic, we assigned an upper limit probability of 0.1 to a V sequence or steam generator tube rupture as a consequence of the LOCA. Finally, we assumed a 0.1 probability that containment would be completely unisolated at the start of the accident (β failure).

The combination of these three conservative assumptions yields a 30% chance of a catastrophic containment failure. As a further level of conservatism, we assigned all of these failures to the 1A release category (Table 5). Finally, we have assumed that the early fatalities due to a 1A failure are ten times as high as the value given in Table 6. These estimates are 500 early fatalities, 10,000 latent cancer fatalities and 6 x 10<sup>7</sup> person rem.

The calculated risk estimates per reactor year for the upper limit sensitivity case are :  $9 \times 10^{-4}$  early fatalities,  $1.8 \times 10^{-2}$  latent cancer deaths and 100 person-rem. The frequencies for early and latent fatalities are still more than four orders of magnitude below the background risks discussed above. The monetized value of 100 person-rem per reactor year would be \$100 thousand per reactor year, or about \$1 million over the life of the plant. Hence, even with the upper limit analysis of containment response and offsite consequences, one could justify spending only \$1 million over the life of the plant for a design improvement that would eliminate the PTS risk.

### Other Plant Types

Oconee has a large dry containment with heat removal by both fan coolers and sprays. We expect that most plants with a PTS potential are in this class. The two other major containment types used for PWR's are the subatmospheric and ice condenser designs. There are important plant differences between the designs types, and some important differences between plants of the same type, which should be accounted for in a plant specific analysis.

Subatmospherics and ice condensers (and some large dry's) depend entirely on sprays for long term containment heat removal. Consequently, spray unavailability would become a more important issue, including the probability of a loss of recirculation spray due to sump failure. Subatmospheric designs are somewhat smaller than the large dry containments and their failure pressures are lower. Ice condensers are considerably smaller and have much lower failure pressures. Therefore, one has to be more careful in analyzing hydrogen burn failure with sprays operating, particularly for the ice condensers.

On the other hand, the subatmospheric containments are virtually always isolated during an accident; otherwise, the plant could not maintain subatmospheric conditions.

Finally the probability of missile generation should be evaluated on a plant specific basis.

### Summary

The analysis presented here illustrates the logical steps which should be followed in evaluating the risk of pressurized thermal shock for a specific plant. The data used in this paper have been borrowed from many sources, and several rough approximations have been used. Plant specific risk evaluations should be based on plant specific calculations of the containment thermal-hydraulics (MARCH), source term behavior (CORRAL) and offsite consequences (CRAC). (In the near future, the codes we have cited will be replaced with more accurate methods).

For the hypothetical case in which Oconee 1 is assumed to operate beyond the screening criterion, our analysis yields very low estimates of the risk from Pressurized Thermal Shock. Despite the approximate nature of our calculations, the low estimates of risk remain, even when conservative assumptions about containment response are used.

For the actual operation of Oconee 1 (Figure 1), the estimated through-wall crack frequency is considerably lower than for the hypothetical case. The core melt frequency and hence the estimated risk would be proportionately lower. This result supports the conclusion that the screening criterion is conservatively defined.

References:

1. T.J. Burns et al., "Pressurized Thermal Shock Evaluation of the Oconee 1 Nuclear Power Plant," Draft NUREG/CR-3770 (April 13 1984).
2. L.T. Pederson (Pacific Northwest Laboratories) to R. Woods (NRC), "Oconee LOCA Probability from Simulated PTS Events," (July 17, 1984).
3. G.J. Kolb, S.W. Hatch, P. Cybulskis and R.O. Wooton, "Reactor Safety Study Methodology Applications Program: Oconee #3 PWR Power Plant," NUREG/CR-1659 Volume 2 (May 1981).
4. "A Probability Risk Assessment of Oconee Unit 3," NSAC-60 (June 1984).
5. "Reactor Safety Study - An Assessment of Accident Risks in U.S. Commercial Nuclear Power Plants," WASH-1400 (NURUG-75/014), October 1975.
6. Janice E. Moore (NRC) to James P. Gleason (Administrative Judge), Direct NRC Testimony in the Matter of Indian Point Units 2 and 3, (January 24, 1983), P III.C-5ff.

## THE TRAC-PF1/MOD1 COMPUTER CODE\*

Dennis R. Liles  
John H. Mahaffy  
Safety Code Development Group, MS K553  
Los Alamos National Laboratory  
Los Alamos, NM 87545

### INTRODUCTION

The Transient Reactor Analysis Code (TRAC) is an advanced best-estimate systems code for analyzing light-water reactor (LWR) accidents. It is being developed at the Los Alamos National Laboratory under the sponsorship of the Reactor Safety Research Division of the US Nuclear Regulatory Commission (NRC). A preliminary TRAC version consisting of only one-dimensional components was completed in December 1976. This version was not released publicly nor formally documented. However, it was used in the TRAC-P1 development and formed the basis for the one-dimensional loop component modules. The first publicly released version was TRAC-P1, completed in December 1977. It is described in the Los Alamos report LA-7279-MS.

The TRAC-P1 program was designed primarily for the analysis of large-break loss-of-coolant accidents (LOCAs) in pressurized water reactors (PWRs). Because of its versatility, however, it can be applied directly to many analyses ranging from blowdowns in simple pipes to integral LOCA tests in multiloop facilities. A refined version, called TRAC-P1A, was released to the National Energy Software Center (NESC) in March 1979. It is described in the Los Alamos report LA-7777-MS. Although it still treats the same class of problems, TRAC-P1A is more efficient than TRAC-P1 and incorporates improved hydrodynamic and heat-transfer models. It also is easier to implement on various computers. TRAC-PD2 contains improved reflood and heat-transfer models and improvements in the numerical solution methods. Although a large LOCA code, it has been applied successfully to small-break problems and to the Three Mile Island incident.

TRAC-PF1 was designed to improve the ability of TRAC-PD2 to handle small-break LOCAs and other transients. TRAC-PF1 has all of the major improvements of TRAC-PD2 but, in addition, uses a full two-fluid model with two-step numerics in the one-dimensional components. The two-fluid model, in conjunction with a stratified-flow regime, handles countercurrent flow better than the drift-flux model previously used. The two-step numerics allow large time steps to be taken for slow transients. A one-dimensional core component

---

\*This work was funded by the US NRC Office of Nuclear Regulatory Research, Division of Accident Evaluation.

permitted calculations to be made with reduced dimensionality although the three-dimensional vessel option was retained. A noncondensable gas field was added to both the one-dimensional and three-dimensional hydrodynamics. Significant improvements were made to both the trip logic and the input. TRAC-PF1 was publicly released in July 1981. PF1 and PD2 have been sent out to over 60 organizations worldwide and are being used for a very wide variety of applications.

TRAC-PF1/MOD1 was designed to provide full balance-of-plant modeling capabilities. This required addition of a general capability for modeling plant control systems. The steam generator model was replaced to allow a wider variety of feedwater connections and better modeling of steam tube ruptures. A special turbine component also has been added, but new components were not required for adequate modeling of condensers, heaters, and pumps in the secondary system.

In addition to the expanded capabilities just mentioned, MOD1 contains a number of changes in physical models. The most significant of these is the condensation model. During condensation, the liquid-side interfacial heat-transfer coefficient is now sensitive to flow regime and includes a special model for thermally stratified configurations. Wall heat transfer has been improved in the condensation and film-boiling regimes. The motion equations have been expanded to include momentum transport from phase change, and their momentum flux terms have been changed substantially in the three-dimensional flow equations. This latter change substantially alters the computed pressure drop across a vessel from previous codes. These model changes, along with several small changes, make TRAC-PF1/MOD1 not only a superior code for small-break and operational transients, but also the best version of TRAC to use for large-break analysis. Reflood analyses, for example, generally run noticeably faster with MOD1 as a result of these improvements.

## TRAC CHARACTERISTICS

Some distinguishing characteristics of TRAC-PF1/MOD1 are summarized below. Within restrictions imposed by computer running times, attempts are being made to incorporate state-of-the-art technology in two-phase thermal hydraulics.

### Variable-Dimensional Fluid Dynamics

A full three-dimensional ( $r, \theta, z$ ) flow calculation can be used within the reactor vessel; the flow within the loop components is treated one dimensionally. This allows an accurate calculation of the complex multidimensional flow patterns inside the reactor vessel that are important in determining accident behavior. For example, phenomena such as emergency core-coolant (ECC) downcomer penetration during blowdown, multidimensional plenum and core flow effects, and upper plenum pool formation and core penetration during reflood can be treated directly. However, a one-dimensional vessel

model may be constructed that allows transients to be calculated very quickly because the usual time-step restrictions are removed by the special stabilizing numerical treatment.

#### Nonhomogeneous, Nonequilibrium Modeling

A full two-fluid (six-equation) hydrodynamics model describes the steam-water flow, thereby allowing important phenomena such as countercurrent flow to be treated explicitly. A stratified-flow regime has been added to the one-dimensional hydrodynamics, a seventh field equation (mass balance) describes a noncondensable gas field, and an eighth, solutes moving with the liquid.

#### Flow-Regime-Dependent Constitutive Equation Package

The thermal-hydraulic equations describe the transfer of mass, energy, and momentum between the steam-water phases and the interaction of these phases with the heat flow from system structures. Because these interactions are dependent on the flow topology, a flow-regime-dependent constitutive equation package has been incorporated into the code. Although this package undoubtedly will be improved in future code versions, assessment calculations performed to date indicate that many flow conditions can be handled adequately with the current package.

#### Comprehensive Heat-Transfer Capability

The TRAC-PF1 program incorporates a detailed heat-transfer analysis capability for both the vessel and the loop components. Included is a two-dimensional (r,z) treatment of fuel-rod heat conduction with dynamic fine-mesh rezoning to resolve both bottom flood and falling-film quench fronts. The heat transfer from the fuel rods and other system structures is calculated using flow-regime-dependent heat-transfer coefficients obtained from a generalized boiling curve based on local conditions.

#### Consistent Analysis of Entire Accident Sequences

An important TRAC feature is its ability to address entire accident sequences, including computation of initial conditions, with a consistent and continuous calculation. For example, the code models the blowdown, refill, and reflood phases of a LOCA. This modeling eliminates the need to perform calculations using different codes to analyze a given accident. In addition, a steady-state solution capability provides self-consistent initial conditions for subsequent transient calculations. Both a steady-state and a transient calculation can be performed in the same run, if desired.

#### Component and Functional Modularity

The TRAC program is completely modular by component. The components in a calculation are specified through input data; available components allow the user to model virtually any PWR design or experimental configuration. This gives TRAC great versatility in the possible range of applications. It also

allows component modules to be improved, modified, or added without disturbing the remainder of the code. TRAC component modules currently include accumulators, pipes, plena, pressurizers, pumps, steam generators, tees, turbines, valves, and vessels with associated internals (downcomer, lower plenum, core, upper plenum, etc.).

The TRAC program also is modular by function; that is, the major aspects of the calculations are performed in separate modules. For example, the basic one-dimensional hydrodynamics solution algorithm, the wall-temperature field solution algorithm, heat-transfer coefficient selection, and other functions are performed in separate sets of routines that are accessed by all component modules. This modularity allows the code to be upgraded readily as improved correlations and experimental information become available.

#### PHYSICAL PHENOMENA TREATED

Because of the detailed modeling in TRAC, most of the physical phenomena important in both large- and small-break LOCA analysis can be treated. Included are

1. ECC downcomer penetration and bypass, including the effects of countercurrent flow and hot walls;
2. lower plenum refill with entrainment and phase-separation effects;
3. bottom flood and falling-film reflood quench fronts;
4. multidimensional flow patterns in the core and plenum regions;
5. pool formation and countercurrent flow at the upper-core support plate (UCSP) region;
6. pool formation in the upper plenum;
7. steam binding;
8. average-rod and hot-rod cladding-temperature histories;
9. alternate ECC injection systems, including hot-leg and upper-head injection;
10. direct injection of subcooled ECC water, without the requirement for artificial mixing zones;
11. critical flow (choking);
12. liquid carryover during reflood;
13. metal-water reaction;
14. water-hammer effects;
15. wall friction losses;
16. horizontally stratified flow;
17. boron injection; and
18. noncondensable gases.

## PLANNED IMPROVEMENTS

TRAC-PF1/MOD1 combines all of the PWR accident analysis capabilities thus far requested by the NRC into a single code. This code represents the final version in the TRAC series although the code will be maintained and some modest improvements will be added.

Work is progressing on planned post critical heat-flux heat-transfer improvements. A users' workshop was held in August and some of the suggested user-convenience improvements will be incorporated into PF1/MOD1 as time and funding permit.

## ASSESSMENT OF PF1/MOD1

Before its release, PF1/MOD1 had undergone developmental assessment. The following Loss-of-Fluid Test (LOFT) and Semiscale experiments have been modeled:

LOFT:	L6-1
	L6-2
	L6-3
Semiscale:	S-UT-6
	S-UT-7
	S-NC-6

These tests emphasize operational transients, small-break LOCAs, and natural-circulation/reflux cooling. In addition, MOD1 has been compared with some Create downcomer data, a test from the Japanese Cylindrical Core Test Facility, and the large-break LOFT L2-3. No results will be shown in this paper although a document with the test results will be published.

During fiscal year 1985, PF1/MOD1 will be independently assessed by Sandia against a variety of separate-effects and integral-system tests. The results will be used to guide model improvements for updated versions of MOD1.

## SUMMARY

TRAC-PF1/MOD1 is the latest and last in a series of advanced best-estimate computer codes. MOD1 can model both primary and secondary loops in a PWR and has noncondensable and boron fields. A full set of trips and controllers allows most transients of interest to be run with this new version. The one-dimensional numerics can permit very large time steps to be taken for slow transients, yet the three-dimensional vessel capability is available if multidimensional effects are deemed important. The result is a very versatile, well-assessed tool for LWR analysis.

## STATUS OF RELAP5/MOD2 DEVELOPMENT AND ASSESSMENT

Gary W. Johnsen

### ABSTRACT

Improvements and refinements made to the RELAP5/MOD2 computer code are described and illustrated. Modifications made to the code since a general release of the first version in April involve vertical phase separation modeling, a water-packing mitigation scheme, a more implicit numerical solution scheme, enhanced code portability, and user conveniences.

### INTRODUCTION

The mission of the RELAP5 project is to provide the United States Nuclear Regulatory Commission (USNRC) with a fast running and user convenient light water reactor (LWR) system transient analysis code for use in rulemaking, licensing audit calculations, evaluating operator guidelines, and as a basis for a nuclear plant analyzer. The code is used extensively at the Idaho National Engineering Laboratory in support of the LWR research projects such as Semiscale and LOF1 where it is used for experiment planning, pretest prediction, and posttest analysis. Nuclear power organizations other than the USNRC (vendors, utilities, and engineering support firms) may use the code for design, safety analysis, and licensing application work.

The RELAP5 project began in 1978 as an effort to surmount the inherent shortcomings of the homogeneous, equilibrium RELAP4 computer code. With the extensive experience of RELAP4 as a guide, a nonhomogeneous, nonequilibrium code was developed, RELAP5/MOD0. This code, released in May of 1979 was intended for blowdown analysis and was relatively incomplete. RELAP5/MOD1, completed about eighteen months later was more complete and is currently in use around the world to study small break loss-of-coolant accidents (LOCAs), large break blowdowns, and operational transients. The currently released version, RELAP5/MOD2 (Cycle 21), became available in

April 1984, and is a generic pressurized water reactor (PWR) code and is applicable to: large and small break loss-of coolant accidents, operational transients, transients in which the entire secondary system must be modeled, and system behavior simulation up to the point of core damage. The controls, turbine, generator, condenser, and feedwater system can be included. The code includes an interactive execution feature and the code output can be coupled with a color graphics terminal to present a color graphic display of computed results. This feature has been used for evaluation of operator guidelines for the USNRC. The color graphic display feature can also be used in a play-back mode using the restart record from a previously run simulation in order to enhance understanding of the result.

The objective of this paper is to describe new features and improvements made to the code since the April release. Development efforts have concentrated on decreasing computational run time, improving the calculation of stratified flow, smoothing the constitutive package, and adding user conveniences. These and other changes are presently undergoing detailed checkout and will be released to recipients of RELAP5/MOD2 (Cycle 21) in the form of updates when that checkout is complete. The remainder of this paper describes the code's changes and their overall effect on modeling performance.

## MODELING IMPROVEMENTS

### Vertical Phase Separation

The developmental assessment of RELAP5/MOD2 as well as results from its early application indicated a need to improve the modeling of stratified liquid/vapor mixtures in vertically-oriented components (e.g., pressurizer, vessel upper head). In particular, the lack of a stratified flow regime for vertical control volumes failed to produce a sharp interface when the situation clearly required one, and generally overpredicted the heat and mass transfer between the phases.

This shortcoming was most pronounced when modeling pressurizer behavior. In particular it was found that the piston-like compression of vapor which occurs during a pressurizer insurge could not be well predicted. Consequently development was initiated on a vertical stratification flow regime model and associated constitutive relationships (i.e., interphase heat and mass transfer, interphase drag, and wall heat transfer to the individual phases).

It was decided at the outset not to develop a model suited only for describing pressurizer behavior. It was recognized that stratified flow situations could arise in many vertically-oriented components of a primary coolant system (for example, the hot leg of a Babcock and Wilcox 2 x 4 plant). Therefore, a model was developed that would function in any vertically-oriented control volume where the conditions would favor stratified conditions.

The criteria for invoking the stratified flow regime is a mass flux less than  $200 \text{ kg/s-m}^2$ . When this condition is satisfied, the interphase drag is reduced to  $10^{-2} \text{ N-s}^2/\text{m}^5$  at the interface which causes the phases to separate in accordance with buoyancy forces and sharpens the liquid/vapor interface. The heat and mass transfer between the phases diminishes substantially under stratified conditions, and this was modeled in RELAP5/MOD2 by reducing the liquid-side and vapor-side interface heat transfer coefficients to  $10 \text{ W/m}^2\text{-K}$  which results from a conduction limited process model with the liquid and a natural convective heat transfer coefficient at the liquid/vapor interface.

Since data from several pressurizer experiments were readily available, assessment of the model focused on them. Included in the assessment were the MIT experiment,<sup>1</sup> the Delft University NEPTUNUS Y05 experiment,<sup>2</sup> and several Semiscale separate effects experiments.<sup>3</sup> In this paper, the performance of the model in modeling an MIT experiment is described.

The MIT experiment consisted of a small-scale, low-pressure test facility utilizing a cylindrical pressure vessel to model a pressurized water reactor pressurizer. By use of compressed air, subcooled water could be forced into the pressure vessel, initially containing a saturated steam/water mixture. Various combinations of insurge rate, initial liquid levels, and degree of subcooling were imposed in the series of experiments.

Test run ST4 was chosen for assessment. The RELAP5/MOD2 input model consisted of 10 equal length control volumes to represent the pressure vessel and a single time-dependent volume and junction to introduce the subcooled water at the vessel inlet at the temperature and rate recorded in the experiment. Figure 1 shows the pressure response measured near the top of the vessel (in the steam space) and compares it to two RELAP5/MOD2 calculations: one with the stratification model included and one without. Without the model, the calculated pressure is seen to drop slightly during the period of insurge. This behavior is indicative of overpredicting the condensation of steam in the vapor space. In this calculation, the uppermost, steam-filled control volumes do show superheating of the steam occurring as a consequence of compression. However, an overall pressure increase is nullified by rapid condensation near the liquid/vapor interface. In contrast, the calculation of the pressure with the stratification model shows a gradual increase in pressure, and agrees very closely with the measured result.

#### Water-Packing Mitigation

One consequence of employing an Eulerian scheme to model physical systems is the occasional occurrence of artificial discontinuities that result from sharp interfaces crossing cell boundaries. For example, the movement of a liquid/vapor interface up or down a vertical pipe causes successive liquid filling or emptying of cells. In the Eulerian framework, the filling and emptying points represent numerical discontinuities. The filling situation is most prone to cause difficulty because of the near incompressibility of the liquid. A slight "overfilling" of a cell in a

# Vertical Stratification Model Produces Good Agreement for MIT Pressurizer Experiment

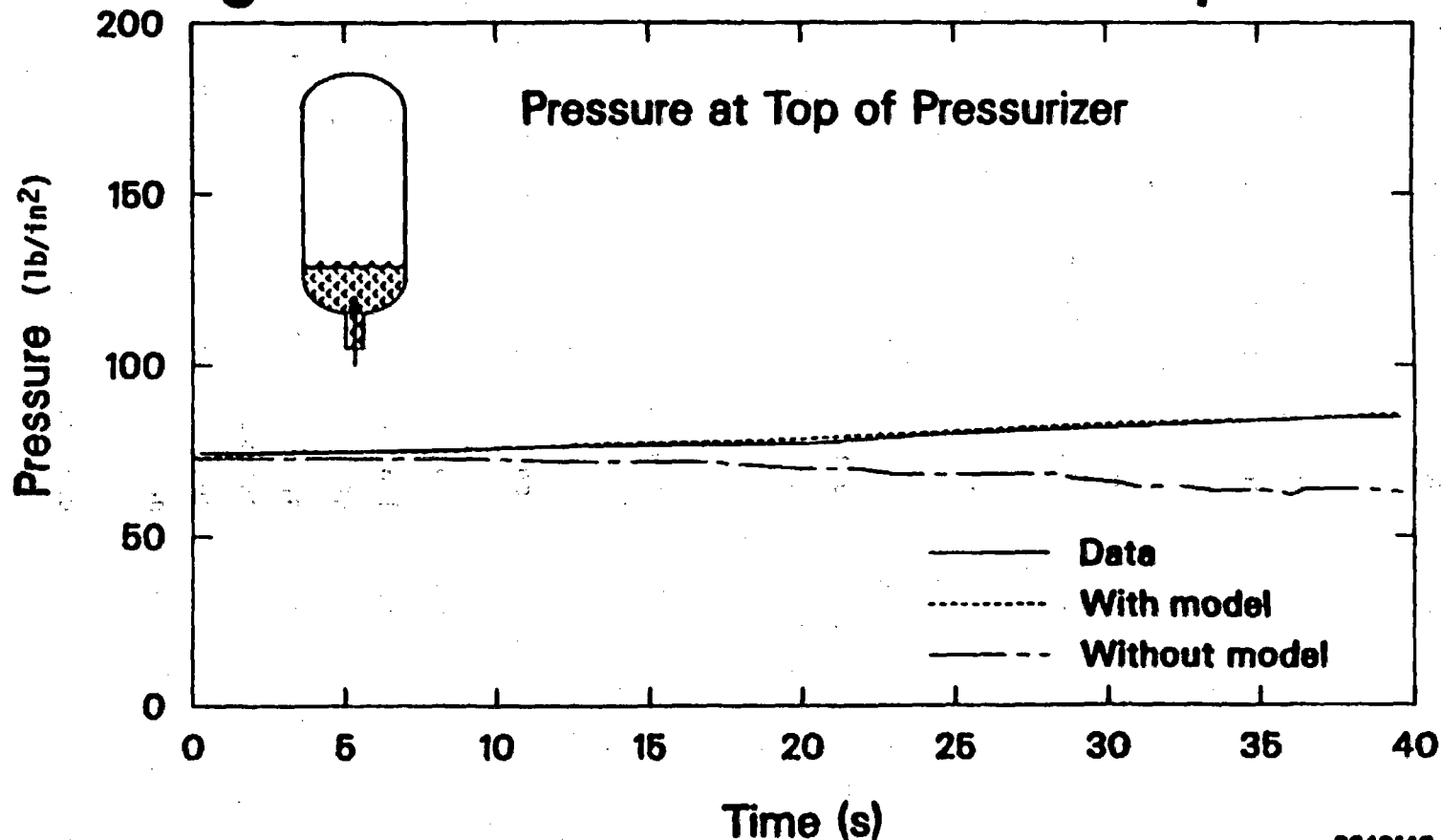


Figure 1. Comparison of pressurizer pressure history from MIT experiment ST4 with that predicted by RELAP5/MOD2 (with and without the vertical stratification model).

RS40140-0

single time step leads to a substantial pressure spike. Reducing time step size diminishes the spike but does not eliminate it and, moreover, makes the calculation costly.

The situation is illustrated by the simple filling problem shown in Figure 2. Subcooled water is introduced at the bottom of a cylindrical tank open at the top and initially containing saturated steam at  $4 \times 10^5$  Pa. Figure 2 shows the calculated pressure for the bottom cell of 10 cells used to model the tank. The overall pressure behavior is as expected, with the pressure increasing due to the hydrostatic head of the liquid above it, once the liquid level passes the volume. Also evident in this calculation are unphysical pressure increases that occur when the liquid level passes through the top of each cell. Although relatively small compared to the absolute value of the pressure ( $4 \times 10^3$  Pa vs  $4 \times 10^5$  Pa), such perturbations are at best cosmetically undesirable and at worst could alter the future course of a calculation under less "forced" circumstances than the file problem illustrated.

The prevention of water-packing is not straightforward within the framework of codes like RELAP5. Since some measure of success had been achieved in mitigating the problem in TRAC,<sup>4</sup> a scheme similar to the one developed for that code was adopted, with some modifications.<sup>5</sup>

The scheme first involves detecting when an abrupt pressure increase occurs in a volume nearly full of liquid. From trial and error, it was found that a pressure change of 0.23% or more at a void fraction less than 0.12 worked best. In addition, the detection criteria require that the liquid temperature be lower than saturation, that the volume be vertically stratified, and that the adjacent volume above not be liquid-full (as would be the case for a true water-hammer).

The damping of the pressure spike is achieved by modifying the momentum equations to flatten the temporal pressure change. The finite difference form of the momentum equation has the form:

## Sample Fill Problem Illustrates Effect of Water-Packing Fix

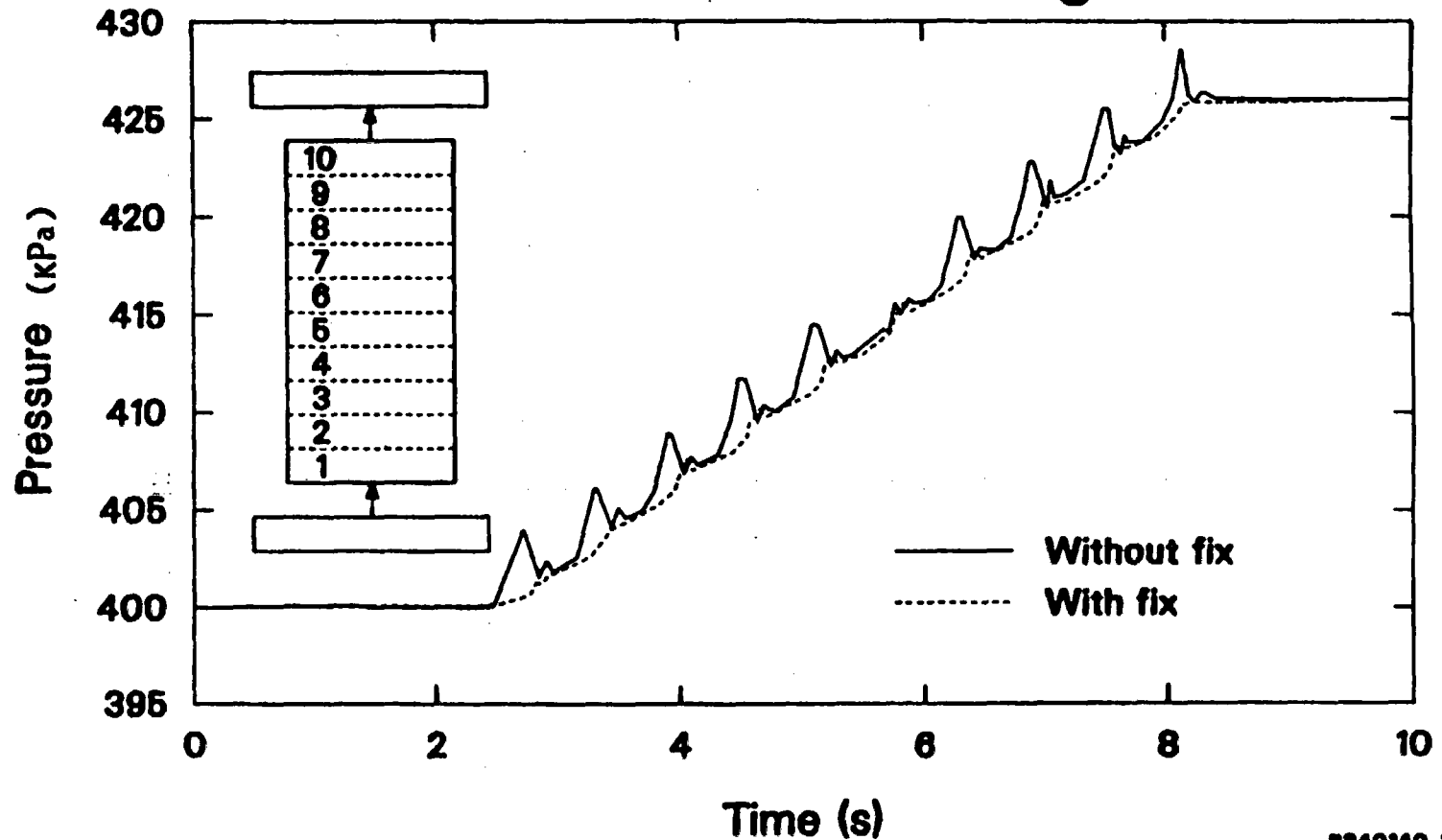


Figure 2. Sample fill problem run on RELAP5/MOD2 with and without water-packing fix.

$$v_{1,j}^{n+1} = v_{1,j}^{exp,n} - (VDP)_{i,j}^n (P_L^{n+1} - P_L^n) + (VDP)_j^n k (P_K^{n+1} - P_K^n) \quad (1)$$

where

- v = phase velocity
- P = pressure
- $v^{exp}$  = old time terms in momentum equation
- VDP = product of terms representing the coefficient for  $\Delta P$  in the momentum equation
- i = phase (one equation for liquid, one for vapor)
- j = junction dividing volumes K and L
- n = old time value
- n+1 = new time value
- k = coefficient used for water-packing mitigation (set to unity under normal conditions;  $10^6$  when a water-pack is detected).

In Equation (1), when water-packing is detected for volume K, the imposition of a large value for k causes the new and old time pressure values to be nearly equal.

The effect of the water-packing mitigation scheme on the filling problem described earlier is shown in Figure 2. The pressure trace is seen to have been smoothed considerably, with pressure spikes limited to approximately  $4 \times 10^2$  Pa.

#### NEARLY-IMPLICIT NUMERICAL SCHEME

The existing numerical solution scheme employed in RELAP5/MOD2 is referred to as the semi-implicit scheme, which has the interphase drag, heat transfer, and mass transfer terms evaluated implicitly. This method eliminates the small time step restrictions associated with the small time

constants of interphase exchange processes. In addition, the terms responsible for acoustic pressure wave propagation are evaluated at the new time value. While the semi-implicit scheme is an efficient and accurate solution method for relatively fast transients, stability considerations require that the time step size not exceed the material Courant limit. Thus, the speed of the code is inherently limited by the relationship between convective velocities and cell length.

For very slow transients (several hours in duration) exhibiting quasi-steady behavior, the dynamic propagation of mass and energy is relatively unimportant. Under these circumstances, by evaluating the convective fluxes implicitly, the time step can be increased beyond the material Courant limit. The nearly-implicit scheme,<sup>5</sup> as it is called, was developed to serve this purpose.

The nearly-implicit scheme is presently installed in a developmental version of RELAP5/MOD2 and is currently undergoing testing. In its present form, the nearly-implicit scheme may be invoked as an option over a user-specified time interval in a transient calculation. The new scheme differs from the semi-implicit one in that the hydrodynamic solution is performed via two fractional steps. The first step solves all six conservation equations (seven if a noncondensable gas is present) treating all interphase exchange processes, the pressure propagation process, and the momentum propagation process implicitly. These equations are the same as those solved in the semi-implicit scheme except that the convective terms in the momentum equation are evaluated implicitly (in linearized form) instead of in an explicit, donored fashion. The second step is used to stabilize the convective terms in the mass and energy equations. This step uses the final (new time) values velocities from the first step along with the interphase exchange terms resulting from the first step. The phasic continuity and energy equations in the second step have the fluxed variables evaluated at the new time level, along with the final new time level velocities and interphase exchange terms from the first step.

With the more implicit hydrodynamic solution scheme, it became necessary to consider the implicitness of the coupling between the hydrodynamics and heat transfer solution. Clearly, large time steps increase the potential for under- or over-extrapolation's of energy from control volumes when the coupling is explicit. Consequently a more implicit coupling technique was developed as an adjunct to the new hydrodynamic solution scheme.

In the existing code, each energy equation contains an explicit term representing the heat flux from the heat slabs connected to a particular hydrodynamic cell. The vapor flux is denoted as  $Q_{wg}^n$ , and for the liquid flux,  $Q_{wf}^n$ . In the new coupling scheme, the heat flux is made implicit in the vapor and liquid temperatures and computed as:

$$Q_{wg}^{n+1} = h_g^n (T_w^{n+1} - \tilde{T}_g^{n+1}) \quad (2)$$

$$Q_{wf}^{n+1} = h_f^n (T_w^{n+1} - \tilde{T}_f^{n+1}) \quad (3)$$

where the new time  $\tilde{T}^{n+1}$  terms are expressed in terms of the new time values of pressure, internal energies and quality using the linearized state equations. The wall heat flux terms are used in the first step of the nearly-implicit scheme, and in the second step the tilde values are used explicitly as is done for the mass and heat exchange terms.

Several simple tests of the more-implicit numerical scheme have been carried out using abstract physical problems. The results of one such problem are shown in Figure 3. The problem consists of a tube into which saturated water at 530 K is introduced at one end. Initially, the tube temperature equals that of the water. At a specified time the tube walls instantaneously begin generating heat internally, which is in turn transferred to the water as it flows down the tube. Figure 3 shows the calculated coolant void at the end of the tube using the semi- and

## Comparison of Semi- and Nearly-Implicit Solution Schemes

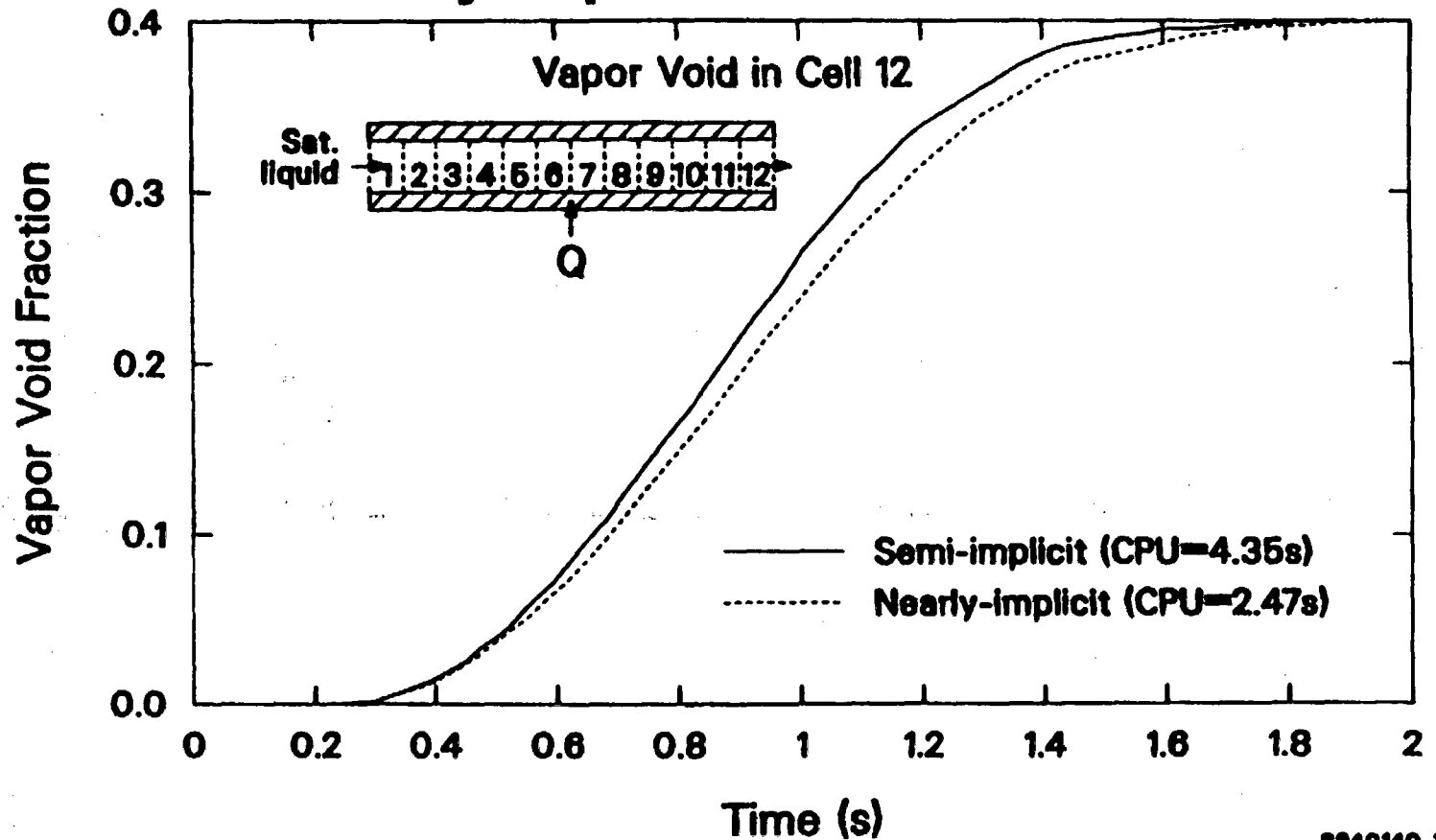


Figure 3. Comparison of void fractions using the semi-implicit and nearly-implicit scheme for the heated tube problem.

nearly-implicit solution schemes. Both calculations produce the same steady-state void fraction after ~2 s. The semi-implicit solution utilized time step sizes restricted by the material Courant limit, and took 111 advancements to reach 3 s of transient time. The nearly-implicit solution only required 30 advancements to reach the same time and ran almost twice as fast. By exceeding the material Courant limit, some of the dynamic response was lost, as evidenced by the difference in the two curves. However, the difference is slight and demonstrates that the nearly-implicit scheme is effectively applied to slow transients.

#### USER CONVENIENCES

Efforts to render the code more convenient to use are primarily instigated by the suggestions made by code analysts. Two such examples were recently incorporated into the code. These are an expanded plot/edit parameter menu and a relief valve model.

The expansion of the parameter list available for editing, plotting, trip control, and control system input adds fifty-five parameters. The parameters include variables associated with control volumes, junctions, heat slabs, and special components. The addition of one or more parameters to the plot/restart tape is a user-option, thereby conserving file space.

A new model to represent the dynamic behavior of a typical light water reactor relief valve was developed. This model accounts for the internal forces and motion of the internals of the valve for determining valve position, flow area, and hysteresis effects.

#### FUTURE PLANS

In FY-1985, efforts will be focused on code maintenance, enhancement, and user support. In the early part of the year, testing of the nearly-implicit solution scheme will be completed. This will involve exercising the new solution scheme with several large problems to gauge

calculational accuracy and speed (by comparison to counterpart calculations using the semi-implicit scheme). User guidelines will be developed and published concerning use of the new scheme.

Data from the INEL's Thermal-Hydraulic Laboratory Tee Critical Flow Experiments<sup>7</sup> will be utilized to improve the modeling of critical flow from stratified, horizontal pipes.

To provide for the support of RELAP5 users outside of the INEL, a Users Group will be formed. This group will provide a mechanism for providing services directly to domestic code users by subscription fee. Services will include periodic newsletters, code update transmittals, workshops, and consultation on code application and problem resolution.

Coordination will continue with the Severe Fuel Damage Program, in the task to link RELAP5 with the Severe Core Damage Analysis Program (SCDAP). The resulting integrated code will be capable of modeling severe accidents from initiation through core meltdown and will be instrumental in assessing the consequences of "terminated" accidents.

## REFERENCES

1. H. R. Saedi and P. Griffith, "The Pressure Response of a PWR Pressurizer During an Insurge Transient," Transactions of the American Nuclear Society, Detroit, Michigan, June 12-16, 1983, pp. 606-607.
2. T. Geomau, Mathematical Modeling of Pressurizer Thermodynamics, WTHD-34, February 1982.
3. J. S. Martinell, "Semiscale Pressurizer Insurge Tests," private communication, 1984.
4. J. H. Mahaffy and D. R. Liles, "Numerically Induced Pressure Excursions in Two-Phase Flow Calculations," 3rd International Topical Meeting on Nuclear Reactor Thermal-Hydraulics, Santa Barbara, California, January 11-14, 1983.
5. L. R. Feinauer et al., Post-Release Improvements for RELAP5/MOD2, EG&G Report SE-CMD-011, August 1984.
6. J. Trapp, R. A. Riemke, and R. J. Wagner, Nearly-Implicit Hydrodynamic Numerical Scheme and Partially-Implicit Hydrodynamic and Heat Slab Coupling for RELAP5/MOD2, EG&G Report EGG-CMD-6715, September 1984.
7. J. S. Martinell, "THL Two-Phase Flow Tests," 12th Water Reactor Safety Research Information Meeting, Garthersburg, Maryland, October 22-26, 1984.

## THE STATUS OF THE TRAC-BWR PROGRAM<sup>a</sup>

Walter L. Weaver, III  
S. Zia Rouhani  
EG&G Idaho, Inc.

The Transient Reactor Analysis Code for Boiling Water Reactors<sup>(1,2)</sup> (TRAC-BWR) is being developed at the Idaho National Engineering Laboratory for the Division of Accident Evaluation, Office of Nuclear Regulatory Research of the United States Nuclear Regulatory Commission (USNRC).

The objective of developing these codes is to provide the USNRC and the public with a best estimate computer code for the analysis of postulated accidents and transients in boiling water reactor (BWR) systems. This program is unique among advanced code development projects in that it focuses on the hardware, thermal-hydraulics, and heat transfer phenomena that distinguish BWR systems and their response during transients from other reactor types. In addition to providing a best estimate analysis capability for BWR systems, the code can also be used to address current licensing concerns such as anticipated transients without scram (ATWS) or the small break loss-of-coolant accident (SBLOCA). The codes also provide analytical support to the USNRC experimental safety programs. The success of this development is attributed in part to the continuing participation of the General Electric Company as a part of the Full Integral System Test (FIST) Experimental Program cosponsored by General Electric, the USNRC, and the Electric Power Research Institute (EPRI).

Work on the TRAC-BWR series of codes began in 1979, starting with a developmental version of TRAC-PD2 received from the Los Alamos National Laboratory. This paper focuses on the work performed during the last year and discusses the latest released version of the code, TRAC-BD1/MOD1, which was released in April 1984, and TRAC-BF1, the code version currently under development.

### TRAC-BD1/MOD1

TRAC-BD1/MOD1, the latest released version in the TRAC-BWR series of codes, was released in April 1984. The code manual in four volumes was published at the time when the code was released. The mission of the TRAC-BD1/MOD1 code is to provide a detailed, best estimate capability for the analysis of design basis loss-of-coolant (DBLOCA) accidents and operational transients (including ATWS) for which point reactor kinetics is applicable. Models of all BWR specific hardware, BWR specific hydrodynamics, and BWR specific heat transfer phenomena are included in the code as well as generalized containment and balance of plant modeling capabilities.

---

a. Work supported by the U.S. Nuclear Regulatory Commission of Nuclear Regulatory Research under DOE Contract No. DE-AC07-76ID01570.

Specific new models in TRAC-BD1/MOD1 include a generalized component to component heat transfer model; a two-phase level tracking model; a separator/dryer component model; a moving mesh reflood heat transfer model; a lumped parameter containment model; a noncondensable gas model; and balance of plant component models such as turbine and feedwater heater/condenser models. A reactivity feedback model has been developed that includes boron tracking and direct moderator heating. An improved interfacial shear model based on the work of Ishii has been implemented. Finally, a comprehensive control systems model has been developed. Before this code version was released, it underwent an extensive developmental assessment. The results of all of the developmental assessment cases are contained in Vol. 4 of the TRAC-BD1/MOD1 manual. The test cases were divided into separate effects tests and systems effects tests. Seven separate effects tests were used to exercise the hydrodynamic models in the code while seven additional separate effects tests investigated the heat transfer models in the code. Six systems effects tests were simulated, two each in the areas of large break LOCA, BWR ATWS and balance of plant. Slides 6, 7, and 8 show selected results from the separate effects tests. Slide 6 shows the comparison of the TRAC-BWR jet pump model with the data from the tests of a 1/6 scale jet pump at the INEL. Slide 7 shows the comparison of the TRAC-BWR counter current flow limiting model (CCFL) with General Electric data for the upper tie plate of an 8 x 8 fuel bundle. Slide 8 shows the comparison between the TRAC computed void fraction in an adiabatic pipe to data taken at CISE. Excellent agreement between the code predictions and the data is obtained for each of these test cases.

Slide 9 shows a schematic of the TRAC-BD1/MOD1 model of the Two Loop Test Apparatus (TLTA). TLTA Run 6423 was used as one of the large break LOCA test cases for TRAC-BD1/MOD1 and has also been used for the developmental assessment to TRAC-BF1. Slide 10 shows the computed peak cladding temperature at the 79 inch elevation along with the maximum and minimum temperatures measured at this elevation. Also shown are the results obtained using TRAC-BWR, Version 12. This slide shows that the moving mesh reflood model has greatly improved the code predictions.

Slide 11 shows the TRAC model that was used to simulate the balance of plant transients. A full balance of plant is simulated with high pressure, intermediate- and low-pressure turbines, three stages of feedwater heating, the main condenser, condensate booster and main feedwater pumps, feedwater pump turbine, turbine bypass system, all piping interconnections, and a complete control system. The reactor vessel is represented by a simple nodalization with a single average fuel channel and a single lumped jet pump and recirculation system. This slide shows the complexity of a balance of plant model. However, the control system model used for this case is far more complex and hence not included here. The transient simulated was an ATWS initiated by the failure of the feedwater flow controller.

The transient begins when the feedwater controller fails in such a way as to increase the steam flow to the feedwater pump turbine to its maximum value, raising the feedwater flow to 120% of the full power steady state value. The downcomer level rises until the high level trip is reached, at

which time the turbine stop valve closes and the bypass valve opens. The scram that normally occurs with the high level signal was disabled. With the closure of the turbine stop valve and the opening of the bypass valve, the reactor pressure begins to increase since the capacity of the bypass system is only 80% of the capacity of the main steam lines. The rising pressure collapses the voids in the core adding positive reactivity, which in turn causes the reactor power to increase rapidly. When the pressure exceeds the safety relief valve settings, the relief valves open, lowering the pressure that causes the fluid in the core to flash. This pressure induced flashing along with void production due to heat transfer from the hot fuel rods, creates voids that introduce negative reactivity, decreasing the reactor power. Slide 12 shows the computed reactor power for this transient. This transient and all of the other development assessment test cases are discussed in more detail in Volume 4 of the TRAC-BD1/MOD1 manual. (The publication of this volume was delayed for revision in some of the calculations.)

### TRAC-BF1

Since the release of TRAC-BD1/MOD1 in April 1984, work has been directed toward the next version of TRAC-BWR, i.e., TRAC-BF1. The mission of the TRAC-BF1 code is to provide a fast running, best estimate capability for all accidents and transients for which one-dimensional neutron kinetics model based on the analytical nodal method has been developed and included in TRAC-BF1. In addition, a Courant limit violating numerical technique similar to the Two Step Method in TRAC-PF1 has been implemented in TRAC-BF1. A code version with these two new capabilities is currently being tested.

As part of the testing of this new code version, the TLTA 6423 simulation that was used for the developmental assessment of TRAC-BD1/MOD1 was repeated twice with this new code version. The first calculation was performed with a maximum Courant number of one to compare the results of the new numerics with the results of the old numerics when they both used the same time step size. The second run was Courant limited in the vessel with a maximum Courant number in the one-dimensional components of ~2. The results of these two runs are shown in Slide 16 along with the results of the calculation using TRAC-BD1/MOD1. Slide 16 shows the steam dome pressure for these three runs. The two runs with TRAC-BF1 are quite similar and are slightly different from the results using the old numerics. This change in results is expected since one effect of the new numerics is to damp out higher frequency response resulting in smoother trends.

The new code when computing with the new numerics is ~2.3 times faster than TRAC-BD1/MOD1 for the same calculation. Obviously, application of the Courant limit violating numerics to the three-dimensional vessel component would further improve the efficiency of such calculations.

## Future Plans

During Fiscal Year 1985, the TRAC-BWR Program will concentrate on increasing the efficiency and speed of the code. This will be accomplished by code cleanup, conversion to a Class VI computer (CRAY or CYBER 205) and by implementation of the Courant limit violating numerics in the three-dimensional VESSEL component. Some model improvements are planned including a boron stratification model and implicit coupling of the conduction and hydrodynamic solutions. Finally, and of more interest to the user community, a TRAC-BWR Code Workshop will be held in the spring of 1985.

## REFERENCES

1. J. Spore et al., TRAC-BD1: An Advanced Best Estimate Computer Program for Boiling Water Reactor Loss-of-Coolant Accident Analysis, NUREG/CR-2178, EGG-2109, Idaho National Engineering Laboratory, Oct. 1981.
2. Dean D. Taylor, ed., et al., TRAC-BD1/MOD1: An Advanced Best Estimate Computer Program for Boiling Water Reactor Transient Analysis NUREG/CR-3633, EGG-2294, Idaho National Engineering Laboratory, April 1984.

## Status of the TRAC-BWR Program

W.L. Weaver

12th Water Reactor Safety  
Research Information Meeting  
October 1984



C4 2073

## Outline

- Introduction
- TRAC-BD1/MOD1
- TRAC-BF1
- Future Plans

C4 2075

171

## TRAC-BD1/MOD1 Mission

To provide a detailed best estimate analysis capability for DBLOCA and transients (including ATWS) for which point kinetics is applicable

C4 2077

## TRAC-BD1/MOD1 Features

- Generalized component to component heat transfer
- Two-phase level tracking model
- Non-condensable gas model
- Containment model

C4 2078

## TRAC-BD1/MOD1 Features (cont'd)

- Separator/dryer component model
- Turbine component model
- Feedwater heater/condenser component model
- Moving mesh reflood model

C4 2079

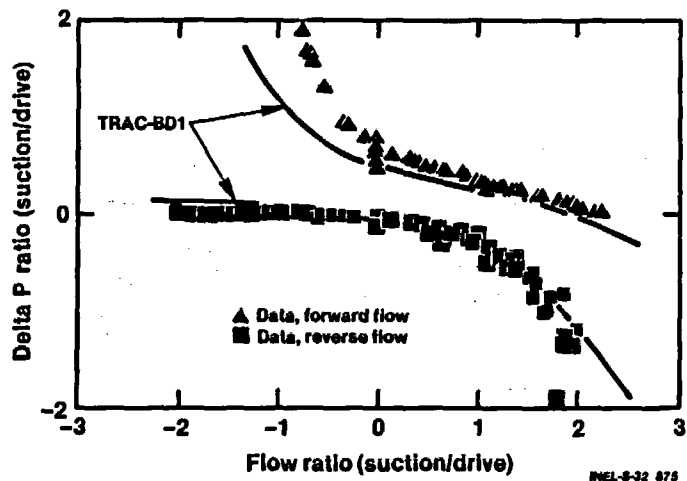
## TRAC-BD1/MOD1 Developmental Assessment

- Separate effects tests
  - 7 hydraulic test cases
  - 7 heat transfer test cases
- System effects tests
  - 2 LOCA transients
  - 2 ATWS transients
  - 2 balance of plant transients

C4 2080

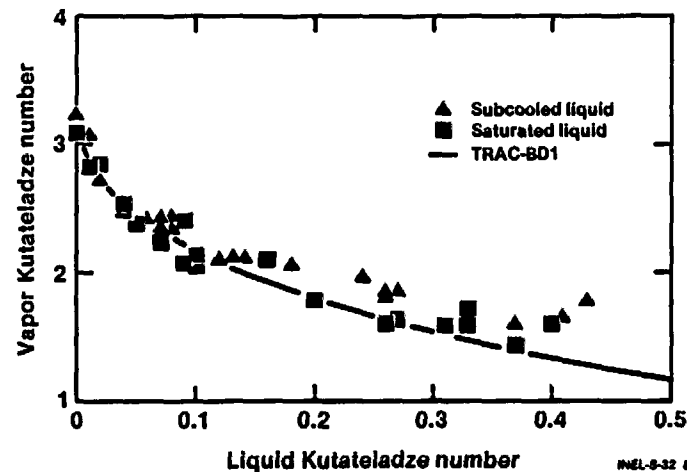
172

### 1/6 Scale INEL Jet Pump



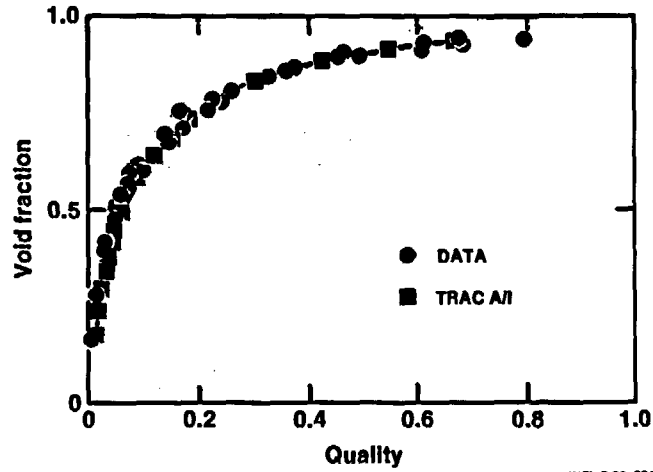
INEL-9-32 875

### GE 8x8 CCFL Bundle Test



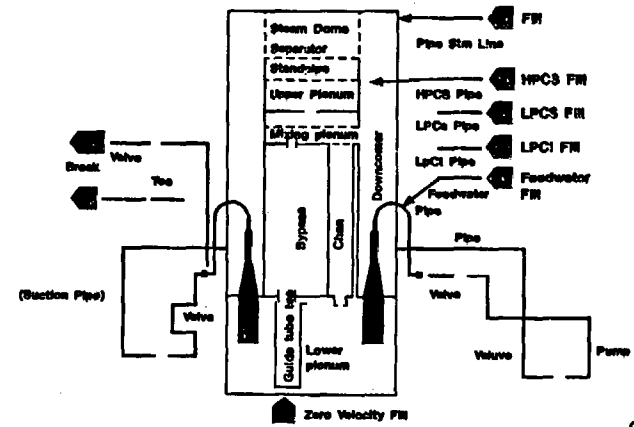
INEL-9-32 879

# Comparison with CISE Void Fraction Data



INEL-8-32 881

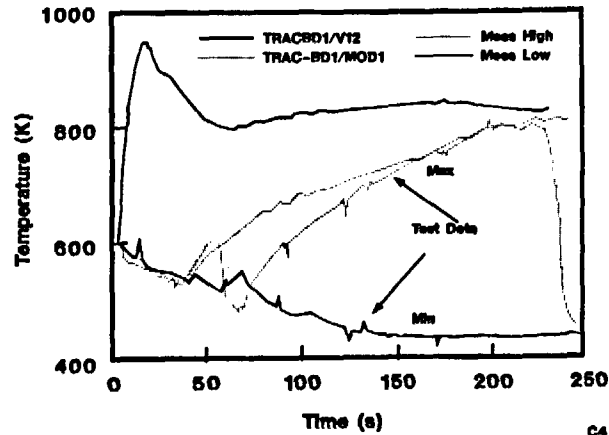
# Schematic of TLTA



C4 1018

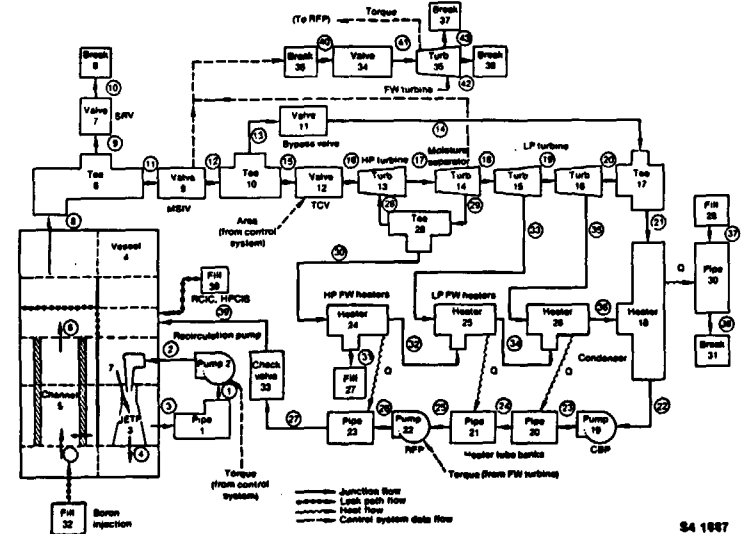
173

# Calculated and Measured TLTA (Case 6423) Rod Temperatures at 2.00m Elevation



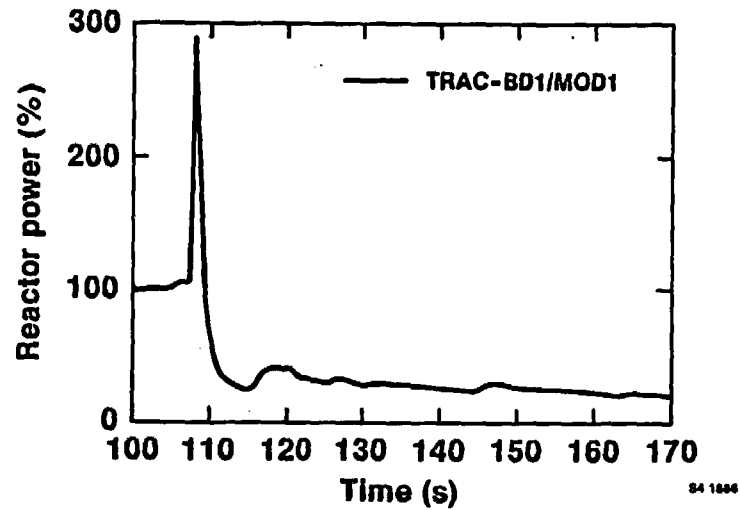
C4 1014

# Feedwater Controller Failure Model



S4 1887

## Reactor Power



174

## TRAC-BF1 Mission

To provide a fast running best estimate analysis capability for accidents and transients for which one-dimensional neutron kinetics is applicable

C4 2081

## TRAC-BF1 Status

- Preliminary version running
- One-dimensional neutron kinetics
- Courant limit violating numerics in one-dimensional components

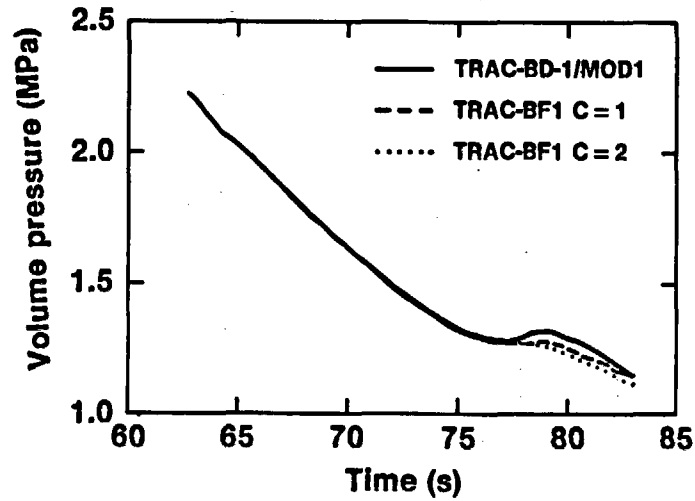
## Developmental Assessment of TRAC-BF1

- TLTA 6423
  - Executed twice
  - Courant limited at break
  - Courant limited in vessel
  - Factor of 2.3 increase in speed

C4 2082

C4 2083

## Steam Dome Pressure



04 1984

## Future Plans

- **Faster running**
  - Code cleanup
  - Conversion to class VI computer
  - Extension of Courant violating numerics to 3-D vessel component
- **Model improvements**
  - Boron stratification model
  - Implicit coupling of conduction and hydrodynamic solutions
- **TRAC-BWR workshop**
  - Spring 1985

C4 2084

INDEPENDENT ASSESSMENT OF THE TRAC-BD1/MOD1 COMPUTER  
CODE AT THE IDAHO NATIONAL ENGINEERING LABORATORY<sup>a</sup>

Gary E. Wilson  
Briant L. Charboneau  
R. Jack Dallman

Craig M. Kullberg  
K. C. Wagner  
Phillip D. Wheatley

ABSTRACT

Under auspices of the United States Nuclear Regulatory Commission, their primary boiling water reactor safety analysis code (TRAC-BWR) is being assessed with simulations of a wide range of experimental data. The FY-1984 assessment activities were associated with the latest version (TRAC-BD1/MOD1) of this code. Typical results of the assessment studies are given. Conclusions formulated from these results are presented. These calculations relate to the overall applicability of the current code to safety analysis, and to future work which would further enhance the code's quality and ease of use.

INTRODUCTION

The latest released version (MOD1)<sup>1</sup> of the Boiling Water Reactor (BWR) Transient Reactor Analysis Code (TRAC-BD1) has been independently assessed with the experimental data identified in Table 1. These data represent transient conditions which include: small, intermediate, and large loss-of-coolant accident (LOCA) blowdown, refill and reflood; natural circulation; anticipated transients without scram (ATWS); and various operational transients. The data were generated in facilities having volumetric scaling ratios ranging between 1/624 and full scale.

---

a. Work supported by the U.S. Nuclear Regulatory Commission, Office of Nuclear Regulatory Research under DOE Contract No. DE-AC07-76ID01570.

## TYPICAL SIMULATION QUALITY

Considering the assessment results as a whole, it is concluded that the code is sufficiently mature to correctly simulate a wide range of BWR behavior. We do note, however, the quality of each simulation is a strong function of the modeling expertise of the analyst. Given adequate modeling, the assessment has shown the code has demonstrated strengths in the simulation of:

- a. Subscale intermediate size break blowdown
- b. Subscale small breaks
- c. Subscale power transients (i.e., ATWS type behavior)
- d. Subscale natural circulation
- e. Full scale containment prior to pool boiling
- f. Full scale operational transients.

Fully detailed documentation of the code's simulation quality is provided in reports available through the Nuclear Regulatory Commission (NRC) staff. Selected examples are discussed in the following three paragraphs.

Figure 1 compares code calculated and experimentally measured natural circulation behavior in the Full Integral Simulation Test (FIST) facility.<sup>2</sup> The data is shown as flow rate as a function of the liquid level in the downcomer. In the experiment, the system was first brought to steady state conditions and then a transient was induced by a step decrease in the feedwater flow which resulted in a mismatch in the steam and feedwater flows. The mismatch induced a falling downcomer level as the test proceeded. In Figure 1 the experimental data is compared with two different code simulations which were identical except for the use, or non-use, of the level tracking model. Note that without level tracking, the code calculated mass flow continued to diverge from the measured data as the downcomer level decreased. In contrast, use of the level tracking model produced more consistent and more accurate mass flows (i.e., calculated flows were well within the experimental data uncertainties). In both simulations, a step change in the mass flow was produced as the

downcomer liquid level passed across a cell boundary in the downcomer model. This behavior is not exhibited in more dynamic transients where the downcomer liquid level falls at a faster rate. The subject behavior is associated with the calculation of static head and it therefore not exhibited when dynamic head effects predominate (faster transients) or in steady state where cell boundaries are not crossed by the downcomer liquid level.

Figures 2 through 5 compare experimental and code data from the Marviken containment during blowdown test 18.<sup>3</sup> Figures 2 and 3 show typical drywell pressure and vapor temperature, respectively. Figures 4 and 5 show similar comparisons for the wetwell. - The comparisons for both drywell parameters, and the wetwell temperature are considered good. The simulated wetwell pressure is considered adequate, but not as accurate as the other simulated parameters. The reader should note the stratified nature of the experimental vapor exhibited in Figure 5. These same effects may also be partially responsible for the larger difference between the experimental and code calculated wetwell pressure (Figure 4). The reader should also be aware that in this experiment, no significant pool boiling occurred in the wetwell. The code's predictive quality during pool boiling is discussed in a subsequent paragraph. Based on the Marviken results, it is concluded the code has high probability of well simulating BWR drywells and secondary containments.

Figures 6 and 7 show comparisons of prototypical BWR/4 operational transient behavior where the recirculation pumps in both loops were tripped off. These figures compare the core inlet flow and core power, respectively. These results are typical of the assessments performed to date and are considered to indicate adequate operational transient simulation quality. It should be noted these studies were conducted with point kinetics representation of the core. It is well recognized that in those transients (such as ATWS) in which significant axial and radial reactivity variations exist, point kinetics may not be sufficient. Those considerations are discussed later in this paper.

## CONTINUED CODE DEVELOPMENT AND ASSESSMENT RECOMMENDATIONS

Based on the recent assessment results it is concluded that the code is sufficiently mature to warrant its application to safety analyses. However, we note that in such applications, certain predicted behavior will in all probability have uncertainties which do not lend themselves to clearly defensible conclusions regarding reactor behavior without further sensitivity studies. These studies can be performed during the safety analyses; however, it may be more efficient to continue with further code development and assessment to reduce the limits of selected uncertainties. Activities considered more important in such a scheme are identified in the following paragraphs.

Simulation uncertainties could be reduced with further code technology development in the areas of:

- a. Level tracking for slow natural circulation transients
- b. Momentum solution scheme (i.e., 3-dimensional reflood)
- c. Water packing
- d. Counter-current flooding (i.e., more general model)
- e. Injected subcooled liquid condensation
- f. Separator behavior (i.e., more mechanistic model)
- g. Containment pool boiling.

A typical example of the work suggested here is illustrated by the containment pool boiling behavior. The containment modeling feature was added to MOD1 to provide a globally adequate feedback function to the models of the nuclear steam supply system (NSSS) and control systems. It was not the intent to provide a tool with which to perform detailed simulations of the containment; such tools are available elsewhere. However, the material presented in the prior section shows good global containment simulation prior to pool boiling. Figures 8 and 9 show similar results for a Mark I containment, as compared with one of the detailed containment codes<sup>4</sup> (experimental data is limited in the public domain). However, Figures 8 and 9 also show that the TRAC-BD1/MOD1 simulation

quality after pool boiling commences is totally inadequate (as was expected because of the code design limitations). Because of the good simulation quality before pool boiling, and because pool boiling behavior is important to severe accident analysis, it seems appropriate to consider further enhancement of the code capability through the addition of a pool boiling model.

Further reduction in the simulation uncertainties could be provided with additional code assessment of:

- a. Fast numerics (also an efficiency consideration)
- b. 1- and 3-dimensional reactor kinetics
- c. Boron transport
- d. Balance of plant
- e. Containment.

Further work for Items a and b is planned during FY-1985. It should be noted that prototypical data for the assessment of Items b through e is extremely limited. These data limitations should be considered primary objectives in further data gathering and experimental tasks.

Simulation uncertainties could be reduced with the continued development of user guidelines for:

- a. Prototypical control system modeling
- b. Break flow modeling.

As an example, consider the rod cladding temperature comparisons shown in Figure 10.<sup>5</sup> The blind simulation was conducted prior to release of the experimental data.<sup>a</sup> The blind simulation missed the initial short term dryout and while producing the second dryout and subsequent heat up, did so

---

a. Actual steady state initial, and transient boundary conditions were, however, used in the blind calculations.

at a delayed time. Subsequent analysis (sensitivity study), after release of the experimental data, showed the discrepancy in the blind simulation was a sole function of underpredicting the break mass flow. By revising the break model discharge coefficient (from 0.7 to 0.9), the sensitivity calculation was able to well capture both the significant behavior and the correct timing. To our knowledge, no single, uniformly good break flow model exists in any code. Thus it appears necessary to provide the user with a good and sufficient set of guidelines for the use of whatever break flow models are incorporated in each code.<sup>6</sup>

The simulation efficiency of each calculation could be improved with:

- a. A more general safety relief valve model
- b. Provision of azimuthal cell to cell heat transfer
- c. Provision of implicitly calculated leak paths

The reader should note these features would improve efficiency by a reduction in modeling complexity and/or run times in contrast to a reduction in the number of simulations, as was previously noted in relation to increased efficiency.

## CONCLUSIONS

Based on the assessment results, it is concluded TRAC-BD1/MOD1 is sufficiently mature to warrant application to safety analyses. In those applications, the current code may require certain sensitivity studies to ensure the analyst has adequately characterized all predicted parameter uncertainties to the level necessary for well founded conclusions. The analyst must also carefully plan the type of simulations to reduce calculational costs.

The preceding restraints could be relaxed with further work in the areas of code development, code assessment and the development of additional user guidelines, as selectively identified in this paper.

## NOTICE

This paper was prepared as an account of work sponsored by an agency of the United States Government. Neither the United States Government nor any agency thereof, or any of their employees, makes any warranty, expressed or implied, or assumes any legal liability or responsibility or any third party's use, or the results of such use, of any information, apparatus, product or process disclosed in this report, or represents that its use by such third party would not infringe privately owned rights. The views expressed in this paper are not necessarily those of the U.S. Nuclear Regulatory Commission.

## REFERENCES

1. INEL TRAC-BD1 Code Development Group, TRAC-BD1/MOD1: An Advanced Best Estimate Computer Code for Boiling Water Reactor Analysis, NUREG/CR-3633, EG&G Idaho, Inc., April 1984.
2. W. S. Hwang et al., BWR Full Integral Simulation Test (FIST), Phase 1 Test Results, GEAP-30496, General Electric Co., November 1983.
3. The Marviken Full Scale Containment Experiments Second Series, Blowdown 18 Results, MXB-101, Studsvik Energiteknik AB, March 1977.
4. Don W. Hargroves, and Lawrence J. Metcalfe, CONTEMPT-LT/028--A computer Program for Predicting Containment Pressure-Temperature Response to a Loss-of-Coolant Accident, NUREG/CR-0255, TREE-1279, EG&G Idaho, Inc., March 1979.
5. O. Sandervag and D. Wennerberg, FIX-II Experimental Results of Test 3025 (ISP-15), Studsvik Technical Report NR-83/283, Studsvik Energiteknik AB, July 1983.
6. D. G. Hall, Empirically Based Modeling Techniques for Predicting Critical Flow Rates in Nozzles, Tubes, and Orifices, EGG-CVAP-TR-78-010, EG&G Idaho, Inc., May 1978.

TABLE 1. TRAC-BD1/MOD1 FY-1984 ASSESSMENT STUDIES

Description	Status
FIST power transient (~ATWS)	Completed 12/83
FIX-II intermediate break blowdown	Completed 3/84
FIST natural circulation	Completed 7/84
SSTF BWR/4 LOCA reflood	Completed 7/84
Containment:	Completed 9/84
Marviken LOCA Mark I ATWS	
ROSA-III small break LOCA	Completed 9/84
BWR/4 operational transients:	To be completed 11/84
One recirculation pump trip Two recirculation pump trip Generator load rejection Feedwater turbine trip	

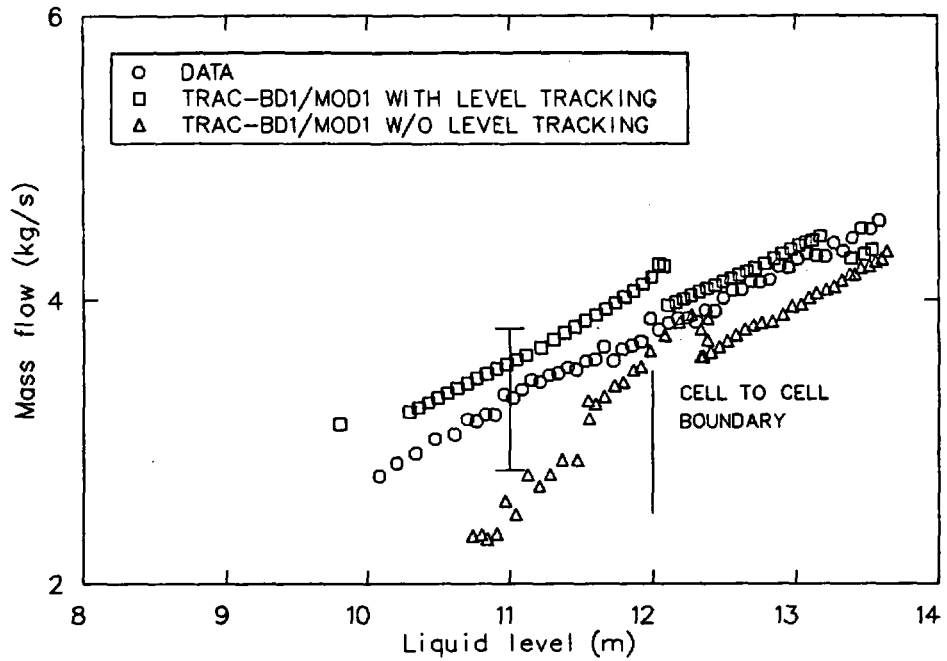


Figure 1. Comparison of the natural circulation flow versus downcomer level for FIST Test 6PNC1-4 (2MW).

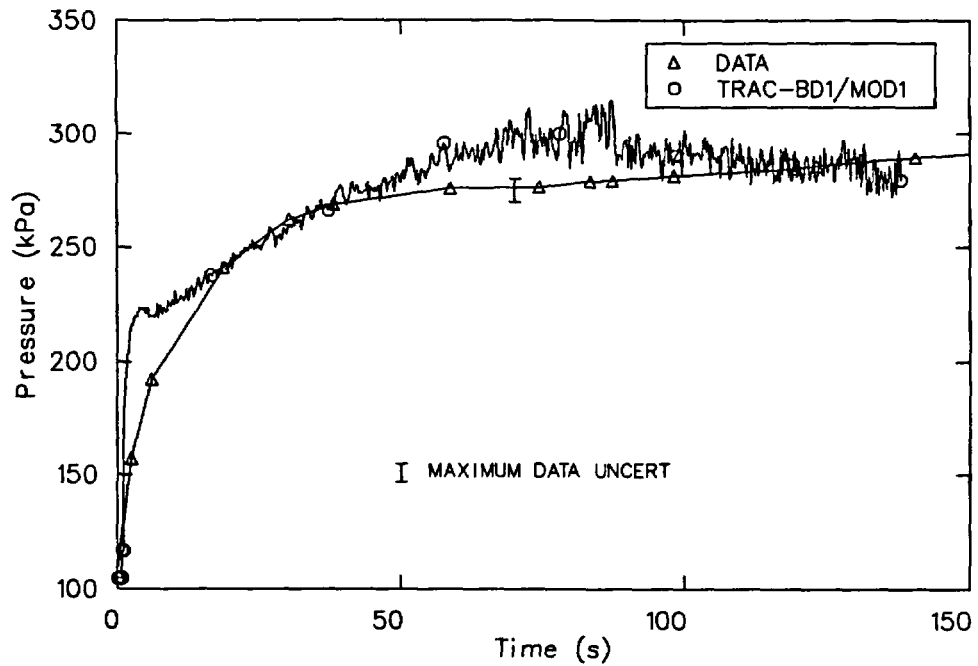


Figure 2. Comparison of typical drywell pressure - Marviken test 18.

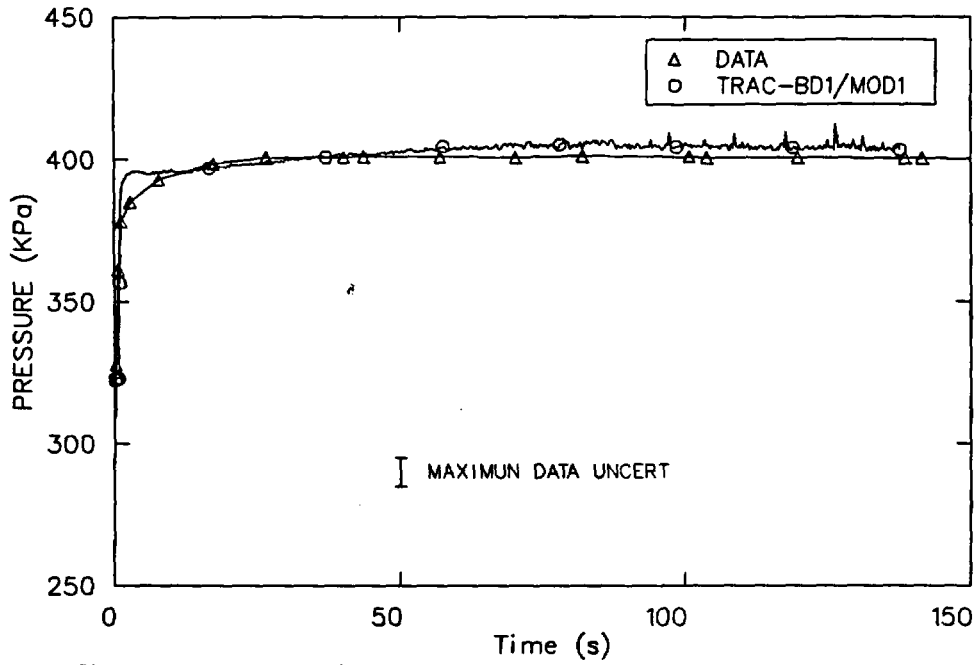


Figure 3. Comparison of typical drywell vapor temperature - Marviken test 18.

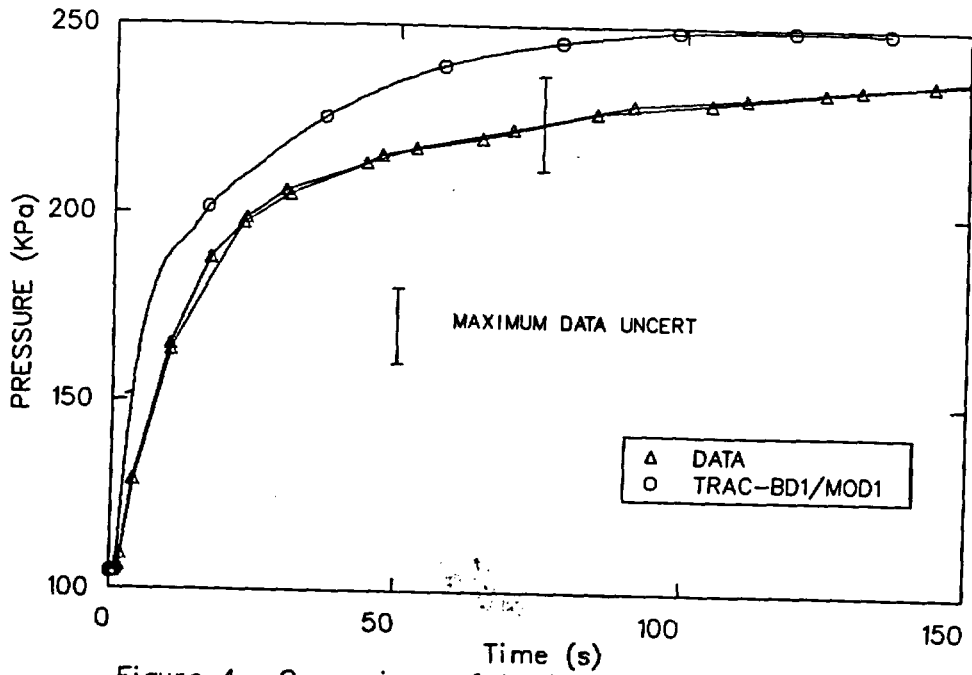


Figure 4. Comparison of typical wetwell pressure - Marviken test 18.

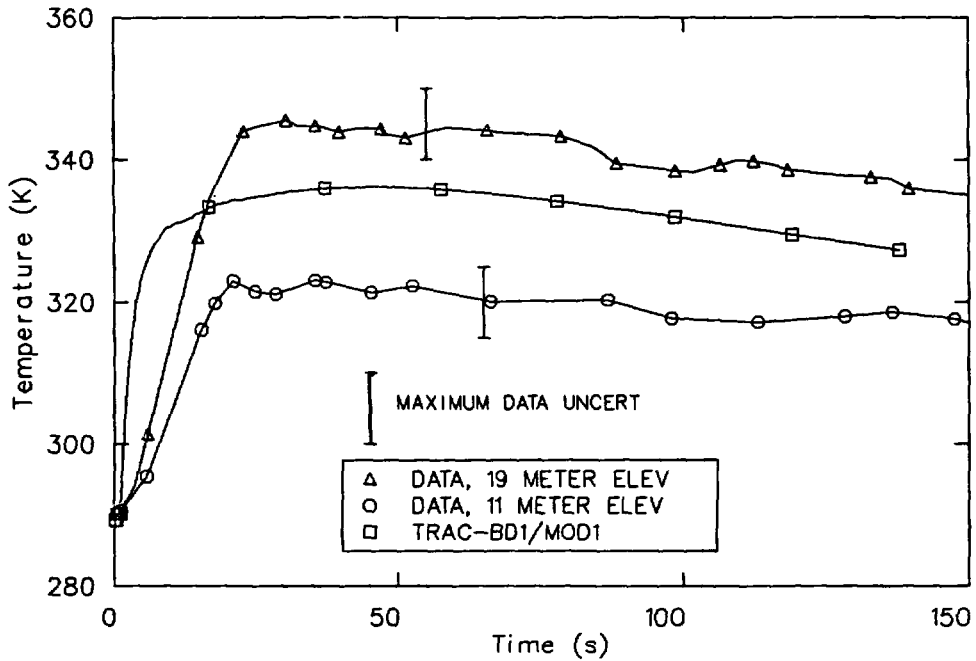


Figure 5. Comparison of typical wetwell vapor temperature - Marviken test 18.

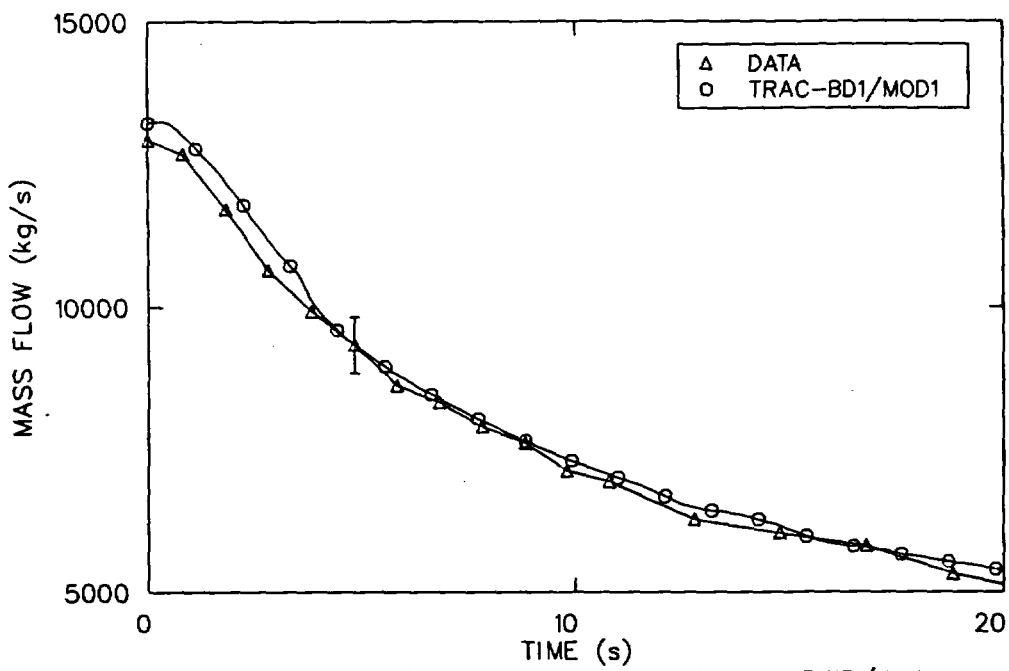


Figure 6. Comparison of core inlet flow - BWR/4 two recirculation pump trip.

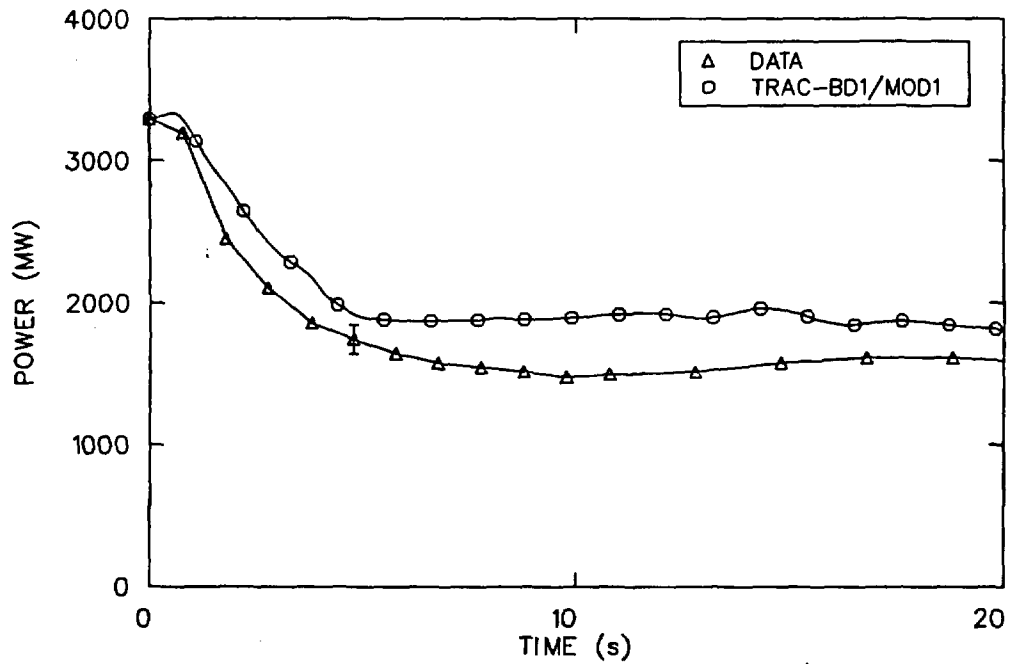


Figure 7. Comparison of core power - BWR/4 two recirculation pump trip.

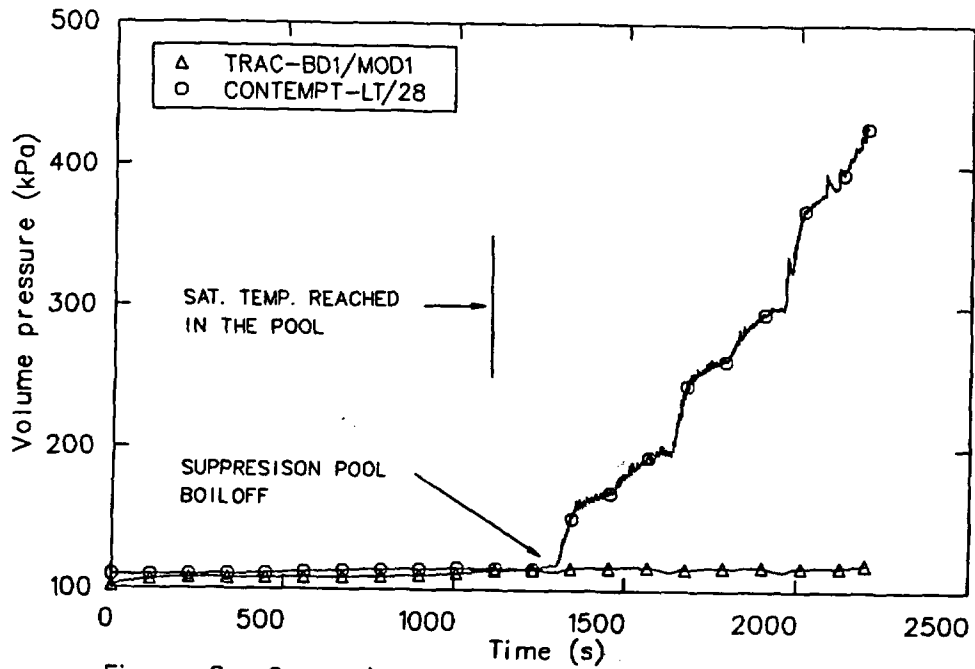


Figure 8. Comparison of Mark I wetwell pressure.

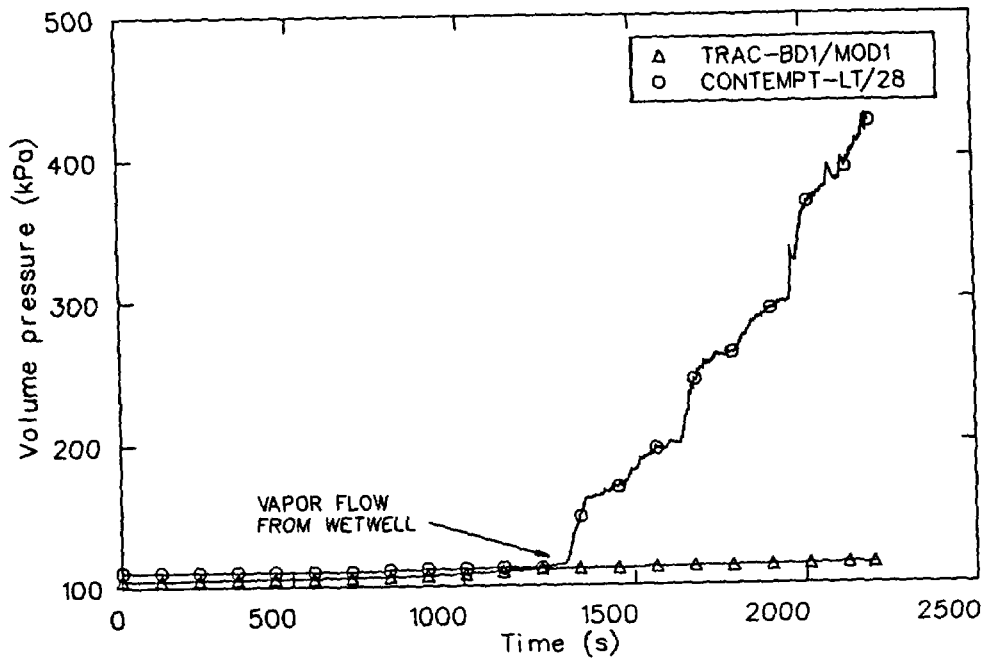


Figure 9. Comparison of Mark I drywell pressure.

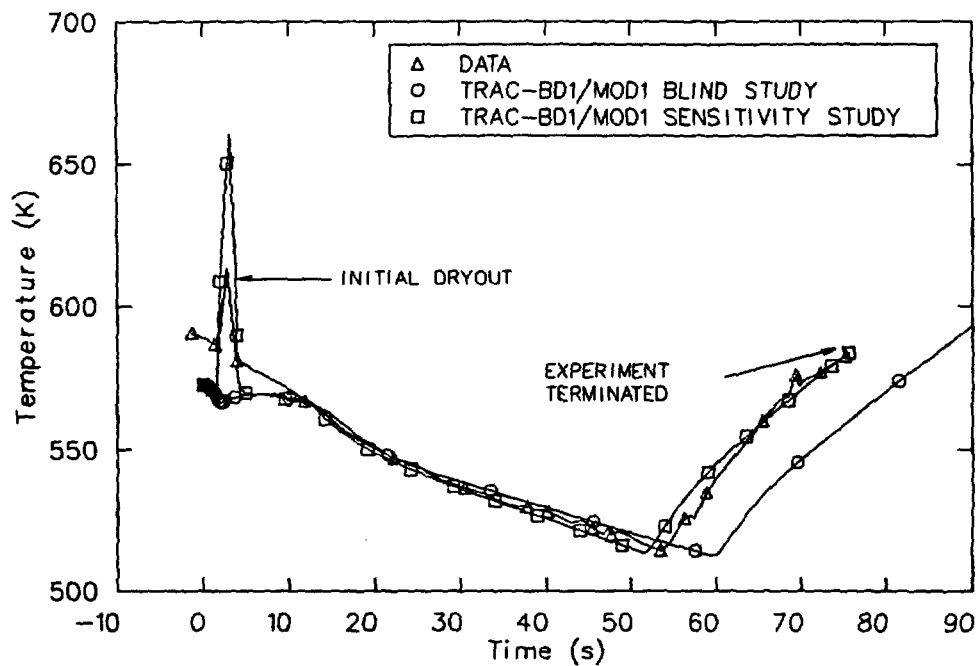


Figure 10. Comparison of experimental and simulated rod cladding temperature - FIX-II blowdown test 3025.

## RELAP5/MOD2 ASSESSMENT CALCULATION OF SEMISCALE TEST S-UT-8

Donald M. Ogden

Cliff B. Davis

EG&G Idaho, Inc.

### Introduction

In support of the United States Nuclear Regulatory Commission's independent assessment of RELAP5, the Idaho National Engineering Laboratory (INEL) has performed analysis of Semiscale Test S-UT-8 using RELAP5/MOD2.

Test S-UT-8, representing a 5% cold leg break, is of interest because an extended core liquid level depression that was related to liquid holdup in the steam generator U-tubes occurred prior to loop seal clearing. Initial subsequent renodalization calculations were performed. Calculation results were compared with experimental data. Assessment of the code's performance relative to the observed test phenomena, including loop seal clearing, steam generator liquid holdup, and core liquid level depression, was performed.

### Facility and Test Description

The Semiscale Mod-2A system (Figure 1) is a two-loop large pressurized water reactor (LPWR) simulator located at the Idaho National Engineering Laboratory. One loop, the intact loop is scaled to simulate three loops of a LPWR, while the other loop, the broken loop, represents a single loop in which a break is simulated. The system primary coolant volume and core power are scaled by approximately 1/1700. Geometric similarity and component layout have been maintained between the Mod-2A system and a LPWR. Specific similarities include a full-length (3.66 m) electrically heated core, full-length upper plenum and upper head, two full-length steam generators, and the preservation of the relative elevations of the various components. Emergency core cooling (ECC) systems include a high pressure injection system, passive accumulators, and a low pressure injection system, each of which inject coolant into the cold legs.

The electrically heated core consists of 25 rods in a 5 x 5 matrix (1.43 cm pitch). Two rods in opposite corners are unpowered and the remaining 23 rods are powered equally yielding a flat radial profile. The axial power profile is a 12-step chopped cosine.

Each steam generator is scaled with respect to both primary and secondary coolant volumes. The intact loop generator contains six U-tubes and the broken loop contains two U-tubes. The secondary side of both generators consists of a rising (boiler) section, steam separator and downcomer. Feedwater enters the downcomer and steam exits the top of the steam generator.

The reactor vessel simulator is multi-sectional consisting of an upper head, upper plenum, heated core region, lower plenum, and an external inlet annulus and downcomer pipe. The complete pressure vessel is approximately 10 m in length. The upper head accounts for about the top 25% of the pressure vessel length and volume. Included in the upper head, are the following: a filler piece to provide proper upper head liquid volume, a simulated control rod guide tube, and two simulated support columns. The simulated upper core support plate forms the boundary between the upper head and upper plenum. The guide tube and the two core support columns penetrate the upper core support plate and extend into the upper plenum region.

A small line connecting the vessel downcomer inlet annulus to the upper head simulates the bypass flow paths within a LPWR vessel. A control valve is installed in the bypass line for adjustment of the bypass flow and bypass line hydraulic resistance. For S-UT-8 the bypass flow was 1.5% of core flow. The bypass standpipe (within the upper head) was shortened in Test S-UT-8, relative to previous UT tests, to obtain a fluid volume above the top of the standpipe equivalent to the scaled inverted top hat volume above the PWR downcomer bypass nozzles. Eight 7.67 mm diameter holes were drilled in a 6.3 cm section of the guide tube below the upper support plate for Test S-UT-8 which were not present in earlier UT tests. An orifice in the guide tube was enlarged in Test S-UT-8 to 9.98 mm diameter to reduce the guide tube hydraulic resistance to 9.3% of the bypass line resistance.

The support columns were plugged in Test S-UT-8 in an attempt to eliminate a flow path between the upper head and upper plenum. However, an unintended flow path from the upper head to the upper plenum through the support tubes still existed in Test S-UT-8 because the instrument holes in the support tubes were not plugged.

Other changes made just prior to Test S-UT-8, which were consistent with a continuing effort to improve Semiscale scaling characteristics, included replacing the 3-inch piping in the intact loop between the hot leg and the pump suction with 2 1/2-inch piping. The 4-inch piping that formed the intact loop pantleg to the steam generator was also replaced by 2 1/2-inch piping and the steam generator plenum was replaced. The broken loop pantleg and steam generator plenum were also replaced, although the piping remained 1 1/2-inch. External heaters were placed on the vessel to mitigate heat losses. The external heaters on the primary piping were modified where the piping size was changed.

Test S-UT-8, which simulated a 5% cold leg break in a LPWR, was a unique test in the UT test series. It was performed after the Natural Circulation test series, eight months after Test S-UT-6, and produced phenomena that none of the previous tests showed. Except for the modifications made in the piping and upper head, it was intended to duplicate Test S-UT-6. However, a substantial core uncover was observed prior to loop seal uncover which was not seen in any of the previous UT series tests.

The experimental data from S-UT-8 were qualified and corrected to the same extent as the rest of the S-UT series data. Some of the data are questionable, however. The broken loop steam generator secondary levels calculated from differential pressure measurements covering the same range give inconsistent results. The U-tubes were, however, probably completely covered by liquid in the secondaries. Since nearly all the primary-to-secondary heat transfer occurs within the first few feet, the

primary response was probably not affected. The differential pressure measurements used to calculate the liquid level in the broken loop steam generator U-tubes, both up and down sides, failed. Furthermore, the flow measurements to and from the upper head were questionable. The bypass flow measurement failed, the support tube flow instrumentation was removed, and the guide tube flow measurement appears unreliable. The high pressure injection flow measurements also failed. Despite the inconsistencies and failed instruments, sufficient qualified data are available to perform an assessment analysis.

### RELAP5 Model Description

RELAP5/MOD2 is an advanced system analysis code under development at INEL for the U.S. Nuclear Regulatory Commission, office of Reactor Safety Research. It is based on a nonhomogeneous, nonequilibrium hydrodynamic model and includes thermal-hydraulic and component models used to describe the processes that occur in a LPWR. The Semiscale Mod-2A system RELAP5 model is represented by the nodalization diagram in Figure 2. This model consists of 154 hydrodynamic volumes, 155 junctions, and 190 heat structures. The nonequilibrium and nonhomogeneous features of the code are applied in all the volumes and junctions of the model. Steam generator secondaries, ECC injection, system environmental heat loss and piping guard heaters are modeled in detail. The core axial power profile is modeled with twelve heat structures over six axial hydrodynamic volumes.

The upper head region is nodalized to allow junctions at the elevations of the top of the control rod guide tube, core bypass line and support columns. Each of these flow paths is modeled individually. Discharge coefficients are applied to the RELAP5 critical flow model at the break. One coefficient (CD1) is applied for single-phase (subcooled) critical flow and another (CD2) is used for two-phase flow. These coefficients are an empirical correction to the critical flow rate to account for parameters such as the multi-dimensional effects due to boundary layer detachment at the orifice throat. A value 0.75 was selected for CD1 and 0.80 for CD2.

An area of uncertainty in Test S-UT-8 relates to the drain rate from the upper head to the upper plenum through the unplugged instrument holes in the support tubes. For the RELAP5/MOD2 calculations, a loss coefficient was imposed upon this flow path which in earlier RELAP5/MOD1.5 calculations gave reasonable agreement with the drain rate seen in the experiment.

### RELAP/MOD2 Assessment Results

The initial calculation of Test S-UT-8 was performed with the Semiscale RELAP5 model described in the previous section. It encompassed the most recent information relative to the facility configuration for Test S-UT-8. The vessel upper plenum and intact steam generator secondary pressure responses are compared with data in Figure 3. As seen in the figure, the comparison with experimental data is quite good. The primary pressure response was controlled by flashing, heat transfer to the steam generators and, to a lesser extent, the break flow. A comparison of calculated and integrated break flows is shown in Figure 4. As evidenced by the figure, the calculated break flow was underpredicted after 80s, corresponding to the two-phase blowdown period, but sensitivity calculations showed that the results between 80 and 250 s were relatively insensitive to the two-phase discharge coefficient. A comparison of upper head collapsed liquid levels is shown in Figure 5. The draining of the upper head through the unplugged instrument holes in the support tubes was modeled with appropriate losses to provide the reasonable comparison shown in the figure. This was done to remove one of the uncertainties in the experiment, which previous analysis showed was only of second order importance to the phenomena of steam generator liquid holdup and core uncovering. Figure 6 shows a comparison of calculated and measured liquid levels in the intact loop pump suction piping on the downflow side. The calculation adequately predicted the liquid level transient behavior including the timing of the loop seal clearing seen at approximately 240 s. A comparison of calculated and measured collapsed liquid levels in the vessel is shown in Figure 7. The liquid levels were obtained by dividing calculated and measured differential pressures by the liquid density and acceleration due to gravity. The differential pressures were not reliable indications of collapsed liquid levels until after the flow

effects from the reactor coolant pump trip subsided near 75 s. Early in the transient the comparison was excellent. However, in the test the liquid level decreased until 240 s when the core was almost completely uncovered. In the RELAP5 initial calculation, the level did not drop below the elevation of the bottom of the loop seals, and most of the core remained covered. Calculated and measured collapsed liquid levels in the uphill side of the U-tubes in the intact loop steam generator are shown in Figure 8. One of the interesting features of Test S-UT-8, which was primarily responsible for the unexpected core uncover, was the increase in collapsed liquid level seen in the figure near 50 seconds. The initial RELAP5 calculation was not able to predict this phenomenon. It should be noted, however, that the calculation predicted the draining of the U-tubes quite well as evidenced by the similar rate of level decrease in the calculation and test after 100 s. Analysis of the RELAP5/MOD2 initial calculation suggested that the inability of the model to predict the increase in steam generator U-tube liquid level may be related to the upper plenum modeling. Figure 9 shows a comparison of calculated and measured upper plenum density. The data shows that near 50 seconds, when the liquid level was increasing in the uphill side of the steam generator U-tubes, the density in the upper plenum was rapidly decreasing. The RELAP5 calculation did not predict this decrease until nearly 250 seconds, which was after the observed core liquid level depression and recovery. The upper plenum modeling was the subject of subsequent calculations using a different model for the upper plenum connection to the hot leg inlets.

Figure 10 schematically illustrates the modeling of the upper plenum and hot legs for the initial and subsequent calculations. A possible deficiency of the initial model was the upper plenum to hot leg connection. In the initial calculation, the division between volumes in the upper plenum was at the hot leg centerline, and the hot legs were connected to the volume below the hot leg centerline. Because RELAP5/MOD2 calculates gravity pressure terms between cell centers, a gravity head existed between the upper plenum and hot legs which was dependent on the size of the upper plenum volume. This gravity head retarded liquid flow from the upper plenum into the hot leg during periods of cocurrent flow and

promoted liquid draining from the hot leg to the upper plenum during periods of countercurrent flow. A subsequent calculation was performed in which the hot legs were connected to the upper plenum volume above the hot leg centerline rather than the one below as in the initial calculation. While a gravity head still exists between the upper plenum and hot legs, the gravity head now promotes draining of liquid from the upper plenum to the hot legs during periods of cocurrent, positive flow and retards draining of liquid from the hot legs to the upper plenum during countercurrent flow.

Figure 11 shows a comparison of the upper plenum density for the initial and renodalized model calculations. The renodalized model calculation showed an improvement in the prediction of the upper plenum voiding. The effect of the faster upper plenum voiding on the liquid level in the uphill side of the U-tubes in the intact loop steam generator is shown in Figure 12. While the magnitude of the level increase was not well predicted, the renodalized model calculation did predict a level increase at about the right time. The nodalization change also slowed the average drain rate from the U-tubes. Figure 13 shows vessel liquid levels for the calculation and the test. The calculated and measured levels were in good agreement. The liquid level was depressed to nearly the bottom of the core in both the calculation and the test. Core heater cladding temperatures, corresponding to an elevation near the core midplane, are shown in Figure 14 for both calculations. While the initial calculation showed no heatup because it did not predict core uncover, the renodalized model calculation agreed well with the data. The renodalized model calculation demonstrated the importance of upper plenum modeling in correctly predicting entrainment from the upper plenum, steam generator liquid holdup and, consequently, core uncover.

#### Further Work

A comparison of the initial and subsequent calculations shows that the results are sensitive to the orientation of the connection between the upper plenum and hot legs. With the upper plenum divided at the hot leg centerline, it is arbitrary to choose connecting the hot legs to either the

upper or the lower volume. RELAP5/MOD2 has a new model, the crossflow model, which allows a junction to be connected to the center of a volume rather than the inlet or the outlet. The use of the crossflow model would allow the hot legs to be connected to the center of a volume, as illustrated in Figure 10, and thus would eliminate the arbitrary gravity term between the upper plenum and hot legs. Some S-UT-8 calculations have been performed with the crossflow model and it appears that the model has the potential to improve the representation of the upper plenum.

### Conclusions

The results of the RELAP5/MOD2 calculations of Test S-UT-8 were sensitive to upper plenum modeling. For Test S-UT-8, the best results were obtained when the hot legs were connected to an upper plenum volume above the hot leg centerline. However, additional assessment calculations, such as of Test S-UT-6, should be performed to determine the general applicability of the model. Additional Semiscale tests should be performed to further investigate the effects of liquid holdup in the U-tubes and core level depression during small break events.

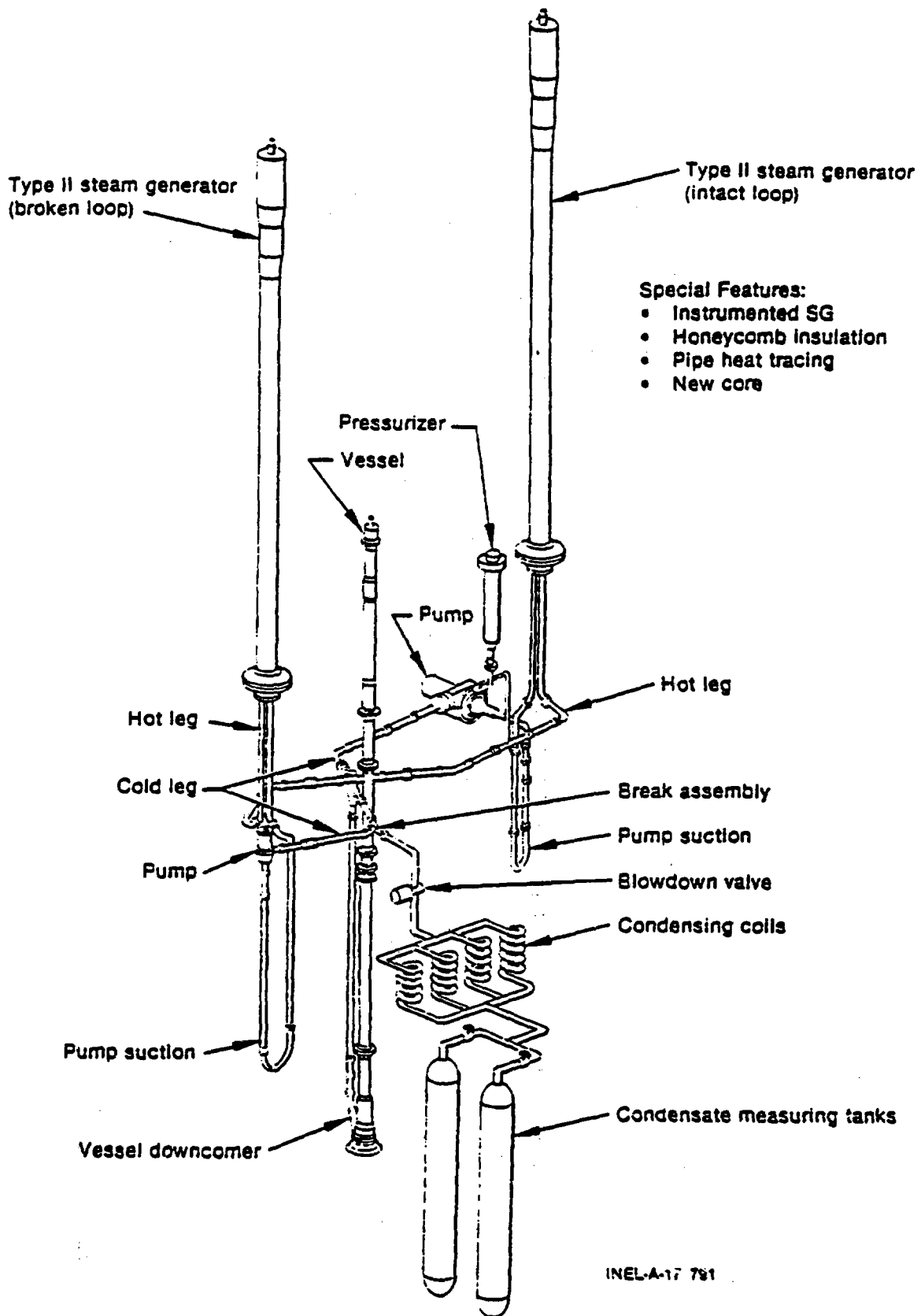


Figure 1. Semiscale MOD-2A system for cold leg break configuration.

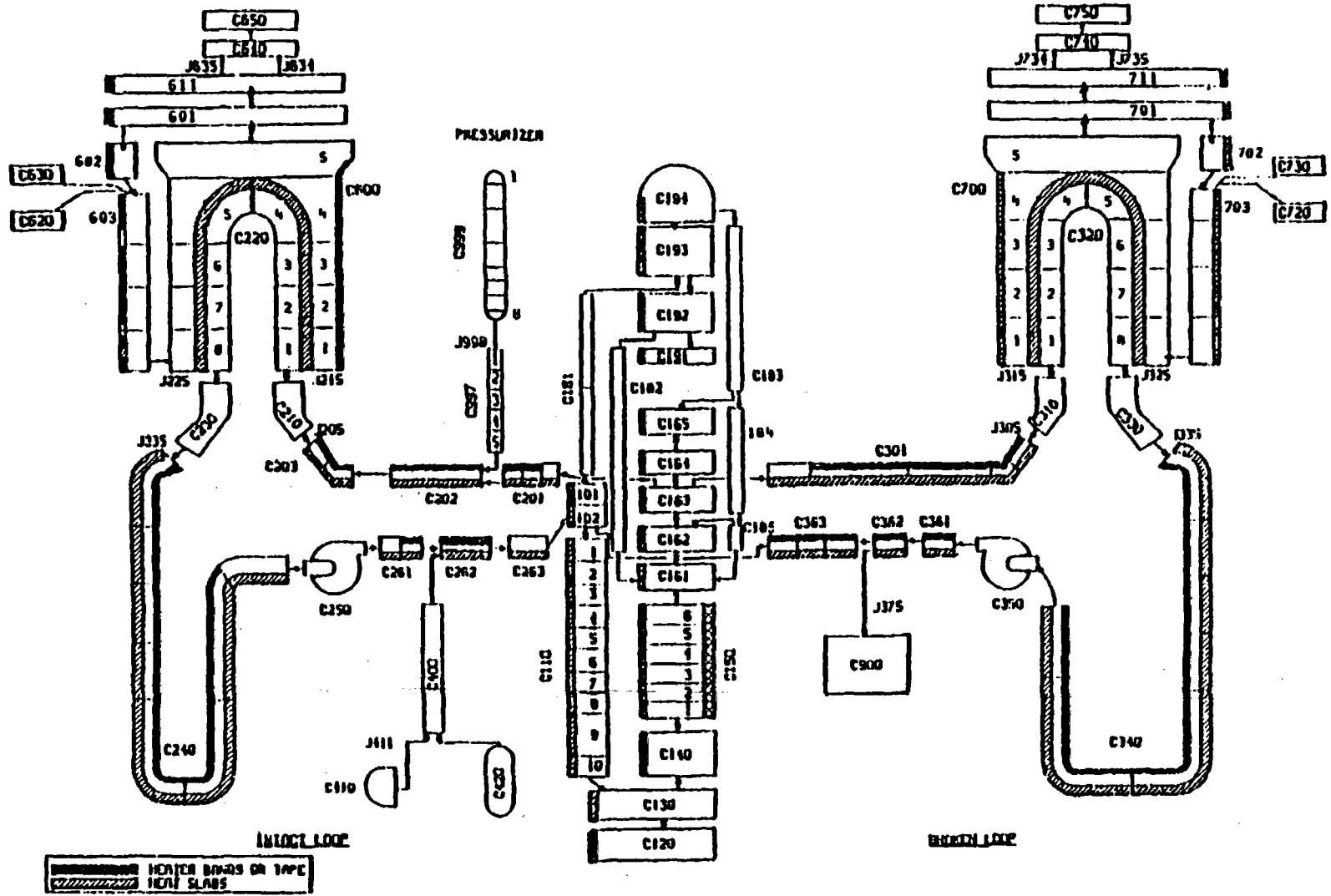


Figure 2. RELAP5/MOD2 model of Semiscale MOD-2A.

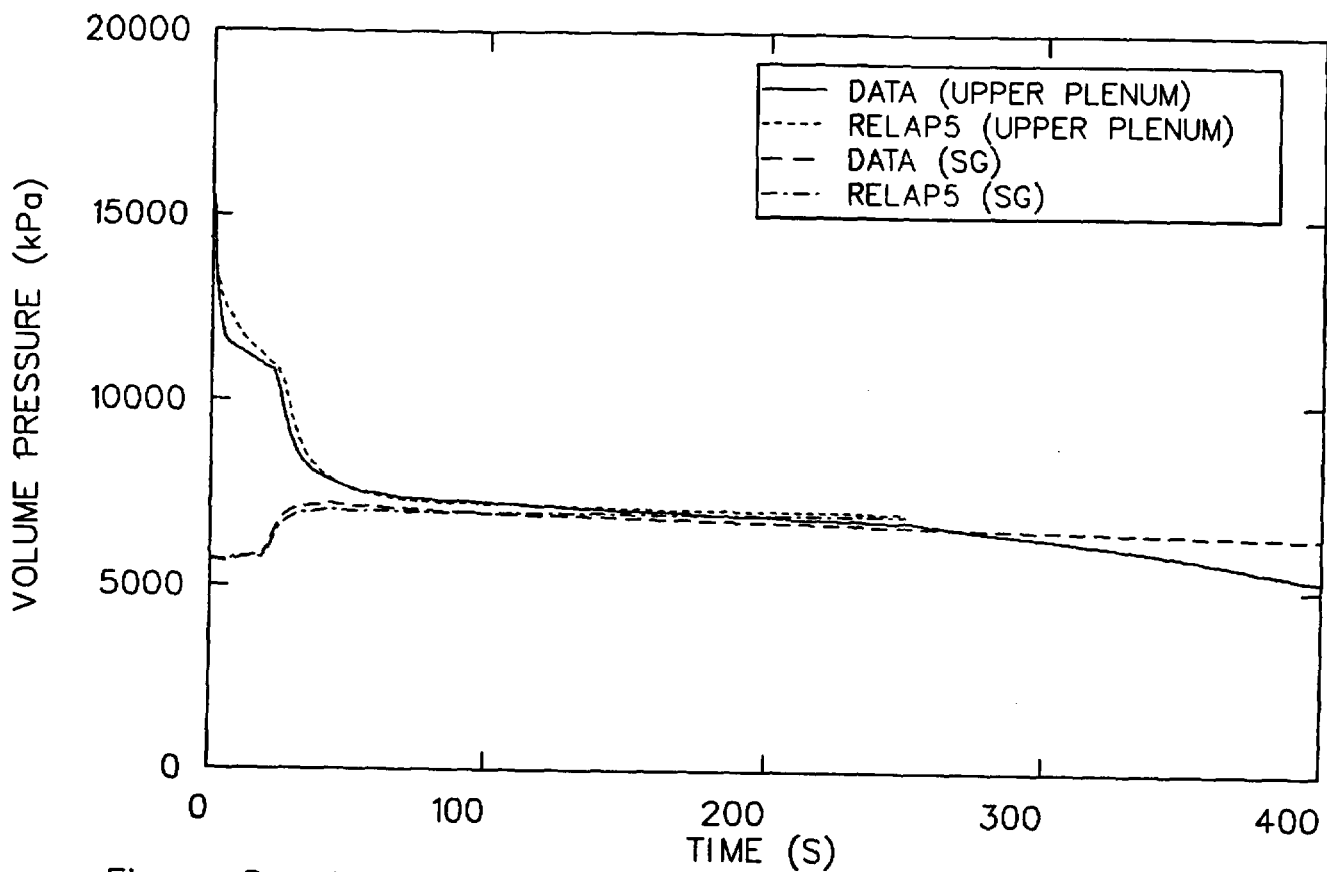


Figure 3. Upper plenum and intact loop steam generator pressure.

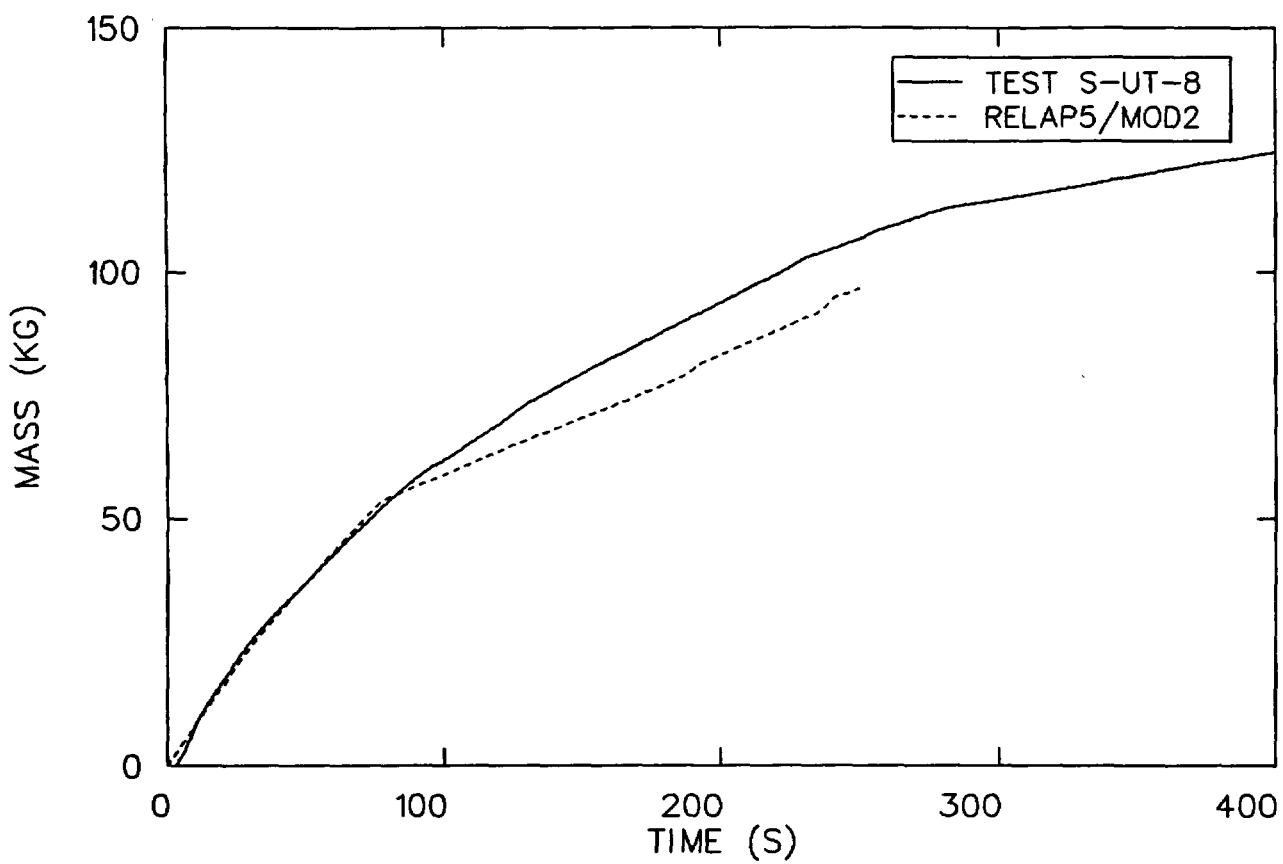


Figure 4. Integrated break flow.

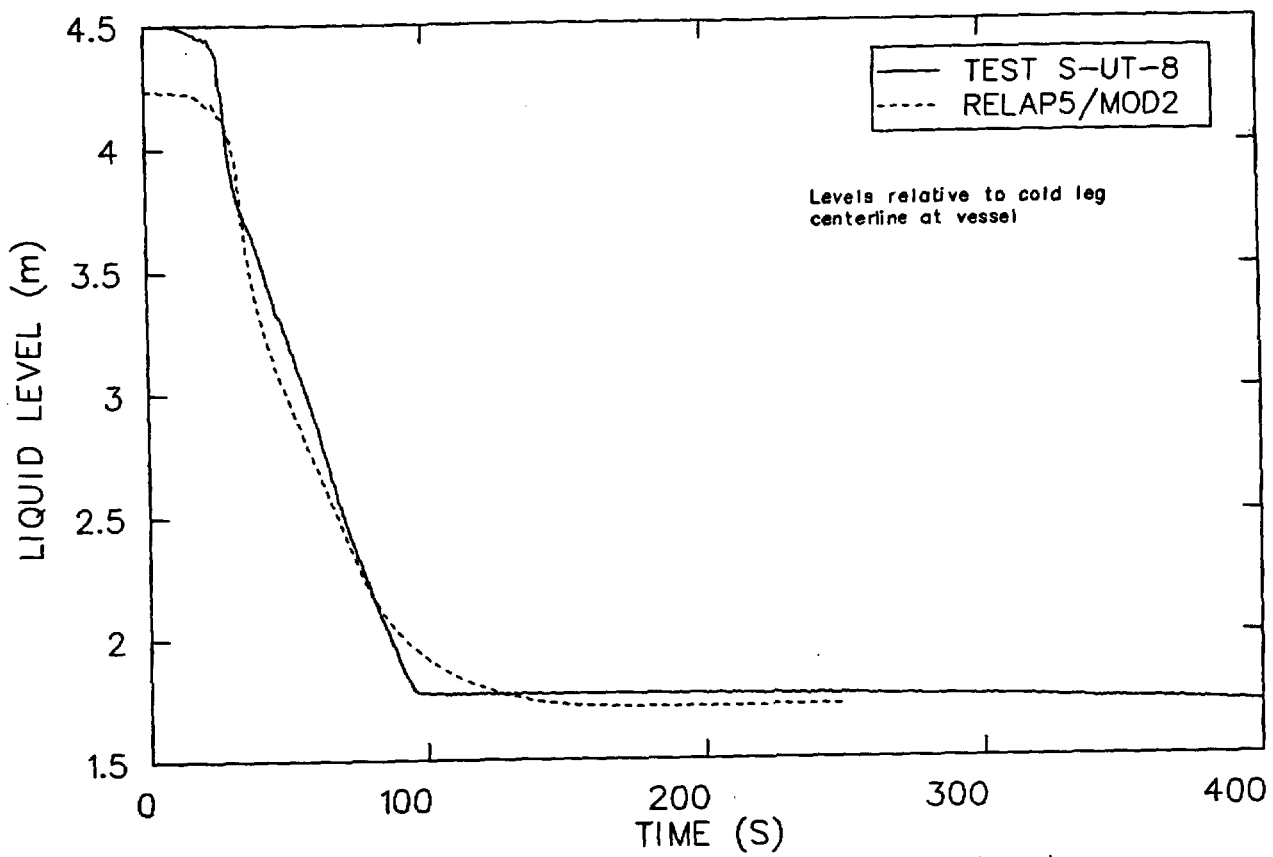


Figure 5. Collapsed liquid levels in the upper head.

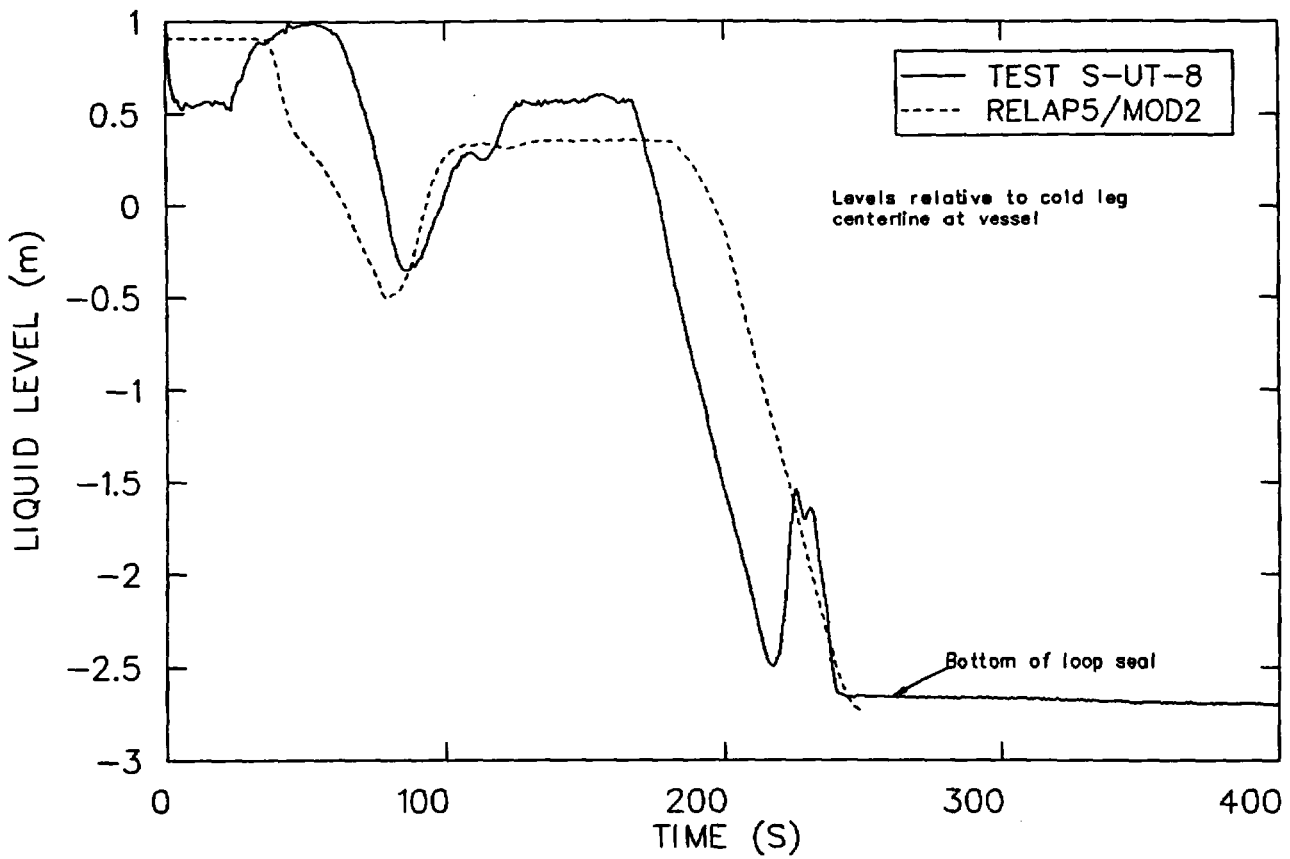


Figure 6. Collapsed liquid levels on the downflow side of the intact loop seal.

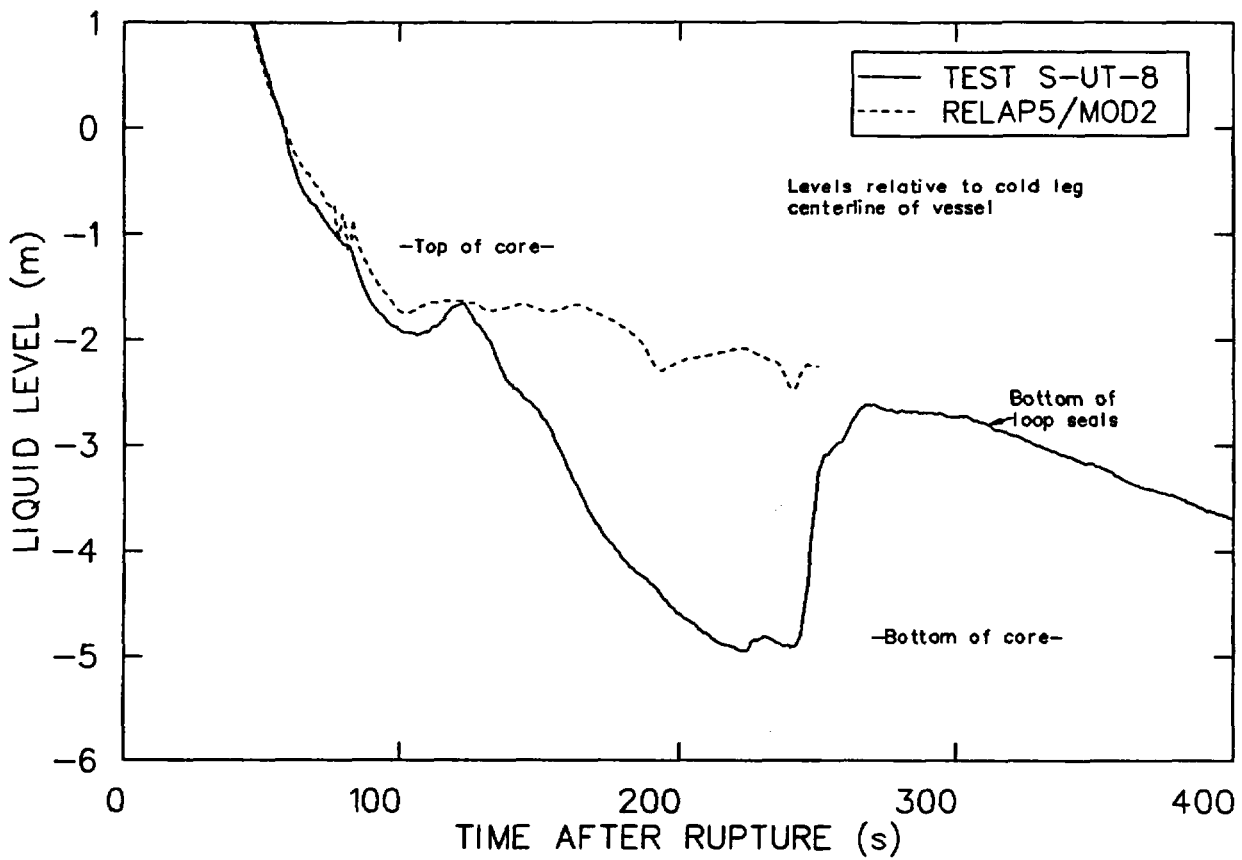


Figure 7. Collapsed liquid levels in the core.

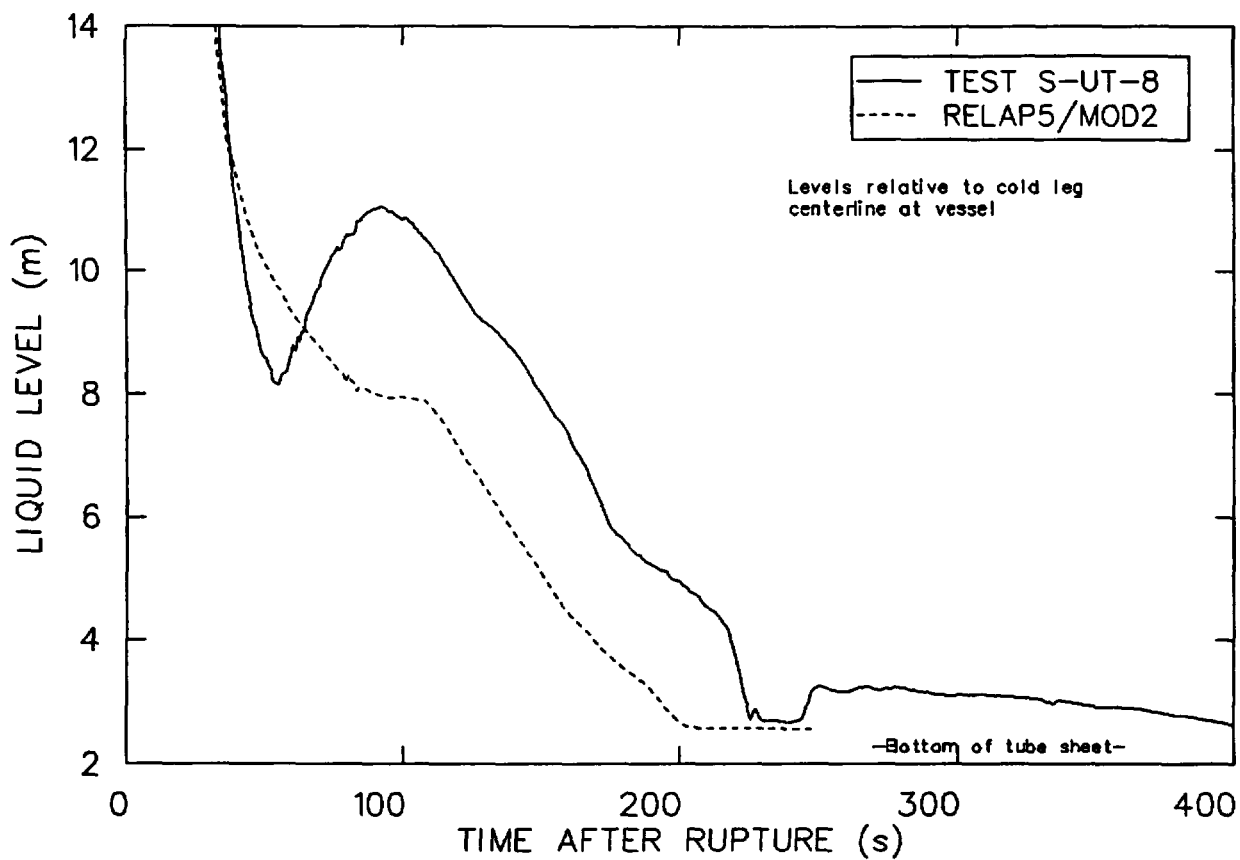


Figure 8. Collapsed liquid levels on the uphill side of the intact loop steam generator.

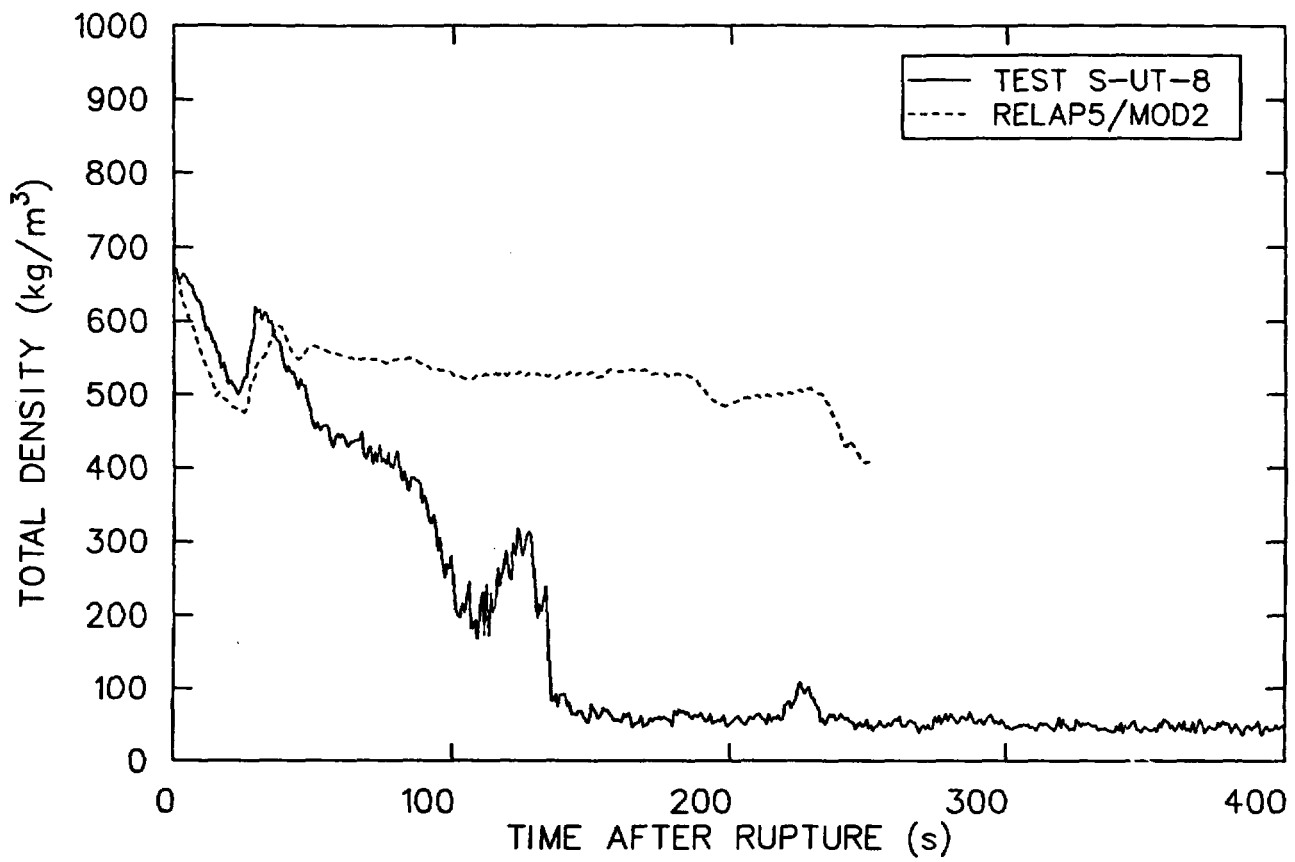


Figure 9. Upper plenum fluid density.

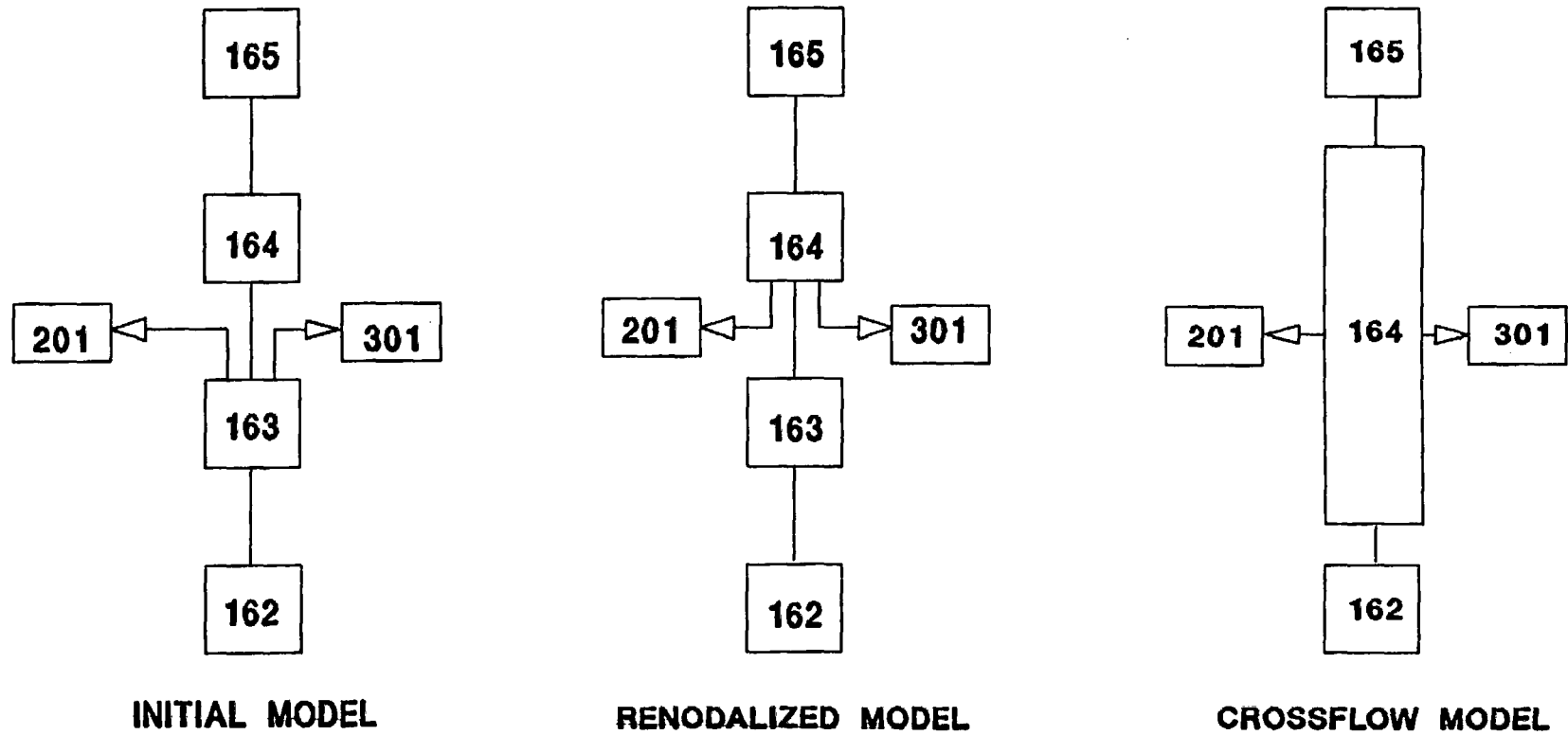


Figure 10. Upper plenum nodalizations.

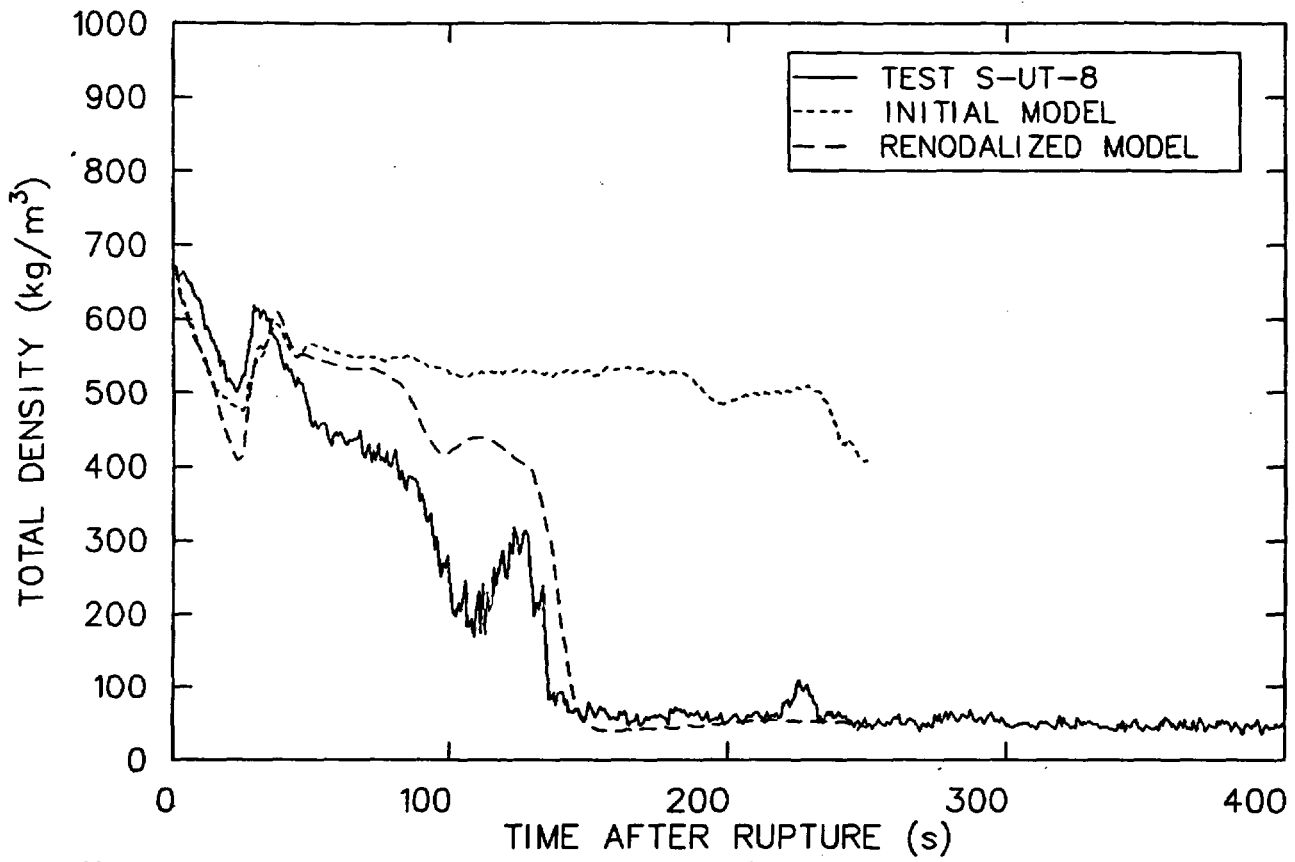


Figure 11. Upper plenum fluid density.

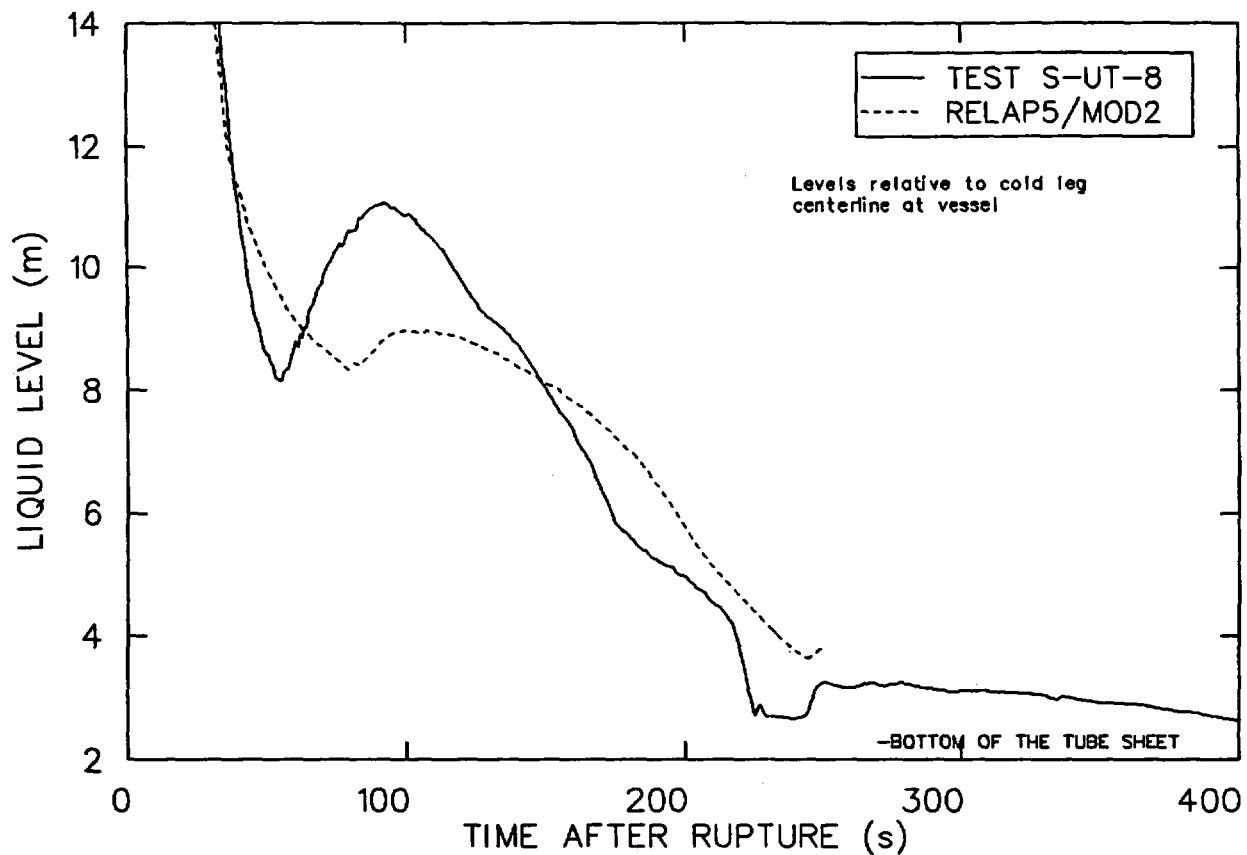


Figure 12. Collapsed liquid levels on the uphill side of the intact loop steam generator.

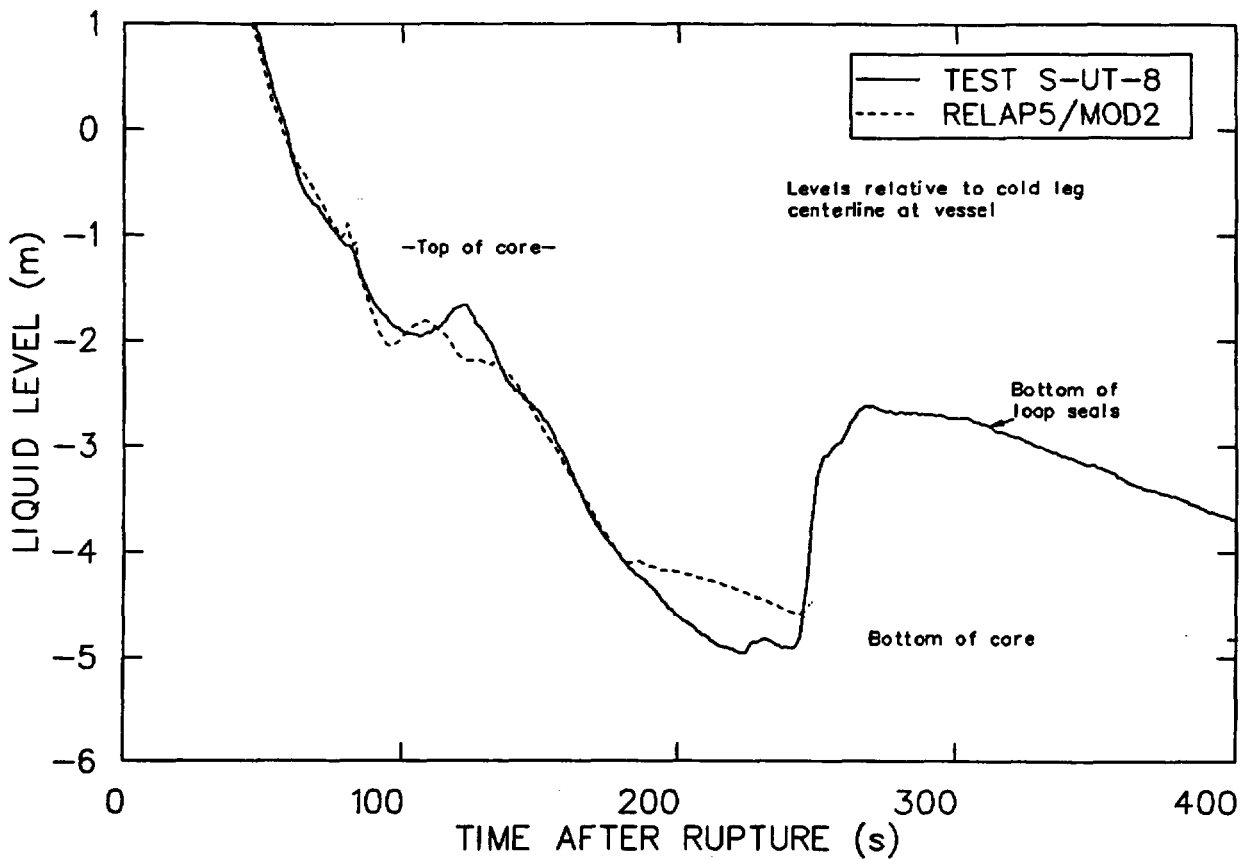


Figure 13. Collapsed liquid levels in the core.

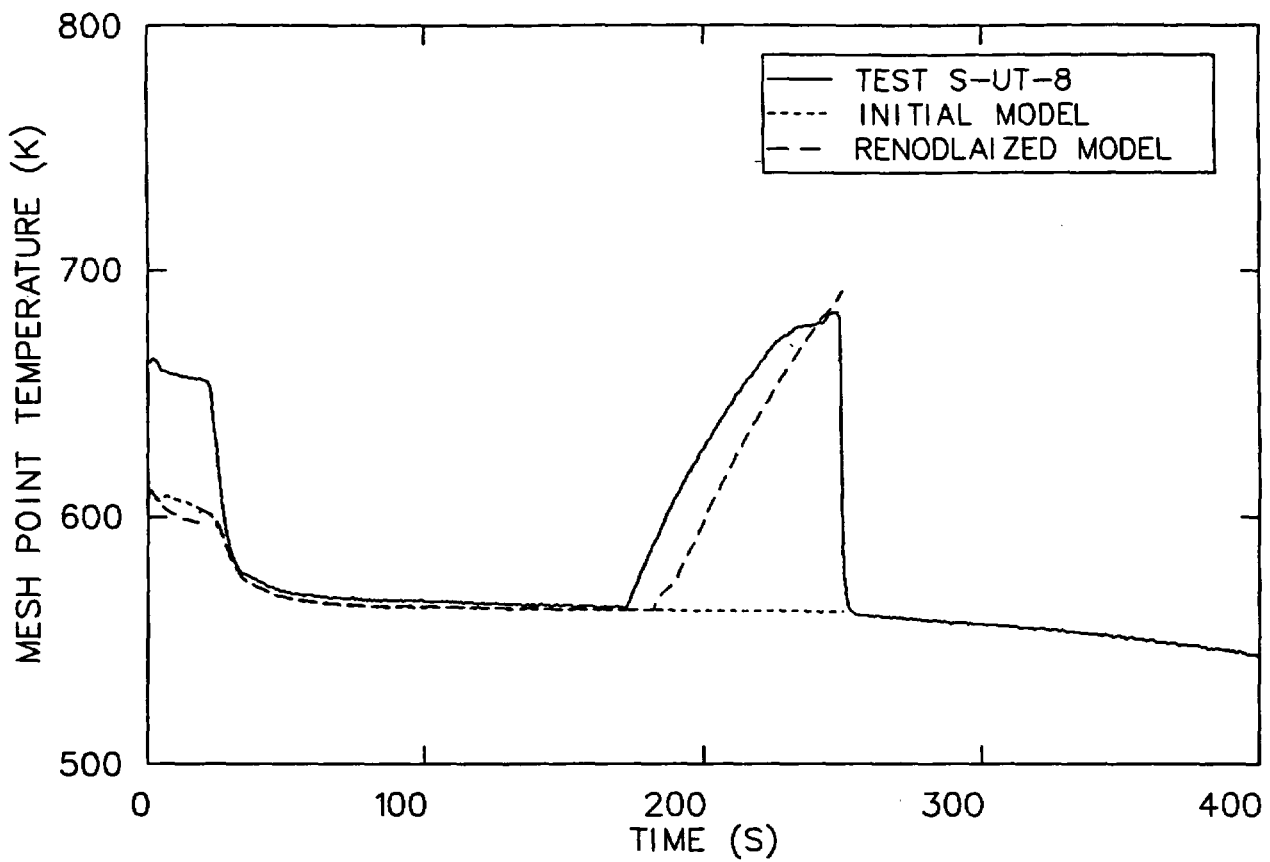


Figure 14. Core heater rod temperatures.

## TRAC-PF1/MOD1 ASSESSMENT AT LOS ALAMOS\*

by

Thad D. Knight  
Safety Code Development Group  
Energy Division  
Los Alamos National Laboratory  
Los Alamos, New Mexico 87545

The Los Alamos National Laboratory is developing the Transient Reactor Analysis Code (TRAC) to provide an advanced best-estimate predictive capability for the analysis of postulated accidents in pressurized water reactors (PWRs). Over the past several years, four distinct versions of the code have been released; each new version introduced improvements to the existing models and numerics and added new models to extend the applications of the code. The first goal of the code was to analyze large-break loss-of-coolant accidents (LOCAs), and the TRAC-PLA and TRAC-PD2 codes<sup>1,2</sup> primarily addressed the large-break LOCA. (The TRAC-PD2/MOD1 code is essentially the same as the TRAC-PD2 code but it also includes a released set of error corrections.) The TRAC-PF1 code<sup>3</sup> contained major changes to the models and trips and to the numerical methods. These modifications enhanced the computational speed of the code and improved the application to small-break LOCAs. The TRAC-PF1/MOD1 code,<sup>4</sup> the latest released version, added improved steam-generator modeling, a turbine component, and a control system together with modified constitutive relations to model the balance of plant on the secondary side and to extend the applications to non-LOCA transients. The TRAC-PF1/MOD1 code also contains reasonably general reactor-kinetics modeling to facilitate the simulation of transients with delayed scram or without scram.

As a part of the code-development process, Los Alamos also conducts developmental assessment of the code before public release. References 5-8 describe the formal developmental assessment for each of the four publicly released code versions. We perform developmental assessment during the later stages of the development process to determine a range of validity for a particular code version, to demonstrate the modeling and calculational capability of the code, and to assist in the setting of empirical constants contained in the constitutive relations in the code. The analyses described in Refs. 5-8 were performed with the final, released code versions.

Independent assessment of a particular code version begins when the code is released. The code version is frozen with the exception that we permit correction of coding errors and updates to improve the handling of boundary conditions as necessary. The purposes of independent assessment are essentially the same as those for developmental assessment except that we change the empirical constants only in sensitivity analyses to investigate discrepancies between the calculated results and the data. The findings of the independent assessment are transmitted to the code developers to aid in

---

\* This work was funded by the USNRC Office of Nuclear Regulatory Research, Division of Accident Evaluation.

correcting errors in the current released code version and to improve the modeling in future code versions.

In the sense that independent assessment involves only released versions of the code and because the results reported in the developmental assessment reports<sup>5-8</sup> were obtained with the final, released versions of the codes, these references constitute the initial independent assessment of the various code versions. The formal independent assessment<sup>9</sup> of the TRAC-PLA code investigated the behavior of that code in a variety of separate-effects and integral tests important to the large-break-LOCA calculational capability. Reference 10 describes the independent assessment of the TRAC-PD2 code (including the TRAC-PD2/MOD1 version); this independent assessment investigated the effects of code improvements on the large-break LOCA capability and extended the applications of the code to small-break LOCAs.

As indicated previously, the TRAC-PF1 code contained many improvements to enhance the application of the code to small-break LOCAs. The developmental assessment mainly investigated the application of the code to small-break LOCAs and tested the new one-dimensional modeling capability. Only a single analysis tied the code back to the large-break LOCA capability in the TRAC-PD2 code that had been tested thoroughly. The independent assessment<sup>11</sup> of TRAC-PF1 provided more testing of the small-break LOCA and began the applications of the code to non-LOCA transient tests.

During the past year, we have completed our independent assessment of the TRAC-PF1 code and begun the independent assessment of the TRAC-PF1/MOD1 code. For the independent assessment of the TRAC-PF1/MOD1 code, we are using several experiments from the Loss-of-Fluid Test (LOFT) and the Semiscale facilities. We also are participating in the International Standard Problem 18 exercise, a Loop Blowdown Investigations (LOBI) small-break LOCA test (for which data currently are unavailable). The developmental assessment<sup>8</sup> of TRAC-PF1/MOD1 consists of analyses of small-break LOCA and natural-circulation tests in the Semiscale Mod-2A facility and non-LOCA transients in the LOFT facility. The independent assessment supports applications of the code to large- and small-break LOCAs and non-LOCA transients and, thus, aids in the resolution of current licensing issues.

We have tested the small-break LOCA capability of TRAC-PF1/MOD1 by analyzing Semiscale Test S-UT-8 (Ref 12). This test simulated a 5% cold-leg break with reduced leakage flow between the cold-leg and hot-leg sides of the system. The test results indicate that the core liquid level drops to the bottom of the core, significantly below the minimum elevation in the pump-suction piping, before the loop seals clear; the extent of the core dryout is enhanced by the formation of liquid levels in the steam-generator tubes on the primary side.

We used a one-dimensional representation of the Semiscale system in our analysis because of the large length-to-diameter ratios throughout the entire system and because of the enhanced calculational speed of the one-dimensional modeling over the three-dimensional modeling (which is only applicable to the pressure vessel). The input model consists of 45 TRAC components, which are subdivided into a total of 198 hydrodynamic cells. Although there are small timing differences between the TRAC-PF1/MOD1 analysis and the data, the code

correctly predicts the phenomena driving the core dryout and the extent of that dryout. Figure 1 compares the calculated and measured upper-plenum pressures. This comparison is quite good. The code correctly represented the effect of the increased pressurizer surge-line resistance that permitted the primary system to decouple from the hot fluid in the pressurizer and to saturate at ~11 MPa initially. The calculated depressurization continues in good agreement with the data until ~360 s, at which time the code begins to underpredict the data slightly. At ~550 s, the calculated rate of depressurization decreased abruptly as liquid from the accumulators reached the core and vapor generation increased. This change in the course of the transient is not reflected in the data.

Figure 2 shows the calculated and measured collapsed liquid levels in the core. The discrepancy between the two liquid levels during the first 100 s is due to flow effects in the measurement and to a difference in the draining of the upper head as shown in Fig. 3. The difference in the draining of the upper head also may impact the comparison as the core drains after 100 s, resulting in a timing offset when the minimum core inventory is reached and in the fact that the data indicate that the level drops below the bottom of the core whereas the calculated minimum level is ~3 cm. Figure 4, a comparison of fluid densities just below the bottom of the core, clearly shows that the difference in minimum core levels is real; the data indicate that shortly after 200 s the liquid drops below this measurement location, but the calculation continues to indicate only liquid during this time. Clearing of

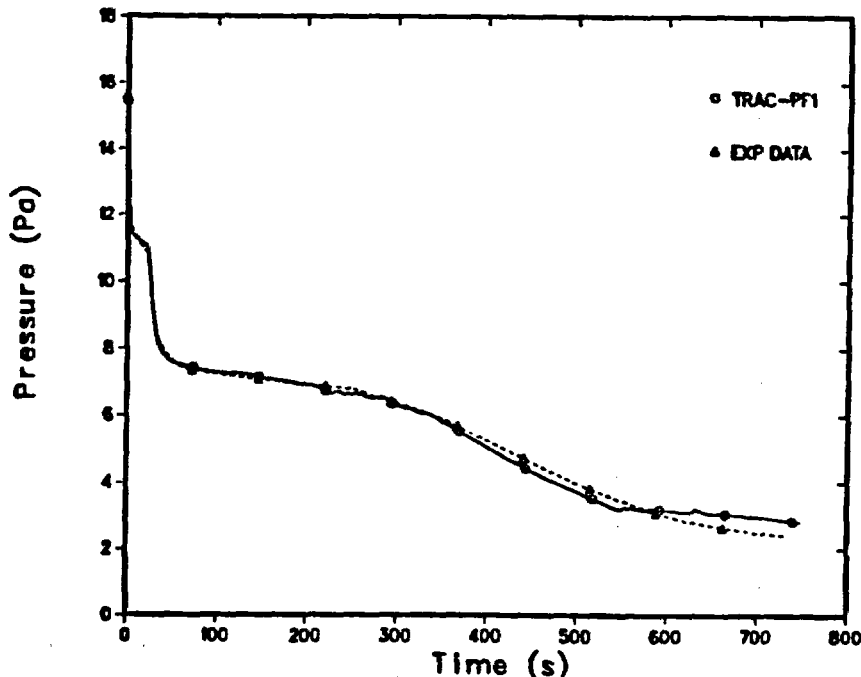


Fig. 1. Comparison of the TRAC-calculated and measured upper-plenum pressures for Semiscale Test S-UT-8.

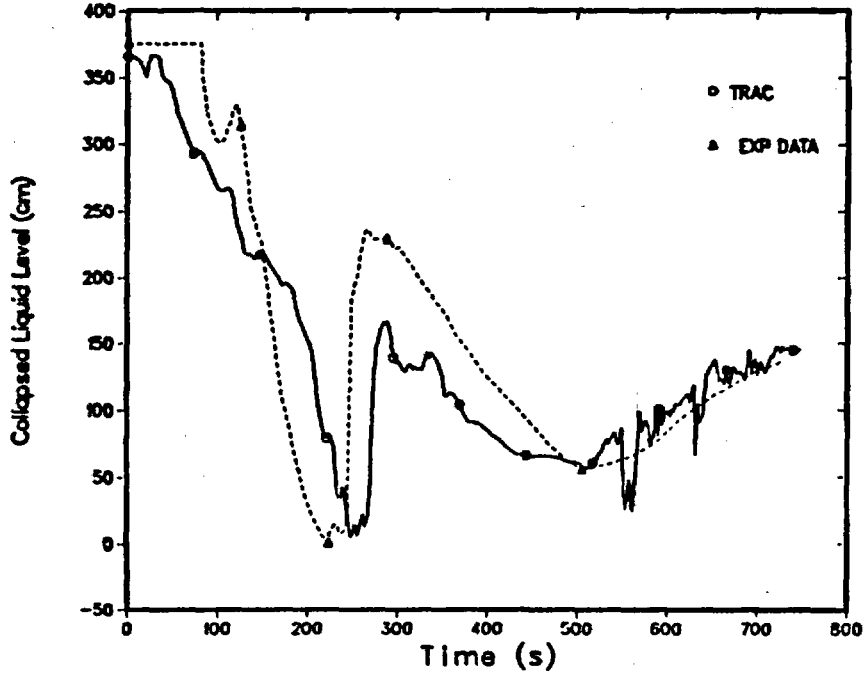


Fig. 2.

Comparison of the TRAC-calculated and measured core collapsed liquid levels for Semiscale Test S-UT-8.

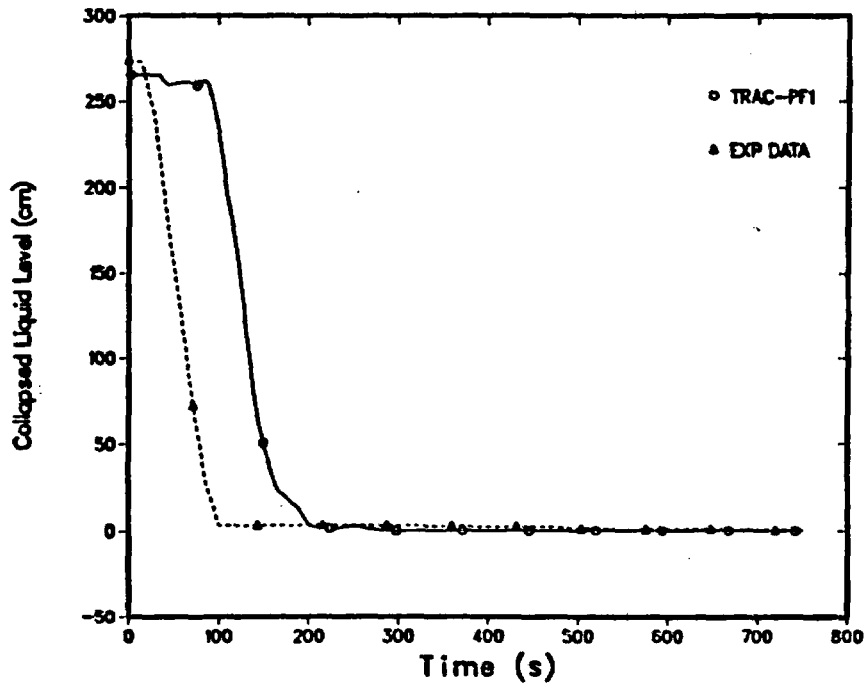


Fig. 3.

Comparison of the TRAC-calculated and measured upper-head collapsed liquid levels for Semiscale Test S-UT-8.

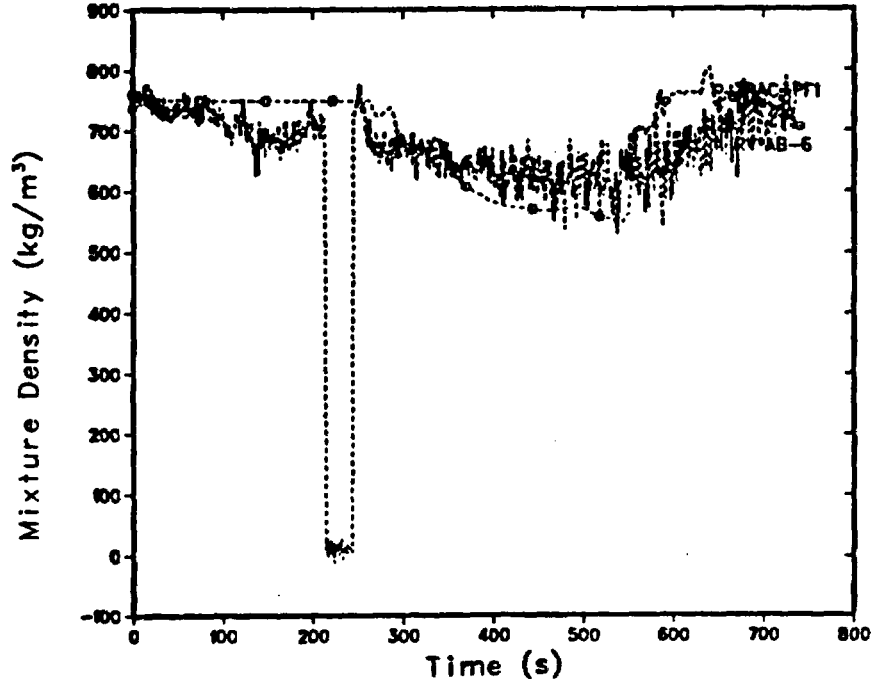


Fig. 4.  
Comparison of the TRAC-calculated and measured fluid densities below the core for Semiscale Test S-UT-8.

the intact-loop seal provides the liquid inventory to drive the rapid and large increase in core inventory. Then, a slow boil-off of core inventory occurs until liquid from the accumulators arrives. As the test ends, the code is calculating the correct magnitude and trend in the core level.

Figures 5-7 compare cladding temperatures at three core elevations. At the 1.37-m elevation, the code calculates both dryouts to occur late and underpredicts the magnitude of the temperature excursions; these discrepancies, in light of the approximately correct core-level calculation (this elevation is well above the two minimums in the core level shown in Fig. 2), indicate that the code distributes the liquid inventory over too much height during the time the dryouts occur. At the 2.08-m elevation, the comparison is improved and the code overpredicts the magnitude of the temperature excursion following the second dryout. At the 3.55-m elevation, near the top of the core, the comparison is excellent although the code predicts that the final quenching process proceeds too rapidly. (It is interesting to note that at this elevation, the data do not show any effect of the early core-level depression even though the measured core liquid level goes to zero.)

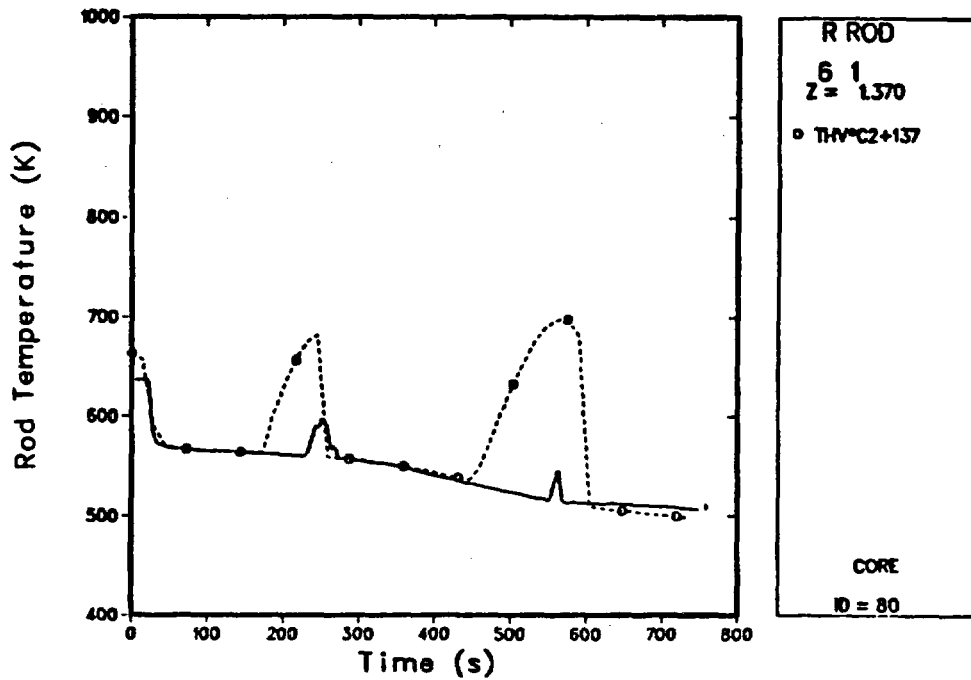


Fig. 5.  
Comparison of the TRAC-calculated and measured cladding temperatures at the 1.37-m elevation for Semiscale Test S-UT-8.

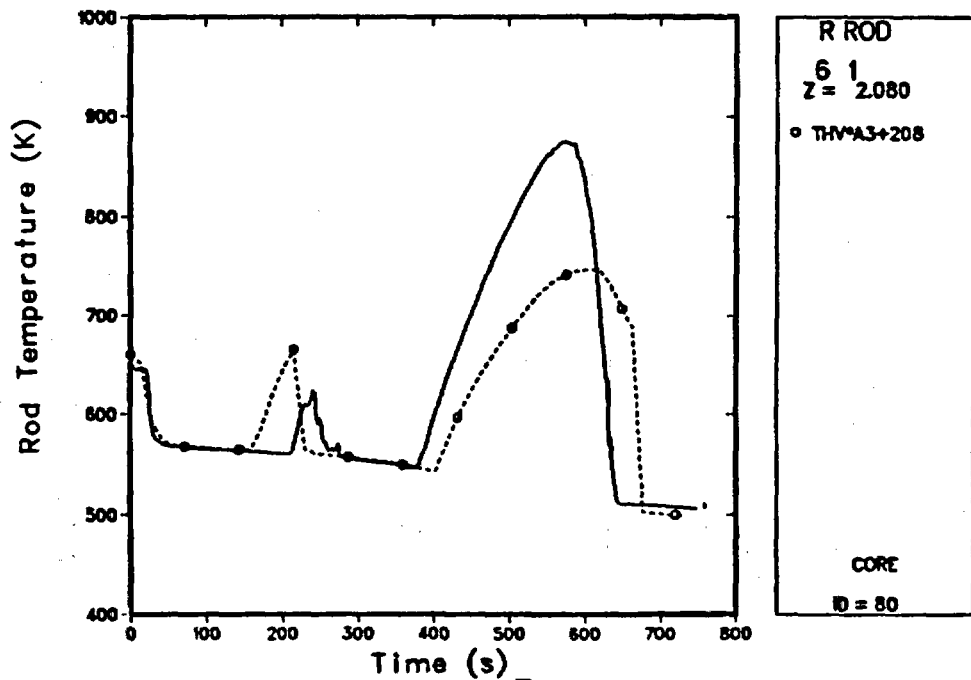


Fig. 6.  
Comparison of the TRAC-calculated and measured cladding temperatures at the 2.08-m elevation for Semiscale Test S-UT-8.

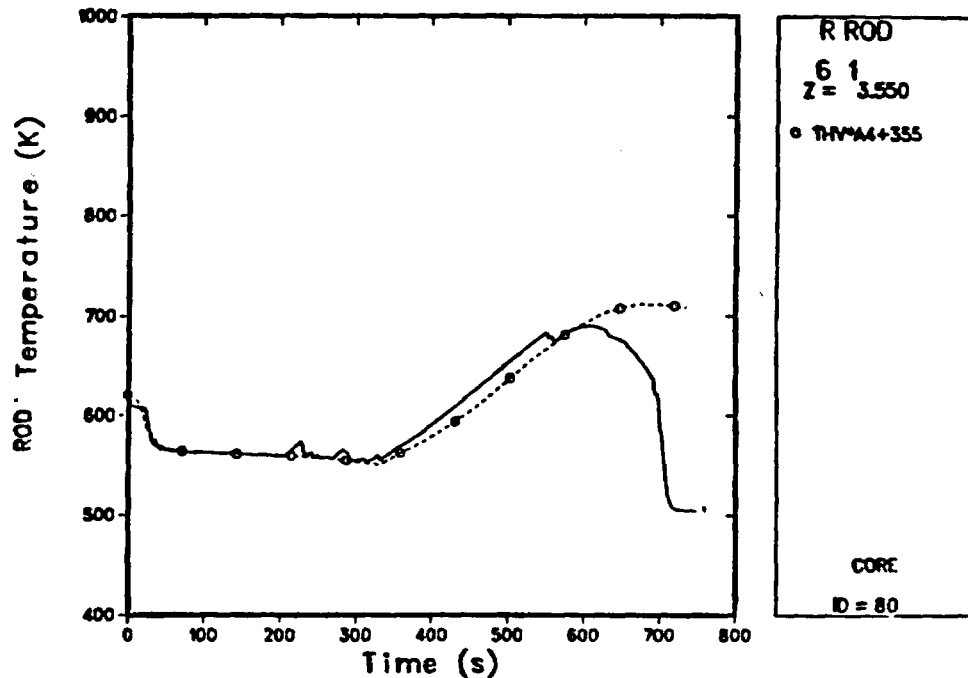


Fig. 7.  
Comparison of the TRAC-calculated and measured cladding temperatures at the 3.55-m elevation for Semiscale Test S-UT-8.

Figure 8 shows the calculated and measured liquid levels in the intact-loop steam-generator tubes. The upside of the tubes is connected to the steam-generator inlet plenum, and the downside of the tubes is connected to the outlet plenum. The data for the first 100 s are influenced strongly by flow effects and should be ignored. The code calculates the correct, at least qualitatively, level formation and disappearance in the tubes, and its predictions are in good agreement with the data quantitatively. The differences in the upside and downside levels during the first 250 s drive the core levels below the minimum elevation in the pump-suction piping. The code calculates a similar behavior in the broken-loop steam generator. A sensitivity calculation in which we increased the steam-generator secondary noding adjacent to the tubes by a factor of two (halved cell sizes) shows that the TRAC-PF1/MOD1 calculated levels before ~250 s are insensitive to the change and that the core liquid level during this time is relatively unchanged. After ~250 s, the levels in the sensitivity calculation do change slightly, and the core-level increase after the initial minimum is reduced.

Figure 9 shows the central-processor-unit (CPU) time on a Cray-1S computer as a function of transient time. On average, this calculation required ~6 s of CPU time for each transient second.

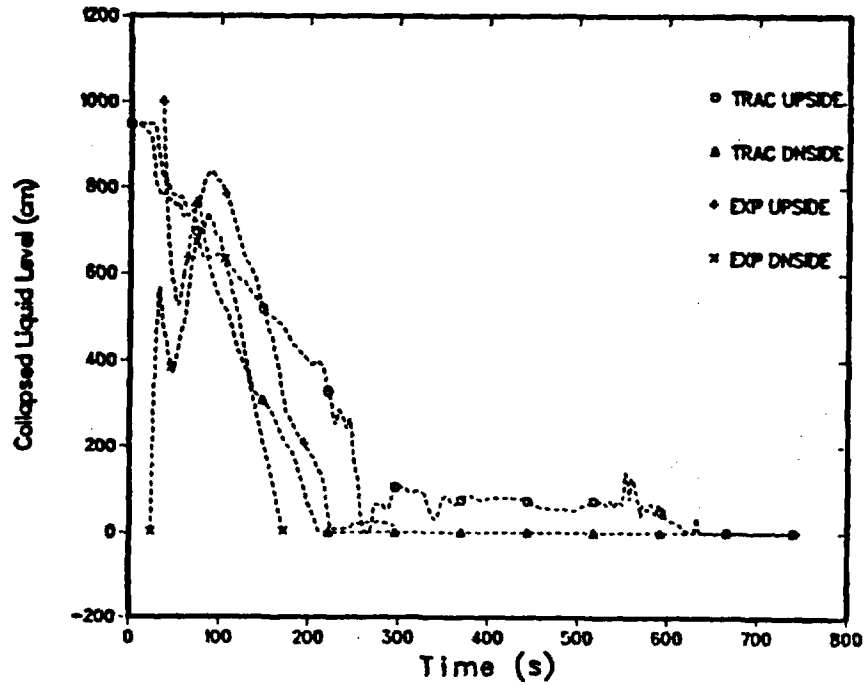


Fig. 8.  
 Comparison of the TRAC-calculated and measured intact-loop steam-generator-primary collapsed liquid levels for Semiscale Test S-UT-8.

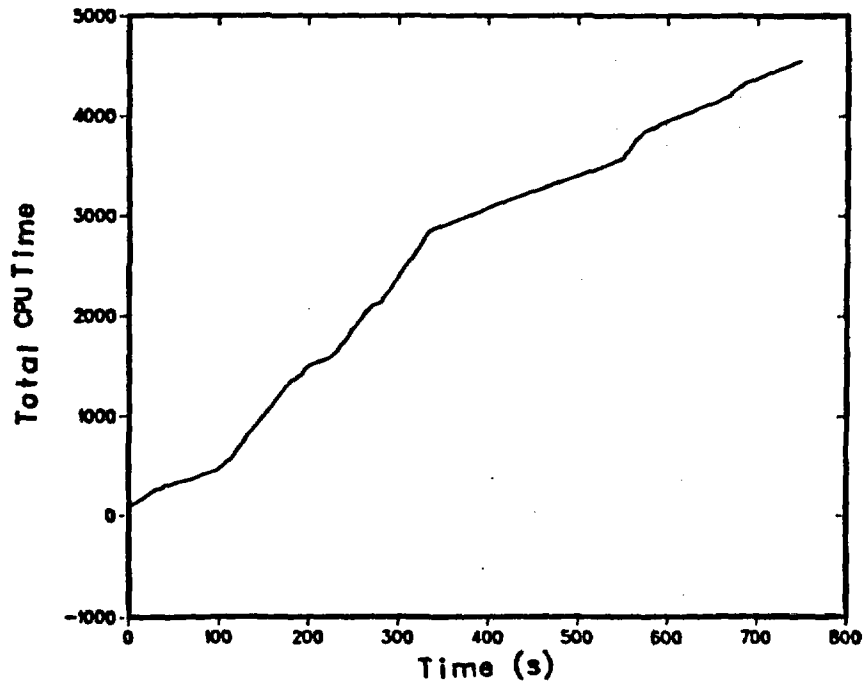


Fig. 9.  
 CPU time required for the Semiscale Test S-UT-8 transient analysis.

We tested the reactor kinetics and the hydraulics in TRAC-PF1/MOD1 by analyzing LOFT L9-4 (Ref. 13), an anticipated transient without scram (ATWS). This test is initiated by tripping the primary-coolant pumps and the main-feedwater pump and by closing the main steam-flow control valve. We discovered several errors in the programming of the reactor-kinetics models and in the reactivity feedback that provided the impetus to add a time-step control and time-step backup (repeat) based on the kinetics calculation. With these corrections and changes, the TRAC-PF1/MOD1 code correctly calculates the course of the L9-4 transient until the reactor scram occurs. We used the one-dimensional hydraulic modeling to obtain increased calculational speed. The input model consists of 39 TRAC components subdivided into 161 hydraulic cells.

Figure 10 shows the calculated and measured pressurizer pressures. This figure, as well as the remaining figures in this paper, shows a portion of the steady-state calculation (and data as appropriate). Following the initiation of the transient, the pressure rises until the safety-relief valve (SRV) begins to open and close cyclically to control the pressure. In the data, the SRV stops cycling at ~580 s, but the calculated SRV behavior continues to cycle until ~663 s. After the SRV stops cycling, the divergence in the measured and calculated pressures may be caused by small differences in the heating and cooling of the primary liquid and to leakage through the SRV.

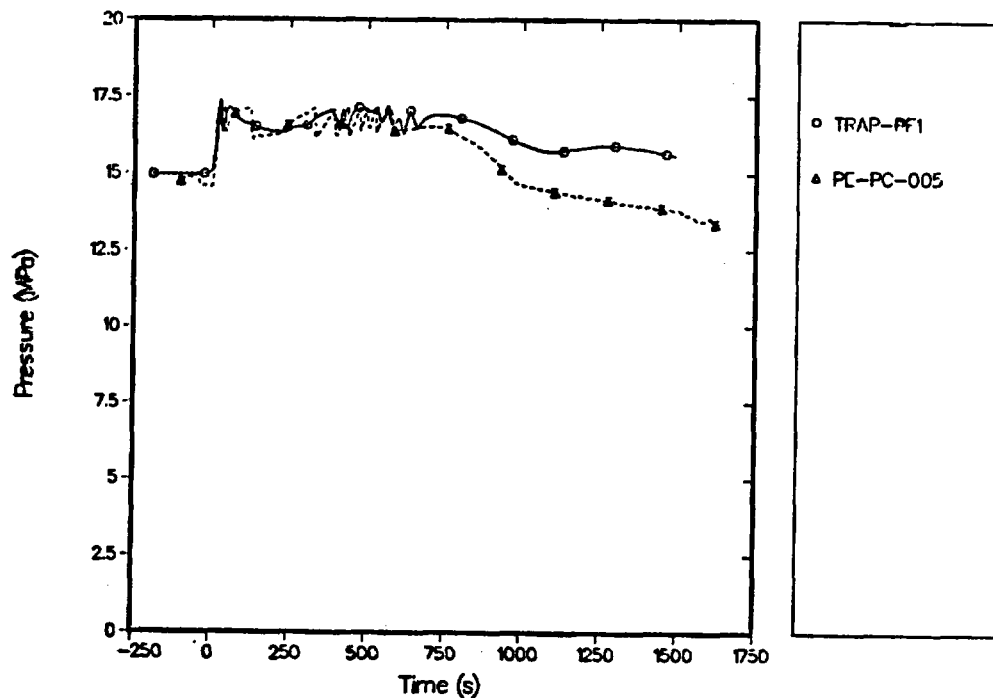


Fig. 10.  
Comparison of the TRAC-calculated and measured pressurizer pressures for LOFT L9-4.

Figures 11 and 12 compare the measured and calculated liquid temperatures in the intact-loop hot and cold legs, respectively. Although there is some variation among the fluid-temperature measurements in the upper plenum, in the intact-loop hot leg, and in the steam-generator inlet plenum, Fig. 11 does show that the calculated temperature in the intact-loop hot leg is underpredicted following the initial rise after the beginning of the transient. Together, Figs. 11 and 12 indicate that the temperature rise across the core may be low during the first ~600 s. The temperature rise in the intact-loop cold leg that begins at ~250 s is caused by the degradation of the steam-generator-secondary heat transfer as the secondary liquid inventory is depleted. A corresponding rise in the intact-loop hot leg is not observed because the increased fluid temperature in the core reduces the core power.

Figure 13 shows the calculated and measured liquid velocities in the intact-loop hot leg. We adjusted the scale on this figure to show the detailed comparison after the pump trip. The calculated result lies within the indicated data uncertainty throughout the transient, although after ~800 s the calculation is near the upper extreme of the data uncertainty. Figures 14 and 15 show the calculated and measured primary-coolant pump speeds during the transient. The code correctly calculates the prolonged coastdown of pump number 1 and the rapid coastdown of pump number 2. The differences in the pump speeds reflect differences in the geometry and the hydraulic resistance associated with the flow paths through the two pumps.

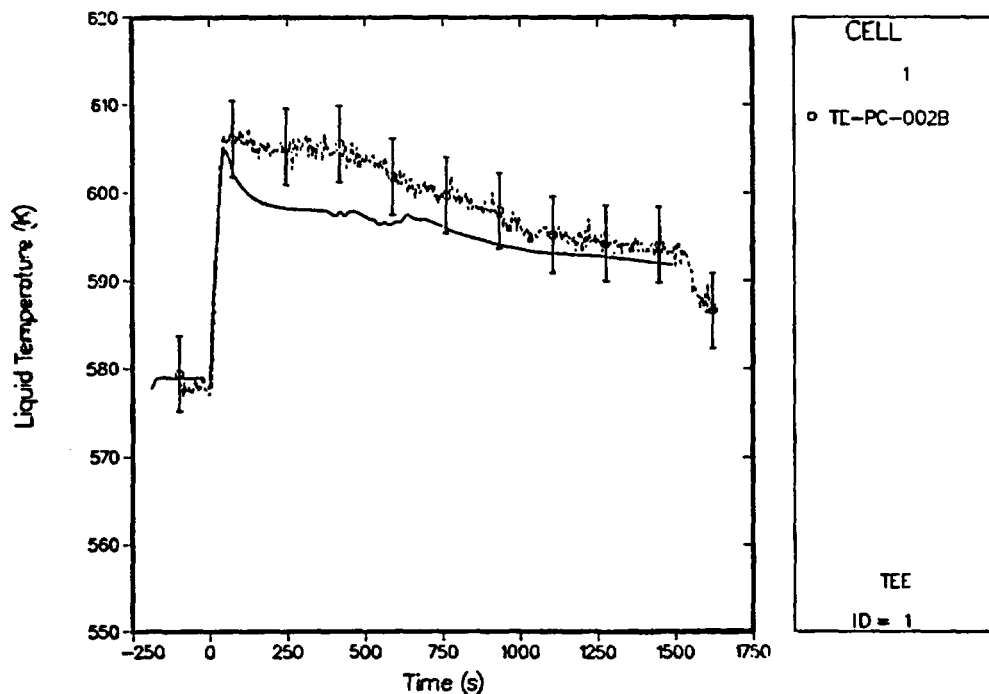


Fig. 11.  
Comparison of the TRAC-calculated and measured intact-loop hot-leg liquid temperatures for LOFT L9-4.

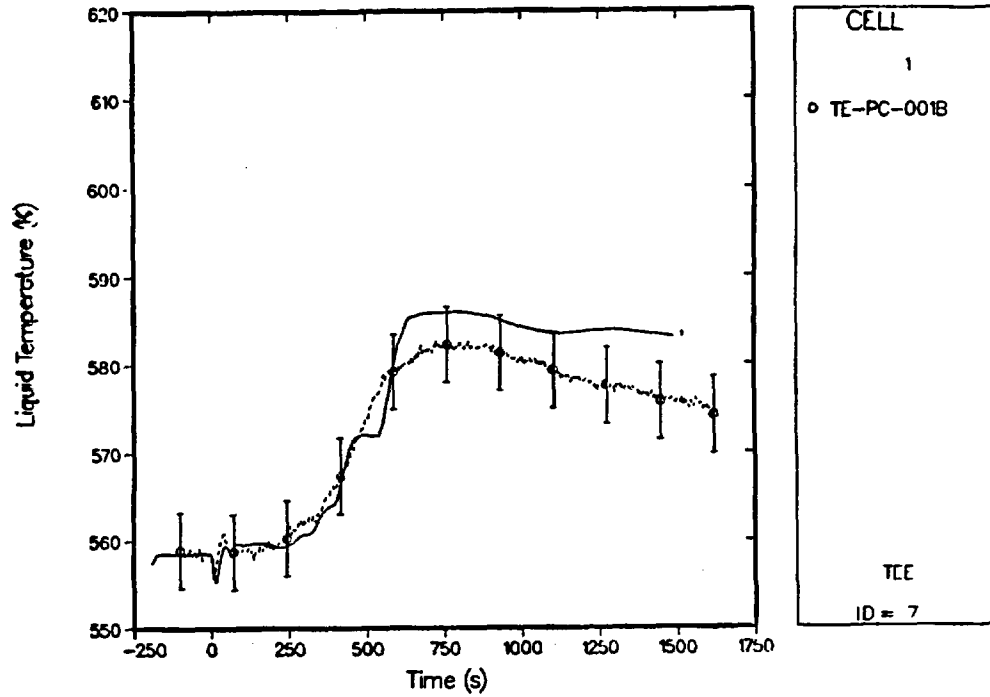


Fig. 12.  
Comparison of the TRAC-calculated and measured intact-loop cold-leg liquid temperatures for LOFT L9-4.

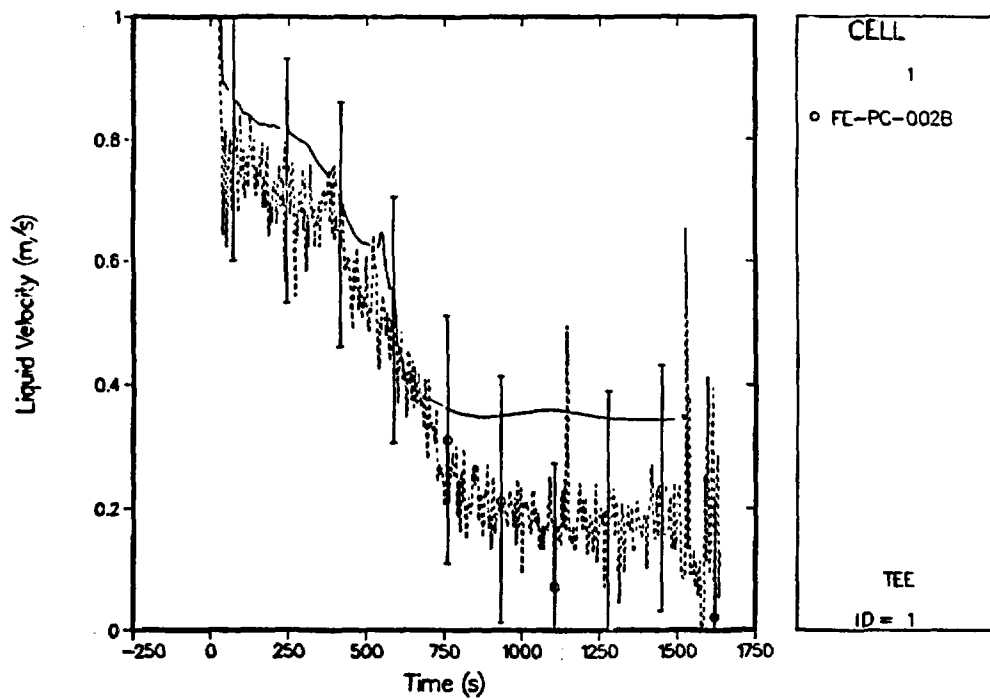


Fig. 13.  
Comparison of the TRAC-calculated and measured intact-loop hot-leg liquid velocities for LOFT L9-4.

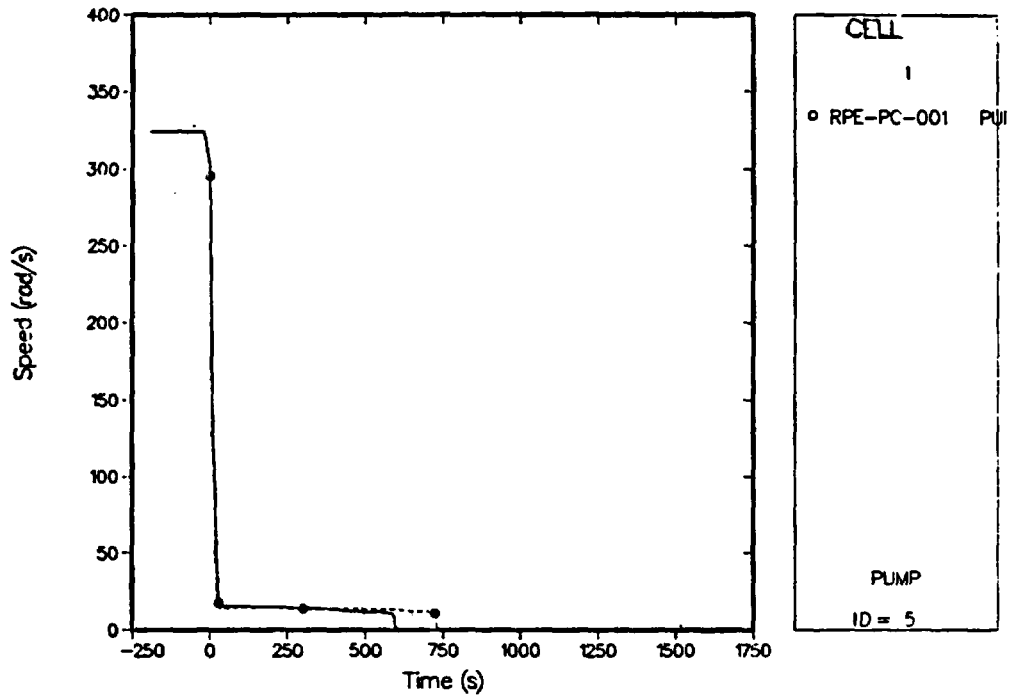


Fig. 14.  
Comparison of the TRAC-calculated and measured primary-coolant pump speeds for pump number 1 for LOFT L9-4.

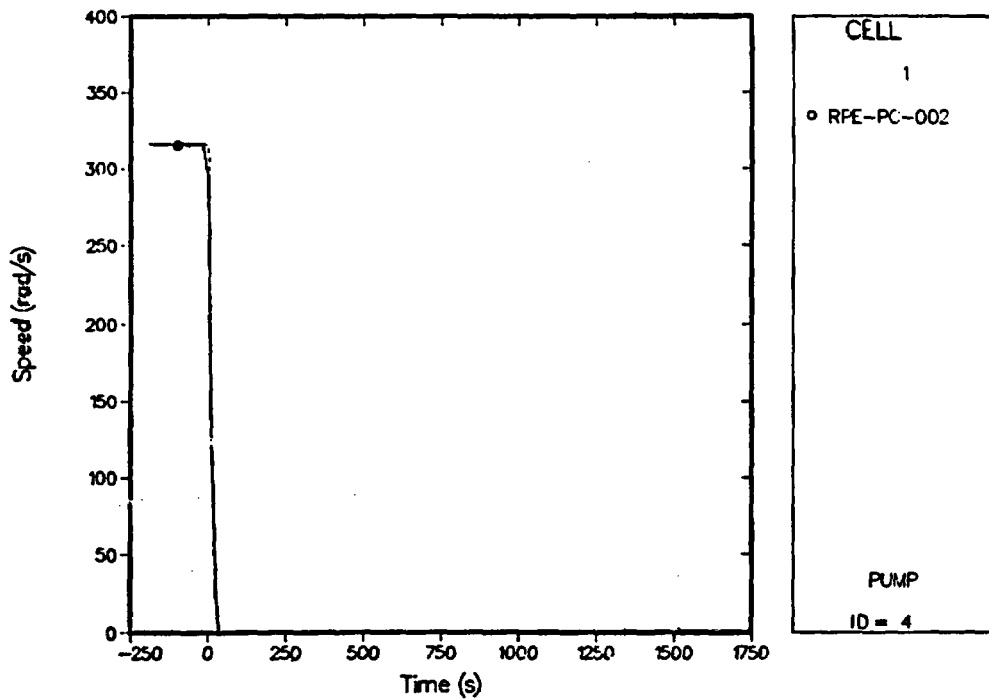


Fig. 15.  
Comparison of the TRAC-calculated and measured primary-coolant pump speeds for pump number 2 for LOFT L9-4.

Figures 16 and 17 compare the calculated steam flows from the steam-generator secondary with two different measurements, the main steam-line flow and the bypass-line flow, respectively. Because of the relatively complex and varying control of the steam-generator-secondary pressure, we specified the secondary pressure as a boundary condition; the secondary pressure rises as the main steam-line valve closes until the steam-generator bypass valve controls the pressure (manually controlled by the operator). Figures 16 and 17 show that the steam flow decreases rapidly as the main steam-line valve closes and then increases as the steam-bypass valve opens. The comparisons in both figures are excellent, but the more accurate bypass-line measurement suggests that the steam flow between ~50 and ~100 s is slightly high.

Figure 18 shows the calculated and measured core powers. Again, we adjusted the scale of this figure to show more detail in the comparison. The comparisons in Figs. 10-18 are very good with the calculation generally lying within or near the data uncertainties; the major discrepancies occur in the broken-loop hot and cold legs and reflect a large uncertainty in the leakage through the reflood-assist bypass valves connecting the two piping legs and possibly the lack of a model to represent the thermal stratification of hot and cold liquid. The variations between the calculated curves and the data traces in Figs. 10-18, although small, are consistent and point to very small errors in the analysis.

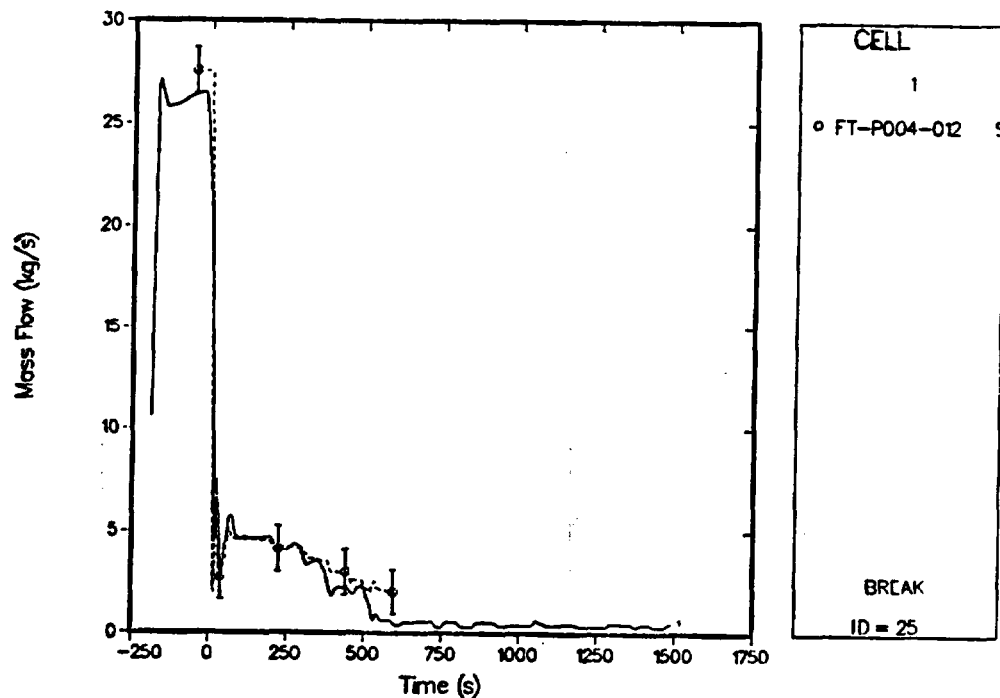
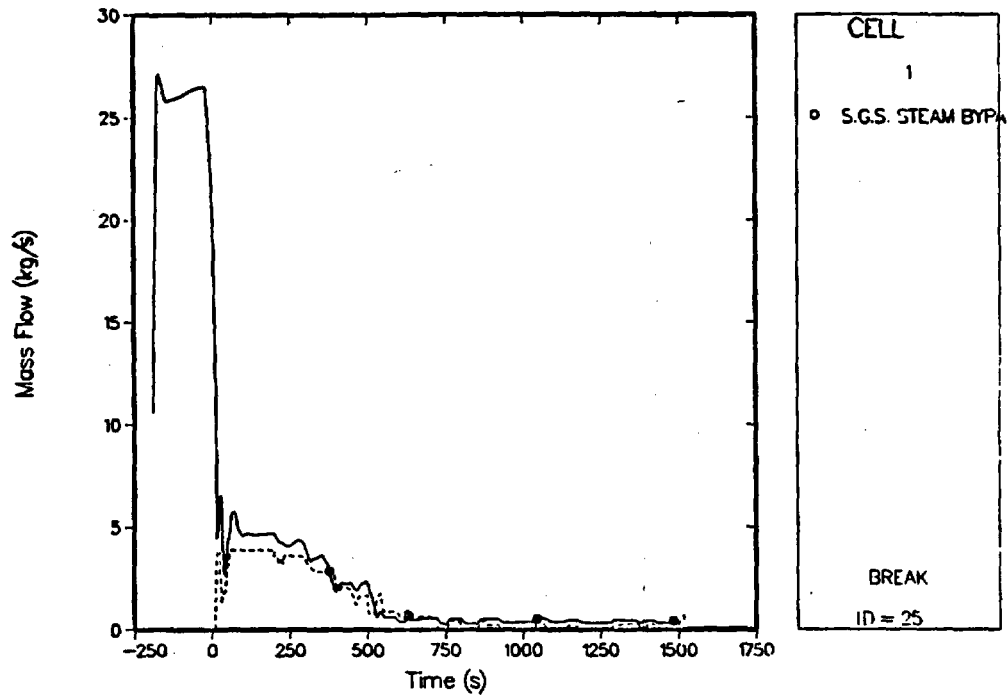
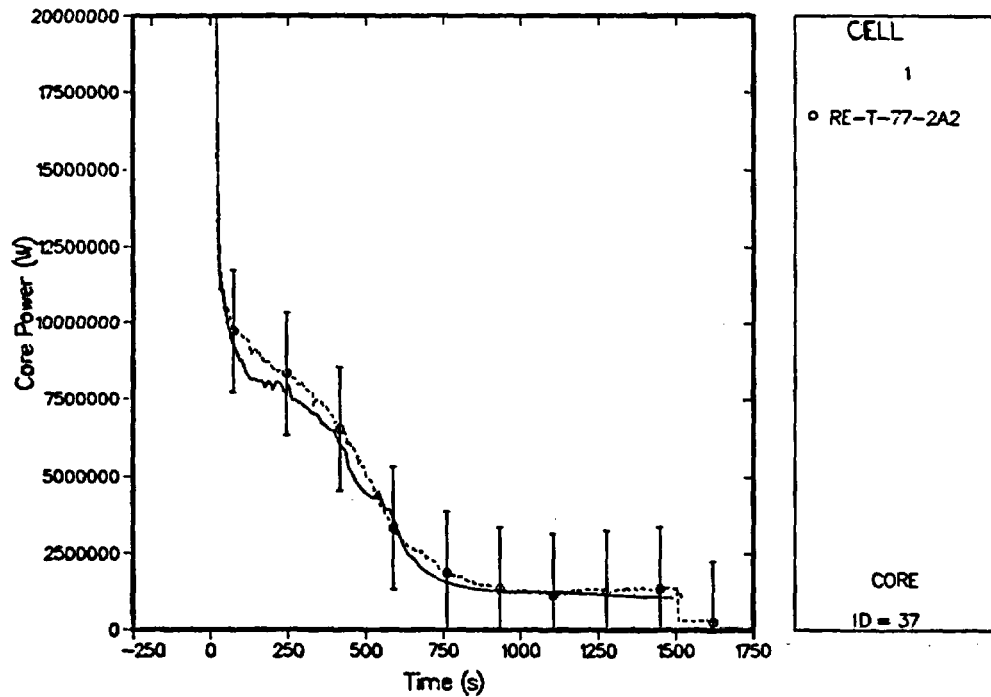


Fig. 16.  
Comparison of the TRAC-calculated and measured steam-generator-secondary steam flows (with the main steam-line flow data) for LOFT L9-4:



**Fig. 17.**  
**Comparison of the TRAC-calculated and measured steam-generator-secondary steam flows (with the steam-bypass flow data) for LOFT L9-4.**



**Fig. 18.**  
**Comparison of the TRAC-calculated and measured core powers for LOFT L9-4.**

Figures 19-22 summarize the reactor-kinetics calculation during the transient. The fuel-temperature reactivity (Fig. 19) becomes positive as the transient begins and remains positive throughout the transient because the fuel temperature drops and the reactor power decreases. The coolant-temperature reactivity in Fig. 20 becomes negative as the transient begins because the average coolant-temperature in the core increases after the primary-coolant pumps trip and the main steam-line valve closes; this figures reflects the changes in the intact-loop hot- and cold-leg liquid temperatures in Figs. 11 and 12. Because there is no core voiding, the void-fraction reactivity is not modeled. The programmed reactivity in Fig. 21 is used to account for the increased concentration of xenon as the power decreased; without this slight negative reactivity, the calculated core power late in the transient exceeded the data. These various contributions to the total reactivity combine to influence the reactor multiplication constant  $k$  (Fig. 22). The changes in the reactor multiplication constant directly affect the core power (Fig. 18). As expected, whenever the reactor multiplication constant approaches one, the calculated power tends to become constant.

Figures 23 and 24 show the CPU time on a Cray-1S computer and the time-step size as functions of the transient time.

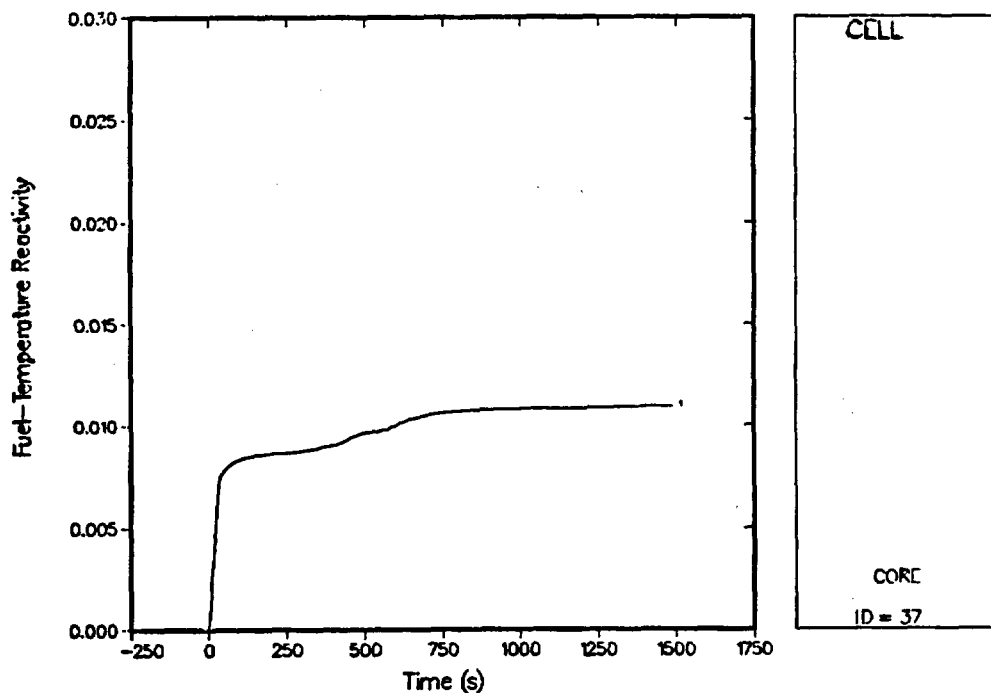
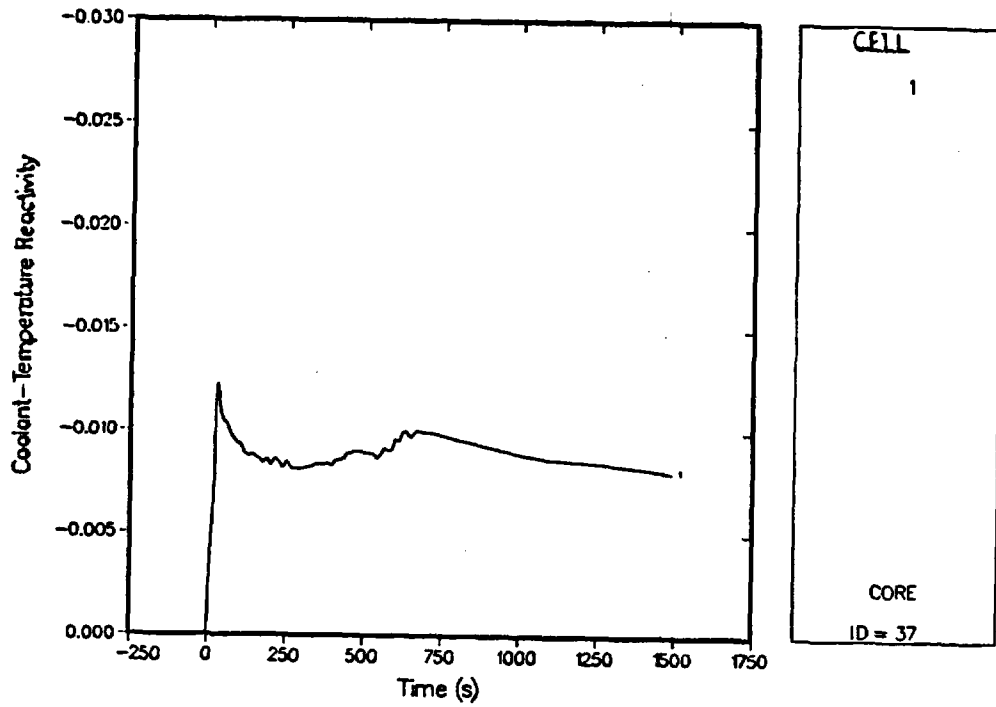
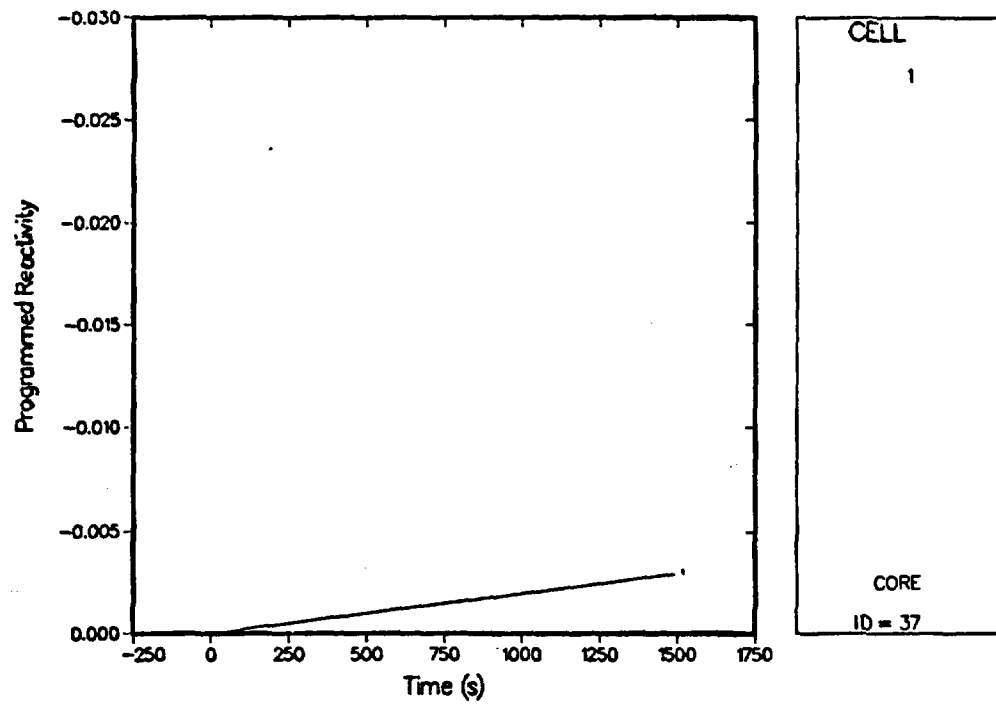


Fig. 19.  
Calculated fuel-temperature reactivity for LOFT L9-4.



**Fig. 20.**  
**Calculated primary-temperature reactivity for LOFT L9-4.**



**Fig. 21.**  
**Programmed reactivity representing xenon poisoning for LOFT L9-4.**

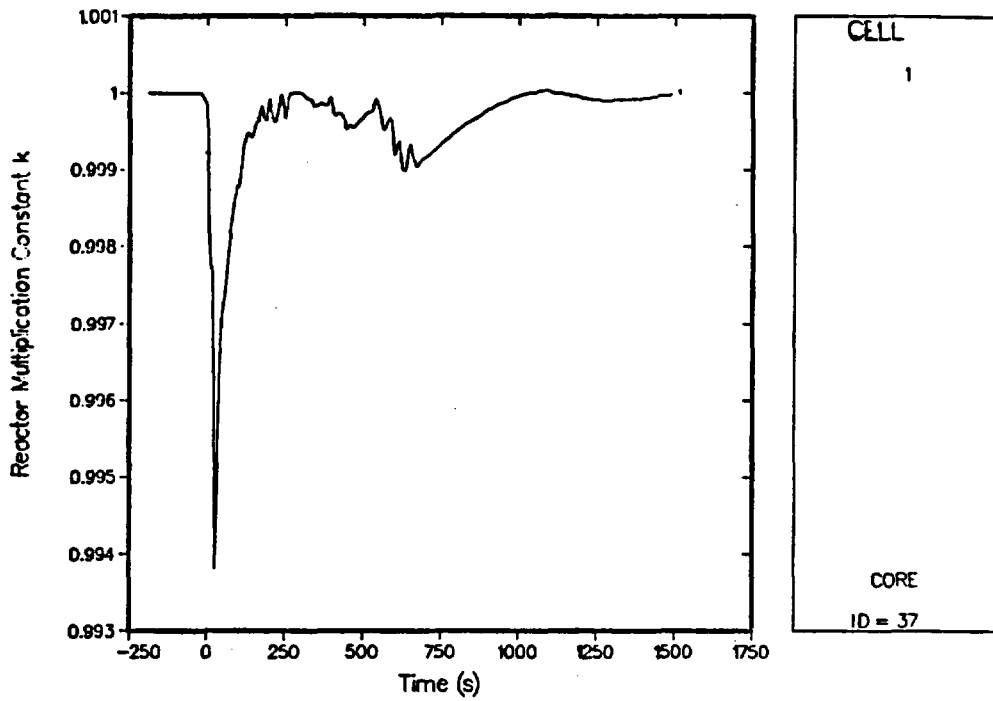


Fig. 22.  
Calculated reactor multiplication constant k for LOFT L9-4.

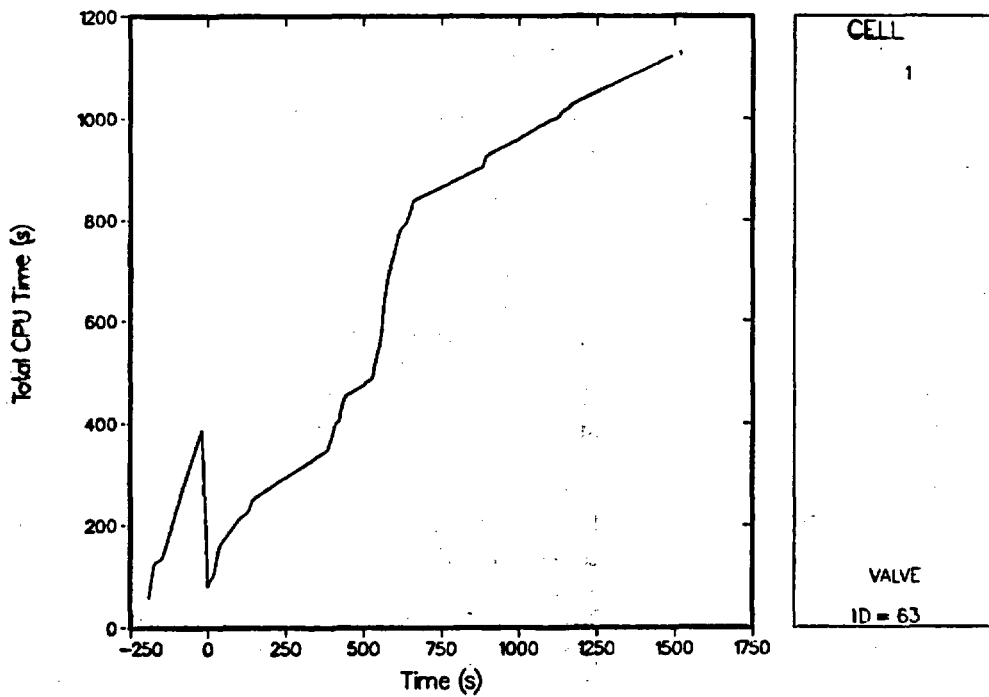


Fig. 23.  
CPU time required for the LOFT L9-4 analysis.

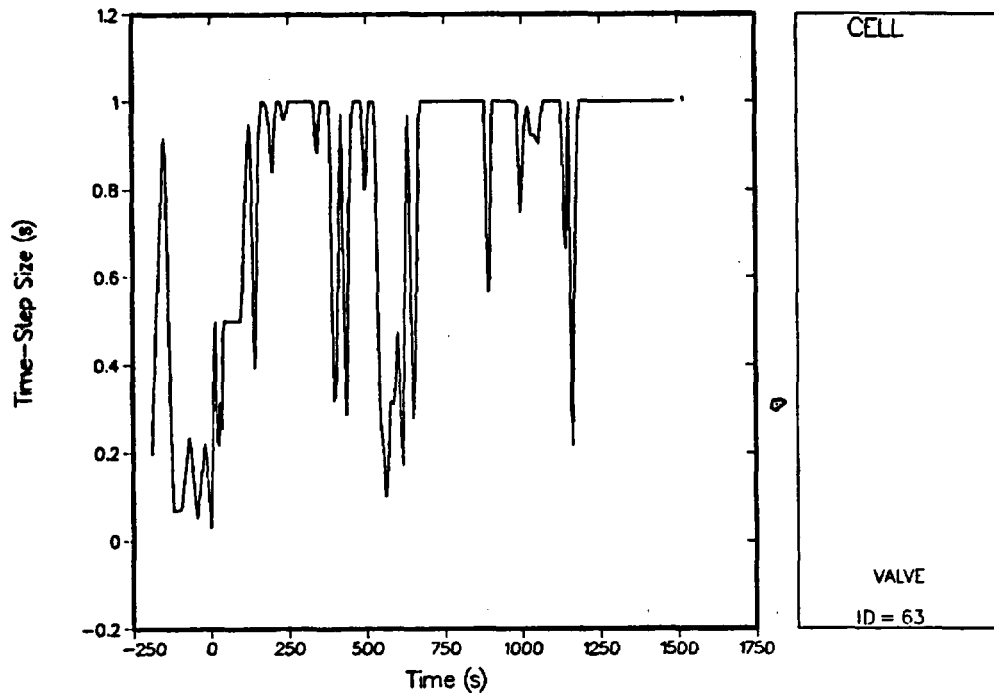


Fig. 24.  
Time-step size used for the LOFT L9-4 analysis.

We currently are analyzing Semiscale tests from the steam-line and feed-line rupture test series to benchmark that capability in the code. These tests show the effects on the primary system of a severe transient in the secondary system and represent a rigorous test of the steam-generator modeling; the hydraulics to calculate level swell, phase separation, and liquid holdup; and the heat transfer.

In the past, we have analyzed LOFT large-break LOCAs L2-3, L2-5, and LP-02-6 with the TRAC-PD2 code. The LOFT Consortium conducted the LOFT LP-02-6 transient to represent the double-ended offset shear of the cold-leg piping from a condition of maximum power with an early pump trip. Our TRAC-PD2/MOD1 analyses of this test indicated that the code could calculate correctly the hydraulic phenomena early in the transient, but that the heat-transfer correlations prevented the calculation of the early core rewet and distorted the remainder of the transient. We are calculating this transient with the TRAC-PF1/MOD1 code to benchmark the large-break LOCA capability against the TRAC-PD2/MOD1 results. We also are using the reactor kinetics to calculate the core power instead of specifying the decay power as a function of time as in the TRAC-PD2/MOD1 calculation. The LOFT large-break LOCAs indicate that the final quenching of the core occurs shortly after the accumulator empties; however, the TRAC-PD2/MOD1 analyses show a later quenching. We have attributed at least part of this difference to the inability of previous code versions to inject the nitrogen from the accumulator as it empties and to force the final reflood of the core. Because

the TRAC-PF1/MOD1 code contains an air field, we are modeling the nitrogen injection in our TRAC-PF1/MOD1 analysis.

In conclusion, the TRAC-PF1/MOD1 analyses of Semiscale Test S-UT-8 compares very well with the data in general, and the code calculates all of the phenomena driving the depletion of core inventory during the transient. However, some of the differences observed in the comparison support the addition of a TRAC plenum component to represent in a straightforward manner multiple connections to a single cell and to avoid complex modeling with tee components. The LOFT L9-4 analyses have led to the correction of several errors in the reactor kinetics and subsequently demonstrated that capability.

The Los Alamos assessment effort indicates that the quality of the code improves as new code versions are released. And, although the work continues to indicate needed improvements in the code, the TRAC series of codes and specifically TRAC-PF1/MOD1 currently provide a very flexible tool for analyzing a wide variety of transients pertinent to PWRs.

## REFERENCES

1. "TRAC-PIA: An Advanced Best-Estimate Computer Program for PWR LOCA Analysis," Los Alamos National Laboratory report LA-7777-MS, NUREG/CR-0665 (May 1979).
2. "TRAC-PD2: An Advanced Best-Estimate Computer Program for Pressurized Water Reactor Loss-of-Coolant Accident Analysis," Los Alamos National Laboratory report LA-8709-MS, NUREG/CR-2054 (April 1981).
3. "TRAC-PF1: An Advanced Best-Estimate Computer Program for Pressurized Water Reactor Analysis," Los Alamos National Laboratory report LA-9944-MS, NUREG/CR-3567 (February 1984).
4. "TRAC-PF1/MOD1: An Advanced Best-Estimate Computer Program for Pressurized Water Reactor Thermal-Hydraulic Analysis," Los Alamos National Laboratory report LA-10157-MS, NUREG/CR-3858 (to be published).
5. J. C. Vigil and K. A. Williams, "TRAC-PIA Developmental Assessment," Los Alamos National Laboratory report LA-8056-MS, NUREG/CR-1059 (October 1979).
6. Thad D. Knight and Vera B. Metzger, "TRAC-PD2 Developmental Assessment," Los Alamos National Laboratory report LA-9700-MS, NUREG/CR-3208 (to be published).
7. B. E. Boyack, "TRAC-PF1 Developmental Assessment," Los Alamos National Laboratory report LA-9704-M, NUREG/CR-3280 (July 1983).
8. M. S. Sahota and F. L. Adessio, "TRAC-PF1/MOD1 Developmental Assessment," Los Alamos National Laboratory report (to be published).
9. T. D. Knight, "TRAC-PIA Independent Assessment - 1979," Los Alamos National Laboratory report LA-8477-MS, NUREG/CR-1652 (January 1981).
10. Thad D. Knight, "TRAC-PD2 Independent Assessment," Los Alamos National Laboratory report LA-10166-MS, NUREG/CR-3866 (to be published).
11. C. P. Booker, B. E. Boyack, P. Coddington, T. D. Knight, J. K. Meier, and J. R. White, "TRAC-PF1 Independent Assessment," Los Alamos National Laboratory report (to be published).
12. Robert K. Fujita, "TRAC-PF1/MOD1 Posttest Analysis of Semiscale Small-Break Test S-UT-8," Los Alamos National Laboratory report LA-UR-84-2079 (May 1984).
13. John K. Meier, "TRAC-PF1/MOD1 Posttest Analysis of LOFT L9-4, an Anticipated Transient without Scram," Los Alamos National Laboratory report (to be published).

TRAC-PF1/MOD1 Independent Assessment  
at Sandia National Laboratories

L. D. Buxton, L. N. Kmetyk, D. Dobranich,  
R. K. Byers, A. C. Peterson, and M. G. Elrick

Sandia National Laboratories  
Albuquerque, New Mexico

INTRODUCTION

TRAC-PF1/MOD1 is the latest in the Transient Reactor Analysis Code (TRAC) series developed by the Los Alamos National Laboratory (LANL) during the last decade. The development of this series of codes was directed towards performing advanced, best-estimate analyses of the thermal/hydraulic response of pressurized water reactor (PWR) systems to a wide variety of hypothesized and/or actual accidents. Sandia's TRAC-PF1/MOD1 independent assessment program is part of a multi-faceted effort sponsored by the Nuclear Regulatory Commission (NRC) to evaluate the ability of the current generation of such systems codes to predict the response of light water reactors (LWRs) to off-normal conditions. This assessment program is a successor to the RELAP5/MOD1 independent assessment project carried out at Sandia during FY82 and FY83.

TRAC-PF1/MOD1 is being assessed at Sandia against data from various integral and separate effects experimental test facilities. The calculated results will also be compared with results from our previous RELAP5/MOD1 independent assessment analyses whenever possible. Our TRAC-PF1/MOD1 matrix includes:

- LOFT large break test L2-5,
- LOFT loss-of-feedwater test LP-FW-1,
- Semiscale Mod-2A intermediate break test S-IB-3,
- Semiscale Mod-2A feedwater line break test S-SF-3,
- Semiscale Mod-2A steam line break test S-SF-5,
- Semiscale Mod-2B loss-of-power test S-PL-3,
- two Semiscale Mod-2B steam generator tube rupture tests,
- PKL natural circulation test series ID1,
- LOBI large break test A1-04R,
- LOBI intermediate break test B-R1M,
- FLECHT SEASET natural circulation test 8,
- B&W OTSG steady state test 28 and loss-of-feedwater test 29,
- NEPTUNUS pressurizer test Y05,
- FLECHT SEASET reflood tests 31504 and 31701,
- a Dartmouth University 3-tube CCFL test,
- Northwestern University horizontal, stratified, cocurrent condensing flow tests, and
- Northwestern University perforated plate CCFL tests.

TRAC input models for most of the integral test facilities have now been developed. Many steady state calculations have been completed and several transient calculations have been begun. Some of the separate effects test analyses have been finished. Table 1 indicates more clearly the state of progress of the individual calculations. The rest of this paper will discuss what we have learned so far about the code and its supporting documentation.

## CODE STATUS

Early in FY84, the then-latest available version (11.0) of TRAC-PF1/MOD1 was installed on Sandia's CDC Cyber-76 (SCOPE operating system) and Cray-1S (COS operating system) computers. Soon thereafter, we upgraded the supporting plot package we had previously developed for TRAC-PF1 so that it worked properly with the slightly altered plot files generated by MOD1. We also modified an early TRAC-PF1 version of the EXTRACT utility program obtained from LANL to recognize the new steam generator secondary nodding scheme used by TRAC-PF1/MOD1. (EXTRACT is a user-convenience utility program used to create new input decks from the current problem information contained in the normal TRAC dump/restart file.)

Several updates to MOD1 have been received from LANL since our assessment effort began. Most of those code updates were directed towards either the addition of user conveniences or the correction of newly discovered code errors; therefore, they have all been implemented in our version of the code as soon as practical after they were received.

One major set of updates recently received from LANL involves a TRAC model change via the addition of a PLENUM component which allows multiple connections at a single 1-D piping junction. Those updates are not expected to affect the results obtained unless the PLENUM component is actually used. Although we have not yet built a model which uses the PLENUM, we definitely plan to assess that new component logic after its development has stabilized. We feel very strongly that it should represent an extremely valuable addition to the code if it functions as intended. The user's ability to build a totally 1-D TRAC system model is quite limited without such a branching component.

The version of TRAC-PF1/MOD1 currently being used for our assessment analyses is 11.9. Several intermediate versions between 11.0 and 11.9 have been used for the calculations reported here; however, a single version of the code is normally used to complete any given analysis or set of analyses once those production calculations have been initiated. If code

updates are generated at some point later in time which we feel will have a significant impact on conclusions drawn from our earlier analyses, we can always rerun a calculation with the newer code, but that situation has not been encountered to date.

One final point should be made concerning the code's current status. As with most large computer codes which are undergoing more or less continuous development, published formal documentation for the code is out of date. At this time, there are no final documents generally available which describe the details of the TRAC-PF1/MOD1 code itself, the developmental assessment analyses performed with it, or the user guidelines utilized by the code developers and analysts doing plant or other applications calculations, even though such documentation does exist in varying forms. An almost complete draft version of the code manual [1], which describes the models and input, is available and furnished to the people who need to exercise the code. That draft manual, however, contains several known errors, does not describe some of the newer code features and user-convenience options, and is often difficult to interpret, particularly in the areas of control block logic and kinetics input which are new for MOD1. The specific documentation deficiencies which we have noted as part of our assessment effort at Sandia have been discussed at great length with the code developers and we expect the final documentation to be much improved.

#### MODEL DEVELOPMENT AND STEADY STATE INITIALIZATION

TRAC input models for most of the integral test facilities have now been developed and many steady state calculations have been completed.

Developing satisfactory nodalizations was somewhat cumbersome and time-consuming, due to the lack of code models for generalized heat slabs and multiple connections to a single cell, at least in the versions used for most of the analyses performed so far. (Although the PLENUM component has recently been released for general use, it is not clear if the final version of MOD1 will have a generalized heat slab capability other than for the steam generator secondary.) These deficiencies forced us to "model around" many important features, such as structural material heat transfer, and details such as pump seal leakage, in some of the facilities. The scarcity of published user guidelines and occasional lack of logically and consistently ordered input also hindered nodalization development.

All of the input models being used for our TRAC assessment were developed at Sandia from system information such as blueprints and other basic system description documents. In some cases, the TRAC models were based on those developed earlier in our RELAP5 assessment project; much of the data manipulation had already been performed in developing those RELAP5 models, but the two codes are sufficiently different that exact translation was not possible. Furthermore, although the same facility may have been modelled with both codes, the tests analyzed are frequently quite different in nature and require more or less modelling detail in different portions of the system.

We developed our own user guidelines for modelling abrupt area changes with TRAC; these guidelines were tested for single-phase flow conditions in our PKL ID1-4 analyses and for two-phase flow conditions in our B&W OTSG study [2]; they are currently being used in all our nodalizations, with good resulting agreement for system pressure drops. Early B&W OTSG and LOBI calculations with TRAC showed that using the minimum tube-to-tube spacing for the secondary-side heated equivalent diameter, as was discovered in the RELAP5 assessment project, gave better agreement with steam generator tube differential temperature data than that obtained using the geometrically based hydraulic diameter.

Our Semiscale and LOBI models were used to develop and test guidelines on how to best use the "perfect" separator in TRAC [3]. One major problem we discovered was that, during steady state calculations, overflowing of the secondary beyond the desired inventory was an extremely difficult condition from which to recover, although this problem caused fewer difficulties for complicated secondary geometries with various possible liquid return paths. We later discovered that this problem was already recognized by LANL but, prior to that, we independently developed a guideline that the desired inventory should always be approached from "below" when using the separator model. Another solution we found was to abandon the special separator logic completely and instead use an artificially large junction area to reduce, but still allow some, liquid entrainment by the steam flow. This approach was ultimately used in some of our Semiscale and LOFT decks with acceptable results.

#### SEPARATE EFFECTS TEST ANALYSES

As mentioned in the Introduction, most of the completed calculations are for separate effects tests. These calculations were performed first to help us gain some basic experience with the code, using the more simple geometries and faster running problems. The separate effects calculations gave acceptable agreement between data and calculations in general, but did

indicate some possible problems with condensation and some deficiencies in TRAC's time step control algorithms. Some effects of nodalization detail were also observed in these calculations.

One set of separate effects test analyses already completed is for the Northwestern University cocurrent condensing flow tests [4]. In these tests, steam and water mixtures were injected into one end of a horizontal flow channel at varying flow rates and temperatures. Our analyses [5] of selected experiments from that test series indicated that too much condensation was being predicted by TRAC, particularly at the lower steam flow conditions; however, those conditions under which the code did most poorly are not expected to be prevalent in PWR accidents. This strong condensation at low steam flow occurred for steady state stratified flow situations; it manifested itself most obviously by the presence of countercurrent steam inflow at the pipe outlet rather than cocurrent steam outflow as measured. Despite these quantitative differences, the correct trends were predicted for variations in the relative flow rates of steam and water and in the water temperature.

The Northwestern cocurrent condensing flow tests were also valuable in that they showed unexpected convergence sensitivities of the final steady state conditions to the time step selected. Because the tests were two-phase steady state tests, the time step sensitivities exhibited may be unimportant during the majority of PWR analyses, but certainly indicate that the convergence criteria used internally in the code need to be more carefully studied by the code developers.

Another separate effects test for which we have completed our TRAC analyses is the NEPTUNUS Y05 pressurizer test performed at the University of Delft [6]. In that test, a 1/40th scale simulated pressurizer was subjected to a series of flow insurges and outsurges; during the insurges, a spray system was also simulated. Our TRAC analyses [7] of this test predicted too much pressurization during insurges when the spray was operational, possibly due to problems with wall and/or bulk condensation, but good pressure recovery during the outsurges.

The NEPTUNUS results were found to be dependent on the time step used, particularly for the liquid temperature calculated in the upper cells of the pressurizer. If the code-selected time step was used, unphysically low liquid temperatures were often calculated; this effect could be remedied by reducing the time step. There were no obvious detrimental effects of using the code-selected time step on any of the results other than the liquid temperatures in the topmost cells when the spray was active. The results were not particularly sensitive to either the types of TRAC components used to model the pressurizer or the number of cells used in the nodalization.

The final set of separate effects experiments for which TRAC PF1/MOD1 analyses are complete is a companion set of steady state and loss-of-feedwater (LOFW) transient tests performed in the B&W 19-tube once-through steam generator (OTSG) facility [8]. Our TRAC calculations [9] showed that, if the correct steady state conditions were obtained, most of the important transient behavior was easily calculated. The actual dryout elevation in the boiler during the steady state test was under-predicted by about 30% when using the standard criterion in TRAC, and was still underpredicted by about 15% after the dryout criterion was modified to force dryout at a quality of 0.9. (Similar dryout elevation discrepancies were seen in the analyses of these same tests with RELAP5/MOD1.)

Noding sensitivity studies for these B&W OTSG tests indicated that the overall good agreement with data deteriorated somewhat as the number of nodes was reduced to values more typical of those used in full-scale PWR analyses. The total primary-to-secondary heat transfer rate prediction was still good, but the detailed behavior as a function of position was not as good; therefore very coarse noding may not be adequate for certain PWR applications.

#### INTEGRAL TEST ANALYSES

As mentioned earlier, the base-case TRAC nodalizations for many of the integral test facilities considered in our assessment matrix have been developed, but most of the transient analyses for those integral tests have only recently been started and conclusions based on them are just becoming available.

An initial set of calculations has been completed for the PKL ID1 series of natural circulation tests [10]. These preliminary analyses indicate that TRAC correctly predicts all modes of natural circulation, but that the peak two-phase natural circulation flow rate is too high and occurs at a slightly higher inventory than measured in the tests. The TRAC results are quite similar to those obtained with RELAP5/MOD1 during our earlier assessment project with that code, even though the manner in which we established the initial two-phase conditions in preparation for performing further system drains to get to the lower inventories was quite different.

Time step difficulties were also encountered in the PKL analyses. We found that the behavior of some of the calculated results was more stable at a certain fixed value of the time step than it was at either half or twice that time step. The time step problem in the PKL calculations was somewhat different than those seen in the separate effects analyses mentioned

above, in that the situation did not improve as the time step was reduced. The oscillatory behavior noted was not sufficient to cause code aborts, but nevertheless was extremely peculiar. We have not been able to determine the cause for this behavior.

The individual PKL analyses discussed above were not all done with a single version of the code, so we intend to rerun them with the latest code version for the sake of consistency. We do not expect the final results to change much, if at all, from the earlier results since no code modifications have been made which would obviously affect these test analyses.

Analysis of the LOFT L2-5 [11] large-break transient has also been started, but has only been carried out through the initial blowdown phase. In that short period, we saw relatively good agreement for pressure and break flow, but the early time core temperatures were all higher than measured. Since the same problem was seen with our RELAP5 analyses for this test, we suspect the problem involves calculating too much stored energy in the fuel rods during the steady state. We are currently investigating the effects of gap width and other fuel parameters on the initial stored energy and the transient PCT.

In the LOBI A1-04R [12] large-break LOCA calculations performed so far, we saw good agreement with measured system pressure, break flow and blowdown PCT prior to accumulator injection. The detailed thermal/hydraulic behavior in the vessel, however, was calculated relatively poorly early in the transient. A core rewet was observed to occur early in the test, but no such core rewet was calculated. This core rewet is caused by reestablished positive core flow; a slug of liquid is indeed predicted to pass through the core at the correct time, but it is apparently smaller in magnitude than the slug in the test and does not cool the heater rods sufficiently for rewet to occur. The lack of this early-time core rewet and associated lack of stored energy removal results in a significant overprediction of late-time core temperatures. We initially thought that the miscalculation of the slug behavior could be the result of the special interface sharpener used in the lower plenum and core regions of the 3-D vessel in TRAC, but a rerun of the analysis with that feature deactivated gave very similar results.

In the LOBI B-R1M [13] intermediate-break LOCA transient, we saw generally good agreement with measured system depressurization, break flow and core temperatures, but some details of early-time broken loop flow behavior were not being calculated correctly. The data showed that positive flow through the broken loop was quickly reestablished, while the calculation predicted reversed flow in the broken loop cold leg at all times for the portion of transient calculated. Another minor discrepancy was the lack of

a calculated preliminary clearing of the intact loop pump suction several seconds before it finally cleared. The calculation also predicted reverse heat transfer from the steam generators to start somewhat later than experimentally observed.

Integral system assessment analyses involving steam generator secondary system transients have also been initiated. Several analyses have already been performed for Semiscale test S-SF-3, a feedwater-line break simulation [14]. In the first analyses, the break flow was greatly underpredicted by TRAC, as it was in RELAP5 post-test analyses performed by staff at the Idaho National Engineering Laboratory (INEL). Several possible explanations exist for this problem, including an inadequate representation of the detailed break geometry. This disagreement will be investigated further when more detailed information concerning the geometry of the Semiscale Mod-2A steam generators is received from the INEL.

The more important problem observed in the initial TRAC S-SF-3 analysis was an early degradation of the heat transfer in the intact loop steam generator. That degradation caused a primary system pressurization which resulted in a system scram considerably earlier than measured. Sensitivity studies indicated that considerably better agreement with data was obtained when the intact loop steam generator's initial inventory was increased about 20% from the reported value. Careful study of the results from those sensitivity studies indicated that the inventory distribution between the downcomer and boiler regions of the steam generator was almost as important as the amount of inventory itself, and that although it might be possible to improve the original results by steam generator modelling changes, insufficient data was available in the tests to determine the actual steady state inventory distribution.

#### SUMMARY

As noted in the previous sections, our assessment of TRAC-PF1/MOD1 is far from complete at this point. Most of the finished calculations are for separate effects tests which do not necessarily exercise all aspects of the code. Because of the incomplete integral test calculations, a disproportionate number of our preliminary assessment conclusions are concerned with details of the documentation and use of the code rather than the physics contained in the code.

Most of the results obtained so far in our assessment effort have been in good overall agreement with the available data. We have found no gross errors in predicted behavior which would indicate that the physical models or correlations contained in

TRAC-PF1/MOD1 were totally inadequate for the range of parameters of interest in full-scale PWR analyses. The most serious deficiency noted could well be the apparent inability of the code to predict early time quench behavior during large-break LOCAs. That problem has been recognized for some time with earlier versions of TRAC and is still being worked on by the code developers.

Many of the coding, documentation and modelling inadequacies identified in the course of our assessment calculations are being or have already been addressed by the code developers. Many of the deficiencies have been extremely bothersome from a user standpoint and have required an extraordinary effort to resolve, but have had little effect on the actual calculated results once the problem was finally identified and fixed or bypassed. More complete documentation would be invaluable to the analyst, particularly in the user-guideline area. Implementation of those new models currently under development at LANL should also make TRAC much more user-convenient and flexible.

#### REFERENCES

1. TRAC-PF1/MOD1: An Advanced Best-Estimate Computer Program for Pressurized Water Reactor Thermal-Hydraulic Analysis (DRAFT), Safety Code Development Group, Energy Division, Los Alamos National Laboratory, 1983.
2. S. L. Thompson et al., Thermal/Hydraulic Analysis Research Program Quarterly Report, January-March 1984, NUREG/CR-3820 (Vol. 1 of 4), SAND84-1025/1 of 4, Sandia National Laboratories, June 1984.
3. S. L. Thompson et al., Thermal/Hydraulic Analysis Research Program Quarterly Report, April-June 1984, NUREG/CR-3820 (Vol. 2 of 4), SAND84-1025/2 of 4, Sandia National Laboratories, August 1984.
4. I. S. Lim et al., Cocurrent Steam/Water Flow in a Horizontal Channel, NUREG/CR-2289, Northwestern University, August 1981.
5. R. K. Byers, TRAC-PF1/MOD1 Independent Assessment: Condensation in Stratified Cocurrent Flow, NUREG/CR-4027, SAND84-2161, Sandia National Laboratories, to be published.
6. H. A. Bloemen, Verification of the Pressurizer Model in RELAP5/MOD1, Energieonderzoek Centrum Nederland, Memo No. O.375.10 GR 26 (OD 79-24), May 1983.

7. A. C. Peterson, TRAC-PF1/MOD1 Independent Assessment: NEPTUNUS Pressurizer Test Y05, NUREG/CR-3919, SAND84-1534, Sandia National Laboratories, to be published.
8. H. R. Carter and D. D. Schleappi, Nuclear Once-Through Steam Generator (OTSG and IEOTSG) Loss of Feedwater Flow (LOFW) Tests, Report No. 4707, Babcock & Wilcox Co., March 1978.
9. D. Dobranich and L. D. Buxton, TRAC-PF1/MOD1 Independent Assessment: B&W 19-Tube Once-Through Steam Generator Tests, NUREG/CR-3877P, SAND84-1229, Sandia National Laboratories, July 1984.
10. D. Hein et al, PKL-Small Breaks (Test Series ID): Results of the Steady-State Test PKL ID1 in a Four-Loop Operation with 30 Bar System Pressure, KWU Tech. Rept. No. R 513/18/81, April 1981.
11. P. B. Bayless and J. M. Divine, Experimental Data Report for LOFT Large Break Loss-of-Coolant Experiment L2-5, NUREG/CR-2826, EGG-2210, Idaho National Engineering Laboratory, August 1982.
12. E. Ohlmer, Experimental Data Report on LOBI Test A1-04R, Communication LEC 80-03, Commission of the European Communities, J.R.C.-Ispra, December 1980.
13. T. Fortescue, LOBI Test B-R1M: Preliminary Data Report, Techn. Note No. I.06.01.81.153, Commission of the European Communities, J.R.C.-Ispra, December 1981.
14. T. M. O'Connell, Experiment Data Report for Semiscale Mod-2A Feedwater Line Break Experiments (Tests S-SF-1, S-SF-2, and S-SF-3), NUREG/CR-2912, EGG-2216, Idaho National Engineering Laboratory, September 1982.

Table 1 Sandia's TRAC-PF1/MOD1 Assessment Status

Test	Completed	Underway	Not Begun
LOFT			
L2-5		X	
LP-FW-1			X
Semiscale Mod-2A			
S-IB-3		X	
S-SF-3		X	
S-SF-5		X	
Semiscale Mod-2B			
S-PL-3			X
S-SG-?			X
PKL			
ID1-4	X		
ID1-8 to 13		X	
LOBI			
A1-04R		X	
B-R1M		X	
FLECHT SEASET			
31504			X
31701			X
B&W OTSG			
28	SAND84-1229		
29	NUREG/CR-3877P		
FLECHT SEASET			
8			X
NEPTUNUS			
Y05	SAND84-1534 NUREG/CR-3919		
Dartmouth			
3-tube CCFL			X
Bankoff/Northwestern Condensation			
253			
259	SAND84-2161		
293	NUREG/CR-4027		
479			
Bankoff/Northwestern CCFL		X	

ASSESSMENT OF TRAC-BD1 AND RAMONA-3B CODES  
FOR BWR ATWS APPLICATION\*

L. Neymotin, C. J. Hsu and P. Saha  
Department of Nuclear Energy  
Brookhaven National Laboratory  
Upton, New York 11973

1. ABSTRACT

Analysis of a typical BWR/4 Anticipated Transient Without Scram (ATWS) has been performed at BNL with both TRAC-BD1<sup>1</sup> and RAMONA-3B<sup>2</sup> codes within the scope of the NRC code assessment program. The objective of the program is to evaluate performance of various codes such as TRAC, RELAP5<sup>12</sup>, and RAMONA-3B in predicting plant operational/accident transients or separate effect tests. Work is currently underway on modeling an ATWS-type experiment conducted in the FIST facility<sup>3</sup>. Results obtained in these calculations will be complementary (in thermal-hydraulics area) to those produced in the present typical BWR/4 ATWS calculations.

Of all various ATWS events, the Main Steam Isolation Valve (MSIV) closure ATWS sequence is the most severe one because of its relatively high frequency of occurrence and its challenge to the heat removal and containment integrity systems. Therefore, this transient has been, and is still being, analyzed by different organizations using various computer codes<sup>4,5</sup>.

The transient was initiated by an inadvertent closure of all MSIVs with subsequent failure to scram the reactor. However, all other plant safety features, namely, the safety and relief valves, recirculation pumps trip, high pressure coolant injection and the standby liquid (boron) control systems were assumed to function as designed. No operator actions were assumed except for activation of the boron injection system. The calculations have been run until the reactor reached the hot shutdown mode of operation.

It was found that both TRAC-BD1 and RAMONA-3B produced similar results for the global parameters such as reactor power, system pressure, and the suppression pool water bulk temperature. Both calculations showed that the reactor can be brought to hot shutdown in approximately 20 to 25 minutes with the borated water mass flow rate of 2.78 kg/s (43 gpm) with 23800 ppm of boron. The suppression pool temperature (assuming no pool cooling) at this time could be in the range of 77 - 96°C (170 - 205°F).

An additional TRAC-BD1 calculation performed with RAMONA-3B power indicates that the thermal-hydraulic models in RAMONA-3B, although simpler than those in TRAC-BD1, can adequately represent the system behavior during an ATWS-type transient. Moreover, for reactor power calculation, RAMONA-3B with three dimensional space-time neutron kinetics is preferable to TRAC-BD1 with point kinetics since, as it was found in the RAMONA-3B calculations, the

\*Work performed under the auspices of the U.S. Nuclear Regulatory Commission.

spatial core power distribution varies strongly during a BWR ATWS. The computer running time for RAMONA-3B was also significantly less than that for TRAC-BD1. Therefore, it is recommended that RAMONA-3B be used for best-estimate BWR ATWS analysis.

Further assessment of both codes is needed to resolve certain differences found in the predictions. Basically, they are related to: a) void distribution calculations in the vessel and, b) condensation on ECC water jets after the feedwater spargers are uncovered.

## 2. INTRODUCTION

Anticipated Transient Without Scram (ATWS) is known to be a dominant accident sequence for possible core melt in a Boiling Water Reactor (BWR). A recent Probabilistic Risk Assessment (PRA) analysis<sup>6</sup> for the Browns Ferry, Unit 1, nuclear power plant indicates that ATWS is the second most dominant transient for core melt in a BWR/4 with Mark 1 containment (the most dominant sequence being the failure of long term decay heat removal function of the Residual Heat Removal (RHR) system).

Of all the various ATWS events, the Main Steam Isolation Valve (MSIV) closure ATWS sequence is the most severe one because of its relatively high frequency of occurrence and its challenge to the heat removal and containment integrity systems. Therefore, this transient has been, and is still being, analyzed by various organizations using various computer codes<sup>4,5</sup>.

The main objective of this paper is to provide a comparative analysis of a BWR/4 MSIV closure ATWS calculation using two advanced, best-estimate codes namely, RAMONA-3B/MODO/Cycle 6<sup>2</sup> and TRAC-BD1/Version 12<sup>1</sup>. Although both are BWR codes, they were conceived from two different stand-points: RAMONA-3B was developed primarily for analyzing operational transients with an emphasis on three-dimensional reactor kinetics and multi-channel core thermal hydraulics, whereas, TRAC-BD1 was developed primarily for analyzing loss-of-coolant accidents with an emphasis on three-dimensional thermal hydraulics with point reactor kinetics.

In a BWR, vapor void fraction varies significantly in space, particularly in the vertical or axial direction. Because of strong void-reactivity feedback, the space-time neutron kinetics, as employed in the RAMONA-3B code is expected to be very important in the ATWS analysis. However, the thermal-hydraulic models of RAMONA-3B must also be adequate, at least for the operational transients such as ATWS. Thus, the second objective of this paper is to verify the thermal-hydraulic models of RAMONA-3B with those of TRAC-BD1 for the same reactor power history.

Before details of the particular calculation are presented, it is worthwhile to point out some specific (common and different) features of the RAMONA-3B and TRAC-BD1 codes. For the sake of brevity, this is accomplished with Table 1.

### 3. TRANSIENT SCENARIO

The transient was assumed to be initiated by an inadvertent closure of all Main Steam Isolation Valves (MSIVs) in a typical BWR/4 with rated power of 3293 MWt and operating pressure of approximately 7 MPa. As a result, the pressure in the reactor vessel increased rapidly causing void collapse in the core and increase in reactor power. The relief and safety valves were assumed to operate as designed, and the recirculation pumps were tripped at the high pressure set point (8.03 MPa).

The feedwater was assumed to be lost at 35 seconds into the transient. The basis of this assumption is explained later. Since RAMONA-3B did not yet include a feedwater control system, the feedwater flow rate was calculated by using the TRAC-BD1 code with its control system, and was imposed on the RAMONA-3B calculation as a boundary condition. As the downcomer water level dropped, the High Pressure Coolant Injection (HPCI) and the Reactor Core Isolation Cooling (RCIC) systems were activated and cold water at a rate of 337 kg/s and 37.8°C was continued to be introduced through the feedwater sparger. At 120 seconds into the transient, the operator was assumed to start one of the two Standby Liquid Control System (SLCS) pumps. After a delay of 45 seconds, the highly concentrated borated water at a rate of 2.78 kg/s (43 gpm) with 23800 ppm of boron started to enter the reactor vessel to achieve the final hot shutdown condition. No other operator action was assumed during this transient.

It should be noted that the selected transient is just one of the many possible sequences during an MSIV closure ATWS event. The intent here is to examine RAMONA-3B and TRAC-BD1 capabilities for analyzing BWR ATWS-type transients, not to recommend corrective actions during all possible ATWS sequences. Thus, the selected transient is sufficient to serve the main purpose of this study.

### 4. INPUT MODEL DESCRIPTION

The modeling of a typical BWR/4 reactor system was performed by modifying a plant data set used at Idaho National Engineering Laboratory for the analysis of the Browns Ferry generator load rejection operational transient. The thermal-hydraulic part of the data was carefully checked and compared with the information given in Peach Bottom 2 and 3 FSAR<sup>7</sup> and the EPRI report NP-563<sup>8</sup>. Effort was made to ascertain that the reactor vessel geometric data were correct, and the thermal-hydraulic steady-state conditions for both RAMONA-3B and TRAC-BD1 adequately described a typical BWR/4 nominal full power operating condition, as shown in Table 2.

Since the RAMONA-3B code was developed specifically for the analysis of Boiling Water Reactors, the system under investigation was already "preassembled" in the code using major components typical for BWRs. However, the geometric and operational data had to be specified to represent the particular BWR being modeled.

The RAMONA-3B representation of the BWR/4 system is shown in Figure 1 which includes a Reactor Pressure Vessel with a Steam Dome Region, Downcomer, Lower Plenum, Core, Riser and Steam Separator, Steam Line with the Main Steam Isolation Valves, and four banks of Safety and Relief Valves. The reactor vessel has one combined recirculation loop with jet and recirculation pumps.

In the RAMONA-3B calculation the fuel assemblies in the core were represented by assuming a half-core mirror symmetry with 16 neutronic channels; all control rod groups were assumed to be completely withdrawn from the core region and remained so throughout the calculation. Six parallel hydraulic or heated channels and one bypass channel each with 12 axial nodes were used.

The TRAC-BD1 model of the reactor system utilized 20 components each consisting of a number of cells as shown in Figure 2. Only one CHAN component was used to represent the core region which was divided into 12 axial nodes. Although the input requirements for the TRAC-BD1 and the RAMONA-3B codes were considerably different, care was taken to ensure that all the geometric input data and the various trip signals used in the two codes were consistent with each other. No balance-of-plant modeling was necessary for the MSIV closure ATWS analysis presented in this paper.

Modeling of the core region is more elaborate in RAMONA-3B (with 192 neutronic and 84 hydraulic cells for half-core) because the code performs a three-dimensional time-dependent neutron kinetics calculation. Two group cross sections generated for the Peach Bottom 2 End-of-Cycle 2 conditions have been used in the present RAMONA-3B calculation. To be consistent, the reactivity feedback coefficients<sup>9-10</sup> developed from the BNL-GWIGL calculations of the Peach Bottom 2 turbine trip tests were used in the TRAC-BD1 calculation.

Table 3 compares the RAMONA-3B and TRAC-BD1 input models for the same BWR/4 plant. Information on recirculation pump trip, HPCI, RCIC, and boron injection is also included. The opening and closing set points and the rated flow rates for the S/R valves are given in Table 4.

## 5. COMPARISON BETWEEN RAMONA-3B AND TRAC-BD1 RESULTS

The RAMONA-3B and TRAC-BD1 predictions for the initial part of the transient following the MSIV closure but before boron injection, will be discussed first. Selected results for the first 150 seconds are depicted in Figures 3 through 9 (comparison of sequence of events for the entire transient is shown in Table 5). The results are discussed below with emphasis on system parameters considered to be the most important from the plant safety viewpoint.

### 5.1 Short Term (0-150 sec) Results

As expected, immediately after the MSIV closure initiation, the reactor vessel pressure experienced a rapid increase (Figure 3) which in turn, caused void collapse in the core (Figure 4). This introduced a positive reactivity insertion, and a rapid increase of the power (Figure 5) in the first 4 seconds of the transient. Differences in peak power predictions (230% in RAMONA-3B vs. 520% in TRAC-BD1) as well as the reactor power up to approximately 30 seconds can be attributed to the differences in the void fraction predictions, difference in the void reactivity feedback parameter and the three-dimensional neutronics in RAMONA-3B vs. point kinetics in TRAC-BD1. Since TRAC-BD1 predicted a higher reactor power, opening of three banks of relief valves could not arrest the pressure rise as it occurred in the RAMONA-3B calculation; so even the fourth bank, i.e., the safety valves, had to open in the TRAC-BD1 calculation (Figure 6). Note that the higher peak pressure (Figure 3) predicted by TRAC-BD1 was consistent with the higher reactor power (Figure 5) calculated by the code during the first 30 seconds. However, due to the strong pressure-void-reactivity coupling, it is difficult to determine the exact

reason for this prediction. An additional TRAC-BD1 calculation has, therefore, been performed with RAMONA-3B reactor power to separate the thermal-hydraulic and neutronic effects. This is discussed later in the paper.

At approximately 30 seconds, the S/RVs actions together with the recirculation pump trip brought the power, pressure, and other system parameters to a quasi-steady-state condition with reasonable agreement between the two calculations (Figures 3, 5, 6 and 7). However, as shown in Figure 4, the core average void fraction including the bypass was an exception. Some possible reasons for this discrepancy are discussed later. No critical heat flux (CHF) condition was experienced in either calculation.

As seen in Figure 5, the reactor power started to increase slightly after 100 seconds. This was due to positive reactivity insertion when the cold HPCI and RCIC water reached the core. There was no boron in the HPCI and RCIC systems. The cold water injection was activated by a low water level signal at slightly different times in these two calculations (Figure 8) in accordance with the water level predictions as shown in Figure 9. In the TRAC BD1 calculation, the collapsed water level dropped at a faster rate because of higher reactor power.

One of the major reasons for the differences observed in the detailed results produced by the RAMONA-3B and TRAC-BD1 codes was due to the differences in the neutronics and power calculation area. As indicated in Tables 1 and 3, TRAC-BD1 calculation was performed with point kinetics assuming the same axial power distribution as the RAMONA-3B steady-state distribution. The power distribution had to be kept invariant in the TRAC-BD1 calculation throughout the transient, whereas RAMONA-3B used a three-dimensional time dependent neutron kinetics. The effect of this difference can be seen in Figure 10 where the RAMONA-3B axial core power distributions at different times are presented. The corresponding axial void fraction profiles are shown in Figure 11. It is seen that a slight variation in axial void profile can indeed produce a large change in the axial power distribution which a point kinetics code like TRAC-BD1 cannot predict.

Another area of concern is the differences in the void predictions as shown in Figure 4. A large difference in the core average void fraction (including bypass) can be seen between the RAMONA-3B and TRAC-BD1 calculations (Figure 4). The difference was present even at the steady-state condition when the reactor power, core flow and temperature conditions were either identical or very close as shown in Table 2. RAMONA-3B uses a slip correlation to calculate the void fraction for a given flow quality. TRAC-BD1, however, solves two phasic momentum equations to calculate the individual phase velocities. Therefore, the correlations which affect the void prediction are completely different in these two codes. Thus some differences in the void fraction prediction should be expected. There were also some differences due to the single channel vs. multi-channel treatment of the reactor core thermal hydraulics in the TRAC-BD1 and RAMONA-3B codes, respectively. However, it should be noted that it is the change in void fraction, rather than the absolute value of void fraction, which is more important in the reactor power calculation. This explains why the total reactor powers as calculated by RAMONA-3B and TRAC-BD1 were in reasonable agreement although the core average void fractions were quite different.

## 5.2 Long Term (0-1500 sec) Results

Both calculations were continued until a hot reactor shutdown condition (~2% of steady state power) was achieved as a result of boron injection. Highly concentrated borated water at a rate of 2.78 kg/s (43 gpm) with 23800 ppm of boron was injected starting at 165 seconds. As the boron concentration in the core started to increase, the power dropped temporarily resulting in a drop in the void fraction which, in turn, increased the power again. These competing effects of negative boron reactivity and positive reactivity insertion due to void collapse kept the reactor critical for a long time. Meanwhile, the downcomer water level reached the high level shut-off point due to continuous injection of HPCI and RCIC water. After this water injection was terminated, the boron concentration in the core started to increase at a higher rate, and it eventually overcame the competing void-reactivity effect. The qualitative behaviors of RAMONA-3B and TRAC-BD1 results were quite similar, and as an example, selected results from the TRAC-BD1 calculations are shown in Figures 12 through 16 for core-average boron concentration, downcomer water level, reactor power, and core-average void fraction. TRAC-BD1 predicted the hot shutdown condition at approximately 1100 seconds, whereas RAMONA-3B predicted the same condition at approximately 1400 seconds. This difference is believed to be mainly due to the differences in the boron reactivity feedback coefficients in the two calculations. No attempt was made to adjust these parameters to achieve a better agreement between the RAMONA-3B and TRAC-BD1 calculations.

As seen in Figure 15 (RAMONA-3B), the reactor remained in hot shutdown condition for approximately 40 seconds. This state was interrupted soon after initiation of the HPCI and RCIC cold water injection on the low downcomer water level had occurred: due to positive reactivity insertion the reactor became critical again.

In the course of this study a question about effects of condensation on the ECCS cold water jets was raised: the condensation starts after the feed-water sparger nozzles are uncovered and the water is injected into predominantly steam environment. This issue may become important because the reactor power depends strongly on the water subcooling at the core inlet. Neither of the two codes had a model for the condensation on cold water jets so that developmental work on such a model for RAMONA-3B was initiated.

## 5.3 Suppression Pool Water Temperature

Since steam released through the S/R valves is dumped into the suppression pool, the pool water temperature starts to increase. To maintain the containment integrity, it is important to keep the suppression pool water temperature at a sufficiently low value. The pool water temperature is, therefore, an important variable from the plant safety viewpoint.

A stand-alone computer program was written to solve the mass and energy conservation equations for the suppression pool water. Steam flow rates and enthalpies calculated by RAMONA-3B and TRAC-BD1 were used as input to this program. The calculated suppression pool temperatures (assuming no pool cooling by the RHR system) are shown in Figure 17. Since RAMONA-3B predicted a longer time for achieving the reactor shutdown condition, the final

suppression pool water temperature calculated by RAMONA-3B was  $-20^{\circ}\text{F}$  compared to  $-170^{\circ}\text{F}$  for TRAC-BD1.

### 5.3.1 Non-Perfect Boron Mixing

It is known that during a low flow or natural circulation cooling mode, all the boron injected into a BWR lower plenum may not be carried into the core. This is because of higher specific gravity of the injected borated water, and the presence of hundreds of control rod guide tubes in the lower plenum. However, in the present calculations no such boron stratification effect was considered. Thus the boron concentration shown in Figure 12 is probably higher-than-actual, which has probably resulted in a shorter-than-actual hot shutdown time.

An attempt has been made to take into account the effect of possible boron stratification based on RAMONA-3B calculation results. Based on the boron mixing efficiency vs. recirculation flow as presented in Reference 11, a value of 0.75 can be assumed for the boron mixing efficiency in the present estimate. Thus, the actual boron concentration in the core would be about 25% lower than the values shown in Figure 12. This would delay the drop in reactor power from  $\sim 1300$  seconds (as shown in Figure 15) to  $\sim 1450$  seconds. Even with the assumption of no HPCI and RCIC injection at 1400 seconds (so that the reactor does not regain criticality), the additional reactor power would increase the suppression pool water temperature by another  $12^{\circ}\text{F}$  ( $6.7^{\circ}\text{C}$ ). So without the RHR cooling, the pool water bulk temperature would be  $\sim 217^{\circ}\text{F}$  ( $102.8^{\circ}\text{C}$ ).

### 5.3.2 Suppression Pool Cooling

During a BWR ATWS, the operator could be expected to activate the RHR system to reduce the suppression pool heat-up rate. However, the RHR system is designed to remove only about 3% of the rated power. Therefore, even if the pool cooling is activated at the early stage of the transient, the maximum reduction of pool water temperature would be approximately  $15^{\circ}\text{F}$  ( $8.3^{\circ}\text{C}$ ).

A realistic boron mixing model coupled with maximum pool cooling by the RHR system can, therefore, result in a pool water bulk temperature of  $\sim 202^{\circ}\text{F}$  ( $94.4^{\circ}\text{C}$ ) at the time of reactor hot shutdown. This temperature may still be high from the plant safety viewpoint. Thus, the effects of other mitigative features such as manual rod insertion, use of two SLCS pumps with total capacity of 86 gpm, lowering the downcomer water level to the top of active fuel (TAF), etc., should be investigated. The RAMONA-3B code is already being used for this purpose under the Severe Accident Sequence Analysis (SASA) program.

### 5.4 TRAC-BD1 Calculation with RAMONA-3B Power

Close coupling between the neutronics and thermal-hydraulics in a BWR makes interpretation of the code predictions a very complex task. An attempt to break up the above coupling was made by performing an additional TRAC-BD1 calculation for the first 150 seconds with the RAMONA-3B core power history as a boundary condition. The RAMONA-3B power was imposed because of the code's detailed treatment of the neutronics part of the calculation. Spatial power

variation as a function of time, however, could not be imposed on the TRAC-BD1 code due to code limitation. Therefore, only the total core power was imposed. Results of this calculation answer the questions concerning the differences in the thermal-hydraulic modeling only, and their impact on the code predictions (as it was mentioned earlier, more information on purely thermal-hydraulic performance of both codes at MSIV closure ATWS-type conditions will be available when the BNL code assessment program with FIST results is completed).

A few selected results of the additional TRAC-BD1 calculation are compared with the RAMONA-3B results in Figure 18 through 21. As it is seen now, the system pressures, S/RV flow rates, and the average fuel temperatures (Figures 18 through 20) are in much better agreement. Differences in the void fraction prediction (Figure 21) still remain due to different thermal-hydraulic models used in these codes. Further assessment with experimental data is required to resolve this issue.

## 6. SUMMARY AND CONCLUSIONS

Based on comparisons between the TRAC-BD1 "power imposed" calculation and the RAMONA-3B results, it can be said that the thermal-hydraulic models of both RAMONA-3B and TRAC-BD1 provide adequate representation of an ATWS event in a BWR. However, for the reactor power calculation, RAMONA-3B with space-time neutron kinetics is a superior and preferable tool to the TRAC-BD1 with point kinetics for ATWS type events where the spatial core power distribution varies with time. Also, the computer running time for RAMONA-3B (with 115 hydraulic cells and 192 neutronic cells) has been found to be about four times lower than TRAC-BD1 (with 63 hydraulic cells and point kinetics). Therefore, it is recommended that RAMONA-3B be further used for best-estimate analysis of BWR ATWS-type events.

The following conclusions can be drawn based on the above results:

- a) In the event of a BWR/4 MSIV closure ATWS, the reactor can be shut-down with recirculation pumps trip, safety/relief valves actions, and boron injection in approximately twenty-five minutes. With all safety systems (except reactor scram) working as designed, no core uncover or damage is predicted.
- b) Either the RAMONA-3B or TRAC-BD1 code can be used to predict the global variables such as reactor power, pressure, suppression pool temperature during a BWR ATWS event. However, for a best-estimate analysis, the use of the RAMONA-3B code with space-time neutron kinetics is preferable since the spatial core power distribution significantly varies during an ATWS event. Moreover, it is difficult to determine the point kinetics feedback coefficients (as required for a TRAC-BD1 calculation) a priori. Computer running time is also significantly lower for RAMONA-3B than for TRAC-BD1.
- c) The thermal-hydraulic models of RAMONA-3B, although simpler than those of TRAC-BD1, are adequate for analyzing abnormal BWR plant transients such as ATWS. Further assessment of both codes is needed to establish the correctness of core void distribution predictions.

## REFERENCES

1. Spore, J. W., et al., "TRAC-BD1: An Advanced Best-Estimate Computer Program for Boiling Water Reactor Loss-of-Coolant Accident Analysis," NUREG/CR-2178, October 1981.
2. Wulff, W., et al., "A Description and Assessment of RAMONA-3B: A Computer Code with Three-Dimensional Neutron Kinetics for BWR System Transients," NUREG/CR-3664, BNL-NUREG-51746, 1984.
3. Stephens, A. G., "BWR Full Integral Simulation Test Program," NUREG/CR-2576, EPRI NP 2314, GEAP 22054, December 1982.
4. Aronson, A., et al., "Status Report on BNL Calculations of ATWS in BWRs," BNL-17608, RP1022, 1973.
5. General Electric Company, "Assessment of BWR Mitigation of ATWS," Volume II, (NUREG-0460 Alternate No. 3), NEDO 24222, February 1981.
6. Mays, S. E., et al., "Interim Reliability Evaluation Program: Analysis of the Browns Ferry, Unit 1, Nuclear Plant," NUREG/CR-2802, EGG-2199, July 1982.
7. "Final Safety Analysis Report, Peach Bottom Atomic Power Station Units No. and 3," Philadelphia Electric Company, 1971-1973.
8. Larsen, N. H., et al., "Core Design and Operating Data for Cycles 1 and 2 of Peach Bottom 2," EPRI NP-563, Project 1020-1 Topical Report, June 1978.
9. Cheng, H. S., and Diamond, D. J., "Core Analysis of Peach Bottom-2 Turbine Trip Tests," BNL-NUREG-24903, September 1978.
10. Cheng, H. S., Private Communication, July 1983.
11. Dente, T. J., "Schedule for BWR Owner's Group Compliance with NUREG-0737, Item II.K.3.18," Letter to D. G. Eisenhut, NRC, BWROG-8204, February 5, 1982.
12. Ransom, V. H., et al., "RELAP5/MOD1.5: Models, Developmental Assessment, and User Information," EGG-NSMD-6035, October 1982.

## ACKNOWLEDGEMENTS

This work was sponsored by the Office of Nuclear Regulatory Research of the U.S. Nuclear Regulatory Commission. Special thanks are due to Dr. F. Odar, the NRC program monitor, for his encouragement and suggestions. Technical help provided by Dr. C. J. Hsu and Ms. H. R. Connell, both of BNL, is highly appreciated. Finally, thanks are due to Mrs. A. C. Fort for her fine typing of this manuscript.

Table 1. GENERAL FEATURES OF RAMONA-3B AND TRAC-BD1 CODES

Item	RAMONA-3B	TRAC-BD1
A. Neutronics	Two-group, three-dimensional neutron kinetics.	Point kinetics.
B. Thermal hydraulics		
1. Balance equations	One-dimensional, four-equation modeling.	Three-dimensional, six equation modeling.
2. Core hydraulics	Set of parallel coolant channels and one bypass channel.	Same as RAMONA-3B.
3. Phasic velocities	Slip model ( $v_g = S v_l + V_o$ ).	$V_g$ and $V_l$ are calculated separately.
4. Subcooled boiling	Present	Present
5. Fuel conduction	Present	Present
6. Safety systems	Present	Present
7. Plant controls	BWR-specific	General

Table 2. Steady State Conditions of RAMONA-3B

	RAMONA-3B	TRAC-BD1
Thermal Power, Mwt	3293	3293
Pressure, Pa	$6.99 \times 10^6$	$6.99 \times 10^6$ (steam done)
Mass Flow Rate of Coolant at:		
Core Entrance, kg/sec	12780	12880
Steam Line/Feedwater, kg/sec	1639	1679
Feedwater Temperature, °C	191.2	191.4
Core Inlet Fluid Enthalpy, kcal/kg	288.39	288.88
Core Bypass Flow/Total Core Inlet Flow, %	11.32	11.20
Recirculation Drive Flow Rate, kg/sec	4356	4306

Table 3. Comparison of the RAMONA-3B and TRAC-BD1 Models

	<u>TRAC-BD1</u>	<u>RAMONA-3B</u>
Core Region (Hydraulics)	1 heated + 1 bypass channel, 14 (12 active) axial nodes.	6 heated + 1 bypass channel, 12 axial nodes
Core Region (Neutronics)	Imposed axial power shape; reactivity feedback coefficients were developed from BNL-GWIGL and RELAP-3B calculation of Peach Bottom 2 turbine trip tests <sup>9-10</sup> .	16 channels 192 nodes
Downcomer	1D, 3 axial nodes.	1D, 11 axial nodes.
Automatic Control System	Used to control downcomer water level, turbine inlet pressure & recirculation loop flow.	Not used. Feedwater flow rate taken from TRAC-BD1 calculations.
Recirculation Pump Trip Set Point	8.0324 MPa with 0.53 sec. delay.	Same as TRAC-BD1
HPCI + RCIC Initiation Set Point	Time at which the downcomer level reaches Level 2 with 30 sec. delay.	Same as TRAC-BD1
Boron Injection Set Point	t=120 sec with 45 sec. delay.	Same as TRAC-BD1
Boron Injection Rate and Concentration	2.79 g/s, 23800 ppm.	Same as TRAC-BD1
Initial Pressure Suppression Pool Water Volume	3859 m <sup>3</sup> .	Same as TRAC-BD1

Table 4. Safety and Relief Valves Set Points

<u>Bank #</u>	<u>1</u> <u>(4 Relief)</u>	<u>2</u> <u>(4 Relief)</u>	<u>3</u> <u>(3 Relief)</u>	<u>4</u> <u>(2 Safety)</u>
High Pressure (opening), 10 <sup>5</sup> Pa	75.50	76.19	76.88	85.84
Delay Time (opening), sec	0.4	0.4	0.4	0.4
Low Pressure (closing), 10 <sup>5</sup> Pa	73.23	73.90	74.57	83.22
Delay Time (closing), sec	0.0	0.0	0.0	0.0
Rated Flow/ Valve (kg/sec)	98.86	98.86	98.86	117.60

Table 5. Sequence of Events

<u>EVENT</u>	<u>RAMONA-3B</u>	<u>TRAC-BD1</u>
MSIVs closure starts, sec	0.0	0.0
S/RVs start to open, sec	2.62	3.57
Recirculation pumps trip on high pressure, (8.03 Mpa), sec	3.7	3.95
MSIVs are completely closed, sec	4.0	4.0
Maximum fuel temperature is reached, sec	4.5 (773°C)	5.7 (835°C)
Maximum system pressure reached, sec	8.5 (8.56 MPa)	11.0 (9.30 MPa)
HPCI + RCIC flow starts on low water level signal, sec	86.6	75.8
Boron Injection begins (43 gpm, 23800 ppm), sec	165.0	165.0
HPCI + RCIC turned off on high water level signal, sec	980.0	1275.0
Hot shutdown achieved, sec	1400.0	1100.0
HPCI and RCIC reactivated on low downcomer water level, sec	1400.0	

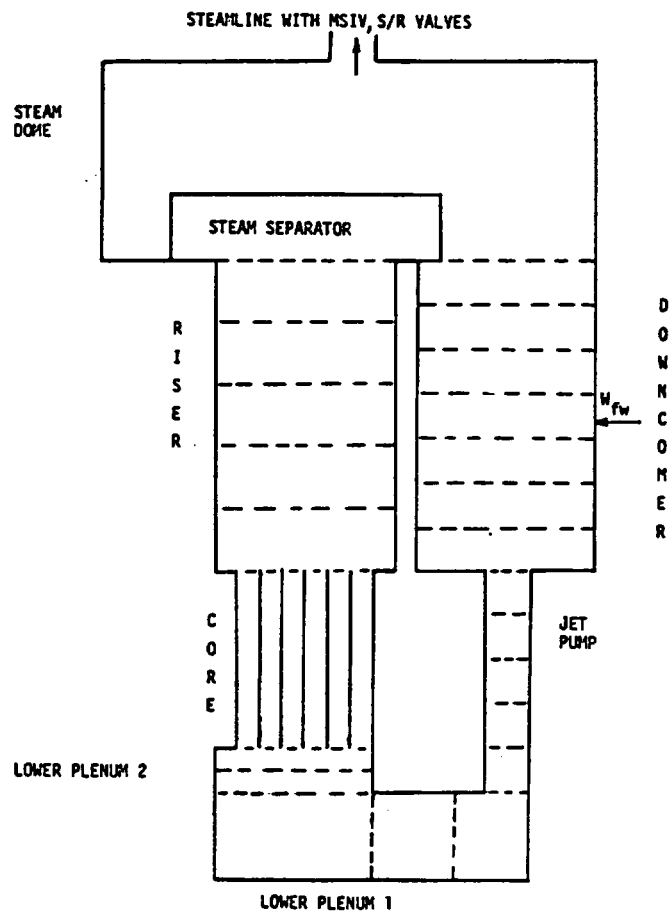


Figure 1 RAMONA-3B Representation of a Boiling Water Reactor Vessel

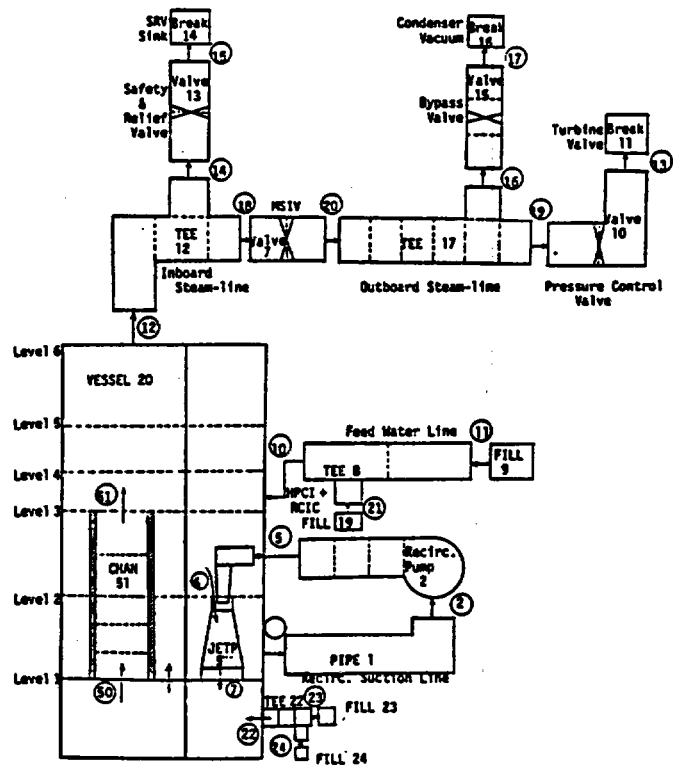


Figure 2 BWR/4 Noding Diagram for TRAC-BD1

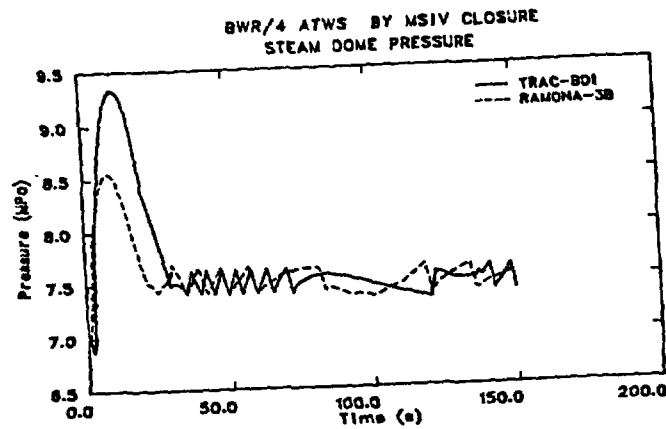


Figure 3. Comparison of Steam Dome Pressures as Calculated by RAMONA-3B and TRAC-BD1

Figure 3 Comparison of Steam Dome Pressures as Calculated by RAMONA-3B and TRAC-BD1

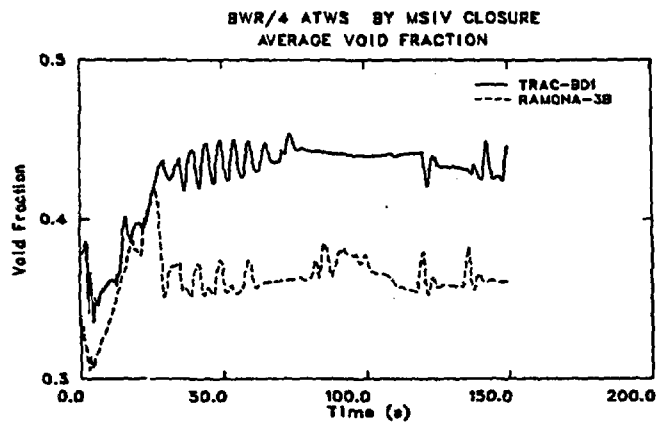


Figure 4. Comparison of Core Average Void Fractions (Including Bypass) as Calculated by RAMONA-3B and TRAC-BD1

Figure 4 Comparison of Core Average Void Fractions (Including Bypass) as Calculated by RAMONA-3B and TRAC-BD1

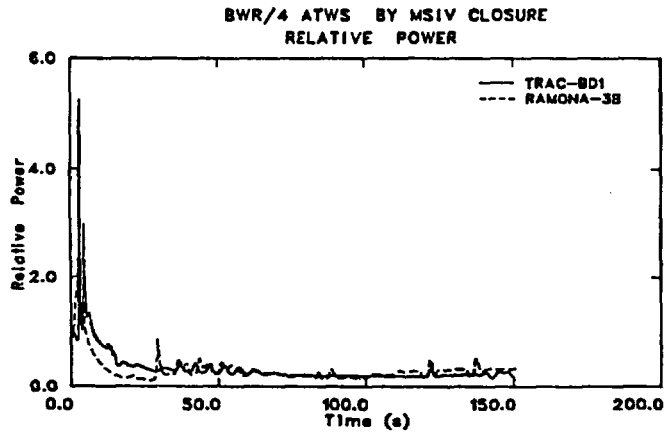


Figure 5 Comparison of Relative Core Powers as Calculated by RAMONA-3B and TRAC-BD1

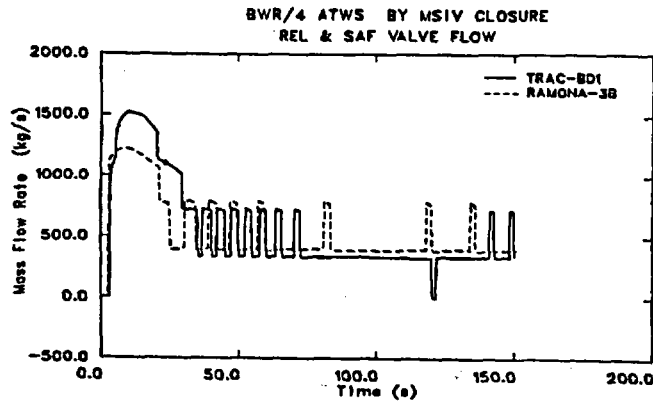


Figure 6 Comparison of Steam Discharge Rates Through Relief and Safety Valves as Calculated by RAMONA-3B and TRAC-BD1

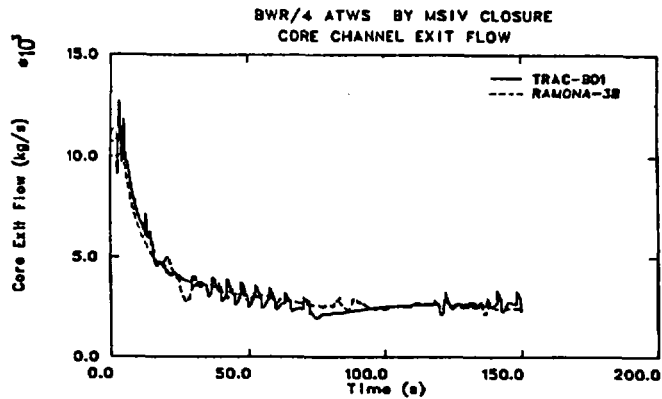


Figure 7 Comparison of Core Exit Flow Rates as Calculated by RAMONA-3B and TRAC-BD1

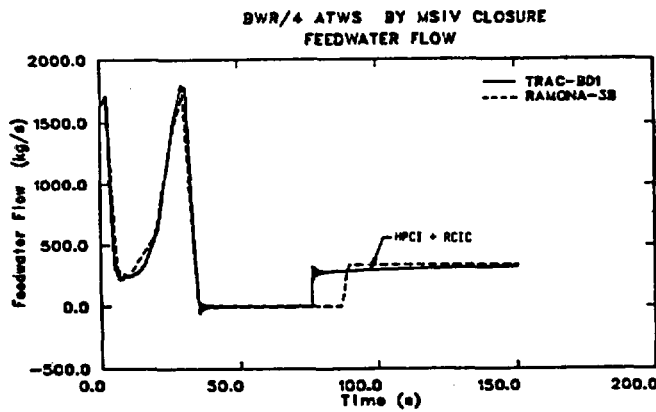


Figure 8 Comparison of Feedwater Sparger Flow Rates as Calculated by RAMONA-3B and TRAC-BD1

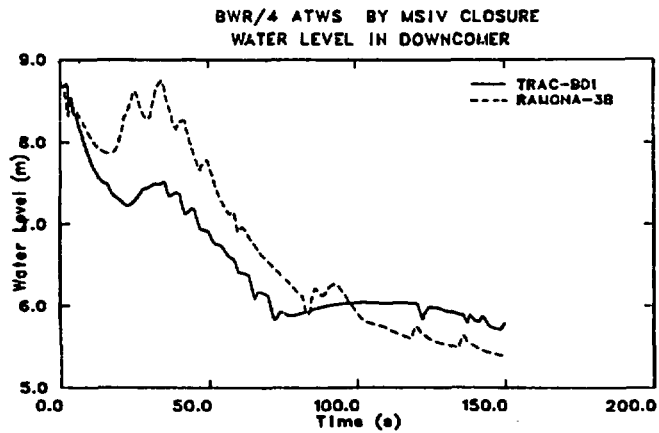


Figure 9 Comparison of Collapsed Downcomer Water Levels as Calculated by RAMONA-3B and TRAC-BD1

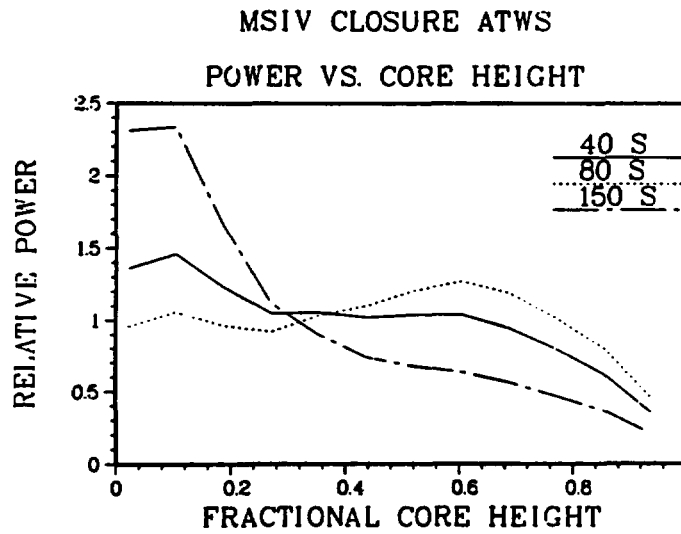


Figure 10 Axial Core Power Distributions as Calculated by RAMONA-3B

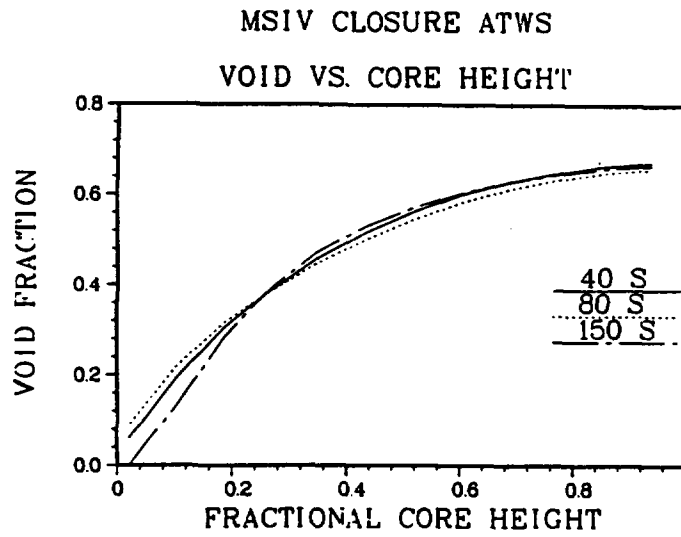


Figure 11 Axial Core Void Fractions as Calculated by RAMONA-3B

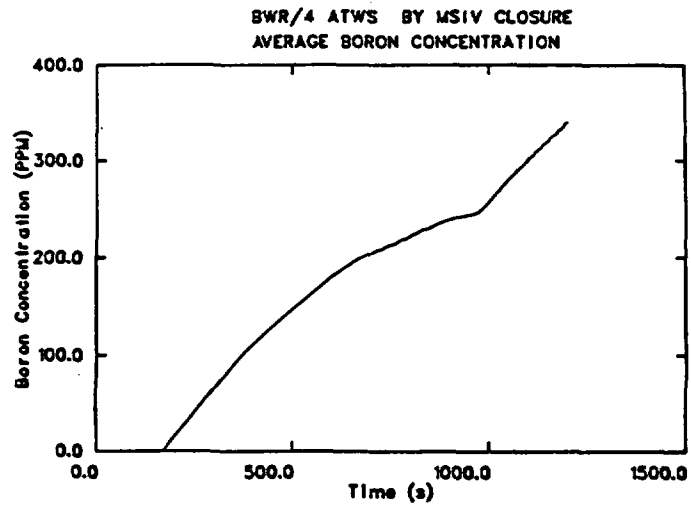


Figure 12 Core Average Boron Concentration (Including Bypass) as Calculated by TRAC-BD1

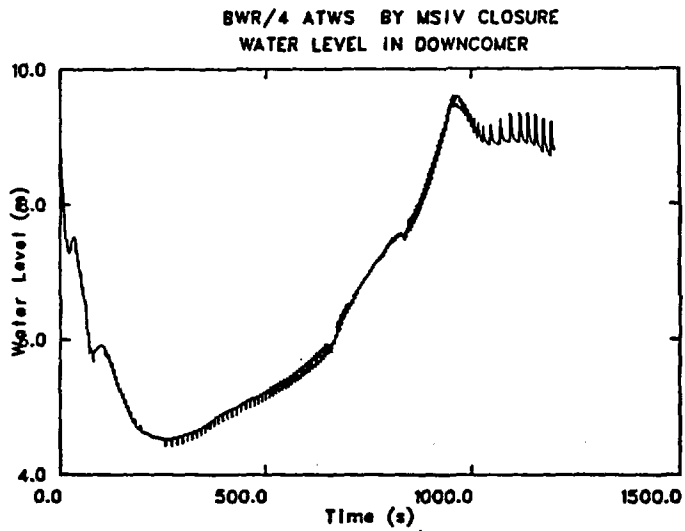


Figure 13 Collapsed Water Level in Downcomer as Calculated by TRAC-BD1

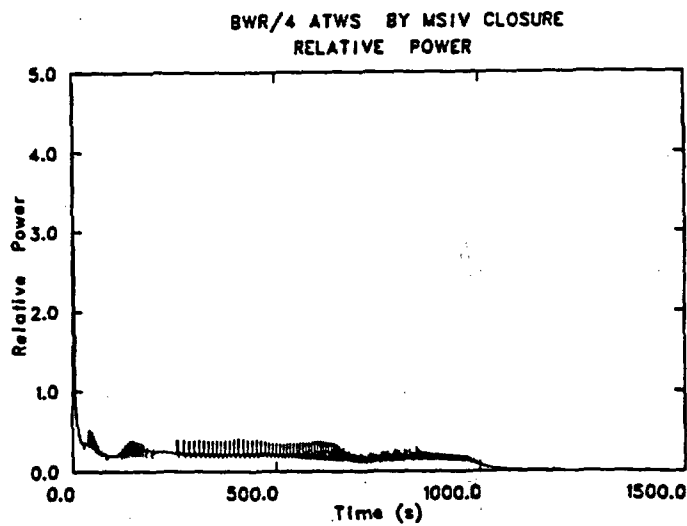
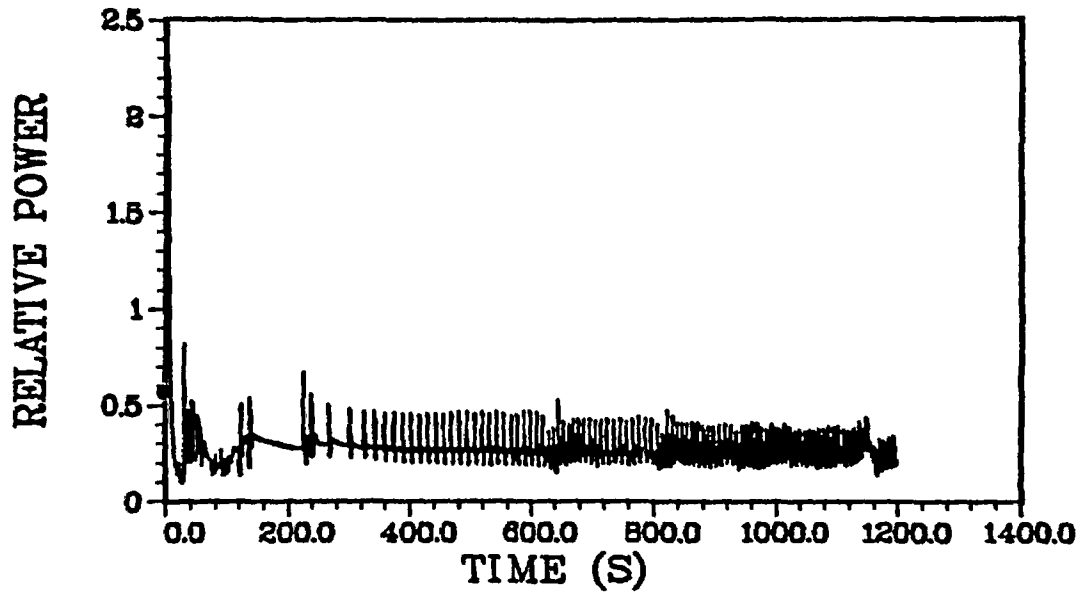


Figure 14 Long Term Reactor Power (Relative to Steady State) as Calculated by TRAC-BD1

MSIV CLOSURE ATWS  
RELATIVE POWER VS. TIME



MSIV CLOSURE ATWS  
RELATIVE POWER VS. TIME

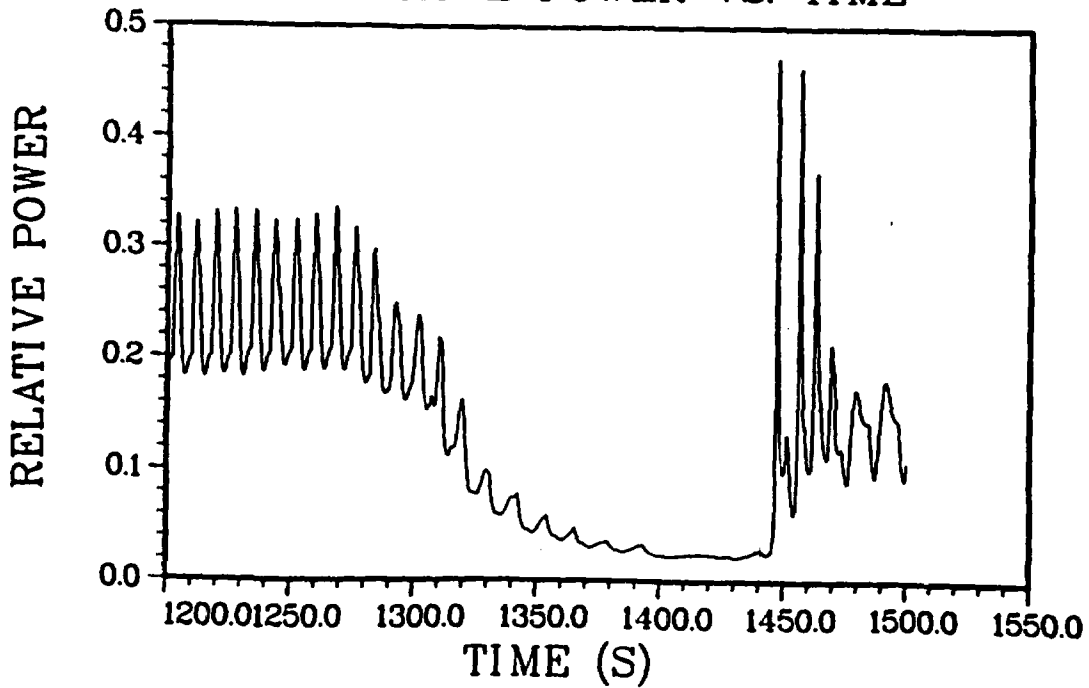


Figure 15 Long Term Reactor Power (Relative to Steady State)  
as Calculated by RAMONA-3B

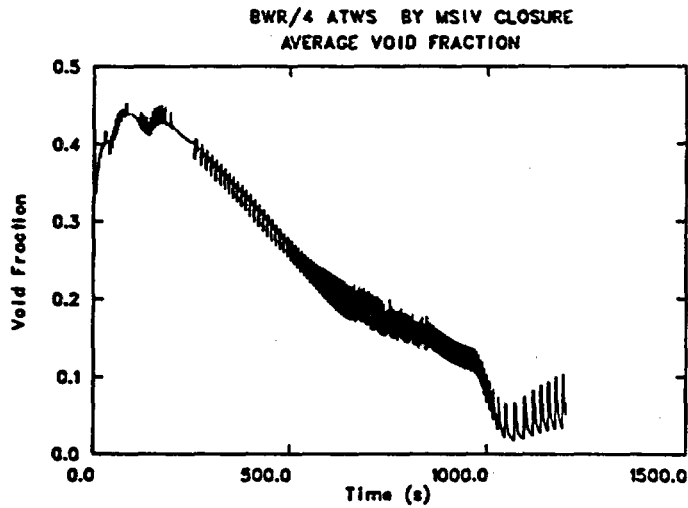


Figure 16 Core Average Void Fraction (Including Bypass) as Calculated by TRAC-BD1

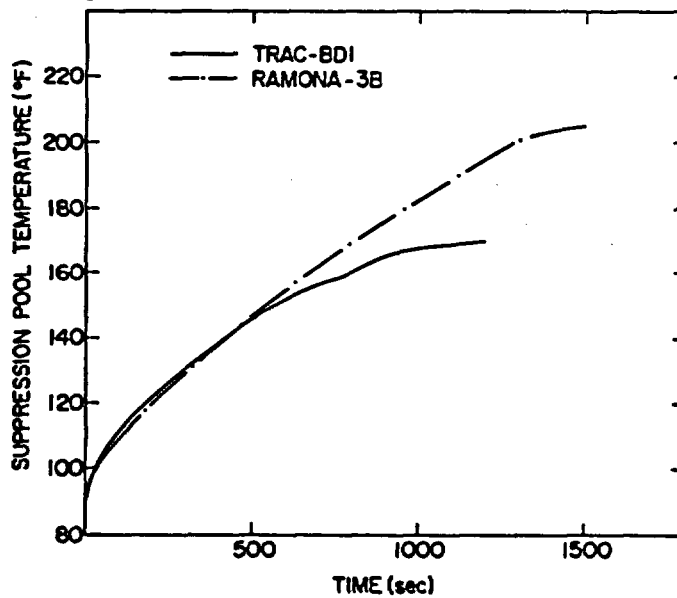


Figure 17 Comparison of Suppression Pool Water Temperature as Calculated by RAMONA-3B and TRAC-BD1

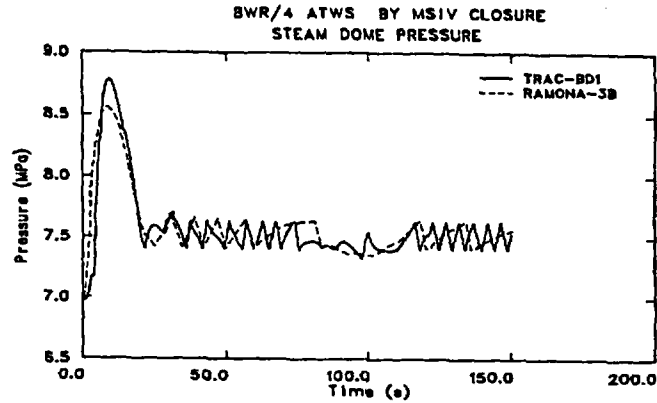


Figure 18 Comparison of Steam Dome Pressure as Calculated by RAMONA-3B and TRAC-BD1 with RAMONA-3B Reactor Power

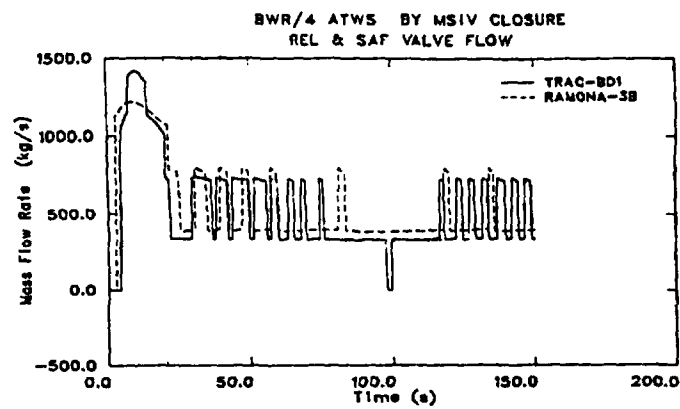


Figure 19 Comparison of Steam Discharge Rates Through Relief and Safety Valves as Calculated by RAMONA-3B and TRAC-BD1 with RAMONA-3B Reactor Power

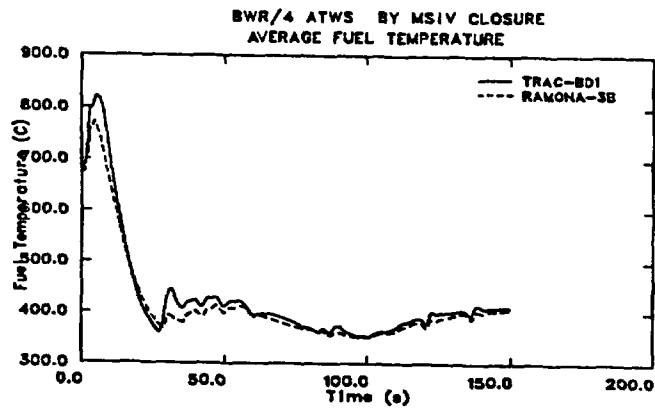


Figure 20 Comparison of Average Fuel Temperatures as Calculated by RAMONA-3B and TRAC-BD1 with RAMONA-3B Reactor Power

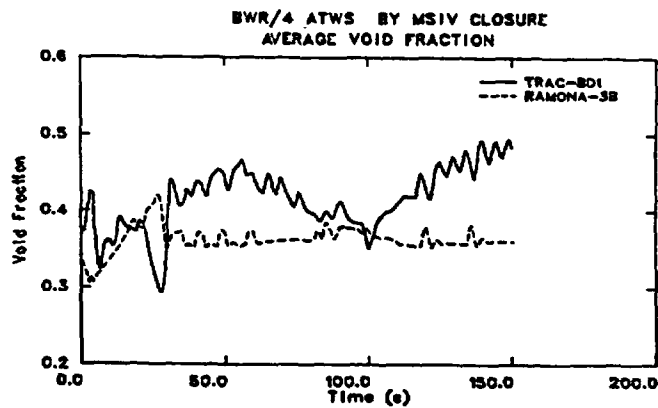


Figure 21 Comparison of Core Average Void Fractions (Including Bypass) as Calculated by RAMONA-3B and TRAC-BD1 with RAMONA-3B Reactor Power



**Investigation of Dispersed Flow  
Heat Transfer Phenomena  
and  
Assessment of TRAC-PF1/MOD1  
Heat transfer correlations**

---

**I. Vojtek  
Gesellschaft für Reaktorsicherheit mbH  
Garching, FRG**

## Objectives

### 1 Assessment and improvement of existing TRAC-PF1/MOD heat transfer model

The first part of this investigation has been performed using a "Driver computer code" which was developed by the author at LANL. The "driver program" BOILTRC consists of all TRAC-PF1/MOD1 heat transfer and properties routines and calculates heat transfer coefficients in all TRAC heat transfer regims as a function of independent variables ( $G$ ,  $X$ ,  $\Delta T$ ,  $p$  or  $V_v$ ,  $V_l$ ,  $\alpha$ ,  $\Delta T$ ,  $p$ ).

The next part of the assessment, that was focused mainly at the post-CHF heat transfer regime has been also performed at LANL using TRAC PF1/MOD1 computer code for the post-test analysis of simple separate effects heat transfer experiments.

### 2. Evaluation of alternative post-CHF heat transfer models

Three different post-CHF heat transfer models were implemented into the TRAC PF1/MOD1 and have been applied for the calculation of wall-mixture heat transfer components:

- Forslund-Rohsenow
- Kendall-Varone-Rohsenow
- Vojtek

## Description of test facilities and experiments

### 1. German transient 5x5 rod bundle heat transfer test facility and experiments

The German blowdown heat transfer test facility is a nonnuclear experimental apparatus with a test section that contains a 5x5 bundle of

electrically heated rods. This facility was designed for a pressure up to 17 MPa and maximum power of 5 MW. The test section is schematically shown in Fig. 1. It consists of a pressure vessel and inlet and outlet control valve stations. A detailed description of the test facility can be found in /1/.

The heater rod design and geometry is shown in Fig. 2. The stepwise variation of the heater wall thickness resulted in a nonuniform axial power distribution which is similar to a PWR profile and is shown in Figure 2. All 25 rods were uniformly heated which produced a flat radial power profile in the bundle. The following important parameters have been measured during each test:

- Inlet and outlet pressure
- Differential pressure between inlet and outlet
- Inlet and outlet fluid temperature
- Inlet single phase mass flow rates
- Electrical power
- Test-section wall temperature
- 80 heater wall temperatures (Fig. 3)

The experimental program has been divided into two groups of experiments called "DNB" and "Post-DNB" tests /2/.

Two specific DNB-tests were selected for the assessment of post-CHF heat transfer models. The results of the post-test analysis of test DNB-3 are described in /3/. In this paper results of the analysis of test DNB-9 are presented.

The boundary conditions for this experiment are shown in Table 1 and Figure 4.

## 2. Lehigh University heat transfer facility and experiments

The Lehigh University forced convection boiling two-phase experimental test facility is shown schematically in Figure 5. The test section for post-CHF measurements consists of a vertical heat channel that is 1.5m in length with 0.0141m inside diameter tube. The test section is located

above a "hot patch" designed to ensure post-CHF flow conditions. Wall temperature measurements are provided at 7.5 cm intervals along the test section. Joule heating of the tube is supplied by direct current through the walls using a variable d-c power supply. The vapor superheat probe is located 130 cm above the inlet to the copper hot patch. The high quality, intermediate mass flux and power test 138 has been selected for the assessment of TRAC PF1/MOD1 post-CHF heat transfer model. The boundary conditions for this test are summarized in Table 2.

### Results of previous analysis

The first part of the post-experimental analysis of 5x5 rod bundle heat transfer tests has been performed by the Gesellschaft für Reaktorsicherheit using computer code BRUDI-VA a modified version of the German blowdown code, BRUCH-D /4, 5/. The computer code BRUDI-VA /6/ is based on the homogeneous equilibrium model of the two-phase fluid flow and the lumped parameter technique was used for the nodal representation of the test section. The basic set of the differential equations of BRUDI-VA is shown in Table 3.

The heater wall temperatures and the heat generation in the wall of electrically heated rods have been calculated using one-dimensional transient heat conduction model with internal heat sources.

The following correlations have been used for the calculation of heat transfer coefficients in the film boiling regime.

#### Equilibrium correlations:

- Modified Dougall-Rohsenow /8/
- Groeneveld 5.7 /10/
- Condie-Bengston IV /11/

#### Nonequilibrium correlations:

- Groeneveld-Delorme /12/
- Chen, Ozkaynak, Sundaram /13/

The wall-vapor heat transfer coefficients predicted with the nonequilibrium correlations have been compared to those predicted by the vapor Dittus-Boelter correlation.

The time histories of wall temperatures and heat transfer coefficients which were obtained using equilibrium correlations, are shown in Figs. 6 through 9. The calculated wall temperatures as obtained from the analysis of test DNB-3 are compared with experimentally determined values. Heat transfer coefficients computed using correlations are compared with those calculated directly from the measurements.

The results of the evaluation of nonequilibrium correlations are shown in Figs. 10 through 12. The time histories of heat flux were used for this comparison rather than effective values of heat transfer coefficients. Additional comparison of calculated vapor temperatures can be also found in these figures.

These results were found to be representative for all DNB experiments and also for Post-DNB experiments with higher mass flow rates - i.e., for experiments where the equilibrium quality varied in the range between 0.3 and 1.0. A comprehensive overview of results obtained by the analysis of all experiments using equilibrium correlations can be found in /14/.

### Assessment of TRAC PF1/MOD1 CHF and Post-CHF heat transfer correlations

#### Brief description of TRAC-PF1/MOD1 computer code.

The Los Alamos National Laboratory is developing a best-estimate computer code for the PWR accidents analysis which is known as the Transient Reactor Analysis Code - TRAC. The TRAC code is based on the full two-fluid nonequilibrium thermal and fluid dynamic model with a flow-regime dependent constitutive equations and the rewet capability for both bottom flood and falling film quench fronts. The TRAC-PF1/MOD1 incorporates detailed heat transfer analysis of the vessel and the loop components. Included is also two-dimensional ( $r,z$ ) treatment of fuel rod heat conduction. The heat transfer from the fuel rods and other system structures is calculated using flow-regime dependent selection of correlations for the calculation of heat transfer coefficients. Because of the purpose

of this investigation, only the TRAC-PF1/MOD1 calculation of heat transfer coefficients in transition and film boiling regime will be described in this paper. The detailed description of all TRAC-PF1/MOD1 heat transfer regimes can be found in /15/. The change from nucleate to the transition boiling occurs in the TRAC-calculation if the wall temperature exceeds the so called CHF-temperature. The CHF-temperature ( $T_{CHF}$ ) is calculated using a Newton-Raphson iteration to determine the intersection of the heat flux found by using the nucleate boiling heat transfer coefficient and the value of critical heat flux which is calculated by the Biasi correlation /16/. The total wall-to-fluid heat flux in the transition boiling regime is obtained from a quadratic interpolation between the Biasi CHF and the minimum stable film-boiling heat flux which is calculated using the value of minimum stable film boiling temperature ( $T_{MIN}$ ) from the homogeneous nucleation temperature correlation. The wall-to-fluid heat flux in this heat transfer regime is then given by:

$$q_{TRANS} = \delta \cdot q_{CHF} (1 - \delta) \cdot q_{MIN}$$

$$\delta = \left( \frac{T_W - T_{MIN}}{T_{CHF} - T_{MIN}} \right)^2$$

In the film boiling heat transfer regime ( $T_W > T_{MIN}$ ) the wall-vapor and wall-liquid heat transfer are treated separately using the following calculational scheme. The wall-liquid heat transfer coefficient is assumed to be the sum of three components:

$$h_{w,l} = (h_{RAD} + h_{PFB}) \cdot \left( \frac{T_W - T_S}{T_W - T_l} \right) + h_{DF}$$

where  $h_{RAD}$  is a radiative HTC,  $h_{PFB}$  is a pool boiling HTC, and  $h_{DF}$  is a dispersed flow HTC. The pool boiling  $h_{PFB}$  is decreasing from its actual value to zero in the void fraction range between  $0.5 < \alpha < 0.75$  and in the same void fraction range the dispersed flow  $h_{DF}$  is increased from zero to its actual value. If the value of actual  $h_{PFB}$  is smaller than  $h_{DF}$  than  $h_{PFB}$  is taken for the calculation of wall-liquid HTC. The wall-vapor heat transfer coefficient in this heat transfer regime is calculated using the

Dougall-Rohsenow correlation and the turbulent natural convection correlation. The greater value predicted with these two correlations is taken for the calculation of wall-vapor heat flux:

$$q_{wv} = \text{MAX} ( h_{DR}, h_{NC} ) \cdot ( T_w - T_v )$$

$$q_{wi} = h_{wi} \cdot ( T_w - T_i )$$

TRAC-PF1/MOD1 model of the German 5x5 rod bundle test facility and important input for the analysis of test DNB-9.

The TRAC-PF1 model of the test section of the German heat transfer test facility is shown in Fig. 13. Five one-dimensional-core components are representing the five axial power regions of the test section. The measured single phase mass flow at the test section inlet has been prescribed as a input time function in the fill component which is connected to the inlet of the first core component. The measured pressure at the test section outlet has also been input as a second boundary parameter in the break component. The power generation for each power region has been calculated separately using the temperature-dependent resistivity and measured electrical current and was also input as a time function for each of the core components.

#### Calculation of test DNB-9 using original and improved TRAC-PF1/MOD1 heat transfer model

The first computer run has been performed using the original set of TRAC PF1/MOD1 (Version 11.5) post-CHF heat transfer correlations i.e.:

Wall - Vapor : Dougall - Rohsenow

$$h_{w,v} = 0.023 \left[ \frac{\rho_v \cdot [\alpha \cdot V_v + (1 - \alpha) \cdot V_l] \cdot D_h}{\mu_v} \right]^{0.8} \cdot Pr_v^{0.4} \cdot \frac{k_v}{D_h}$$

Wall - Liquid :

$$h_{w,l} = (h_{RAD} + h_{PFB}) \cdot \left[ \frac{T_w - T_s}{T_w - T_l} \right] + h_{DP}$$

$$h_{rad} = (1 - \alpha) \cdot \sigma \cdot \varepsilon \cdot \left[ \frac{T_w^4 - T_s^4}{T_w - T_s} \right]$$

$$h_{PFB} = K_1 \cdot \left[ \frac{\rho_v \cdot k_v^3 \cdot (\rho_l - \rho_v) \cdot g \cdot h_{fg}^*}{\mu_v \cdot (T_w - T_s) \cdot \lambda} \right]^{0.25} \quad K_1 = 0.61$$

$$\lambda = 2 \cdot \pi \cdot \left[ \frac{\sigma}{g (\rho_l - \rho_v)} \right]^{0.5}$$

The comparison of calculated and measured wall temperatures (Figure 14) shows that the time to CHF has been predicted late at all elevations in the bundle. At the elevation 377 cm, where DNB occurred 0.2s after the beginning of the transient, TRAC PF1/MOD1 predicted it with a 1.5s delay. Since there is no possibility in the present version of TRAC to prescribe the time of DNB as an input value, following computer runs have been performed to determine a correction of max. critical heat flux that will result in better agreement between calculated and measured time to CHF. The best fit value of this multiplier has been found to be 0.78 (Figure 15). The next calculation has been performed using the improved post-CHF heat transfer model. The comparison of measured and calculated wall temperatures (Figure 16) shows much better agreement.

## Results of TRAC PF1/MOD1 analysis of Lehigh University test No. 138

The comparison of calculated and measured wall and vapor temperature (Figure 17) shows that the improved TRAC-PF1/MOD1 post-CHF heat transfer model overpredicted slightly the measured wall temperature in the upper part of the test section. The measured value of vapor temperature at the elevation 130 cm is about 50 K higher than the calculated value.

### Evaluation of correlations for the calculation of minimum film boiling temperature

Two different correlations were applied for the calculation of minimum film boiling temperature:

TRAC-PF1/MOD1 correlation:

$$T_{MIN} = T_{NH} + (T_{NH} + T_1) \cdot R^{0.5} \quad R = \frac{(K \cdot \rho \cdot c)_l}{(K \cdot \rho \cdot c)_v}$$

$$T_{NH} = 705.44 - (4.722 \cdot 10^{-2}) \cdot DP + (2.3907 \cdot 10^{-5}) \cdot DP^2 \\ - 5.8193 \cdot DP^3 \quad [^{\circ}F]$$

$$DP = 3203.6 - P$$

Groeneveld correlation for  $p < 9\text{MPa}$  and no liquid subcooling:

$$T_{MIN} = 284.7 + 0.0441 \cdot P - 3.72 \cdot 10^{-6} \cdot P^2; \quad P = [\text{kPa}]$$

The comparison of calculated and measured wall temperatures has shown that none of these two correlations predicted the return to nucleate boiling (RNB) in the first 13s of DNB-9 experiment. The measured wall temperature at the elevation 259 cm shows that RNB occurs at about 10.5s after initiation of transient.

### Evaluation of alternative post-CHF heat transfer models

#### 1. Forslund-Rohsenow correlations /17/

Wall-vapor heat transfer coefficient

$$h_{w,v} = 0.019 \cdot \frac{k_v}{D_h} \cdot \left( \frac{G_T \cdot D_h}{\mu_v} \right)^{0.8} \cdot Pr_v^{0.4} \left[ x_A + (1 - x_A) \cdot \left( \frac{\rho_v \cdot v_v}{\rho_l \cdot v_l} \right) \right]^{0.8}$$

Wall-liquid

$$h_{w,l} = K_2 \cdot K_1 \cdot (1 - \alpha)^{2/3} \cdot \left[ \frac{g \cdot \rho_l \cdot \rho_v \cdot h_{fg} \cdot k_v^3}{(T_w - T_s) \cdot \mu_v \cdot d_d} \right]^{1/4} \cdot C_1$$

$$K_1 \cdot K_2 = 1.5 \text{ and } C_1 = 1.27$$

The comparison of results (Figure 18) shows that the application of Forslund-Rohsenow correlations for the calculation of both, wall-vapor and wall-liquid heat transfer coefficients, results in too high wall temperatures at all elevations.

## 2. Kendall-Varone-Rohsenow correlations /18/

Wall-vapor heat transfer coefficient - modified Hadaller correlation

$$h_{w,v} = 0.008348 \cdot \Gamma \cdot \frac{k_v}{D_h} \cdot Re_v^{0.5774} \cdot Pr_v^{0.6112}$$

Wall-liquid

$$q_{w,l} = \varepsilon \cdot n_p \cdot \frac{\pi}{6} \cdot d_d^3 \cdot \rho_l \cdot h_{fg}$$

$$n_p = v_p \cdot N_T$$

where  $\varepsilon$  is effectiveness of wall-droplet heat transfer.

The values of the Nusselt number multiplier  $\Gamma$  for the typical thermo- and fluiddynamic conditions in the post-CHF part of test DNB-9 are summarized in Table 4. It can be seen that the value of  $\Gamma$  is less than unity the entire post-CHF part of the experiment. Therefore the first calculation was performed without any correction of wall-vapor heat transfer coefficient ( $\Gamma = 1$ ). The results of this computer run are shown in Fig. 19. Since the calculated wall temperatures were much too high, any further reduction of wall-vapor heat transfer coefficient ( $\Gamma < 1$ ) would result in larger disagreement between analysis and experiment. Therefore no further calculations have been performed.

### 3. Vojtek correlation

Wall-vapor heat transfer coefficient

$$Nu_{MOD} = 0.023 \cdot Re_v^{0.8} \cdot Pr_v^{0.4}$$

The correction of Nusselt number is based on the reduction of boundary layer thickness due to heat transfer between vapor and droplets in boundary layer.

Wall-Liquid

Kendall-Rohsenow effectiveness model.

The comparison of calculated and measured results (Fig. 20) shows good agreement in the first portion of the transient. In the later part of the experiment ( $t > 13s$ ) also this correlation underpredicts the wall-vapor heat transfer coefficients.

Comparison of different heat transfer models.

This final comparison of calculated results which were obtained using different post-CHF heat transfer models and correlations has been performed to investigate the influence of the splitting of the total wall-mixture heat flux into the individual heat transfer components of dispersed flow heat transfer regime. The schematic of dispersed flow heat transfer process is shown in Fig. 21. The quantities  $Q_{TOT}$  and  $Q_{V,sup}$  can be calculated from the measurement (experiments with measurements of vapor temperature). There are still three unknown quantities  $Q_{w,v}$ ,  $Q_{w,l}$  and  $Q_{v,l}$ .

For the investigation of the influence of the splitting of  $Q_{TOT}$  following heat transfer models have been selected:

	$Q_{w,v}$	$Q_{w,l}$
Forslund-Rohsenow ( $K_1 * K_2 = 2.25$ )	small	large
TRAC-PF1/MOD1	intermed.	intermed.
Vojtek correlation	large	small

The comparison of wall-vapor and wall-liquid heat transfer coefficients as calculated using these heat transfer models is shown in Figs. 22 and 23. The coefficient in Forslund-Rohsenow wall-liquid correlation had to be increased ( $K_1=2.25$ ) in order to get approximately the same wall temperatures (Fig. 24). The comparison of the calculated results in Figs. 25, 26 and 27 shows that the splitting of total wall-mixture heat flux into the wall-vapor and wall-liquid components has no significant influence on the calculated void fraction, vapor velocity and vapor temperature.

## CONCLUSIONS

- The improved TRAC PF1/MOD1 post-CHF heat transfer model was shown to predict wall and vapor temperatures with reasonable accuracy.
- The calculational methods for the prediction of the transition from nucleate to film boiling and vice versa need further improvement.
- The application of three alternative post-CHF heat transfer models did not improve the overall agreement between calculated and measured results.
- The results of this investigation indicated difficulties of the experimental determination of individual heat transfer components in dispersed flow heat transfer regime.

## NOMENCLATURE

A	area, cross section	$m^2$
$c_p$	specific heat capacity	$J/(K \cdot kg)$
d	diameter	m
$d_{equ}$	equivalent diameter	m
G	mass flux	$kg/(m^2 \cdot s)$
g	acceleration of free fall	$m/s^2$
h	specific enthalpy	$J/kg$
$\Delta h$	latent heat of vaporization	$J/kg$
l	length	m
m	mass	kg
$N_D$	number of droplets	$1/m^3$
P	pressure	$N/m^2$
Q	heat per unit of area	$W/m^2$
q	heat flux density	$W/m^2$
r	radius	m
T	temperature	$K(^{\circ}C)$
U	velocity	$m/s$
X	equilibrium quality	

### Greek letters

$\alpha$	void fraction	
$\eta$	dynamic viscosity	$kg/(s \cdot m)$
$\lambda$	thermal conductivity	$W/(K \cdot m)$
$\rho$	mass density	$kg/m^3$
$\sigma$	surface tension	$N/m$

### Dimensionless parameters

$$Pr = \frac{c_p \mu}{a} \quad \text{Prandtl number}$$

$$Re = \frac{c_l d_l}{\mu} \quad \text{Reynolds number}$$

### Subscripts

D	droplet
E	equilibrium
f	film
l	liquid
M	measurement
MAX	maximum
MIN	minimum
SAT	saturation
TOT	total
V	vapor
W	wall

## REFERENCES

- /1/ Agemar, Brand, Emmerling, Flittner, Köhler, Loser  
Abschlußbericht über die Inbetriebnahme des Versuchsstandes für gesteuerte Bündelmessungen und über die ersten Versuche mit einem DWR-25-Stab-Bündel  
Technischer Bericht KWU R52-3015
- /2/ Agemar, Brand, Emmerling  
DWR Hauptversuche mit einem 25 Stabbündel, Teil 1:  
Experimentelle Durchführung und Dokumentation der Meßergebnisse  
KWU RE23/012/77
- /3/ I. Vojtek, Gesellschaft für Reaktorsicherheit, Garching, FRG  
Investigation of Dispersed Flow Heat Transfer using different Computer Codes and Heat Transfer Correlations  
Paper presented at the International Workshop on Post-CHF Heat Transfer, Abstract April, 1984, Salt Lake City
- /4/ Karwat, H., Wolfert, K.  
BRUCH-D A Digital Program for PWR-Blowdown Investigations  
Nucl. Eng. Des. 11 (1970), p 241-254
- /5/ Liesch, K.J., Steinhoff, F., Vojtek, I., Wolfert, K.  
BRUCH-D -02. Ein Rechenprogramm zur Analyse der fluid- und thermodynamischen Vorgänge im Primärkreis von Druckwasserreaktoren bei schweren Kühlmittelverluststörfällen  
MRR-P-3, Laboratorium für Reaktorregelung und Anlagensicherung, Garching
- /6/ Vojtek, I.  
Auswertung der 25 Stabbündel-Versuche mit dem Rechenprogramm BRUDI-VA  
GRS-A-208, September 1978

- /7/ Smith, R.A., Griffith, P.  
A simple model for estimating time to CHF in PWR LOCA  
Trans. of American Society of Mechanical Engineering, paper no.  
76-HT-9, 1976
- /8/ Liesch, K.J., Raemhild, G., Hofmann, K.  
Zur Bestimmung des Wärmeüberganges und der kritischen Heizflächen-  
belastung im Hinblick auf besondere Verhältnisse in den Kühlkanä-  
len eines DWR bei schweren Kühlmittelverluststörfällen  
MMR 150, Laboratorium für Reaktorregelung und Anlagensicherung,  
Garching, 1975
- /9/ Steinhoff, F.  
Vergleich theoretischer und experimenteller Ergebnisse der  
SWR-Notkühlversuche mit einem Vierstabbündel  
MMR-I-37, Laboratorium für Reaktorregelung und Anlagensicherung,  
Garching, 1975
- /10/ Groeneveld, D.C.  
An investigation of heat transfer in the liquid deficient regime  
AECL-3281, 1969
- /11/ Condie, K.G., Bengston, S.J., Richlen, S.L.  
Post-CHF heat transfer data-analysis, comparison and correlation  
EG&G, Idaho Falls
- /12/ Groeneveld, D.C., Delorme, G.G.J.  
Prediction of thermal nonequilibrium in the post-dryout regime  
Nucl. Eng. Des. 36 (1976) 17-26
- /13/ Chen, J.C., Ozkaynak, F.T., Sundaram, R.K.  
Vapor heat transfer in post-CHF region including the effect of  
thermodynamic nonequilibrium  
Nucl. Eng. Des. 51 (1979) 143-155

**/14/ Vojtek, I.**

**Untersuchung der Wärmeübergangsverhältnisse in der Hochdruckphase  
eines Kühlmittelverluststörfalls mit mittlerem und großem Bruch-  
querschnitt**

**GRS-A-709, Gesellschaft für Reaktorsicherheit, März 1982**

**/15/ TRAC-PF1/MOD1 User Manual, to be published**

**/16/ Biasi, L. et al.**

**Studies on Burnout**

**Part 3 Energia Nucleare, Vol. 14, No. 9, Sept. 1967**

Table 1: Variation of test parameters - DNB tests

TEST NUMBER	INITIAL MASS FLOW RATE [KG/M <sup>2</sup> S]	REDUCED MASS FLOW IN POST-CHF REGION [KG/M <sup>2</sup> S]	INLET ENTHALPY [KJ/KG]
DNB-1	3300.	1419.	1284.
DNB-2	3300.	957.	1284.
DNB-3	3300.	660.	1284.
DNB-4	3300.	1450.	1233.
DNB-5	3300.	990.	1233.
DNB-6	3300.	660.	1233.
DNB-7	3828.	1378.	1284.
DNB-8	3828.	957.	1284.
DNB-9	3828.	689.	1284.
DNB-10	3300.	660.	1233.
DNB-11	3300.	660.	1233.

Table II. Summary of Lehigh University Post-CHF Tests

Test Number	P (bar)	G (kg/s-m <sup>2</sup> )	Q (kw/m <sup>2</sup> )	x <sub>e,0</sub> (z)	x <sub>e,L</sub> (z)	x <sub>e,a</sub> (z)	$\frac{\Delta x_a}{\Delta x_e}$	Tv,data (K)
138	3.6	37.33	49.32	55.8	79.1	62.2	0.27	692
134	3.5	37.35	64.73	57.4	87.1	66.8	0.32	725
50	3.8	29.94	23.39	6.6	19.4	14.5	0.62	764

Table 3. Basic differential equations of computer code BRUDI-VA.

$$\dot{p} = \frac{-\dot{M} \cdot (h + \frac{v}{\epsilon_h}) - (G \cdot h)_A + (G \cdot h)_E + Q}{M(\frac{\epsilon_p}{\epsilon_h} + v)}$$

$$\dot{h} = \frac{v \cdot \dot{M} - \epsilon_p \cdot \dot{p} \cdot M}{M \cdot \epsilon_h}$$

$$\epsilon_p = \left(\frac{\partial v}{\partial p}\right)_h \quad \epsilon_h = \left(\frac{\partial v}{\partial h}\right)_p$$

$$\dot{G} = \frac{1}{\int_i^{i+1} \frac{dz}{F}} \cdot [p_i - p_{i+1} - g \cdot S (H_{i+1} - H_i) - K \cdot G \cdot |G|]$$

Table 4 : Values of Nusselt number multiplier  $\Gamma$

$\Gamma$	$T_w - T_b [k]$	$\mu_b / \mu_w$	$\chi_a$	$p [MPa]$
0.91	400	0.561	0.4	8.0
0.8	400	0.561	0.5	8.0
0.74	400	0.561	0.7	8.0
0.99	200	0.72	0.4	8.0
0.92	200	0.72	0.5	8.0
1.08	200	0.72	0.7	8.0
0.98	300	0.618	0.4	6.0
0.85	300	0.618	0.5	6.0
0.85	300	0.618	0.7	6.0



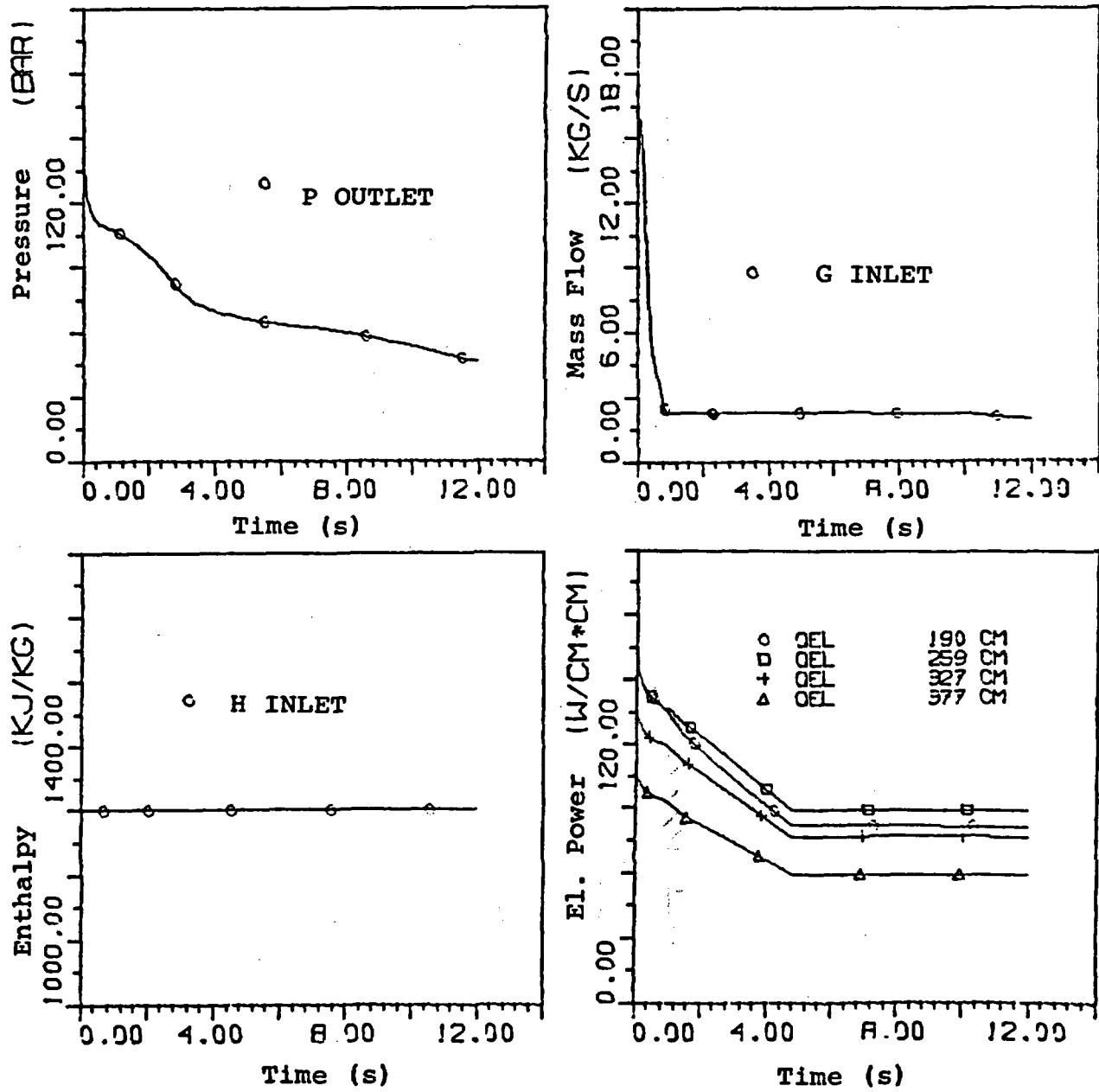


Fig. 4 Boundary conditions for test DNB-9

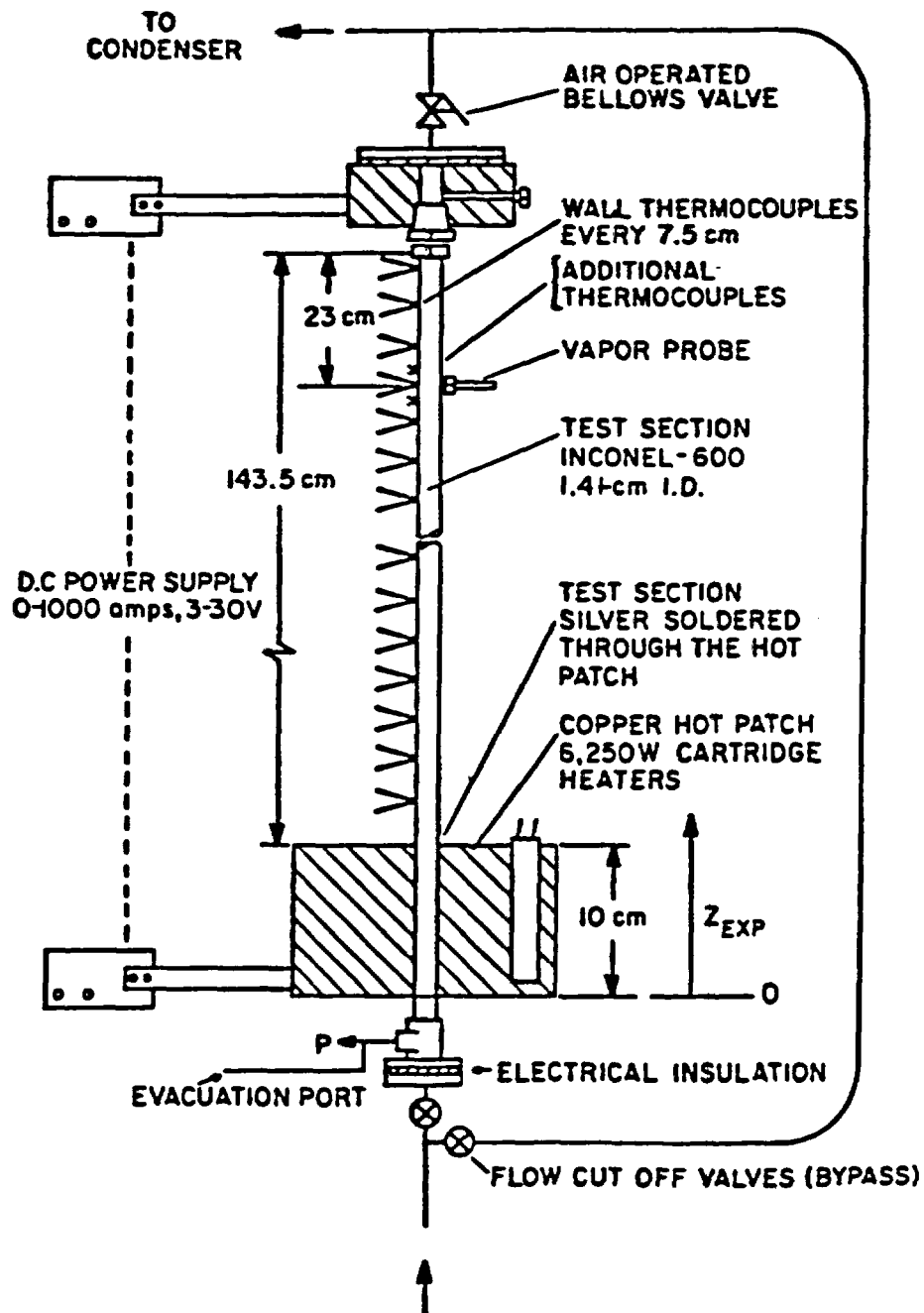


Fig. 5. Lehigh University experimental test facility for post-CHF heat transfer.

Test DNB-3 Corr. Comparison

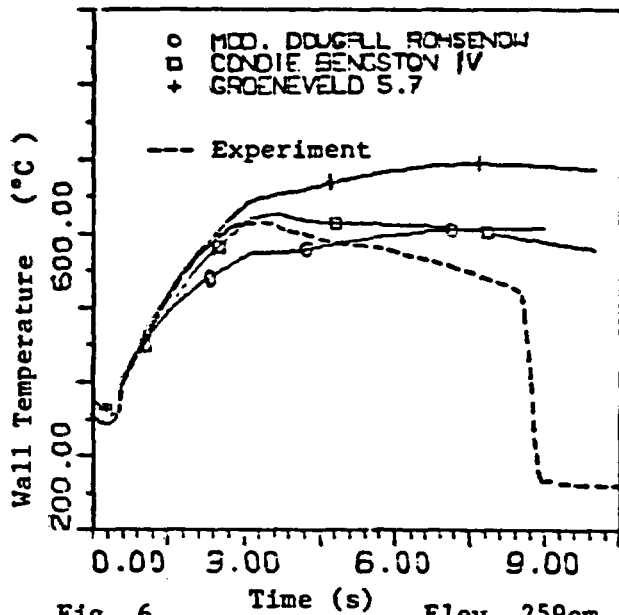


Fig. 6 Time (s) Elev. 259cm

Test DNB-3 Corr. Comparison

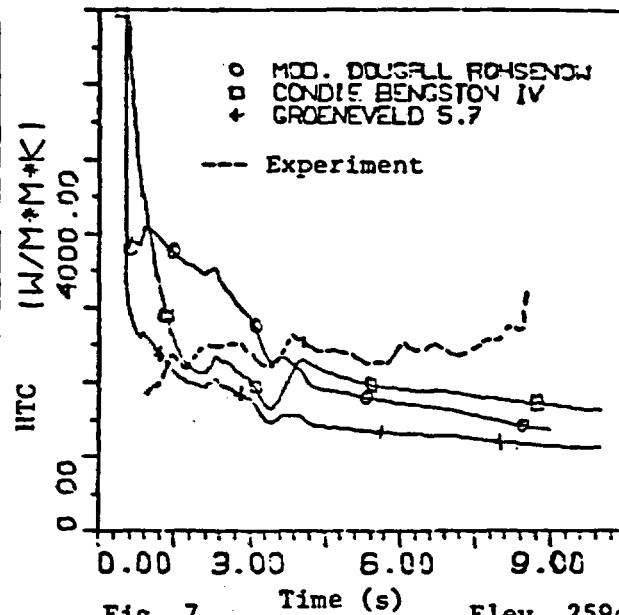


Fig. 7 Time (s) Elev. 259cm

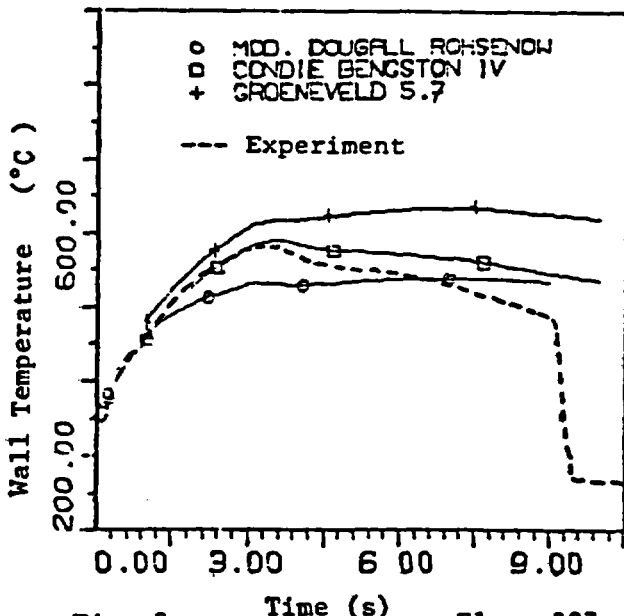


Fig. 8 Time (s) Elev. 327cm

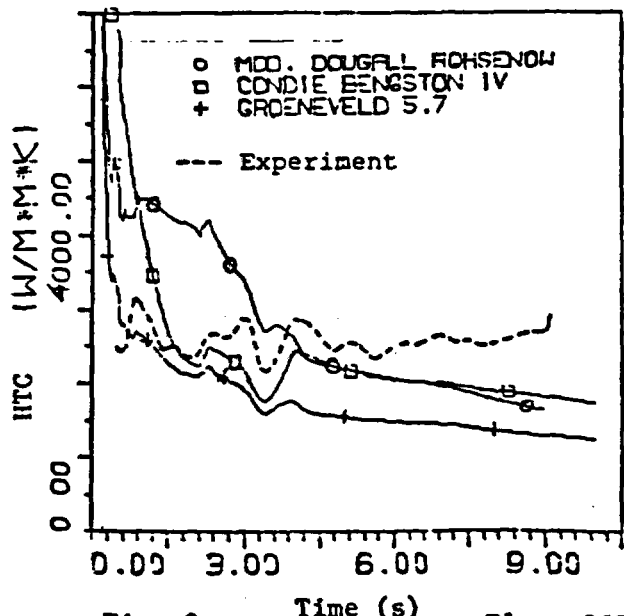


Fig. 9 Time (s) Elev. 327cm

Test DNB-3 Neq. Correlations

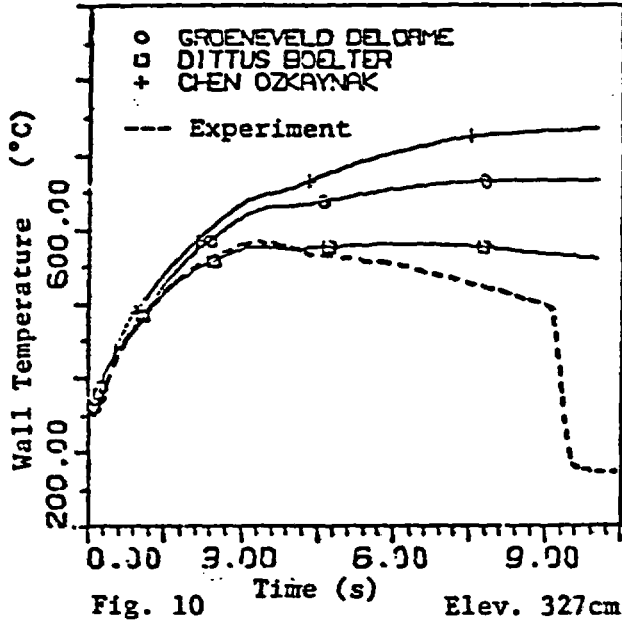


Fig. 10 Time (s) Elev. 327cm

Test DNB-3 Neq. Correlations

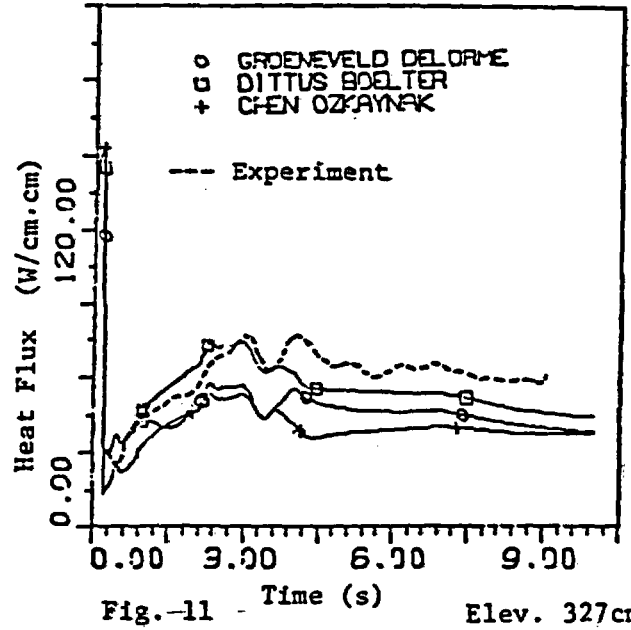


Fig. 11 Time (s) Elev. 327cm

Test DNB-3 Neq. Correlations

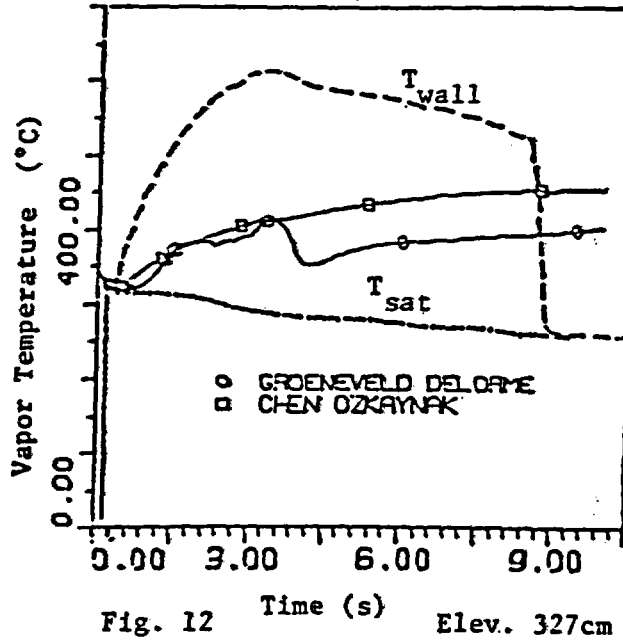


Fig. 12 Time (s) Elev. 327cm

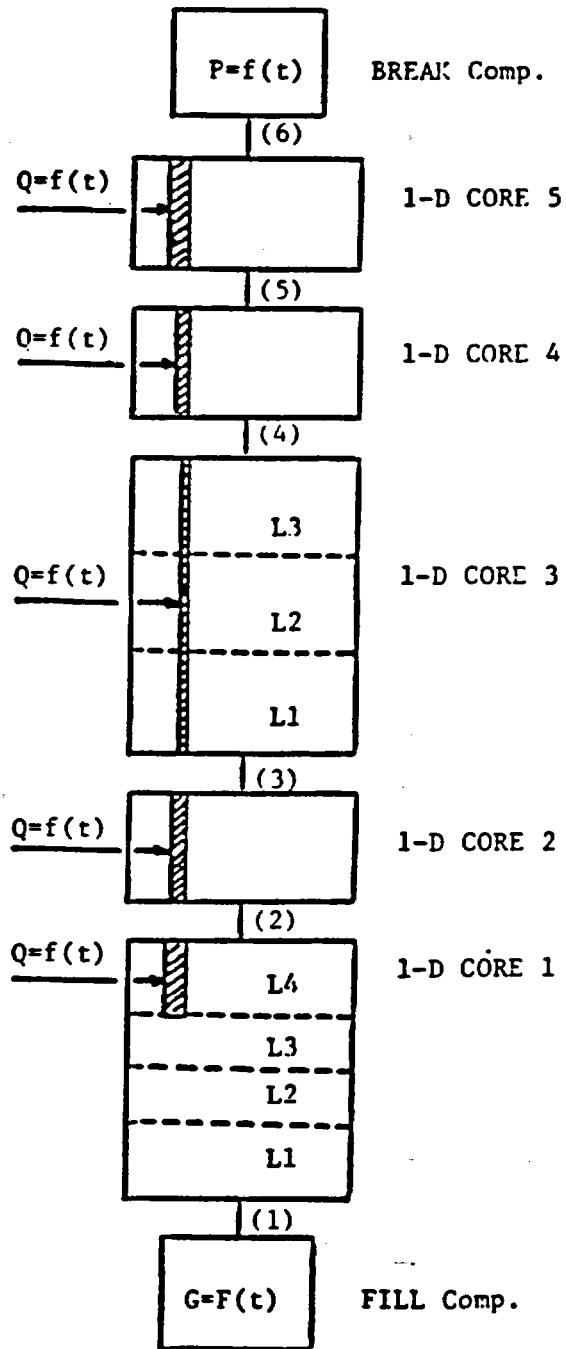


Fig. 13 TRAC-PF1/MOD1 Model of the test section

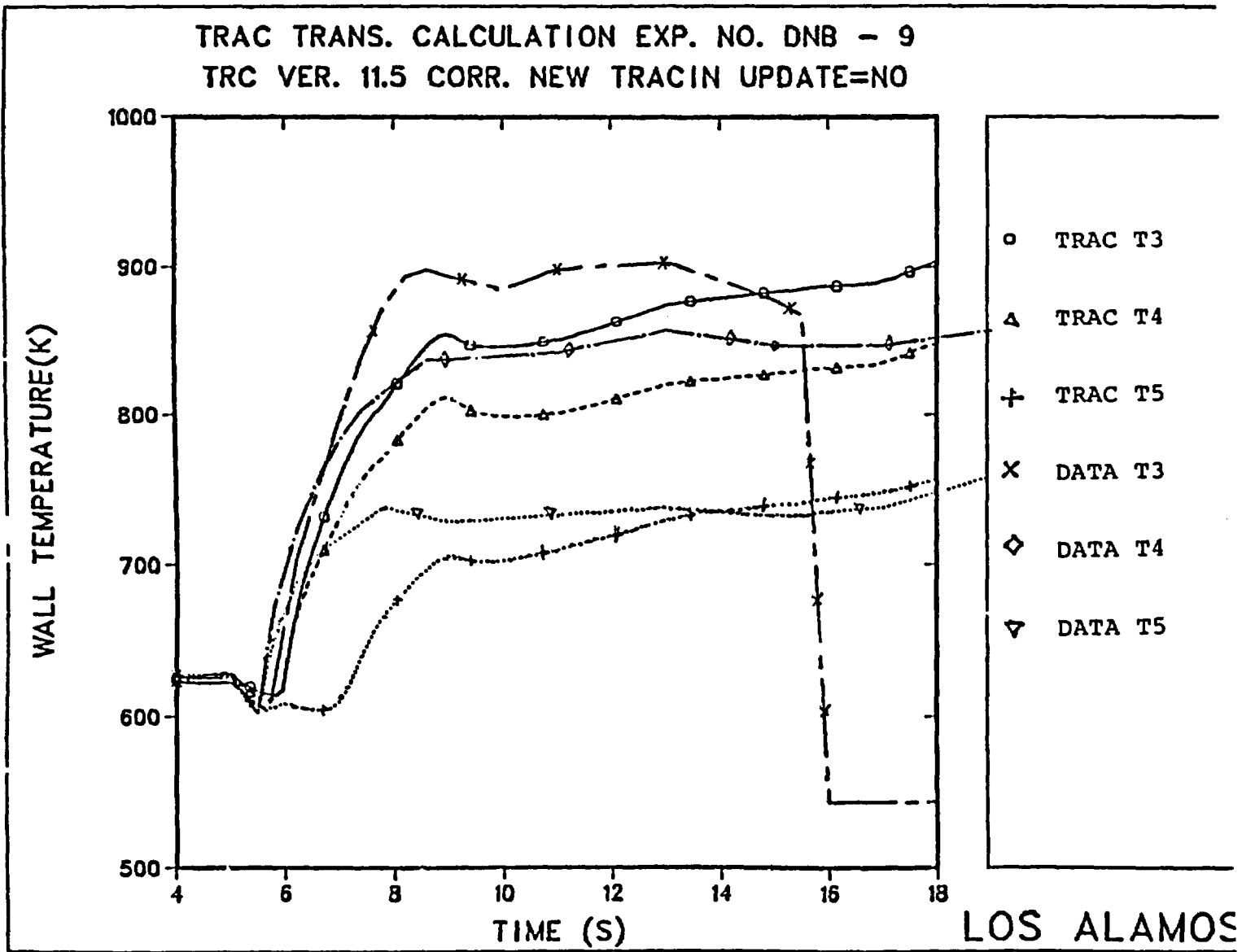


Fig. 14 Comparison of calculated and measured wall temperatures  
Original TRAC PF1/MOD1 heat transfer korrelations

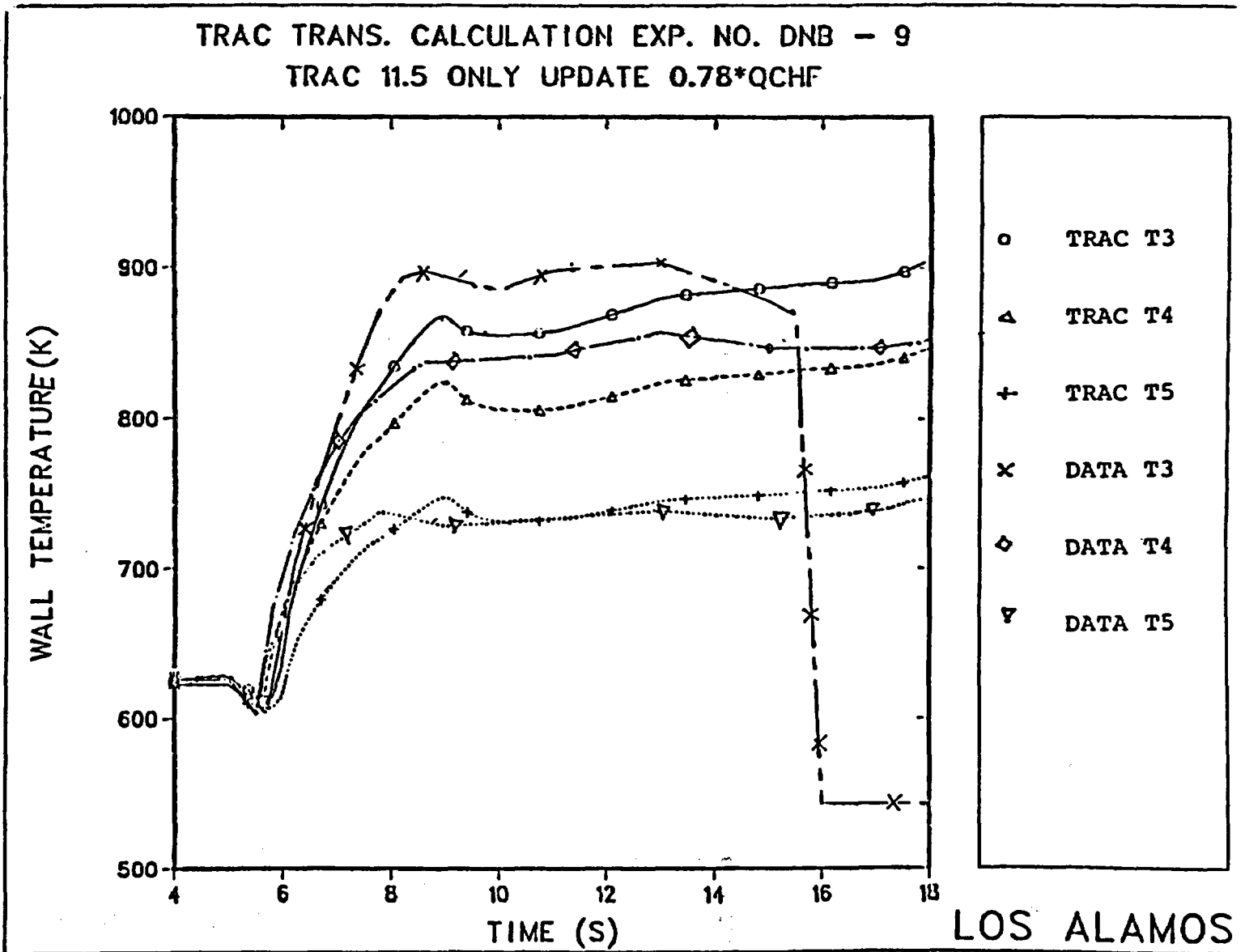


Fig.15 Comparison of measured and calculated wall temperatures  
(Orig. TRAC heat transfer model with  $QCHF \cdot 0.78$ )

TRAC TRANS. CALCULATION EXP. NO. DNB - 9  
 TRAC 11.5 FINAL UPDATES FOR H-T ROUTINES 0.78 CHF

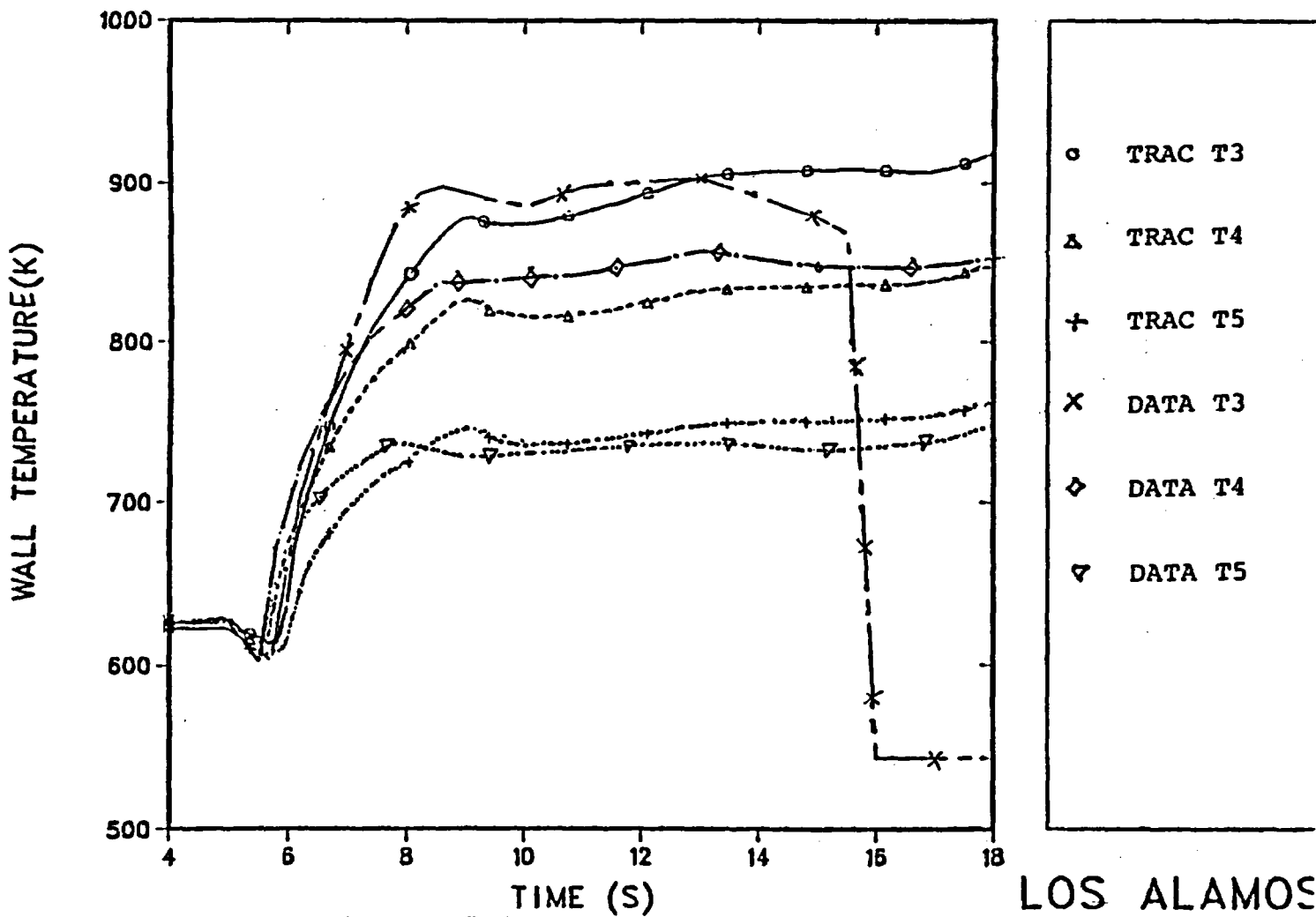


Fig. 16 Comparison of calculated and measured wall temperatures  
 (Improved TRAC PF1/MOD1 heat transfer model)

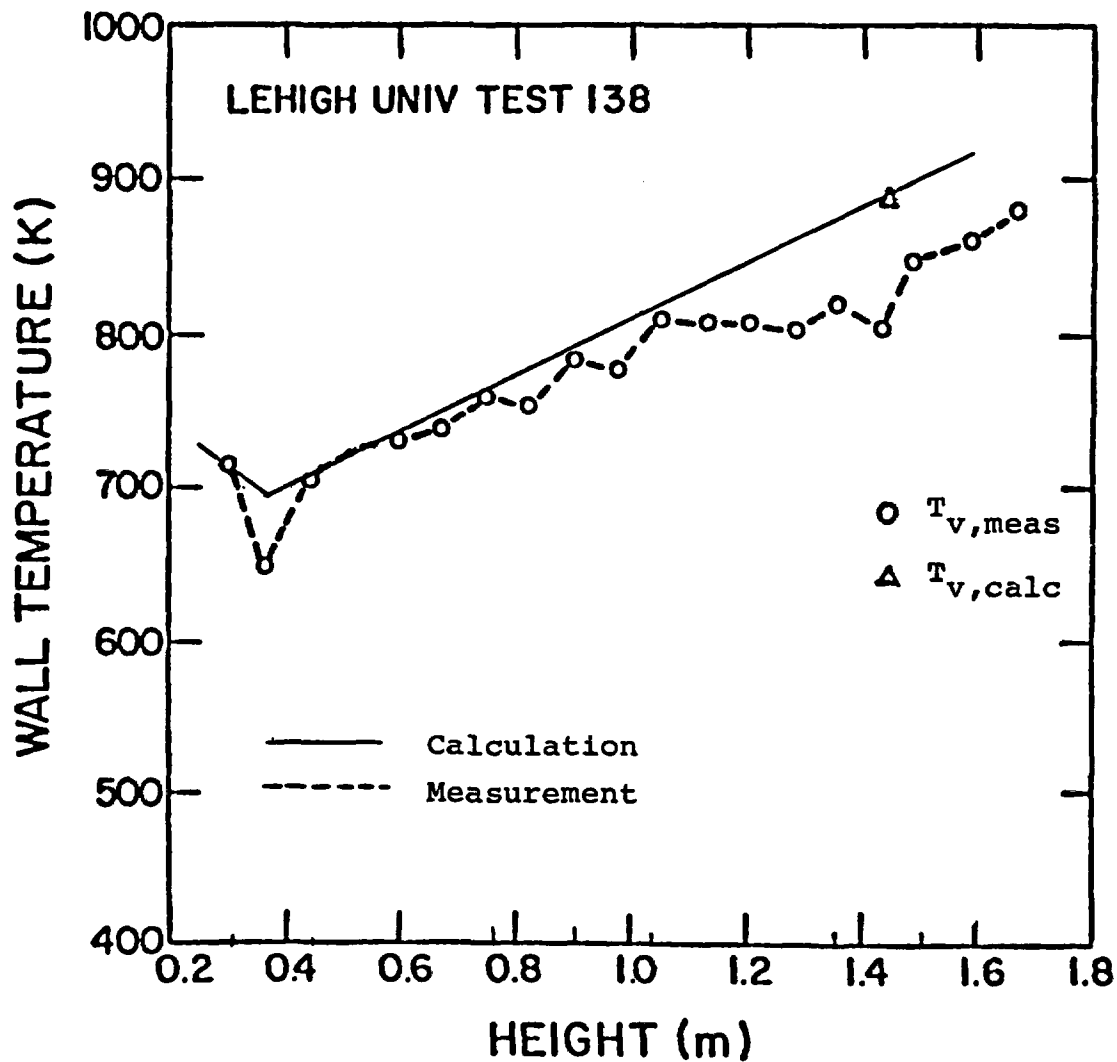


Fig.17 Comparison between calculated and measured wall temperature for test 138.

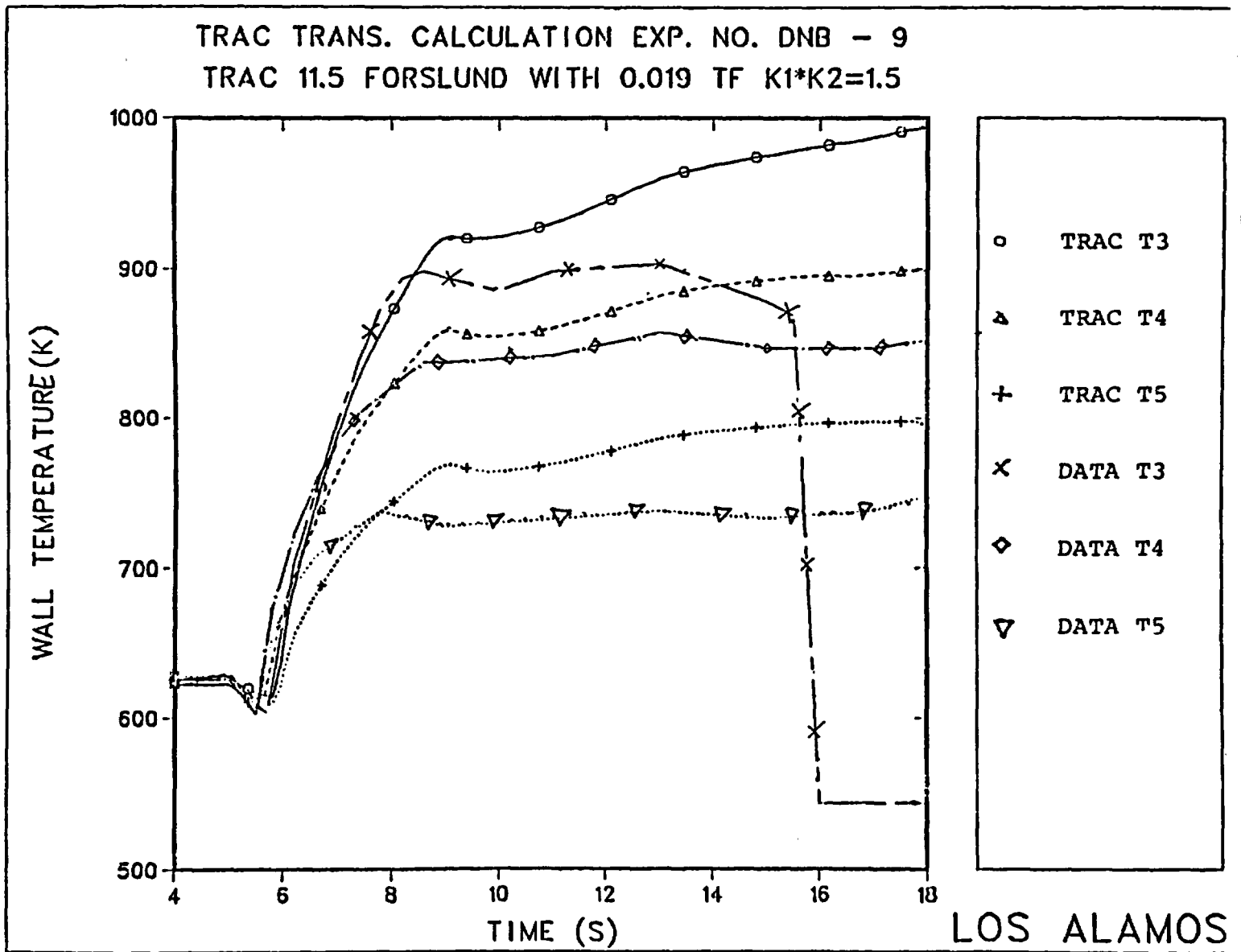


Fig. 18 Comparison of calculated and measured wall temperatures (Forslund - Rohsenow heat transfer correlations)

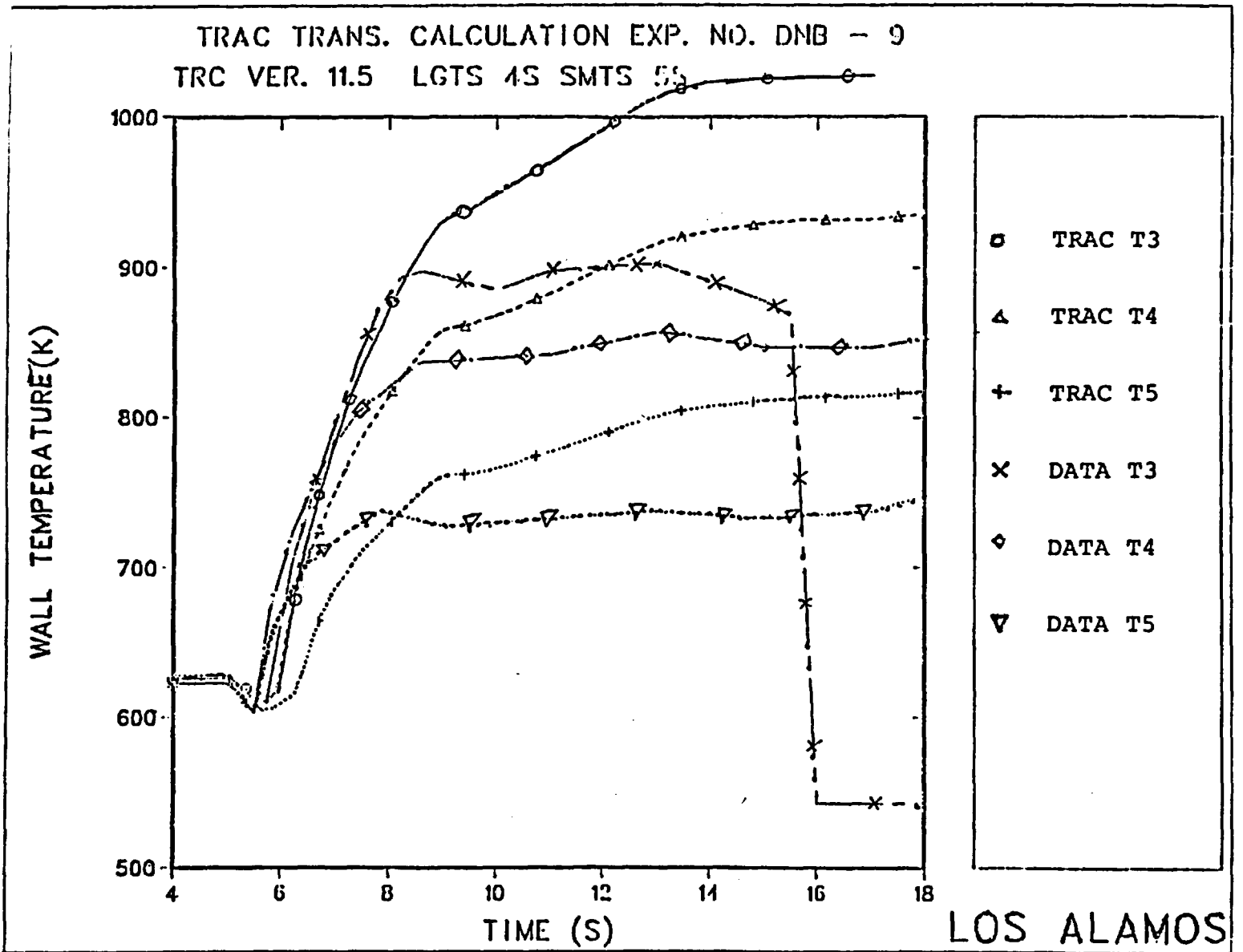


Fig.19 Comparison of calculated and measured wall temperatures  
(Kendall-Varone-Rohsenow heat transfer correlations)

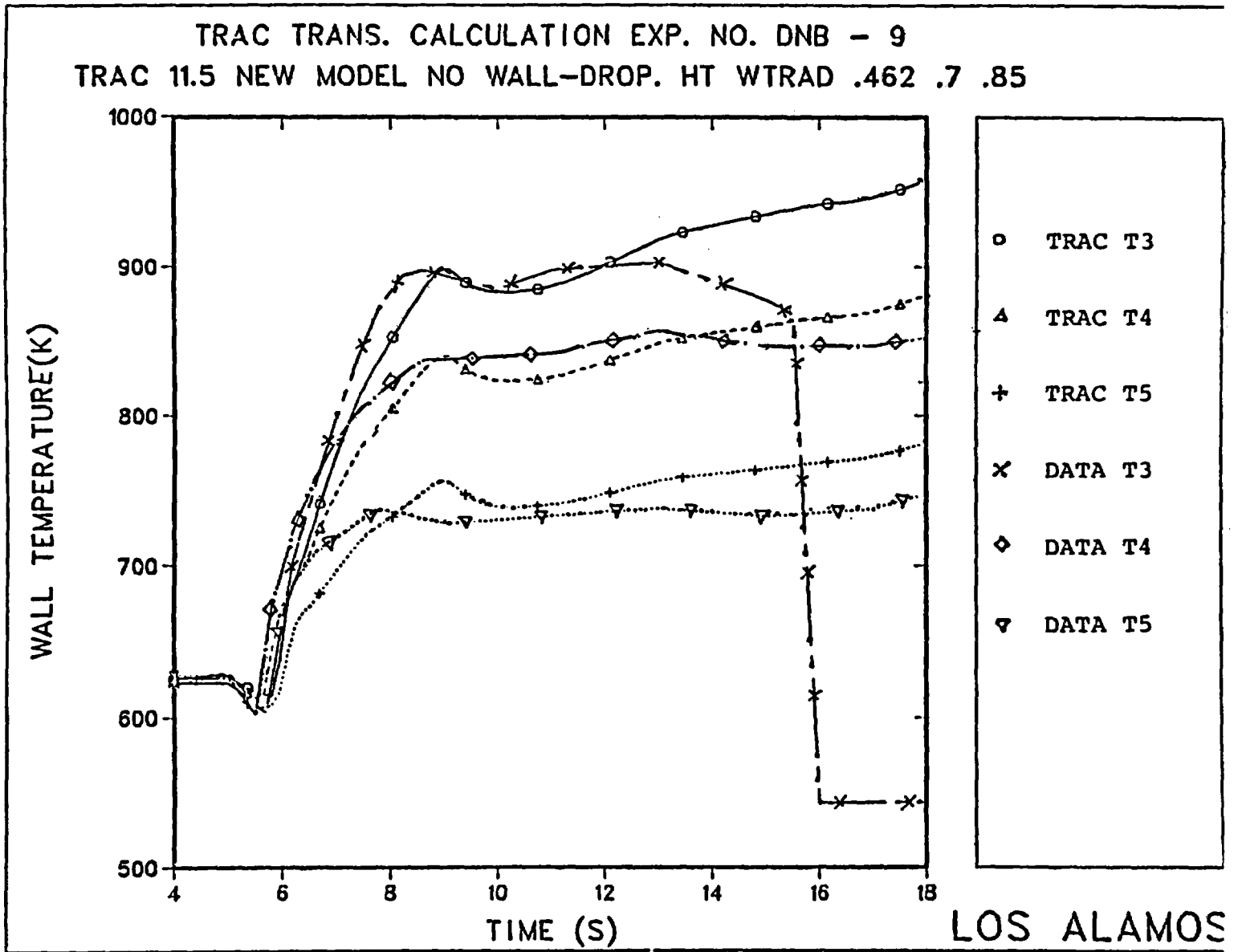


Fig.20 Comparison of calculated and measured wall temperatures (Vojtek and Kendall het transfer correlations)

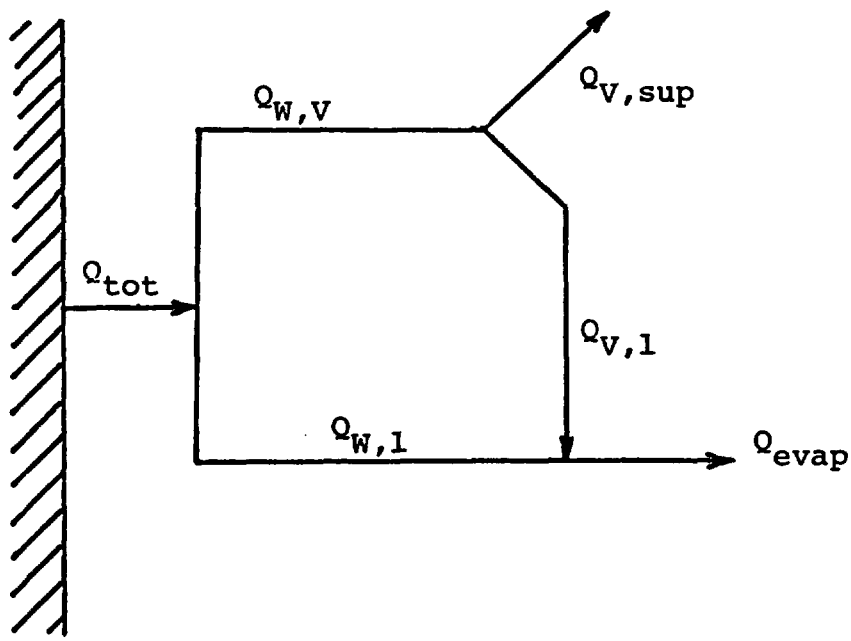


Fig.21 Dispersed flow heat transfer components

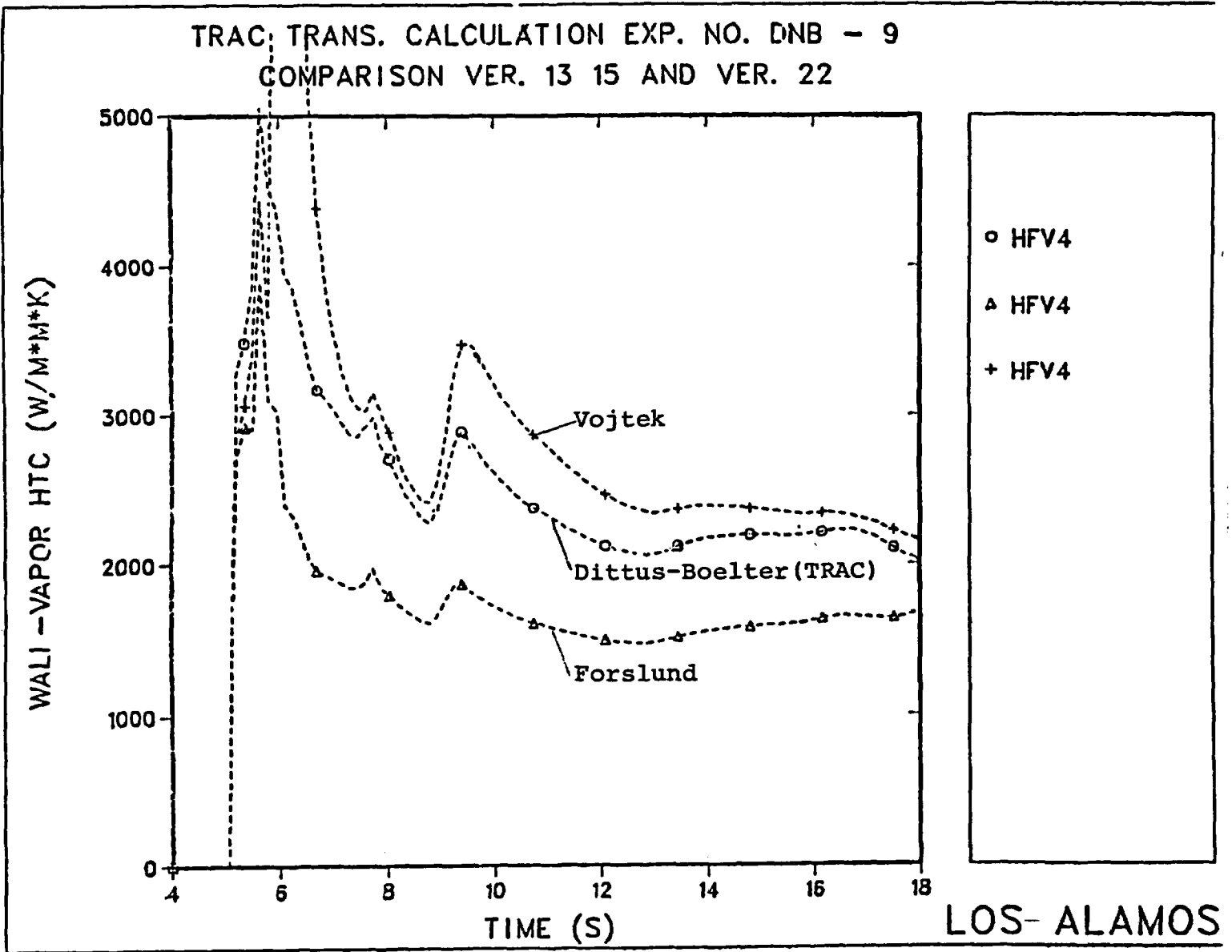


Fig.22 Comparison of wall vapor HTC's from different heat transfer models

TRAC TRANS. CALCULATION EXP. NO. DNB - 9  
 COMPARISON VER. 13 15 AND VER. 22

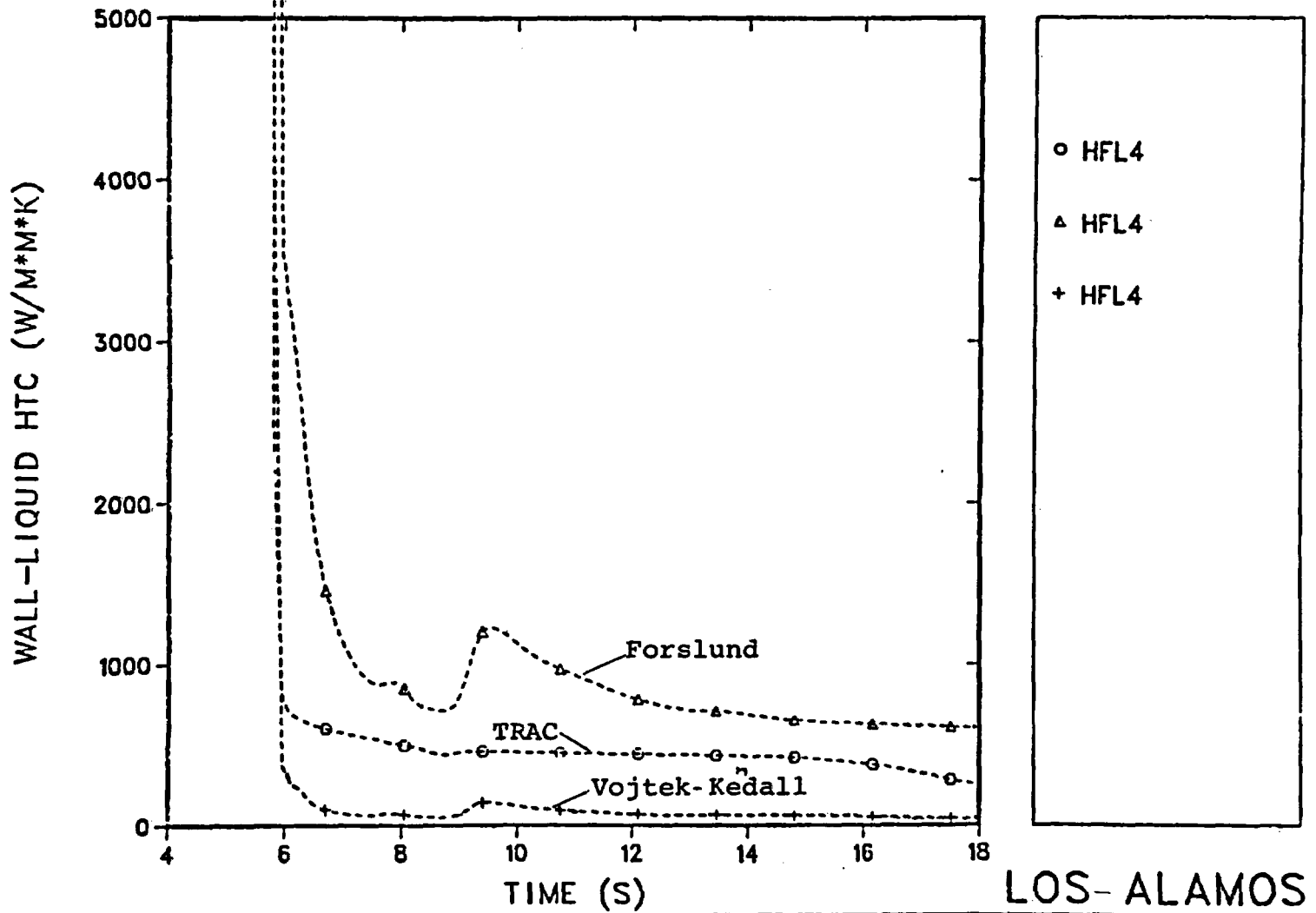


Fig.23 Comparison of wall liquid HTC's from different heat transfer models

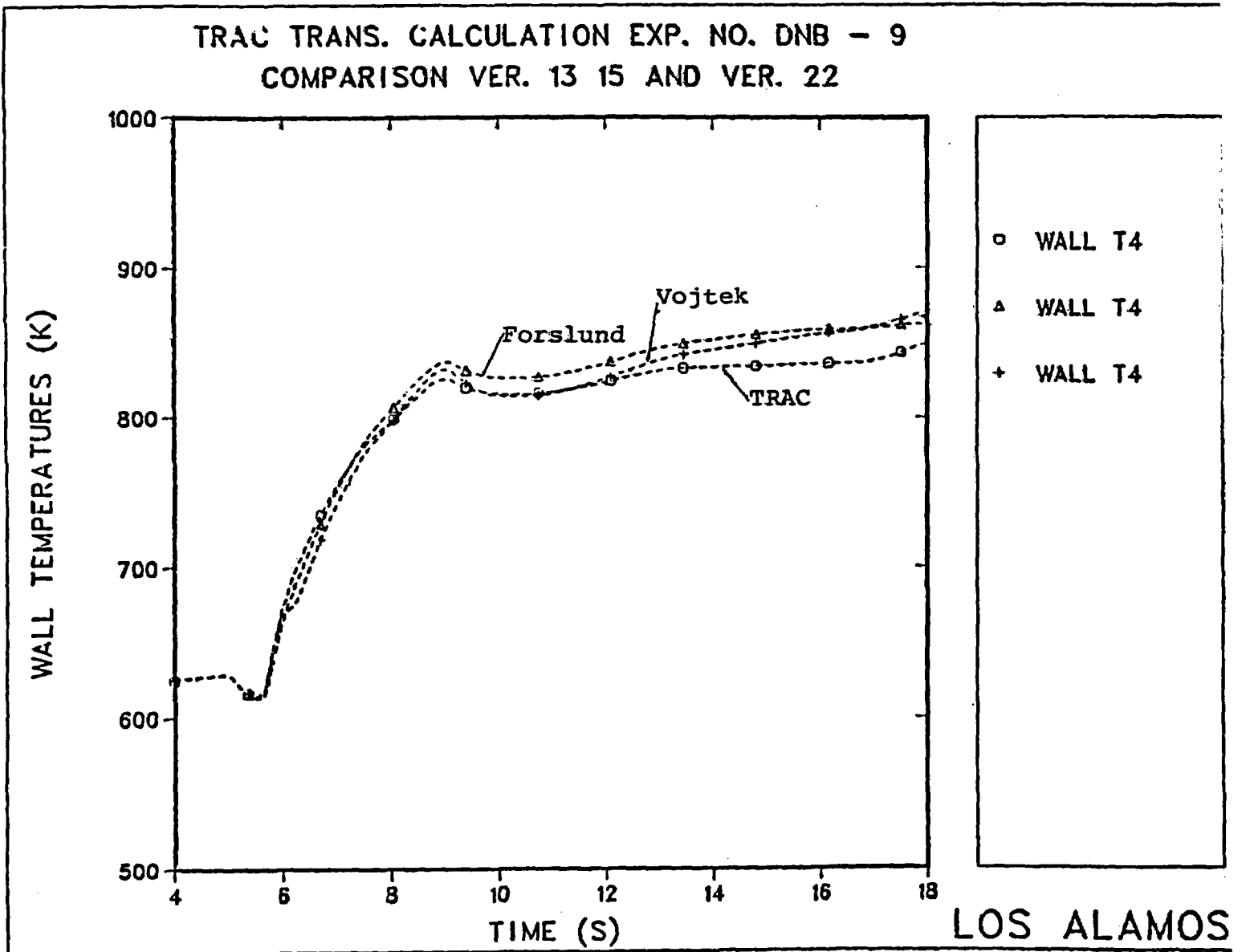


Fig.24 Comparison of calculated wall temperatures  
(Three different heat transfer models)

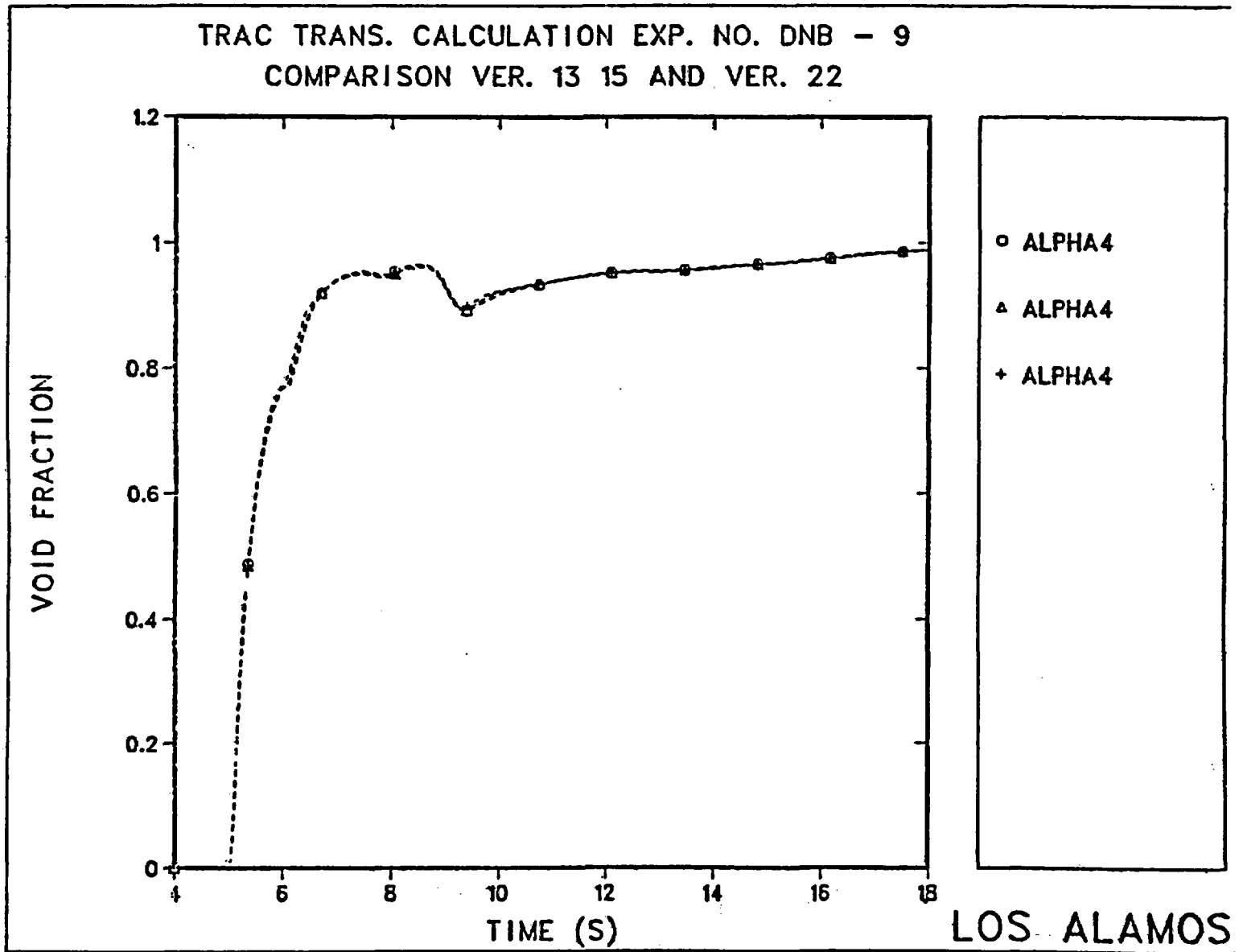


Fig.25 Comparison of calculated void fractions  
(Different post-CHF heat transfer models)

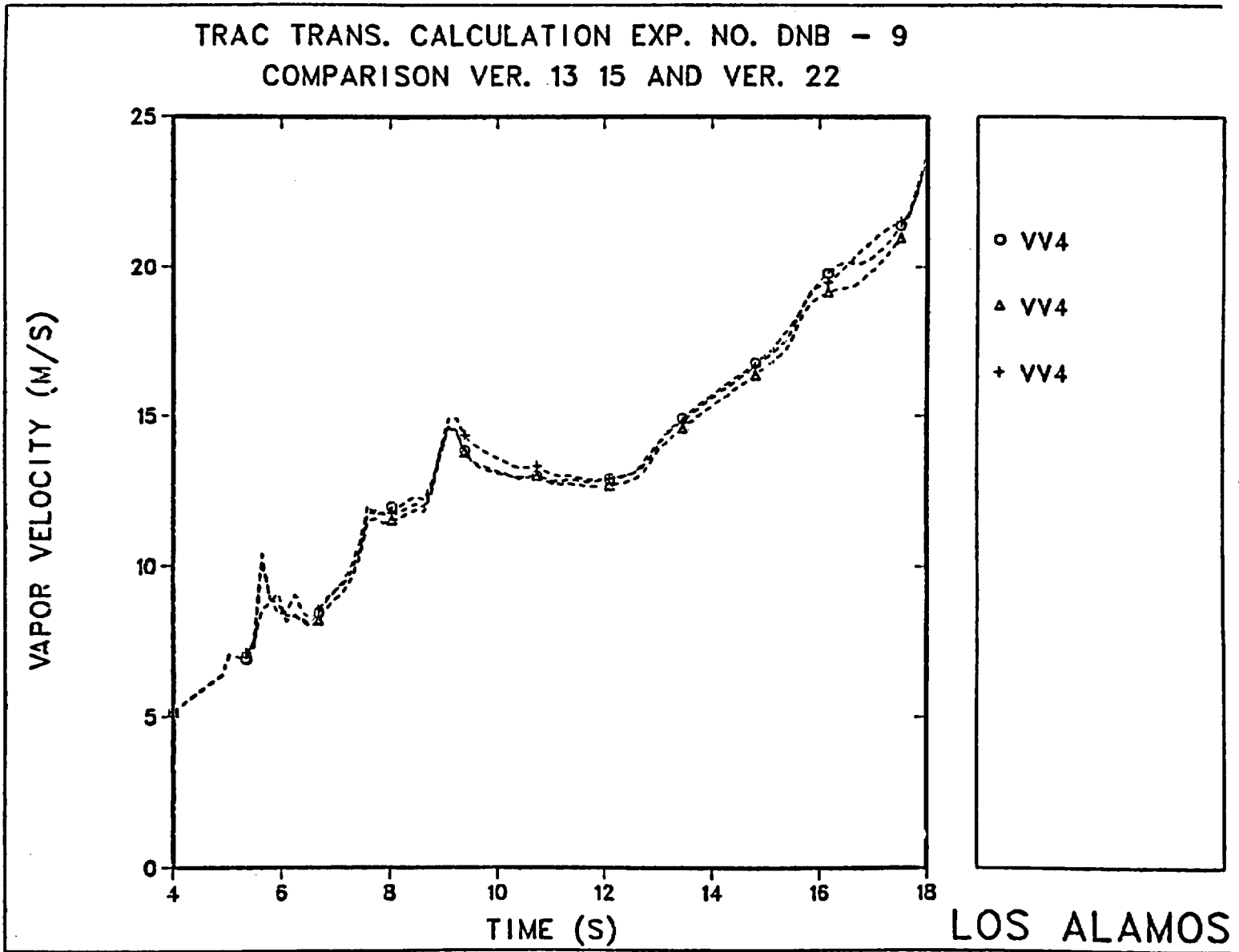
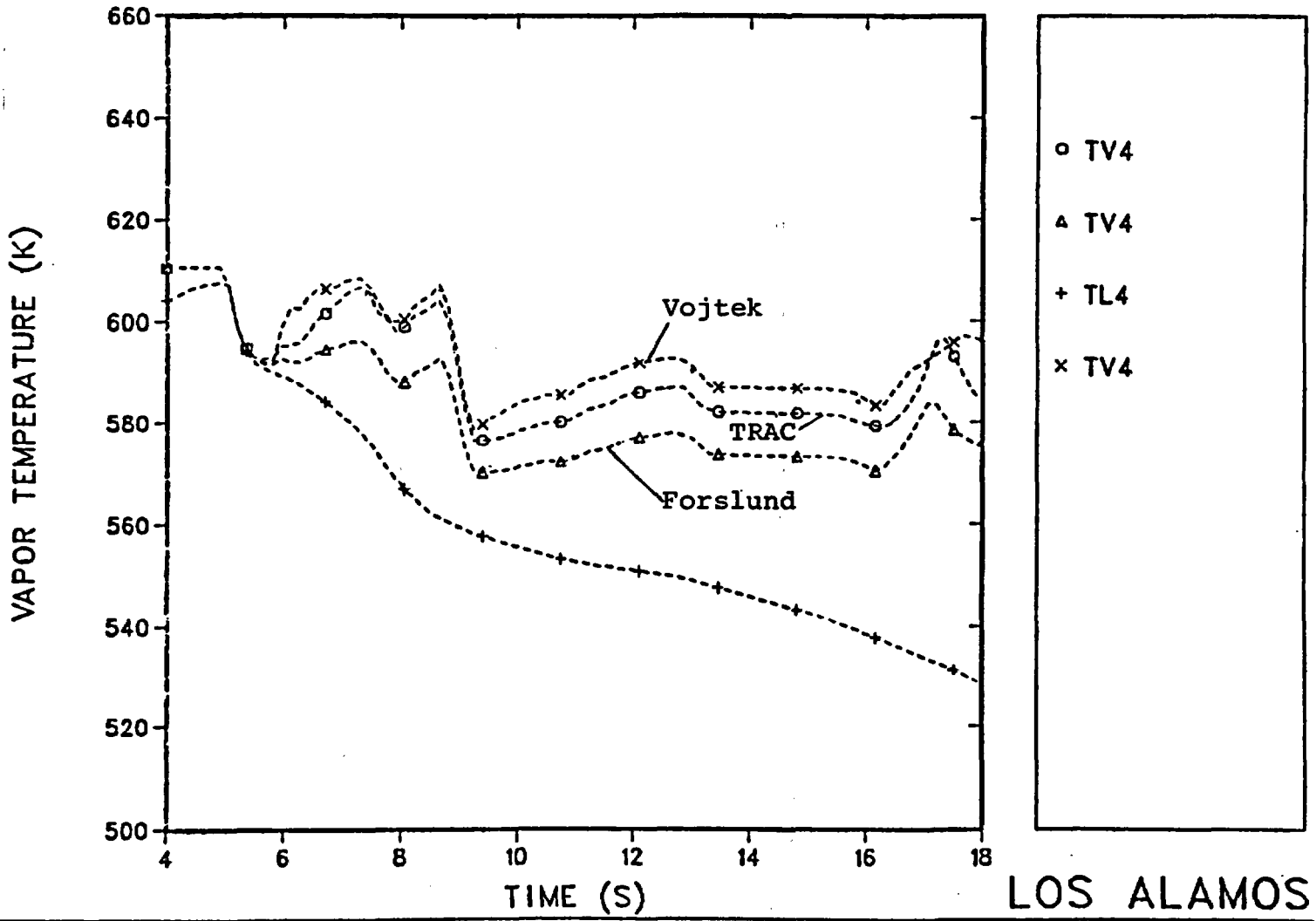


Fig.26 Comparison of calculated vapor velocities  
(Different post-CHF heat transfer models)

TRAC TRANS. CALCULATION EXP. NO. DNB - 9  
 COMPARISON VER. 13 15 AND VER. 22



LOS ALAMOS

Fig.27 Comparison of calculated vapor temperatures  
 (Different post-CHF heat transfer models)

## Results of CCTF Upper Plenum Injection Tests

Yoshio MURAO, Tadashi IGUCHI, Kazuharu OKABE,  
Jun SUGIMOTO, Hajime AKIMOTO, Tsutomu OKUBO

Japan Atomic Energy Research Institute

### 1. Introduction

By using the Cylindrical Core Test Facility (CCTF), many tests have been performed in Japan Atomic Energy Research Institute (JAERI) in order to investigate the thermo-hydrodynamic phenomena in the refill and reflood phase during a PWR-LOCA. Most of tests have been conducted by using Cold Leg Injection (CLI) type ECCS for three- or four-loop PWRs. Some two-loop PWRs, however, equip the Upper Plenum Injection (UPI) type ECCS instead of CLI type ECCS. In the UPI type ECCS, the Low Pressure Coolant Injection (LPCI) water is injected into the upper plenum and Accumulator (Acc) and High Pressure Coolant Injection (HPCI) water into the cold legs, while in CLI type ECCS, the LPCI, Acc and HPCI water is injected into the cold legs alone. It has been found in tests for CLI type ECCS that the higher mass flow rate at the primary pump caused higher steam binding which caused poorer core cooling due to induced reduction of core inlet mass flow rate.

In the reactor with UPI type ECCS, it is estimated that the most of the water injected into the upper plenum is held on the tie plate above the core due to ascending steam from the core and accumulates in the upper plenum up to the level of the hot leg and then begin to enter the hot leg, if assumed are the same core cooling as the core of the reactor with CLI type ECCS and the validity of the Bankoff's correlation for the counter-current flow limitation (CCFL). The steam binding in the primary loops is increased by entering water into the hot legs, if the water enters the heat transfer tubes of the steam generators and resultant evaporation causes the increase of the mass

---

The work was performed under contract with the Atomic Energy Bureau of Science and Technology Agency of Japan.

flow rate at the primary pump. Therefore, the following two possibilities are considered in the UPI type ECCS.

- (1) The larger steam binding and the resultant poorer core cooling appears than those in referential CLI type ECCS.
- (2) The higher upper plenum injection rate causes the poorer core cooling in the UPI type ECCS.

In order to investigate the possibilities, two UPI tests were performed. One was a test under no failure assumption of two LPCI pumps (denoted as no failure UPI test), and the other was a test under a single failure assumption (denoted as single failure UPI test). The results from two UPI tests and a referential single failure CLI test are compared and analyzed.

## 2. Experiment

### 2.1 Facility

The CCFT is designed to provide the capability to reasonably simulate the flow conditions in the primary system of a PWR during the refill and reflood phases of a LOCA, and models a four-loop 1000 MWe class PWR with the flow area scaling ratio of 1/21.4. It has a scaled pressure vessel and four loops with passive and active component simulators, eg. active steam generators, primary pump simulators and containment tanks, as shown in Fig. 1. A cold leg break situation is simulated in this test facility.

The pressure vessel consists of the full height heated core, the upper and the lower plena, and the annulus downcomer with a gap of 61.5 mm surrounding the core.

The core has thirty-two 8×8 electrically heated rod bundles arranged in a cylindrical configuration. The location of each bundle is identified by the bundle number 1 ~ 32, as shown in Fig. 2(1). Each heated rod is modelled a full-size fuel rod for 15×15-rod-type PWR fuel assembly and has a cosine axial power distribution with a peaking factor of 1.4. The electric power can be supplied to the subdivided three regions of the core indivisually to achieve a desired radial power distribution, namely, A, B and C regions as indicated in Fig. 2(1). The upper plenum has a scaled (scaling ratio: 8/15) upper plenum internals, i.e. control rod guide tubes, support columns and so on, arranged as shown in Fig. 2(2).

The tie plate and the upper core support plate (UCSP) are located between the core and the upper plenum. The tie plate is simulating the flow area of the end box and is a 10 mm thick perforated plate with totally 1408 round flow holes of 12.8 mm diameters. The blockage ratio of the plate is 0.48. Plugging devices are installed on the tie plate to simulate the flow resistance correctly. The UCSP is 60 mm thick and has the perforation analogous to that of an actual reactor.

The ECC water can be injected into the lower plenum, cold legs and upper plenum. Figure 3 shows the upper plenum injection devices. Two ECC water injection pipes are provided for the upper plenum injection and the inside diameter of the pipe is 49.5 mm. Each water injection

pipe has a flow hole of 3 mm diameter at the elevation of the hot leg center line. The radial location of the water injection pipes is shown in Fig. 2(2). The arrows in the figure show the injection direction of the ECC water. The ECC water is injected horizontally into upper plenum through the flow holes. The injected ECC water impinges on the control rod guide tubes, as noticed from Fig. 2(1). In order to keep the same flow rates between the flow holes, orifices with 33 mm diameter are installed between the header and the water injection pipes.

As described later, since the ECC water flow rate through an injection pipe was 60% higher than through the other pipe in the single failure UPI test, additional orifice was installed at the lower part of each injection pipe to equalize the flow rates through the injection pipes in the no failure UPI test.

## 2.2 Test conditions and procedure

Table 1 gives the major test conditions for two UPI tests and a referential CLI test. The test conditions are basically identical for the three tests, namely single failure UPI, no failure UPI and single failure CLI test, respectively, except for the locations and flow rates of the ECC water injections.

In UPI tests, the Acc and HPCI waters were injected into cold legs after short injection into the lower plenum. The LPCI water was injected through two injection pipes into the upper plenum during whole transients for both UPI tests. On the other hand, in the CLI test, the LPCI water as well as Acc and HPCI waters was injected into cold legs alone through whole transients after short injection into the lower plenum.

In the no failure UPI test, LPCI flow rate is twice as large as one of the single failure UPI tests. The single failure CLI test was performed to simulate the single failure assumption of the LPCI pumps in CLI type PWR. The LPCI water injection rate through one injection pipe denoted A in Fig. 2(2) is 60% higher than one through the other injection pipe in single failure UPI test, and both LPCI water injection rates through two injection pipes are equal with each other in the no

failure UPI test. Figure 4 shows the flow rates of the ECC water.

The test procedures were as follows: The lower plenum was initially filled with saturated water to 0.9 m from the bottom of the vessel. The electric power was then applied to the heater rods in the core. When the clad temperatures were scheduled to reach the specified value at the highest power location, the injection of the Acc and HPCI waters into the lower plenum was initiated. Simultaneously, the LPCI water was injected into the upper plenum through two injection pipes in the UPI tests, and into the lower plenum in the CLI test, respectively. The power input to the rods began to decay at the reflood initiation when the water reached the bottom of the heated region of the heater rods (2.1 m high from the bottom of the vessel). The injection location for Acc and HPCI waters was switched from the lower plenum to the three intact cold legs shortly after the reflood initiation. The LPCI water was still injected into the upper plenum in the UPI tests, while the injection location for LPCI water was also switched from the lower plenum to the three intact cold legs in the CLI test. The generated steam and the entrained water flowed through broken and intact loops to the containment tanks. The pressure of the containment tank-2 shown in Fig. 1 was kept constant (0.2 MPa) during each test. When all heater rod temperatures showed complete cooling of the core, the power supply to the heater rods was turned off, terminating the test.

### 3. Results

#### 3.1 Core cooling

Figure 5 shows the clad temperatures and the differential pressures across the bottom and the top of the upper plenum for the early transient. Since the gravity term is a dominant factor for the differential pressure in the upper plenum because of the low water mass flow rate, the differential pressure means the static head of the accumulated water on the upper core support plate (UCSP), or in the upper plenum.

The water injected into the upper plenum fell down into the core before the reflood initiation in both UPI tests, since less water accumulation rate in the upper plenum was observed than the estimated from the one-hundred percent water accumulation of the injected water, as shown in Fig. 5, and no water is considered to be carried over into the hot legs because of the reverse steam flow (direction from steam generators to upper plenum) induced by the steam condensation in the upper plenum.

The core cooling was observed in both UPI tests even before the reflood initiation, that is, the temperatures at the reflood initiation were 30 K lower for single failure UPI test and 50 K lower for no failure UPI test respectively than the temperature estimated for no core cooling, and is attributed to the effect of the falling water from the upper plenum.

During the short period after the reflood initiation, the 100% water accumulation is observed, suggesting the occurrence of CCFL at the interface between the core and the upper plenum. In this period, the core cooling is almost not observed in the UPI tests. After this period, the core cooling is observed again.

Figure 6 shows the clad temperature through the whole transients at the highest power bundle. The core cooling behavior in the core, specially in the lower half of the core, for single failure UPI test is roughly the same as that for the single failure CLI test. However, precisely speaking, in the period from the reflood initiation to the turnaround time the core cooling is slightly poorer for single failure UPI test than for single failure UPI test. This is judged from the fact that

the peak clad temperatures (PCT) are nearly the same between the two tests although the core is pre-cooled in UPI test before the reflood initiation. The core cooling in the no failure UPI test is judged to be better than that in the single failure CLI test from the PCTs in two tests.

The clad temperature transients in the lower half of the core, the characteristics of the bottom quench were similar between the UPI and CLI tests, namely the bottom quench advancement was radially uniform and the advancing rate was the same for both tests. However, the top quench remarkably appeared in UPI tests. The top quench appeared even at the midplane of the core and down to lower elevation in no failure UPI test than in single failure UPI test. The occurrence of the top quench was not horizontally uniform and was observed in the roughly half of the core bundles. Figure 7 shows the example concerning the ununiformity of the top-quench occurrence by hatching. In the top-quench region, (2.44 m elevation and 3.05 m elevation) the better pre-cooling is observed prior to the top-quench occurrence as shown in Fig. 8, while in the bottom quench region (1.83 m elevation), no difference of the pre-cooling or the uniform core cooling is observed. Therefore, three-dimensional analysis is necessary to be applied to get the accurate prediction of the phenomena, such as ununiform core cooling and the ununiform top-quench occurrence in the upper part of the core, while the one dimensional thermo-hydraulic model can be applied to the clad temperature analysis in the lower part of the core.

Figure 9 shows the comparison of the heat transfer coefficients among no failure UPI, single failure UPI and single failure CLI tests. The heat transfer coefficients in UPI tests are almost equal to that in CLI test in the lower half of the core, as shown in Fig. 9(1), although the PCT was lower in no failure UPI test than those in single failure UPI and CLI tests. It should be noted that the heat transfer coefficient in UPI tests are almost equal to that in CLI test nevertheless the net flow direction of the water is completely different, namely positive flow (from the lower plenum to the core) in CLI test and negative flow in UPI tests, as will be discussed later. The heat transfer coefficient in the upper half of the core is clearly higher in no failure UPI test

than those in single failure UPI and single failure CLI tests, as shown in Fig. 9(2). This can be explained by the higher water accumulation in the upper core in no failure UPI test, which is shown in 3.2 Thermo-hydrodynamic behavior in pressure vessel.

### 3.2 Thermo-hydrodynamic behavior in pressure vessel

As shown in Fig. 10 the much water accumulation in the upper plenum is observed in both UPI tests in comparison with the CLI test. The fluid temperature measurement indicated that the water was saturated in the upper plenum except for the vicinity of the water injection nozzle in single failure UPI test. On the other hand in no failure UPI test, the saturation temperature in the upper plenum except for the vicinity of the water injection nozzle was observed only up to 40 s after the re-flood initiation. After the time, the fluid temperature was saturated roughly in the radially half of the upper plenum and subcooled in the other half, as seen in Fig. 11. In single failure UPI test the potential subcooled energy of the ECC water into the upper plenum was estimated to be less than the energy of the steam ascending from the core, while in no failure UPI test the potential subcooled energy was estimated to be less in the early transient ( $< 50$  s) and more in the later transient ( $> 60$  s) than the steam energy. Thus, it can be summarized that under the complete condensation condition (the later transient of the no failure UPI test) the co-existence of both the saturated and the subcooled bulk waters is attained, while under the non-complete condensation condition the condensation occurs in the region of the vicinity of the nozzle and the subcooled water is limited only in this small region.

From the mass balance calculation, the direction of the net water flow rate was estimated to be downward at the tie plate and at the bottom of the core. The readings of the turbine meters installed just above the tie plate indicates the ununiform upward steam flow from the core as shown in Fig. 12 for no failure UPI test. Since subcooled water was detected at the tie plate above the remarkable top quench region and the steam flow was inferior in the remarkable top quench

region, it is considered that subcooled water flowed downward at the tie plate in the inferior steam flow region. The ununiformity of turbine meter readings was observed even in single failure UPI test. The above mentioned fact suggests that the water falling region and the dominantly steam ascending region tend to discrete with each other.

The net water flow rate estimated from mass balance calculation was compared to the predicted with Bankoff's CCFL correlation under the uniform steam upflow assumption. The estimated for the single failure UPI test is much larger than the predicted, as shown in Fig. 13. The disagreement on the flow rate of falling water between the estimated and the predicted is considered to be caused by the ununiformity effect on the CCFL phenomena. It is necessary to study further this ununiformity effect on the CCFL phenomena for a large size perforated plate.

The static head of the accumulated water in the upper plenum was predicted, based on the above mentioned findings and the following assumptions:

- (1) Under the complete condensation condition, the condensation occurs below the upper core support plate (UCSP) and the water with no void accumulates on the UCSP up to the hot leg elevation.
- (2) Under the non-complete condensation condition, the condensation occurs at the elevation of the ECC water injection nozzle and two phase mixture accumulates on UCSP.
- (3) The void fraction in two phase mixture can be predicted with Wilson's void fraction correlation.
- (4) The steam flow rate, based on the energy balance calculation in the core, can be given as the boundary condition in the above prediction.

Figure 14 shows the comparison of the static head of the water accumulated on UCSP up to the hot leg elevation. The prediction agrees well with the data in single failure UPI test and after 100 s in no failure UPI test. The difference of the water accumulation between the measured and the prediction, which is appeared before 100 s in no failure UPI test, is mainly caused by the simplified treatment of the condensation phenomena, such as the condensation elevation and the horizontal ununiformity of the fluid temperature distribution (or co-existence of the subcooled and saturated bulk waters).

Shown in Fig. 15 are the core sectional differential pressures measured at four azimuthally different directions in the upper part of the core. Although the thermal behavior in the upper core was horizontally ununiform (eg. ununiform top quenching) and the CCFL phenomena was horizontally ununiform, the ununiformity of the core sectional differential pressure is very small in both UPI tests. However, in detail, the more core sectional differential pressure (+ 10% of the others from 50 s to 250 s) is recognized at the top quench region (shown by symbol  $\Delta$ ). The upper plenum differential pressure is more scattering than the core sectional differential pressure, as shown in Fig. 15. The higher upper plenum differential pressure is noticed above the top quench region.

Figure 16 shows the core sectional differential pressures at various elevations. The water accumulation in the upper core in no failure UPI test is higher than those in single failure UPI and CLI tests.

### 3.3 Thermo-hydrodynamic behavior in primary loop

#### Single failure UPI test

Figure 17 shows the mass flow rates in the system for the single failure UPI test and the referred CLI test. These values were obtained with the direct measurement or the mass and energy balance calculation. In the single failure UPI test, the major part of the water which is injected into the upper plenum falls down through the core except for the short period after the reflood initiation, flows up in the downcomer, and overflows through the break. Two thirds of the steam from the core condenses in the upper plenum, so that the steam flow rate through loops is lower than that in the referential CLI test, although the steam generation rates in the core are nearly equal with each other.. And, the water flow rate through loops is higher.

Figure 18 shows the rate of the evaporation in the steam generator, which is estimated from the fluid temperature transient in the steam generator secondary side. The more evaporation in the steam generator is observed in single failure UPI test than CLI test. This is because in the UPI test more water passed through the steam generators and transferred the heat from their secondary side. The two phase mixture was

observed through the viewing windows downstream the steam generator, so that the complete evaporation cannot be assumed for the accurate estimation of the differential pressures across the primary pumps, although the complete evaporation in the steam generator can be assumed in CLI case.

#### No failure UPI test

By comparing with thermo-hydrodynamics in primary loop for both UPI tests, the following phenomenological similarities and differences have been found between the two UPI tests: Before 50 s, the thermo-hydrodynamics in primary loop, such as the negative core inlet flow after short positive flow, the small steam flow to hot legs, the large water flow to hot legs and the large evaporation in the steam generator, are generally the same between both UPI tests, mainly due to the no complete condensation situation in the upper plenum. However after 60 s, the steam flow rate in the hot legs became null, as shown in Fig. 19, due to the complete condensation in the upper plenum. The water stagnated in the hot legs and the inlet plenums of the steam generators. The static head of this stagnated water balanced the static heads of waters in the upper plenum, the core and the downcomer. The core inlet flow remained negative under the complete condensation condition. Figure 20 shows the transients of the core inlet flow rate, which are almost entirely negative in both UPI tests.

Figure 21 shows the conceptual figure of the hydrodynamic behavior in the primary loop, which is derived from the above findings.

#### 3.4 Steam binding effect

Figure 22 shows the comparison of the pressure drop across the intact loop. It is seen that the pressure drop is smaller in the higher UPI water flow rate (No failure UPI test) than in the lower UPI water flow rate (Single failure UPI test). This shows that the sequence described in 1. Introduction (The larger intact loop pressure drop at the higher UPI water flow rate) is not attained as far as the complete condensation is established in the upper plenum as in case of no failure UPI test.

It should be noted that the major term of the intact loop pressure drop is different between two UPI tests. The major term was the pressure loss due to the flow resistance in the intact loop in case of non-complete condensation condition while the major term was the static head of water accumulated in the riser part of the intact hot leg and the steam generator in case of complete condensation condition.

The reason of the lower intact loop pressure drop at the higher UPI water flow rate is that the CCFL phenomena is different from the case of the small scale model and that the much water can fall down into the core smoothly.

#### 4. Conclusion

- (1) The CCFL characteristics in large scale tie plate is different from those in small scale one, and it is not possible to be predicted with Bankoff's correlation.

In the radially half region of the core, the water fell down from the upper plenum to the core, and the top quench occurred. In the other half region, the steam ascended dominantly.

- (2) The net water flow rate at the core inlet became negative ( from the core to the lower plenum ), shortly after the reflood initiation.

- (3) Before the reflood initiation, the water injected into the upper plenum fell down to the core and caused the core cooling. The peak clad temperature in single failure UPI test was nearly equal to one in single failure CLI test. The peak clad temperature in no failure UPI test was lower than one in single failure CLI test.

- (4) Steam binding effect was not so large. In the complete condensation situation, the water stagnated in the hot leg and the steam generator, and the loop differential pressure was caused mainly by the static head of the stagnated water.

Table 1 Test conditions

Test name	No failure UPI	Single failure UPI	Single failure CLI
Injection rate			
To lower plenum	96 kg/s from -8.5 to 4s	94 kg/s from -9 to 0s	104 kg/s from -8.5 to 5s
To cold legs	81 kg/s from 4 to 15.5 s	79 kg/s from 0 to 15s	88 kg/s from 5 to 15.5s
To upper plenum	2.8 kg/s from 15.5 to 912s	2.8 kg/s from 15 to 1008s	11 kg/s from 15.5 to 939s
	22 kg/s from -8.5 to 912s	11 kg/s from -9 to 1008s	None

Other conditions:

Power	Total initial power	7.9 ~ 8.1 MW
	Average linear power	1.18 ~ 1.21 kW/m
	Radial distribution (A:B:C)	1.37:1.20:0.76
Pressure	Containment tank	0.2 MPa
Temperature	Initial peak clad temperature	974 ~ 1074 K
	ECC liquid	308 K

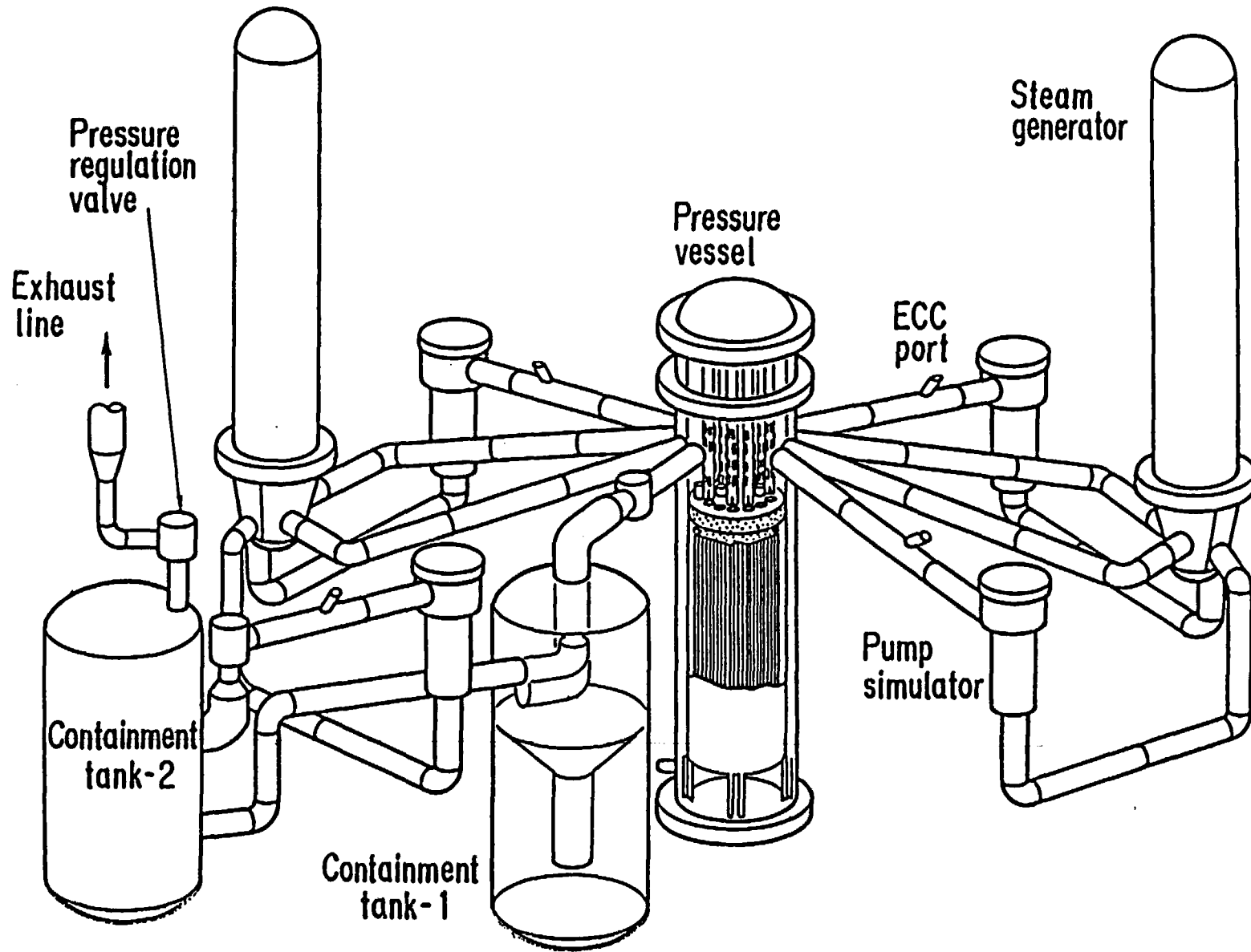


Fig. 1 Bird's-eye view of CCTF

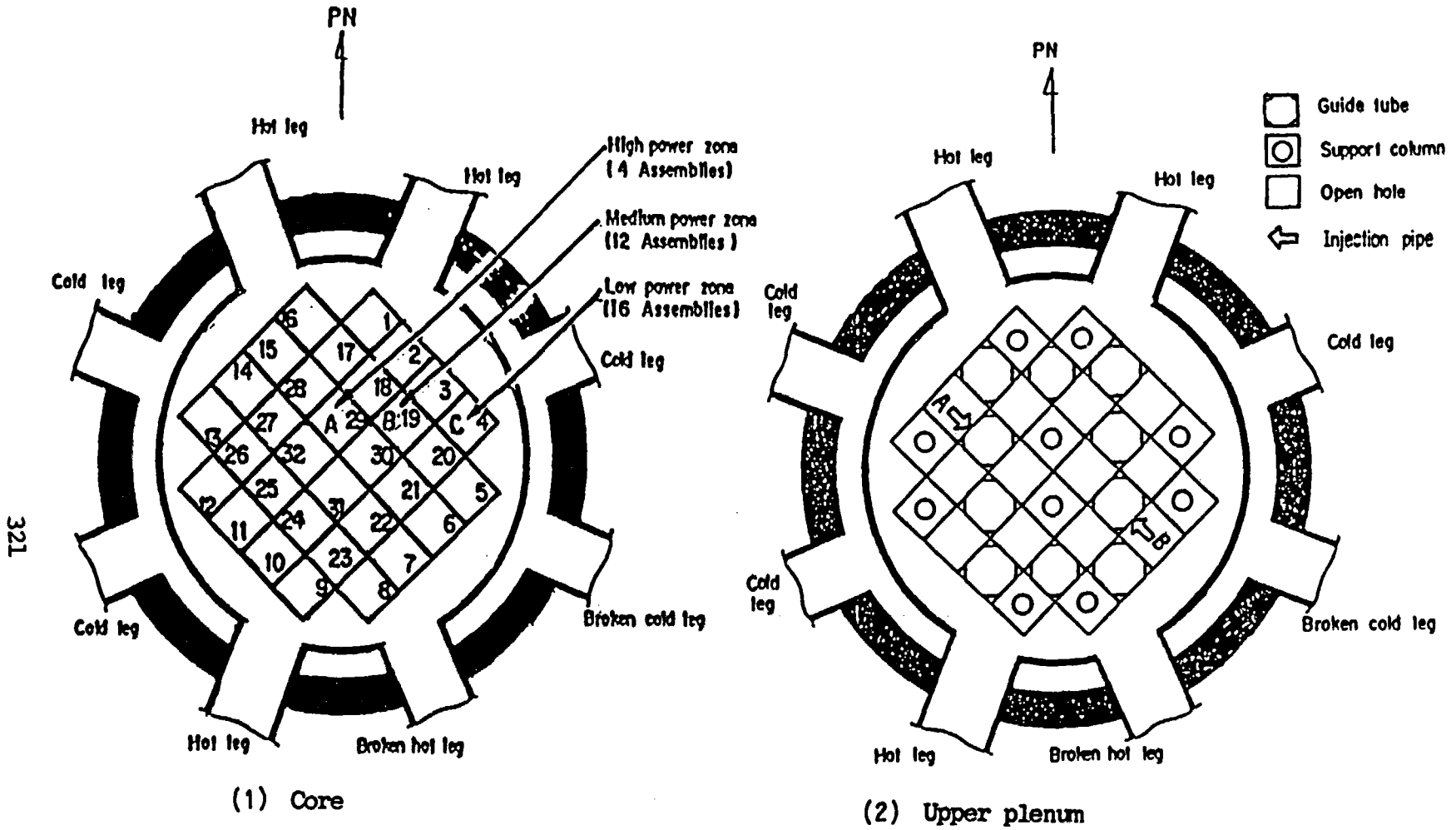


Fig. 2 Cross section of OCTF and upper plenum

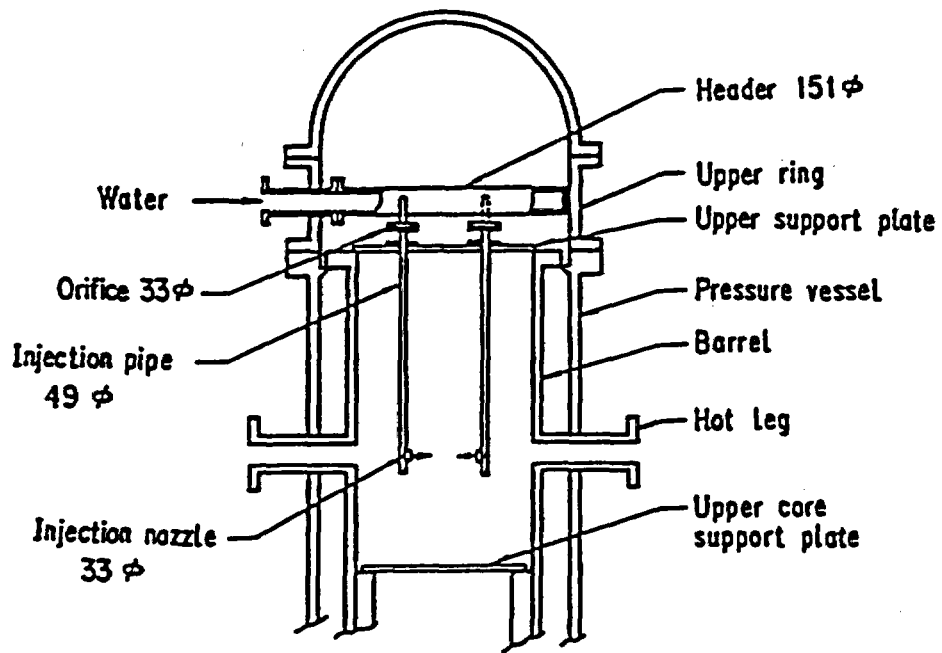


Fig. 3 Configuration of upper plenum injection pipe

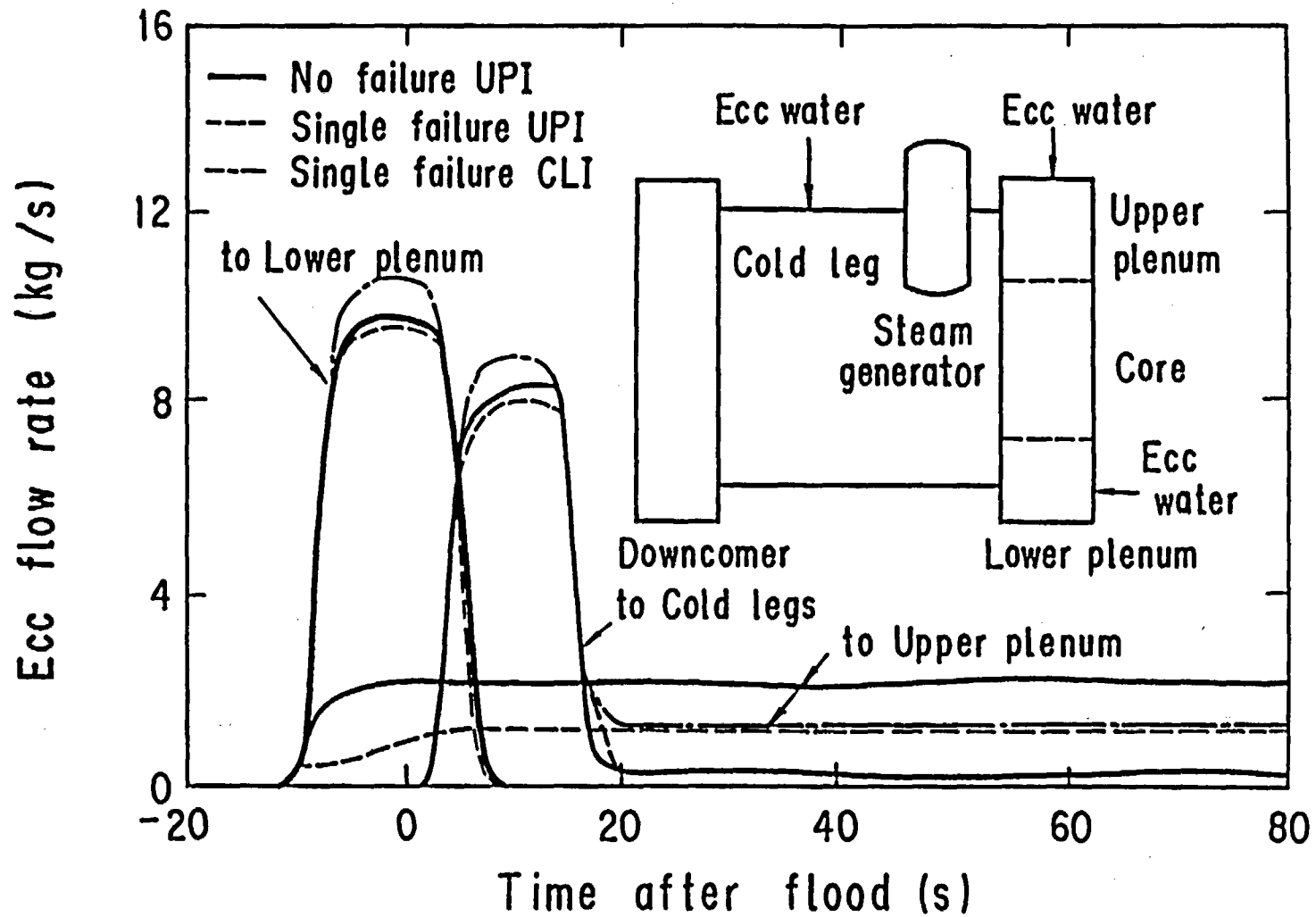


Fig.4 Comparison of ECC injection flow rate

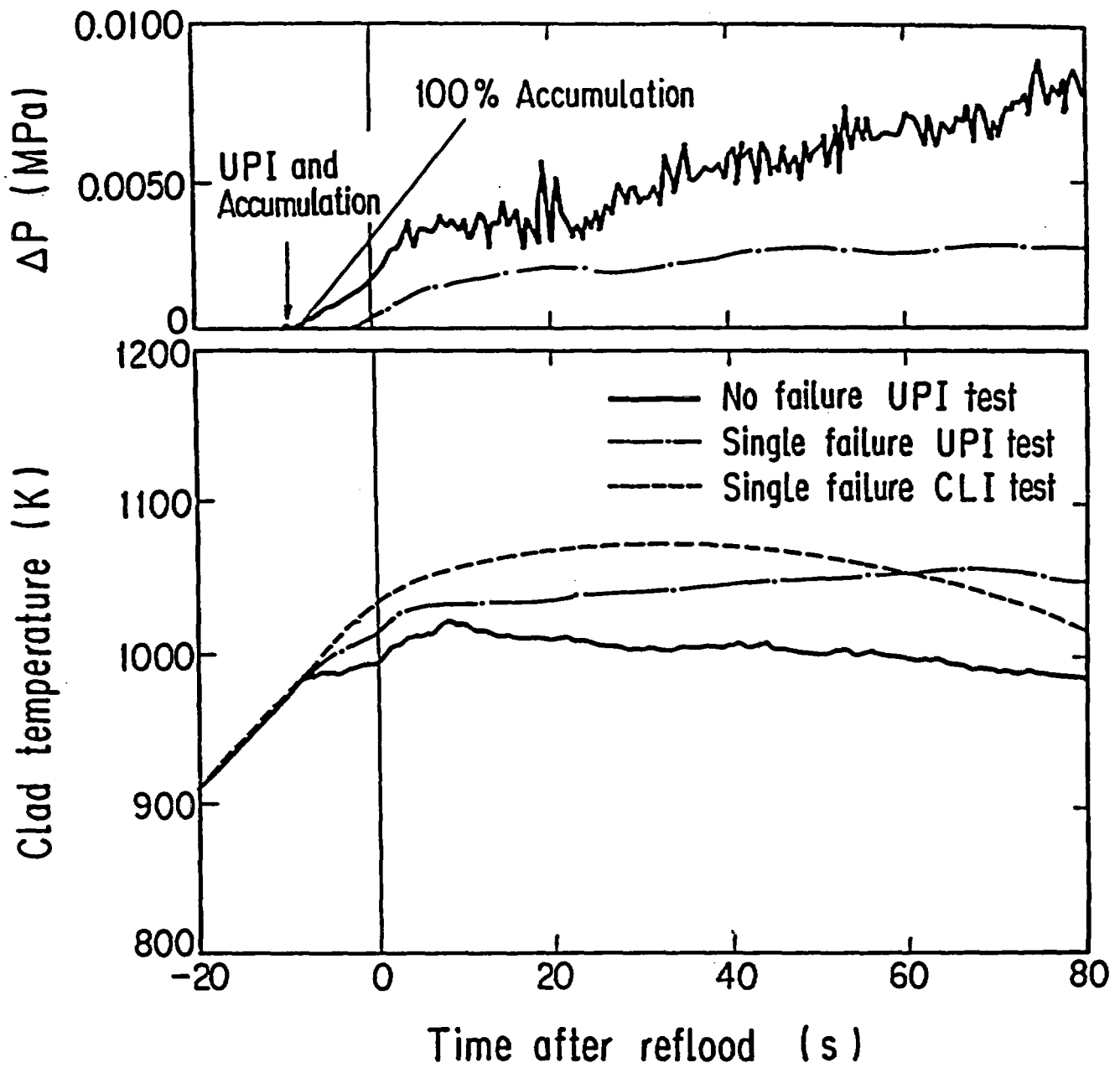


Fig. 5 Clad temperatures and  $\Delta P$  in upper plenum during early transient

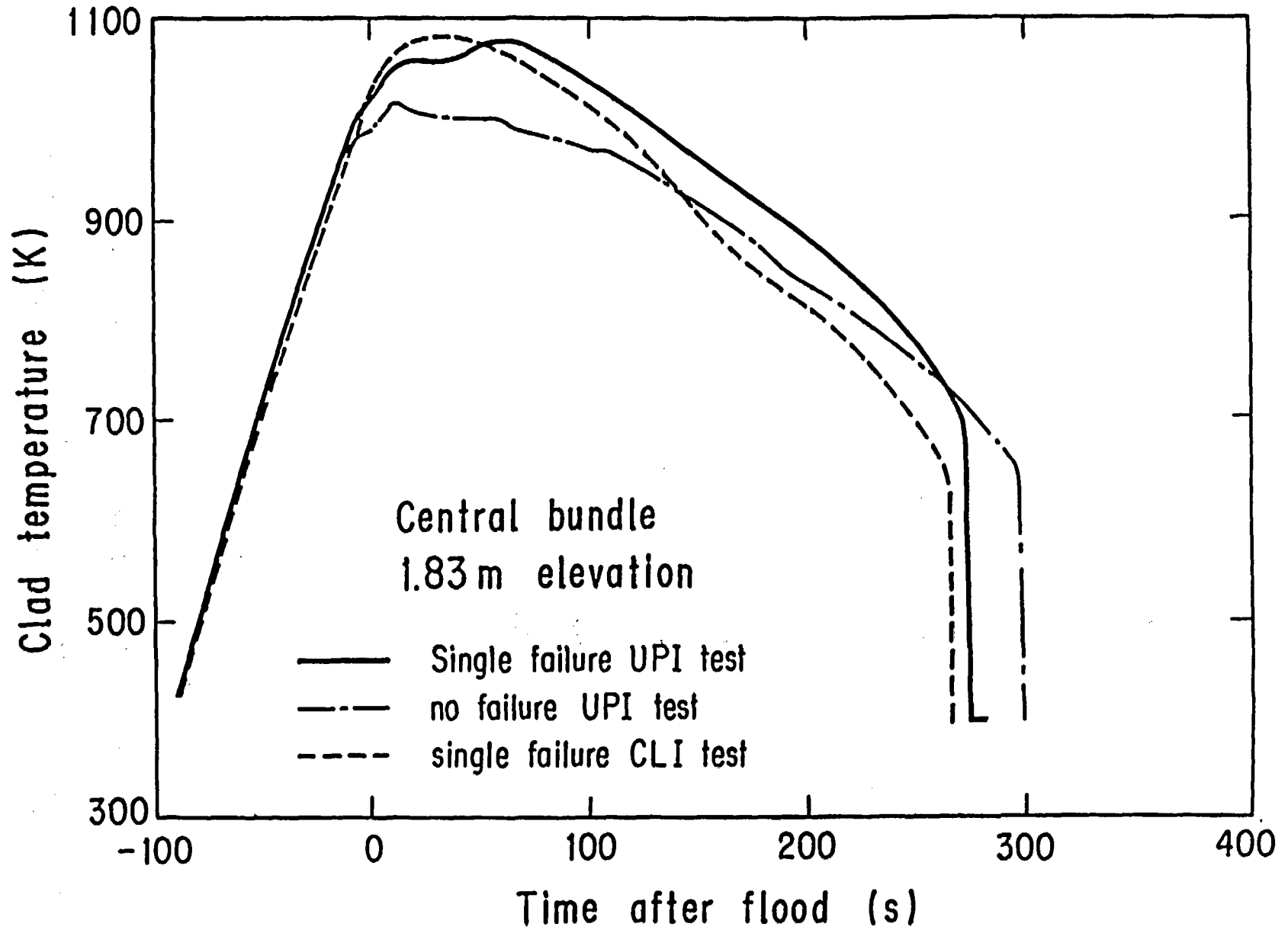


Fig. 6 Comparison of clad temperature

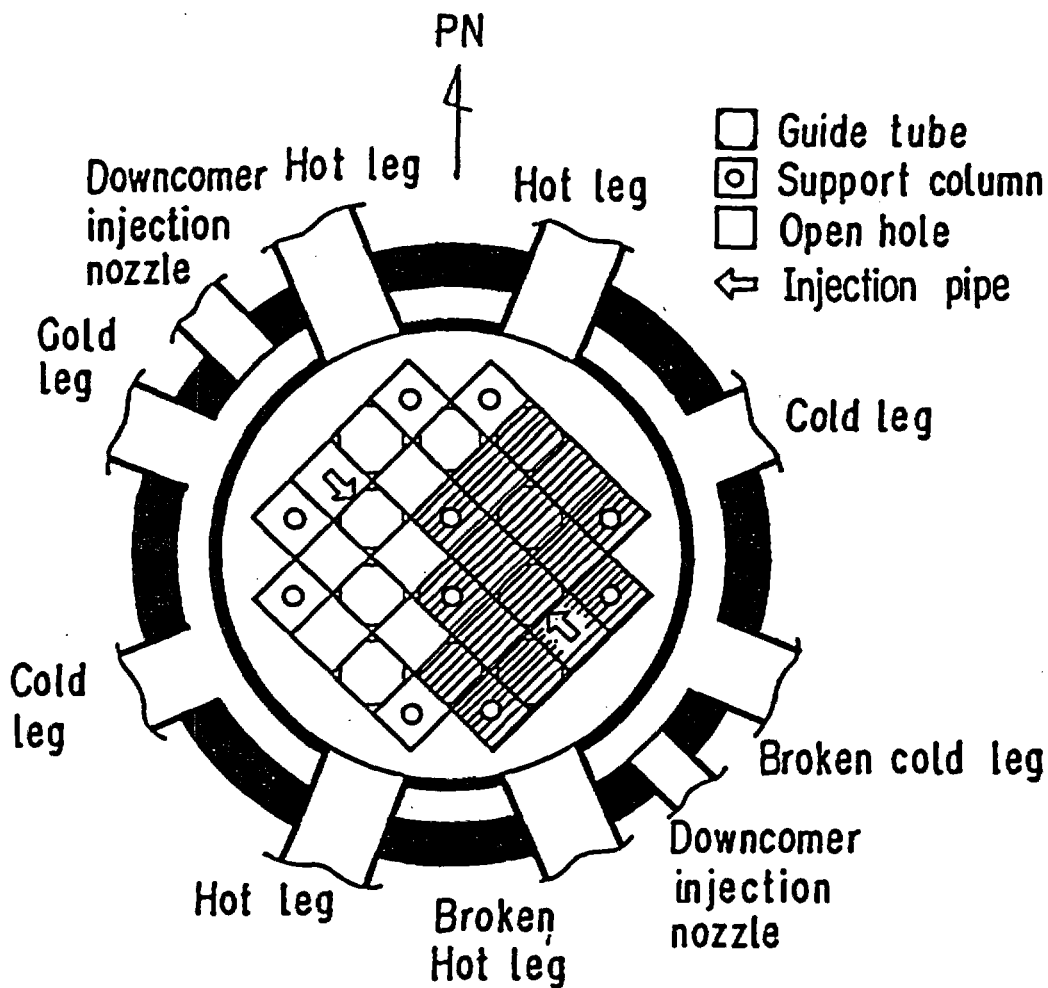


Fig.7 Ununiform top quench occurrence  
 (No failure UPI test at 3.05m elevation)

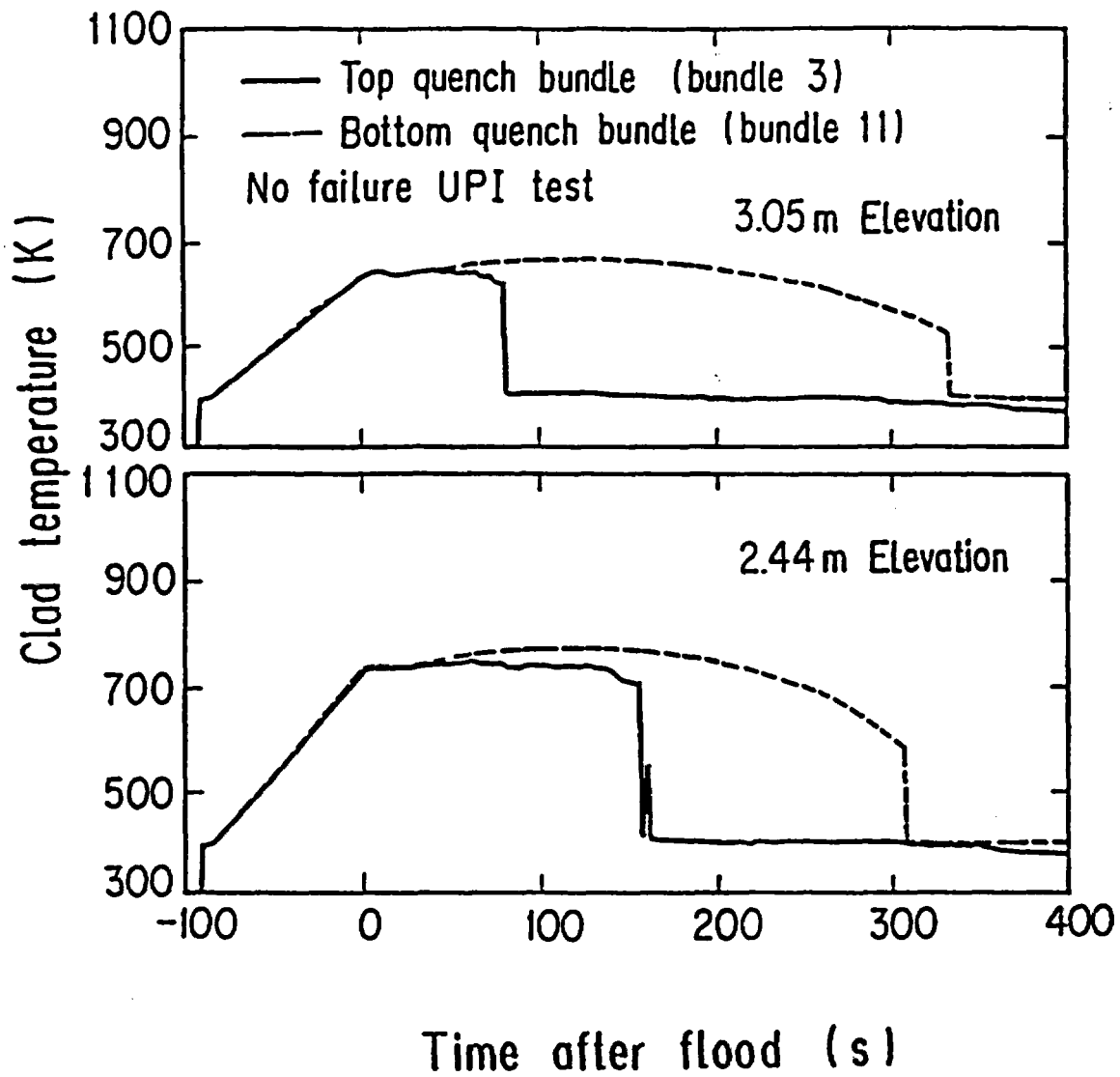


Fig. 8 Clad temperatures on rods in top-quench region and bottom quench region

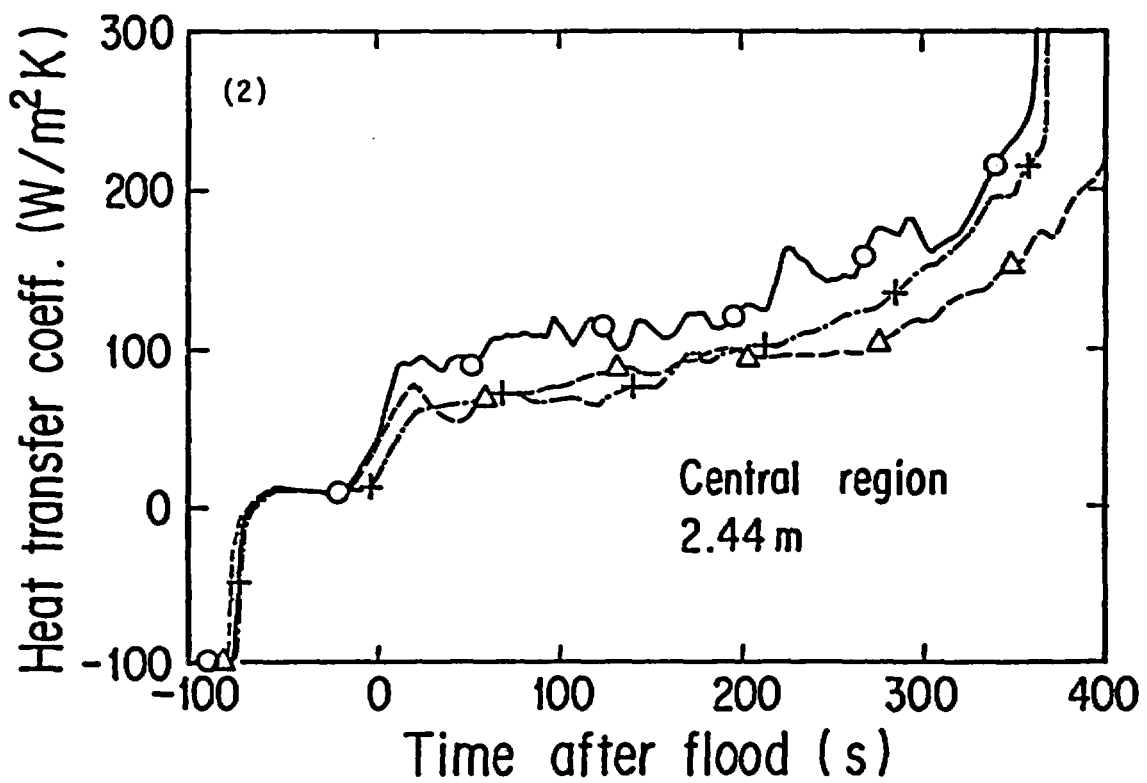
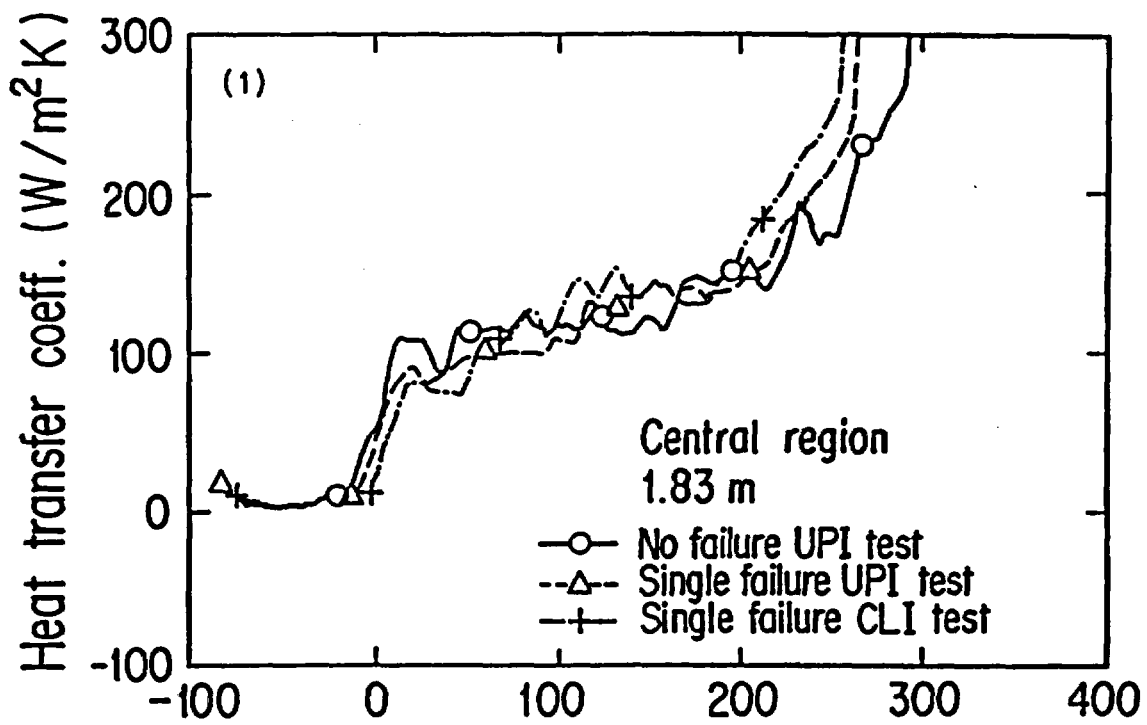


Fig.9 Comparison of heat transfer coefficient

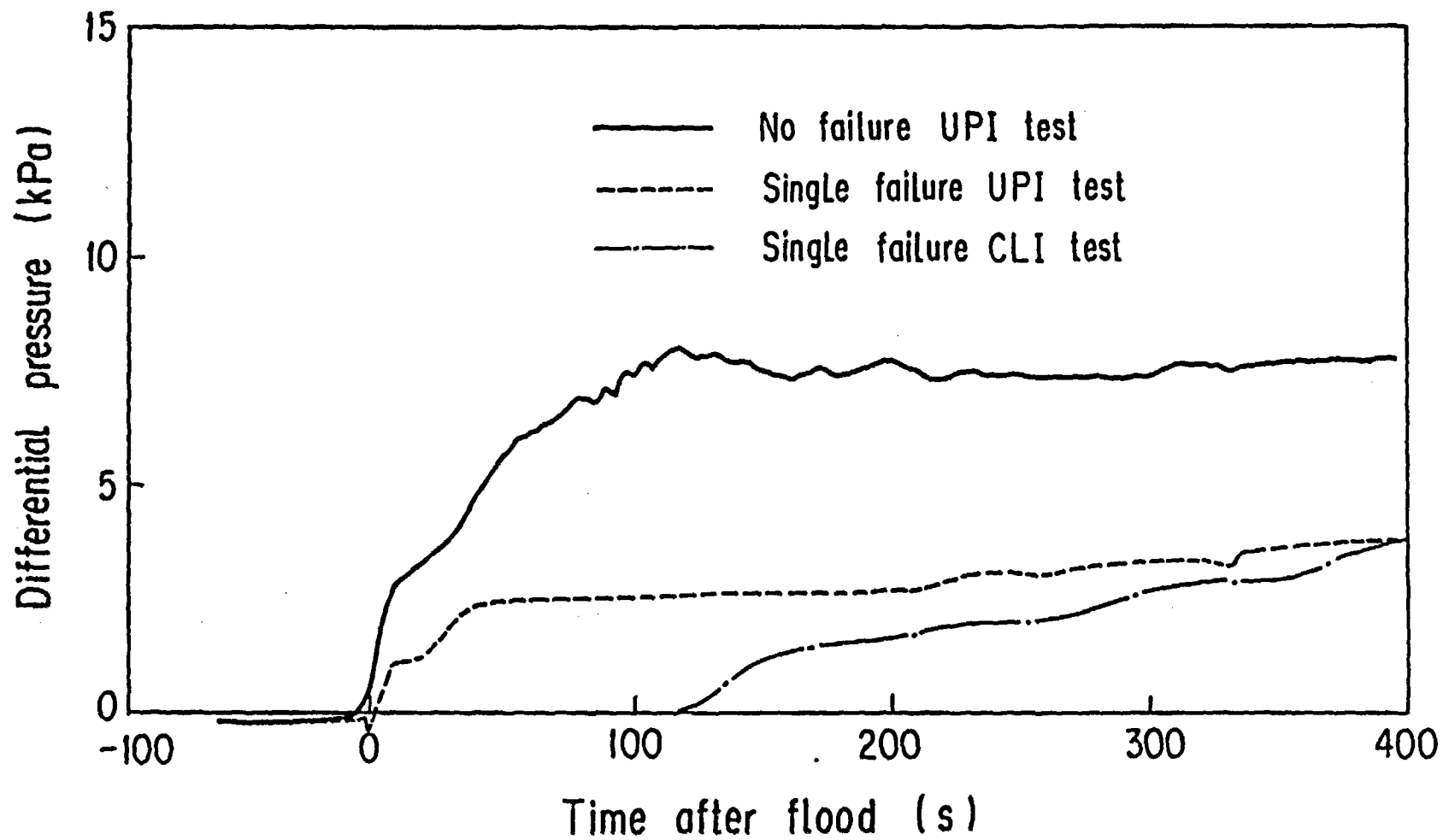


Fig. 10 Water accumulation in upper plenum

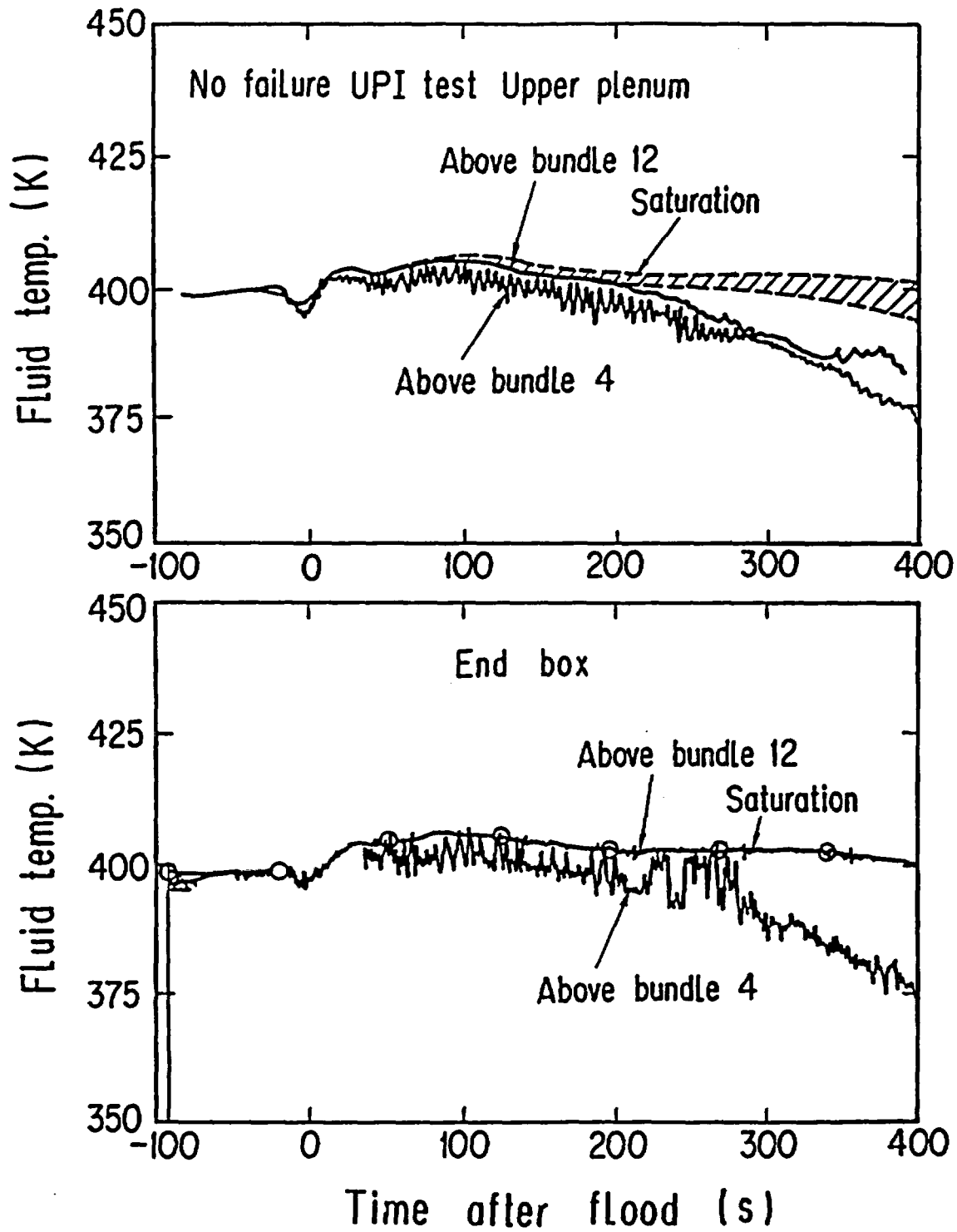


Fig. 11 Fluid temperature in upper plenum

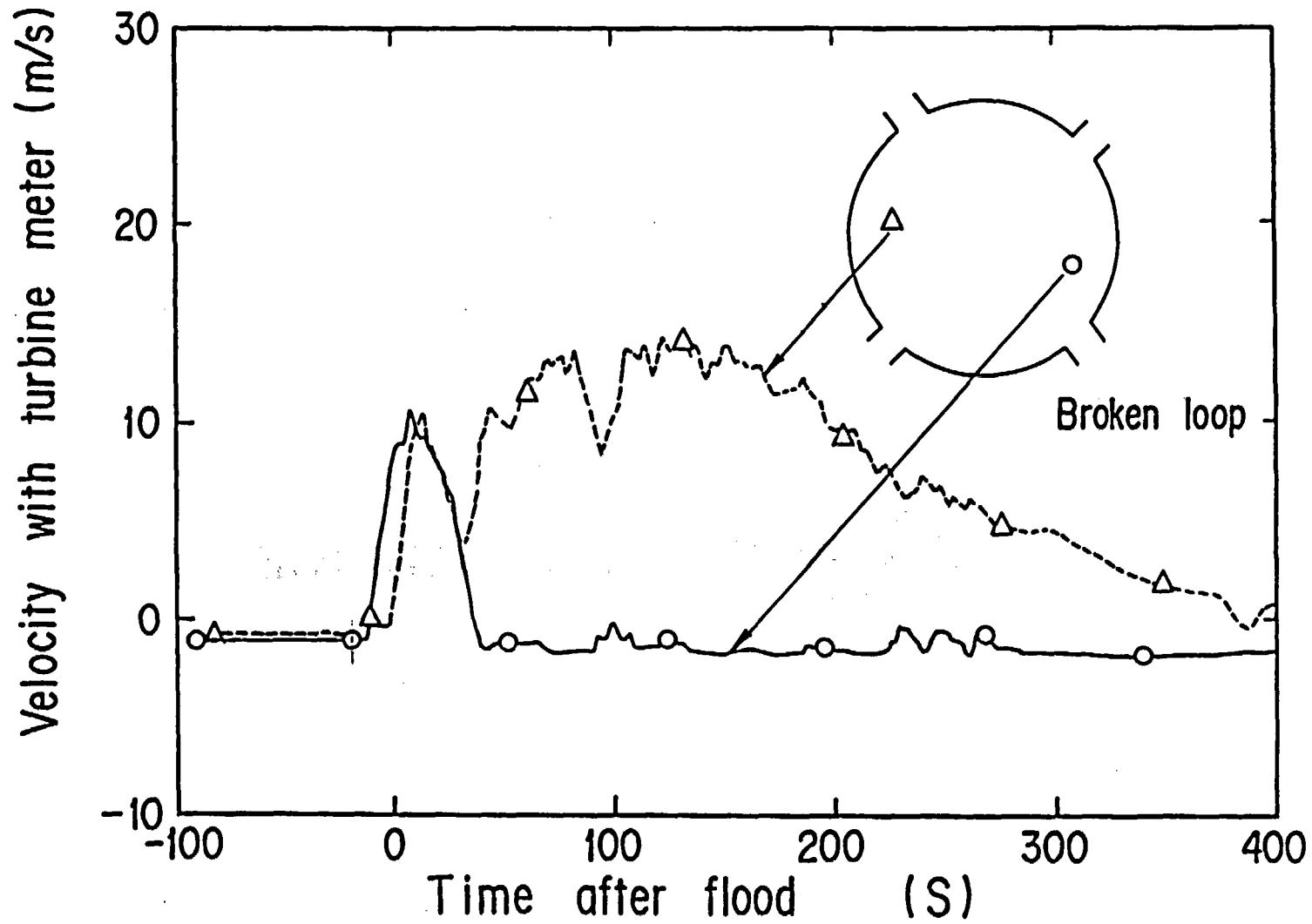


Fig. 12 Ununiformity of mass flow at end box

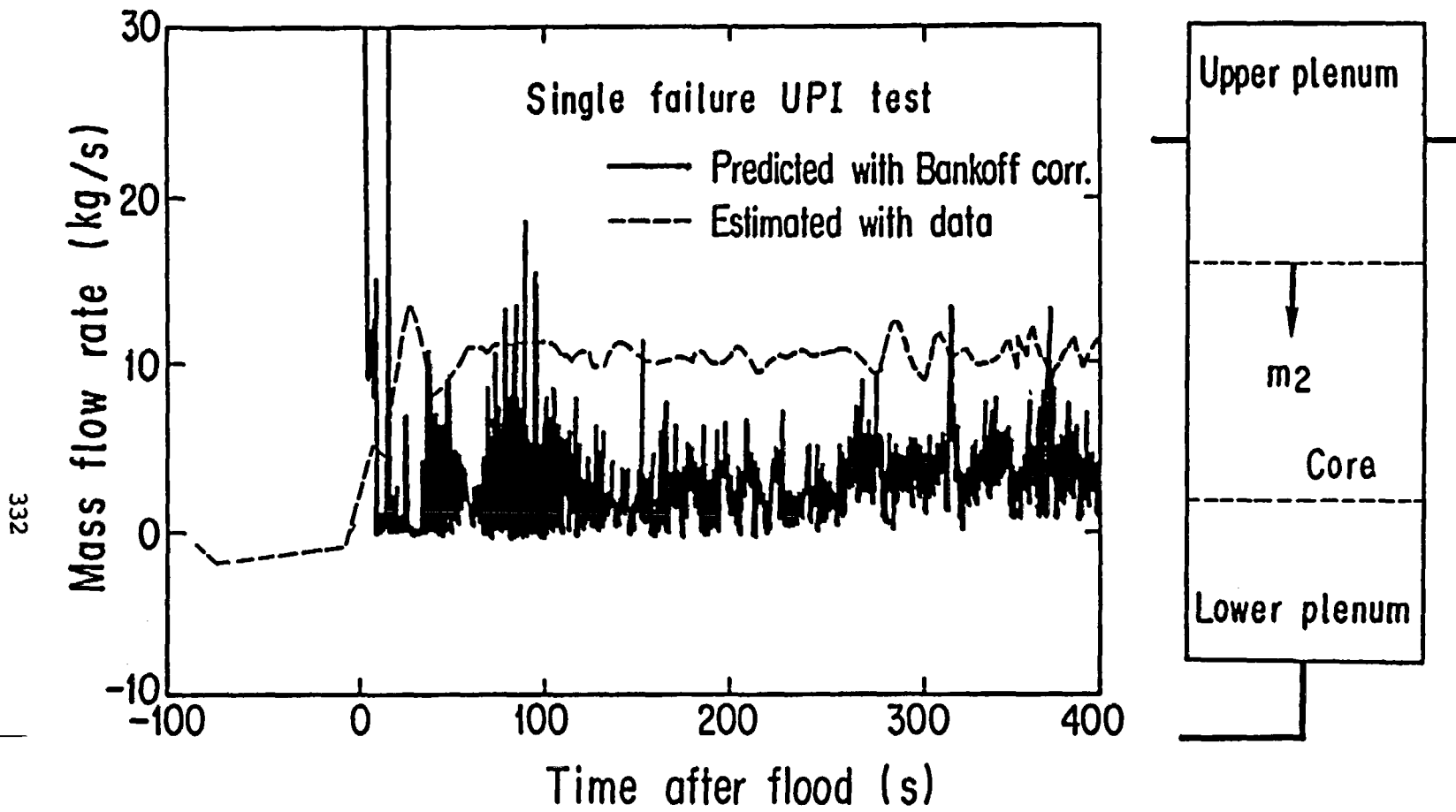


Fig. 13 Comparison of water downflow rates between the estimated and the predicted

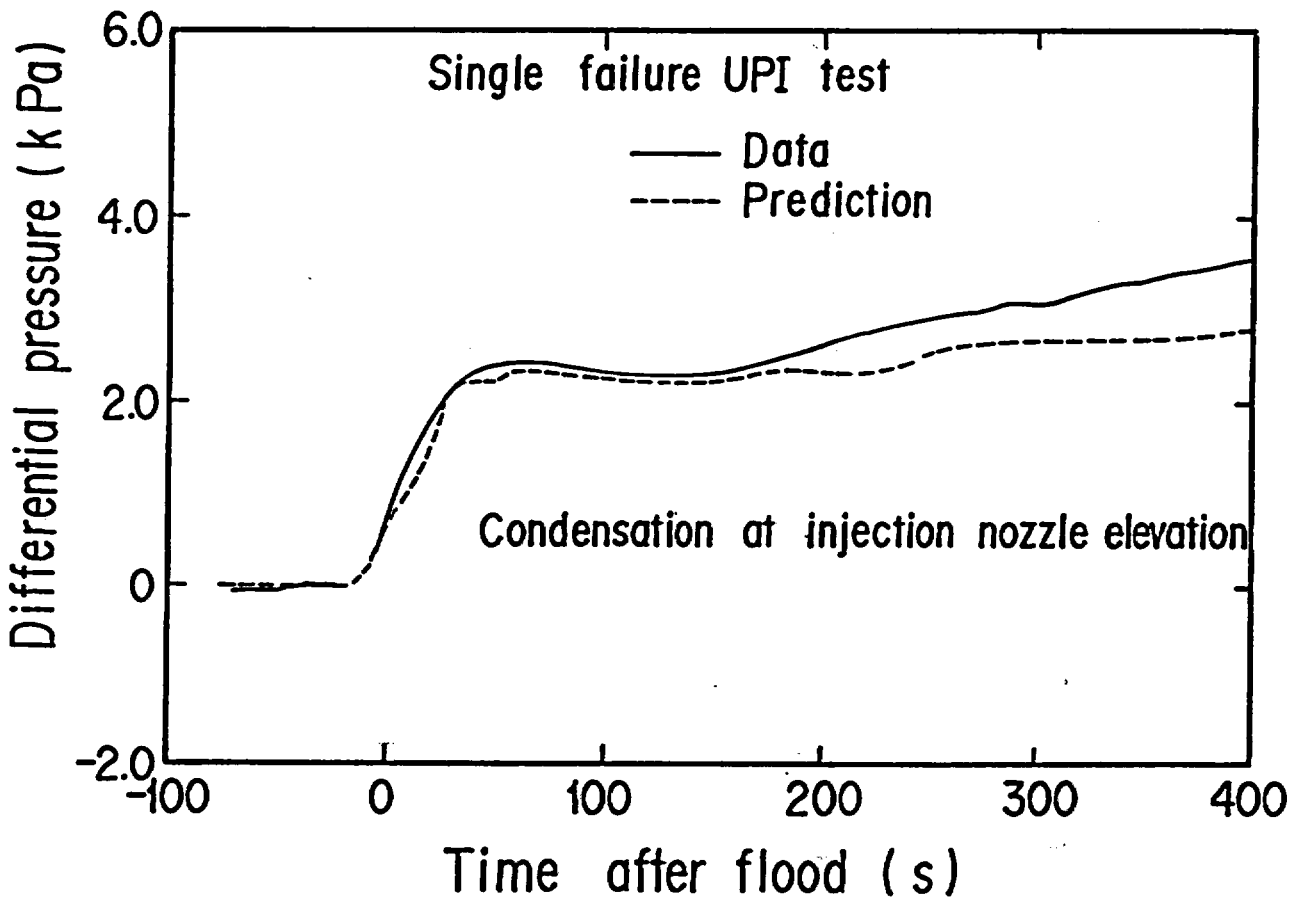
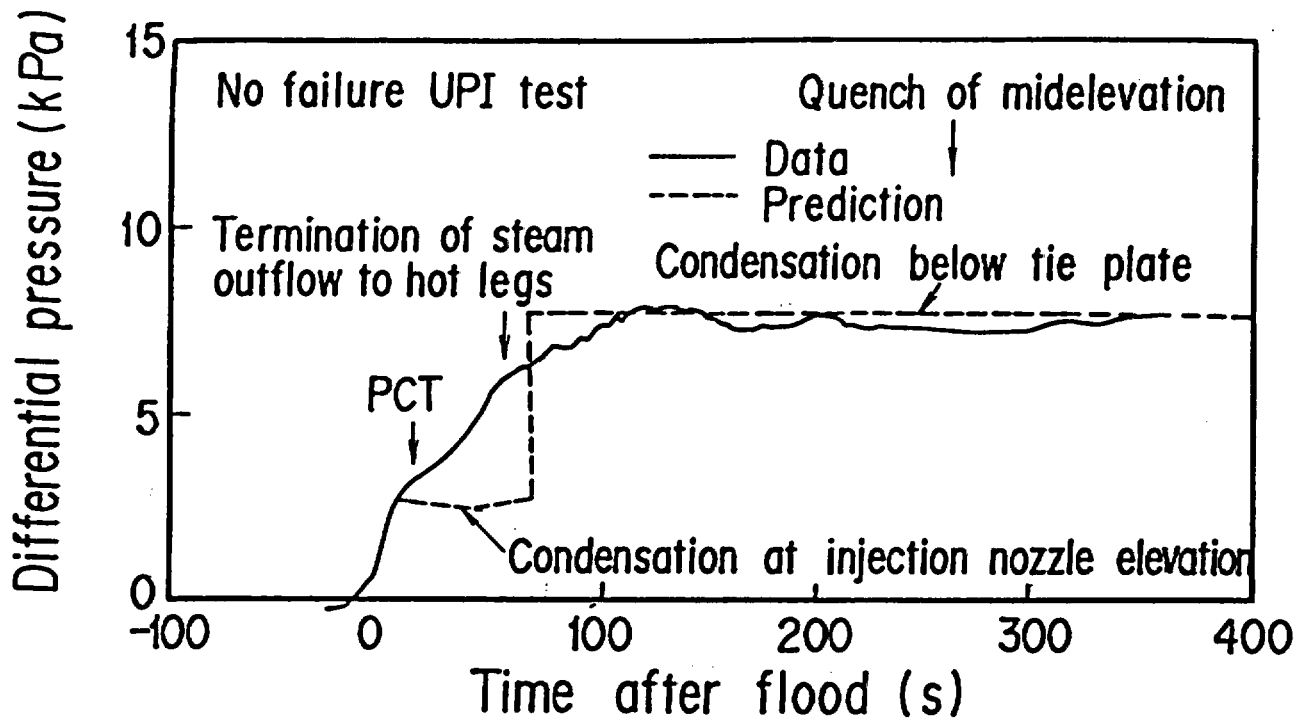


Fig. 14 Comparison of the static head of the water accumulated in the upper plenum between the data and the prediction for the UPI tests

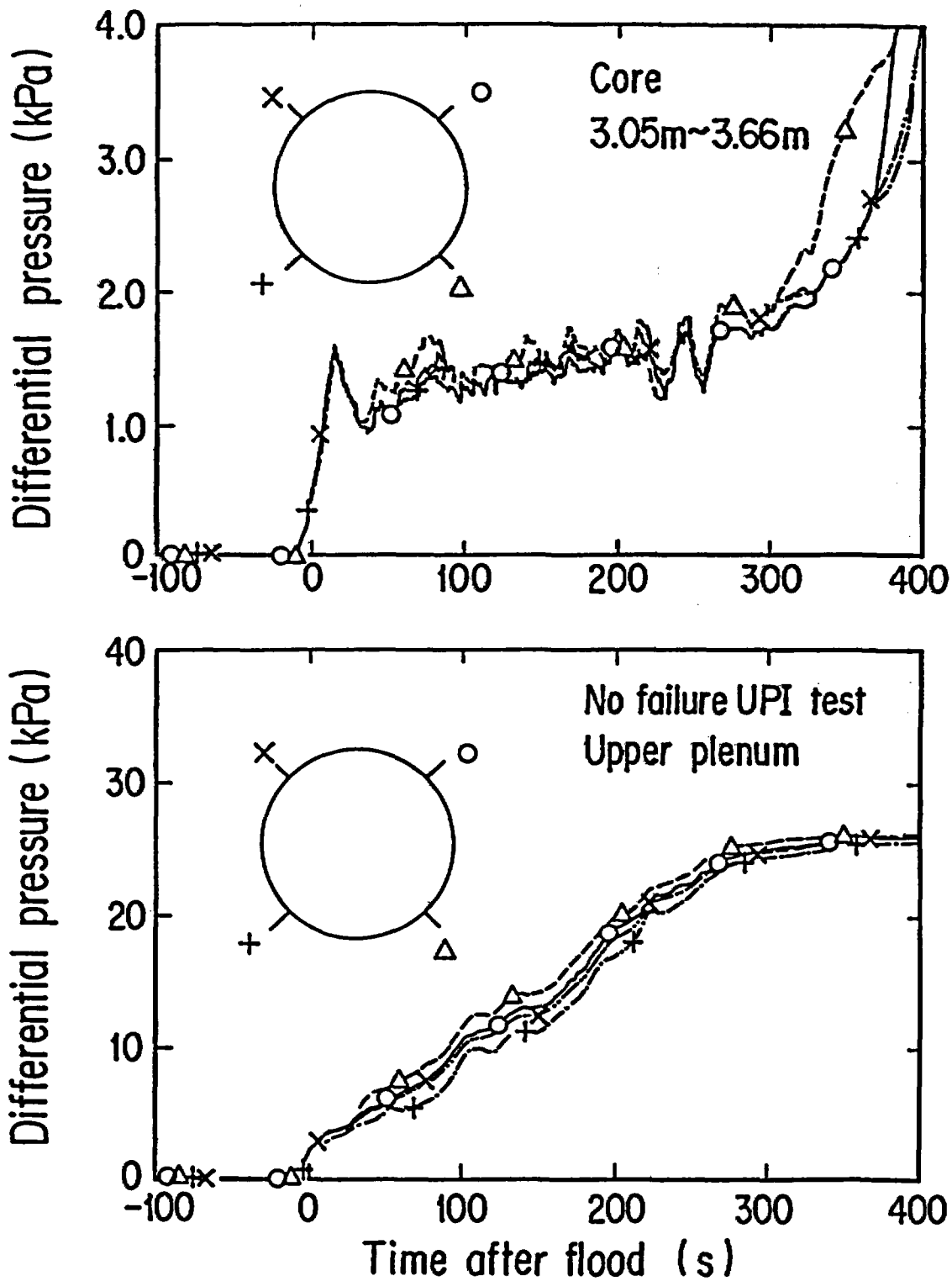


Fig.15 Radial uniformity of differential pressures in core and upper plenum

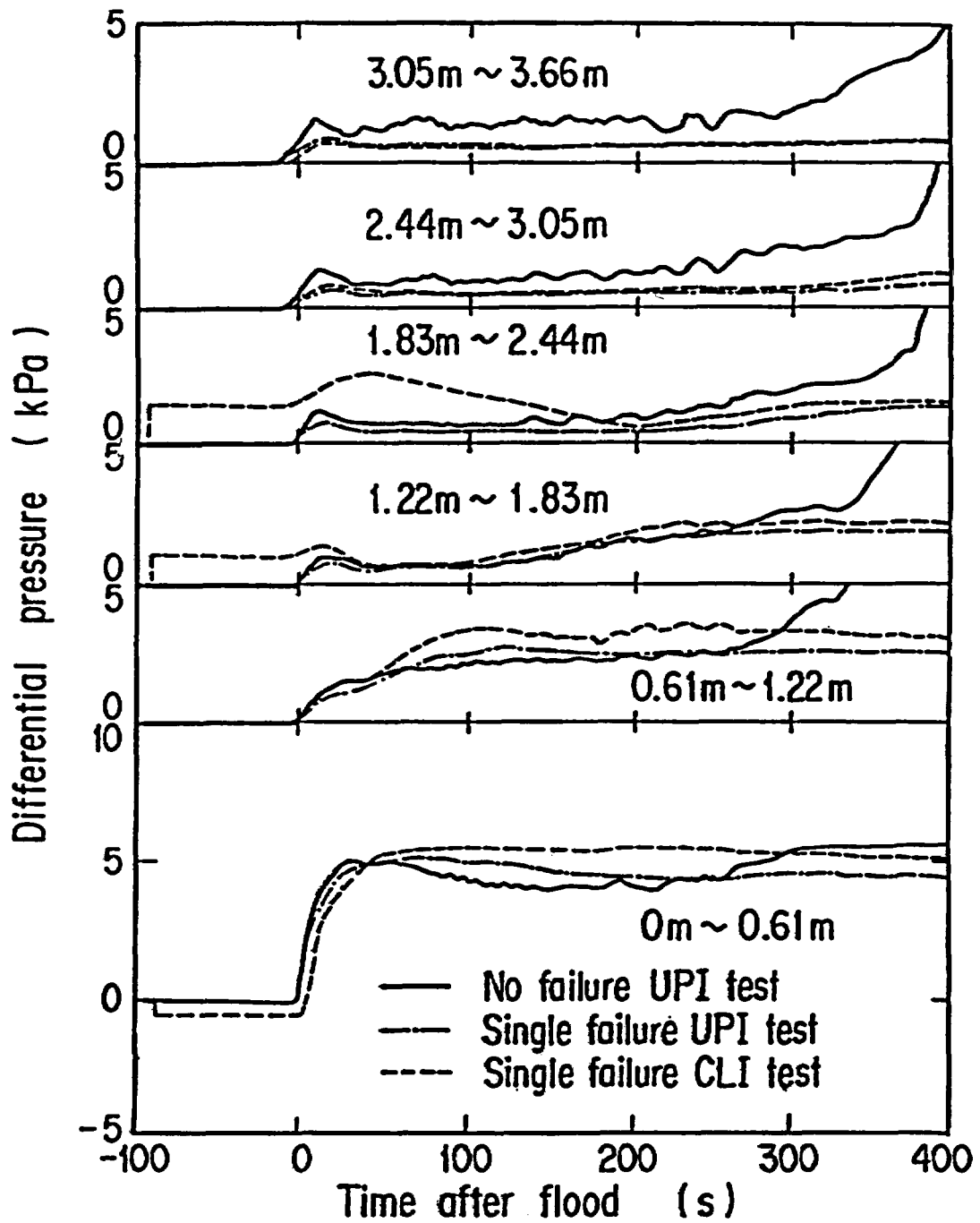
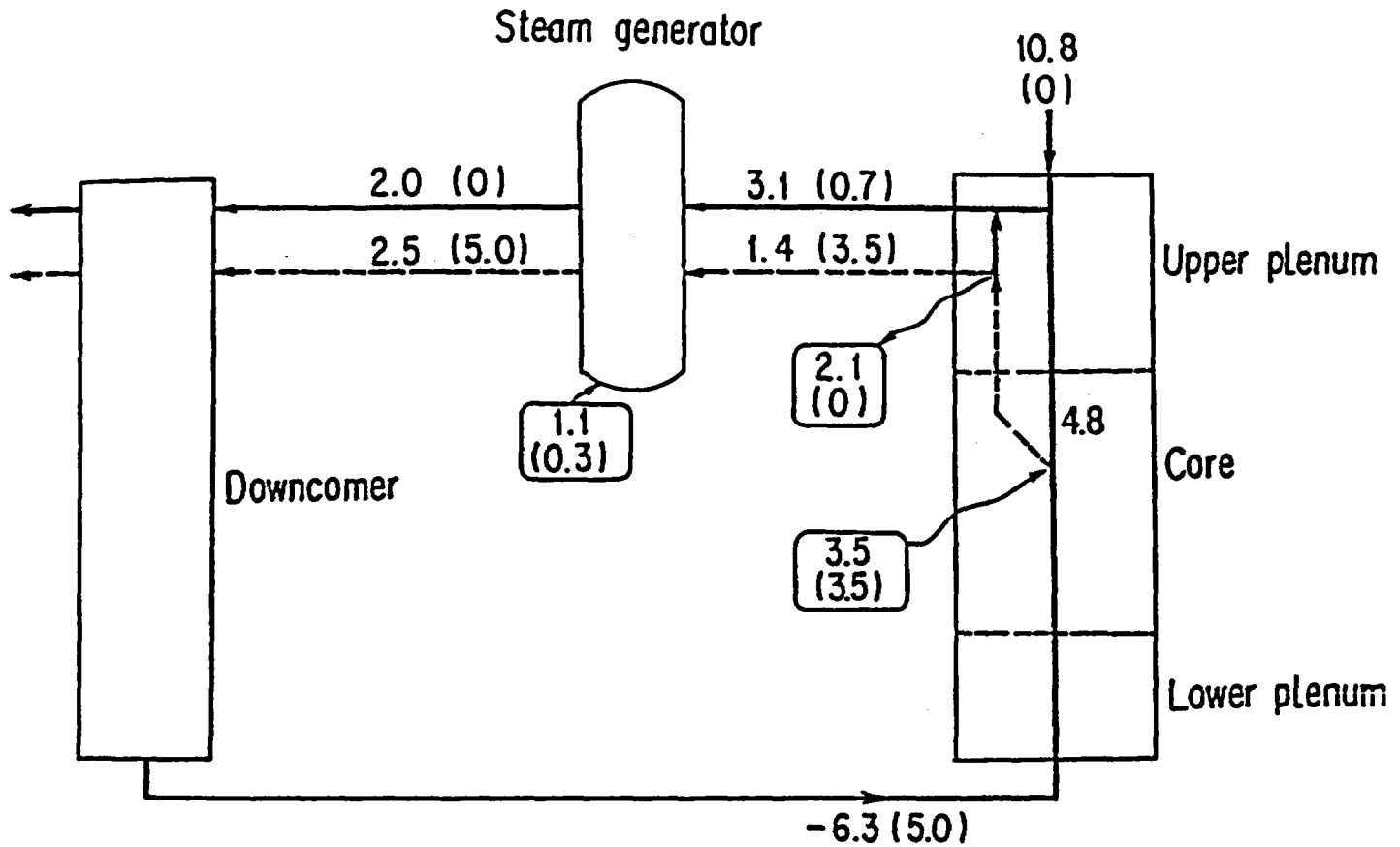


Fig.16 Comparison of core sectional differential pressure



**Notation**

xxxx (kg/s) for Single failure UPI test at 300s~400s

(yyyy) (kg/s) for Single failure CLI test at 300s~400s

— Water flow

- - - Steam flow

□→ Heat source

□← Heat sink

**Fig.17** Comparison of mass flow rate distributions in system between UPI test and CLI test

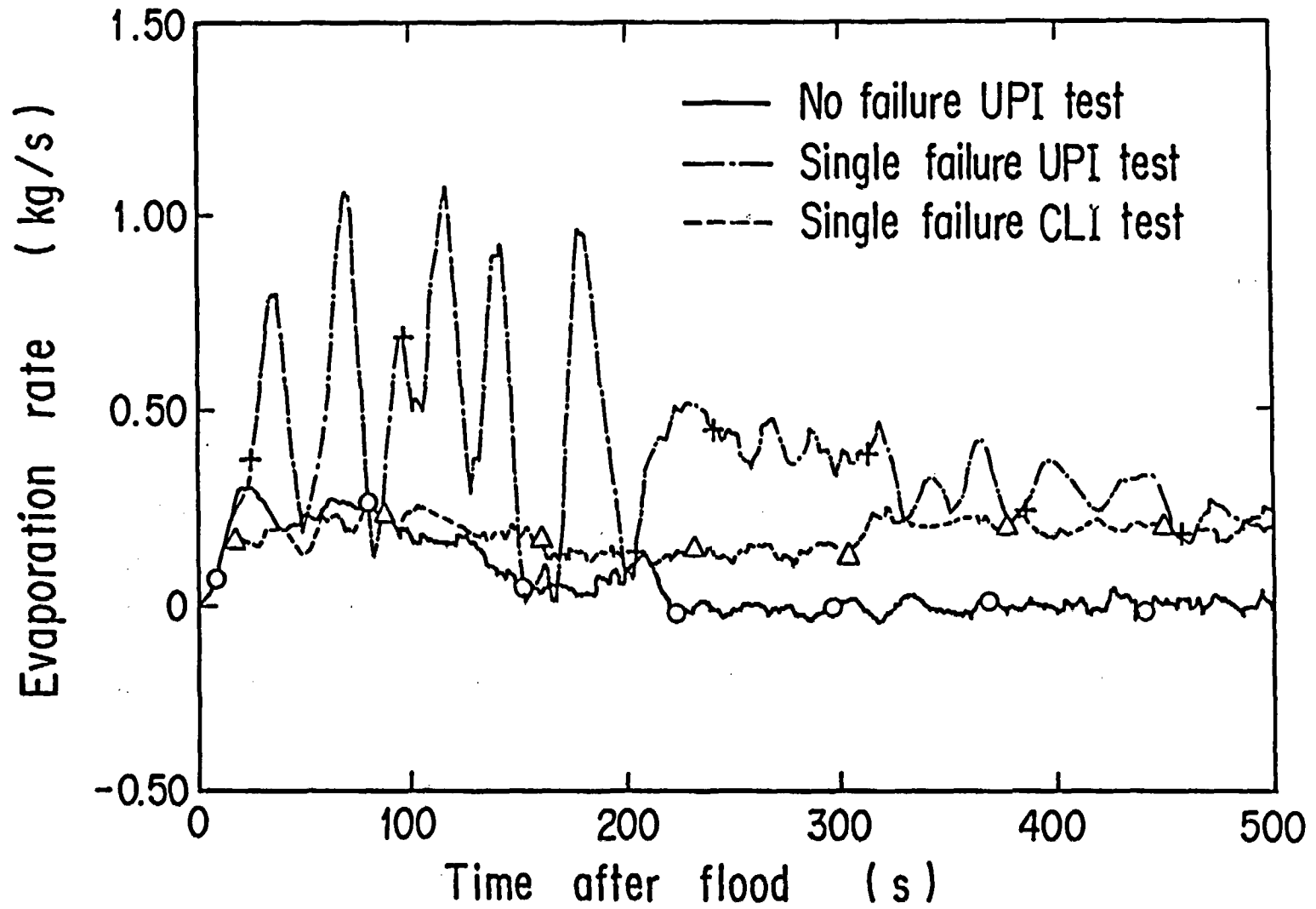


Fig. 18 Comparison of evaporation rate in a steam generator

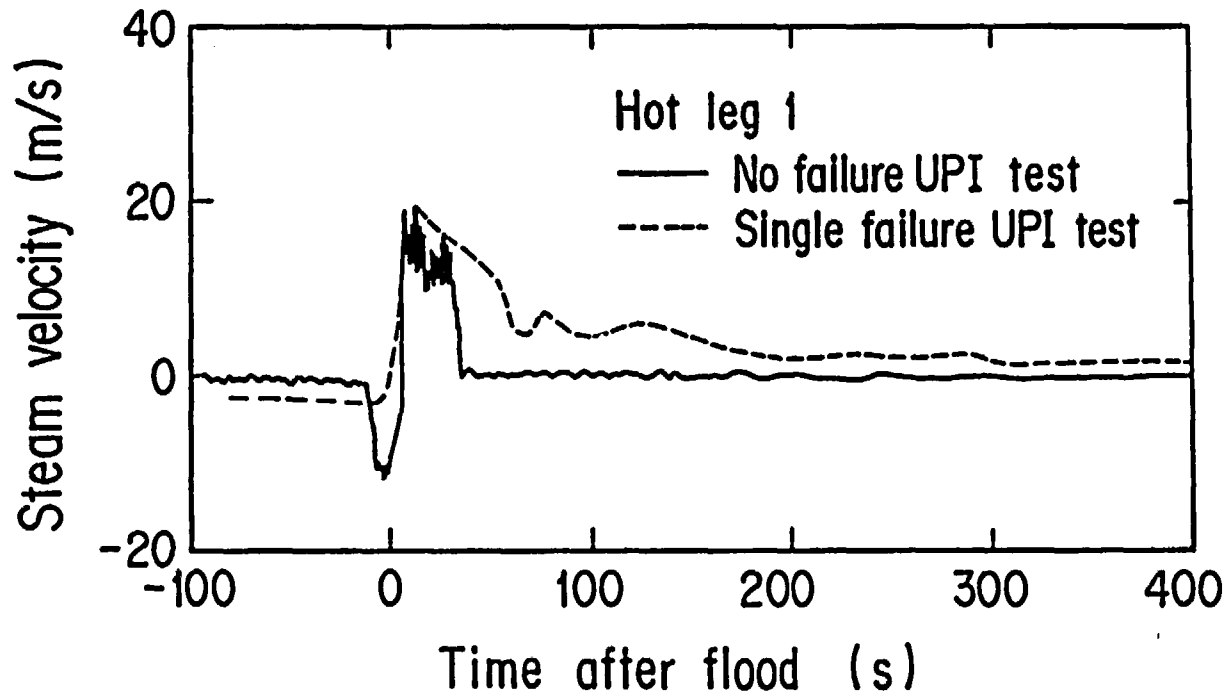


Fig.19 Comparison of Steam velocity in an intact hot let

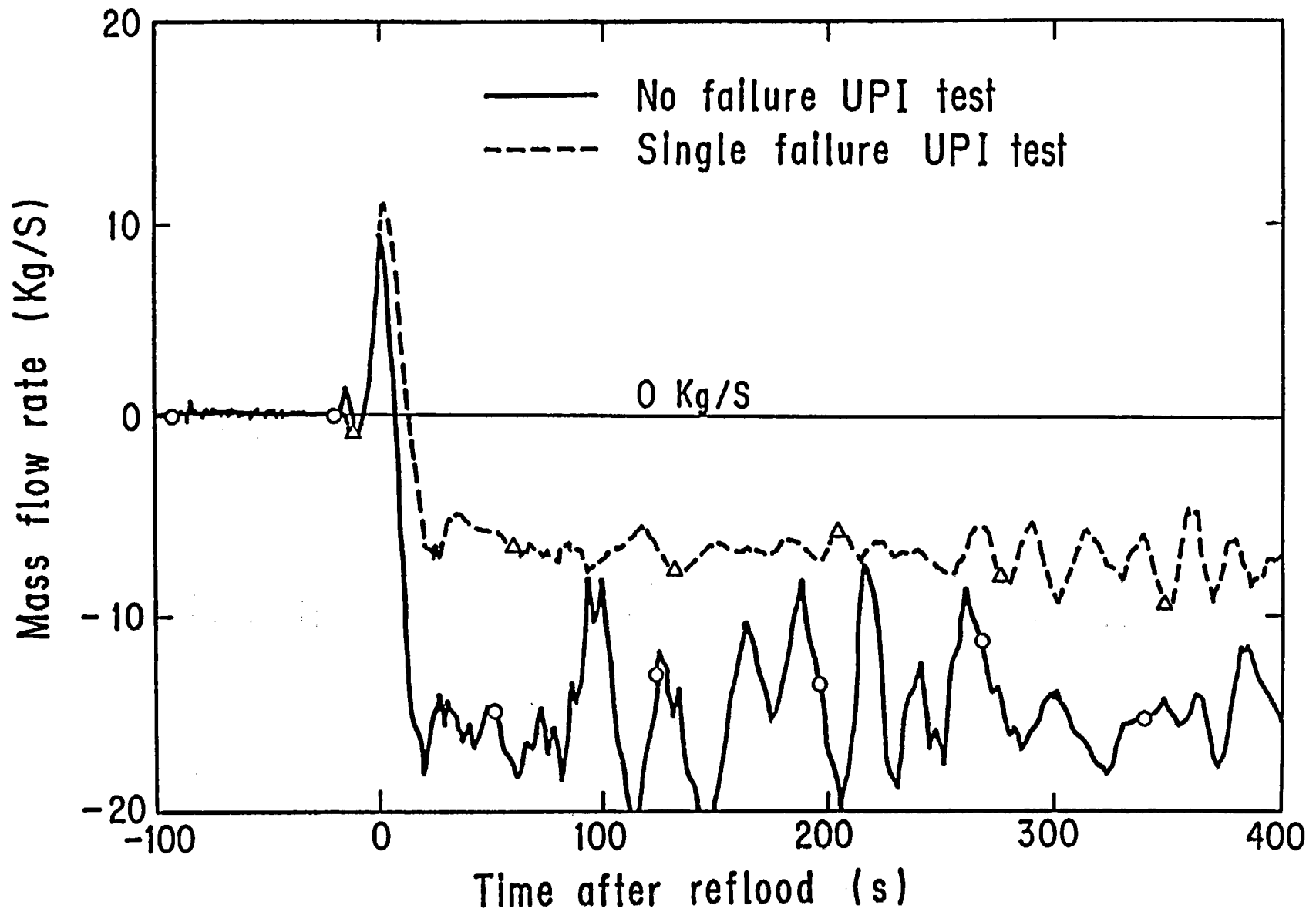
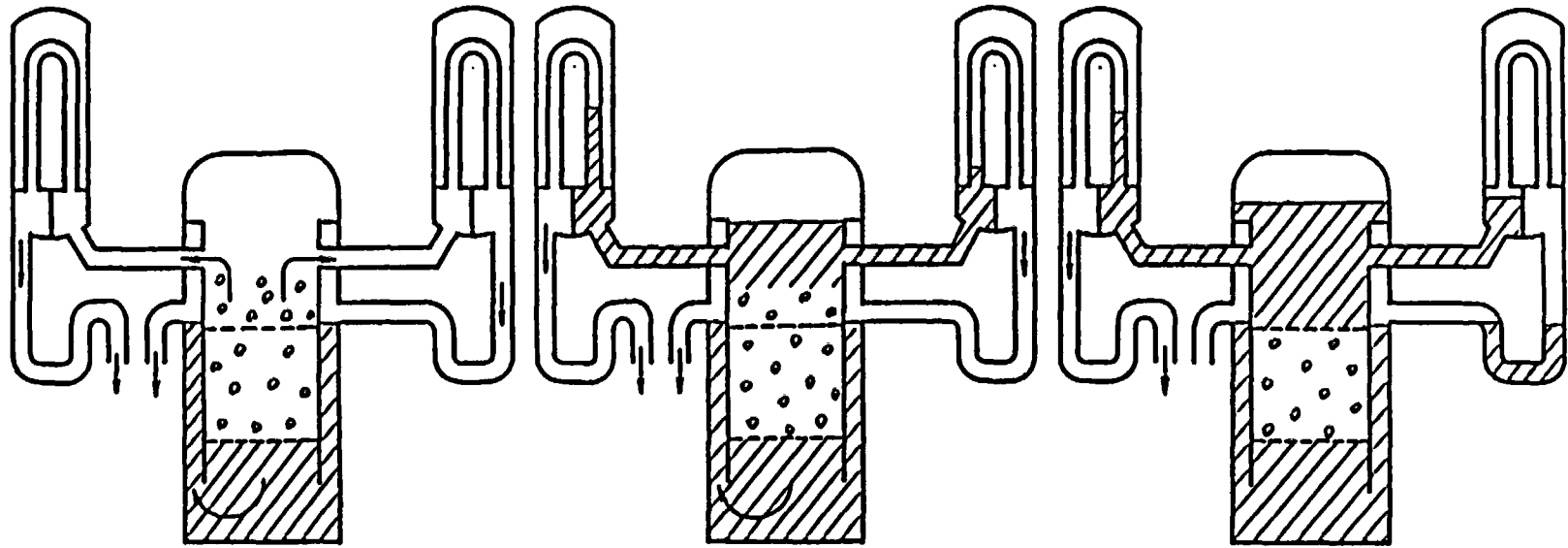


Fig.20 Negative core inlet mass flow rates in UPI tests



(1) No complete condensation  
in upper plenum

(2) Complete condensation  
in upper plenum

(3) Complete condensation  
in upper plenum  
(Blocked intact loops)



Water



Two phase flow

Fig.21

Conceptual hydrodynamic behavior in primary system

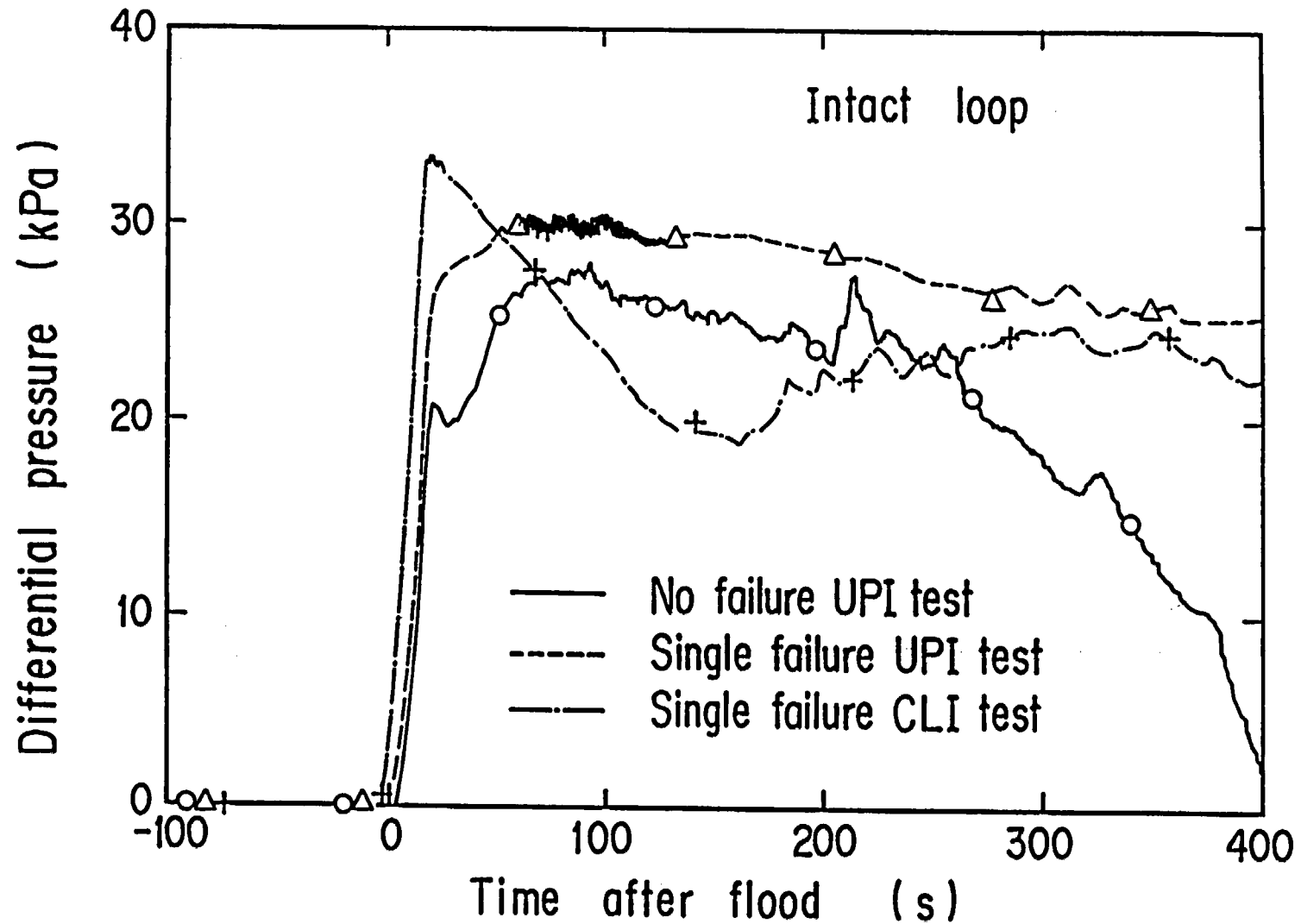


Fig. 22 Comparison of differential pressure across intact loop

## Status of CCTF/SCTF Test Programs

Yoshio MURAO, Hiromichi ADACHI, Tadashi IGUCHI,  
Makoto SOBAJIMA, Kazuharu OKABE, Jun SUGIMOTO,  
Hajime AKIMOTO, Takamichi IWAMURA, Tsutomu OKUBO, Yutaka ABE

Japan Atomic Energy Research Institute

### 1. Introduction

The Cylindrical Core Test Facility (CCTF) and the Slab Core Test Facility (SCTF) are the facilities of the Large Scale Reflood Test Program which was initiated in April, 1976. This program has been built in the 2D/3D project which is performed by USNRC, BMFT and JAERI. The CCTF is designed to model a four-loop 1000MWe PWR with the flow area scaling ratio of 1/21.44 and has a scaled pressure vessel with a full length core and four loops with passive and active components. Using CCTF, the core thermo-hydrodynamic behavior coupled with the system behavior in the primary loops has been investigated for the refill and reflood phases of a PWR-LOCA.

The SCTF is being operated to complement the results from CCTF specially in the field of the multi-dimensional thermo-hydrodynamic behavior in a radially wide core and upper plenum. The SCTF has a full length, full radius and one-bundle depth PWR simulated core which is composed of in-line eight bundles, and has downcomer, upper plenum, lower plenum and simplified loop with passive components.

In this presentation, the following topics are explained;

- (1) CCTF Best Estimate (BE) test,
- (2) CCTF Refill test
- (3) CCTF Multi-dimensional test,
- (4) SCTF Multi-dimensional test and
- (5) Related code development.

### 2. Facility

#### 2.1 CCTF

The CCTF is designed to provide the capability to reasonably simulate the flow conditions in the primary system of a PWR during the refill and reflood phases of a LOCA, and models a four-loop 1000 MWe PWR with the flow area scaling ratio of 1/21.44. It has a scaled pressure vessel with a full height core and four loops with passive and active component simulators, eg. active steam generators, pump simulators and containment tank, as shown in Fig. 1.

The core has about 2000 electrically heated rods arranged in cylindrical configuration, as shown in Fig. 2. Each heated rod is a full-size 15 x 15 - array fuel rod simulator and has an axial power distribution with a peaking factor of 1.4. The core can be subdivided into three regions to achieve a desired radial power profile, as indicated by A, B and C regions in Fig. 2.

The broken hot and cold legs have blowdown valves to simulate the end of blowdown period by quickly opening the valves which function as pressure boundaries.

---

The work was performed under contract with the Atomic Energy Bureau of Science and Technology Agency of Japan.

## 2.2 SCTF

The Slab Core Test Facility (SCTF) is being operated to complement the results from CCTF specially in the field of the multi-dimensional thermo-hydraulic behavior in a radially wide core and upper plenum. SCTF has a full length, full radius and one-bundle depth of a PWR simulated core which is composed of in-line eight bundles and has downcomer, upper and lower plena and simplified primary loop components as shown in Figs. 3 and 4. One full-height hot leg represents all four hot legs in the flow area and connects the upper plenum and a steam water separator. The separator is provided instead of active steam generators. One intact loop with a pump simulator connects the separator and a downcomer and represents 3 loops. The vessel side and the separator side broken cold legs are connected to respective containment tanks. A core bundle has  $16 \times 16$  heater rods including 22 non-heated rods. The upper plenum structure are of a half scaled ones for proper flow simulation as shown in Fig. 4.

## 3. Experimental

### 3.1 CCTF best estimate reflood test

Initial and boundary conditions of this test are based on the best estimate (BE) LOCA analysis by TRAC-PF1 code. On the other hand, test parameters of most of previous CCTF tests including base case test are derived from LOCA analysis by the safety evaluation model (EM). Table 1 compares test conditions of the BE test and the base case of CCTF-II. Parameters of BE test are characterized by its lower power, higher containment pressure, higher ECC flow rate (after ACC period) and lower initial clad temperature than those of the base case.

### 3.2 CCTF refill tests

Refill tests were conducted at CCTF-II to investigate the thermo-hydraulic behavior from the end of blowdown to the bottom of core recovery in large break LOCA. Table 2 shows the test parameters. At each refill test, lower plenum was filled with saturated water to the specified level before the test and the blowdown valves were then opened. Subcooled ECC water was injected into the intact cold legs. The intact loops were closed in Test C2-11 by replacing orifices with blind plates at the pump simulator in order to simulate the direction of the steam flow from the core to the lower plenum. This downward steam flow is expected to occur at the end of blowdown phase of the cold leg large break LOCA.

### 3.3 CCTF multi-dimensional tests

In order to investigate the multi-dimensional effect in CCTF, tests with the flat and steep radial power profiles were performed. Table 3 and Figure 5 show comparisons of test conditions between two test. Both the averaged linear power and the initial stored energy in the core were almost identical in the steep radial power test and the flat radial power test, respectively. When the reflood phase is initiated, therefore, the average clad surface temperatures for all heater rods in the core are

900 and 901 K at the midplane in the steep radial power test and the flat radial power test, respectively.

### 3.4 SCTF multi-dimensional tests

In order to examine the effect of multi-dimensional flow due to radial power distribution, two tests were performed in SCTF. Test S2-SH2 has a radially flat power profile whereas Test S2-06 has a radially steep power profile. The normalized radial power is 1.0 for Bundle 1, 2, 5 and 6, 1.2 for Bundle 3 and 4, and 0.8 for Bundle 7 and 8. Total power in both tests was 7.12 MW at the reflood initiation (time: 0 second) and was decreased afterward to simulate the decay heat.

Coolant was injected into the lower plenum for the accumulator injection period of 55 seconds at the rate of 19.3 kg/s and the injection port was switched from the lower plenum to the cold leg for the low pressure injection period at the rate of 5.4 kg/s. Each coolant temperature was 363 K and 350K, respectively. The containment pressure was kept almost constant at 0.2 MPa.

## 4. Test result

### 4.1 CCTF BE test

Figure 6 shows the clad temperature transient of the central bundle at various elevations. Peak clad temperature of this test (648 K) was much lower than one of the base case test (1132 K), whereas short re-dryout was observed after the first core quench. Quench times at various elevations are compared in Fig. 7 (second quench of BE test is neglected in this figure) and it is found that the quench at BE test occurred earlier than one of the base case test at each elevation and also that the quench propagation from the top of the core are clearly observed at the higher elevation than 2.44 m of BE test.

Figure 8 shows the oscillatory behavior of the differential pressures of the core, upper plenum and the intact loop (between upper plenum and the top of the downcomer). Such oscillation was not observed in the base case test.

The re-dryout of the core of BE test shown in Fig. 6 occurred at about 140 s. At the time, the core water inventory, shown in core differential pressure (dp), decreased with the increase of the intact loop pressure loss. The mechanism of this oscillation is estimated as follows:

Water accumulated in the upper plenum overflowed to the hot leg and entered into the heat transfer tube of the steam generator (SG). Then the water was evaporated by the heat from the SG secondary side and the evaporation caused the increase of the intact loop dp that reduced the water inventory of core due to steam binding effect. Decrease of the CORE water inventory terminated the overflow to the hot leg and decreased the loop dp. Then the increase of core water inventory and also the water accumulation in the upper plenum were considered to be initiated again. This hydraulic oscillation of the BE test disappeared when ECC flow rate was reduced at about 160 sec. Reduction of ECC flow rate also terminated the complete condensation of steam flow in the intact cold legs.

This termination of the complete condensation was considered to the potential cause on the disappearance of the hydraulic oscillation. However, the detailed mechanism should be studied in future.

## 4.2 CCTF refill tests

Figure 9 shows the pressure transient of the upper plenum and containment. High depressurization rate continued after the blowdown valves opened, depressurization rate decreased and then pressure became a steady state. Pressure of the upper plenum increased again after 30 seconds in the test C2-14 (0.5 m initial water inventory) because the reflood phase of heated core was simulated in this test and the steam was generated in the core after the bottom of core recovery (BOCREC). Pressure difference between containment and the upper plenum in the later period of test C2-11 (2.0 m) was caused by the mechanical seal at the pump orifice and the water seal in the lower plenum after the refill period.

Start times of ECC injection are also shown in Fig. 9, and it is found that the depressurization is not so influenced by subcool water injection.

Figure 10 shows the differential pressure of the lower plenum that corresponds to the water inventory. In each test, the saturated water in the lower plenum flashed due to depressurization and the two phase mixture swelled into the downcomer. When the depressurization rate became lower, two phase mixture collapsed and then refill of the lower plenum was initiated. Succeedingly, when the depressurization and the pressure difference between the pressure vessel and containment continued, counter current flow condition (ascending steam flow and falling water) was observed in the downcomer. And then, complete penetration of ECC water into the lower plenum continued until the initiation of the reflooding of the core.

At the test C2-2 (2.0 m) and C2-11 (2.0 m), swelling of two phase mixture into the downcomer continued for rather long time and during this period, ECC water was carried to the break point by the swelled two phase mixture, in other words, ECC water bypass was continued. On the other hand, early initiation of the refill was observed at test C2-14 (0.5 m) because its initial water inventory in the lower plenum was small. The initial rapid decrease of water inventory at C2-11 (2.0 m) was caused by the loop mechanical seal at pump orifices which prevented the expanded steam release through loops, but suppressed the mixture level to the lower level than the core barrel.

Figure 11 shows the fluid temperature of the lower plenum and it is found that the subcool water appear after the complete ECC water penetration except C2-2 (2.0 m) in which ECC flow rate at later period was much lower than the others.

In these CCTF refill tests, ECC water bypass due to swelling of two phase mixture, and succeeding refill behavior was clearly observed, and these results will be applied for the improvement of the best estimate code in future.

## 4.3 CCTF Multi-dimensional tests

Figure 12 shows comparisons of the core inlet mass flow, pressure and subcooling between the flat and steep radial power tests. The core inlet mass flow was estimated using the mass balance relation in the pressure vessel. The error of the mass flow rate was estimated within  $\pm 15\%$ . It is found that the radial power profile in the core has weak effect on the net flow through the core inlet. For the core inlet pressure and subcooling, no significant discrepancy is observed between two tests.

Figure 13 shows quench envelopes in the flat and steep radial power test. The quench front propagates one-dimensionally in the flat radial power test. On the other hand, the quench front in the central region propagates slower than that in the peripheral region due to higher initial temperature and supplied power. The result shows that the radial power effect still exist inside the core although the radial power profile has weak effect on the thermal hydraulic behavior in the primary system beside core.

Figure 14 shows the averaged heat transfer coefficient at the midplane in the central, intermediate and peripheral regions from the flat and steep radial power tests. In the flat radial power test, the heat transfer coefficient in the central region is slightly higher than that in the peripheral region between 20 and 150 seconds. The difference of the heat transfer coefficient may be attributed to the wall effect in the periphery of the core and/or the nonuniform condition at the boundary between the core and the upper plenum.

Although some slight multi-dimensional effect was observed in the flat radial power test, more clear difference is observed in the steep radial power test as shown in Fig. 14. The heat transfer coefficient in the central region is 25 % higher at 100 s than that in the peripheral region. The difference should be caused by the radial power profile itself and/or the profile of the clad temperature in a horizontal cross section. The heat transfer coefficient in the central (high power) region was higher at the other elevations than that in the peripheral (low power) region. These results indicate that the core cooling is enhanced in the high power region of the core with the steep radial power profile.

#### 4.4 SCTF multi-dimensional test

The isobar of every 0.5 kPa step is indicated in Fig. 15. The figure shows the nonuniformity in void fraction since the difference of the gaps between two adjacent contours means the difference of the fluid density. The fluid density in the peripheral bundle (Bundle 8) is lower than the central bundle (Bundle 1). In the upper part of the core, the pressure in the peripheral bundle is higher than that in the central bundle at the same elevation. The pressure distribution is considered to strongly depend on the radial pressure distribution at the top of the core which is related to the radial distribution of water accumulation in the upper plenum. Therefore the figure shows the more water accumulation in the periphery.

The distortion of the isobars in Fig. 15 show that the fluid in the upper part of the core does not flow strictly upward but drift to the left side (opposit side of the hot leg) of the tie plate.

Judging from the more water accumulation in the periphery even for the flat radial power test with similar magnitude to those for the steep radial power test, the water accumulation is supposed to be affected by an asymmetric fluid flow in the upper plenum, since the hot leg is connected to a peripheral side of the upper plenum. Observations through view windows exhibit recirculation flow in the upper plenum. The flow is considered to be accelerated by the falling fluid near the periphery which is caused by the de-entrainment of water droplets near the hot leg and by the reflux water from the steam generators through the hot leg.

The quench propagation in each bundle is not identical as shown in Fig. 16 even in the flat radial power test in the later period of the transient (after 300 seconds). This is attributed to poorer heat

transfer due to less water accumulation and the drift of the fluid flow which causes reduction of the mass flow rate in the upper part of the core. In the case of the steep radial power test, the effect of the slower quench propagation in higher power bundle is superimposed on the effect mentioned above.

Heat transfer coefficients (HTCs) were evaluated and indicated in Fig. 17 for the two tests. The difference of HTCs among three bundles for the flat radial power test is small whereas the HTC for high power bundle (Bundle 4) is higher and the HTC for low power bundle (Bundle 8) is lower. This fact suggests the improvement of HTC due to a secondary flow caused by the radial power profile. Actually the measurement of horizontal differential pressure indicates larger gradient of pressure and hence an existence of a secondary flow for the steep radial power test.

In order to evaluate the effect of the improvement in the heat transfer due to the potential secondary flow, compared are two clad surface temperatures calculated with HTC histories obtained in the flat and steep radial power tests. The difference of the turnaround temperature (peak temperature) shows the increase of the safety margin expected in the analysis in consideration with the secondary flow due to the radial power profile. It can be concluded that the expected increase of the safety margin is the order of 100 K.

Further study on the secondary flow effect will be continued to explain the mechanism of the enhancement of the core heat transfer.

## 5. Related code development

The REFLA code is best estimate (BE) oriented code for the refill and reflood phase analysis. JAERI is performing the verification of the REFLA code and the development of necessary models, based on the CCTF/SCTF results. The applicability of the REFLA code to the reflood phase analysis under the evaluation model (EM) conditions has been confirmed and the result was presented at the last WRSRI meeting. Recently, the applicability of the REFLA code to the reflood phase analysis under the BE conditions has been studied and the local power effect model installed in the code has been studied.

### 5.1 Reflood phase analysis under BE conditions

REFLA code predictions for the core thermo-hydrodynamics of the BE and the base case tests were conducted. The core inlet boundary conditions were taken from the CCTF experimental data. Figure 19 shows the comparison about the quench envelopes. The good agreements between the data and the prediction are obtained.

Good agreement of clad temperature histories between REFLA code prediction and the measured indicated its predictability under BE condition. However, it did not predict a re-dryout of the core.

Improvement of REFLA-system model about the two phase flow in the loop and the heat transfer at SG is required for the quantitative prediction of the hydraulic oscillation causing the re-dryout of the core.

## 5.2 Local power effect model

A radial peaking factor of typical initial loading core is 1.15 and the typical maximum radial peaking factor for the safety evaluation is 1.55.

The REFLA local power effect model, which was developed based on the CCTF thermally asymmetric tests (C1-17 and C1-20), was applied to CCTF tests with various radial peaking factors. The model treats  $U_g$ ,  $U_l$ ,  $T_g$ ,  $T_l$  and  $\alpha$  on the average of the core and treats  $Z_q$ ,  $h$  and  $T_w$  with the local value depend on the local power. ( $U_g$ ,  $U_l$ : Steam and water velocities,  $T_g$ ,  $T_l$ : Steam and water temperatures,  $\alpha$ : void fraction,  $Z_q$ : quench front elevation,  $T_w$ : clad temperature)

Figures 20 and 21 show the comparison of the clad temperature transients between the CCTF data and the prediction. Figure 20 is a case of a typical initial loading core (Peaking factor  $F = 1.15$ ), and Figure 21 is a case of a more steep power profile ( $F = 1.28$ ). The prediction is better in a initial loading core case than in a more steep power profile case.

Figure 22 show the comparison of the turnaround temperature between the REFLA prediction and the CCTF results. The predicted turnaround temperature is higher than the measured in the high power region of the core with the steep power profile (EM test). This indicates that the present local power effect model in the REFLA code can conservatively predicts the power profile effect.

## Summary

(1) The thermo-hydrodynamics under the following extended reflood conditions were studied.

(i) Best Estimate (BE) condition

(ii) End of Blowdown (EOB)/Refill condition

It was found in the BE condition that the core quenched rapidly and that hydraulic oscillation with a long period ( $\sim 50$  seconds) occurred. The oscillation caused a short re-rise of the clad temperatures after the first core quench.

It was confirmed in the EOB/Refill condition that ECC water bypass due to swelling of two phase mixture and succeeding refill behavior occurred. The larger initial lower plenum inventory caused a greater delay in refill initiation.

(2) The multi-dimensional effect on reflood phenomena was studied.

It was confirmed that the radially steep power profile of the core enhanced the core cooling.

(3) The reflood analysis code REFLA succeeded in the prediction of the reflood phenomena under BE condition and local power distribution effect.

Table 1 Comparison of test conditions between CCTF BE test and Base case test

Item	BE test	Base case test
Total power	7.12 MW	9.37 MW
Radial power distribution	flat	1.37/1.19/0.76
Containment pressure	0.3 MPa	0.2 MPa
ECC flow rate to cold legs		
0 - 20 sec	324 m <sup>3</sup> /hr	324 m <sup>3</sup> /hr
20 - 160 sec	70 m <sup>3</sup> /hr	40 m <sup>3</sup> /hr
160 sec-	30 m <sup>3</sup> /hr	40 m <sup>3</sup> /hr
Initial clad temperature at the bottom of core recovery	580 K	1060 K

Table 2 Test conditions of CCTF refill tests

Item	C2-2	C2-11	C2-14
Initial system pressure (MPa)	0.53	0.60	0.58
Containment pressure (MPa)	0.20	0.20	0.20
Initial lower plenum water level (m)	2.0	2.0	0.5
Blowdown valve opening time (sec)			
PV side	0	0	0
SG side	10	not used	0
ECC injection			
start time (sec)	6	5	4
flow rate (kg/s)	80	90	90
	10 (after 22 sec)		
water temperature (K)	309	309	309
Loop isolation	No	Yes	No

Table 3 Comparison of test conditions between flat and steep radial power tests

Item	Flat radial power test	Steep radial power test
Total power (MW)	7.11	7.12
Decay curve type	ANS×1.0+Actinide×1.1 (40 s after scram)	ANS×1.0+Actinide×1.1 (40 s after scram)
Radial power profile A : B : C	0.99 : 1.00 : 1.00	1.36 : 1.19 : 0.76
Containment pressure (MPa)	0.20	0.20
Acc flow rate into cold legs (kg/s)	86	84
LPCI flow rate into cold legs (kg/s)	10	10

352

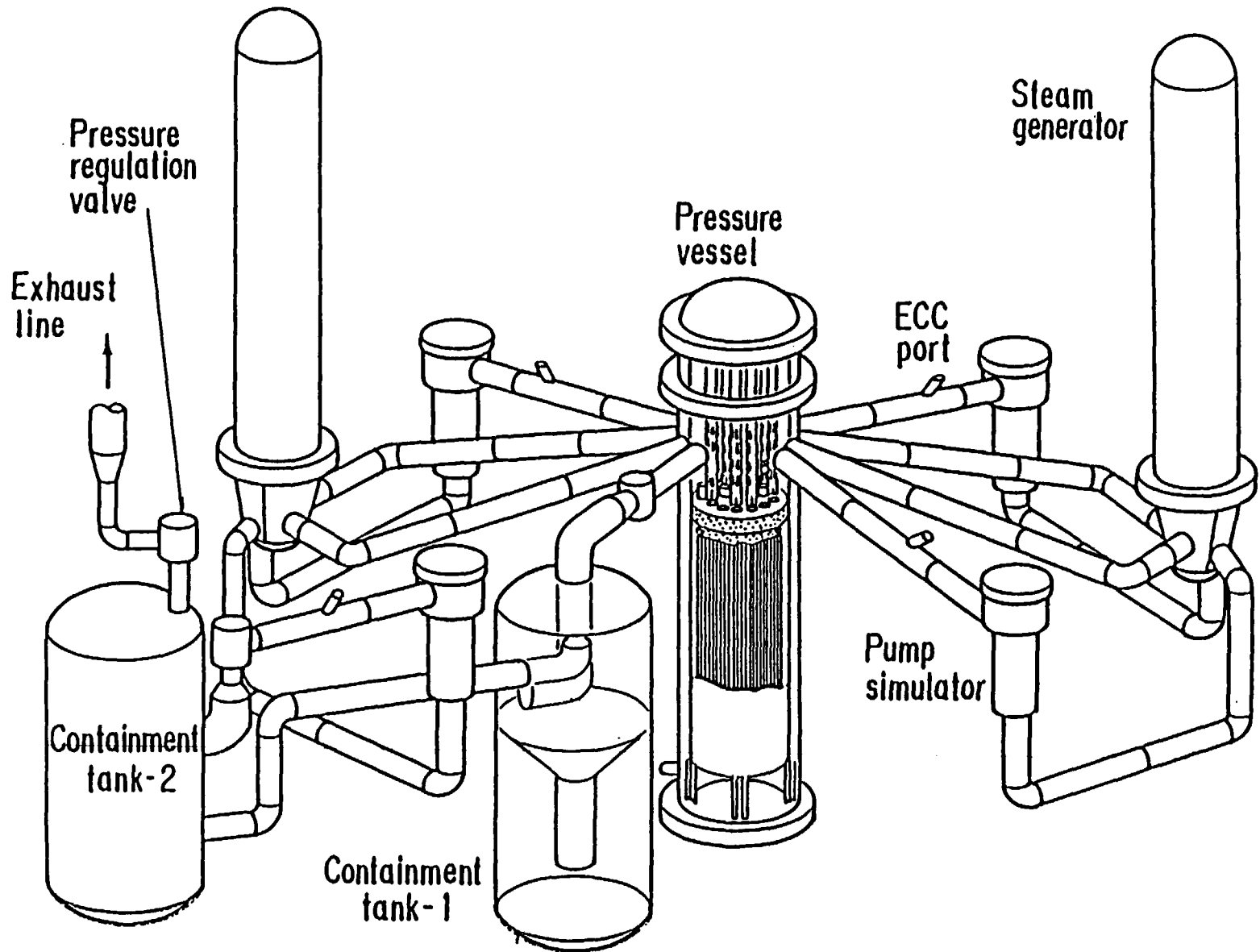


Fig. 1 Bird's-eye view of CCTF

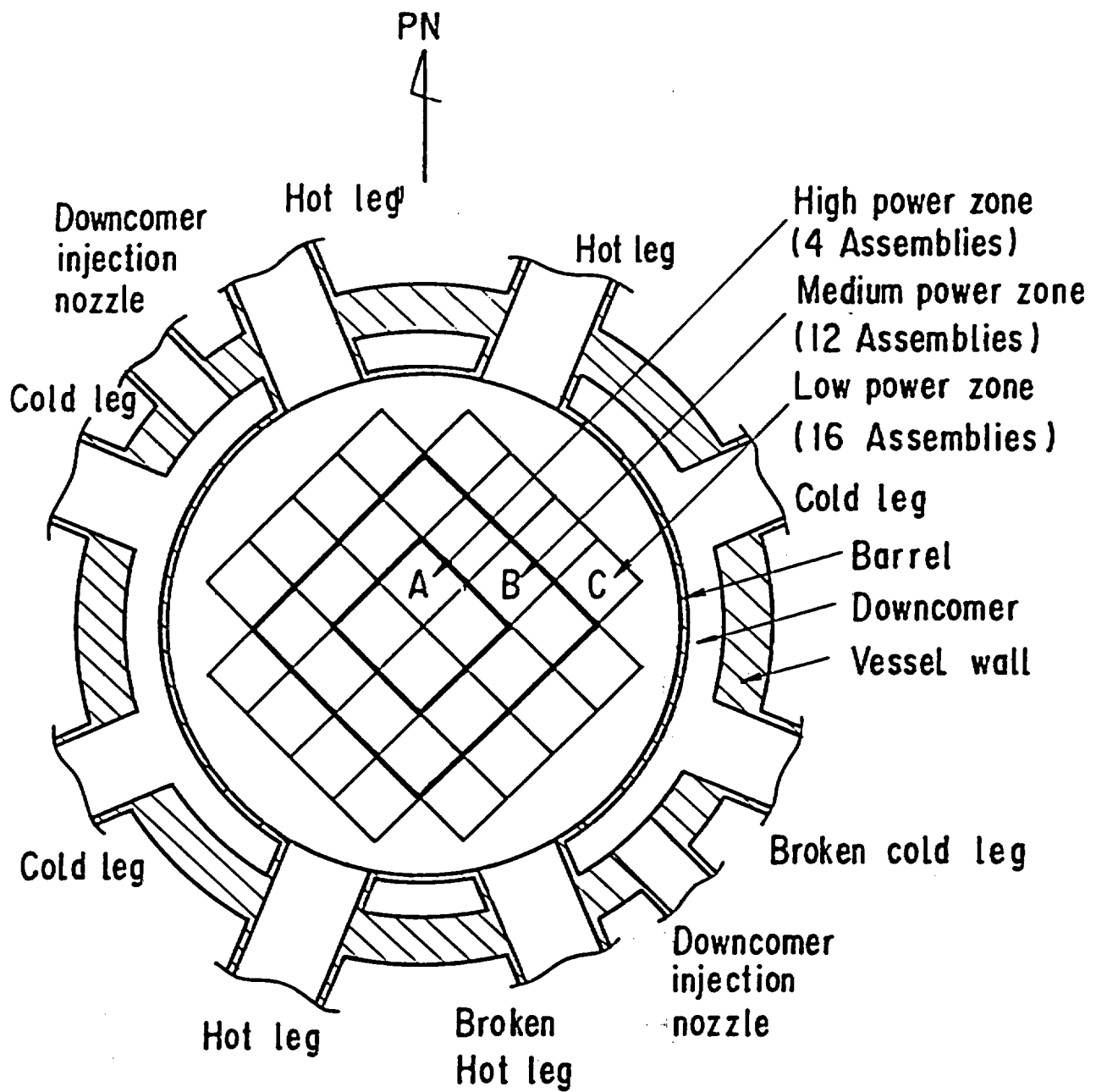


Fig.2 Cross section of CCTE Core-II

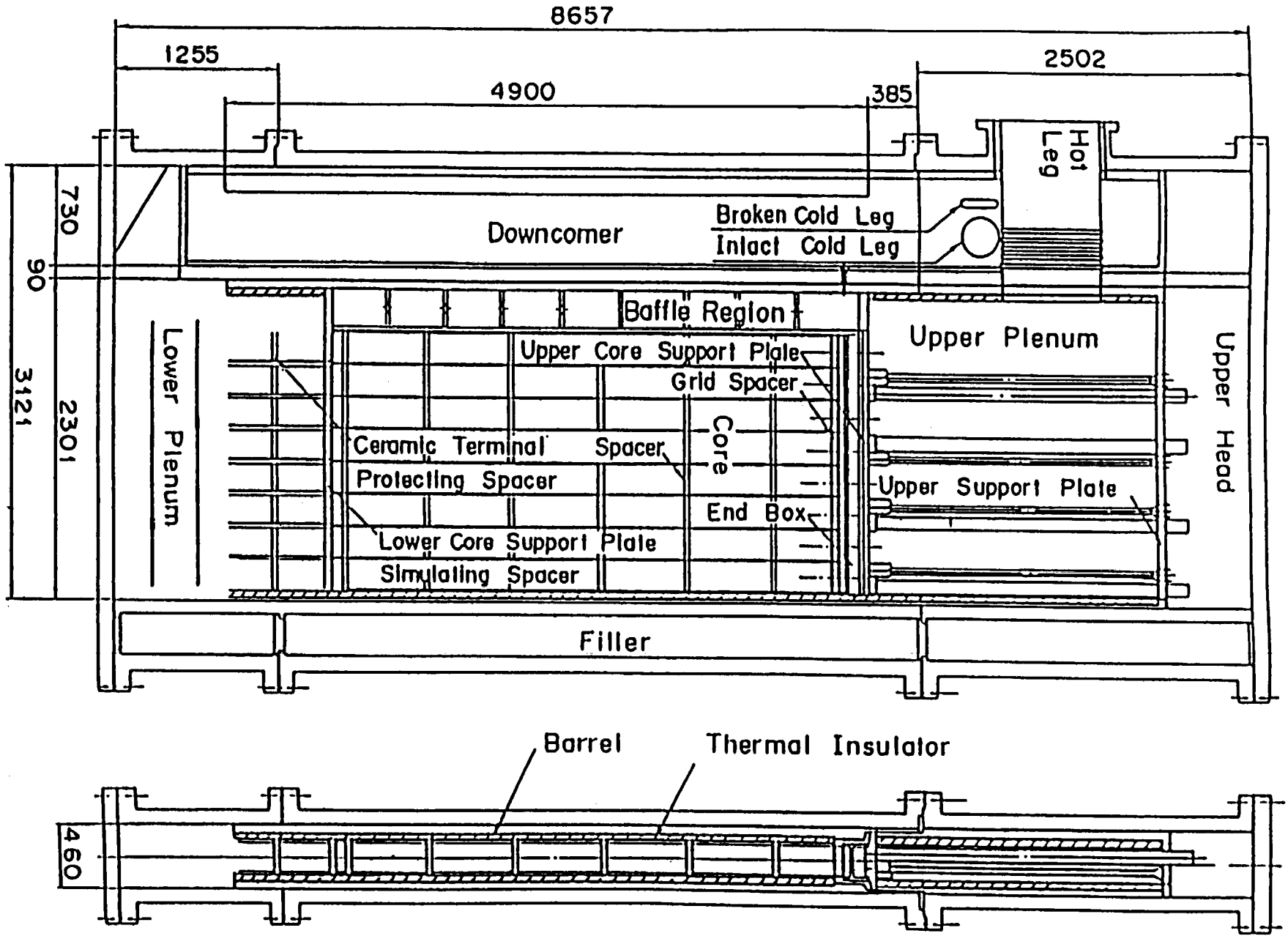


Fig. 3 Vertical Cross Section of the Pressure Vessel

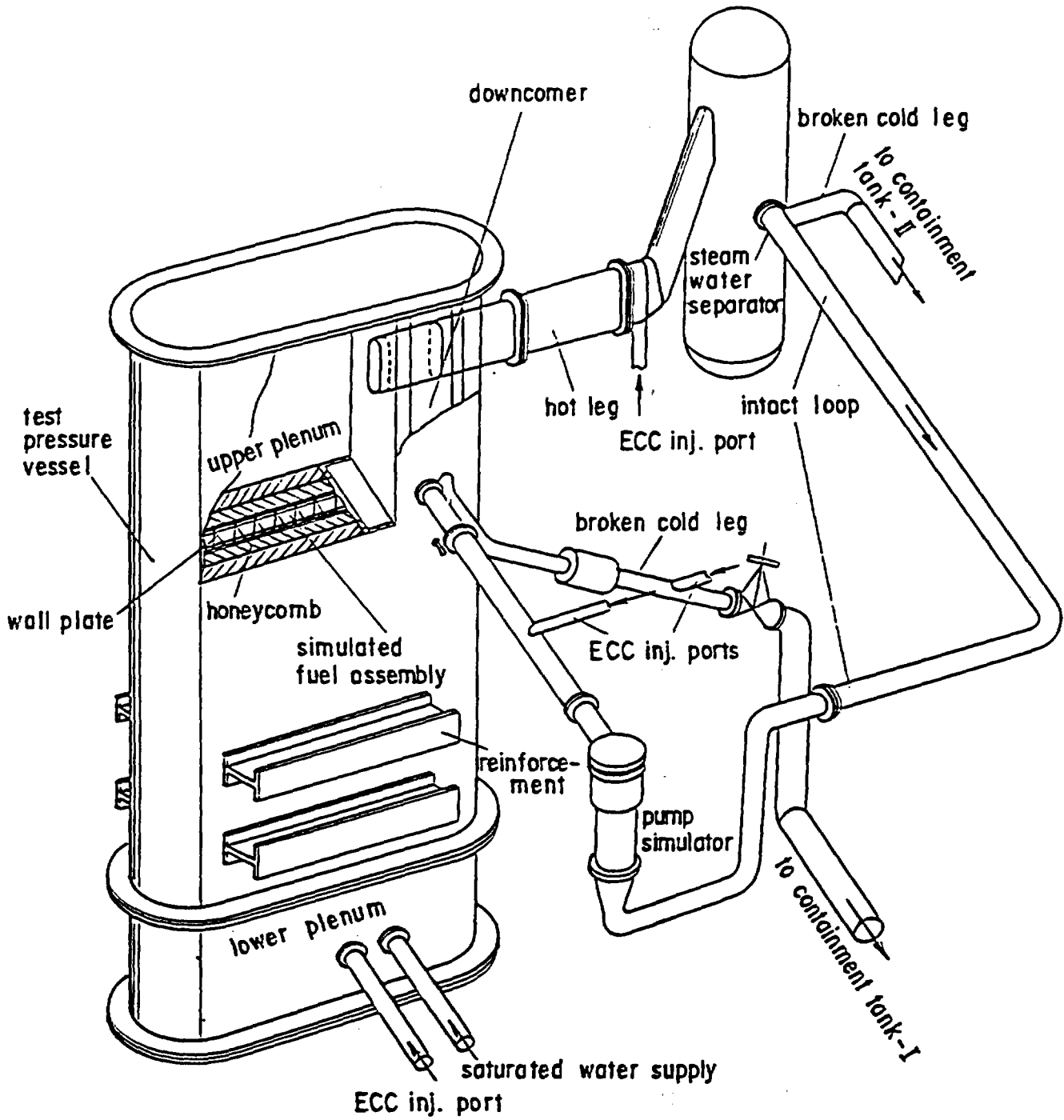
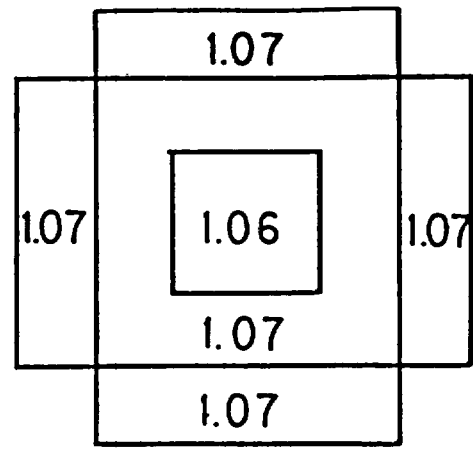
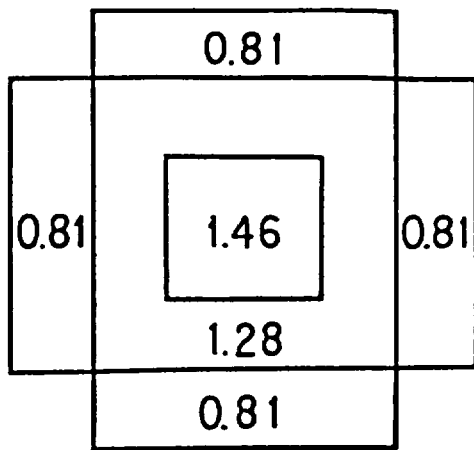


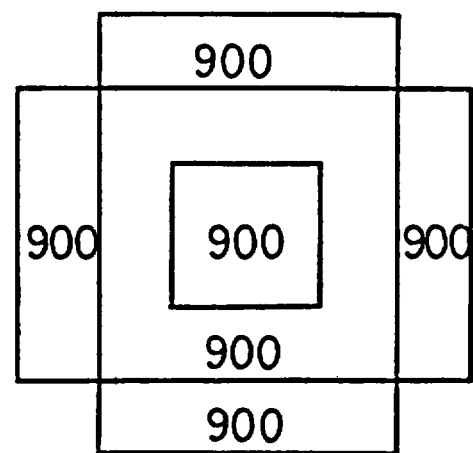
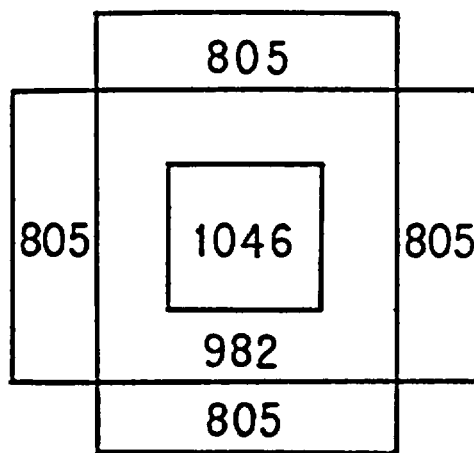
Fig. 4 Artist's View of the SCTF



(1) Steep radial power test

(2) Flat radial power test

(a) Initial Linear power ( in kW/m )



(1) Steep radial power test

(2) Flat radial power test

(b) Initial clad surface temperature  
at midplane of core ( in K )

Fig.5 Comparisons of radial power and temperature profiles at reflood initiation between flat and steep radial power tests

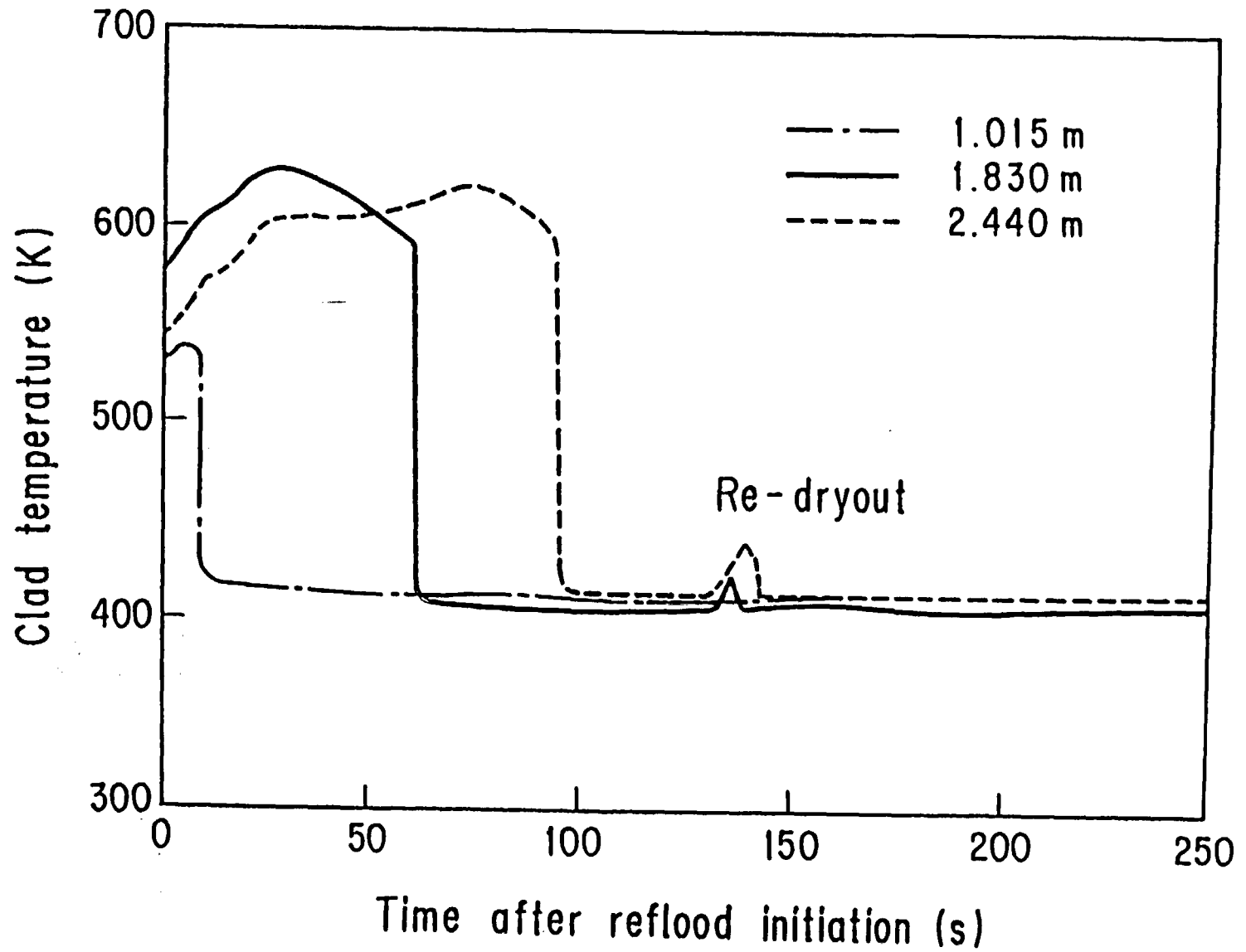


Fig.6 Clad temperature in CCTF BE test

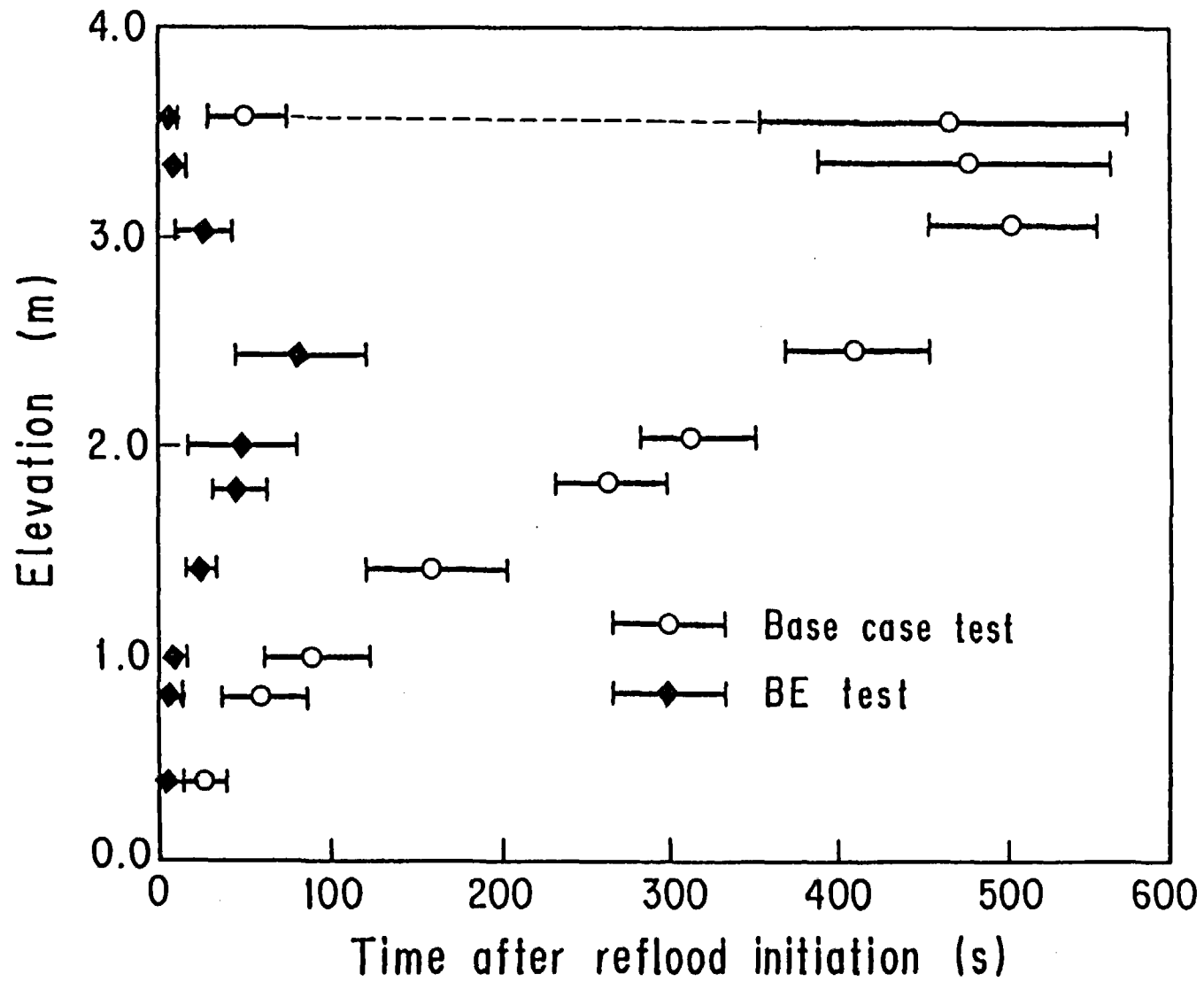


Fig. 7

Comparison of quench front elevation between BE test and base case test

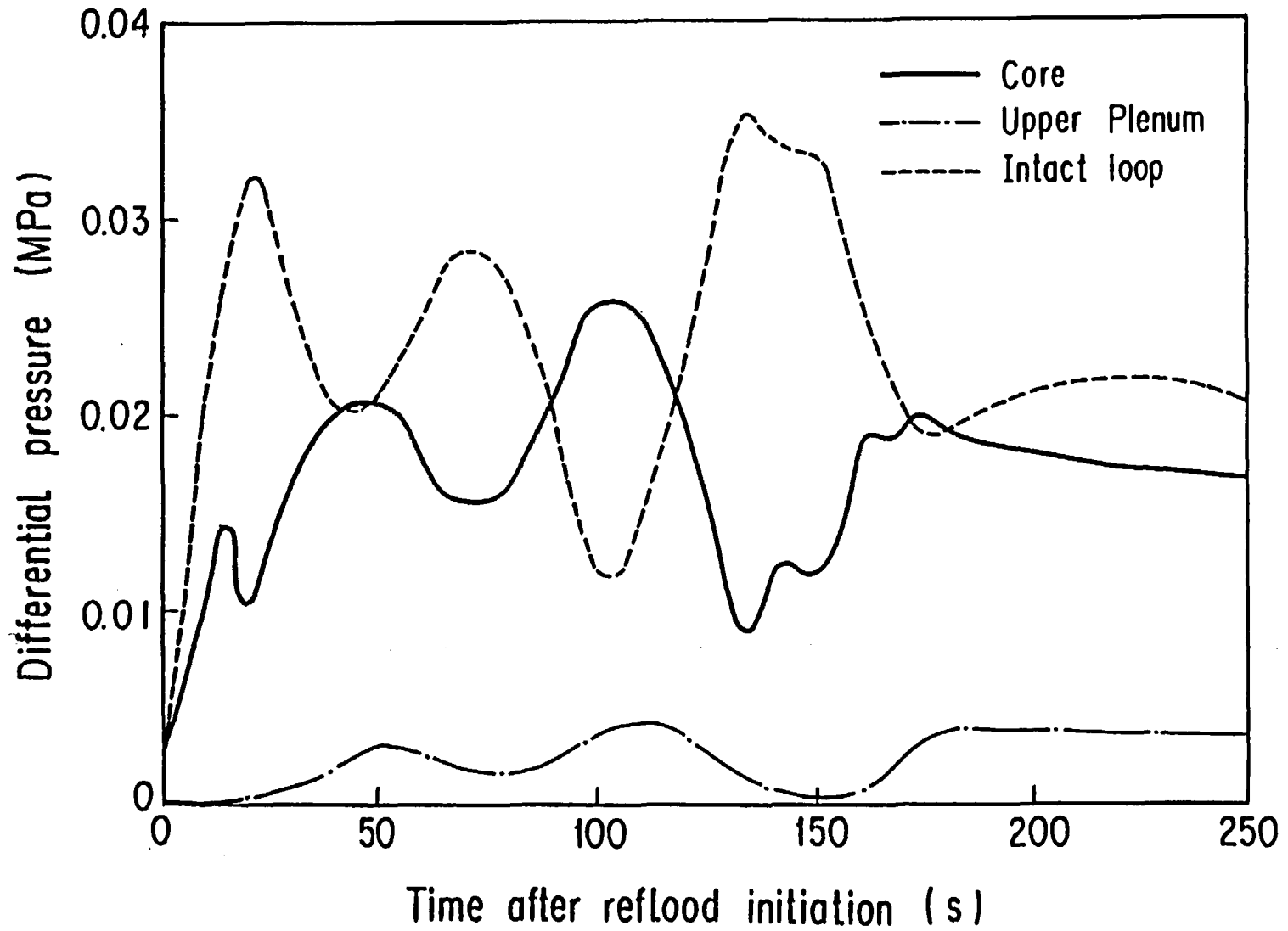


Fig. 8 Oscillatory differential pressure in BE test

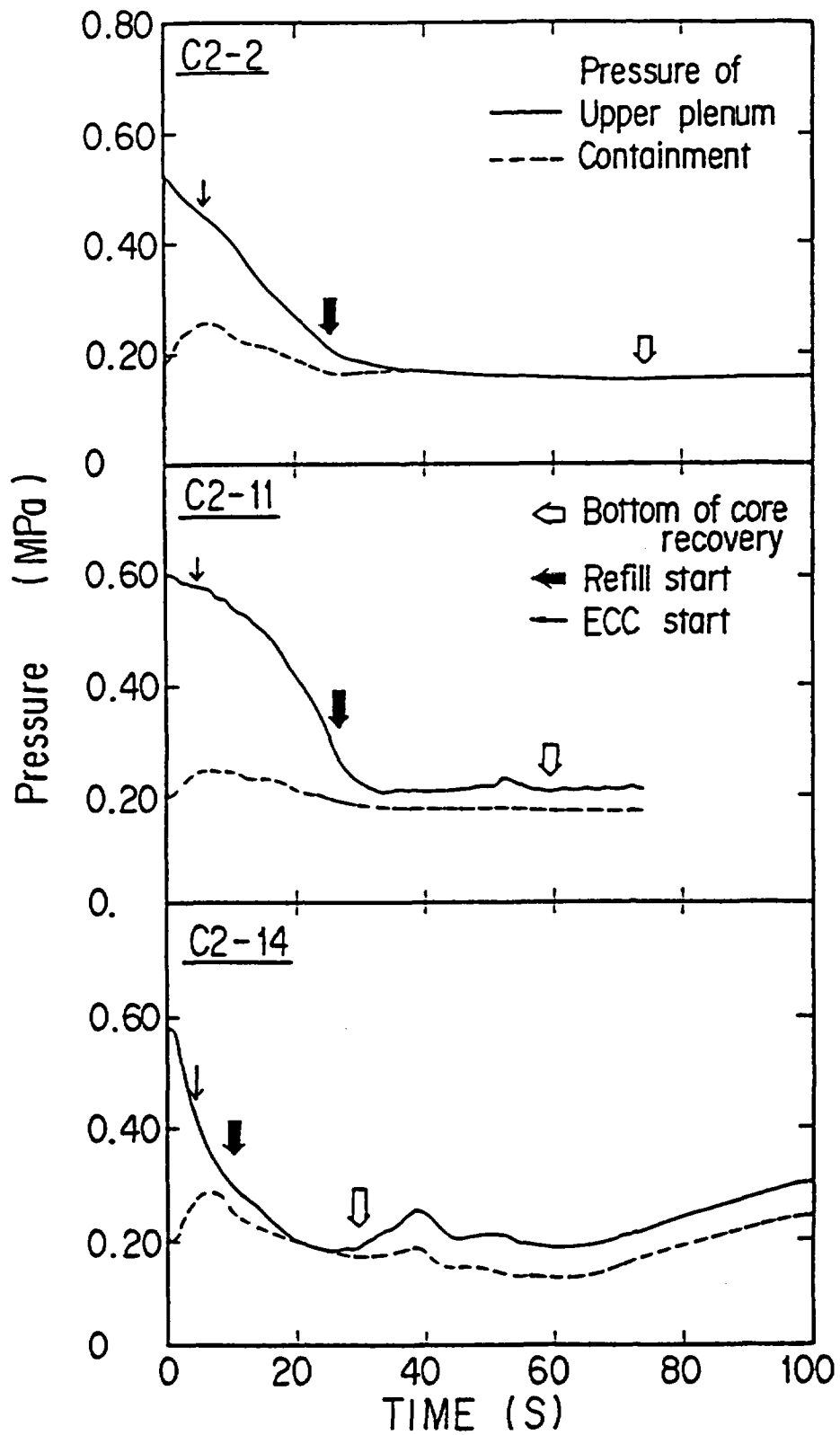


Fig. 9 Comparison of pressure transient in CCTF refill tests

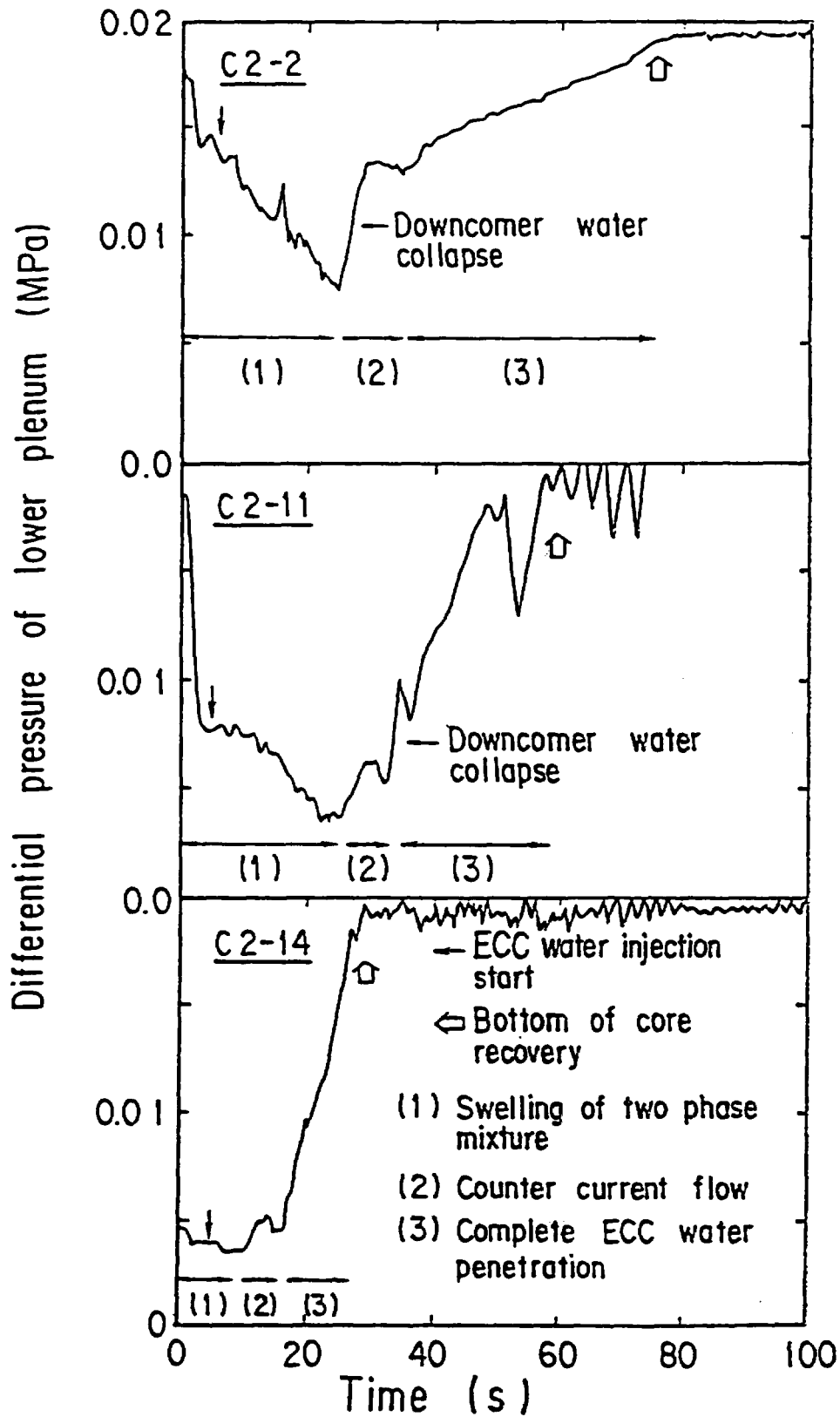


Fig. 10 Comparison of differential pressure in lower plenum in CCTF refill tests

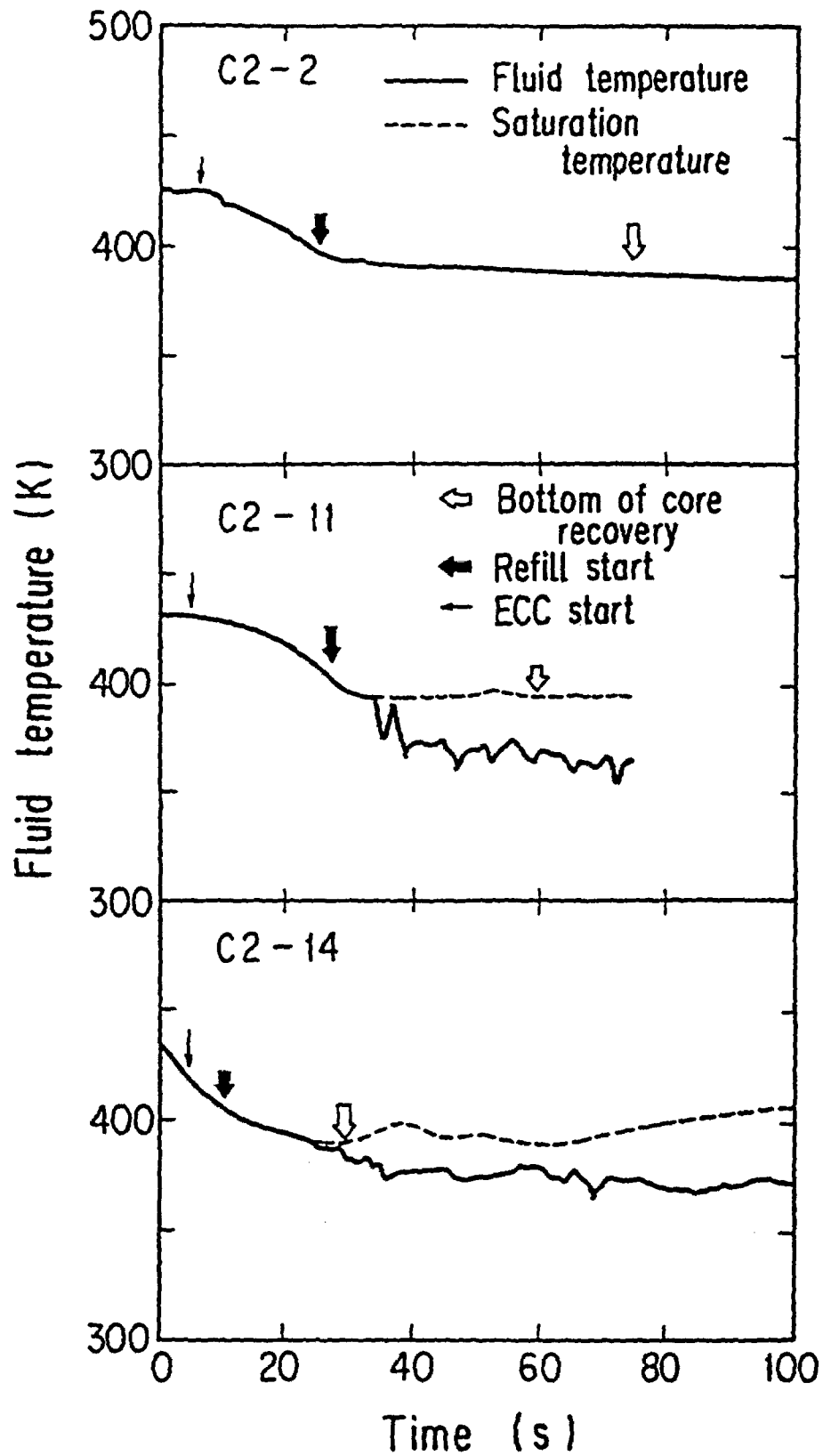


Fig. 11 Transient of fluid temperature in lower plenum

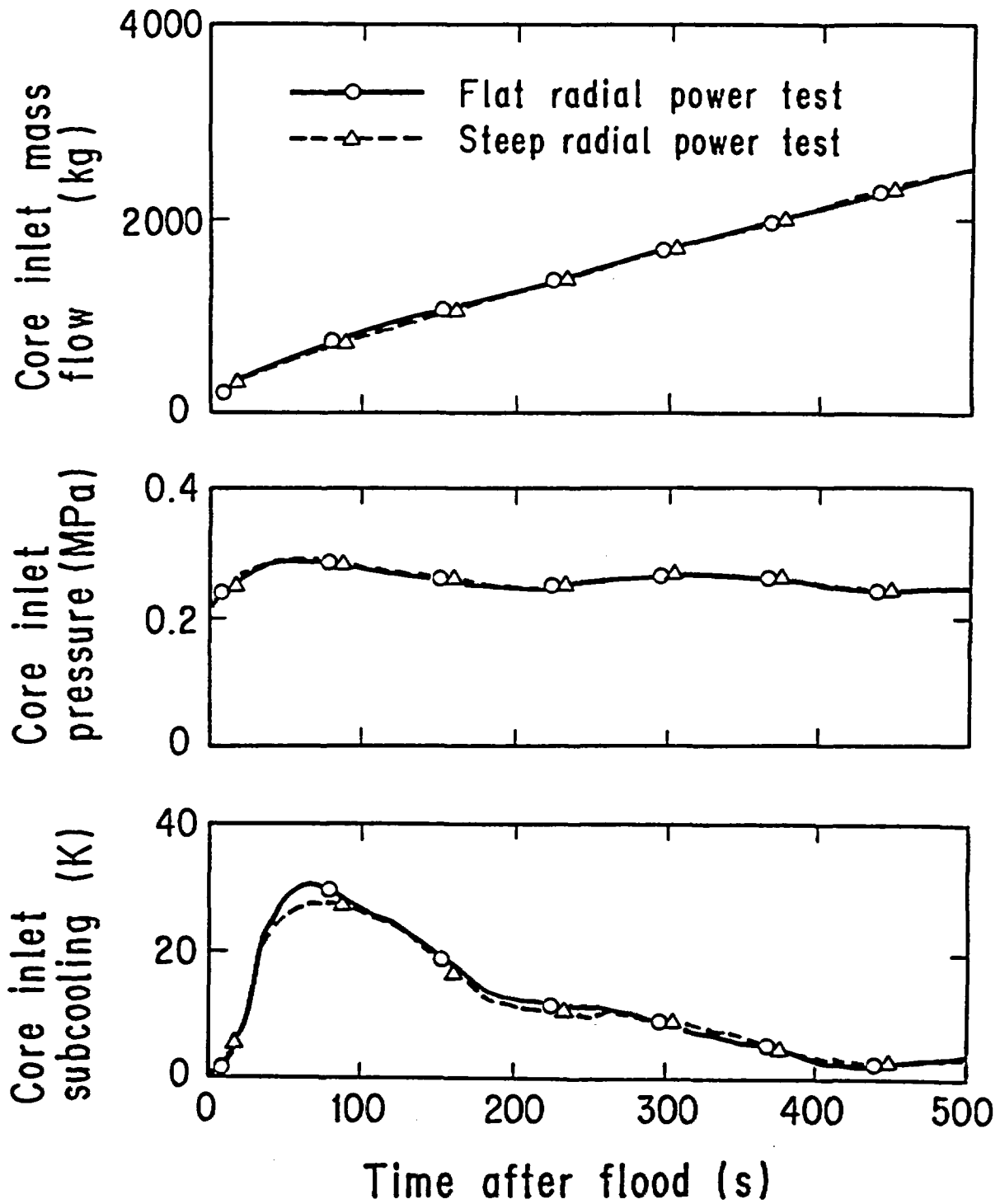
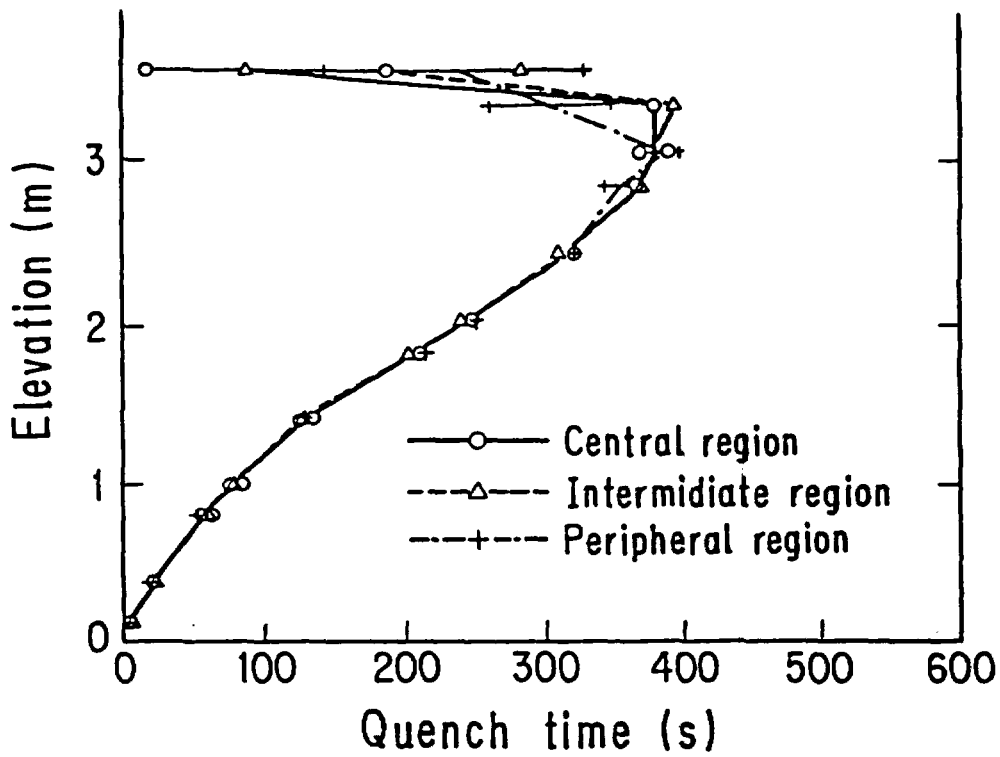
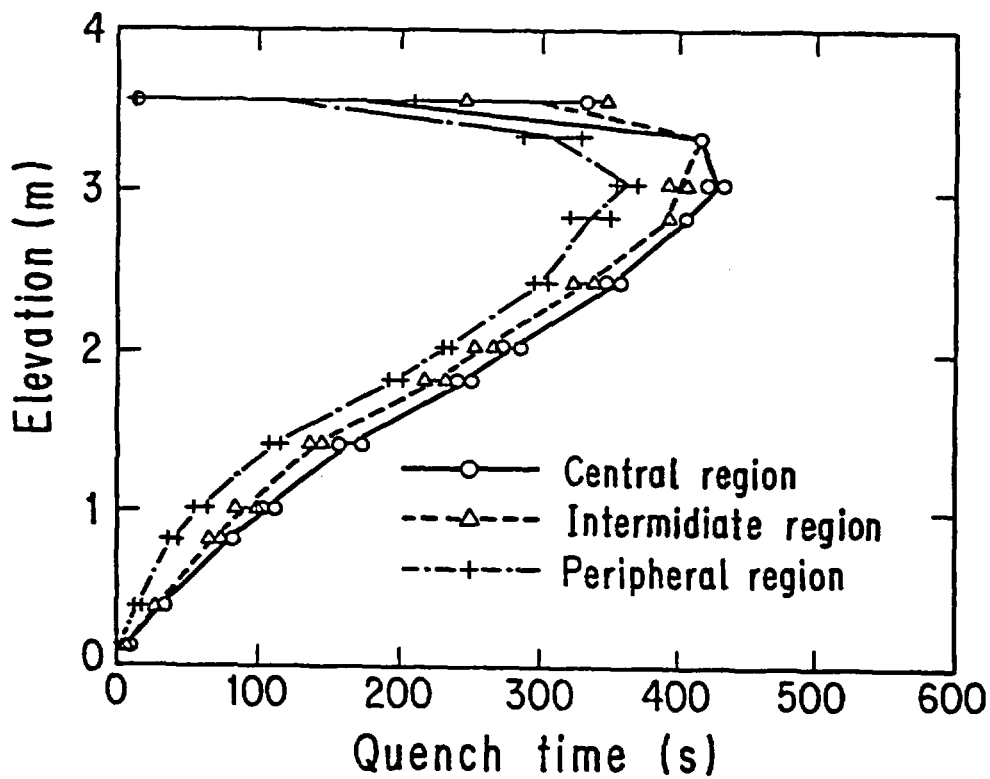


Fig. 12 Comparison of flow variables at core inlet between flat and steep radial power tests



(a) Flat radial power test



(b) Steep radial power test

Fig.13 Comparisons of quench envelopes between flat and steep radial power tests

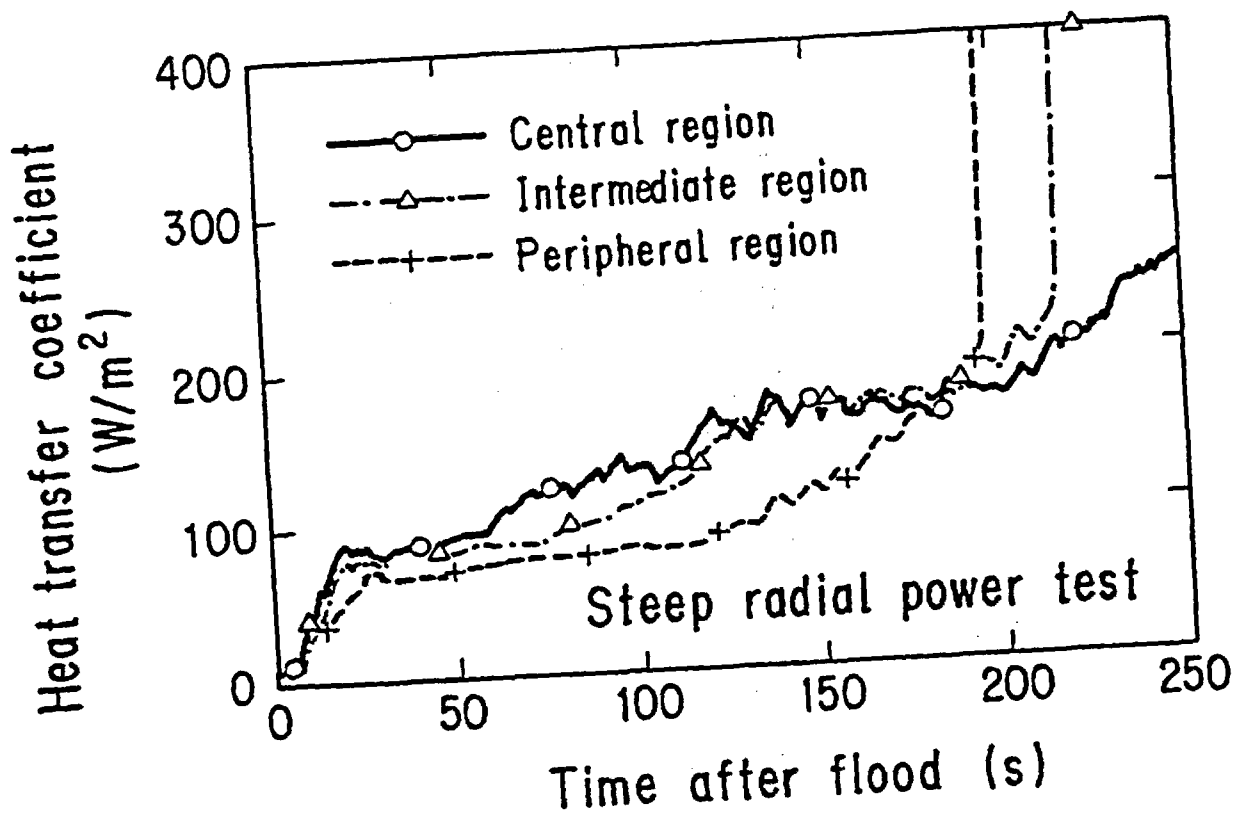
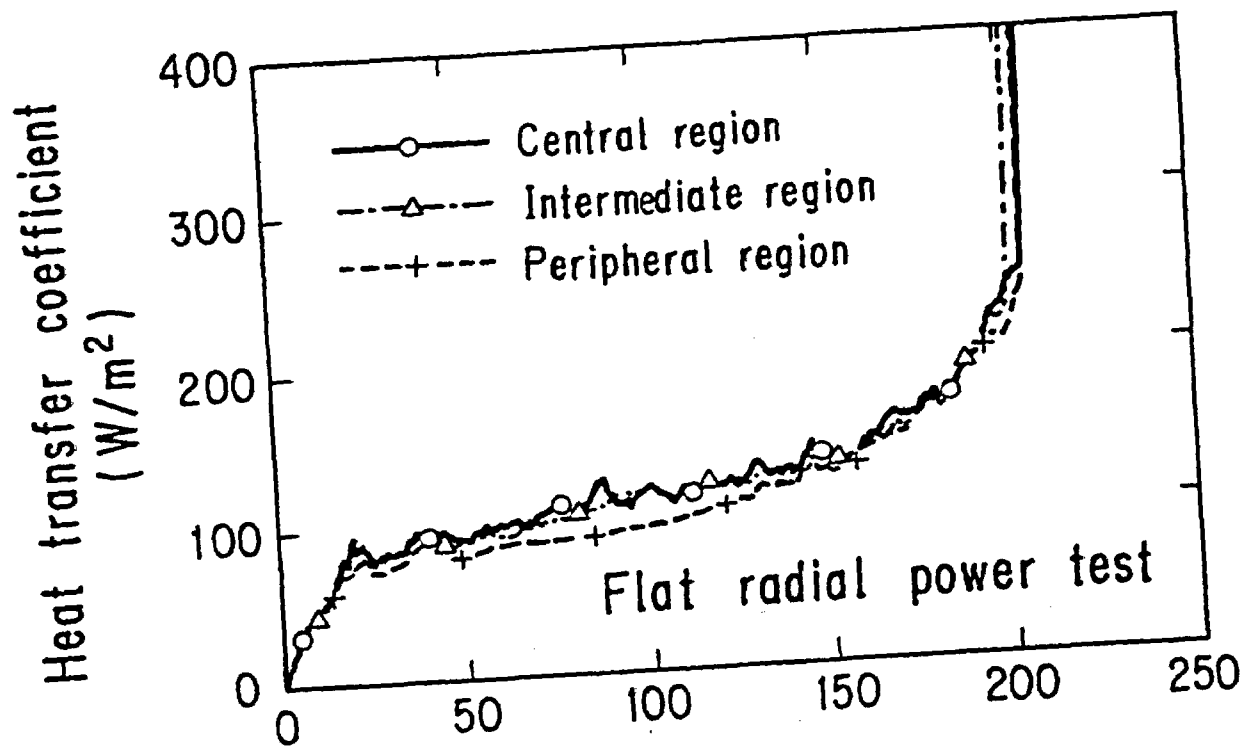


Fig. 14 Radial power effect on heat transfer coefficient at midplane of core

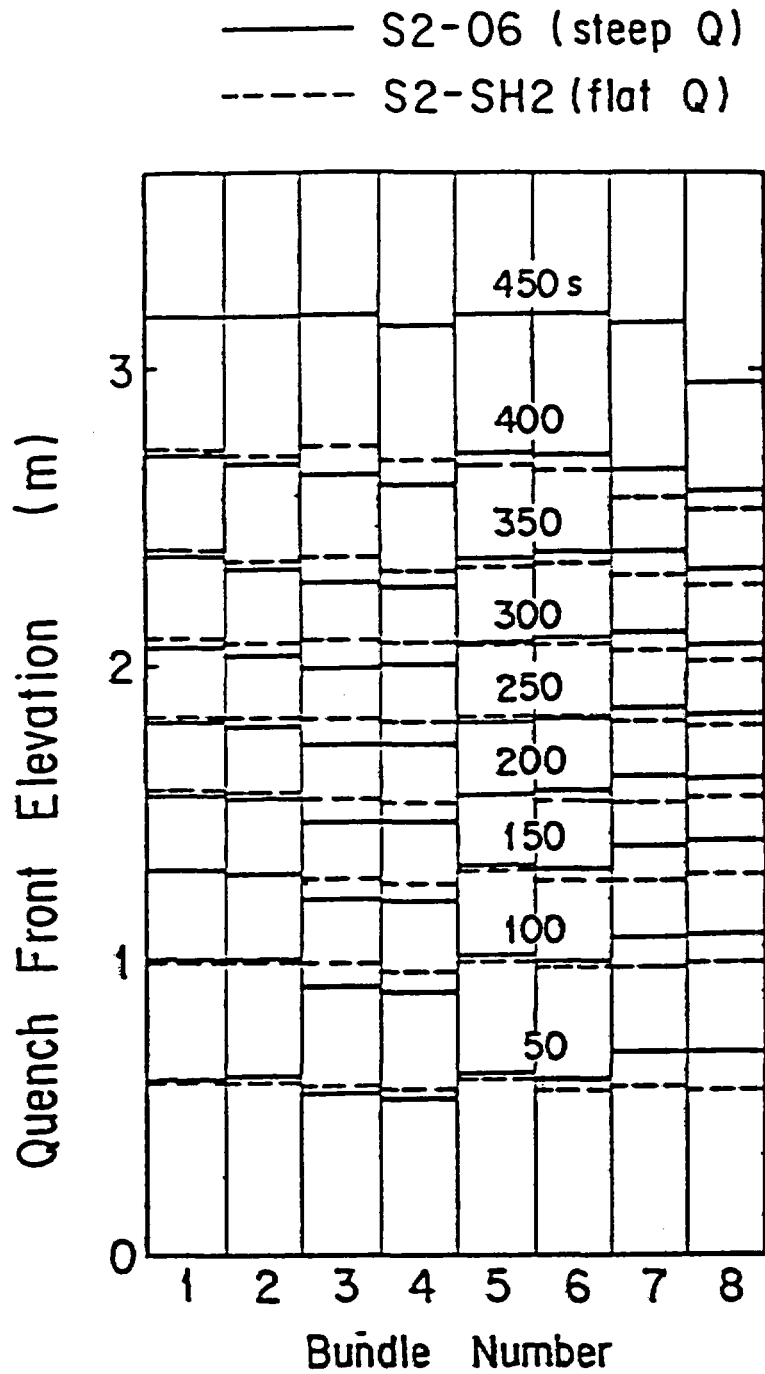


Fig. 16 Two-Phase Convection Effect on Quench Front Propagation

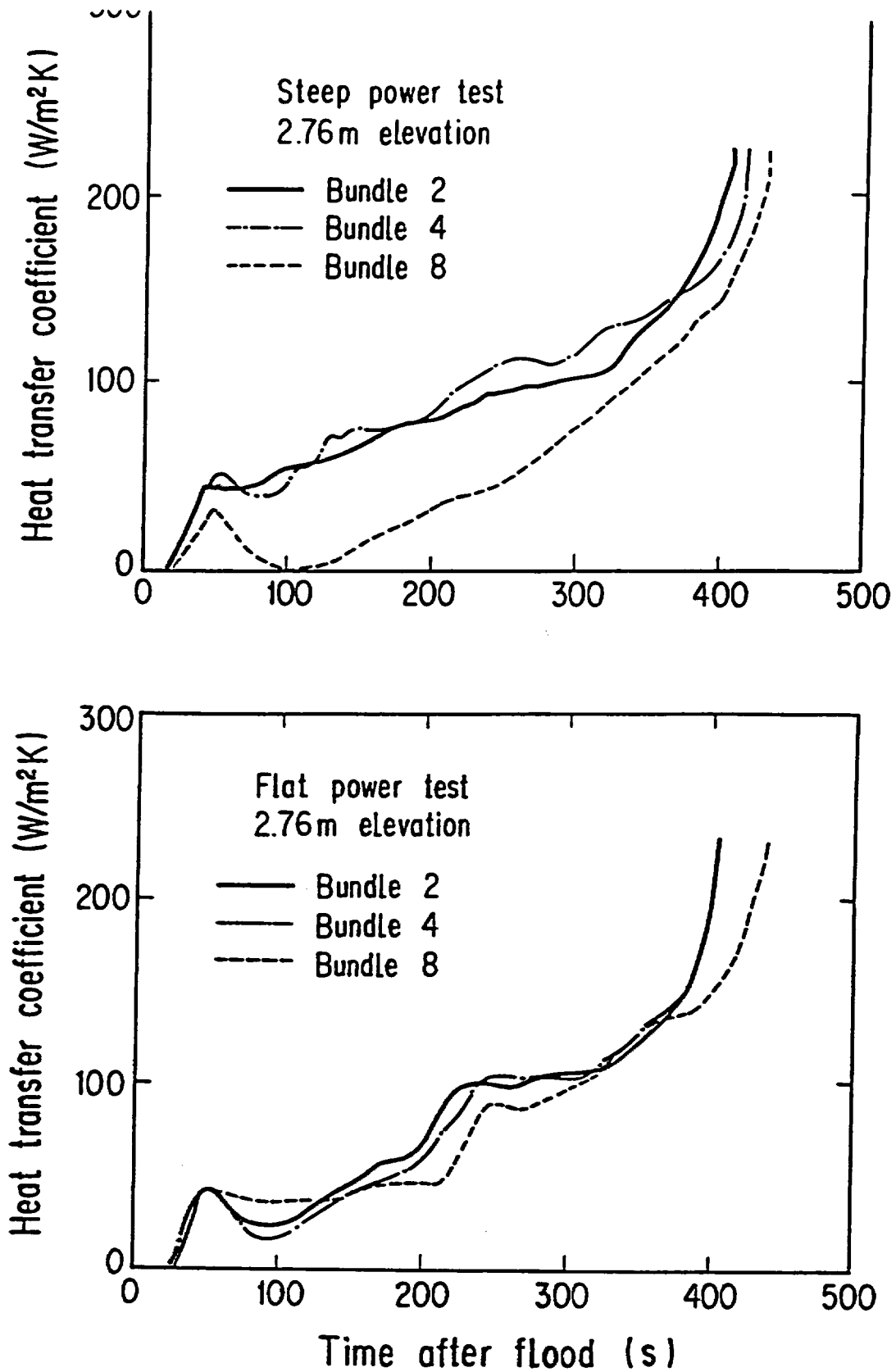


Fig. 17 Heat transfer coefficients in SCTF steep and flat tests

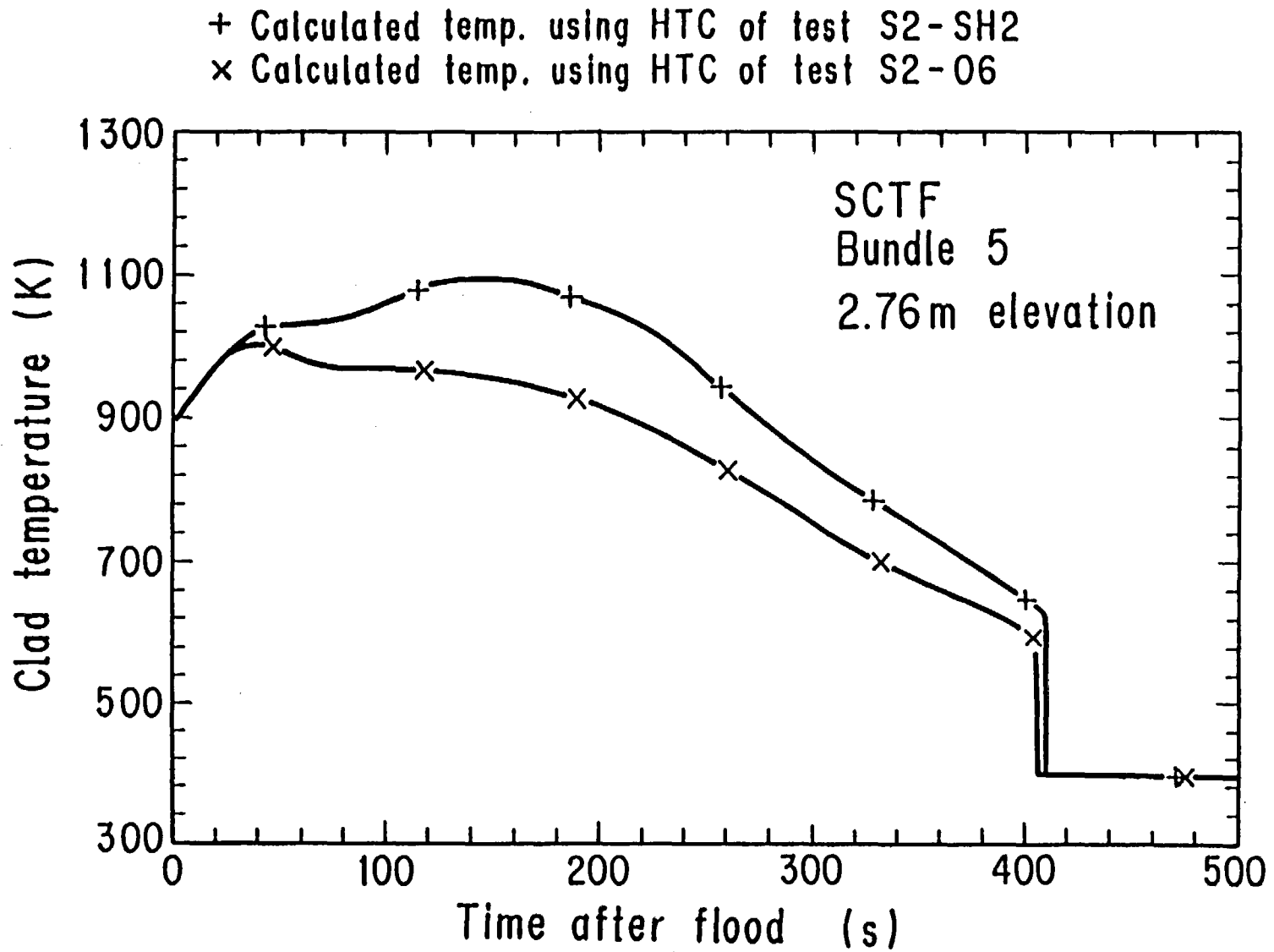


Fig. 18 Calculated results with the use of obtained heat transfer coefficients at high elevation

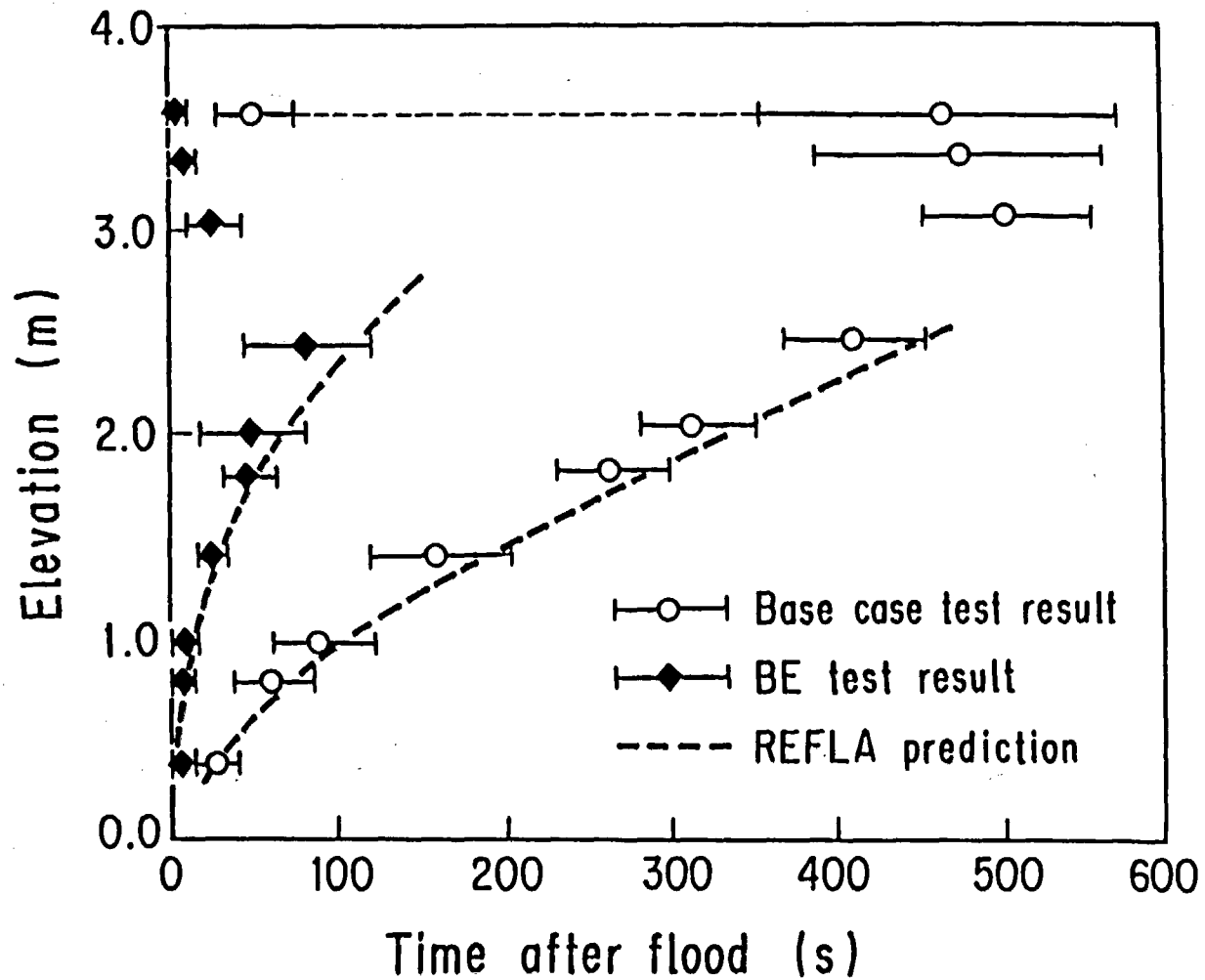


Fig.19 Comparison of the quench front elevation between CCTF data and REFLA prediction

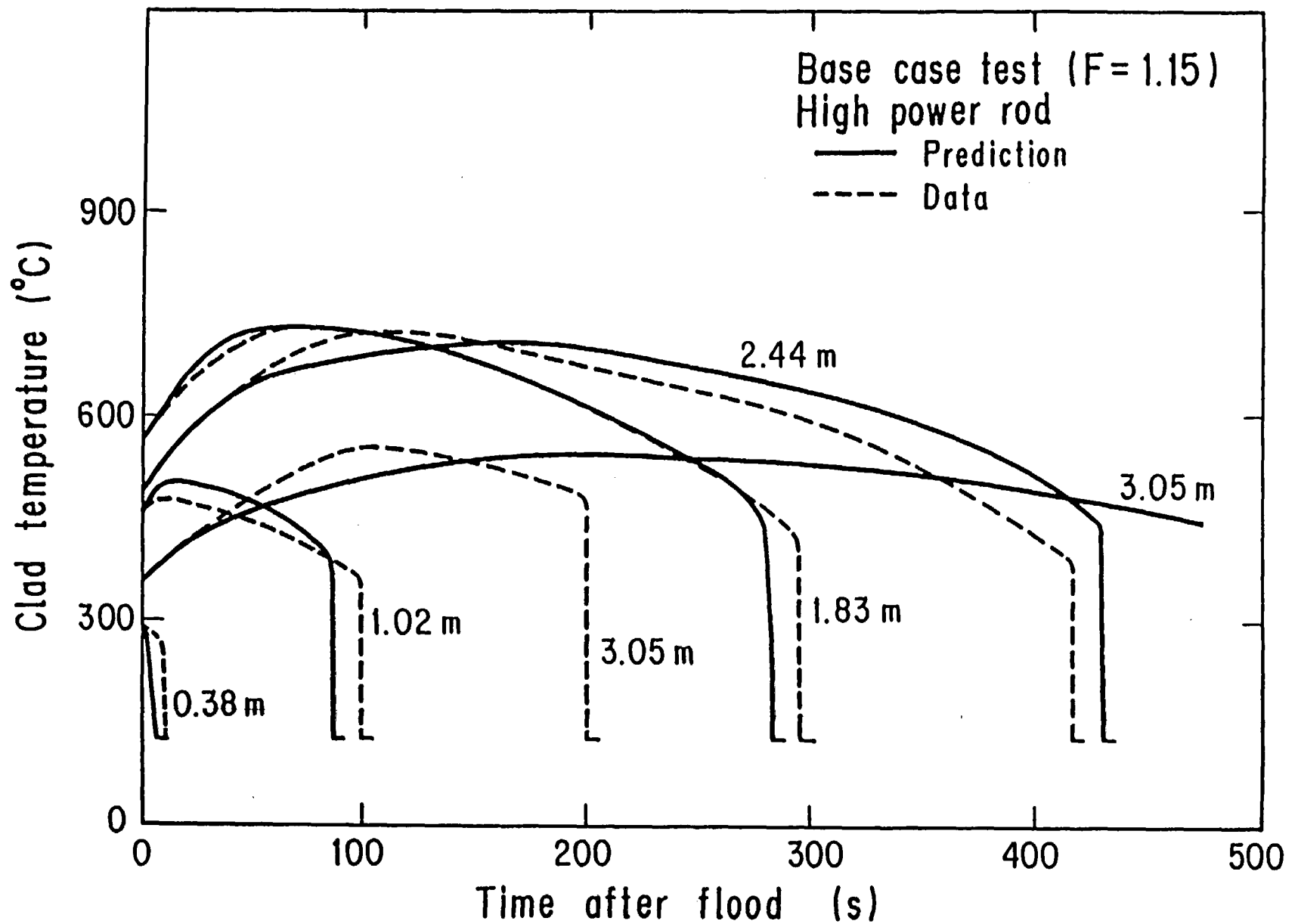


Fig. 20 Comparison of clad temperature between CCTF data and REFLA prediction (Base case test :  $F = 1.15$ )

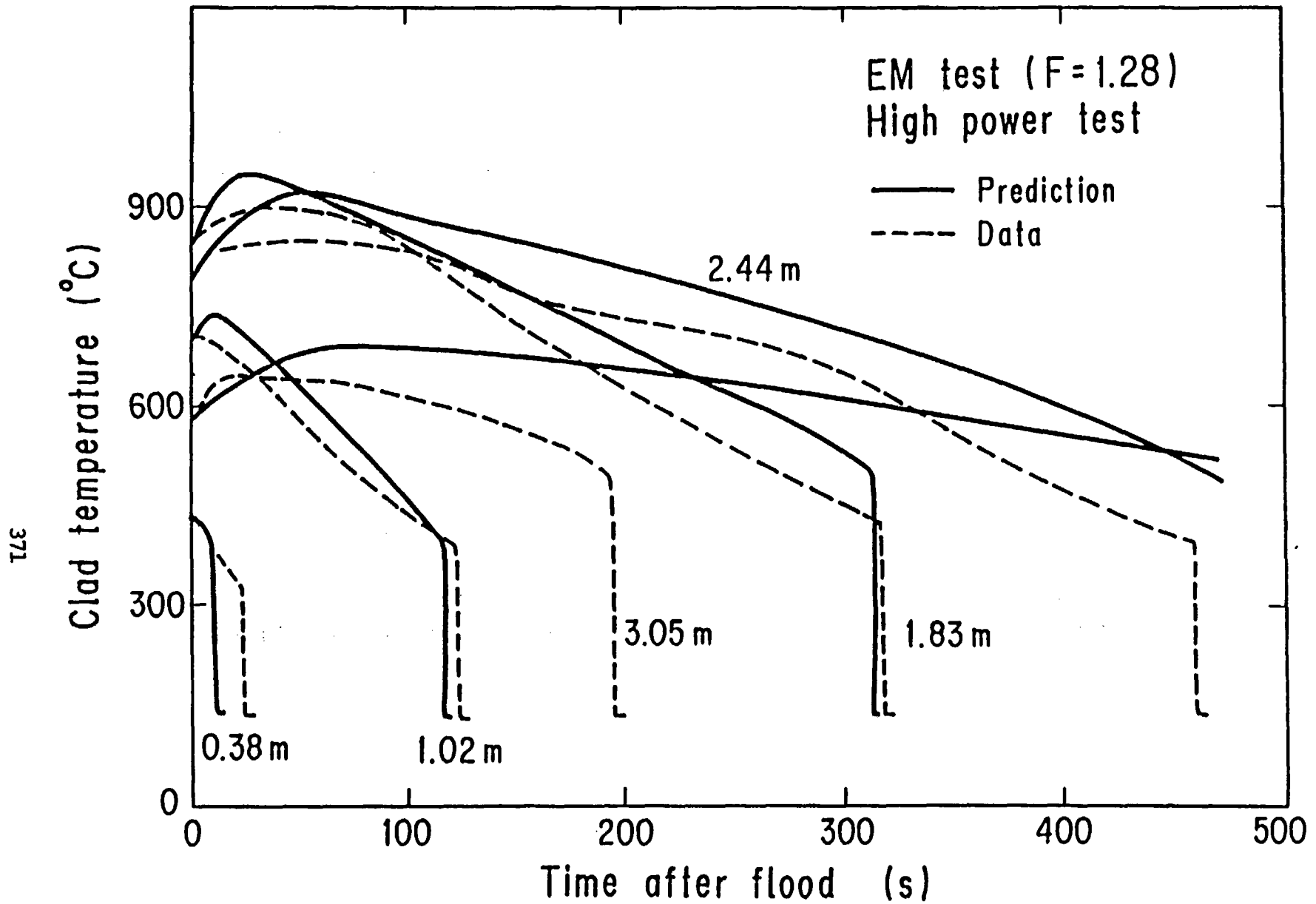


Fig. 21 Comparison of clad temperature between CCTF data and REFLA prediction (EM test : F = 1.28 )

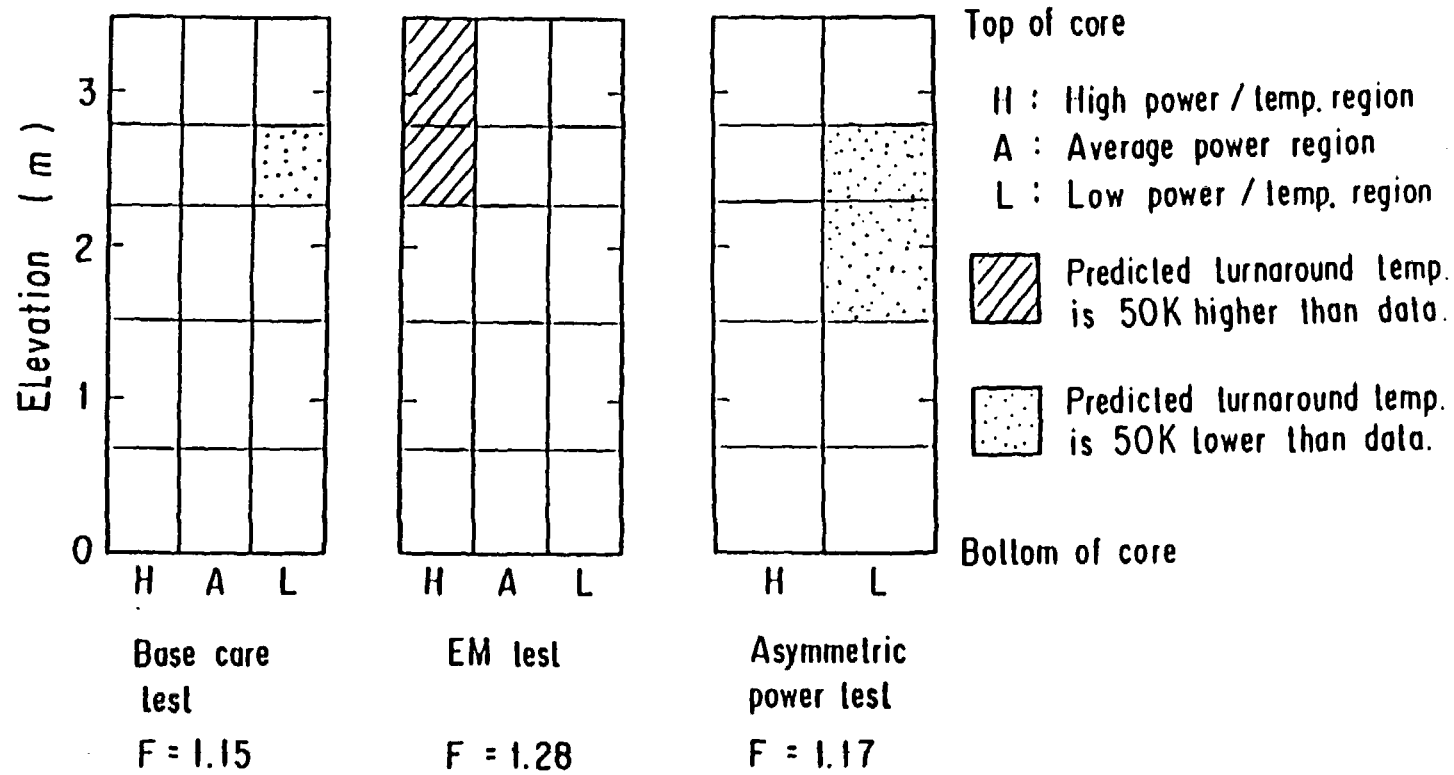


Fig. 22 Comparison of the turnaround temperature between the predicted and the measured (F : Radial peaking factor)

**TRAC ANALYSES FOR CCTF AND SCTF TESTS  
AND UPTF DESIGN/OPERATION\***

by

**F. E. Motley  
Thermal Hydraulics Group  
Energy Division  
Los Alamos National Laboratory  
Los Alamos, New Mexico 87545**

The 2D/3D Program is a multinational (Germany, Japan, and the United States) experimental and analytical nuclear reactor safety research program. Its main purpose is the investigation of multidimensional thermal-hydraulic behavior in large-scale experimental test facilities having hardware prototypical of pressurized water reactors (PWRs). The Japanese are presently operating two large-scale test facilities as part of this program: the Cylindrical Core Test Facility (CCTF) and the Slab Core Test Facility (SCTF). The CCTF is a 2000-electrically-heated-rod, cylindrical-core, four-loop facility with active steam generators primarily used for investigating integral system reflood behavior. The SCTF is a 2000 electrically-heated-rod, slab-core (one fuel assembly wide, eight across, and full height), separate-effects reflood facility. Both facilities have prototypic power-to-volume ratios preserving full-scale elevations, and are much larger than any existing facilities in the United States (including LOFT). The German contribution to the program is the Upper Plenum Test Facility (UPTF), a full-scale facility with vessel, four loops, and a steam-water core simulator under construction in Mannheim, Germany. All of these facilities have more instruments than any existing facilities: conventional instrumentation data channels alone are in excess of 1500 in each facility. The United States contributions to the program are the provision of advanced two-phase flow instrumentation and analytical support.

The Los Alamos National Laboratory is the prime contractor to the US NRC in the latter activity. The main analytical tool in this program is in the Transient Reactor Analysis Code (TRAC), a best-estimate, multidimensional,

---

\*Work performed under the auspices of the US Nuclear Regulatory Commission.

nonequilibrium, thermal-hydraulics computer code developed for the US NRC at Los Alamos. Through code predictions of experimental results and calculations of PWR transients, TRAC provides the analytical coupling between the facilities and extends the results to predicting actual PWR behavior.

During Fiscal Year 1984, TRAC-PF1/MOD1 analyses were provided for five CCTF-II experiments. Prediction of the upper plenum injection (UPI) tests 54 and 59 demonstrated that TRAC can correctly predict the multidimensional phenomena occurring with this type of emergency core-cooling (ECC) system. This analysis will be discussed later in this paper. TRAC also adequately predicted the vent-valve test (Run 69), the high LPCI test (Run 68) and the refill test (Run 70). For the SCTF, TRAC predictions were provided for five tests including the gravity-feed ECC parametric effects tests (Runs 531), 531-M, 614), a steep radial power-profile test (Run 514), and a combined-ECC-injection test (Run 529). TRAC was used to aid in developing operating procedures for the UPTF, and to investigate the expected integral system transients including the core simulator feedback control system. Finally, a fine-node 200% LOCA calculation of a Westinghouse 3411 Mwt PWR assuming licensing-type boundary and initial conditions was completed. This calculation predicted that a peak cladding temperature of 1035K (1403<sup>o</sup>F) occurs at 3 s into the blowdown phase. Last year Los Alamos completed a fine-node, large-break loss-of-coolant-accident (LOCA) calculation of a US/Japanese PWR reference reactor using most probable boundary and initial operating conditions. This year a similar calculation was completed using licensing boundary and initial conditions. The results of this calculation were used as part of the Appendix K conservatism evaluation also presented at this meeting. JAERI has run a CCTF test (Run 71) during the past year with boundary conditions similar to these two PWR calculations. After describing the latest calculation (licensing boundary conditions), the TRAC results will be compared to the test results.

The TRAC model uses 953 cells to model a Westinghouse 3411 Mwt plant with twelve feet 17 x 17 fuel assemblies. A schematic of the complete system model used for the transient calculation is shown in Fig. 1. All the loop components such as the hot leg, steam generator, loop seal, circulating pump,

cold leg and emergency core cooling system (ECCS) were modeled as physically complete as possible. A schematic of the vessel component is shown in Fig. 2. The vessel has been subdivided into 17 axial levels, 4 radial rings, and 8 azimuthal sectors for a total of 544 hydrodynamic cells. The core region consists of the 2 inner radial rings and the 5 axial levels extending between levels 4 to 9. The barrel baffle region extends from level 4 to 10 and occupies the 3rd radial ring within these levels. The fourth radial ring represents the downcomer region from level 3 to 15. At the top of level 15 in each azimuthal sector open flow area passages are located to model the upper head spray nozzles. Flow paths between the upper head and upper plenum were represented by the modeling of the control rod guide tubes that reversed these two regions. These guide tubes were modeled with pipe components within the vessel. Three guide tubes were combined for each sector of the inner ring and 4.5 guide tubes for each sector of the outer ring.

This PWR analysis simulates a 200% guillotine break of a cold leg. The break is located between the cold leg nozzle and the ECC injection port immediately outside of the biological shield.

The predicted cladding temperature response of a high powered rod (12.9 kW/ft local peak) is shown in Fig. 3. This figure shows the temperature transient at six axial elevations measured from the bottom of the heated core. Figure 4 shows the temperature for an average power rod. The rapid cooldown of the entire rod after peaking during the first seconds of the transient is due to a rapid refilling of the core, shown in Fig. 5. The core flow returned to positive because the mass flow from the three intact loops (with pumps tripped but still spinning) exceed the choked flow out the single broken loop. The fuel rods continued to cool until 20 to 25 s into the transient. This longer term cooling resulting partially from the blowdown of the upper head water through the control rod guide tubes. Although a reheat of the core occurred during the refill/reflood phase, the maximum temperature never exceed the earlier blowdown peak of 1035 K (1403°F) for the hot rod and 900°K (1160°F) for the average rod. During the core reflood phase there were significant manometer-type oscillations between the core and downcomer. The downcomer mass is shown in Fig. 6. These oscillations were predicted primarily because of the very short time (60 s) required to reflood

and quench the entire core. This calculation also modeled the noncondensable gas (nitrogen) field that entered the system after all accumulator water was discharged. When nitrogen entered the system at 50 s it pressurized the upper downcomer region and locally lowered the condensation rates. This increased the core reflooding rate and damped the manometer oscillations after nitrogen was in the primary system.

The predicted cladding temperature response in the previous "most probable" calculation is shown for the peak and average power rods in Fig. 7 and 8, respectively. Inspection of these figures and Fig. 3 and 4 at the time of core reflood shows that at close to the midplane (1.73 m) the temperatures are between 700 K for the licensing calculation and 650 K for the hot rod in the most probable calculation. The temperatures showed very little heatup after reflood started. Quenching at this elevation takes place 50 s after reflood in the licensing calculation and 30 s after reflood in the most probable case. Figure 9 shows the temperature response of the midplane (1.83 m) thermocouple in CCTF test Run 71. The response is very similar to that predicted by TRAC in the PWR. The high power level of the experiment accounts for the longer heatup after reflood initiation and the longer quench time. Similar comparisons can be made at the upper core elevations (2.44 m and 3.05 m).

Redryout occurred in the experiment at 130 s after reflood began. This occurred because there were oscillations between the downcomer and the core that partially emptied the core as shown in Fig. 10. This did not occur in the TRAC calculation probably because of the effect of the nitrogen injection that pressurized the top of the downcomer and damped the oscillations.

In summary, the PWR calculations have shown a significant safety margin in PCT and that the stored energy level at the start of reflood is low so that core quenching can occur within a minute after reflood initiation. A CCTF experiment with low initial stored energy verifies this finding.

One of the upper plenum injection (UPI) tests (CCTF Run 59) was analyzed by TRAC-PF1/MOD1 during the past year. The model of the CCTF facility is similar to other CCTF calculations except that two injection nozzles were placed in the upper plenum at the hot leg elevation and since the nozzles spray against guide tubes the flow area on the opposite side of the injection cells was blocked off. This is shown in the vessel nodding diagram (Fig. 11).

One of the most interesting findings of the UPI test is the negative flow at the core inlet. JAERI has calculated a mass balance in the facility. The results are shown in Figs. 12 and 13. In Fig. 12 the values in parenthesis are flow for a matching cold-leg injection run. The core inlet flow is shown in Fig. 13. In the UPI test after an initial positive value during the accumulator flow period, the core inlet flow has an average negative value of 6 or 7 kg/s for the remainder of the transient. The integral of the TRAC predicted core inlet mass flow is shown in Fig. 14. After an initial positive flow period during accumulator flow, the slope of the integral was a fairly consistent value of -6.5 kg/s. This is an excellent agreement with the value calculated by JAERI. The slope of the integral of the TRAC predicted mass exiting the vessel at the hot legs is also in good agreement with the JAERI calculated value. TRAC calculated an average of 4.6 kg/s and JAERI calculated 4.5 kg/s (3.1 kg/s water and 1.4 kg/s steam). As you would expect with the flow rates properly predicted by TRAC the liquid inventories in the lower plenum, downcomer, core, and upper plenum are also in good agreement with the data.

The heater rod temperature response during this experiment showed fairly wide variation among the 32 bundles especially at the top elevation (3.1 m). The TRAC model only has 6 different zones so that it is very difficult to choose the appropriate test bundle to compare with the TRAC prediction. One rod from each power zone was selected and they are shown in Figs. 17 through 19.

In general all the comparisons at the lower two elevations (0.4 and 1.1 m) are very good. At midplane the predicted quench is late but the peak temperatures are correct for the high and intermediate power zones and too high for low power zones. At the 2.4 m and 3.05 m elevations the variation from bundle to bundle is extensive but in general the high and intermediate power zones are well predicted. The low powered outer zone shows poor agreement.

In summary the flow behavior during a UPI test is quite different than a cold leg injection test but the core flood and cooling process are quite similar. The TRAC code correctly predicts the flow behavior.

In conclusion, the Los Alamos analysis effort is functioning as a vital part of the 2D/3D program. Results from this program already have addressed, and will continue to address, key licensing issues including scaling, multidimensional effects, downcomer bypass and refill, reflood, steam binding, core blockages, alternate ECC systems, and code assessment. The CCTF and SCTF analyses have demonstrated that TRAC-PF1 can correctly predict multidimensional, nonequilibrium behavior in large-scale facilities prototypical of actual PWRs. Through these and future TRAC analyses, the experimental findings can be related from facility to facility; and more importantly, the results of this multinational research program can be directly related to licensing concerns affecting actual PWRs.

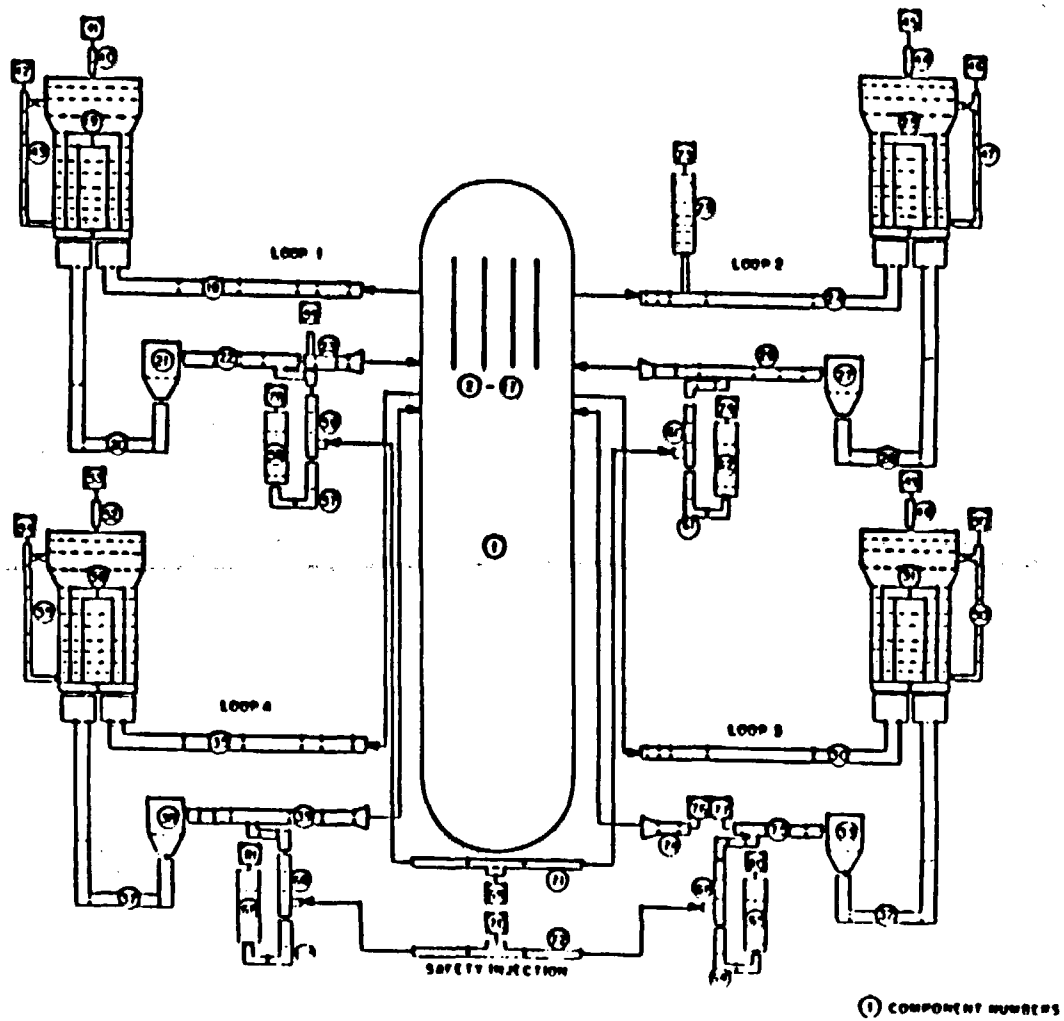


Figure 1. TRAC system model of Westinghouse four-loop PWR

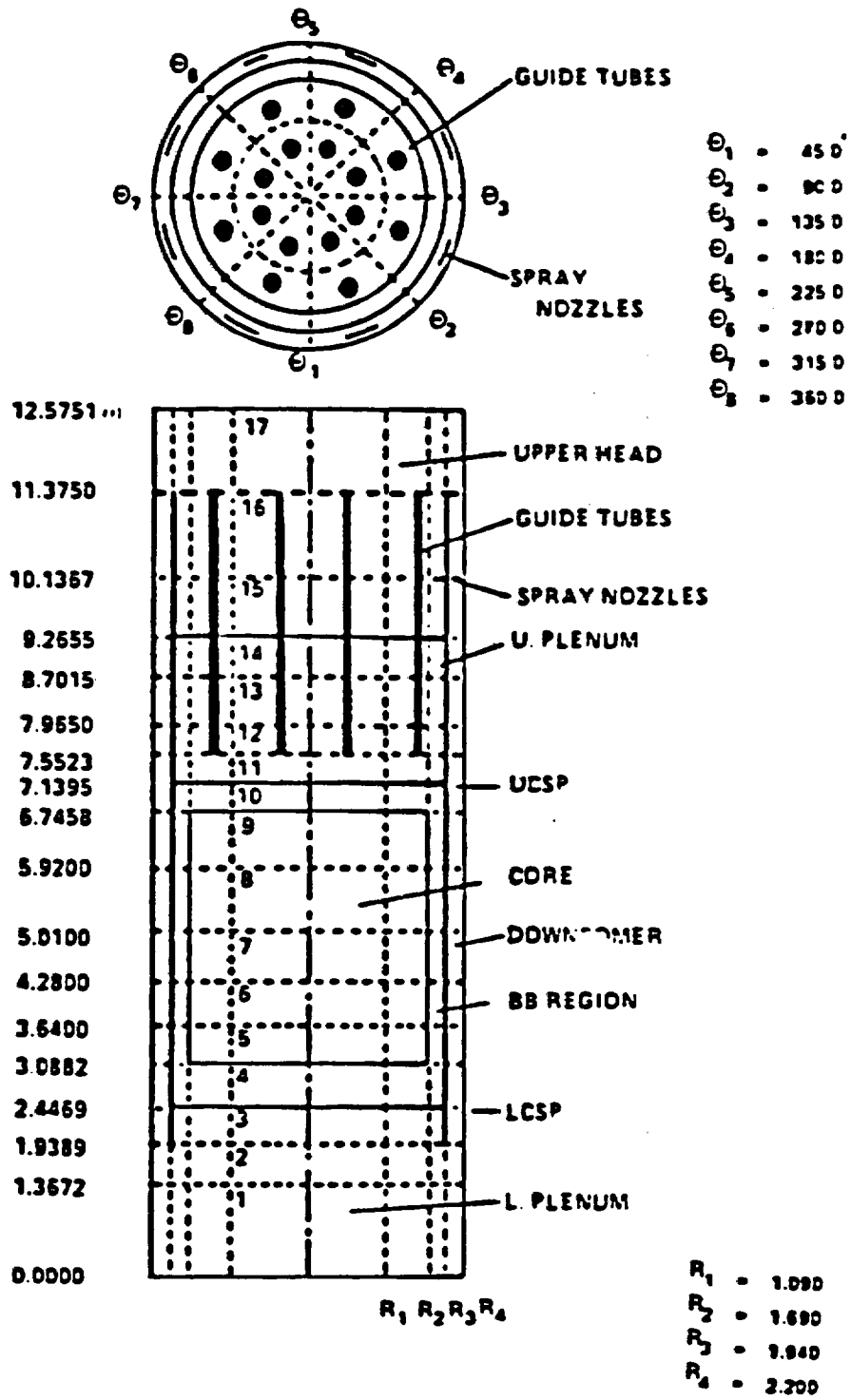


Figure 2. TRAC vessel model of Westinghouse PWR

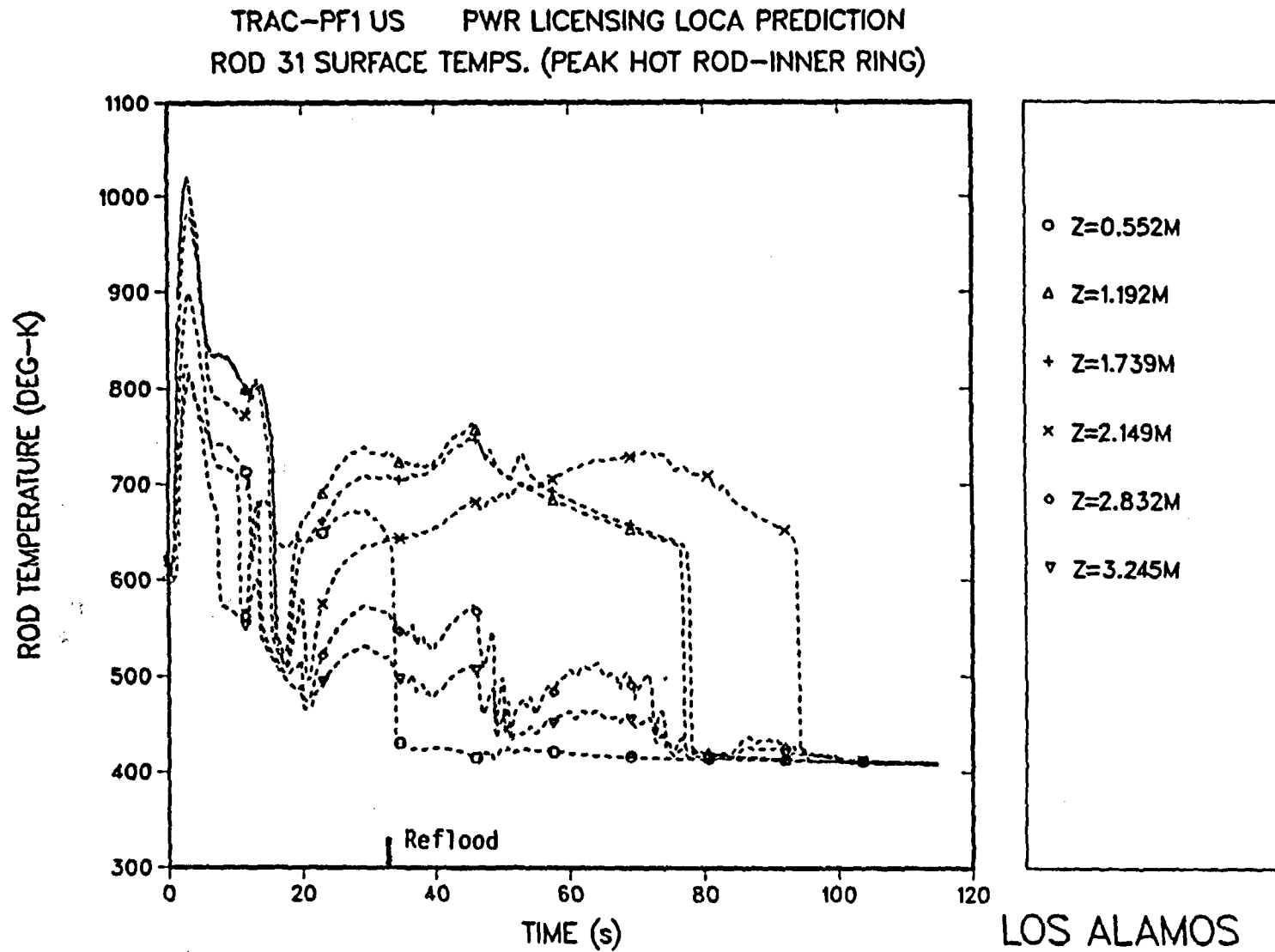


Fig. 3. Cladding temperature history of a high powered rod in the Westinghouse Licensing LOCA calculation.

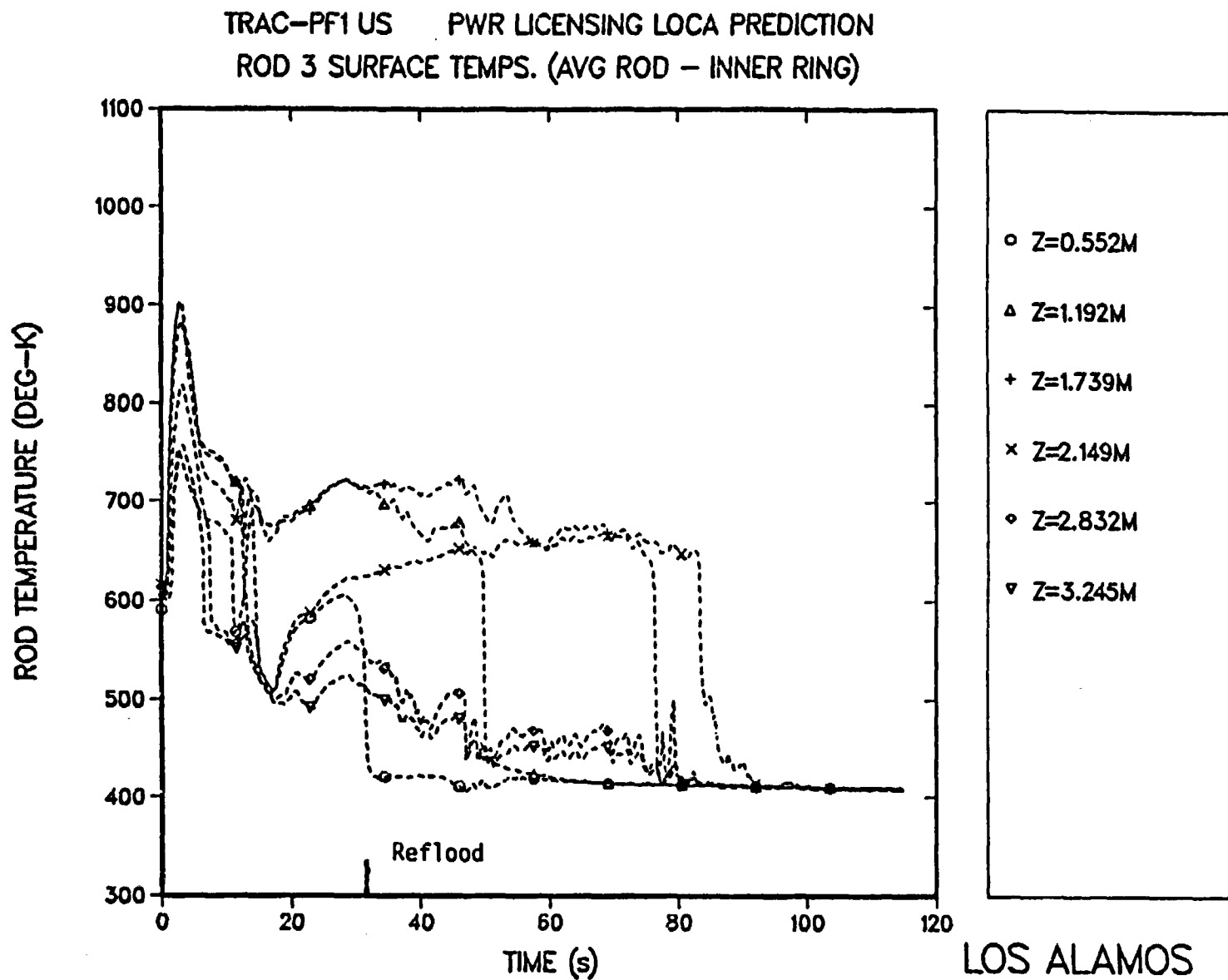


Fig. 4. Cladding temperature history of an average powered rod in the Westinghouse Licensing LOCA calculation.

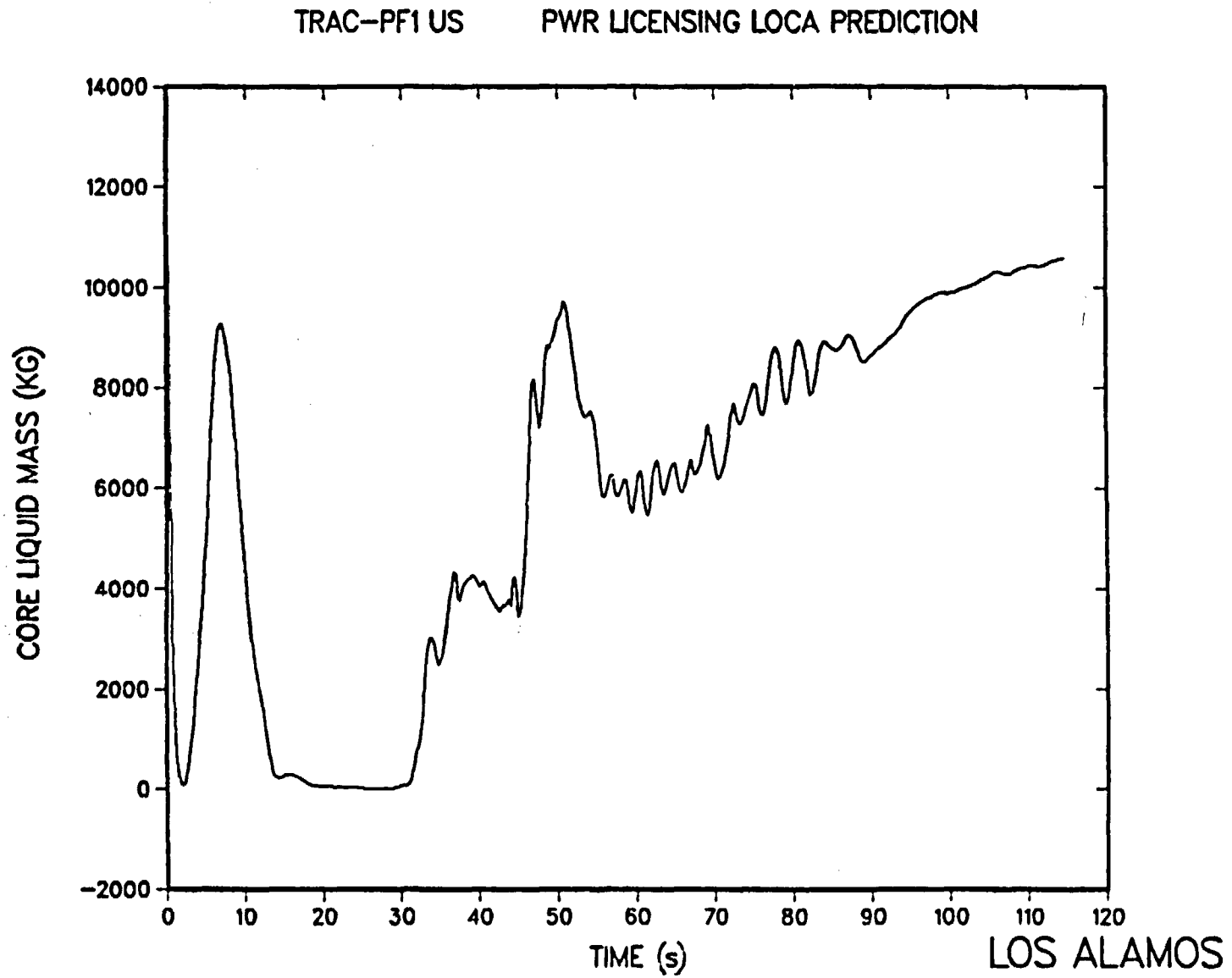
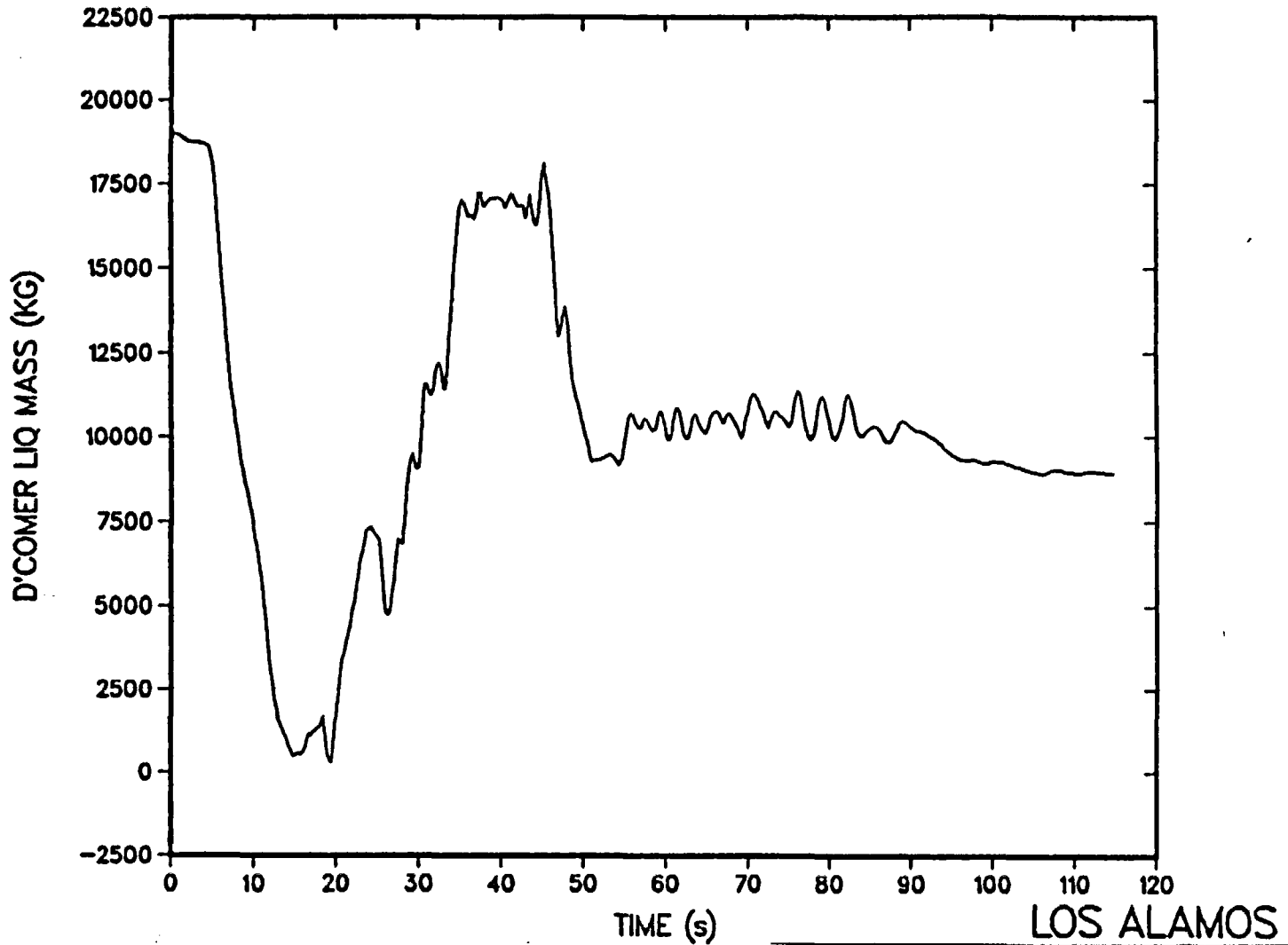


Fig. 5. Core liquid mass history in the Westinghouse Licensing calculation.

TRAC-PF1 US PWR LICENSING LOCA PREDICTION



384

Fig. 6. Downcomer liquid mass history in the Westinghouse Licensing calculation.

LOS ALAMOS

TRAC-PF1 US PWR BEST ESTIMATE LOCA PREDICTION  
ROD 38 SURFACE TEMPS. (HOT ROD - OUTER RING)

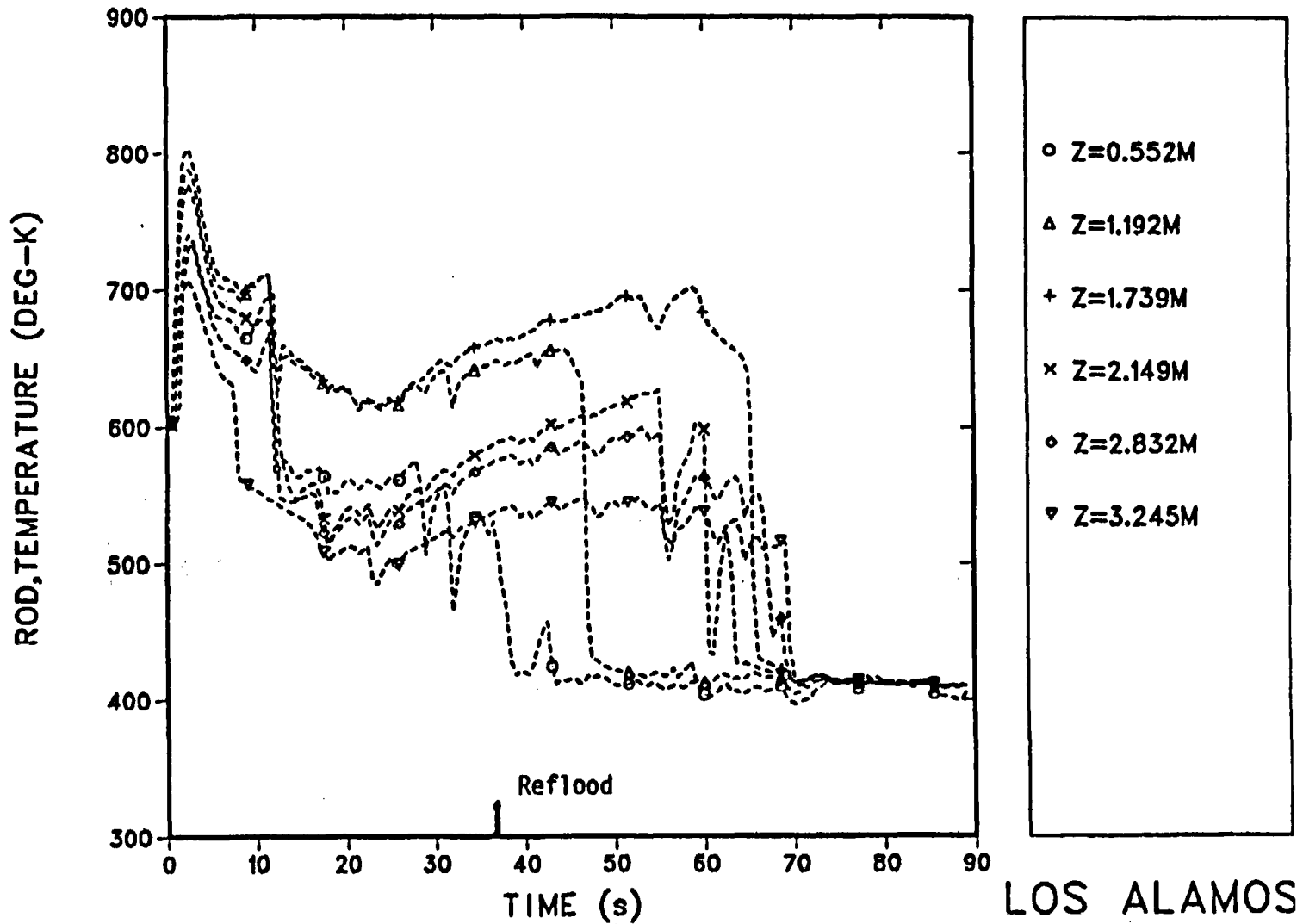


Fig. 7. Cladding temperature history of a high powered rod in the Westinghouse most probable calculation.

TRAC-PF1 US PWR BEST ESTIMATE LOCA PREDICTION  
ROD 3 SURFACE TEMPS. (AVG ROD - INNER RING)

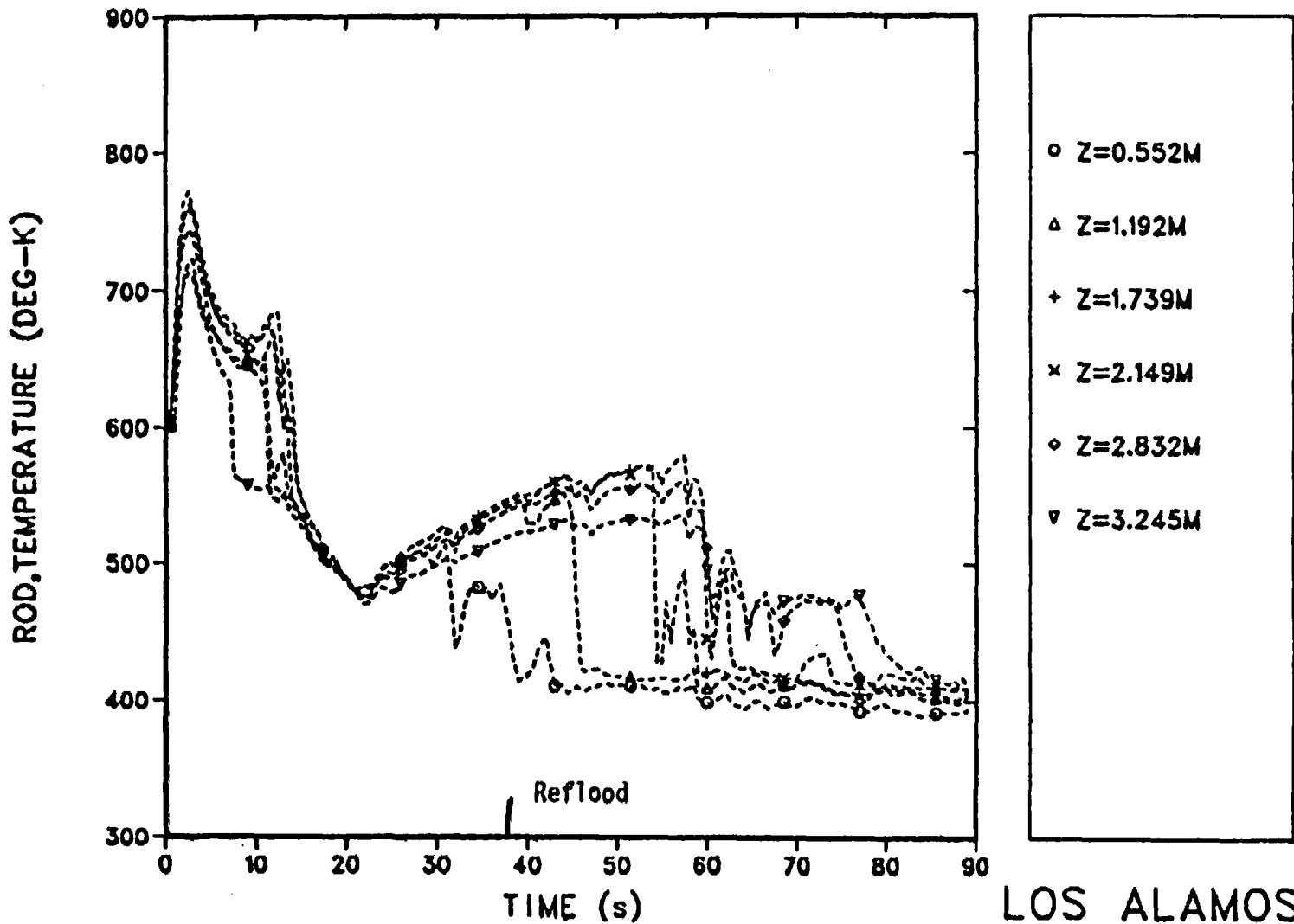


Fig. 8. Cladding temperature history of a high powered rod in the Westinghouse most probable calculation.

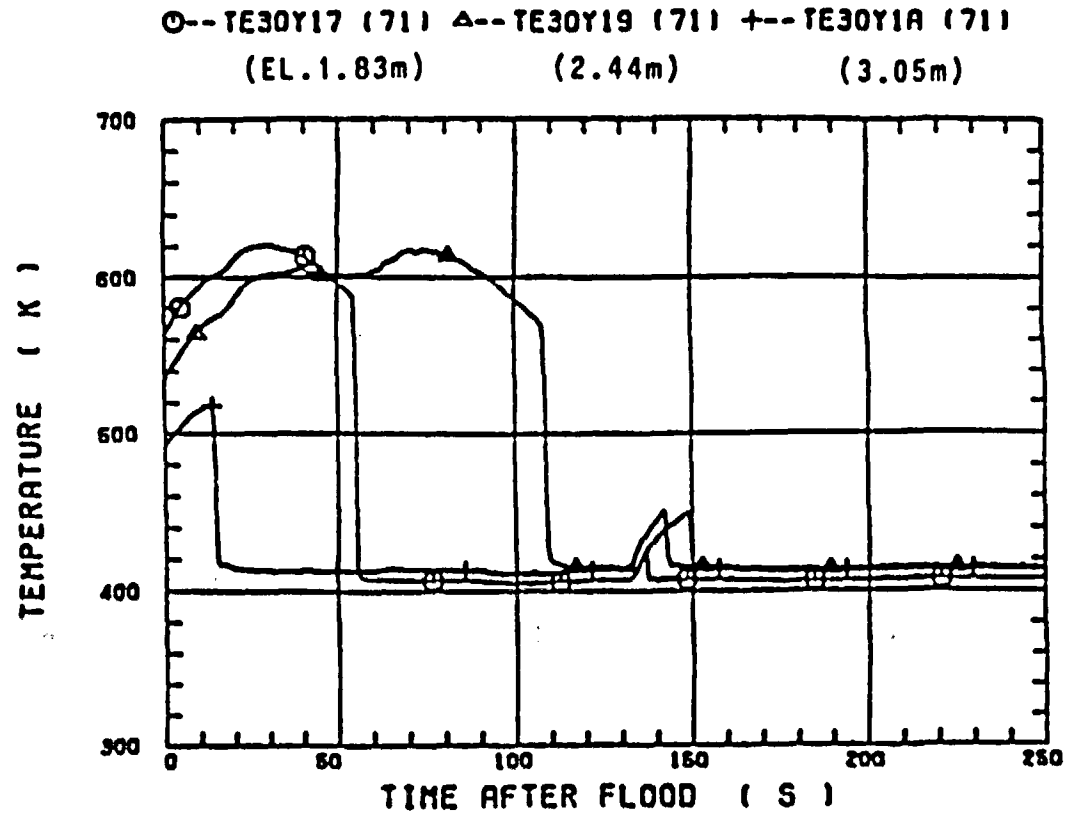


Fig. 9. Clad surface temperature at various elevations along a heater rod in Bundle 30 (Run 71).



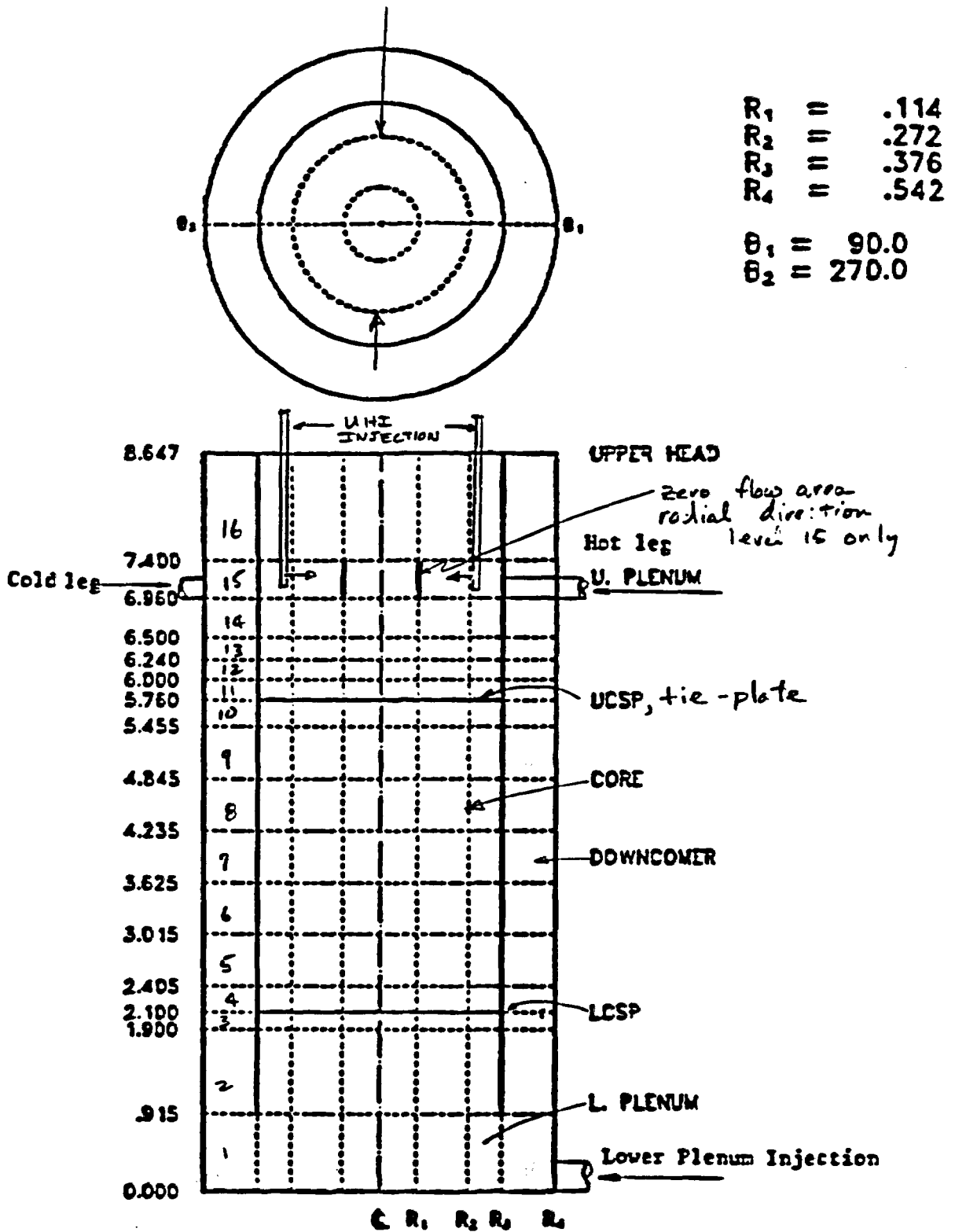


Fig. 11. TRAC noding for the CCTF vessel.

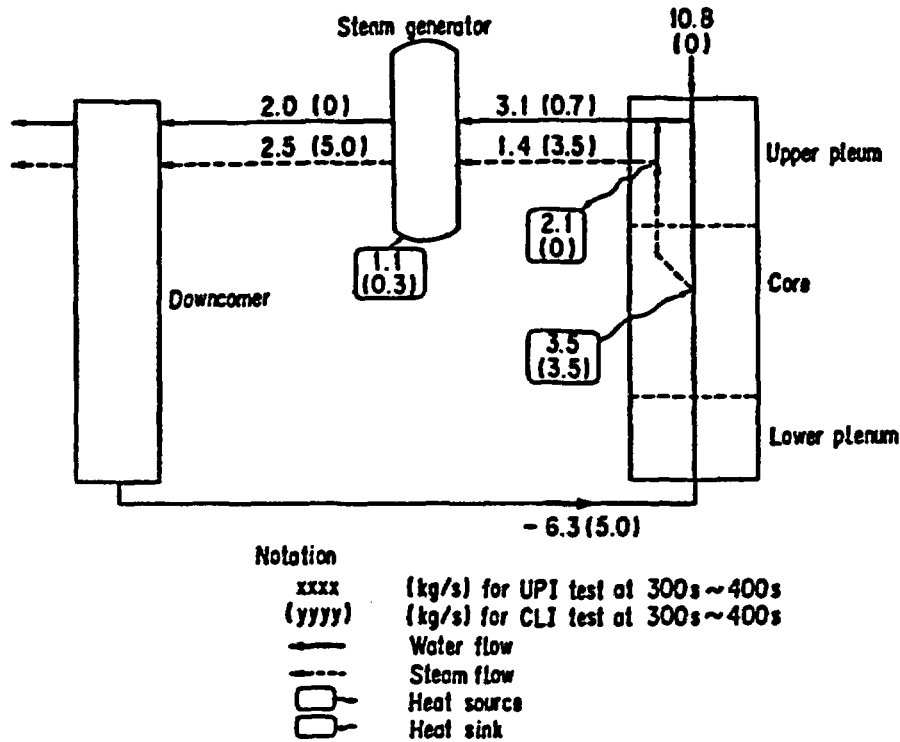


Fig. 12. Mass flow rate in system for UPI test and CLI test.

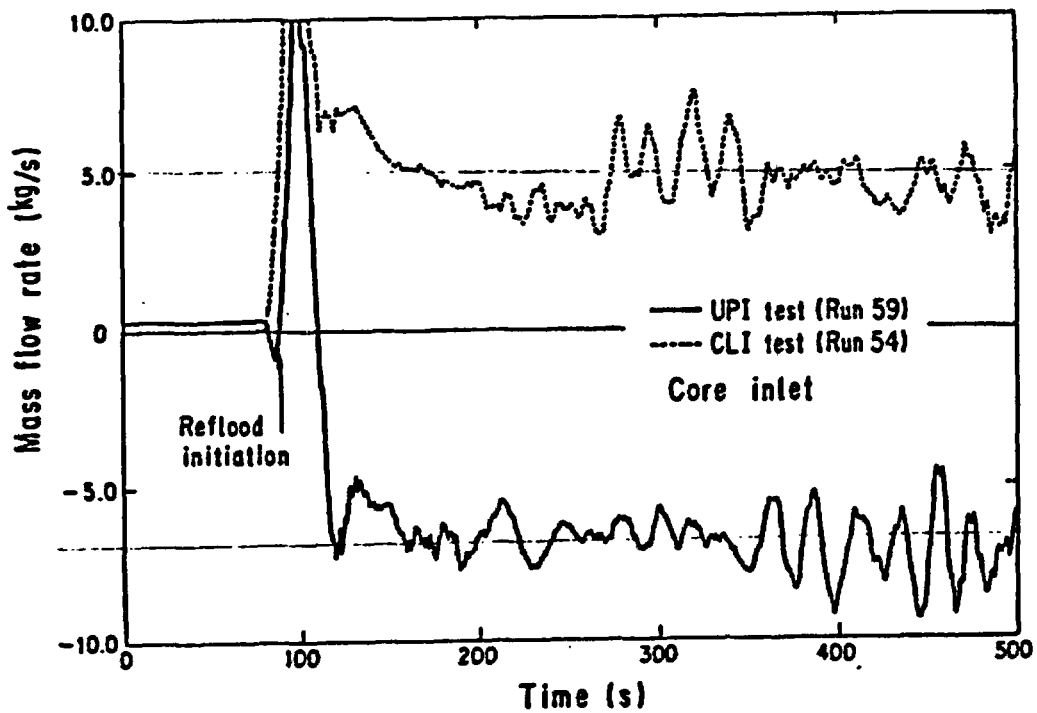


Fig. 13. Comparison of mass flow rate at core inlet between UPI test (Run 59) and CLI test (Run 54).

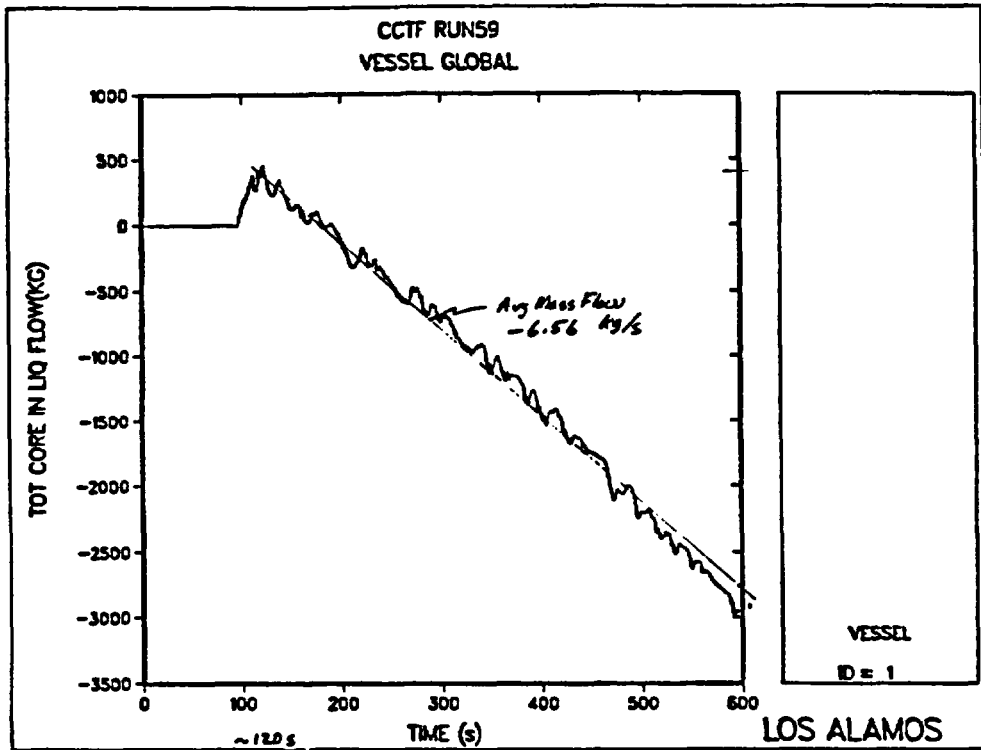


Fig. 14. Integral of calculated core inlet mass flow (positive is into the core).

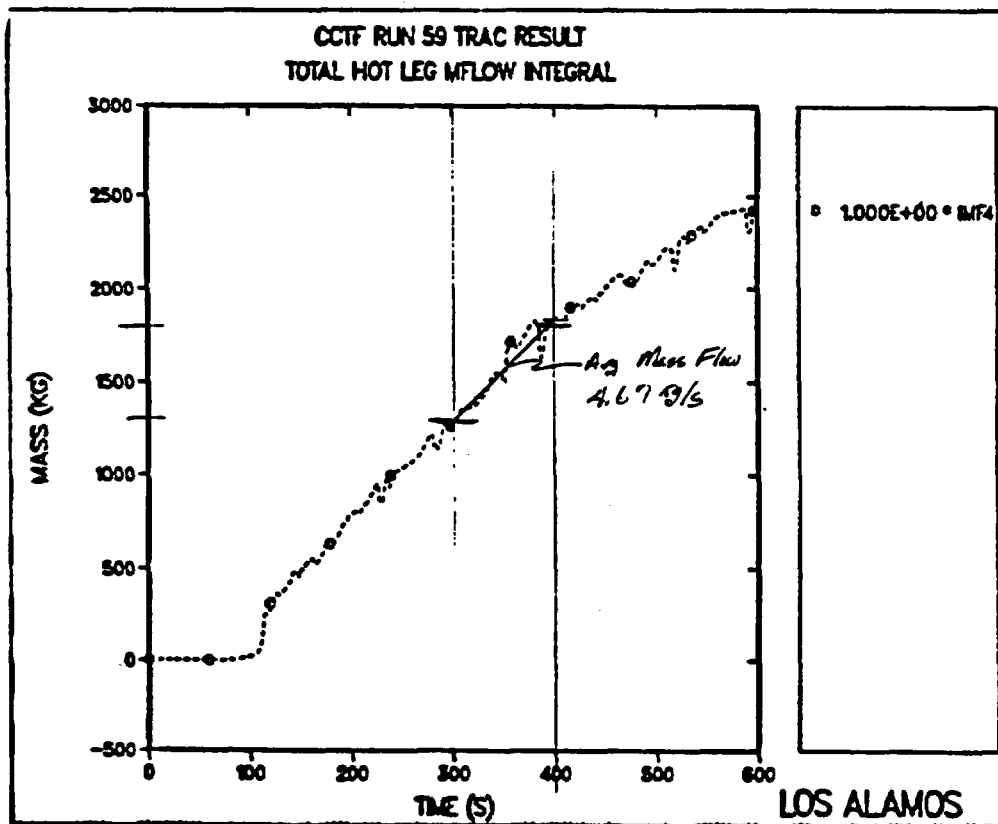


Fig. 15. Integral of calculated mass exiting the vessel through the hot legs.

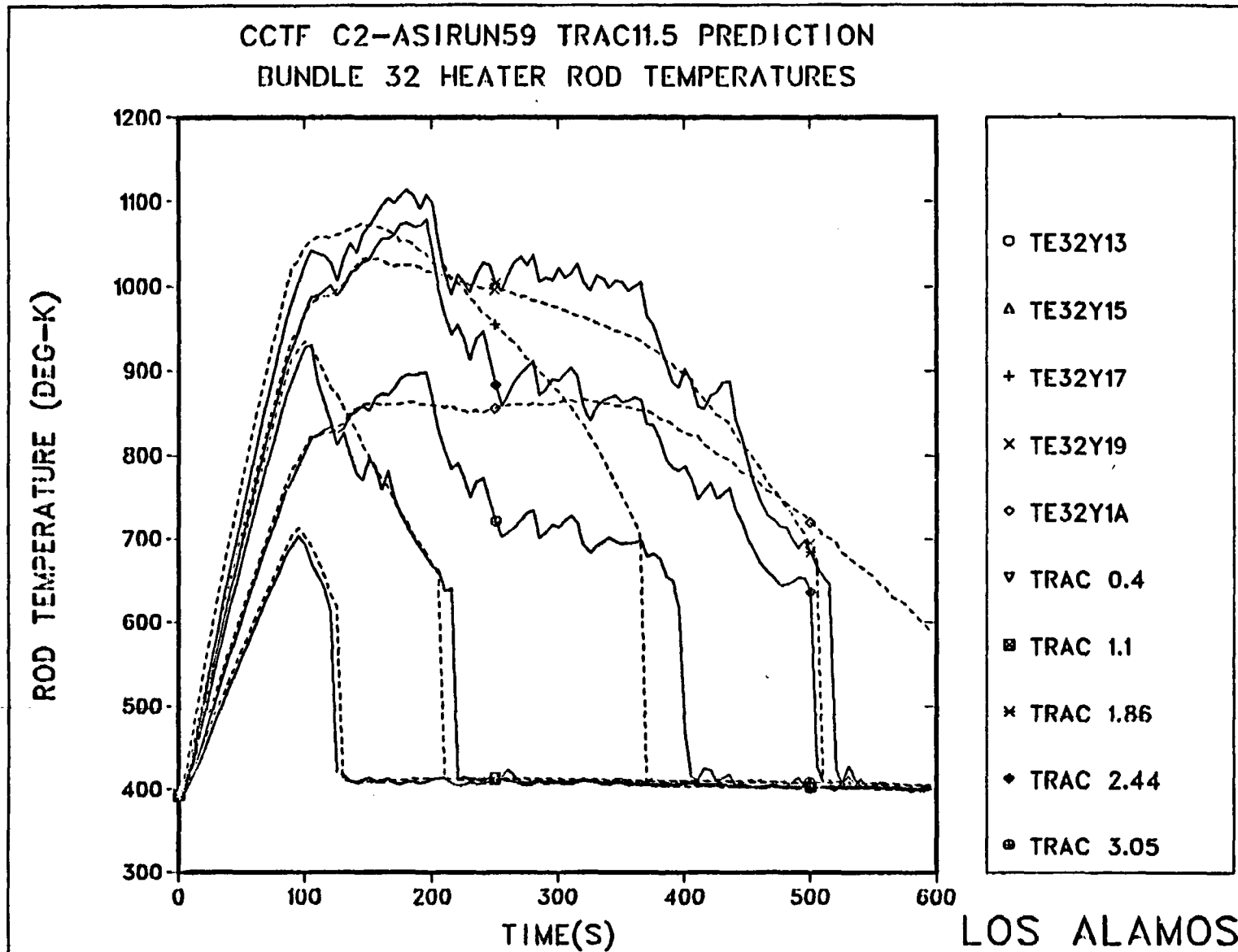


Fig. 16. Comparison of measured to calculated rod temperature in the high powered inner zone.

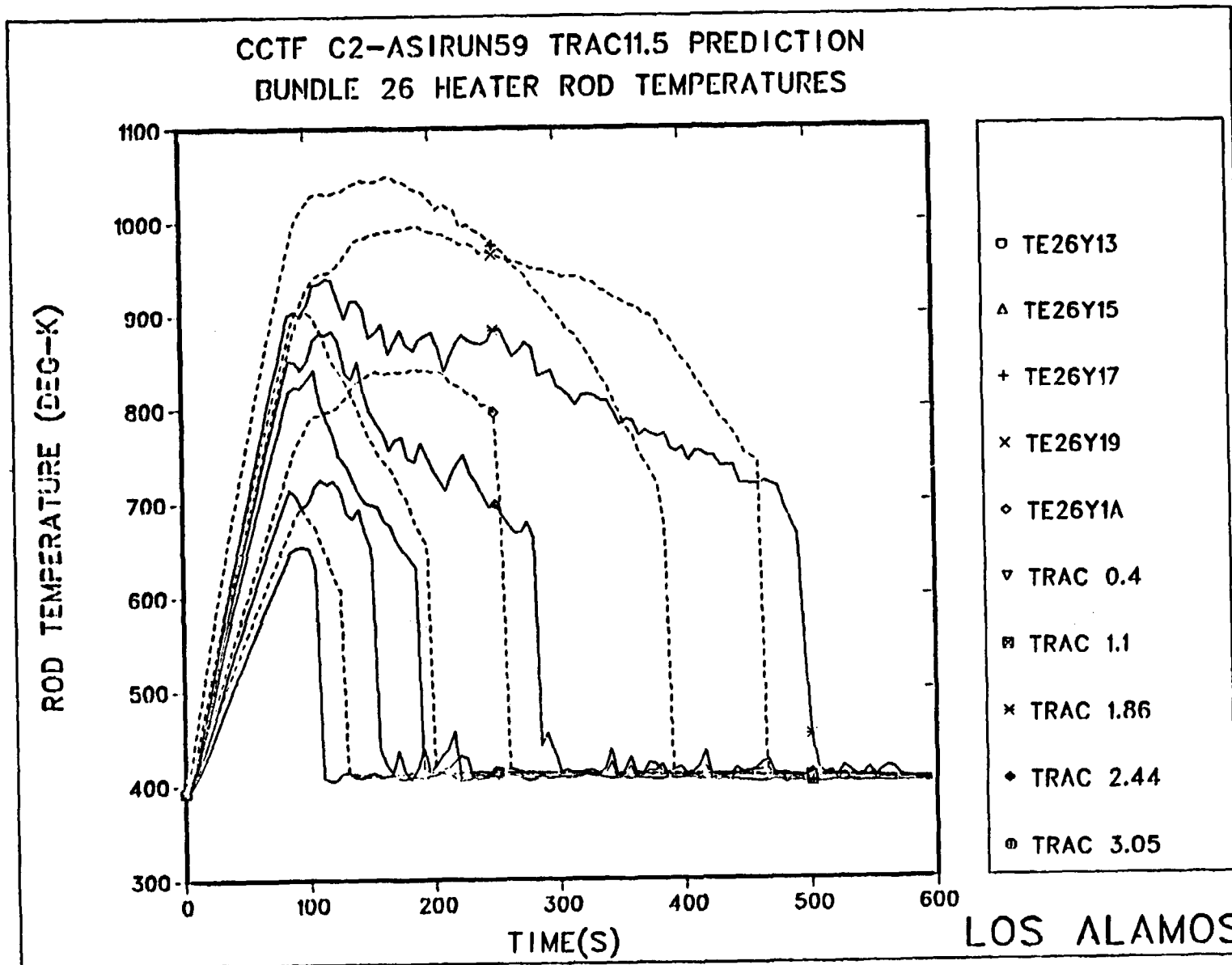


Fig. 17. Comparison of measured to calculated rod temperatures in the medium powered intermediate zone.

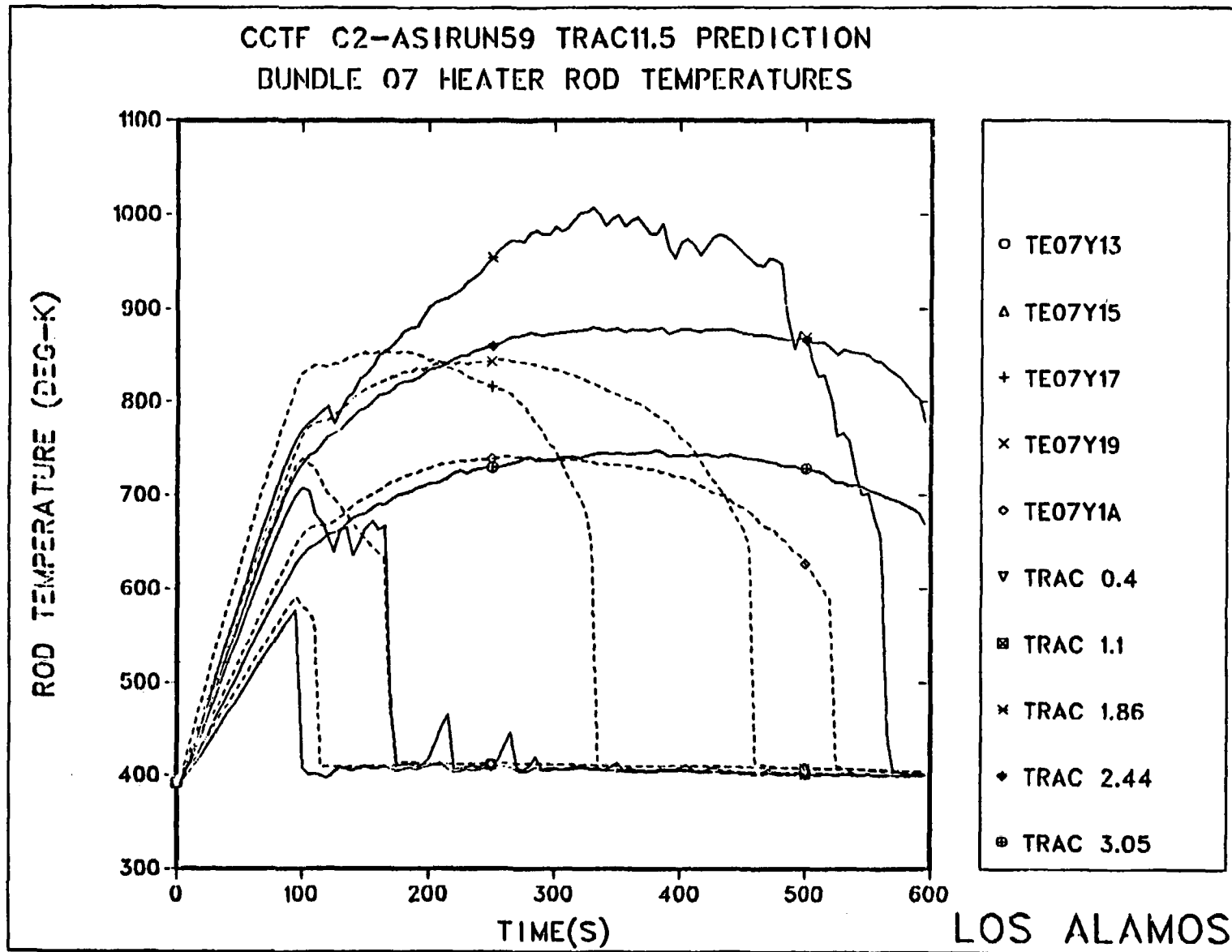


Fig. 18. Comparison of measured to calculated rod temperatures in the low powered outer zone.

## SAFETY ANALYSIS CODE INPUT AUTOMATION USING THE NUCLEAR PLANT DATA BANK

H. Kopp  
J. Leung  
A. Tajbakhsh  
F. Viles

### INTRODUCTION

The Nuclear Plant Data Bank (NPDB) is a computer-based system that organizes a nuclear power plant's technical data, providing mechanisms for data storage, retrieval, and computer-aided engineering analysis. It has the specific objective to describe thermohydraulic systems in order to support:

- Rapid information retrieval and display
- Thermohydraulic analysis modeling

The system performs the above two functions so that NO COMPUTER SKILL is presumed on the part of the user. The intent is to permit the user to be able to focus on the data displayed and on engineering analysis problems. The user only needs to know what data-oriented results are desired to be successful with the system.

The Nuclear Plant Data Bank (NPBD) system fully automates the storage and analysis based on this data. The system combines the benefits of a structured data base system and computer-aided modeling with links to large scale codes for engineering analysis. Emphasis on a friendly and very graphically oriented user interface facilitates both initial use and longer term efficiency.

Specific features are:

- Organization and storage of thermohydraulic data items
- Ease in locating specific data items
- Graphical and tabular display capabilities
- Interactive model construction
- Organization and display of model input parameters
- Input deck construction for TRAC and RELAP analysis programs
- Traceability of plant data, user model assumptions, and codes used in the input deck construction process.

The major accomplishments of this past year were the development of a RELAP model generation capability and the development of a CRAY version of the code.

OVERALL DESIGN

The Nuclear Plant Data Bank (NPDB) system consists of the following five major subsystems:

- A hierarchically structured data base
- A data display system
- Thermohydraulic modeling system
- Data input system
- TRAC and RELAP program interfaces

Figure 1 illustrates the overall design

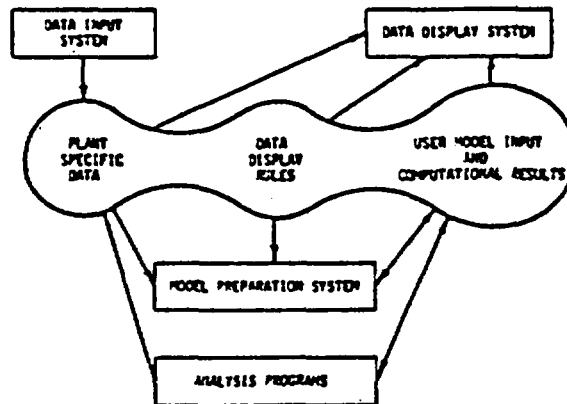


FIGURE 1. NUCLEAR PLANT DATA BANK ARCHITECTURE



## STRUCTURED DATA BASED

The structured data base subsystem used a hierarchic index. The uppermost level of the index is the name of the nuclear reactor power plant; and the level immediately under that consists of summary information for the previous level, categories for the major plant subsystems and categories for model input to specific analysis program (Figure 2). Within each of the major categories, data is stored for the physical plant descriptions, plant system performance and plant operating parameters. This data is stored in sufficient detail to perform state-of-the-art reactor safety analysis.

Data is organized by "engineering" systems so that engineers can rapidly locate and use the data in ways already familiar to them. An important element of user convenience is that screen displays can be obtained simply by positioning a horizontal cross-hair over the hierarchical name of the item to be displayed and hitting the "SPACE" key followed by the "RETURN" key. This cross-hair approach allows one to proceed further from the top of the hierarchy to retrieve greater detail about the nuclear reactor power plant. It also allows one to return to the top levels of the hierarchy as desired. For example, by placing the cross-hair through the name element "RXCOOL" illustrated in Figure 2, one obtains a display of the data structure for the reactor cooling system (Figure 3). The reactor cooling system index indicates that the following types of data are available.

INFO	Summary data
SKETCH	System process flow diagram
OPER-TH	Operating plant parameters (temperature, pressure, etc.)
COMPONENTS	Detailed technical data about individual components
MODEL	Capability to interactively generate an analysis model

Greater detail can be obtained by using the cross-hair to select a specific component. Figure 4 illustrates the hierarchic index that results when detail is required regarding the reactor vessel (selection of VESSEL by the cross-hair). Selection of the D.ZION-1.RXCOOL.VESSEL hierarchic index displays sublevel selections which will result in the display of technical information. The number of levels varies from index branch to index branch, depending upon the intrinsic complexity of the engineering system being described. Note that summary information, a process flow diagram, component technical data, and modeling capability are available just as they were at the preceding index level. Because the same scheme is used throughout the data structure, engineering users are expected to have little difficulty in locating the information they desire.

```

D.ZION-1.INFO
  .RXCOOL
  .SECOND
  .ESAFETY
  .CONTAIN
  .AUXPOWER
  .TRAC-PO2
  .RELAP5
  
```

FIGURE 2. TOP OF THE HIERARCHIC INDEX FOR ZION 1  
HIERARCHIC STRUCTURE FOR THE  
REACTOR COOLING SYSTEM

```

D.ZION-1.RXCOOL.INFO
  .SKETCH
  .MODEL
  .OPER-TH
  .PUMP
  .VESSEL
  .CORE
  .STMGEN
  .PIPESYS
  .PRESSURE
  .VALVE
  
```

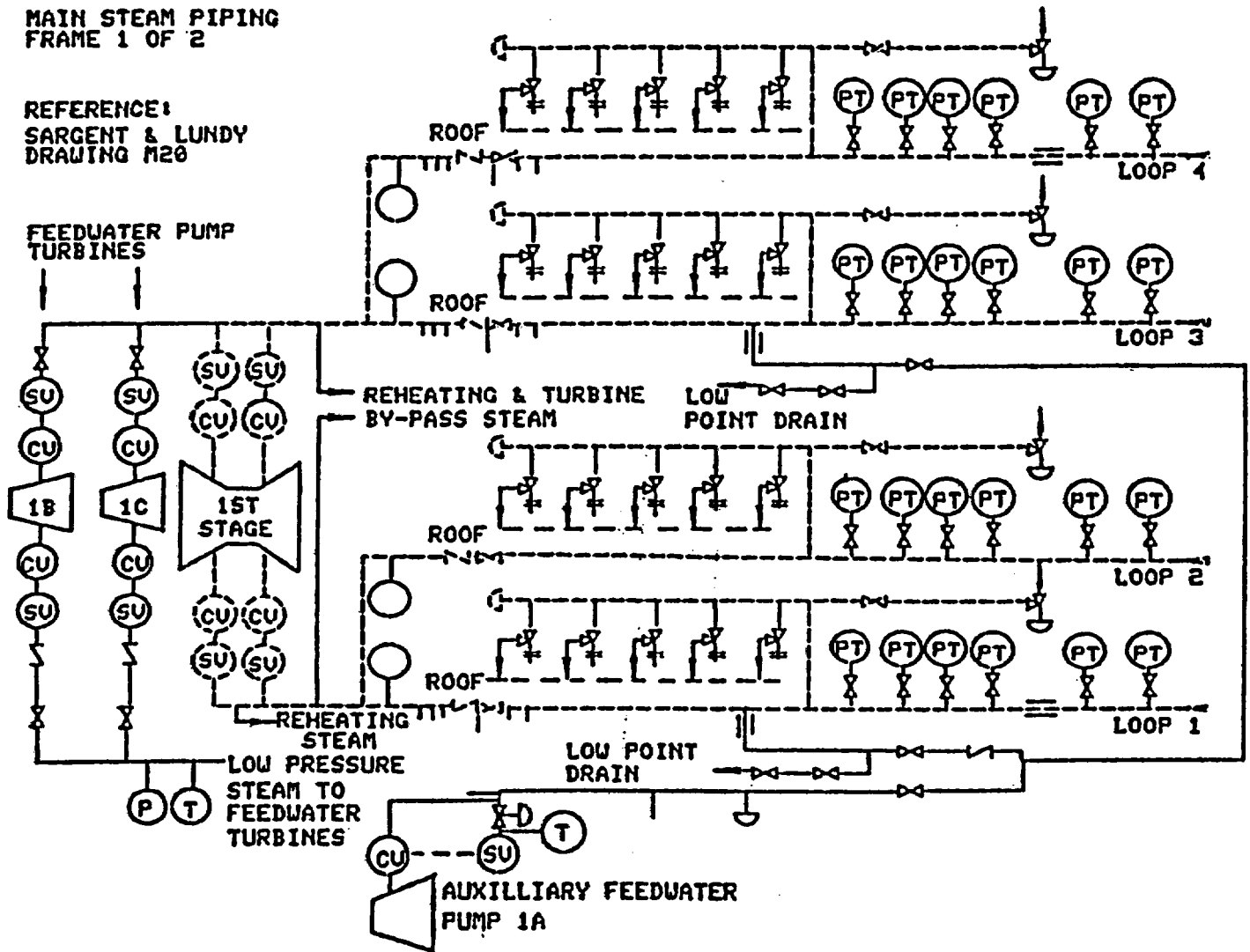
FIGURE 3. REACTOR COOLING SYSTEM HIERARCHIC INDEX

```

D.ZION-1.RXCOOL.VESSEL.SKETCH
  .MODEL
  .INFO
    .ELEV
    .DIM
    .VOLUMES
    .DESIGN
  .CR-DRIVE.INFO
  .US-PLATE.DRAWING
  .INFO
  .UC-PLATE.DRAWING
  .INFO
  .T-SHIELD.INFO
  .BARREL.INFO
  .FORMER.INFO
  .BAFFLE.INFO
  .LC-PLATE.DRAWING
  .INFO
  .D-PLATE.DRAWING
  .INFO
  .SUP-CAST.DRAWING
  .INFO
  .OUT-NOZZ.INFO
  .IN-NOZZ.INFO
  .SLICE.DRAWING
  .OPER-TH.START-3
  .START-85
  .RATED
  
```

FIGURE 4. REACTOR VESSEL HIERARCHIC INDEX

An addition that has been made to supplement data retrieval from the structured data base is to allow the user to point to a sketch in order to identify the data that is desired. This has been implemented for piping systems such that the user may point to a pipe run in order to obtain isometric drawings of the run or to model the run. Figure 5 illustrates the type of P&ID sketch used to select a pipe run. Control system models also combine the use of the hierarchic structure and pointing to sketches.

**D.ZION-1.SECOND.MAINSTM.PIPESYS.SKETCH**
**MAIN STEAM PIPING  
FRAME 1 OF 2**
**REFERENCE:  
SARGENT & LUNDY  
DRAWING M20**

**FIGURE 5. MAIN STREAM PIPING SKETCH**



## DATA DISPLAY SYSTEM

Data is maintained in the Data Bank according to the hierarchic index previously described. This may be operated upon by the data display system to generate video screen displays. In some cases, the same data can be operated upon by more than one display program. It is important to understand that data, not displays of data, are maintained in the data structure and that displays are generated from these data. The following types of displays are currently generated:

Data Tables	Screen displays of data
Sketches	Displays of qualitative data
Plots	Graphic interpretation of tabular data (linear, logarithmic, contour, perspective)
Piping Isometrics	Scaled isometric drawings at user-selected rotation angles
Planar Geometry	Slices through three-dimensional geometry

## MODEL INPUT PREPARATION SYSTEM

The display subsystem, in conjunction with the structured data base subsystem provides the capability to generate analysis models in a very short time span and with very little labor. This represents a major step in improving one's ability to respond to an incident. Not only can models be created from scratch with this system, but the model decisions are stored in such a manner that an engineer other than the original modeler can safely modify the input in a very short time. Graphic displays are used extensively for illustrating the modeling decisions.

Modeling capability has been developed for the following components:

- PWR reactor vessel
- Steam generators
- Pumps
- Piping systems
- Accumulators
- Tanks
- Valves

The control and trip system modeling is partially complete and is expected to be available by the end of November, 1984. Additional components that should become available on the same time frame are:

- Turbine
- Heat exchangers
- Condensers



The data needed to generate models is maintained in the data structure, and programs operate upon this data to generate the models. The engineer must still exercise judgement regarding engineering model decisions. Figures 12 through 14 illustrate the type of screen displays currently used for the modeling of piping, a reactor vessel, and a steam generator. Note that the piping model display provides scaled lengths and elevations and is also useful in obtaining an understanding of pipe systems. Most of the model generation steps are independent of the analysis code that is to be used. However, code specific menus are provided to the user for those features that are dependent upon each code. Very little effort is required to change from a TRAC to a RELAP model (less than a 1/2 hour task).

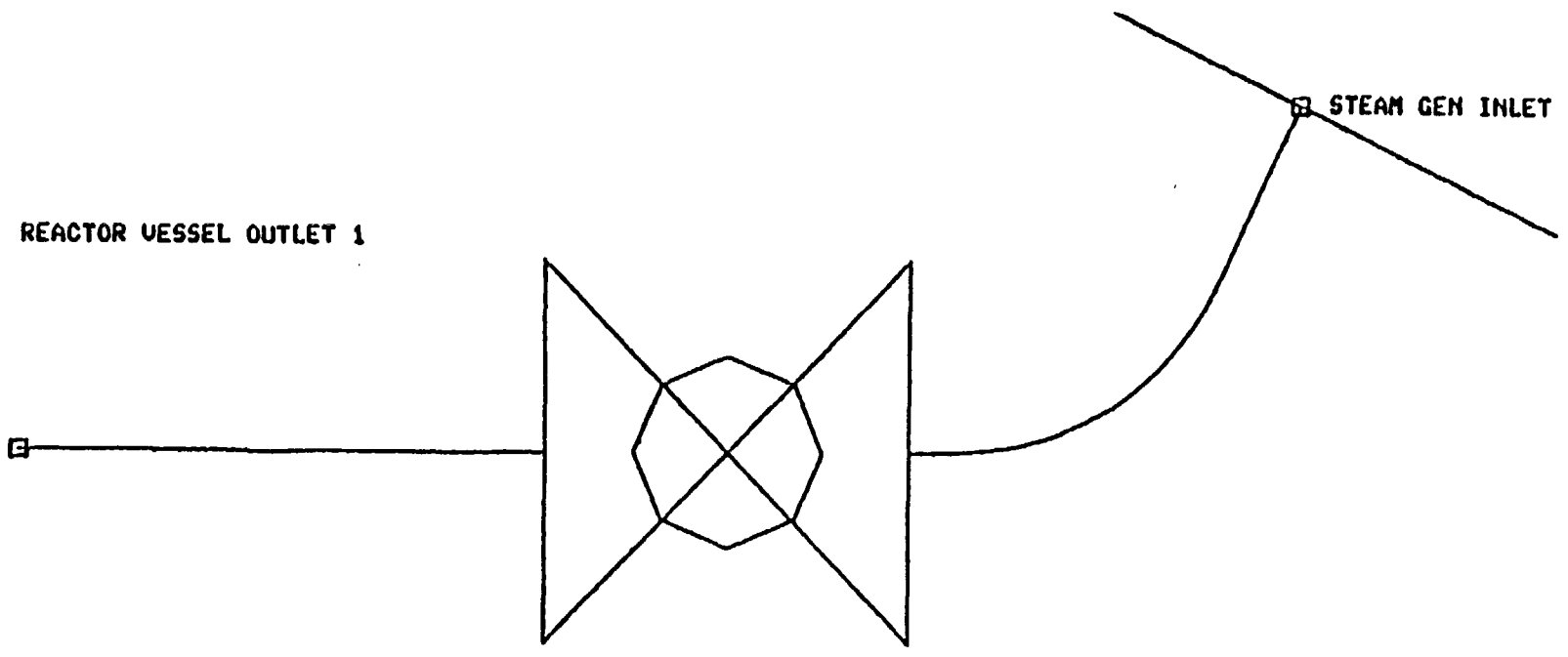


Figure 4. - Main Coolant Loop Model

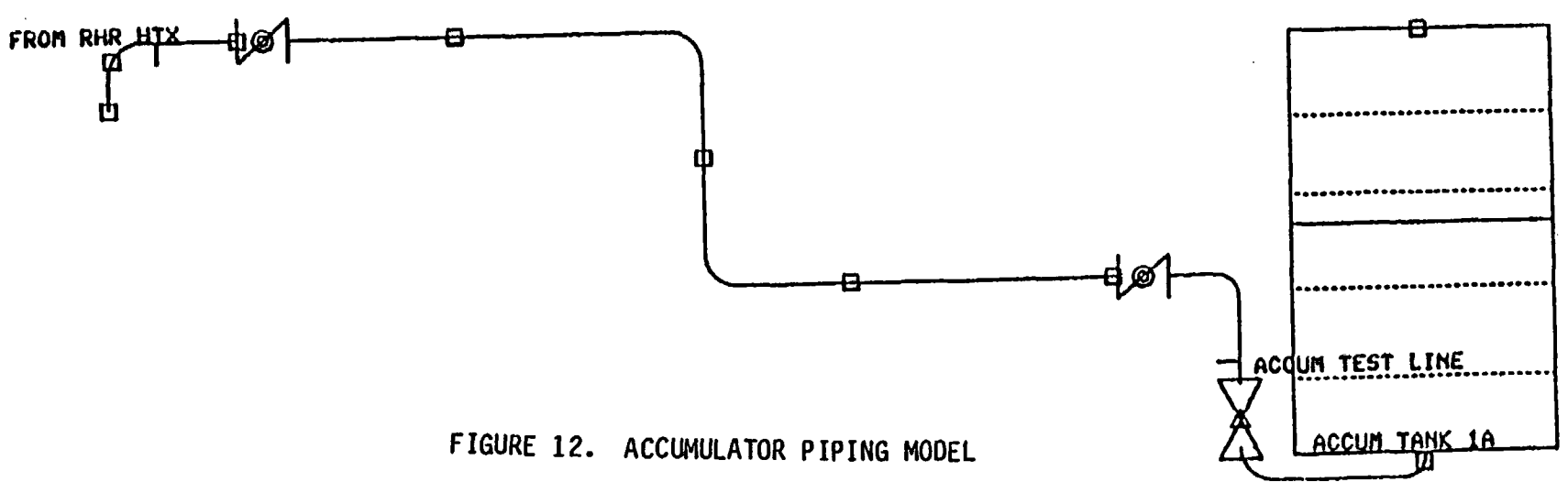


FIGURE 12. ACCUMULATOR PIPING MODEL

D.ZION-1.RXCOOL.VESSEL.MODEL

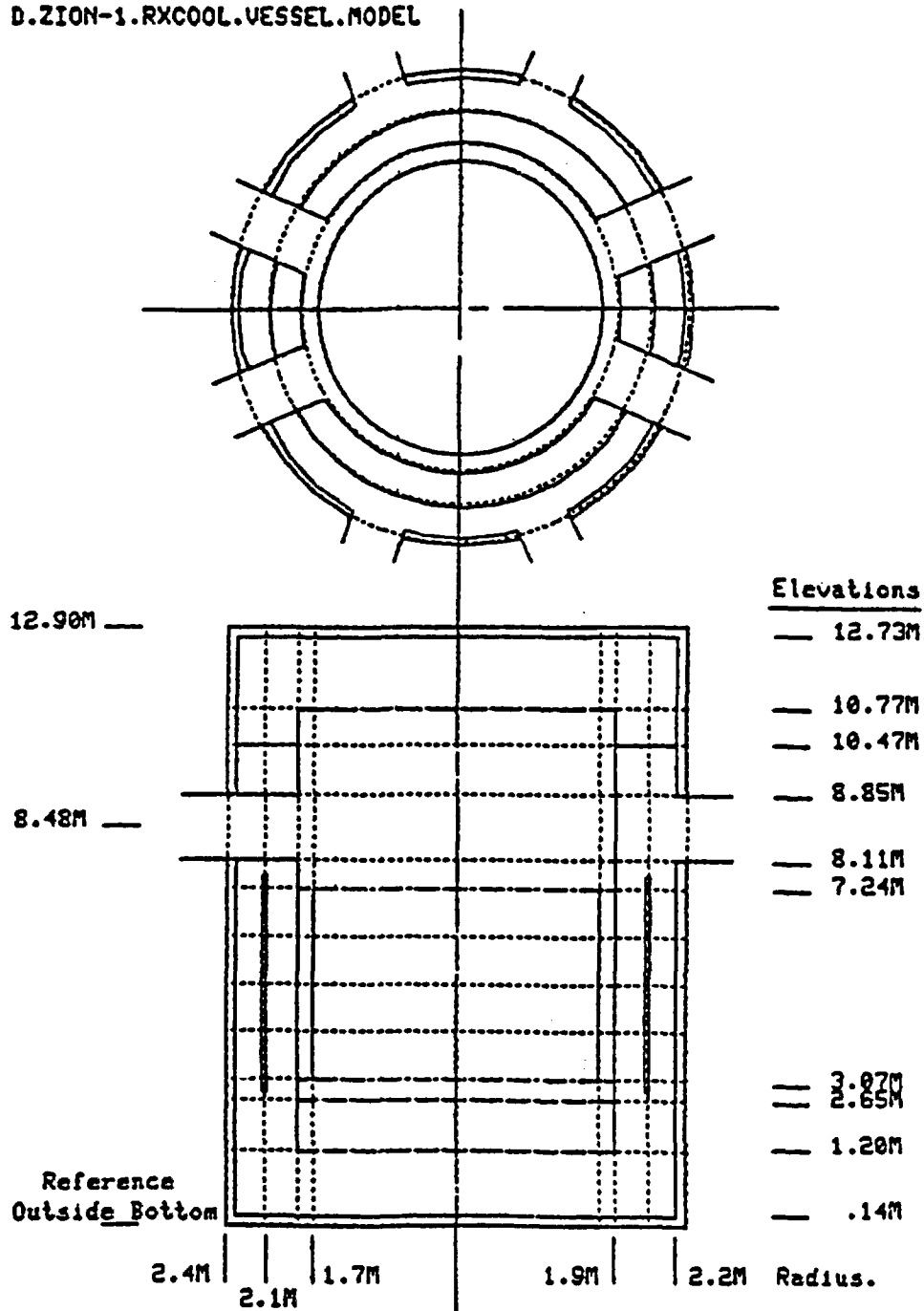


FIGURE 13. REACTOR VESSEL MODEL

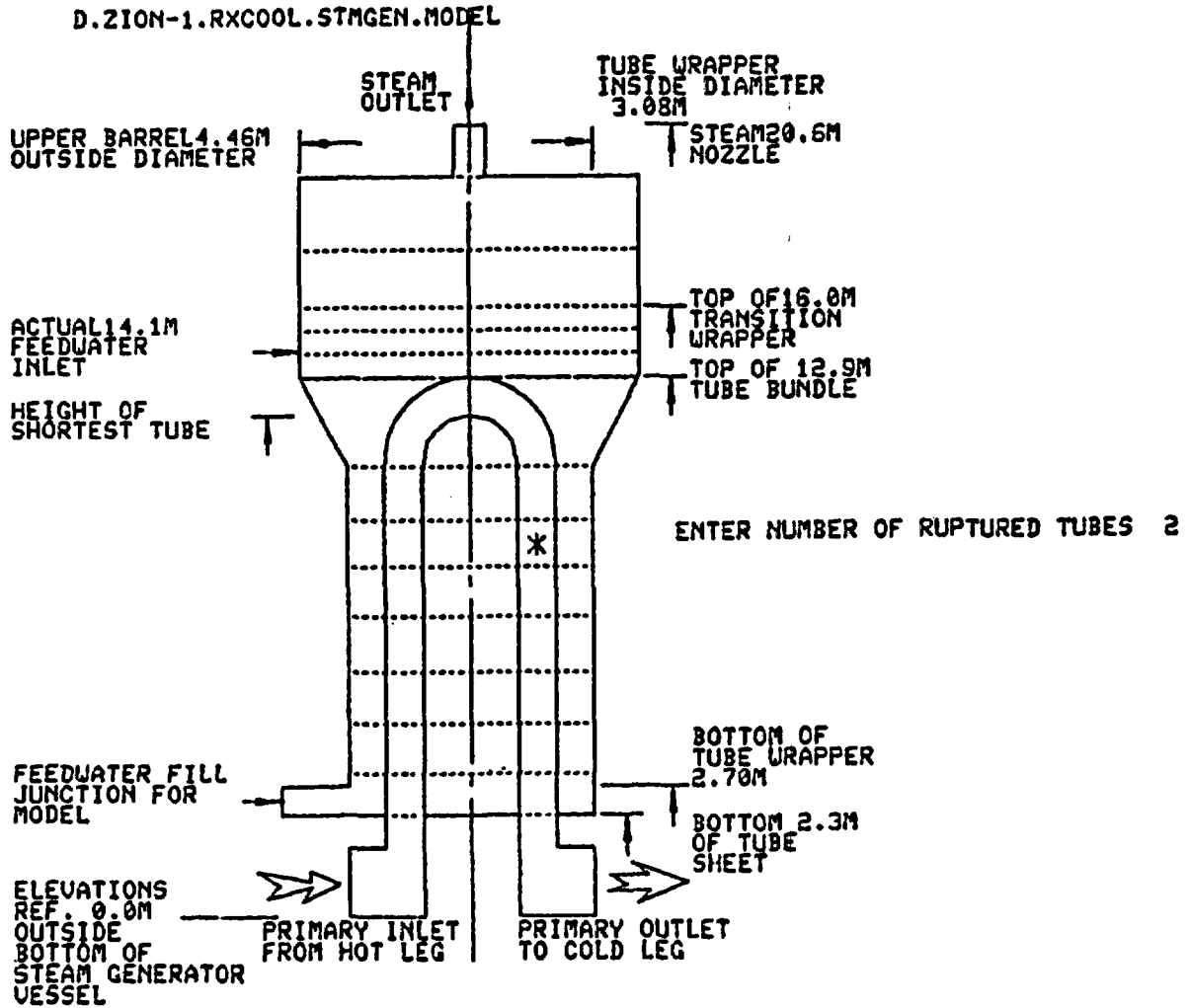


FIGURE 14. STEAM GENERATOR WITH RUPTURE



## TRAC AND RELAP PROGRAM INTERFACES

The modeling capability described in the previous section generates data that is formatted by the NPDB into 'input card decks' for either TRAC-FP1, (the TRAC capability was discussed at the last safety information meeting) or RELAP5, MOD2. These decks contain extensive comments so that the input deck developer can understand them. Since the thrust of the system is to permit the user to model separate components, node numbers are assigned by the NPDB when an input deck is requested. The comment cards in the deck assist the user in understanding the node number assignment.

## TRACEABILITY

An entry is provided on every data collection and display form to provide a reference to basic source documentation. A history is maintained of the use of each group of data including user modeling decisions, and the version of the codes that process the data into the final input deck. The NPDB provides the capability of determining at a later time if the most current data or codes have been used for any specific model. If only data parameters have been modified since the deck was originally created, the process of generating an input deck based on more current data is only a matter of a few keystrokes. However, if a significant change has been made to the plant such as the addition of a component, then an engineer must modify the model for that plant addition prior to generating an up-to-date input deck. Figure 15 illustrates a summary table generated by the NPDB that identifies the data and the computer codes used to create an input deck.

**NPDB Model Status Report  
of ZION-1**

**DATA SETS**

Current SEQ	Used SEQ	Still Current
1	1	D.ZION-1.RXCOOL.CORE.INFO
1	1	D.ZION-1.RXCOOL.VESSEL.OUT-NOZZ.INFO
1	1	D.ZION-1.RXCOOL.VESSEL.IN-NOZZ.INFO
1	1	D.ZION-1.RXCOOL.VESSEL.US-PLATE.INFO
1	1	D.ZION-1.RXCOOL.VESSEL.UC-PLATE.INFO
1	1	D.ZION-1.RXCOOL.VESSEL.LC-PLATE.INFO
1	1	D.ZION-1.RXCOOL.VESSEL.D-PLATE.INFO
1	1	D.ZION-1.RXCOOL.VESSEL.SUP-CAST.INFO
1	1	D.ZION-1.RXCOOL.VESSEL.T-SHIELD.INFO
1	1	D.ZION-1.RXCOOL.VESSEL.BARREL.INFO
1	1	D.ZION-1.RXCOOL.VESSEL.INFO.ELEV
1	1	D.ZION-1.RXCOOL.VESSEL.INFO.DIM
1	1	D.ZION-1.E SAFETY.S-INJECT.ACCUM.PIPESYS.HYDRO
1	1	D.ZION-1.E SAFETY.S-INJECT.ACCUM.PIPESYS.GEOM
		<b>No longer Current</b>
2	1	D.ZION-1.RXCOOL.PIPESYS.HYDRO
3	1	D.ZION-1.RXCOOL.PIPESYS.GEOM

**CODES**

Current version id	Used version id	Still Current
U1	U1	UESGEO
U1	U1	MSCALE
		<b>No longer Current</b>
U2	U1	MODEL3

FIGURE 15. NPDB MODEL STATUS REPORT OF ZION-1



## COMPUTER CONFIGURATION

The NPDB has been implemented at Idaho National Engineering Laboratory on a CDC CYBER-176 using NOS/BE operating system. It is currently being revised to function under the NOS operating system. The NPDB has also been implemented to function at Los Alamos National Laboratory using a CRAY1S computer using the CTSS operating system. At the specific direction of the NRC, a Tektronix 4014 has been used as the NPDB terminal. The high resolution provided by this terminal is used for detailed drawings and P&ID drawings. Terminal technology has evolved very rapidly and many alternatives are possible.

Technology Development of California has developed a microprocessor workstation product which provide the interactive portion of the NPDB. This provides quicker response to the engineer than the larger mainframe computer version. The background portion of the NPDB resides on the host mainframe computer in this configuration and interfaces to the workstation. Technology Development of California also offers enhanced data entry capabilities on microprocessor workstations.

## FUTURE PLANS

The thrust of the NRC sponsored NPDB project is:

- Validation of capability of INEL and LANL
- Entry of additional plant data
- Dissemination of the NPDB to Nuclear Electric Utilities

The validation and data entry phases noted above have already begun at various NRC contractors.

The Electric Power Research Institute currently plans to enhance the NPDB by sponsoring an interface to the RETRAN safety analysis computer program.

## REFERENCES

1. Kopp, HJ, "Nuclear Plant Data Bank (NPDB) and Input Deck Preparation", Tenth Water Reactor Safety Research Information Meeting, October 12-15, 1982, NUREG/CP-0041, Volume 2, pp. 29-38.
2. Kopp, HJ, et al. "Automating TRAC decks using the Nuclear Plant Data Bank", Eleventh Water Reactor Safety Research Information Meeting, October 24-28, 1983, NUREG/CP-0048, Volume 3, pp. 357-369.

THE LOS ALAMOS NUCLEAR PLANT ANALYZER:  
AN INTERACTIVE POWER-PLANT SIMULATION PROGRAM\*

Robert Steinke, Clay Booker, Paul Giguere, Dennis Liles,  
John Mahaffy, and Michael Turner  
Safety Code Development Group  
Los Alamos National Laboratory  
Los Alamos, New Mexico 87545

ABSTRACT

The Nuclear Plant Analyzer (NPA) is a computer-software interface for executing the TRAC or RELAP5 power-plant systems codes. The NPA is designed to use advanced supercomputers, long-distance data communications, and a remote workstation terminal with interactive computer graphics to analyze power-plant thermal-hydraulic behavior. The NPA interface simplifies the running of these codes through automated procedures and dialog interaction. User understanding of simulated-plant behavior is enhanced through graphics displays of calculational results. These results are displayed concurrently with the calculation. The user has the capability to override the plant's modeled control system with hardware-adjustment commands. This gives the NPA the utility of a simulator, and at the same time, the accuracy of an advanced, best-estimate, power-plant systems code for plant operation and safety analysis.

INTRODUCTION

The Nuclear Plant Analyzer (NPA), a US Nuclear Regulatory Commission (NRC) sponsored project, provides a more powerful and convenient user interface for executing the major power-plant systems codes: the Transient Reactor Analysis Code (TRAC) (Ref. 1) and the Reactor Leak and Power Safety Excursion Code (RELAP5) (Ref. 2). Los Alamos National Laboratory and Idaho National Engineering Laboratory (INEL) jointly are developing the NPA. Technology Development of California (TDC) Inc. is developing the Nuclear Plant Data Bank (NPDB) to be used by the NPA for TRAC or RELAP5 input data preparation.

TRAC and RELAP5 are advanced, best-estimate, thermal-hydraulic systems codes used to analyze the operation and safety of nuclear, as well as conventional, power plants. Weeks to months of human effort are required to prepare and quality-assure input data, to execute TRAC or RELAP5 utilizing that data, and to interpret the results of the calculation. The NPA is designed to automate most of this procedure. In addition, the NPA provides interactive capability to the user during the calculation. Calculational results are

---

\* This work was funded by the US NRC Office of Nuclear Regulatory Research, Division of Accident Evaluation.

presented in graphics displays as the calculation proceeds. Control of the plant, as defined by the input data, can be overridden at any time during the calculation by hardware-adjustment commands issued by the NPA user. The NPA handles all interaction with the computing environment. This allows the user's attention to be devoted fully to the transient event being analyzed.

The NPA provides TRAC and RELAP5 users with an analysis tool that can reduce significantly the time and effort required to analyze power-plant transients. Opportunities for introducing human error into the analysis are reduced greatly through automating most of the data manipulation. No experience is needed to run these complex computer codes with the NPA. Reading and understanding a sizable user's manual are no longer prerequisites. Now, analysts need only the expertise to understand the complex thermal-hydraulic phenomena occurring in power-plant transients.

The NPA has been under development for two years. Several more years will be required to develop its full capability. Thus far, an NPA to drive TRAC has been developed at Los Alamos, and a separate NPA to drive RELAP5 has been developed at INEL using common guidelines. This was done to facilitate the programming and testing of NPA interactive coupling to each code. With this now completed, the next step will be to combine these two NPA versions utilizing the best features of each and to incorporate software to access and utilize the NPDB. In this paper, the current TRAC-based NPA developed at Los Alamos will be described.

#### HARDWARE

The Tektronix 4115B, intelligent, high-resolution color-graphics terminal has been selected as the NPA workstation. In addition, it has data storage configured as two hard-disk drive units and two floppy-disk drive units, a color hard-copy unit, and a 4800/9600-baud modem to communicate with the mainframe computers at Los Alamos or INEL. The TRAC/RELAP5 thermal-hydraulic calculation is executed on a Cray-1 or a Control Data Corporation 7600/Cyber 176 mainframe computer.

Currently, the NPA software and graphics-data manipulation are executed on the mainframe computer as well. In this form, the NPA can be run on a Tektronix 4105, 4107, or 4109 nonintelligent, color-graphics terminal. Eventually, when the two NPA versions are combined, these functions will be downloaded to execute on the 4115B intelligent workstation. The capability for executing everything on the mainframe computer, however, will be maintained so that a less expensive, nonintelligent workstation can be used as well.

#### SOFTWARE STRUCTURE

A block diagram of the Los Alamos NPA software structure is shown in Fig. 1. Computer programs are shown as boxes, and data files are shown as ellipses. There are three programs that execute on the same computer using different execution suffixes in a time-shared computing environment. The NPA executive program executes on suffix A; it generates the terminal's graphics display and communicates with the NPA user, TRAC, and the Common File System (CFS) for accessing and permanently storing files. The IOGRF program executes on suffix D; it reads data from the TRAC graphics-data output file TRCGRF1 and writes a selected portion of that data to the NPA executive graphics-data

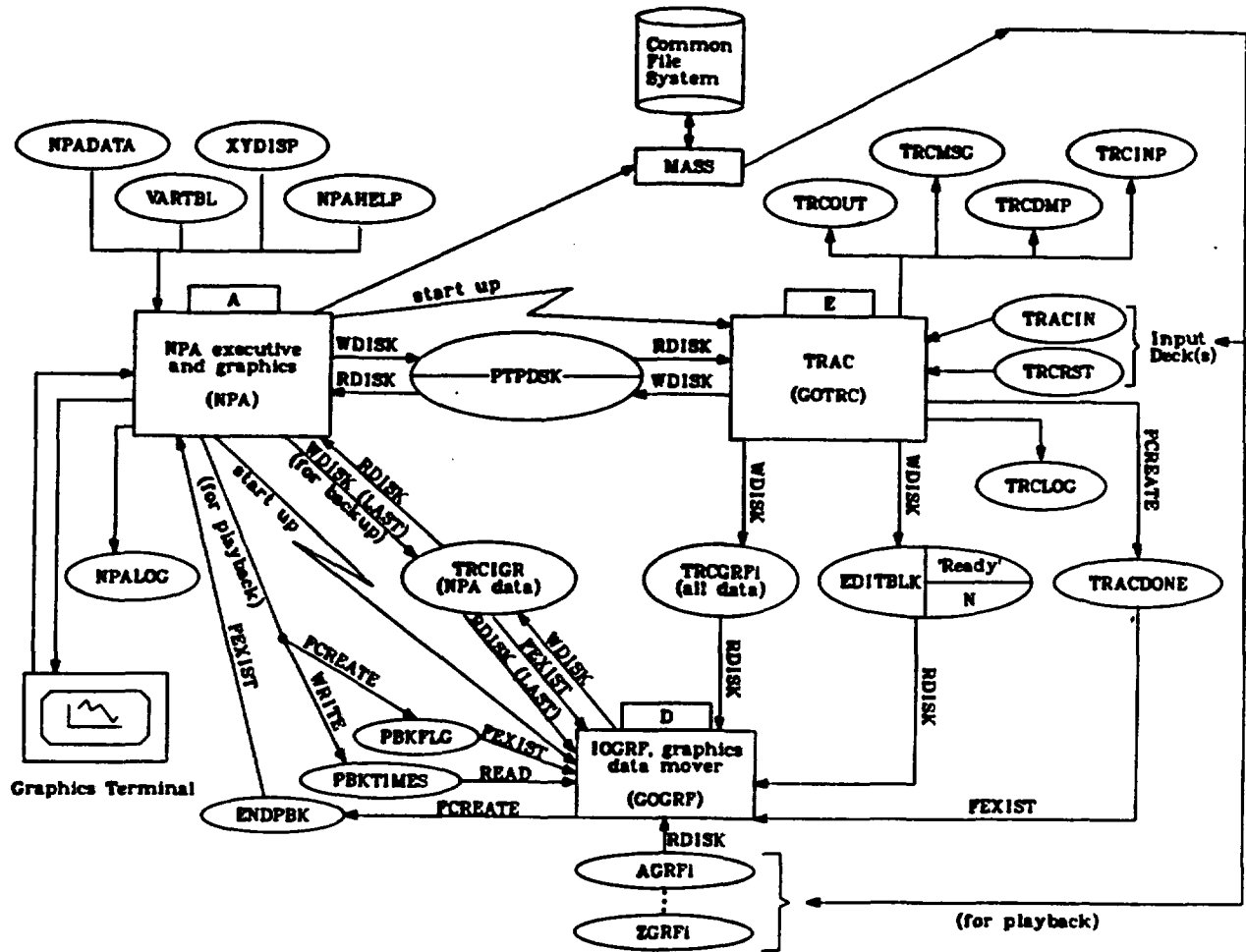


Fig. 1.  
A block diagram of the NPA software structure.

input file TRCIGR. The TRAC program executes on suffix E; it performs the power-plant, thermal-hydraulic calculation.

The data files reside on a local storage disk and perform three functions: to communicate data and information between programs, to provide input data to a program, and to store output data from a program. The files TRCGRF1, TRCIGR, EDITBLK, TRACDONE, PTPDSK, PBKTIMES, PBKFLG, and ENDPBK communicate between programs. Files NPADATA, VARTBL, XYDISP, NPAHELP, TRACIN, and TRCRST provide input data to the NPA and TRAC programs. Files NPALOG, TRCLOG, TRCGRF1, TRCOUT, TRCMSC, TRCDMP, and TRCINP store output data from the NPA and TRAC programs.

Files TRCGRF1 and TRCIGR, as described earlier, are used to transfer graphics data from the TRAC program to the NPA executive program using the IOGRF program. The NPA executive program also uses file TRCIGR to send to program IOGRF the number of time edits of graphics data (LAST) to be retained in file TRCIGR for a backup/branch calculation. File EDITBLK sends to program IOGRF the message 'Ready' and the number of time edits already written by TRAC

on file TRCGRF1. File TRACDONE is created by TRAC just before terminating a TRAC run. Its presence serves as a flag to program IOGRF to terminate execution as well because no further data will be written to the TRCGRF1 file by TRAC.

File PTPDSK communicates information between the TRAC and NPA executive programs. The NPA sends user commands affecting TRAC and NPA messages to the TRAC program; TRAC sends its status data and TRAC messages to the NPA executive program. At present, PTPDSK is a disk file. Communications with it, however, have been designed to allow it to be replaced eventually with a direct process-to-process (PTP) protocol communication path between the TRAC and NPA executive programs. A direct PTP path would eliminate much of the time delay experienced with disk read/write operations and with written data being buffered in blocks for efficiency.

Files PBKTIMES, PBKFLG, and ENDPBK communicate the problem time intervals that graphics data in previously generated TRCGRF1 files (renamed AGRF1, BGRF1, ..., ZGRF1) are to be played back through file TRCIGR to the NPA executive program. In this NPA operating mode, the TRAC program is not executed. The creation of file PBKFLG flags the IOGRF program to read the problem time intervals from file PBKTIMES; to read the desired graphics data from TRCGRF1 files AGRF1, BGRF1, ..., ZGRF1; and to write it to file TRCIGR. Program IOGRF signals completion of this task to the NPA executive program by creating file ENDPBK.

The remaining files provide input data to and store output results from the NPA executive and TRAC programs. Files NPADATA, VARTBL, and XYDISP contain problem-dependent information that the NPA executive program uses to create the graphics displays. Information for an on-line help package for the NPA user is contained in file NPAHELP. The two input files, TRACIN and TRCRST, are the standard TRAC input and restart data files, respectively. The NPALOG and TRCLOG files contain a record of all communications between the NPA user, the NPA executive program, and the TRAC program. This encompasses commands, messages, and responses (when the message is a question). Files TRCGRF1, TRCOUT, TRCMSG, TRCDMP, and TRCINP are the standard TRAC output files containing graphics data, thermal-hydraulic state edits, execution messages, data dumps, and TRAC input-format data, respectively.

#### PROBLEM STARTUP

The NPA is run by executing the NPA executive program. Input-data files NPADATA, VARTBL, XYDISP, and NPAHELP must be created or retrieved from CFS storage by the user before the run. Eventually, the NPA executive program will be automated to do this. A menu system is available to allow the user to select a desired power plant and to have the NPA executive program access the plant's TRAC input-data files TRACIN and TRCRST from CFS storage. At present, these files are available for only the Three Mile Island (TMI) Unit 2 and Calvert Cliffs power plants. An example sequence of four menu displays is shown in Fig. 2. Positioning the + cursor nearest to an item and hitting the space-bar key or typing the number of the item brings up its subdirectory menu on the video screen. The screen displays shown in Fig. 2 and in subsequent figures are black and white copies of actual screen displays made by the color hard-copy unit.

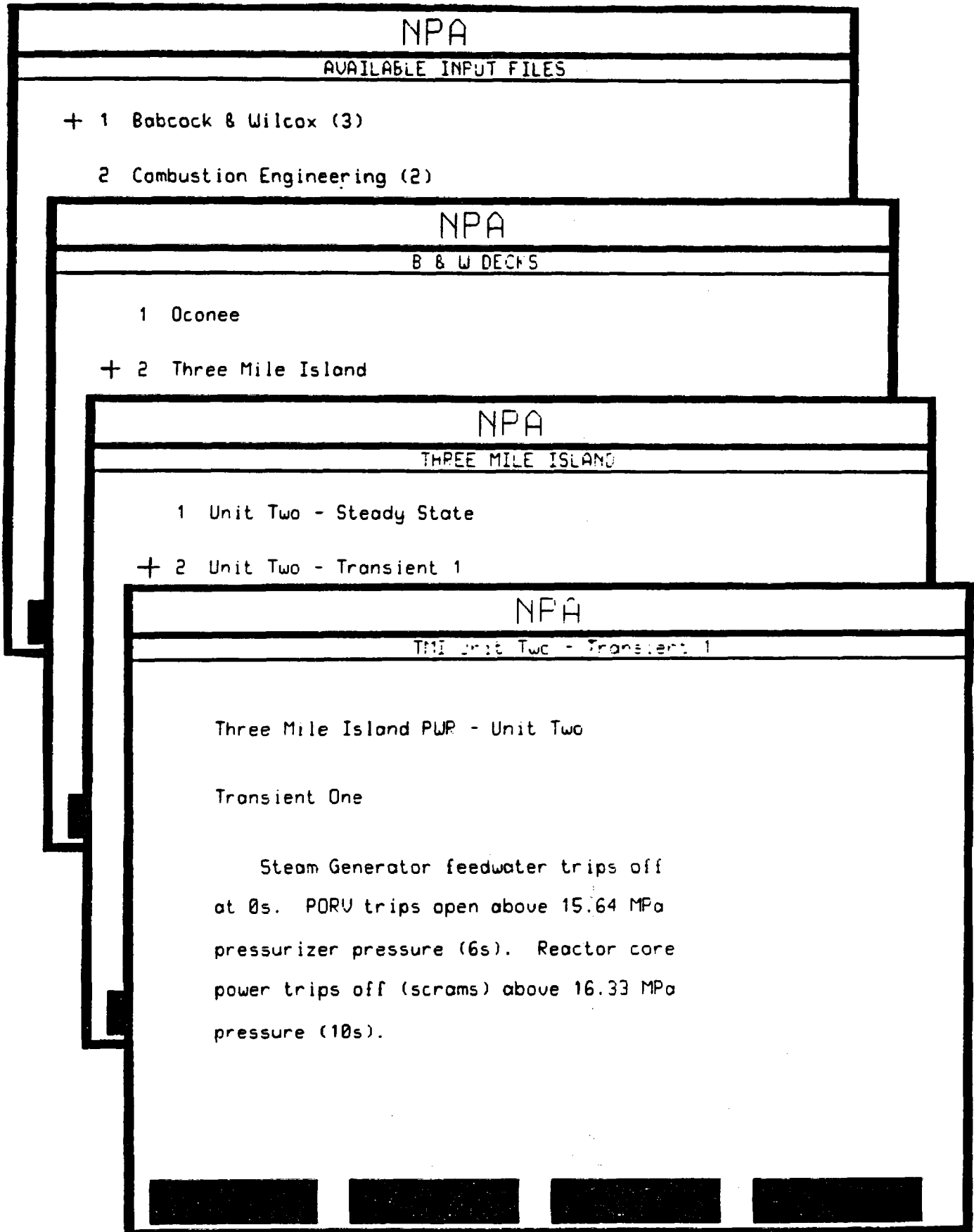


**Fig. 2.**  
Four sequential screen displays selected by the + cursor from the hierarchical menu system.

For each power plant, steady-state and transient input-data files are available. There is only the TRACIN file for steady-state analysis, because it is an initial TRAC calculation. Transient analysis requires file TRCRST as well as TRACIN, because it is the restart of a previous TRAC run (the end of the steady-state calculation or the restart at some time during a transient calculation). Restart-data file TRCRST is the renamed data-dump file TRCDMP created by TRAC in a previous run. The menu system may be bypassed if files TRACIN and TRCRST were created or accessed from CFS storage by the user before the run. Eventually, the menu system will provide the user with the capability to create file TRACIN using the geometric and operational data from a desired power plant stored in the NPDB. Numerical modeling information, which also is required to create TRACIN, would be obtained through interactive dialog with the user.

With TRACIN and TRCRST as local files, the NPA executive program starts the IOGRF and TRAC programs on execution suffixes D and E, respectively. It then pauses execution until TRAC and IOGRF execute far enough to create and write graphics data to the TRCGRF1 and TRCIGR files, respectively. At this point, TRAC and IOGRF pause execution as well. The NPA executive program then initializes the graphics display and the TRAC status as being "paused" on the video screen. The problem setup and calculation startup are now complete. An NPA-user command is needed now to continue with the interactive TRAC calculation.

#### SCREEN DISPLAYS

The video-screen display is subdivided into two areas: the upper 84% of the screen is for the graphics display and the lower 16% is for five lines of data communications with the NPA user. Three different types of graphics displays currently are available: time-history plots, a power-plant display of generic data, and a TRAC-noding display of detailed data. The five communication lines consist of two lines for TRAC-status information, one line for messages or questions to the NPA user, and two scrolling dialog lines for entering NPA-user commands and responses.

An example display of six time-history (x-y) plots is shown in Fig. 3. This display can have from one to six time-history plots with one to three function curves (in green, yellow, and white) on each plot. The number of such displays and the form of each is defined by file XYDISP. The NPA user is given the capability to define or modify the form of these displays interactively at the terminal.

Examples of a TMI Unit 2 power-plant display of generic data and a TRAC-noding display of detailed data are shown in Figs. 4 and 5, respectively. Generic and detailed data, defined by files NPADATA and VARTBL and written to file TRCIGR by program IOGRF, are shown in Table I. The form and content of these schematic displays are programmed currently in the NPA executive program. Eventually, they will be generated internally by the NPA executive program from the geometric and numerical-modeling information in the TRACIN and TRCRST files and from the NPA user's interactively selected parameters. In these displays, the numerical values of generic data are shown and vary as TRAC problem time advances. The detailed-data parameter's value (void fraction of water in Fig. 5) is represented by color with a spectrum of colors spanning the parameter's value range. If Fig. 5 was shown in color as it is on the video-screen display, it would be easy to locate where steam and liquid

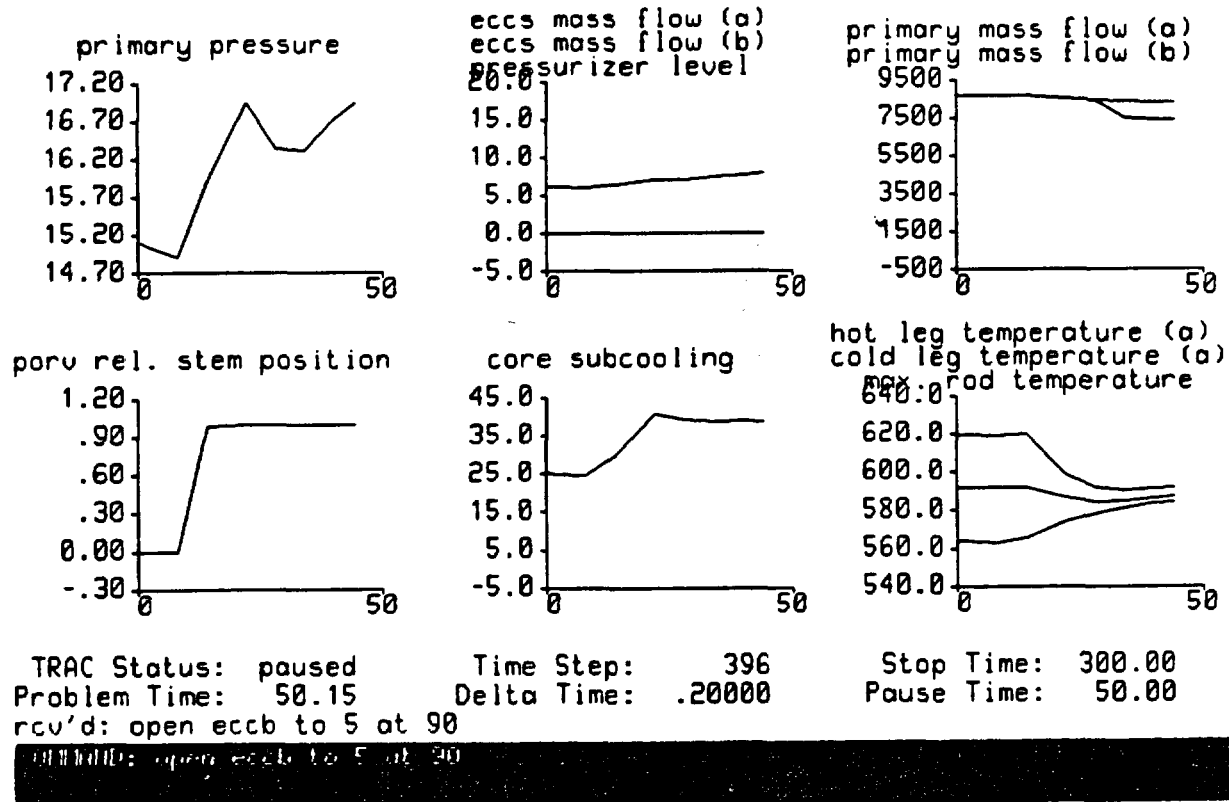
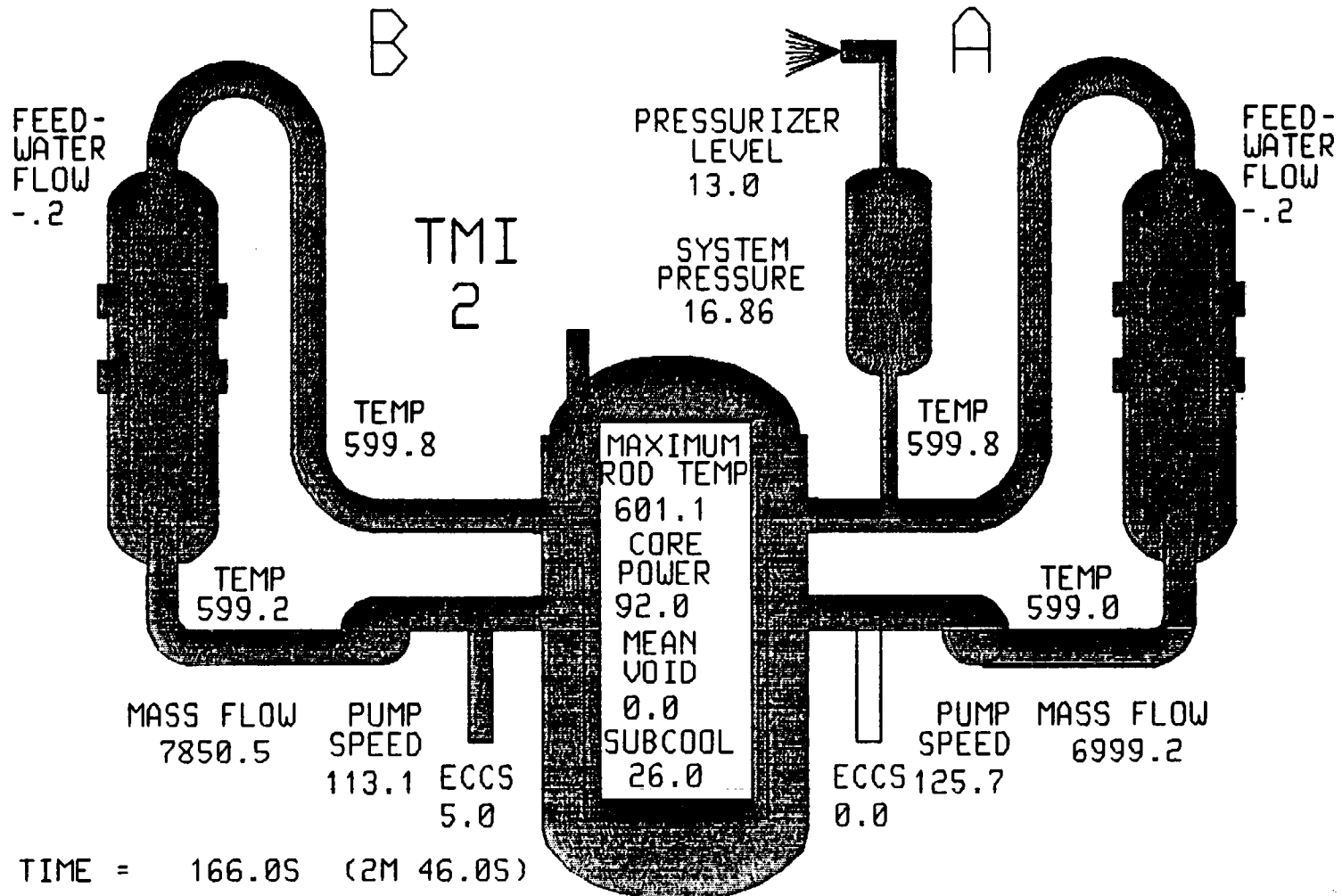


Fig. 3.  
Time-history (x-y) plot display.

water reside and where change of void fraction is occurring (when viewed over time).

The TRAC-status information shown in the first two communication lines of the display is transferred from TRAC to the NPA executive program by file PTPDSK. This information consists of the execution state of TRAC (running, paused, end exit, or err exit), current TRAC problem time, current time-step number, size of the last time step, the NPA user-defined TRAC stop time, and the next pending TRAC pause time. While TRAC problem time also is shown in the graphics displays, the TRAC-status time is more current with the TRAC calculation. Eventually, when the PTPDSK file is replaced by a PTP protocol communication path between the TRAC and NPA executive programs, the time delay between the TRAC calculation and its status display will be reduced to only a few time steps. Having current TRAC-status information can be very important when issuing commands to TRAC "on the fly" (when TRAC is running).

The message/question line and the two dialog lines for NPA-user commands/responses provide the window for communication between the NPA executive program and the NPA user. Commands available to the NPA user are discussed in the next section. When the NPA executive program processes a command, the command in the form that it was received is displayed on the message line (see Figs. 3 and 4). Many possible messages and questions may appear on this line. Figure 5 provides an example of a backup question. When

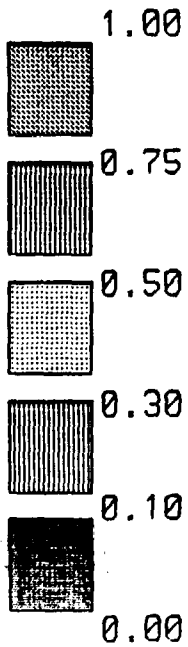


TRAC Status: paused      Time Step: 671      Stop Time: 300.00  
 Problem Time: 170.05      Delta Time: .50000      Pause Time: 170.00  
 rcv'd: set pumpa to .2  
 COMMAND: set pumpa to .2

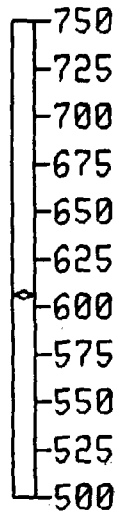
Fig. 4.  
 Power-plant display of generic data.

TIME = 273.35 (4M 33.3S)

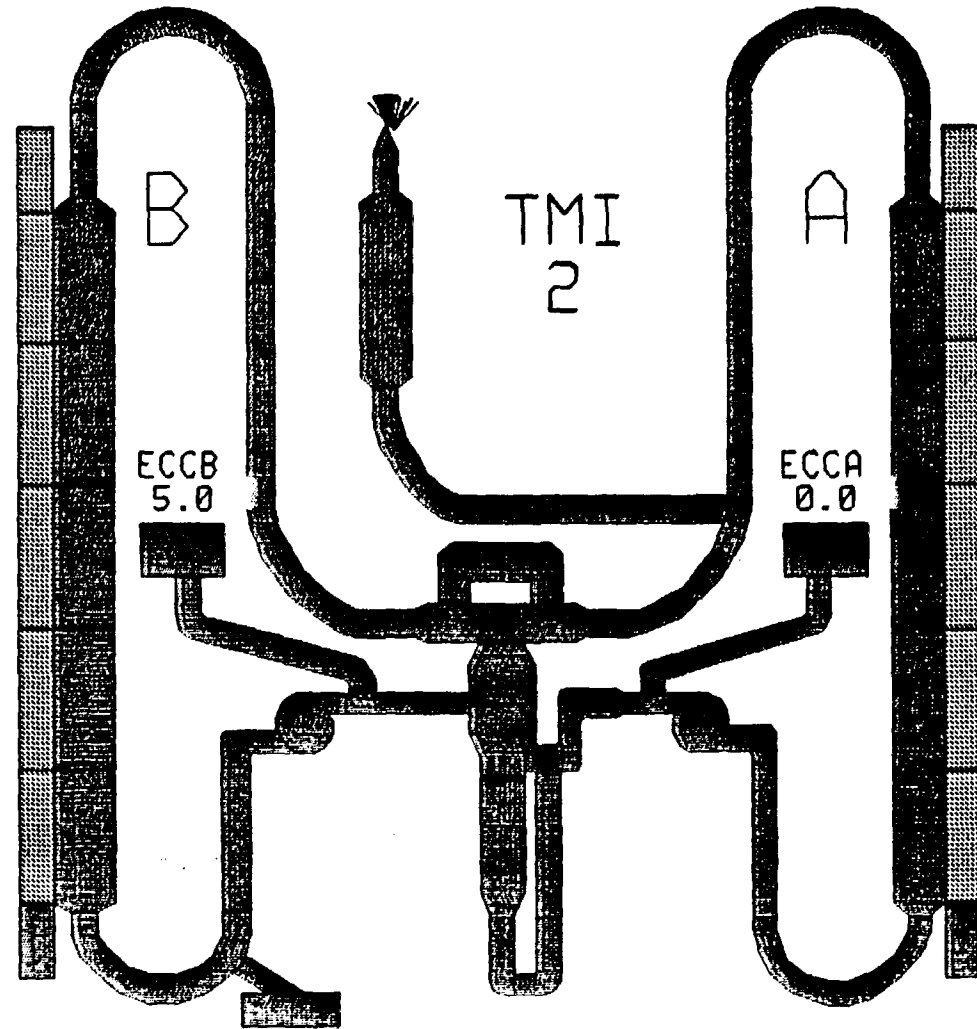
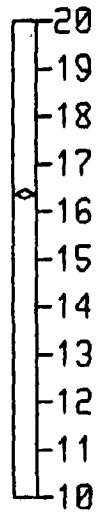
Void Fraction



Max  
Clad  
Temp



System  
Press-  
ure



TRAC Status: paused      Time Step: 815      Stop Time: 300.00  
Problem Time: 280.33      Delta Time: 1.00000      Pause Time: 280.00  
Is a backup to be done to time 200.00 s for the close command (y or n)?

COMMAND: close parv at 300

Fig. 5.  
TRAC-noding display of detailed data.

TABLE I  
NPA GRAPHICS-DATA PARAMETERS

Generic Data, Two-Loop (A and B) Plant

<u>Name</u>	<u>Description</u>	<u>Name</u>	<u>Description</u>
CLTA	Cold-leg temperature (A)	PRZRLV	Pressurizer level
CLTB	Cold-leg temperature (B)	PUMPSPA	Pump speed (A)
COREVOID	Core void fraction	PUMPSPB	Pump speed (B)
ECCSMFA	ECCS mass flow (A)	SECPA	Steam-generator secondary pressure (A)
ECCSMFB	ECCS mass flow (B)	SECPB	Steam-generator secondary pressure (B)
HLTA	Hot-leg temperature (A)	SGPRIMFA	Steam-generator primary mass flow (A)
HLTB	Hot-leg temperature (B)	SGPRIMFB	Steam-generator primary mass flow (B)
LDMFB	Let-down mass flow (B)	SGSECLVA	Steam-generator secondary level (A)
MAXRT	Maximum rod-cladding temperature	SGSECLVB	Steam-generator secondary level (B)
PORV	PORV relative stem position	SGSECMFA	Steam-generator secondary mass flow (A)
POWER	Reactor-core thermal power	SGSECMFB	Steam-generator secondary mass flow (B)
PRIMFA	Primary mass flow (A)	SUBCOOL	Reactor-core subcooling
PRIMFB	Primary mass flow (B)	SUPHEATV	Reactor-core vapor superheat
PRIP	Primary pressure		

Detailed Data

ALPHA	Void fractions in all mesh cells	TL	Liquid temperatures in all mesh cells
MFLOW	Mass flows at all mesh-cell interfaces		

a question is asked, the expected responses are shown within parentheses by the question mark. For a question with "(y or n)?", for example, the NPA user should respond with "y" for yes or "n" for no.

**NPA-USER COMMANDS**

After problem startup is completed, the TRAC and IOGRF programs are paused and the NPA executive program issues a "COMMAND:" prompt on the lower dialog line. Now, the NPA user controls execution of the NPA executive and TRAC programs with the commands shown in Table II. At some point, a RUN or STEP command must be entered to restart TRAC (and IOGRF) execution. The use of all other commands is optional. Commands can be entered at any time, even when TRAC is running. When TRAC is "running", the RETURN key must be hit first to get a "COMMAND:" prompt before entering a command. When TRAC is in a "paused", "end exit", or "err exit" state, the "COMMAND:" prompt appears automatically.

A command is implemented either by the NPA executive program or the TRAC program, as noted in Table II. The commands that the NPA executive program sends to TRAC through file PTPDSK are used to control hardware adjustment (currently valve closure, pump speed, reactor-core thermal power, and boundary-condition pressure and mass flow), TRAC output affecting the NPA, and TRAC execution. The quantities "value", "time", and "interval" in the commands are user-defined numbers (values). The quantity "command name" or "component name" is a word or letter string: "command name" is the first word of any command in Table II; "component name" is one of the letter-string names in Table III defining a hardware component or an adjustable action. Currently, the names in Table III are programmed in the NPA executive program

TABLE II  
NPA-USER COMMANDS

To the NPA Executive Program

<u>Command</u>	<u>Description</u>
ADD value	Add a new x-y display numbered "value"
CANCEL (or C)	Cancel previous command entered
CHANGE (or CH) value	Change existing display numbered "value"
COPY	Make a color hard copy of the screen display
DISPLAY (or D) value	Bring up the screen display numbered "value"
END (or E)	End the NPA interactive run
HELP command name	Get help information on "command name"
RESET (or RESCALE or RS) keyword TO (or =) value/s	Rescale or redefine x-y plot coordinates or format
WCOPY	Make a color hard copy of the screen display with black and white reversed

To the TRAC Program

For Hardware-Adjustment Control

CLOSE component name TO (or =) value AT time	Close a valve, pump, or fill to its "value" state
OPEN component name TO (or =) value AT time	Open a valve, pump, or fill to its "value" state
SCRAM AT time	Shut down the reactor-core thermal power
SET component name TO (or =) value AT time	Set the hardware-action state to "value"
TRIP component name AT time	Set the hardware-action state to its zero-value state

For TRAC-Output-Affecting-NPA Control

DUMP AT time EACH interval	Redefine the TRAC data-dump time and interval
EDIT AT time EACH interval	Redefine the TRAC graphics-data edit time and interval

For TRAC-Execution Control

BACKUP TO time	Perform a backup/branch procedure
PAUSE (or P) AT time	Pause the TRAC program
RUN (or R) TO (or FOR) time	Restart TRAC and set the TRAC-run end time
SPEED RATIO value	Limit TRAC to execute no faster than "value" times real time
STEP value	Restart TRAC and implement a PAUSE AT "present time plus value" command
STOP AT time	Set the TRAC-run end time

TABLE III

NPA "COMPONENT NAME" FOR HARDWARE COMPONENTS OR ADJUSTABLE ACTIONS

<u>Name</u>	<u>Description</u>	<u>Name</u>	<u>Description</u>
CONPA	Containment pressure at Loop A PORV	LDB	Letdown mass flow or velocity, Loop B
CORE	Reactor-core component	PORV	Pressure-operated relief-valve component
ECCA	ECC <sup>a</sup> mass flow or velocity, Loop A	PUMPA	Primary pump component, Loop A
ECCB	ECC <sup>a</sup> mass flow or velocity, Loop B	PUMPB	Primary pump component, Loop B
FWA	SGS <sup>b</sup> feedwater mass flow or velocity, Loop A	SGSECPA	SGS <sup>b</sup> pressure, Loop A
FWB	SGS <sup>b</sup> feedwater mass flow or velocity, Loop B	SGSECPB	SGS <sup>b</sup> pressure, Loop B

<sup>a</sup>ECC is emergency core coolant.

<sup>b</sup>SGS is steam-generator secondary side.

for a two-loop plant. Eventually, the user will be able to define these names and the hardware-adjustment actions they represent interactively.

For the TRAC commands, the "AT time", "TO (or =) value", and "EACH interval" are optional parts of the command. If "AT time" is not specified, the time for implementing the command's action defaults to the current TRAC problem time. If "TO (or =) value" is not specified, the default value is 0.0 for the CLOSE command and 1.0 for the OPEN command. An exception is the SET command that requires a "value" to be specified. The number "value" is either the physical value of the action (in SI units) or the fractional value (when between 0.0 and 1.0) of the 'fully deployed' operating state. If "EACH interval" is not specified, the default time interval is a very large number.

Commands received by TRAC are stored in a 'stack' arrangement. The commands are ordered first by type of command and then by implementation time. This allows the NPA user to enter any number of commands to TRAC with any number of the same type (PAUSE, for example) to be implemented at different future problem times. The user is able to 'stack' up commands for future implementation. While the NPA user adds commands to the stack, TRAC removes them from the stack after they have been implemented. The user can remove a command that has not been implemented from the stack by entering the same command again but with the four letters "AUTO" for its "value". This command also can be used, when there is not a similar command in the stack (same type and time), to return control of the hardware action to the hardware's AUTOMATIC control procedure defined by TRAC's input data.

#### BACKUP/BRANCH AND PLAYBACK

During an NPA run, there are three occasions when TRAC is not executed on suffix E: problem setup, backup/branch, and playback. Problem setup was described earlier. Backup/branch and playback are user-convenient features of the NPA that will be described now. They greatly extend the analysis capability of the NPA for the user.

Backup/branch is a procedure implemented at any time during TRAC execution wherein the NPA user can stop the TRAC calculation and restart it at some earlier problem time. Restarting TRAC produces a separate identifiable run with its own TRAC input/output files; thus, it is a branch calculation. The NPA user initiates a backup/branch procedure by entering a "BACKUP TO time" command or one of the TRAC hardware-adjustment commands with an "AT time" that is before TRAC's current problem time. TRAC responds to the latter commands by sending a message to the NPA executive program asking if the user wishes to do a backup. The question is displayed to the NPA user (see Fig. 5). If answered "y" for yes, a backup procedure is initiated; if answered "n" for no, the "time" in the command is changed to the current problem time, the command is implemented, and TRAC continues its execution.

The NPA executive program performs the backup/branch procedure under interactive-dialog control from the NPA user. The NPA executive program sends a STOP command to TRAC. TRAC terminates execution with an "end exit" status; IOGRF terminates as well. The NPA user is given the options of renaming the terminated TRAC-run output files and storing them on the CFS. The actual renaming and storing are done by the NPA executive program. Files TRACIN and TRCRST are renamed by adding the number of this backup/branch (1, 2, 3, ...) to the end of their names. Then, a new TRACIN file is generated for the

branch calculation; file TRCDMP is copied and named TRCRST. Only the graphics data before the backup time are saved in file TRCIGR by redefining the total number of time points of graphics data in TRCIGR to this lesser number. The NPA executive program then starts up TRAC and IOGRF to begin the branch calculation. When reading the TRAC command-stack parameters from file TRCRST, all commands to be implemented at and after the backup time are discarded. The TRAC data dump just before the backup time is used. To complete the backup/branch procedure, the NPA executive program automatically sends a "PAUSE AT backup time" command and the hardware-adjustment command that caused the backup (if such is the case) to TRAC.

Playback is a procedure for interactively analyzing on NPA graphics displays all the graphics data in existing TRCGRF1 files (renamed AGRF1, BGRF1, ..., ZGRF1) from previous TRAC runs with the NPA. At present, only the generic and detailed data parameters in Table I can be accessed from the AGRF1, BGRF1, ..., ZGRF1 files by program IOGRF during a playback. Data from any time frame of the transient can be displayed. Data from successive branch calculations can be concatenated for display by renaming the TRCGRF1 files from the initial TRAC run and subsequent branch calculations with the names AGRF1, BGRF1, CGRF1, ... The time intervals for data to be extracted from each of these files and then combined are interactively specified by the user to the NPA executive program that then writes it to file PBKTIMES for program IOGRF.

In the future, when the NPA executive and IOGRF programs are downloaded to execute on the Tektronix 4115B intelligent workstation, the playback procedure would be executed entirely on the workstation. A telephone link to the mainframe computer would not be needed when operating the NPA in the playback mode. Analyzing the results of previous TRAC runs with this interactive graphics-display capability would be inexpensive and convenient. The TRCGRF1 files from such runs could be copied by the workstation onto a floppy disk and mailed to other NPA workstation sites for further analysis and evaluation.

#### FUTURE DEVELOPMENT

The basic capabilities of the NPA are programmed and operational on both the TRAC-based and RELAP5-based NPA versions. Many of the desired enhancements to this capability for the TRAC-based NPA version are mentioned throughout the text of this paper. A list of future developments for the NPA follows:

1. Combine the best features of the Los Alamos TRAC-based and INEL RELAP5-based NPA versions into one NPA for running either code.
2. Download most functions of the NPA executive and IOGRF programs for execution on the Tektronix 4115B intelligent workstation. While doing this, maintain as an option the current capability to execute the entire NPA on a mainframe computer so that a less expensive, nonintelligent color-graphics terminal can be used as well.
3. Implement a menu-driven data-base management system to provide convenient storage and retrieval of NPA files. Currently, only specific predetermined files can be accessed interactively.

4. Produce a special NPA thermal-hydraulic code with a three-dimensional two step numerics and vectorization for fast running.
5. Incorporate into the NPA the software being developed by TDC to create TRAC or RELAP5 input-data files using the NPDB and numerical-modeling information obtained interactively from the NPA user.
6. Provide interactive capability to renode a TRAC or RELAP5 input-data file. When coupled with the backup/branch procedure, this would allow, among other advantages, arbitrary placement of breaks for loss-of-coolant analysis (LOCA) studies.
7. Provide batch-execution capability for the NPA so that a more cost-effective TRAC/RELAP5 calculation can be performed when playback analysis of the results is sufficient.
8. Expand the graphics-display capabilities; for example, animation of flow information, three-dimensional displays, automatic generation of plant-noding displays, interactive definition of graphics displays, etc.
9. Give the NPA user the interactive capability to define or modify the names of generic data, detailed data, and adjustable-hardware components or actions.
10. Incorporate additional commands that would be useful to the user.
11. Create as many suitable input-data files as possible for other power plants.
12. Increase flexibility in all areas of NPA user/executive program interaction.

## CONCLUSIONS

Recent advances in computer technology and numerical-solution methods have made it appropriate to develop the user-convenient features of the NPA described in this paper. The computational speed and high-resolution color graphics now available make it possible to evaluate and analyze interactively power-plant thermal-hydraulic behavior with best-estimate computer models. Sufficient computational speed is available when using current-generation mainframe computers to execute the TRAC code. This program uses the recently developed stability-enhancing two-step numerical method (Ref. 3) that allows very large time steps (thus, fewer time steps) to be employed for evaluating slow transients. With a reasonable numerical model of a power plant (several hundred nodes), operational transients can be evaluated by TRAC (PF1/MOD1 version) faster than real time. With such speed, the NPA running TRAC becomes a useful interactive analyzer. The high-resolution color-graphics terminals now available make it possible with graphics to analyze calculational results effectively. Presenting these graphics concurrently with the calculation gives the user the information needed to interact and control the calculation and its solution. While the NPA is a convenient power-plant analyzer, it also can be used as a highly accurate power-plant simulator.

TRAC is an extremely complex fluid-dynamics code for power-plant analysis. Preparing input data and executing TRAC on a computer require considerable expertise, experience, effort, and time. Much of this expertise and experience is being programmed into the NPA. Automating the process with the NPA eliminates most of the effort and the time requirement. Flexibility is maintained by interactive dialog with the user. With the NPA, TRAC is no longer the province of the expert; NPA provides an expert system that allows the user to be the analyst. Under NPA control, TRAC becomes a convenient and useful tool for power-plant operation and safety analysis.

#### REFERENCES

1. "TRAC-PF1/MOD1: An Advanced Best-Estimate Computer Program for Pressurized Water Reactor Thermal-Hydraulic Analysis," Los Alamos National Laboratory report LA-10157-MS, NUREG/CR-3858 (to be published).
2. "RELAP5/MOD1 Code Manual, Volume 1: System Models and Numerical Methods, Volume 2: Users Guide and Input Requirements, Volume 3: Checkout Problems Summary," EG&G Idaho, Inc. report EGG-2070 Draft Revision 1, NUREG/CR-1826 (March 1981).
3. J. H. Mahaffy, "A Stability-Enhancing Two-Step Method for Fluid Flow Calculations," J. Comp. Phys. 46, 329 (1982).

NUCLEAR PLANT ANALYZER DEVELOPMENT AT THE  
IDAHO NATIONAL ENGINEERING LABORATORY<sup>a</sup>

E. Thomas Laats  
Kenneth D. Russell  
Howard D. Stewart  
Robert N. Hagen  
Ronald J. Beelman  
John E. Tolli

EG&G Idaho, Inc.

The Nuclear Plant Analyzer (NPA) was developed for the United States Nuclear Regulatory Commission (USNRC) under the sponsorship of the USNRC's Office of Nuclear Regulatory Research. The NPA is the USNRC's chief computerized tool promoting fast and easy access to accurate computational tools, commercial plant design and behavior data, and experimental data obtained from the NRC's numerous test programs. The NPA development effort is a joint undertaking among the Idaho National Engineering Laboratory (INEL), the Los Alamos National Laboratory (LANL), and Technology Development of California (TDC). The INEL has responsibility for overall project direction, with LANL providing supporting development particularly related to the TRAC-PWR series of codes,<sup>1</sup> and TDC providing development of a major component of the NPA, namely the Nuclear Plant Data Bank (NPDB).<sup>2</sup> This paper addresses the INEL activities during FY-1984. The LANL and TDC activities are covered by other papers at this meeting.

The NPA is a computer software package that integrates large nuclear reactor systems codes, such as RELAP5<sup>3</sup> and TRAC-PF1, with advanced graphics capabilities and numerous data bases of experimental<sup>4</sup> and analytical data, including the NPDB. User friendly interfaces tie these components together to reduce the time and skill level required to utilize these analytical tools that were separate entities before the establishment of the NPA.

Late in 1983, the NPA entered production operation. All functions were performed on the INEL Control Data Corporation mainframe computers and the user interacted with the NPA through a "Type-1" (nonintelligent) workstation. Since that time, NPA development efforts have focused on four areas. The design, specifications, and selection of a microcomputer-based "Type-2" workstation were completed. The Tektronix 4115B color graphics device was selected as the major component of the station. A Type-2 workstation was acquired in July 1984 and initial downloading of rudimentary graphics functions commenced, more to learn the full capabilities and usefulness of the workstation hardware than as a production operation device.

---

a. Work supported by the U.S. Nuclear Regulatory Commission, Office of Nuclear Regulatory Research Under DOE Contract No. DE-AC07-76ID01570.

In parallel, an extensive effort was conducted to modify the TRAC-BD1/MOD1 code<sup>5</sup> to enable on-line interactive control of a calculation through the NPA. That effort was completed in July 1984, and now NPA users have the ability with the appropriate TRAC input model, to interactively control a calculation in a manner similar to the controls available to a power plant operator (e.g., trip pumps and valves).

With the addition of TRAC-BD1, the computer codes whose data have been displayed through the NPA currently include RELAP5, TRAC-BD1, CRAC2,<sup>6</sup> and SCDAP.<sup>7</sup> The libraries containing the graphical display masks have been increasing, also. Eleven graphical depictions representing various Westinghouse, Babcock and Wilcox, and Combustion Engineering pressurized water reactor plants have been developed to date, along with depictions of a General Electric boiling water reactor/4 primary system and a balance of plant configuration.

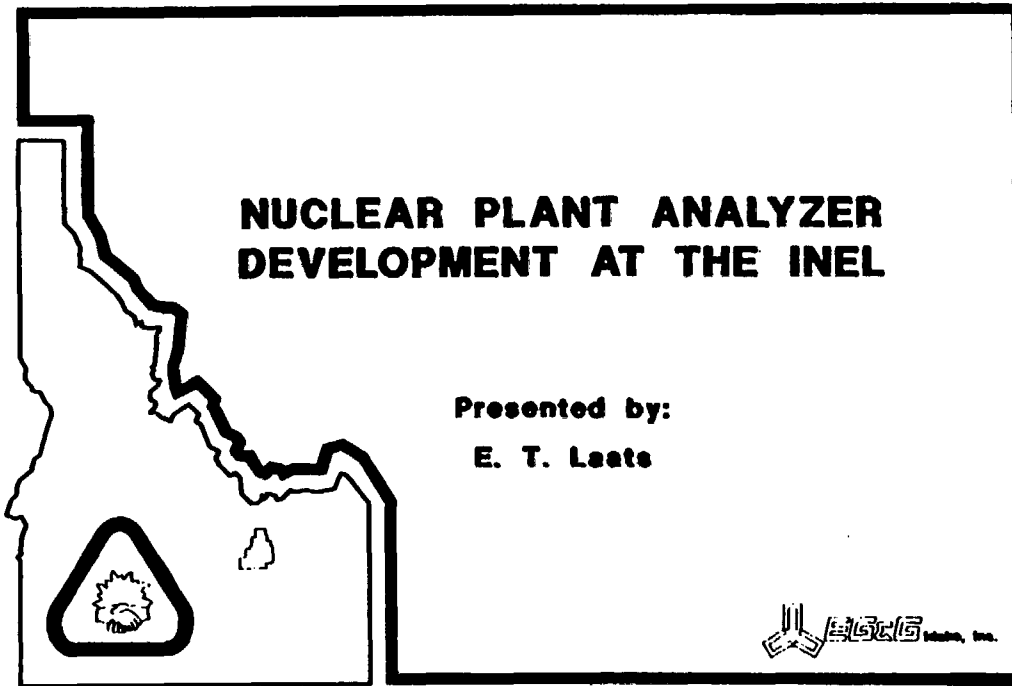
Finally, overall NPA usability and friendliness have been enhanced through numerous software upgrades and the issuance of an easy-to-read users manual<sup>8</sup> that describes how to perform basic NPA functions.

Future directions of the NPA program will be concentrated on first, downloading and enhancing many of the NPA functions on the Type-2 (microcomputer-based) workstation, and second, building the numerous libraries or data bases within the NPA system. Also, greater computational power will be added through improvements to existing codes and models, as well as the incorporation of other computer codes that simulate power plant performance not currently modeled by the existing package of codes.

#### REFERENCES

1. Safety Code Development Group, TRAC-PF1: An Advanced Best Estimate Computer Program for Pressurized Water Reactor Analysis, Los Alamos National Laboratory report (to be published).
2. H. Kopp et al., Automating TRAC Decks Using the Nuclear Plant Data Bank (NPDB), NUREG/CP-0048, Vol. 2, January 1984.
3. V. H. Ransom, "RELAP/MOD2: For PWR Transient Analysis," Proceedings of the Joint CNS/ANS International Conference on Numerical Methods in Nuclear Engineering, September 6-9, 1983, Montreal, Quebec, Canada.
4. N. R. Scofield et al., Introductory User's Manual for the U.S. Nuclear Regulatory Commission Reactor Safety Research Data Bank, NUREG/CR-2531, Revision 2, March 1984.
5. W. L. Weaver et al., TRAC-BD1: An Improved Analysis Code for Boiling Water Reactor Analysis, NUREG/CR-0027, February 1983.
6. L. T. Ritchie et al., Calculations of Reactor Accident Consequences Version 2: CRAC2 Model Description, NUREG/CR-2552, December 1982.

7. G. A. Berna et al., SCDAP/MOD0: A Computer Code for the Analysis of LWR Fuel Bundle Behavior During Severe Accident Transients, WR-NSMD-078, December 1982.
8. E. T. Laats, User's Manual for the U.S. Nuclear Regulatory Commissions' Nuclear Plant Analyzer, EGG-NTP-6657, June 1984.



## Major Contributors

R. J. Beelman	K. D. Russell
D. L. Carlson	H. D. Stewart
J. N. Curtis	D. H. Schwieder
R. N. Hagen	D. N. Tillitt
E. T. Laats	J. E. Tolli
G. E. McConnell	R. J. Wagner

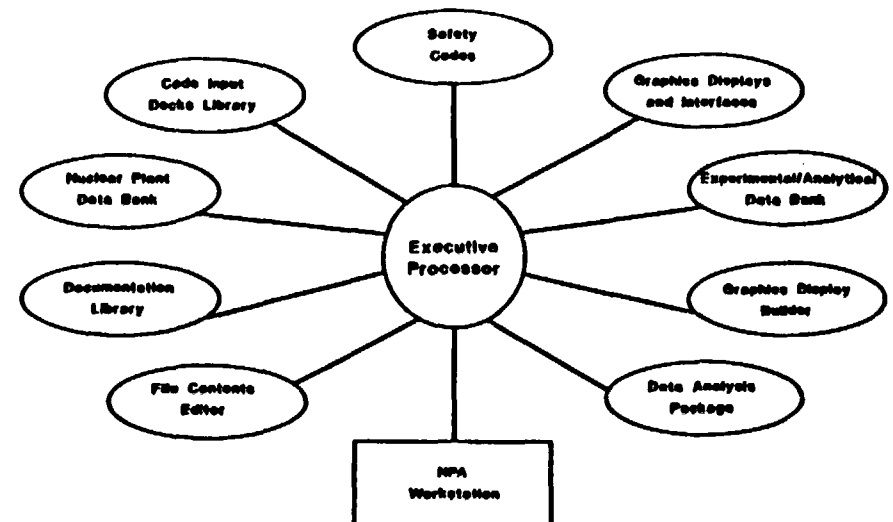
427

CS00000

## Four goals are being addressed.

- Enable diverse application of advanced system codes by broad set of users
- Provide NRC direct and immediate access during emergencies
- Improve contractor responsiveness to NRC technical assistance requests
- Provide integrated package of numerous simulation codes to cover large spectrum of plant conditions

## Nuclear Plant Analyzer Components



CS00000

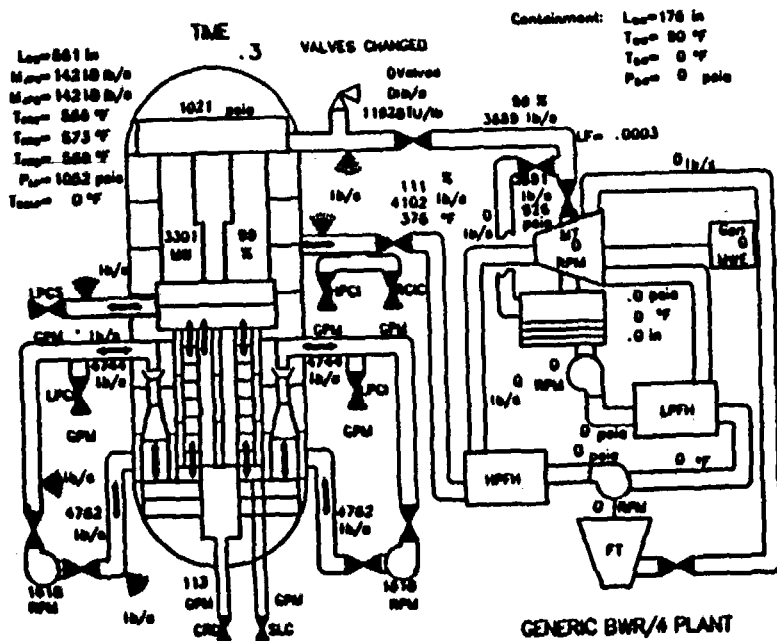
## PART ONE

Movie to demonstrate two new applications.

- BWR/4 ATWS calculation using RELAP5/MOD1.6
- TMI-2 calculation using SCDAP/MOD1

- Boiling Water Reactor/4 model using RELAP5/MOD1.6
- Spurious main steam isolation valve closure 0 to 5s
- Plant follows automatic controls for first 144s, then operator takes control

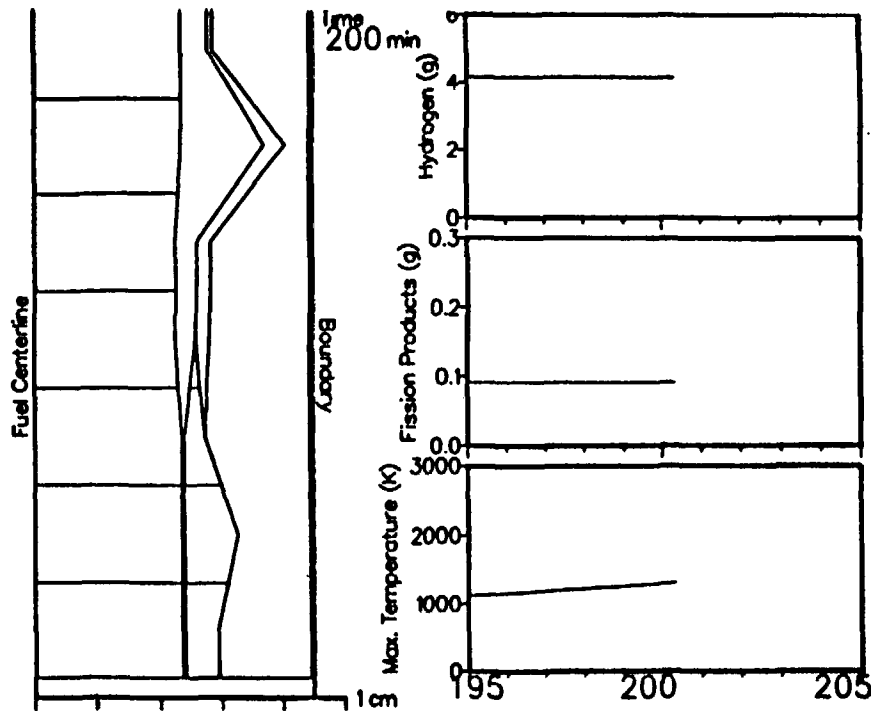
428



## PART TWO

- Three Mile Island - Unit 2 model using SCDAP/MOD1
- Event of March 29, 1979

CA00000



429

Graphical display masks have been developed.

- |                     |   |
|---------------------|---|
| <b>B&amp;W</b>      | - System, ATOG, steam generator masks             |
| <b>C-E</b>          | - System mask                                     |
| <b>GE BWR/4</b>     | - System containment mask                         |
| <b>GE BWR/6</b>     | - System mask                                     |
| <b>Westinghouse</b> | - 3-Loop system mask<br>- Indian Point area masks |
| <b>Semiscale</b>    | - System mask                                     |

**TRAC-BD1 code modified to enable on-line interactive control through NPA.**

- Completed in July 1984.
- Enables interactive control of model similar to plant operator's controls.

CS00001

Noteworthy applications of NPA in FY-1984 include

- Operator guidelines evaluation
- Emergency procedures guidelines evaluation
- Simulation model for drills and critique at NRC Operations Center.

CS00000

CS00004

**Future direction is oriented toward enhanced operations production.**

- **Download and enhance functions on Type-2 workstation.**
- **Build NPA libraries and data bases.**

\*\*\*\*\*

Development of  
BWR PLANT ANALYZER\*

W. Wulff, H.S. Cheng, S.V. Lekach, A. Stritar and A.N. Mallen  
Department of Nuclear Energy  
Brookhaven National Laboratory  
Upton, NY 11973

1. Purpose and Achievements (Slide No. 2)\*\*

The BWR Plant Analyzer has been developed for realistic and accurate simulations of normal and severe abnormal transients in BWR power plants at high simulation speeds, low capital and operating costs and with outstanding user conveniences. The simulation encompasses neutron kinetics, heat conduction in fuel structures, nonequilibrium, nonhomogeneous coolant dynamics, steam line acoustics, and the dynamics of turbines, condensers, feedwater pumps and heaters, of the suppression pool, the control systems and the plant protection systems.

These objectives have been achieved. Advanced modeling, using extensively analytical integration and dynamic evaluation of analytical solutions, has been combined with modern minicomputer technology for high-speed simulation of complex systems. The High-Speed Interactive Plant Analyzer code HIPA-BWR has been implemented on the AD10 peripheral parallel processor.

2. Applications (Slide No. 3)

The Plant Analyzer has been developed to reduce computing time and cost and also the manpower required for safety analyses. The Plant Analyzer is particularly suitable when many transients are to be simulated for a chosen plant, such as for parametric studies, for studies in support of risk assessment, to identify accident signatures, to establish system stability and to assess the consequences from control system failures. We have simulated 37 different transients for a BWR plant in less than four days.

The Plant Analyzer's computing speed and its built-in, high-speed analog-to-digital and digital-to-analog converters for I/O signal processing, makes it a powerful tool for computer-aided power plant operations. Computed signals could be compared with signals from a power plant for the purpose of plant performance monitoring and failure detection. The Plant Analyzer could serve to diagnose component or system failures. The Plant Analyzer could also be locked in-step with the power plant and then initiated at some time to compute in advance the consequences of operator actions contemplated for the mitigation of an accident. The results could be used to optimize remedial strategies before the operator has to act.

\* Work performed under the auspices of the U.S. Nuclear Regulatory Commission.

\*\*Most slides are reproduced at the end of this paper.

The Plant Analyzer can also serve to optimize plant performance, particularly to optimize the control system.

### 3. Recent Achievements (Slide No. 4)

Thirty-seven different transients, induced by both single and multiple failures or events have been carried out in less than four days. The results are documented [1].

Plant Analyzer results have been compared [1] with results from TRAC-BD1 [2], RELAP-5 [3,4], RAMONA-3B [2] and with results published earlier by General Electric [5]. Comparisons were also made with results published in the Final Safety Analysis (FSAR) report, but only to verify the proper functioning of the Plant Analyzer because the FSAR results are not comparable with best estimate results.

The comparisons show good agreement as long as the reference codes perform properly. Differences between Plant Analyzer and reference code results have been analyzed [1].

Models have been improved. The slip flow model required earlier [1] has been replaced by the drift flux model. The Plant Analyzer now simulates countercurrent flows and flow reversal. The level tracking model is now based on mass jump conditions from the level and accounts rigorously for falling films and liquid sprays above the level. A boron tracking model, based on analytical integration of the transport equation, has been implemented successfully.

### 4. The Plant Analyzer Operation (Slides No. 5 to 8)

The BWR/4 plant schematic of the HIPA-BWR/4 model is shown in Slide No. 5. It shows the reactor vessel and the balance of plant systems as well as the systems for feedwater control, pressure regulation and recirculation flow controls.

Almost all malfunctions are entered from the control panel, simply by setting a switch and/or a dial, as shown in Slide No. 6. (Other malfunctions, as well as the geometric and operating parameters, trip set points and control function parameters, are entered from the keyboard without reloading of program.)

By setting only three switches, for example, one sets up the Plant Analyzer for a turbine trip without bypass and without scram. The trips are indicated in the schematic of the plant shown in Slide No. 7.

The results are displayed instantly and while the calculations are being performed. Labeled graphs can be displayed on-line, on the monitor of the IBM personal computer as shown on Slide No. 8.

5. Results (Slides No. 9 through 17, taken from [1] and Slides No. 18 and 19)

Comparisons between TRAC-BD1 results and Plant Analyzer simulations are shown in Slide No. 9 for an MSIV closure-induced ATWS. The top graph shows the comparisons for the system pressure versus time. There are two TRAC curves for the pressure as reported in Reference [2]. The validity of the TRAC curve with the higher peak is in doubt [2], the curve with the lower peak agrees well with that of the Plant Analyzer. The same can be said for the fission power displayed in the bottom part of Slide No. 1.

Comparisons between RELAP-5 results and Plant Analyzer results are shown in Slides No. 10 through 15. The comparisons were carried out for feedwater controller failure at full demand (Slides No. 10 and 11), for MSIV closure with scram operating (Slide No. 12), and for loss of feedwater (Slides No. 13 through 15). The major difference between RELAP-5 and Plant Analyzer results are seen in the bottom graph of Slide No. 15. RELAP-5 was executed by imposing HPCI liquid injection below the falling level in the downcomer. Under this condition, steam cannot condense onto the subcooled liquid, and the pressure remains high. HIPA in the Plant Analyzer permits condensation between the injection nozzles and the level below, and the pressure falls temporarily.

Comparisons between RAMONA-3B and Plant Analyzer results are shown in Slide No. 16 for an MSIV closure-induced ATWS. The comparisons show good agreement.

The same MSIV closure-induced ATWS was also used as one of the ten different transients for the comparisons between GE calculations and Plant Analyzer results. The comparison is shown in Slide No. 17. The GE results show significantly slower depressurization rates than both the Plant Analyzer, TRAC-BD1 and RAMONA-3B. Analysis has shown [1] that the GE calculations are wrong. The differences in peak pressures during valve cycling are due to differences in set points.

Slides No. 18 and 19 show, respectively, the core-averaged boron concentration, the total reactivity, the fission power and the system pressure for an MSIV closure-induced ATWS as simulated by the Plant Analyzer.

6. Plant Analyzer Characteristics (Slides No. 20 through 25)

The high simulation speed has been achieved in the mini-computer of the Plant Analyzer for two reasons: Firstly, five modeling principles have been used that distinguish the Plant Analyzer from all other plant analyzers [6] and reduce drastically the number of arithmetic operations executed during the simulation.

Secondly, the AD10, a special-purpose peripheral processor, has been used. The AD10 is specifically designed for high-speed simulations of complex systems. Its major features are listed on Slide No. 20.

Slide No. 21 shows the AD10 with a standard oscilloscope for size reference. Slide No. 22 shows the PDP host computer, Slide No. 23 the specifically designed control panel from which many combinations of 29 malfunctions can be introduced, and Slide No. 24 shows a schematic of the Plant Analyzer's component configuration. Slide No. 25 shows the arrangement of the control panel, Tektronix storage oscilloscope and IBM personal computer, as they are used to operate the plant analyzer.

#### 7. Program Statistics (Slide No. 26)

HIPA is a detailed BWR systems code. Four equations for nonequilibrium, nonhomogeneous two-phase flow are integrated for 54 computational cells in the reactor vessel alone.

Fifty-five differential equations have been integrated analytically. Their solutions are evaluated dynamically during the transient. Two-hundred additional state equations are integrated by a variety of high-order integration algorithms. Multi-stepping for stiff equations is used, bringing the total number of integrations per time step up to 330.

Over 4,000 subroutine output parameters are computed, including multi-dimensional table interpolations from 200 distinct tables. All I/O channels are scanned 200 times a second.

The simulation is advanced from one time level to the next in only 5.4 milliseconds.

#### 8. Conclusions ( Slide No. 27)

Realistic and accurate LWR simulations are possible. They can be achieved at very low cost, great user convenience and high simulation speeds, provided proper modeling techniques are used and modern minicomputers, designed specifically for high-speed simulations of large, complex systems are selected.

#### 9. Future Plans (Slide No. 28)

We intend to expand the range of applications for BWR simulations in government and industry. We plan also to develop this new technology for the simulation of PWR power plants.

**Development of  
*BWR PLANT ANALYZER***

**at**

**DEPARTMENT OF NUCLEAR ENERGY  
BROOKHAVEN NATIONAL LABORATORY  
UPTON, NEW YORK 11973**

**Slide No. 1**

**H. S. Cheng  
S. V. Lekach  
A. N. Mallen  
A. Stritar  
W. Wulff**

**October 1984**

## 1. PURPOSE AND ACHIEVEMENTS

Slide No. 2

- **Realistic and accurate simulations of normal and severe abnormal BWR transients at:**
    - **High simulation speed (10 times real-time speed),**
    - **Low cost (dedicated minicomputer AD-10), with**
    - **Outstanding user convenience and instant response to changes of input data.**
  - **Simulation includes**
    - Nuclear Steam Supply System**
    - Balance of Plant,**
    - Plant Protection System,**
    - Control Systems.**
- HIP A-BWR**

## 2. APPLICATIONS

Slide No. 3

- ***Safety Analyses:***
  - Parametric Studies,**
  - Risk Assessment,**
  - Accident Signatures,**
  - System Stability,**
  - Consequences from Control System Failures.**
- ***Computer-Aided Plant Operation:***
  - (Potential Application)***
  - Plant Monitoring,**
  - Failure Diagnostics,**
  - Accident Mitigation.**
- ***Optimizations: (Potential Application)***
  - Component Design,**
  - Control Systems.**

### 3. RECENT ACHIEVEMENTS

37 Single- and Multiple-Failure Events  
simulated and documented  
(BNL-NUREG-51812, NUREG/CR-3943).

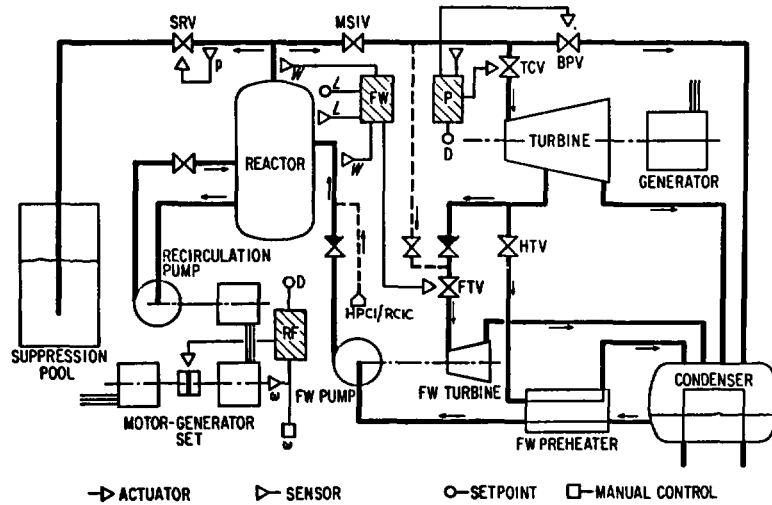
Slide No. 4

Developmental Assessment:

HIPAs Comparisons with:  
TRAC-BD1 (ASME 84-NE-10),  
RELAP-5 (BNL-NUREG-32396),  
RAMONA-3B (ASME 84-NE-10),  
General Electric (NUREG-0460),  
FSAR.

### MODEL IMPROVEMENTS

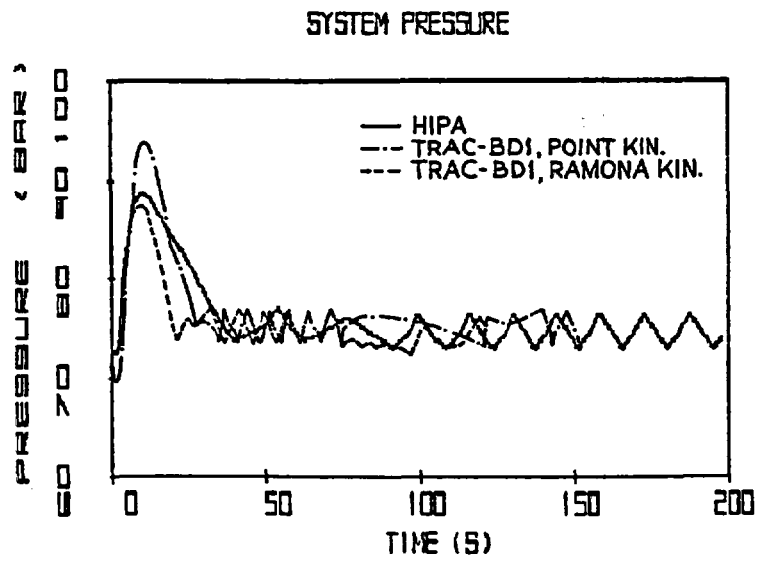
Slide No. 5



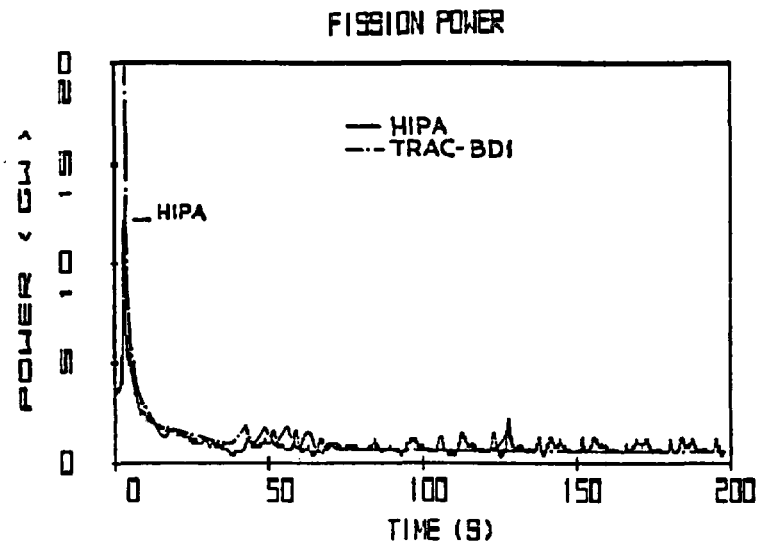
Slide No. 6 Photograph of Control Panel

Slide No. 7 Photograph of Trip Schematic

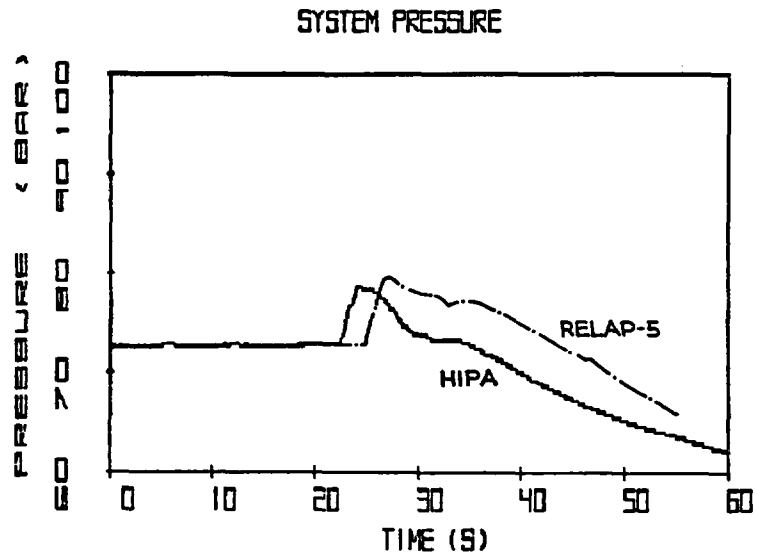
Slide No. 8 Photograph of Graphics Output



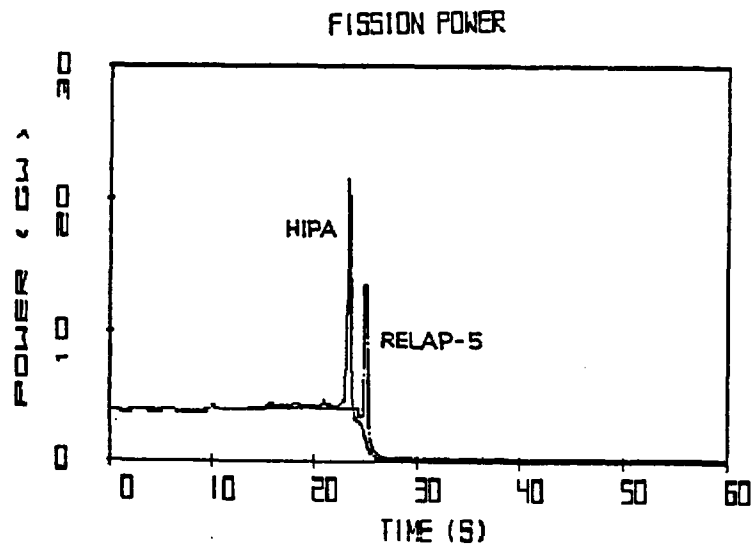
Slide No. 9



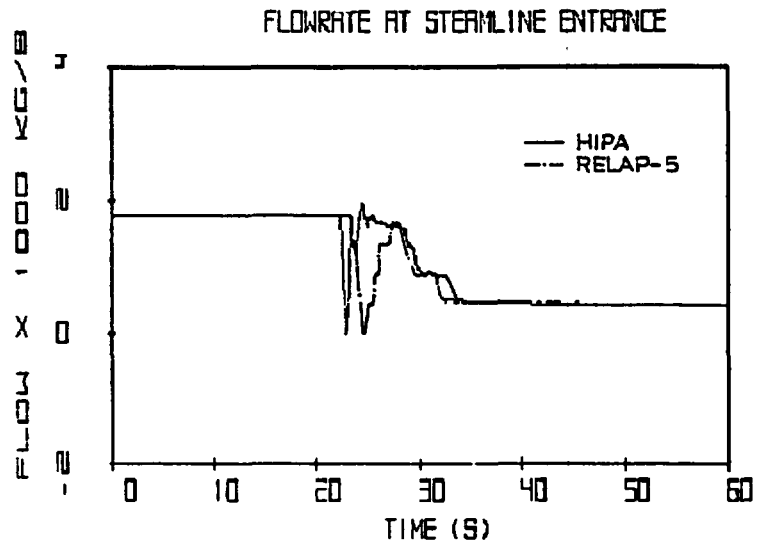
MSIV-ATWS



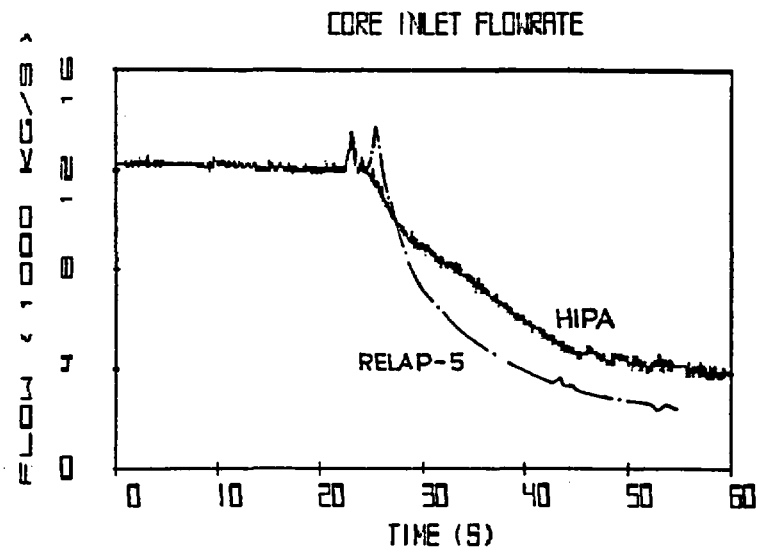
Slide No. 10



Failure of Feedwater Controller at Maximum Demand

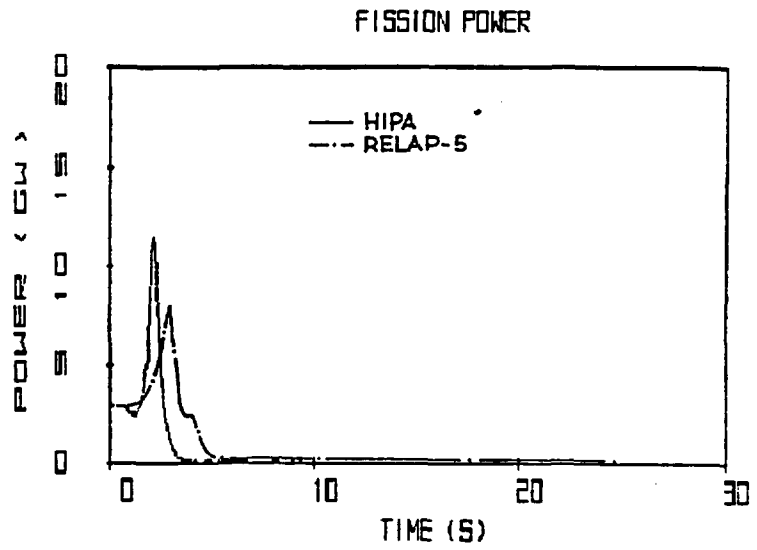
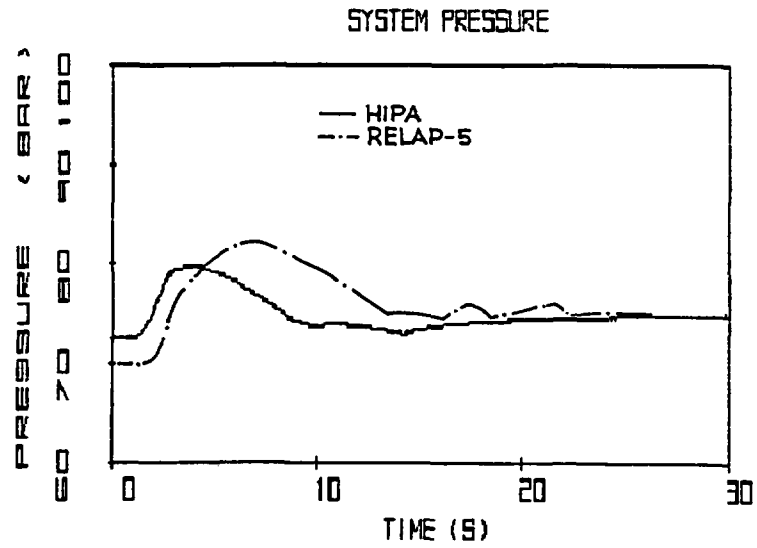


Slide No. 11

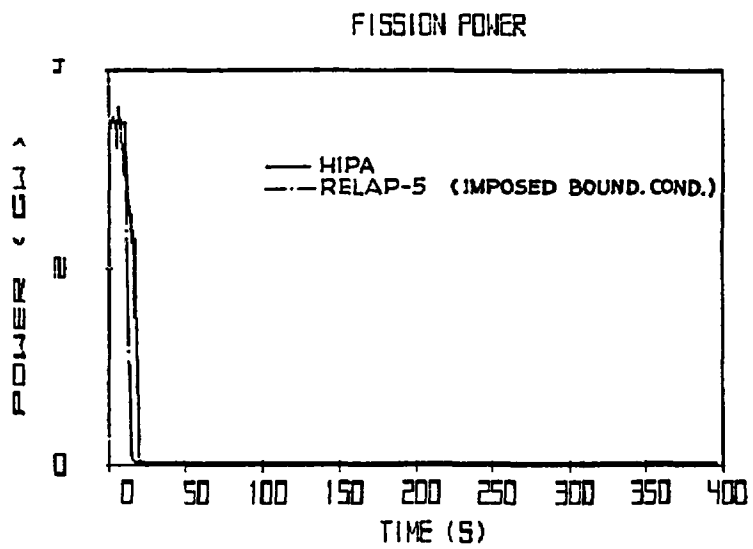


Failure of Feedwater Controller at Maximum Demand

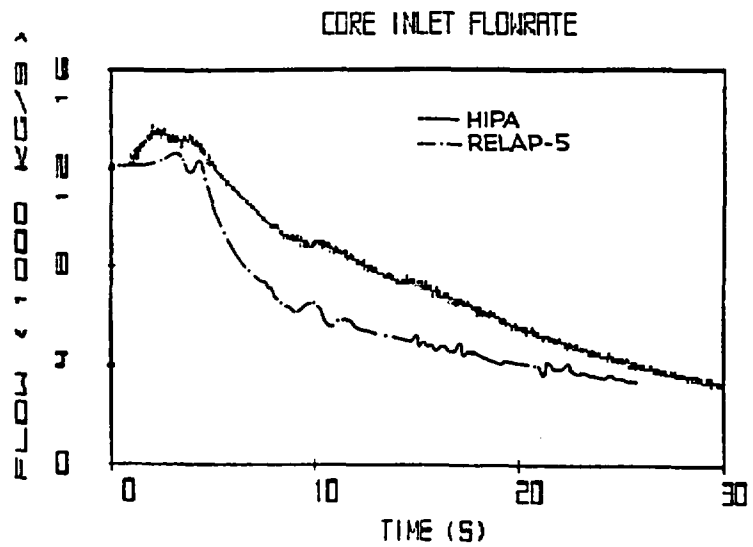
Slide No. 12



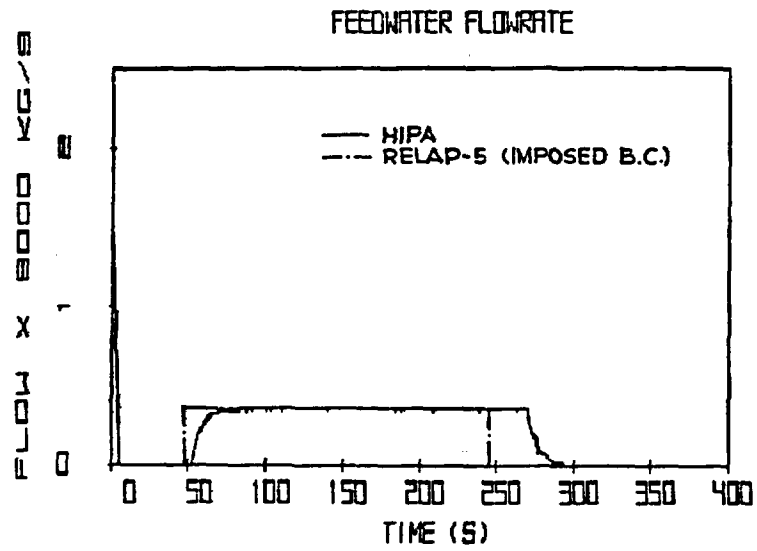
MSIV Closure / Reactor Scram



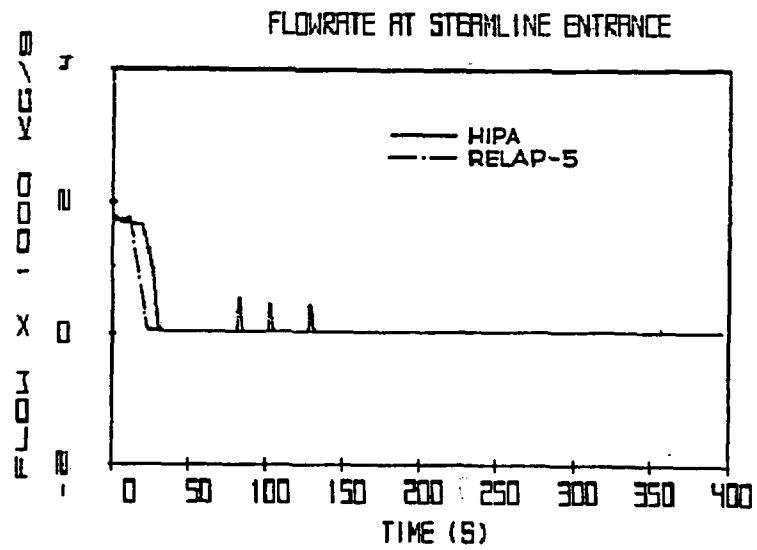
Slide No. 13



Loss of Feedwater Transients

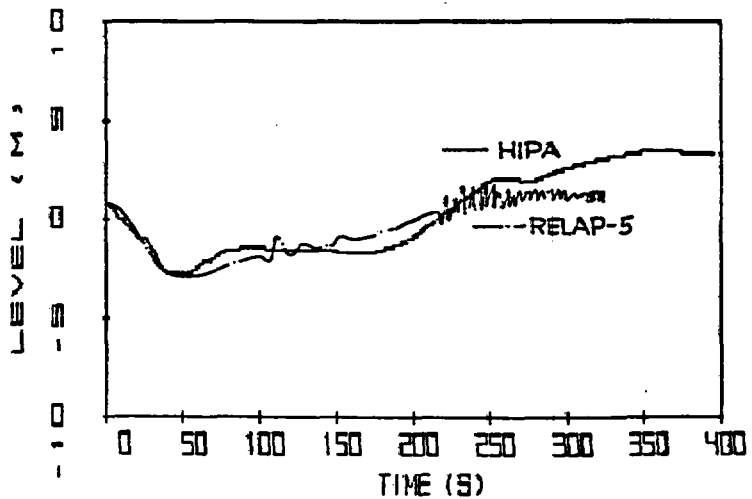


Slide No. 14



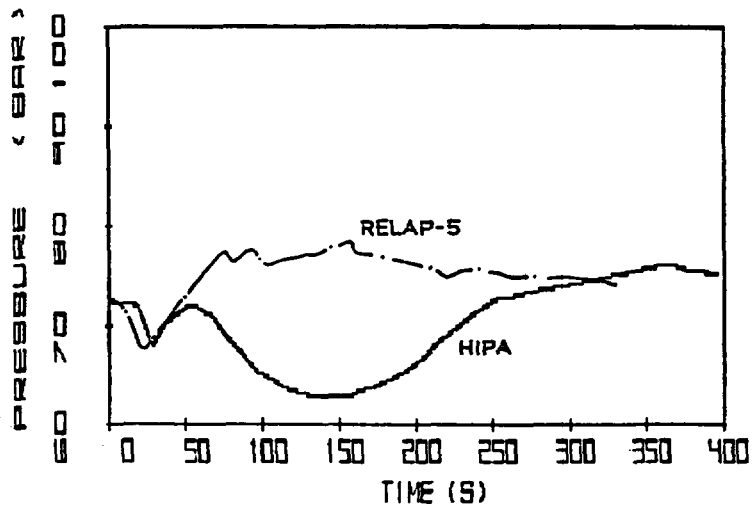
Loss of Feedwater Transients

COLLAPSED VESSEL LEVEL



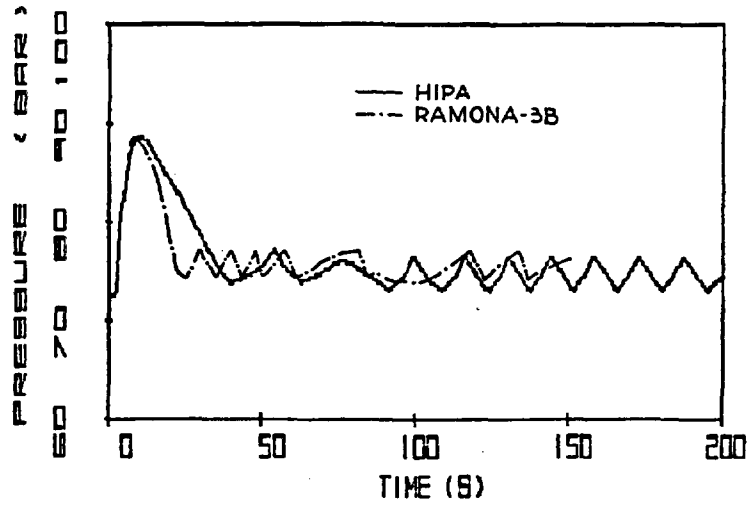
Slide No. 15

SYSTEM PRESSURE



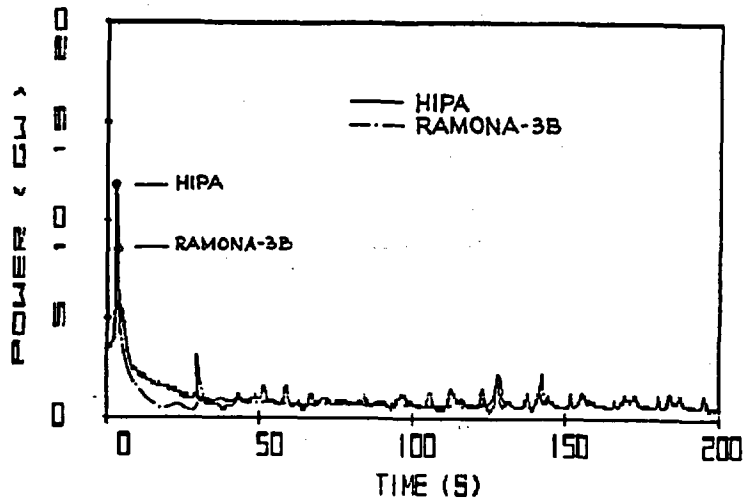
Loss of Feedwater Transients

SYSTEM PRESSURE



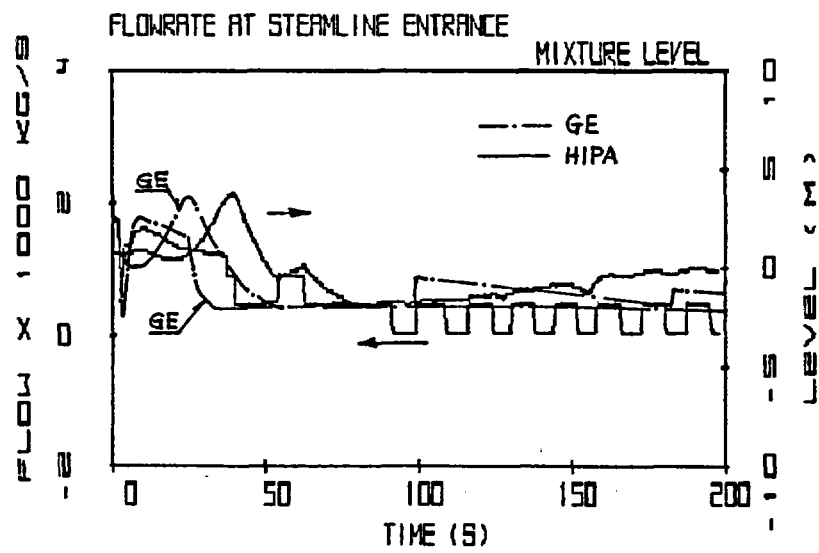
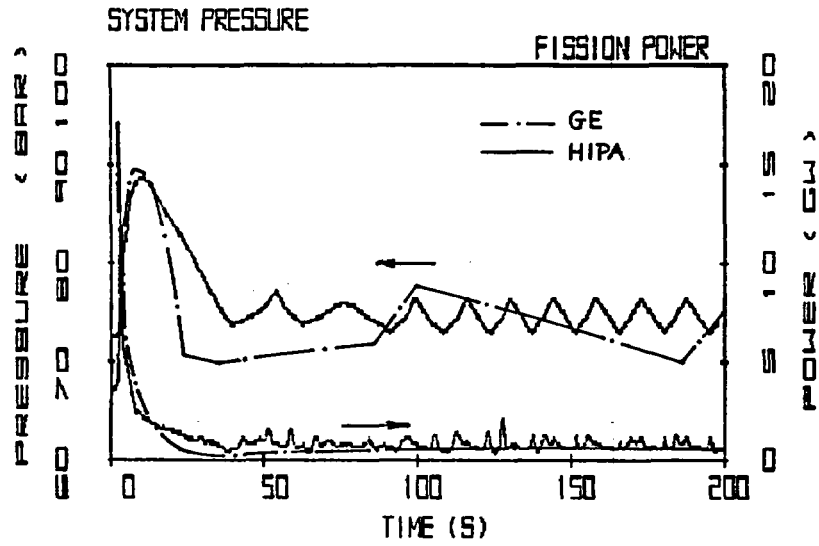
Slide No. 16

FISSION POWER



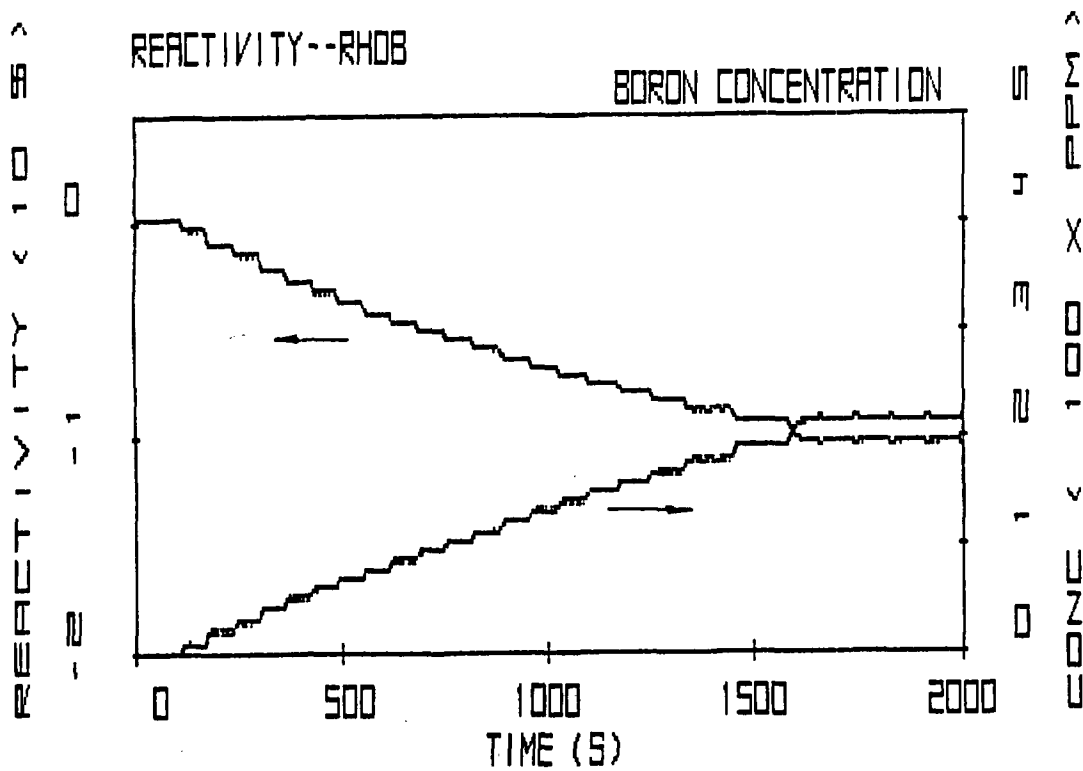
MSIV-AIWS

Slide No. 17

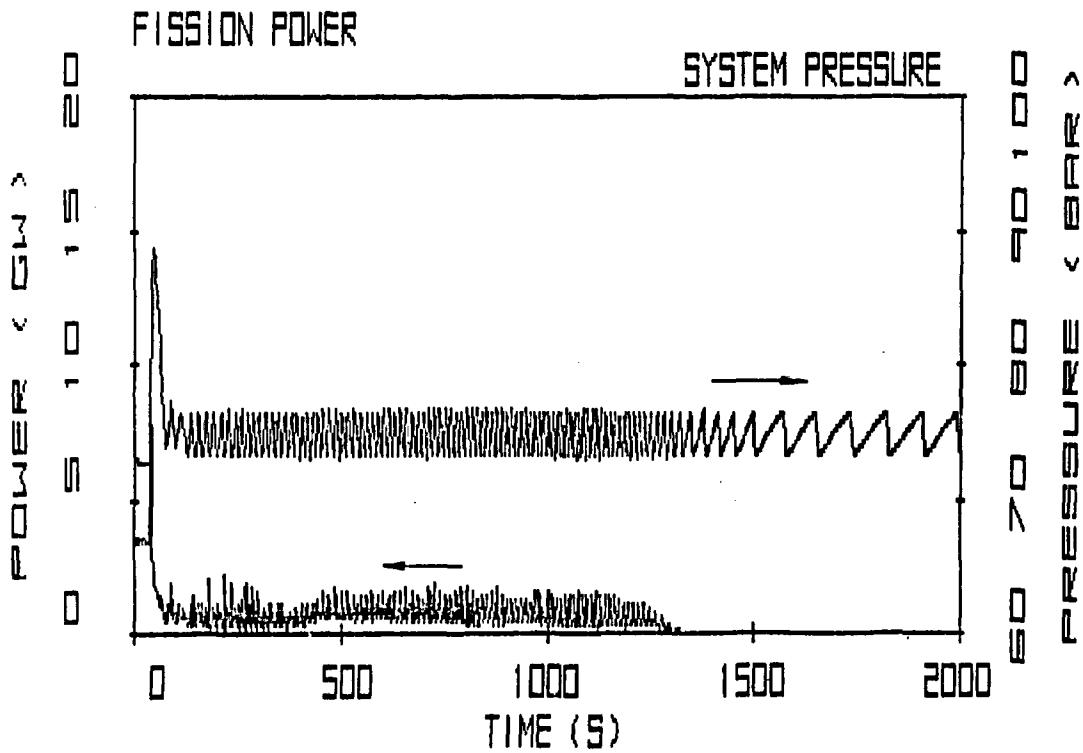


HIPA-GE Comparisons for MSIV-Initiated ATWS

Slide No. 18



Slide No. 19



## 6. PLANT ANALYZER CHARACTERISTICS

- **Modeling:**
  - 5 distinctive modeling principles.
- **SPECIAL-PURPOSE PERIPHERAL PROCESSOR:**
  - 6 distinct, task-specific parallel processors,
  - pipeline architecture,
  - synchronous computing at 10 MHz, up to 30 million operations per second,
  - hard-wired processors for interpolation of multi-dimensional tables,
  - high-speed I/O processing,
  - single programming rule to utilize fully the computer architecture.

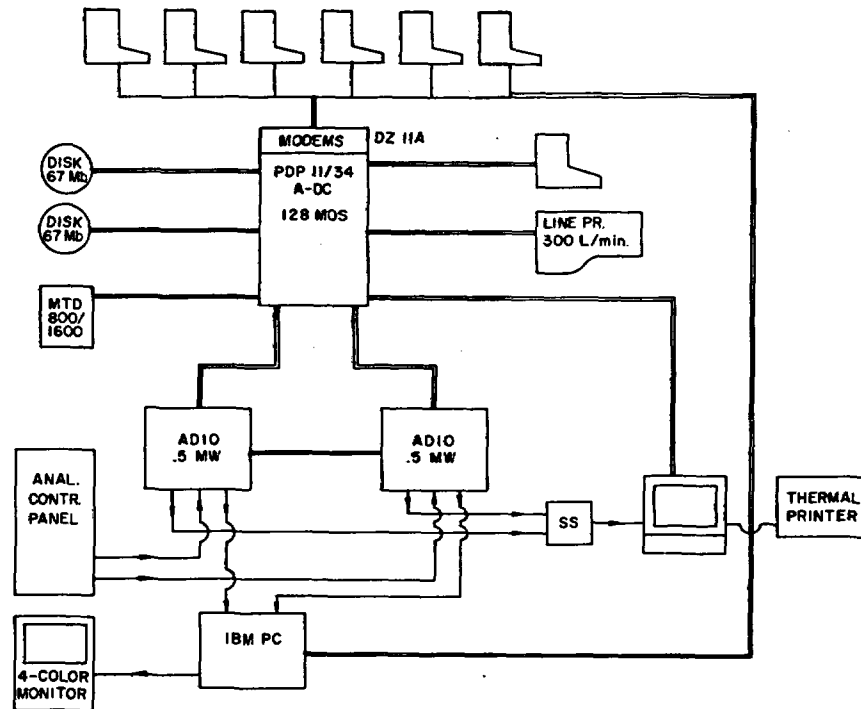
Slide No. 20

Slide No. 21 Photograph of AD10 Peripheral Processor

Slide No. 22 Photograph of Host Computer: PDP 11/34

Slide No. 23 Photograph of Control Panel

Slide No. 24



Slide No. 25 Photograph of Office with Control Panel, Tektronix and PC

## 7. PROGRAM STATISTICS

Slide No. 26

- **255 State Variables**  
**200 Integrators (330 integrations/  
time step)**  
**55 Analytical Integrations**
- **4,000 Module Output Parameters**  
**200 Distinct Multi-Dimensional Tables**  
**(some called 54 times/time step)**
- **All I/O channels scanned 200**  
**times/second**
- **Frame time is 5.4 milliseconds**  
**(independent of function complexity)**

## 8. CONCLUSIONS

Slide No. 27

- **Realistic and accurate LWR simulations**  
**are possible at:**  
**low cost,**  
**great convenience and**  
**high simulation speed by**
- **Advanced modeling and**
- **Use of special-purpose minicomputer**  
**for systems simulation**

## 9. FUTURE PLANS

Slide No. 28

- **Expand applications of BWR simulation**  
**technology,**
- **Develop PWR simulation capability.**

## References

- [1] Wulff, W., Cheng, H.S., Lekach, S.V. and Mallen, A.N., "The BWR Plant Analyzer," Brookhven National Laboratory, BNL-NUREG-51812, NUREG/CR-3943 (July 1984).
- [2] Hsu, C.J., Neymotin, L. and Saha, P., "Analysis of a Typical BWR/4 MSIV Closure ATW Using RAMONA-3B and TRAC-BD1 Codes," Joint ASME/ANS Conference on Design Construction and Operation of Nuclear Power Plants, Portland, Oregon, ASME Paper No. 84-NE-10 (1984).
- [3] Lu, M.S., Levine, M.M. and Shier, W.G., "BWR Loss of Feedwater Transient Analysis," Informal Report, BNL-NUREG-32396, (1984).
- [4] Lu, M.S. and Shire, W.G., "Analysis of Three Rapid Transients for a BWR/4 with the RELAP-5 Code," Informal Report, BNL-NUREG-34507 (1983).
- [5] General Electric Staff report, " Assessment of BWR Mitigation of ATWS," Vol.2, NEDO-24222, (NUREG-0460, Alternate No. 3), (1981).
- [6] Wulff, W., Cheng, H.S., Lekach, S.V., Mallen, A.N. and Stritar, A., "High-Speed LWR Transient Simulation for Optimizing Emergency Response," International Conference on Power Plant Simulation, Cuernavaca, Morelos, Mexico (November 1984).

<b>NRC FORM 335</b> (7-77)		<b>U.S. NUCLEAR REGULATORY COMMISSION</b> <b>BIBLIOGRAPHIC DATA SHEET</b>		<b>1. REPORT NUMBER (Assigned by DDC)</b> NUREG/CP-0058, Volume 2	
<b>4. TITLE AND SUBTITLE (Add Volume No., if appropriate)</b> Proceedings of the Twelfth Water Reactor Safety Research Information Meeting				<b>2. (Leave blank)</b>	
<b>7. AUTHOR(S)</b> Compiled by: Stanley A. Szawlewicz, Consultant				<b>3. RECIPIENT'S ACCESSION NO.</b>	
<b>9. PERFORMING ORGANIZATION NAME AND MAILING ADDRESS (Include Zip Code)</b> Office of Nuclear Regulatory Research U. S. Nuclear Regulatory Commission Washington, DC 20555				<b>5. DATE REPORT COMPLETED</b> MONTH   YEAR December   1984	
<b>12. SPONSORING ORGANIZATION NAME AND MAILING ADDRESS (Include Zip Code)</b> Same as Item 9.				<b>6. (Leave blank)</b>	
<b>13. TYPE OF REPORT</b> Collection of Conference Papers				<b>7. (Leave blank)</b>	
<b>13. TYPE OF REPORT</b> Collection of Conference Papers				<b>PERIOD COVERED (Inclusive dates)</b> October 22-26, 1984	
<b>15. SUPPLEMENTARY NOTES</b>				<b>8. (Leave blank)</b>	
<b>16. ABSTRACT (200 words or less)</b> <p>The papers published in this six volume report were presented at the Twelfth Water Reactor Safety Research Information Meeting held at the National Bureau of Standards, Gaithersburg, Maryland during the week of October 22-26, 1984. The papers describe progress and results of programs in nuclear safety research conducted in this country and abroad. Foreign participation in the meeting included twenty-six different papers presented by researchers from seven European countries, Japan, and Canada.</p>					
<b>17. KEY WORDS AND DOCUMENT ANALYSIS</b>			<b>17a. DESCRIPTORS</b>		
<b>17b. IDENTIFIERS/OPEN-ENDED TERMS</b>					
<b>18. AVAILABILITY STATEMENT</b> Unlimited			<b>19. SECURITY CLASS (This report)</b> Unclassified		<b>21. NO. OF PAGES</b>
<b>18. AVAILABILITY STATEMENT</b> Unlimited			<b>20. SECURITY CLASS (This page)</b> Unclassified		<b>22. PRICE</b> S

**UNITED STATES  
NUCLEAR REGULATORY COMMISSION  
WASHINGTON, D.C. 20555**

**OFFICIAL BUSINESS  
PENALTY FOR PRIVATE USE, \$300**

**FOURTH CLASS MAIL  
POSTAGE & FEES PAID  
USNRC  
WASH. D.C.  
PERMIT No. G-67**